

# Proceedings of the 2004 NASA/ONR Circulation Control Workshop

*Edited by  
Gregory S. Jones  
Langley Research Center, Hampton, Virginia*

*Ronald D. Joslin  
Office of Naval Research, Arlington, Virginia*



## The NASA STI Program Office . . . in Profile

Since its founding, NASA has been dedicated to the advancement of aeronautics and space science. The NASA Scientific and Technical Information (STI) Program Office plays a key part in helping NASA maintain this important role.

The NASA STI Program Office is operated by Langley Research Center, the lead center for NASA's scientific and technical information. The NASA STI Program Office provides access to the NASA STI Database, the largest collection of aeronautical and space science STI in the world. The Program Office is also NASA's institutional mechanism for disseminating the results of its research and development activities. These results are published by NASA in the NASA STI Report Series, which includes the following report types:

- **TECHNICAL PUBLICATION.** Reports of completed research or a major significant phase of research that present the results of NASA programs and include extensive data or theoretical analysis. Includes compilations of significant scientific and technical data and information deemed to be of continuing reference value. NASA counterpart of peer-reviewed formal professional papers, but having less stringent limitations on manuscript length and extent of graphic presentations.
- **TECHNICAL MEMORANDUM.** Scientific and technical findings that are preliminary or of specialized interest, e.g., quick release reports, working papers, and bibliographies that contain minimal annotation. Does not contain extensive analysis.
- **CONTRACTOR REPORT.** Scientific and technical findings by NASA-sponsored contractors and grantees.

- **CONFERENCE PUBLICATION.** Collected papers from scientific and technical conferences, symposia, seminars, or other meetings sponsored or co-sponsored by NASA.
- **SPECIAL PUBLICATION.** Scientific, technical, or historical information from NASA programs, projects, and missions, often concerned with subjects having substantial public interest.
- **TECHNICAL TRANSLATION.** English-language translations of foreign scientific and technical material pertinent to NASA's mission.

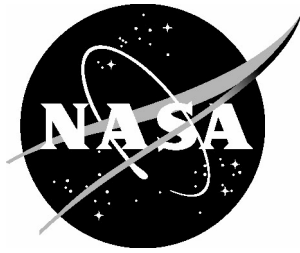
Specialized services that complement the STI Program Office's diverse offerings include creating custom thesauri, building customized databases, organizing and publishing research results ... even providing videos.

For more information about the NASA STI Program Office, see the following:

- Access the NASA STI Program Home Page at <http://www.sti.nasa.gov>
- E-mail your question via the Internet to [help@sti.nasa.gov](mailto:help@sti.nasa.gov)
- Fax your question to the NASA STI Help Desk at (301) 621-0134
- Phone the NASA STI Help Desk at (301) 621-0390
- Write to:  
NASA STI Help Desk  
NASA Center for AeroSpace Information  
7121 Standard Drive  
Hanover, MD 21076-1320



NASA/CP-2005-213509/PT2



# Proceedings of the 2004 NASA/ONR Circulation Control Workshop

*Edited by*  
*Gregory S. Jones*  
*Langley Research Center, Hampton, Virginia*

*Ronald D. Joslin*  
*Office of Naval Research, Arlington, Virginia*

Proceedings of a workshop sponsored by the National Aeronautics and  
Space Administration and Office of Naval Research, Arlington, Virginia  
and held at Radisson-Hampton, Hampton, Virginia  
March 16 – 17, 2004

National Aeronautics and  
Space Administration

Langley Research Center  
Hampton, Virginia 23681-2199

June 2005

Available from:

NASA Center for AeroSpace Information (CASI)  
7121 Standard Drive  
Hanover, MD 21076-1320  
(301) 621-0390

National Technical Information Service (NTIS)  
5285 Port Royal Road  
Springfield, VA 22161-2171  
(703) 605-6000

# TABLE OF CONTENTS

## Part 1

Introduction .....vii

### SESSION 1: CC APPLICATIONS

**1 – Circulation Control in NASA’s Vehicle Systems Program..... 1**  
Paul Rich, Bob McKinley, and Gregory S. Jones – NASA Langley Research Center

**2 – Overview of Circulation Control Pneumatic Aerodynamics: Blown Force and Moment Augmentation and Modification as Applied Primarily to Fixed Wing Aircraft .....37**  
Robert J. Englar – Georgia Tech Research Institute

**3 – Experimental Development and Evaluation of Pneumatic Powered-Lift Super-STOL ..... 101**  
Robert J. Englar – Georgia Tech Research Institute  
Bryan A. Campbell – NASA Langley Research Center

### SESSION 2: NCCR AIRFOIL CFD TEST CASE

**4 – Full Reynolds Stress Modeling of Circulation Control Airfoils..... 141**  
Peter A. Chang, Joseph F. Slomski, Thomas A. Marino, Michael P. Ebert and Jane Abramson– Naval Surface Warfare Center; Carderock Division

**5 – RANS and Detached-Eddy Simulation of the NCCR Airfoil..... 167**  
Eric G. Paterson and Warren J. Baker – Pennsylvania State University

**6 – Numerical Analysis of Circulation Control on a NCCR 1510-7607N Airfoil using RANS Models ..... 197**  
Aroon K. Viswanathan and Danesh K. Tafti – Virginia Polytechnic Institute and State University

### SESSION 3: CFD MODELING

**7 – Aspects of Numerical Simulation of Circulation Control Airfoils..... 227**  
Charlie C. Swanson, Chris L. Rumsey and Scott G. Anders – NASA Langley Research Center

**8 – Role of Turbulence Modeling in Flow Prediction of Circulation Control Airfoils ... 275**  
Greg McGowan, Ashok Gopalarathnam, X. Xiao and Hassan A. Hassan – North Carolina State University

**9 – Computational Evaluation of the Steady and Pulsed Jet Effects on the Performance of a Circulation Control Wing Section ..... 295**  
Yi Liu, Lakshmi N. Sankar, Robert J. Englar, Krishan K. Ahuja and R. Gaeta – Georgia Institute of Technology

**10 – Investigation of Turbulent Coanda Wall Jets Using DNS and RANS..... 337**  
PeteH. Fasel, A. Gross and S. Wernz– University of Arizona

## **SESSION 4: EXPERIMENTS**

**11 – Some Circulation Control Experiments ..... 369**  
D. Cerchie, L. Cullen, J. Goldstein, G. Han, L. Taubert and I. Wygnanski – University of Arizona  
E. Halfon – Tel Aviv University  
L. Trouve – L'Ecole Nationale Supérieure de Mécanique et d'Aérotechnique

**12 – A Wind Tunnel Experiment for Trailing Edge Circulation Control on a 6% 2-D Airfoil up to Transonic Mach Numbers ..... 407**  
Mike G. Alexander, Scott G. Anders and Stuart K. Johnson – NASA Langley Research Center

**13 – Experimental Investigation of a Morphing Nacelle Ducted Fan ..... 435**  
Shayne Kondor – Georgia Tech Research Institute  
Mark Moore – NASA Langley Research Center

**14 – A Novel Airfoil Circulation Augment Flow Control Method Using Co-Flow Jet... 469**  
Ge-Cheng Zha and Craig Paxton – University of Miami

**15 – Noise Reduction Through Circulation Control..... 497**  
Scott E. Munro – Naval Air Warfare Center; Weapons Division  
Krish K. Ahuja and Robert J. Englar – Georgia Tech Research Institute

## Part 2

Introduction .....vii

### SESSION 5: APPLICATIONS AND SYSTEMS

**16 – Circulation Control – Issues for NAVAL Applications ..... 553**

Ron Joslin – Office of Naval Research

**17 – Exploratory Investigations of Circulation Control Technology: Overview for Period 1987–2003 at NSWCCD..... 577**

Robin Imber – Naval Surface Warfare Center; Carderock Division

**18 – Why Have Only Two Circulation-Controlled STOL Aircraft Been Built and Flown in Years 1974–2004 ..... 603**

John Loth – West Virginia University

**19 – Wake Vortex Wingtip-Turbine Powered Circulation Control High-Lift System... 641**

Mark D. Moore – NASA Langley Research Center

**20 – The Use of Circulation Control for Flight Control ..... 657**

Steven P. Frith and Norman J. Wood – University of Manchester, United Kingdom

**21 – Time-Accurate Simulations of Synthetic Jet-Based Flow Control for a Spinning Axisymmetric Body ..... 689**

Jubaraj Sahu – U.S. Army Research Laboratory

**22 – Design and Fabrication of Circulation Control Test Articles..... 723**

Kenneth P. Burdges – Novatek, Inc.

**23 – Selected Topics Related to Operational Applications of Circulation Control ..... 743**

Ernest O. Rogers and Jane Abramson – Naval Surface Warfare Center; Carderock Division

**24 – From Concept to Production of the of the Coanda Driven Exhaust Deflector for the V-22 ..... 771**

Thomas Wood – Bell Helicopter

**25 – Simulation of Steady Circulation Control for the General Aviation Circulation Control (GACC) Wing ..... 791**

Warren J. Baker and Eric G. Paterson – Pennsylvania State University

<b>26 – CFD Analysis of Circulation Control Airfoils Using Fluent.....</b>	<b>813</b>
Gregory McGowan and Ashok Gopalarathnam – North Carolina State University	
<b>27 – Pneumatic Flap for a 2D Circulation Control Airfoil, Steady and Pulsed.....</b>	<b>845</b>
Gregory S. Jones – NASA Langley Research Center	
<b>28 – Experimental and Computational Investigation into the use of the Coanda Effect on the Bell A821201 Airfoil.....</b>	<b>889</b>
Gerald M. Angle, Wade W. Huebsch and James E. Smith – West Virginia University	
<b>29 – Low-Cost, High-Quality Wind Tunnel Testing of a 30% Elliptical Circulation Control Airfoil at Low Blowing Levels for Application to Wind Turbines .....</b>	<b>911</b>
Frederick J. Kelso, Kenneth L. Laubsch and Rikard K. Haraldsson – AdvanTek International	
<b>30 – Commercial Applications of Circulation Control (Wind Turbines, Pumps, Aerosol Sprays, Vacuum Cleaners, etc.).....</b>	<b>921</b>
Terence R. Day – Vortex Dynamics Pty Ltd	
<b>31 – Measurement and Analysis of Circulation Control Airfoils .....</b>	<b>947</b>
F. Kevin Owen – Complere, Inc. Andrew K. Owen – Oxford University	
<b>32 – Application of Pneumatic Aerodynamic Technology to Improve Drag Reduction, Performance, Safety, and Control of Advanced Automotive Vehicles.....</b>	<b>957</b>
Robert J. Englar – Georgia Tech Research Institute	
<b>33 – Aerodynamic Heat Exchanger: A Novel Approach to Radiator Design using Circulation Control.....</b>	<b>997</b>
Richard J. Gaeta, Robert J. Englar and G. Blaylock – Georgia Tech Research Institute	
<b>Summary .....</b>	<b>1023</b>
Ron Joslin – Office of Naval Research Gregory S. Jones – NASA Langley Research Center	
<b>Editorial Remarks.....</b>	<b>1051</b>
Gregory S. Jones – NASA Langley Research Center Ron Joslin – Office of Naval Research	
<b>List of Attendees.....</b>	<b>1055</b>

## Introduction: 2004 NASA/ONR Circulation Control Workshop

Gregory S. Jones<sup>1</sup> and Ronald D. Joslin<sup>2,a</sup>

<sup>1</sup>NASA Langley Research Center, Hampton, Virginia

<sup>2</sup>Office of Naval Research, Arlington, Virginia

This conference proceeding is comprised of papers that were presented at the NASA/ONR Circulation Control Workshop held 16-17 March 2004 at the Radisson-Hampton in Hampton, VA. Over two full days, 30 papers and 4 posters were presented with 110 scientists and engineers in attendance, representing 3 countries.

As technological advances influence the efficiency and effectiveness of aerodynamic and hydrodynamic applications, designs, and operations, this workshop was intended to address the technologies, systems, challenges and successes specific to Coanda driven circulation control in aerodynamics and hydrodynamics. A major goal of this workshop was to determine the state-of-the-art in circulation control and to assess the future directions and applications for circulation control.

The 2004 workshop addressed applications, experiments, computations, and theories related to circulation control, emphasizing fundamental physics, systems analysis, and applied research. The workshop consisted of single session oral presentations, posters, and written papers that are documented in this unclassified conference proceeding. The format of this written proceeding follows the agenda of the workshop. Each paper is followed with the presentation given at the workshop. The editors compiled brief summaries for each effort that is at the end of this proceeding. These summaries include the paper, oral presentation, and questions or comments that occurred during the workshop.

The 2004 Circulation Control Workshop focused on applications including Naval vehicles (Surface and Underwater vehicles), Fixed Wing Aviation (general aviation, commercial, cargo, and business aircraft); V/STOL platforms (helicopters, military aircraft, tilt rotors); propulsion systems (propellers, jet engines, gas turbines), and ground vehicles (automotive, trucks, and other); wind turbines, and other non-traditional applications (e.g., vacuum cleaner, ceiling fan).

As part of the CFD focus area of the 2004 CC Workshop, CFD practitioners were invited to compute a two-dimensional benchmark problem for which geometry, flow conditions, grids, and experimental data were available before the workshop. The purpose was to accumulate a database of simulations for a single problem using a range of CFD codes, turbulence models, and grid strategies so as to expand knowledge of model performance/requirements and guide simulation of practical CC configurations.

The comparison benchmark was the NCCR 1510-7067N circulation control airfoil that was tested at David Taylor Naval Surface Research and Development Center (currently, Naval Surface Warfare Center-Carderock Division). The airfoil is an eight-inch cambered elliptic section foil with thickness-to-chord ratio of 15% and a spiral Coanda trailing edge. It had a blowing slot located on the suction side at  $x/c = 0.967$  and which has a height-to-chord ratio of  $h/c = 0.003$ .

---

<sup>a</sup> The views expressed in this article are those of the authors and do not reflect the official policy or position of the US Office of Naval Research, the US Department of Defense, or the US Government. Distribution Statement A: Approved for public release; distribution is unlimited.



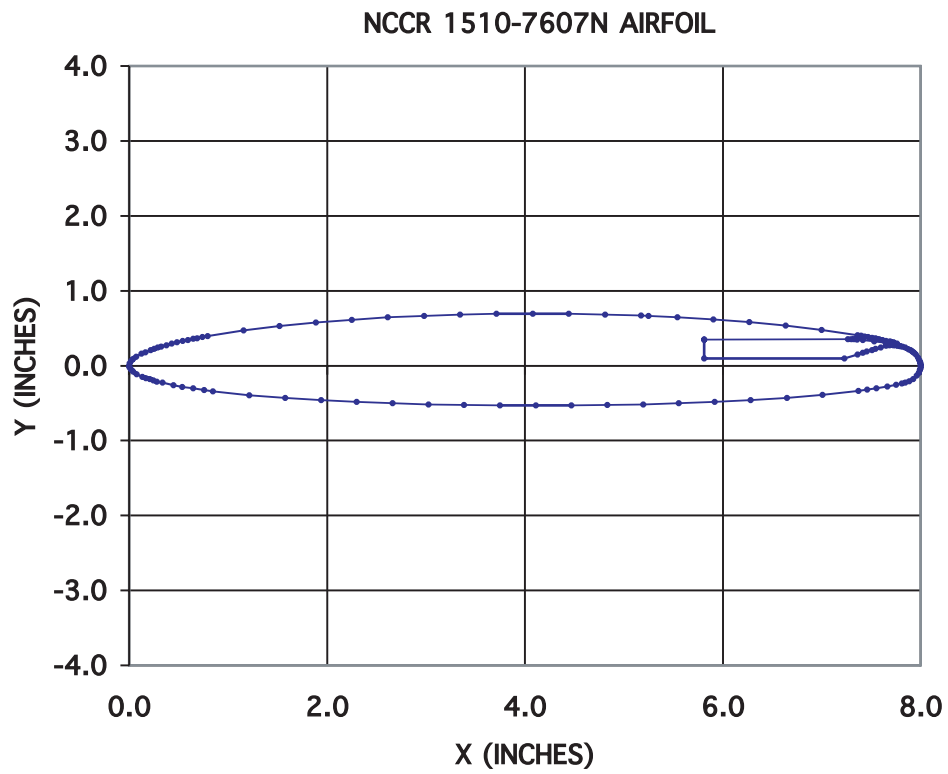


Figure 1. Sketch of the NCCR airfoil used for CFD test case.

**Table 1. Coordinates for NCCR airfoil used in CFD test case.**

1510-7067N Circulation Control Airfoil		h/c=0.0030	
UPPER		LOWER	
X(Inches)	Y(Inches)	X(Inches)	Y(Inches)
5.810000	0.351000	0.000000	0.000000
7.263000	0.356468	0.005000	-0.029000
7.298000	0.356600	0.021000	-0.057000
7.326875	0.352687	0.040000	-0.080000
7.355750	0.348775	0.077000	-0.112000
7.413500	0.340950	0.133000	-0.147000
7.529000	0.325530	0.170000	-0.165000
7.644500	0.309650	0.207000	-0.181000
7.760000	0.294000	0.244000	-0.196000
7.724000	0.310950	0.281000	-0.211000
7.688000	0.322210	0.336000	-0.228000
7.652000	0.333060	0.446000	-0.259000
7.616000	0.343910	0.538000	-0.281000
7.579000	0.353760	0.648000	-0.304000
7.543000	0.363610	0.757000	-0.326000
7.507000	0.372460	0.848000	-0.342000
7.470000	0.381710	1.212000	-0.393000
7.435000	0.390170	1.576000	-0.432000
7.398000	0.399020	1.938000	-0.462000
7.362000	0.406870	2.301000	-0.485000
6.999000	0.479380	2.663000	-0.503000
6.635000	0.535890	3.024000	-0.516000
6.270000	0.581400	3.386000	-0.525000
5.905000	0.616900	3.748000	-0.530000
5.540000	0.646000	4.109000	-0.532000
5.250000	0.664000	4.471000	-0.530000
5.175000	0.668000	4.832000	-0.524000
4.809000	0.684000	5.194000	-0.515000
4.443000	0.693000	5.555000	-0.501000
4.078000	0.695000	5.918000	-0.483000
3.712000	0.692000	6.280000	-0.459000
3.346000	0.683000	6.649000	-0.428000
2.980000	0.667000	7.006000	-0.388000
2.615000	0.644000	7.370000	-0.335000
2.250000	0.614000	7.461000	-0.319000
1.885000	0.576000	7.553000	-0.301000
1.520000	0.529000	7.662000	-0.277000
1.156000	0.469000	7.754000	-0.254000
0.793000	0.394000	7.809000	-0.239000
0.739000	0.381000	7.843000	-0.227000
0.688000	0.368000	7.887000	-0.205000
0.648000	0.358000	7.924000	-0.177000
0.594000	0.343000	7.961000	-0.134000
0.540000	0.328000	7.981000	-0.099000
0.485000	0.312500	7.993000	-0.061000
0.431000	0.294000	7.998000	-0.034000
0.377000	0.275000	8.000000	0.000000
0.323000	0.255000	7.998000	0.019000
0.287000	0.240000	7.994000	0.046000
0.251000	0.225000	7.987000	0.072000
0.215000	0.208000	7.972000	0.110000
0.162000	0.181000	7.952000	0.147000
0.126000	0.160000	7.934000	0.170603
0.073000	0.122000	7.915000	0.190000
0.038000	0.088000	7.897000	0.206049
0.020000	0.066000	7.878000	0.220487
0.004000	0.030000	7.845000	0.240735
0.000000	0.000000	7.816000	0.254000
		7.793000	0.261565
		7.770000	0.267000
		7.748000	0.270347
		7.724000	0.272000
		7.687000	0.270000
		7.652000	0.264000
		7.598000	0.245000
		7.543000	0.224000
		7.507000	0.210000
		7.453000	0.188000
		7.417000	0.174000
		7.363000	0.152000
		7.228000	0.096000
		5.810000	0.096000
		5.810000	0.351000



# Circulation Control: Issues for Naval Applications

Ronald D. Joslin<sup>1</sup>

Office of Naval Research, 800 North Quincy Street, Arlington, VA 22217 USA

## Abstract

The application, investigation, and modeling of circulation control are the focus of this workshop and resulting proceedings. Most of the papers in this workshop either experimentally observe performance gains using circulation control or attempt to predict such performance gains with computational fluid dynamics. This paper will highlight the successful implementation of circulation control for some naval aircraft demonstrations. Issues are then raised for the potential application of circulation control for undersea platforms.

## 1. Introduction

Circulation control implies that the circulation of a lifting or control surface is altered through geometry change or active flow control. The majority of the papers in this workshop use the Coanda effect<sup>2</sup> to actively cause this control. The Coanda effect results from the introduction of a fluidic tangential wall jet at some strategic location of the application. This wall jet causes the flow to remain attached to the

---

<sup>1</sup> The views expressed in this article are those of the author and do not reflect the official policy or position of the US Office of Naval Research, the US Department of Defense, or the US Government. Distribution Statement A: Approved for public release; distribution is unlimited.

<sup>2</sup> Discovered by Henri Marie Coanda (1886-1972). September 1, 1936, H. Coanda *Device for deflecting a stream of elastic fluid projected into an elastic fluid*. US Patent # 2,052,869. (In France on October 8, 1934: *Procedure and device for the deviation of a fluid inside another fluid*, #762688)

surface. For an airfoil, blowing over a rounded trailing edge causes a change in the circulation and results in changes to the lift force. In this paper, circulation control is used synonymously with the Coanda effect.

The majority of this introduction is focused on aircraft configurations because most of the flow control research available in the open literature was developed for aircraft platforms. There are some interesting documents relating circulation control to undersea platforms, but these papers are not available for this discussion. Many of the statements and achievements of circulation control for air-based platforms directly or indirectly contribute to undersea platforms.

### *1.1 Aircraft Platforms*

In 1994, the United States transportation system had over 190 million automobiles, trucks, and vans; 275,000 airplanes operating at 17,500 airports; 18,000 locomotives; 1.2 million cars; and 20 million recreational boats and over 8,000 ships, tugs, and other commercial vessels (1, 2). This complex transportation system produces considerable noise, impacting the traveling and surrounding communities and the environment. Considerable energy is expended each year to operate this system. Hence, any improvement on one platform or subsystem, such as performance improvements with circulation control, can lead to significant global benefits to society and the environment. The impact of one flow control system will be quantified below in terms of a global benefit.

As of May 2000, the US transportation system supported 500 million passenger enplanements (3). Prior to the terrorist attacks in the US on 11 September 2001, the Federal Aviation Administration (FAA) had estimated a 3.4 percent increase in

domestic enplanements (i.e., 17 million) and a 4.0 percent increase in jet aircraft (i.e. 260 aircraft per year) by the year 2010 (3). In 2003, US enplanements were projected to be 1.1 billion by 2013 (4), suggesting that the growth projections persist even after the terrorist events of 2001.

The effects of this growth will be further compounded by the more stringent noise certification requirements and even more severe local restrictions at individual airports. Regulatory constraints of this type have already impacted the present fleet of aircraft which is required to comply with Stage III of the US Federal Aviation Administration (FAA) Federal Aviation Regulations (FAR). For certification, aircraft are required to be nearly 16-20 effective perceived noise Decibels (EPNdB) quieter than the first turbojet powered airliners (5). The Stage IV standards approved by the International Civil Aviation Organization (ICAO) will require an additional reduction of 10 EPNdB on a cumulative basis for new airplanes introduced into service after January 2006 (6). Note, that a 10 EPNdB reduction would half the noisiness experienced by the community. Unless aircraft noise reduction can keep pace with this trend, the projected growth in aviation would be constrained due to the regulations. Circulation control, through performance enhancements, may impact these noise reduction goals for aircraft.

Circulation control has reached the state of high technology readiness level for air-based platforms based on the various wind tunnel experiments and flight tests; however, this flow control technology is a "complex system". Yet, many such complex systems exist on aircraft. The Northrup Grumman F-14 and the General Dynamics F-111 employ crank or swing wings that are pivoted to permit variable

sweep for optimal flight operating conditions, which are different for takeoff conditions versus high-speed cruise conditions. More common, the multi-element high lift system is employed on many large transports for takeoff/landing conditions and is re-configured to form an airfoil for cruise conditions. Arguably, this type of flow control system is passive – no direct energy is input to the flow from the system (although energy is expended to activate the system). Circulation control is then by this definition an active flow control system since energy is introduced into the flow by-way-of the blown fluidic jet.

To be used on a platform, these flow control systems must either be commercially beneficial or resolve a mission critical role. For example, McLean (7) highlights the results of a systems study that quantifies the benefits of active separation flow control to replace a multi-element high lift system on a large transport. Although this analysis is a retrofit which is not optimal for many flow control technologies, the study indicates that the modified aircraft would have 3.3% empty weight, 1.3% part card, 3.3% drag and 0.7% manufacturing cost reductions. As a result, the manufacturing cost, for example, of a \$30M aircraft would be reduced by \$0.4M (not accounting for the actuator costs which are unknown). The consequences of the weight and drag savings are reductions in fuel burn (and emissions) and noise (inferred from weight savings). An airline that typically spends on the order of \$1.0-1.5B on fuel per year would directly recoup \$30-40M per year on a recurring basis as a result of the drag reduction alone. So, perceivably small benefits yield large financial benefits for some industries, such as the air transportation industry. As will be demonstrated in a workshop paper on



tractor trailer drag reduction, smaller scale financial savings in fuel can be realized using circulation control on the trailer. To reach application, circulation control must demonstrate a significant commercial benefit for the platform.

Most often for military applications, satisfaction of a mission critical role “buys” a new technology onto the platform. The use of circulation control on the Bell Boeing V-22 Osprey (figure 1) is an example of mission critical role (see the keynote presentation by Wood for this workshop). While on the ground during flight idle operations, the V-22 engine exhaust impinges on the ground. A portion of these hot gases are directed toward the fuselage causing some of the sensitive subsystems (e.g., avionics) to operate in an undesirable environment (8). The Coanda circulation control system was developed and implemented on the nacelles to deflect these gases away from the fuselage with a penalty of 7% engine bleed to operate the system. Circulation control was incorporated into the platform with a reduced weight and cost compared with the various deflector options. The engine bleed penalty did not detract from the performance of the platform because circulation control is used while on the ground when minimum performance is required from the engine. Hence, circulation control solved a critical platform issue.

## *1.2 Undersea Platforms*

For undersea naval vessels (i.e., submarines), a reduced acoustic signature results in enhanced stealth, leading to desired challenges for those tasked with classification and targeting the platform; hence, controlling the level of noise

contributes to the overall survivability of an undersea vehicle (9). Reduced acoustic signature also results in an improvement in the submarine's own passive sonar performance, which will be further expanded upon in the next section. What are some motivations for the use of circulation control for underwater vehicles? Figure 2 gives a notional submerged operating envelop of a platform with speed and depth. The primary operational limits are imposed by potential controller failures. The use of circulation control on individual controllers may create the opportunity to expand this envelop. Figure 3 shows a platform undergoing a maneuver in shallow (i.e. littoral) environment. In this environment the platform must be aware of the bottom, ships on the surface, and other submersibles. Further, most of these platforms undergo large excursions during maneuvers (hundreds of meters). These excursions occur because of the often large asymmetric forces on the hull and can lead to pitch up or down moments on the boat. In addition to the undesired moments of maneuvering, the signature of the platform increases during maneuvers because of the asymmetric unsteady forces on the propulsor and resulting cavitation. The increased forces and moments resulting from circulation control can potentially resolve some of these platform issues. Enhanced control effectiveness that may result from circulation control would be invaluable in littoral waters for many reasons. So, implementation of circulation control for a submarine may significantly impact the at-sea operations.

One must address other potential issues for the use of circulation control beyond commercial viability or resolving a mission critical role for a platform. This paper introduces, but does not resolve, some of these issues in particular for

underwater vehicles. The next section highlights some of the previous accomplishments for US Navy/Marine platforms in air, followed by a discussion of the use of circulation control for undersea applications. Finally, summary comments are presented.

## **2. Naval Platforms and Circulation Control**

Many of the papers at this workshop clearly show the benefits resulting from circulation control on a variety of applications. In addition, many of these presentations and papers give a review of circulation control. Also, the previous 1986 CC workshop (9), a workshop summary paper (10) and a bibliography (11) summarize some of the historical contributions made by the US Navy.

### *2.1 Aircraft Platforms*

Because other papers in this workshop give historical perspectives, here this introduction is limited to 3 US Navy projects and serve as an introduction to the issues related to undersea platforms. The contemporary V-22 platform has been discussed above. Here, circulation control applied to the Grumman A-6A and Kaman Aerospace HH-2D are discussed because these were successful US Navy projects that clearly demonstrated the effectiveness of this flow control technology.

In the late 1970's, a Navy/Grumman A-6A Intruder was modified to become the A-6A/CCW (figure 4) flight test demonstrator with circulation control wings (CCW) (12). The A-6A/CCW flight test program demonstrated a landing roll of 1,075 ft compared with 1,700 ft of the A-6A (33,400 lb). Touchdowns were conducted at

speeds as slow as 78 kt compared with 120 kt of the A-6A. The reduced landing speed provides an added safety benefit for the pilot and deck crew. The cost of the full trailing edge blowing system was driven by bleeding the dual engines of 12% engine bleed for a maximum flow rate of 24 lbs/second.

Also in the 1970's, the US Navy and Kaman Aerospace modified a HH-2D for a circulation control rotor (CCR) to become a XH-2D/CCR (figure 5) demonstrator (13). The CCR operates at 267 revolutions per minute (rpm) compared with the HH-2D rotor which operates at 298 rpm. The maximum lift coefficient was 4-5 compared with 1.4 for the conventional airfoil. Furthermore, the CCR used a maximum flow rate of 10 lbs/second. The flight test program demonstrated that differential blowing of the advancing and retreating blades can substitute for conventional pitch cycling of the blades to balance the lift forces.

From these earlier flight demonstrations on the A-6A and HH-2D and the inclusion of circulation control on the more conventional V-22 indicate that the technology readiness level (TRL=6 or 7) is high for air based platforms. However, additional issues result from proposing circulation control for undersea systems as will be explored in the next section.

## *2.2 Undersea Platforms*

The most recent underwater application of circulation control was conducted in 2002 (14). The investigation was conducted in the NSW-Carderock Division Large Cavitation Channel (LCC) in Memphis, TN. The fresh water tunnel can operate up to 50 ft/s and has a cross section of 10 ft x 10 ft and test length of 43 ft.

The circulation control model had a chord taper ratio of 0.76 with an effective aspect ratio of 2 to resemble stern-planes and rudders (14). The cross section profile is an ellipse with the thickness ratio of 20% (somewhat larger than a conventional appendage). Unlike previous circulation control experiments which used single slot injection, identical upper and lower ejectors are independently operated. The goal of investigation was to investigate circulation control of a small aspect ratio control surface in order to identify any characteristics unique to three-dimensional effects and to assess the performance of a dual injector system.

The test results indicated that circulation control applied to low aspect ratio wings is just as effective as on high aspect ratio surfaces, relative to finite wing theory. No penalties were found that are unique to the development of lift by a short span slotted Coanda-effect trailing edge. The highest demonstrated sectional lift coefficient was 3.0, which is more than double that of a conventional ship appendage. Substantial increases in the maximum lift are obtained by a slot assisted by a small flow from the second slot. Increased second-slot flow forms a merger of the two wall jets into a vectored planar jet. The dual slots can also be used for a full 0-360 degree thrust vectoring mode.

The results from this experiment demonstrate the use of circulation control in a (fresh) water environment. However, many other issues must be addressed before a large scale demonstration should commence. Many of these issues are discussed in the next section.

### **3. Submarine Platform Circulation Control Issues**

In this section, issues are explored for the practical implementation of a circulation control system on a submarine platform. The issues include acoustics, interference effects, performance, environmental effects, cost, and safety.

Low levels of self-noise are crucial to maintain stealth for the submarine. Therefore, the implementation of circulation control must not introduce an unacceptable level of noise. There is a number of noise sources associated with circulation control (15). These sources include classical trailing edge noise, jet noise, incident turbulent noise, and radiation due to a separating boundary layer. Howe (16) includes noise resulting from the interaction of the boundary layer with a curved surface. The two-dimensional analysis (16) showed that high frequency noise is produced at the Coanda jet slot. The most likely source of noise occurs when the slot lip scatters noise due to turbulence-slot interaction. An example calculation showed the circulation control slot noise can be 20 dB or more greater than a conventional airfoil. However, this number becomes smaller with an increase in the slot lip size.

As shown by the submerged operating envelope (SOE) (figure 2) and littoral operations (figure 3) sketches, maneuvering performance (and safety) are key ingredients for the permitted operations. Figure 6 shows a notional futurist submarine which will serve to pose questions about the use of circulation control on control surfaces. Using circulation control on bow and stern control surfaces would lead to many unknown implications. Using circulation control on the bow planes could introduce desired stability, but how the turbulent water-jet wakes

would impact the sonar, weapons systems, and deployable subsystems is unknown. This use may impose additional operational restrictions on the submarine. Further, these water jet wakes could induce forces on submarine thereby altering the maneuvering characteristics of the submarine. Could the interaction of the water-jet wakes and downstream control surface induce undesired unsteady wakes into the propulsor? Could this interaction also make the stern control surfaces less effective? If circulation control was used on the stern control surfaces, how would these wake structures impact the propulsor acoustics and performance since the inflow would be non-symmetric? The SOE is determined by safety issues. With circulation control, there may have to be a paradigm shift in the assessment of fail modes.

Also similar to air platforms, model to full scale uncertainties arise with circulation control. However, the knowledge gained from the flight demonstrations will contribute to this issue. In addition, power requirements must be scaled up and the uncertainty in these estimates determine the level of risk.

There are many elements to be considered in the cost estimate for circulation control. These include the direct operating costs (i.e., maintenance, fuel or energy), manufacturing cost, and space consideration. The system is comprised of pumps and ducts; so estimates for the operating cost obtainable with minimal risk. Understanding the manufacturing tolerance requirements can support a good estimation of construction costs. Further, the air platform experience and water tunnel experiments can support system space requirements; however, will the platform support this subsystem space requirements is certainly an issue.



An exception to the operating cost estimate consists in uncertainty in environmental issues such as fouling and corrosion. This issue currently exists for other subsystem water intake systems and should not lead to a show-stop situation for the circulation control subsystem. Yet, aspects of fouling have not been addressed for circulation control in terms of performance degradation with fouling. Experiments have demonstrated that with an appropriate fouling release coating and with sufficient shear, fouling can be removed from a surface (17, 18). Yet, the performance must be measured for a circulation control in a fouling environment.

The section has explored some issues related to the practical implementation of circulation control on a submarine platform. Apparently, no show-stoppers are evident in the discussion, yet there is insufficient testing and analysis of circulation control on a scaled platform to fully address some of these issues.

#### **4. Final Comments**

This paper has highlighted the successful implementation of circulation control for some naval aircraft demonstrators and raised some issues for the practical application of circulation control for undersea platforms.

#### **References**

1. Anon. Transportation statistics annual report, US Department of Transportation, 1994.
2. Anon. Strategic planning document – Transportation R&D. National Science and Technology Council, Office of Science and Technology Policy, March 1995.

3. Federal Aviation Administration (FAA), National Aviation Research Plan, 2001.
4. Federal Aviation Administration (FAA), National Aviation Research Plan, 2003
5. Anon. Much tighter aircraft noise limitations to be imposed. ICAO News Release, International Civil Aviation Organization, 1969.
6. Bond D. US EC look past hush kit rule, take issues to ICAO assembly. *Avi Week & Space Tech* 2001;155(13):50-51.
7. McLean JD, Crouch JD, Stoner RC, Sakurai S, Seidel GE, Feifel WM, Rush HM. Study of the application of separation control by unsteady excitation to civil transport aircraft. NASA/CR-1999-209338, 1999.
8. Brand AG, Jenkins JL, Wood TL. Analysis, design, and testing of the Coanda effect exhaust deflector of the V-22 tiltrotor. Twentieth European Rotorcraft Forum, Amsterdam/October 4-7, 1997, 16 pgs. Hess DE, Fu TC. Impact of flow control technologies on naval platforms. AIAA Paper 2003-3568, Jun 2003.
9. Nielsen JN. (editor). Proceedings of the Circulation-Control Workshop 1986, 19-21 February 1986, NASA Conference Proceedings 2432, 1987.
10. Nielsen JN, Biggers JC. Recent progress in circulation control aerodynamics. AIAA Paper 87-0001, Jan. 1987.
11. Englar RJ, Applegate CA. Circulation control – A bibliography of DTNSRDC research and selected outside references. (January 1969 through December 1983). DTNSRDC-84/052, Sept 1984.
12. Mayfield J. Circulation control wing demonstrates greater lift. *Avi Week & Space Tech* March 19, 1979.
13. Mayfield J. Navy sponsors Coanda rotor program. *Avi Week & Space Tech* March 31, 1980.
14. Rogers EO, Donnelly MJ. Characteristics of a dual-slotted circulation control wing of low aspect ratio intended for naval hydrodynamic application. AIAA Paper 2004-1244, Jan 2004.
15. Williams RM, Cheeseman IC. Potential acoustic benefits of circulation control rotors. Fourth European Rotorcraft and Powered Lift Aircraft Forum, Stresa, Italy, September 13-15, 1978.
16. Howe MS. Noise generated by a Coanda wall jet circulation control device. *J Sound and Vibration* 2002 ;249(4) :679-700.
17. Schultz MP, Finlay JA, Callow ME, Callow JA. Three models to relate detachment of low form fouling at laboratory and ship scale. Biofouling

2003 ;19 :17-26.

18. Finlay JA, Callow ME, Schultz MP, Swain GW, Callow JA. Adhesion strength of settled spores of the green Alga *Enteromorpha*. *Biofouling* 2002 ;18(4) :251-256.



Figure 1: Bell Boeing V-22 Osprey transitioning from helicopter to aircraft mode (Photo courtesy US Navy).

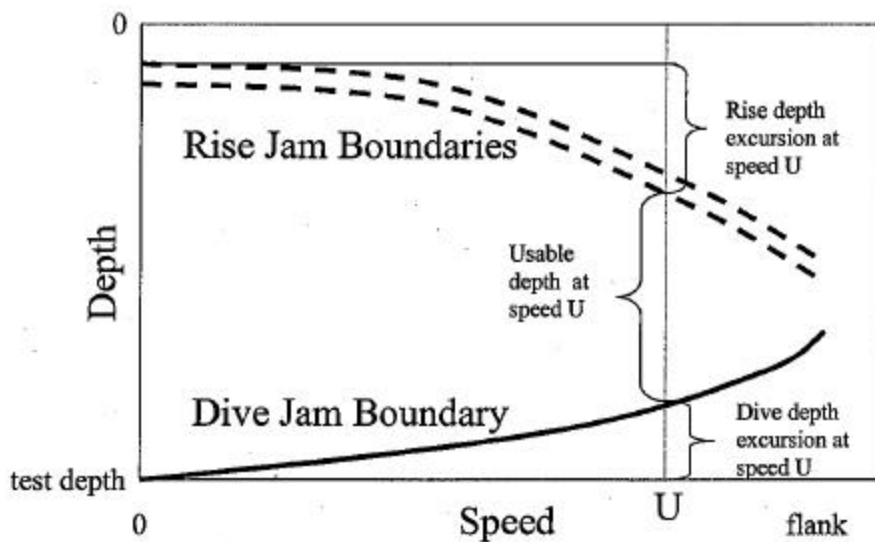


Figure 2: Notional Submerged Operating Envelop resulting from speed versus depth.

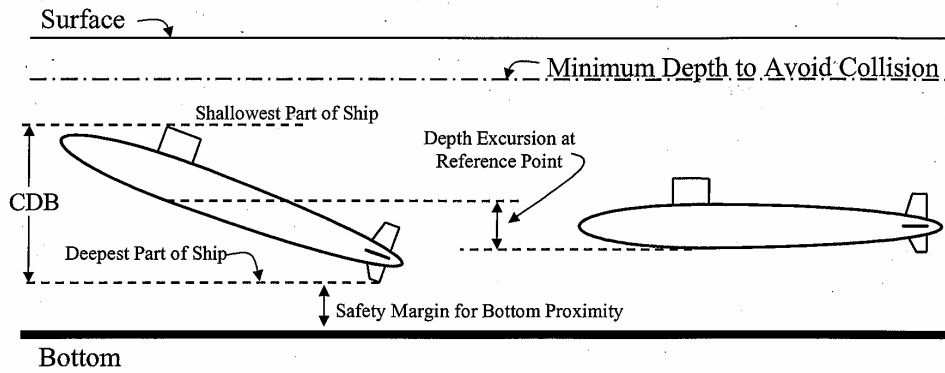


Figure 3: Notional maneuvering limitations and issues resulting from littoral environments.



Figure 4: Navy/Grumman A-6A/CCW flight test demonstrator with circulation control wings (CCW).



Figure 5: Navy/Kaman Aerospace XH-2D/CCR flight test demonstrator with circulation control rotor (CCR).

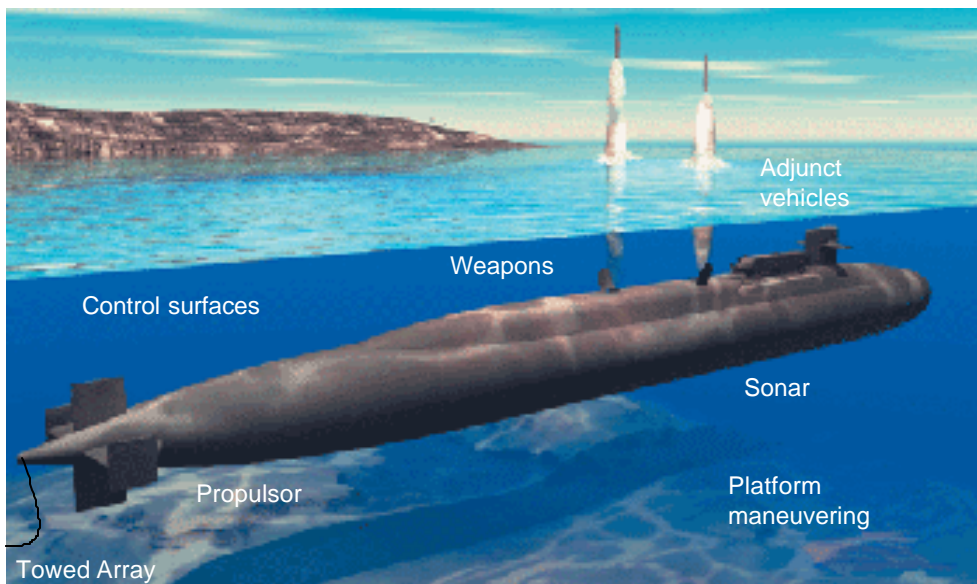


Figure 6: Sketch of futuristic submarine.



Distribution Statement A:  
Approved for public release; distribution is unlimited



## Circulation Control – Issues for Naval Applications

Dr. Ronald D. Joslin  
Code 333

NASA/ONR Circulation Control Workshop, Hampton, VA/17 March 2004



## Circulation Control – Issues for Naval Applications

Dr. Ronald D. Joslin  
Code 333

NASA/ONR Circulation Control Workshop, Hampton, VA/17 March 2004

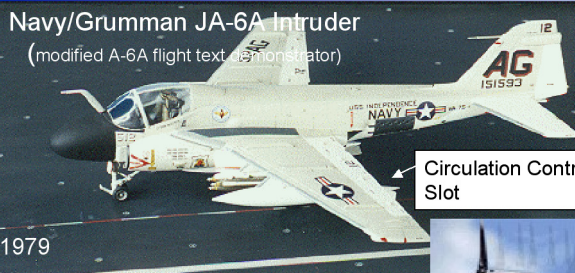
# Outline

CC: ISSUES FOR NAVAL APPLICATIONS

- Navy Hydromechanics Platforms
- Applications & Issues

## Aircraft Platforms

CC: ISSUES FOR NAVAL APPLICATIONS



Circulation Control Slot

### Achievements

- 78 kt touchdown vs 120 kt
- 1,075 ft landing rollout vs 1,700 ft
- 12% engine bleed



Bell Boeing V-22 Osprey



# ONR Hydromechanics Objectives

CC: ISSUES FOR NAVAL APPLICATIONS

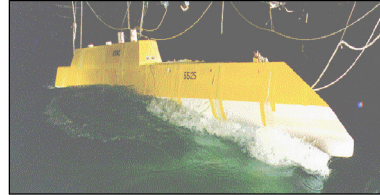
## Subsurface Subthrust:

- > Maneuvering
- > Signature Reduction



## Free Surface Subthrust:

- > Maneuvering and Seakeeping
- > Propulsion and Stealth



## Performers

### Universities:

Stanford, MS State, JHU, Iowa, UCSD, MIT, U Mich, UMD, VA Tech, N. Dame, ...

### Labs:

NSWCCD, ARL/PSU, Panama City, NUWC

### Companies:

Bath I.W., N-G, Anteon, NWRA, Cortana, SAIC, NNS, EB...

# Nonlinear Ship Motions

CC: ISSUES FOR NAVAL APPLICATIONS

**Advanced hulls** → challenge

- Incomplete design/analysis
- Minimal database for empirical design
- Unusual hydro and seakeeping characteristics



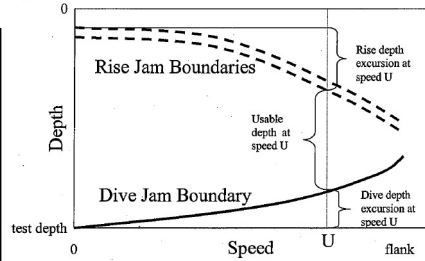
# Submarine Platform Issues

CC: ISSUES FOR NAVAL APPLICATIONS

- **Submarine Stealth and Agility**
- **Advanced Concepts**

## Platform "Realities"

- Limited Submerged Operating Envelope (SOE)
- Hydromechanic "Surprises"



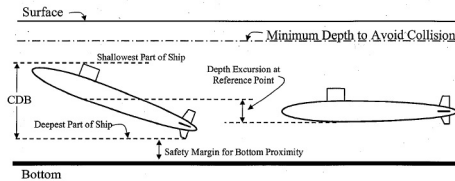
# Platform Issues

CC: ISSUES FOR NAVAL APPLICATIONS

- **Submarine Stealth and Agility**
- **Advanced Concepts**

## Platform "Realities"

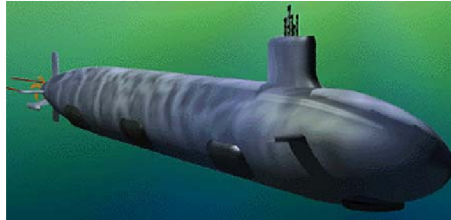
- Littoral Ops
- Large excursions during maneuvers (hundreds of meters)
- Signature increases during maneuvers
- Tactical speed inhibitors



## Focused Goals

CC: ISSUES FOR NAVAL APPLICATIONS

- Develop advanced control effectors and automated control systems for improved M&C
- Develop and validate physics-based design/analysis tools for reduced development costs
- Explore non-BOR hull forms for payload and maneuvering

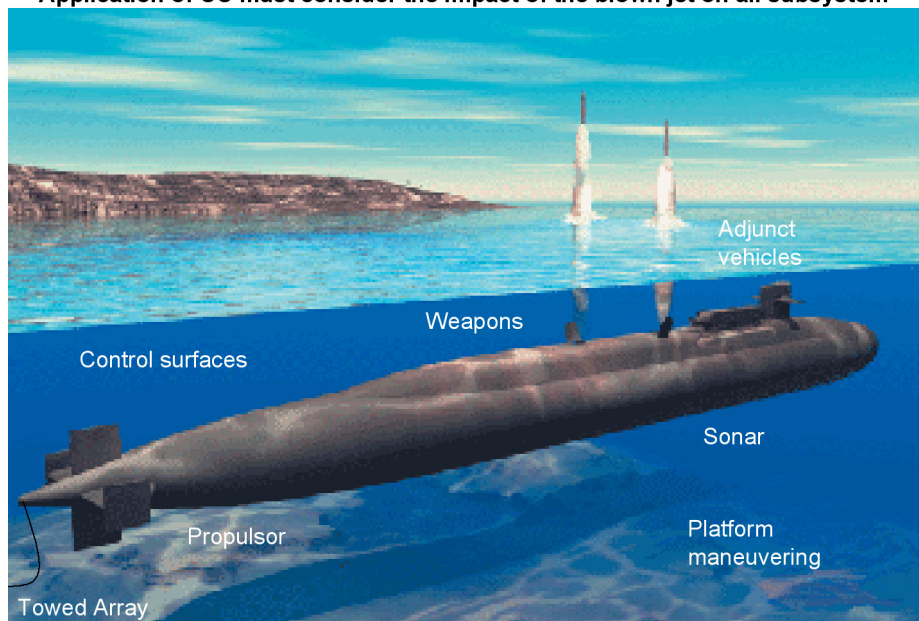


# Outline

CC: ISSUES FOR NAVAL APPLICATIONS

- Navy Hydromechanics Platforms
- Applications & Issues

Application of CC must consider the impact of the blown jet on all subsystem



# Issues

CC: ISSUES FOR NAVAL APPLICATIONS

- Model to Full Scale
- Acoustics (i.e., flow-induced noise)
- DOC (i.e., maintenance, reliability)
- Environmental (i.e., fouling)
- Power requirements
- Intake design (i.e. acoustics/fouling)
- Corrosive Environment



## Exploratory Investigations of Circulation Control Technology: Overview for Period 1987-2003 at NSWCCD

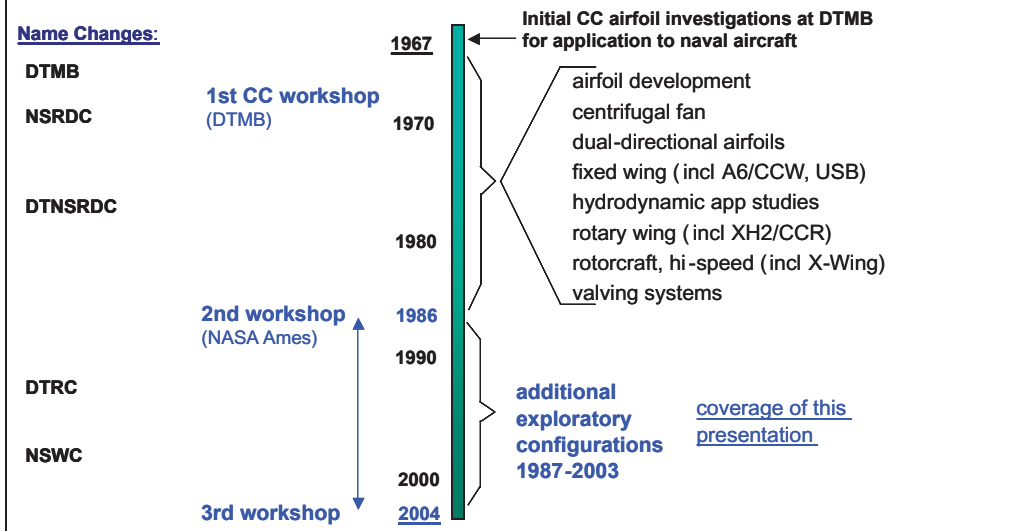
Dual-Slotted Cambered Airfoil (LSB)  
 Rotary Thruster, Self -Driven (Tip-Jet)  
 Annular Wing (Duct)  
 Circular Wing (Disc)  
 System to Cancel Unsteady Loads (Actuator)  
 Low Aspect Ratio CC Wing (Hydrofoil)

presented by

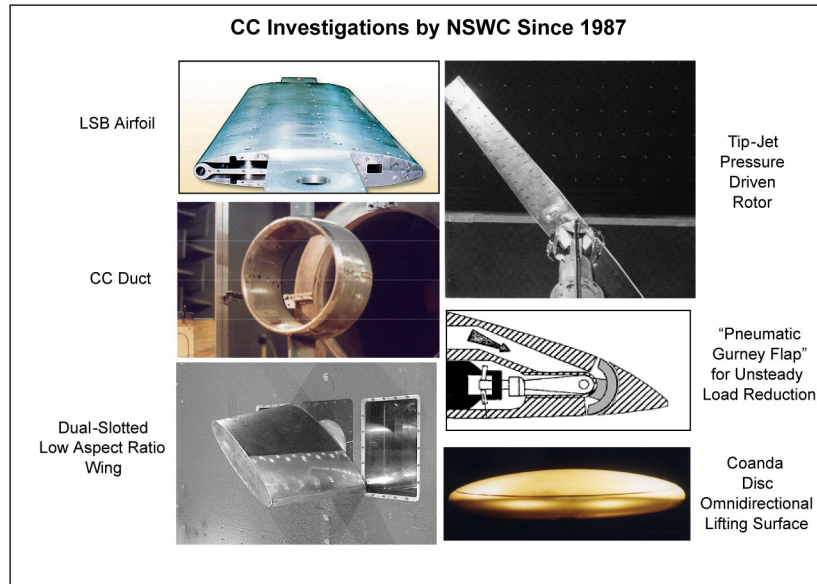
**Robin Imber**

Marine and Aviation Department  
 Naval Surface Warfare Center, Carderock Division

## Overview of NSWC Involvement with CC Technology

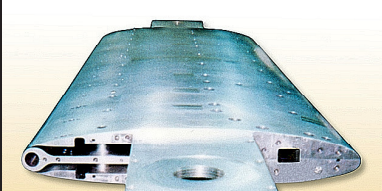
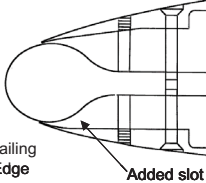


The timeline above shows an overview history of Circulation Control (CC) technology at the Naval Surface Warfare Center, Carderock. Since 1967, when the organization name was David Taylor Model Basin (DTMB), researchers at Carderock have been involved with a number of projects, including fixed wing, rotorcraft, and hydrodynamic applications.



This presentation covers six of the major CC exploratory investigations that have taken place since the last CC workshop that was held in 1986.

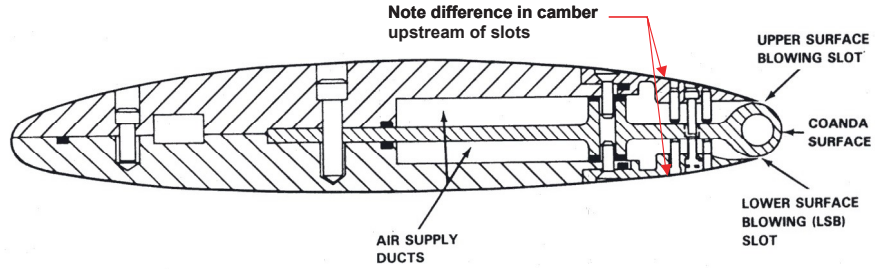
**Dual-Slotted  
Cambered Airfoil  
(LSB)**

<p><u>Investigator:</u> Jane Abramson</p> <p><u>1987</u></p> <p><u>Sponsor:</u> In-house Research</p> <p><u>Facility:</u> NSWC 8x10-ft Wind Tunnel w/ 2-D wall inserts</p> <p><u>Documentation:</u> in preparation</p>	
<p><b>Key Findings</b></p> <ul style="list-style-type: none"> <li>¥ Lower slot did not affect performance of upper slot.</li> <li>¥ Upper and Lower Slots doubled the control range.</li> <li>¥ Augmentation Ratio of 80 for lower slot was obtained.</li> <li>¥ Performance was greater for lower slot.</li> <li>¥ Simultaneous blowing from both slots decreased lift.</li> </ul>	 <p>Trailing Edge</p> <p>Added slot</p>

The 2-D dual slotted airfoil was designed and tested in 1987 by Jane Abramson. Test documentation can be found in NSWCCD-50-TR-2004/030.

The airfoil was the first CC model designed at Carderock to incorporate both upper and lower trailing edge blowing slots. The dual slots provide the ability to produce lift in either direction.

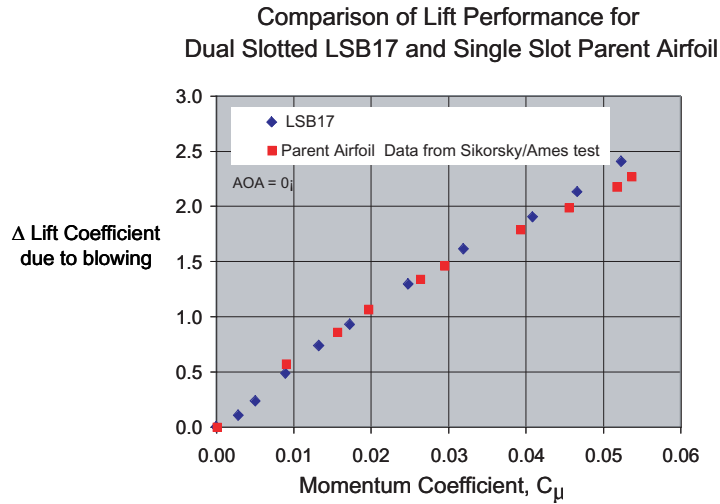




LSB17 Model	
Thickness ratio:	17%
Camber:	1.1% circular arc
Chord:	12 -inch
Span:	36 -inch
Slot location ( $X_s/c$ ):	
upper:	0.968
lower:	0.970

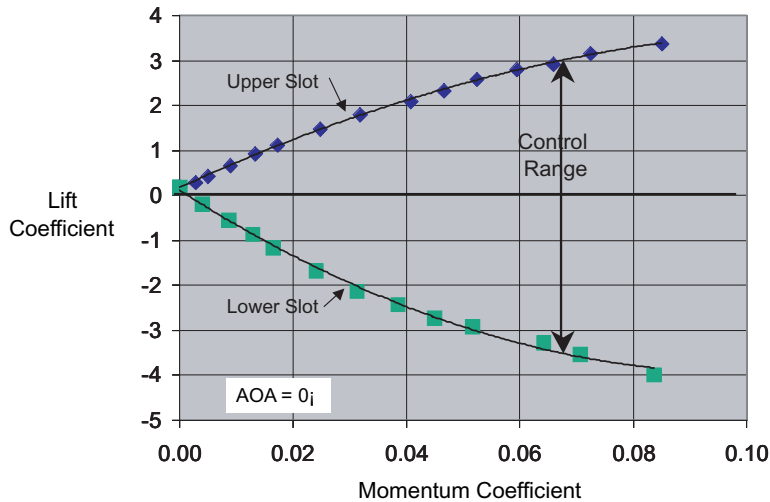
Test Matrix	
Dynamic pressures:	20 to 60 psf
Reynolds number:	0.8 to $1.4 \times 10^6$
Geometric AOA:	-10 to 10 $^\circ$
h/c:	0.0013 and 0.0020
$C_{\mu}$ :	to 0.22

The cross section sketch above shows the LSB17 model. Note that there are differences in both the camber distributions upstream of each slot and in the actual nozzle designs. Testing included three blowing modes: upper surface only, lower surface only and dual blowing.



One of the main design goals was to have the dual slotted model perform as well as the single slotted “parent” model. The comparison shows that there was no detrimental effect of adding the 2nd slot.

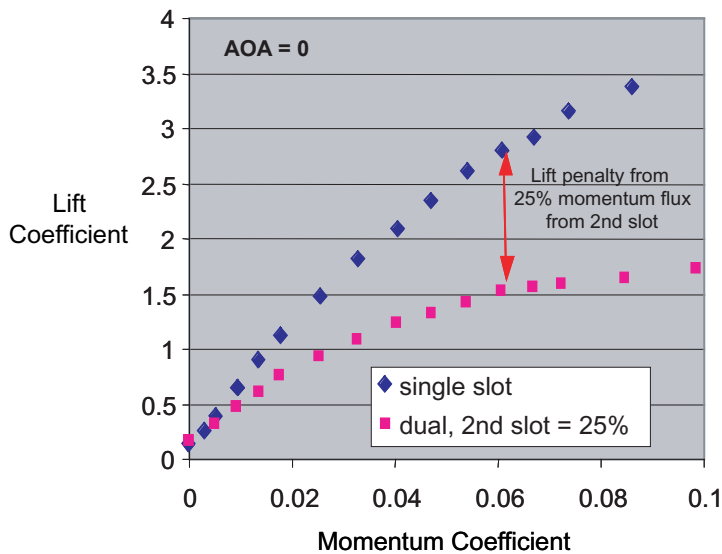
### Control Range Increase Demonstrated With Upper and Lower Slot Capability (LSB17 1986)



The fundamental design objective was to increase the control range so that force control in both directions was available. This plot shows lift coefficient vs.  $C_{\mu}$  and reveals that the goal of doubling the control range was met. An unexpected finding was that the performance of the lower slot, in terms of measured lift augmentation, was noticeably better than the upper slot.

### Dual Blowing Effects on the LSB Airfoil

High level blowing from the 'unblown' slot was detrimental to Lift



For this model, when blowing was applied to the upper and lower surfaces simultaneously (dual blowing), with lower slot  $C_{\mu}$  set to 25% of the upper slot  $C_{\mu}$ , lift developed was considerably lower than the single slot mode.

## Self-Driven Rotary Thruster (Tip-Jet)

Investigators : Al Schwartz, Ernie Rogers,  
Ken Reader, Jane Abramson

1991

Sponsor : In-house Research

Facility : NSWC Hover Test Stand

Documentation : AIAA 92 -0630

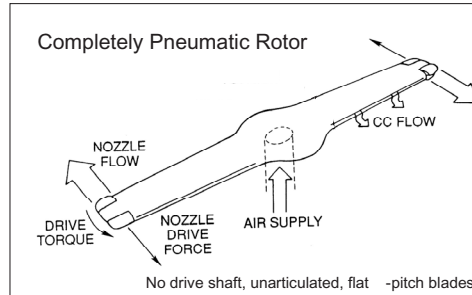
### Key Findings

¥ Lift gain of 29 from slot flow was obtained.

¥ Fully pneumatic rotor inherently seeks an equilibrium, self limiting rotational rate, that is a function of slot to nozzle area ratio. Resulting thrust is a near linear function of the blade pressure.

¥ There is a significant impact on induced power efficiency due to non-lifting tip nozzle region.

¥ The presence of the tip nozzle jet has no discernible impact on the external aerodynamics of the lift (thrust) system.



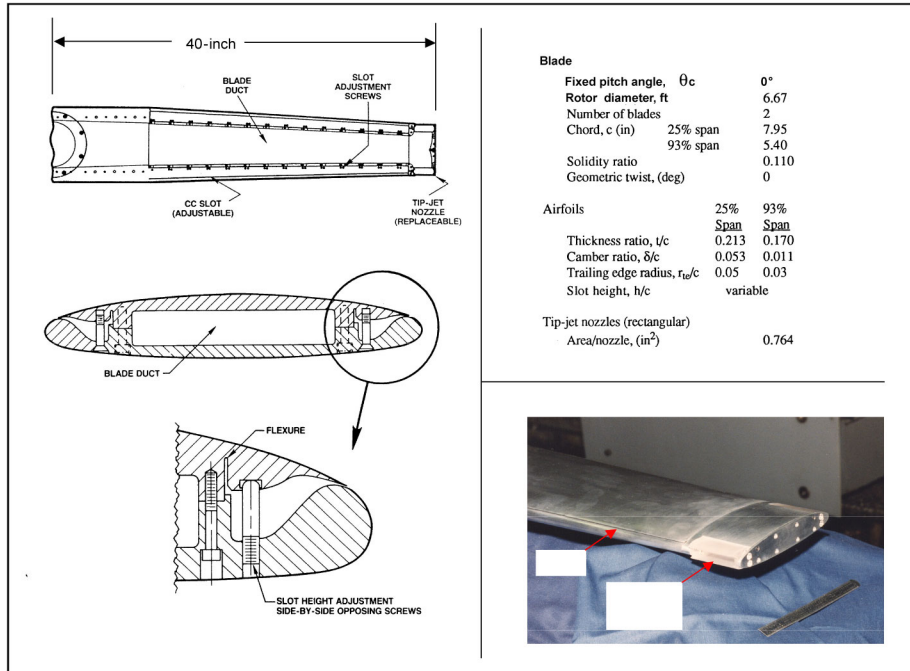
Experimentally investigated in 1991, the Tipjet was the first integrated lift/reaction-drive rotor system combining Coanda circulation control aerodynamics with cold-cycle reaction drive technologies. The hover investigation reviewed in this presentation is extensively documented in AIAA 92-0630.

The sketch of the completely pneumatic rotor shows the circulation control slots located along the span and the drive nozzles located at the tips.

A single source of compressed air flowed radially toward the nozzles at the tip for reaction drive. Along the way, a portion of the air is passed through the circulation control slots to augment the rotor thrust.

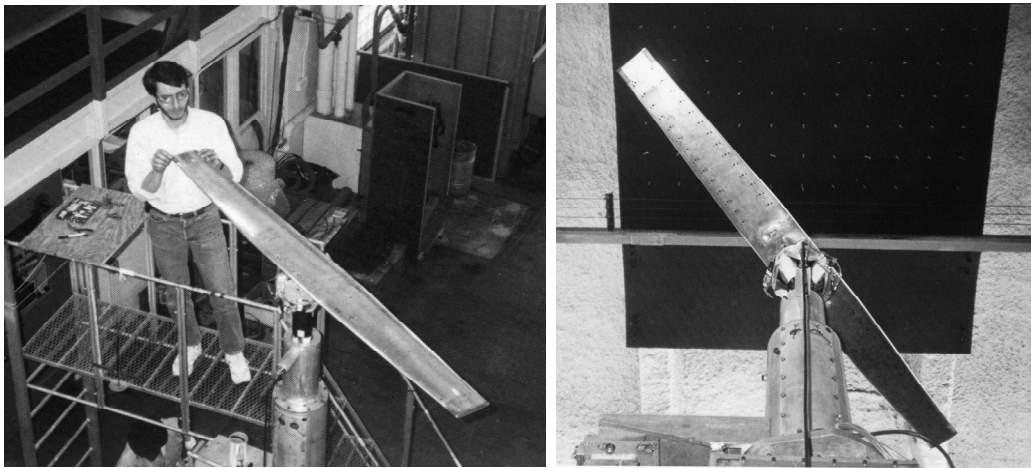
This rotor was developed as part of the Tipjet Unmanned Air Vehicle. The application involved a stoppable rotor concept where, after lifting off vertically in rotary mode, the rotor transitions to fixed wing for high speed forward flight. The compressed air could be supplied by a 'cold cycle' gas generator such as the fan stage of a turbofan engine.

The primary objective of the hover investigation was to evaluate the interactions between the lift and drive systems.



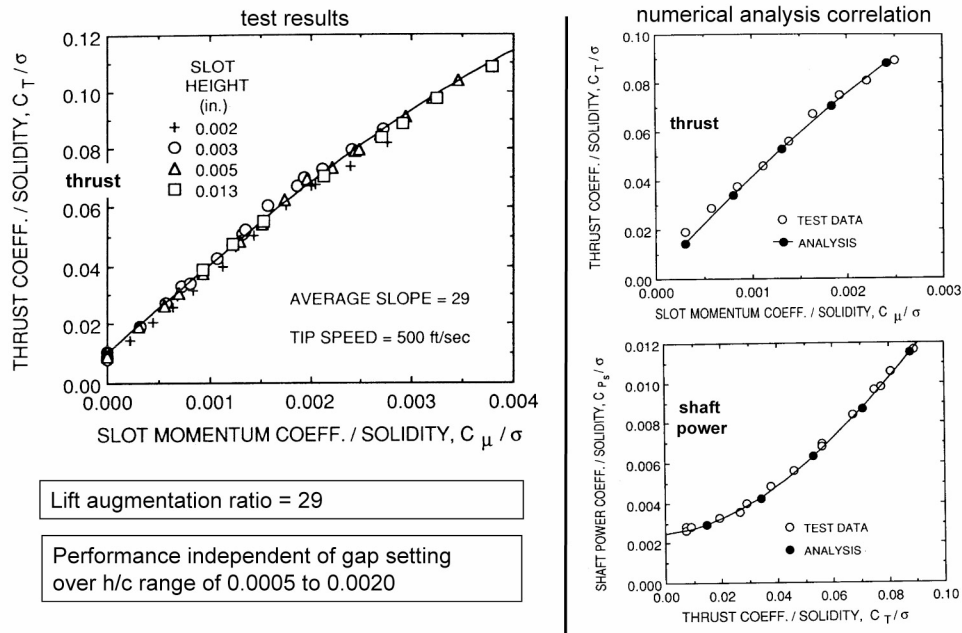
Drawings of the planform view, a 2-D section cut, and close up of the trailing edge are shown above. The photo of the rotor tip shows both the drive nozzle and CC-slot. The 80-inch rotor blade was tapered, but with no twist and no pitch angle. The thickness and camber varied linearly with radius from the 25% to 95% span location.

### Tip-jet Hover Test Set-up



Two photos of the test set-up are shown above. During the test the rotor could be driven by either an electric drive motor that enabled the rotor to be operated at selected rpm settings while investigating specific performance attributes, or by the tip jet reaction drive.

### Thrust Augmentation when Mechanically Driven at Constant RPM



To properly interpret the performance of the integrated lift/drive system, a detailed investigation was first conducted of the rotor model CC lift system with the tip nozzles closed and the rotor mechanically driven.

The figure on the left shows the measured lift in the form of rotor thrust coefficient as a function of  $C_\mu$  for several slot height settings.

Two main things to note are:

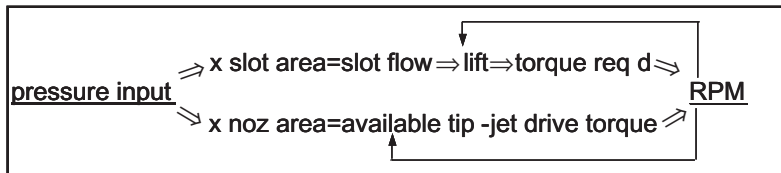
- the slope of the curve, which is the lift gain or augmentation ratio, is 29 and was higher than on any of the previously tested CC rotors.
- this measure of efficiency was independent of the slot heights tested.

An excellent correlation between the experimental performance and a numerical calculation was accomplished. The results of the calculations are shown in the plots on the right for both thrust and shaft power.

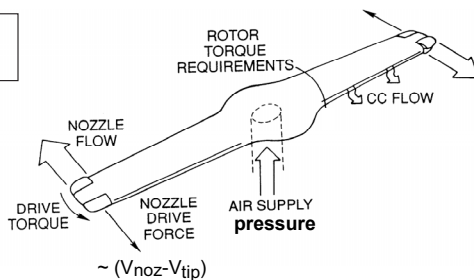
Sufficient understanding of this pneumatic lift/drive system was gained so that successful implementation of this technology into a vehicle system is feasible.

## Fully Pneumatic Operation Concept: Rotational Rate Equilibrium?

factors influencing pressure -RPM equilibrium (conceptual)



major parameter:  
slot / nozzle area



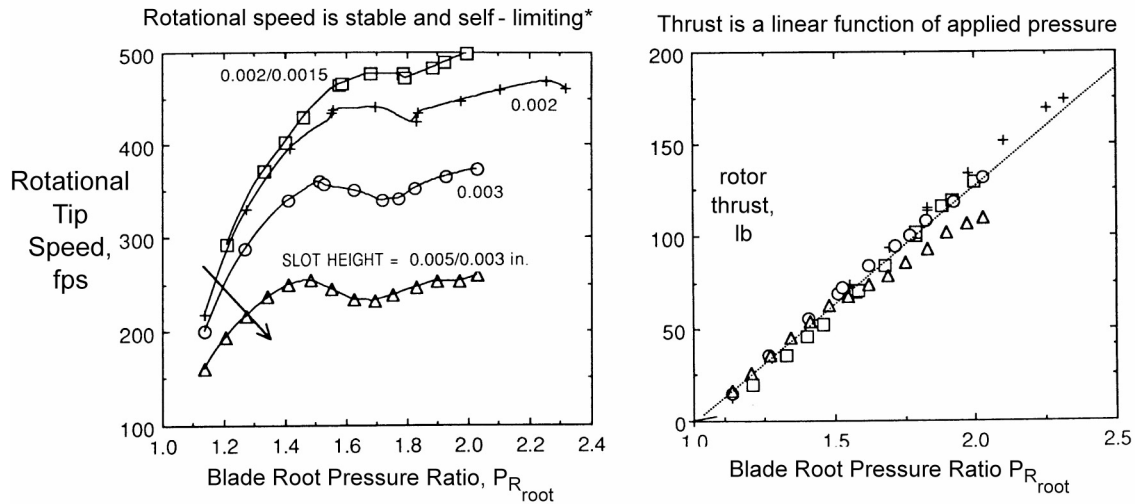
### 2 Bladed Tip-Driven Blown Rotor

The ultimate goal of the test was to determine the aeromechanics of the model rotor in the self-drive mode. The nature of the rotor tip speed response to pressure input was unknown at the outset of the test. With a slot height and tip nozzle area set, the blade duct pressure input is the only determining factor of the operating condition.

Pressure input simultaneously influences the lift and produces torque drive. The two effects are coupled as shown in the schematic. The question was, what is the nature of the simultaneous solution of these equations.

It was discovered that the rotational speed is stable and exhibits a self-limiting maximum for a given slot height to nozzle area ratio.

## Characteristics when Self Driven via Tip-Jet Nozzles



The data showing the nature of the self limiting rotational speed is shown in the figure on the left. Rotational tip speed is shown as a function of blade pressure for several slot height settings.

At each of the slot height settings, the rotor response to increasing blade root pressure is an increasing rotational rate, until a limiting tip speed is reached. Larger slot heights result in a lower limiting tip speed. Although the tip speed for each slot height reaches a limit, the lift due to CC will continue to increase as blade pressure increases. This can be seen in the figure on the right, which shows that the rotor thrust is essentially a linear function of the root pressure throughout the entire range.

A major finding was that a fully pneumatic rotor inherently seeks a rotational rate that results in lift being a near-linear function of the blade pressure input, which is easily controllable by throttling.

Such a capability should have applications to many systems that require a mechanically simple easily controlled thruster.



<h2>Annular Wing (CC Duct)</h2>	
<p><u>Investigators:</u>  Ernie Rogers, NSWC  Dr. Terry Brockett (Arete, Inc)  Dr. Neal A. Brown (AARC)</p> <p><u>1992 —1994 (1972 WVU)</u></p> <p><u>Sponsor:</u>  NSWC In-house  DARPA via Draper Labs  NSWC (ONR) for follow - on tests</p> <p><u>Facility:</u>  <u>Atlantic Applied Research, Acoustic WT.</u></p> <p><u>Documentation:</u>  undistributed contractor reports  1974 WVU report (ONR)</p>	
<p><b>Key Findings</b></p> <ul style="list-style-type: none"> <li>¥ Lift and Side Force is generated using specific blowing segments. At zero AOA, almost 2.5 -times the force is available versus a conventional ring - wing.</li> <li>¥ Braking (lift induced drag) force is available without development of lift.</li> <li>¥ Performance met expectations and can be predicted using a potential flow code</li> </ul>	

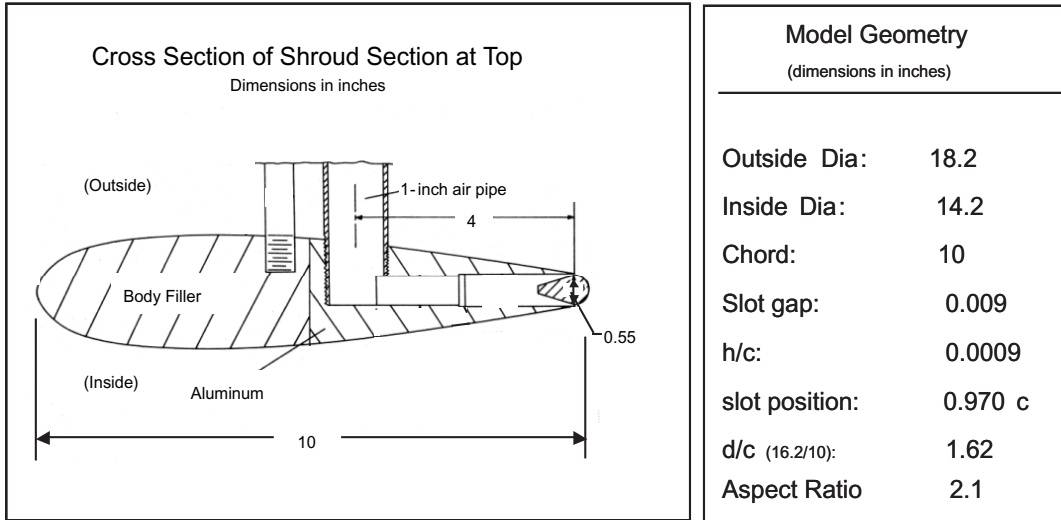
In 1992, Mr. Ernest Rogers initiated a project to investigate specific attributes of a CC circular duct. The focus was on using full or partial perimeter trailing edge CC fluid ejection to provide maneuvering control for watercraft.

Another investigator, Dr. Terry Brockett, independently proposed a similar concept shortly thereafter, under a DARPA program.

It was found that a CC duct model, with the needed inner and outer trailing edge slots, was available from West Virginia University. In the 1970s under ONR funding, the University built and tested the model researching the attribute of variable diffusion for ducted fans on aircraft.

The WVU model was borrowed and is shown in this photo undergoing a wind tunnel evaluation to determine thrust vectoring capability. The motor housing and stator have been removed to provide a pure ring-wing configuration.





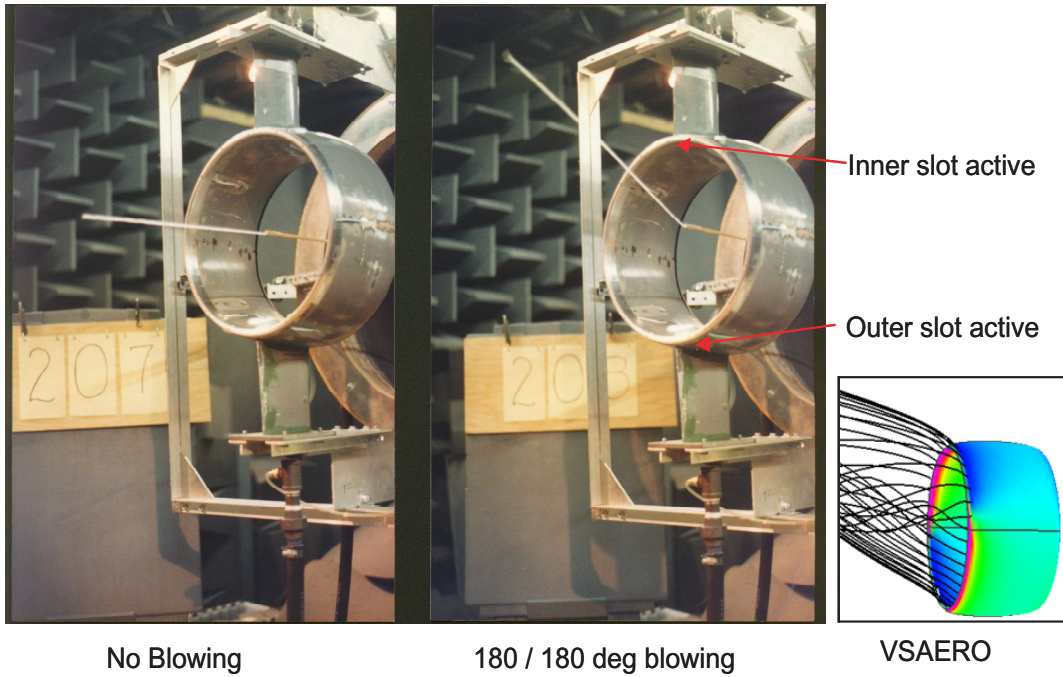
The model was 18-inch in diameter with 10-inch chord. The inner and outer slots continued around the full trailing edge circumference.

### Modes of Operation

	Slot Ejection Configuration	Effect	Operational Benefit
	Inner slot only	Increase duct flow-through: accelerating nozzle	Higher prop efficiency
	Outer slot only	Decreased duct flow: diffusion	Reduced cavitation
	Complementary quadrants	Side-force: yaw	Steerage
	Complementary quadrants	Side-force: pitch	Depth keeping
	Alternating	Vortex generation: very high drag, no side force	Braking: crash-back
	Both slots	Drag reduction, aux thruster	Cruise efficiency, dock side positioning

Aft view of duct  
 Dashed line is trailing edge  
 Solid lines represent active slot

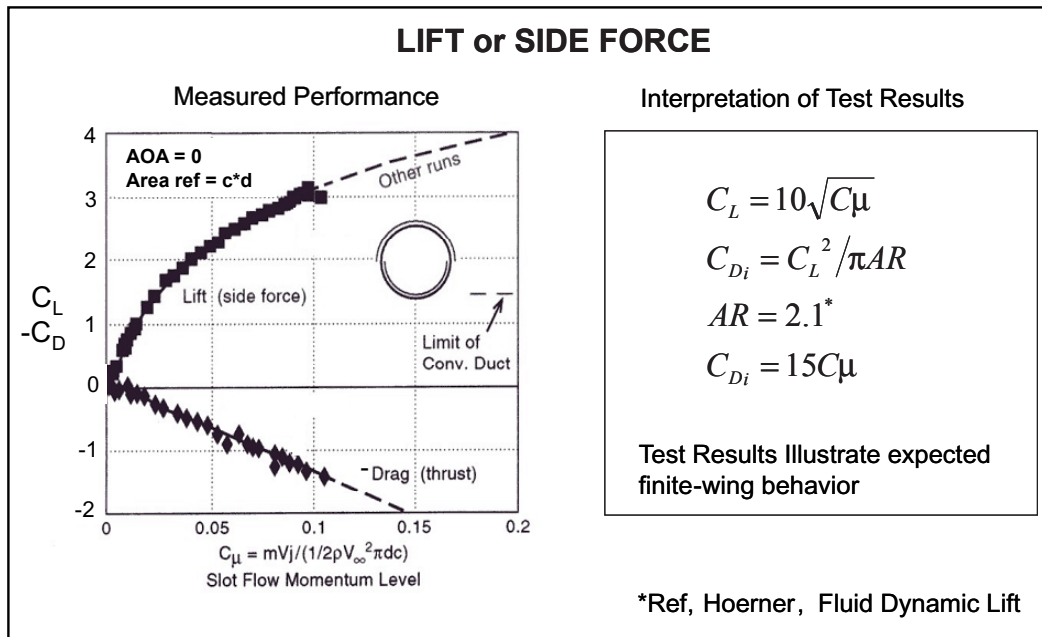
LATERAL FORCE CAPABILITY: PROOF OF CONCEPT  
Wake Deflection with asymmetric trailing edge CC blowing



The photo on the left shows the duct in passive mode. Note the yarn tuft in the center is horizontal and in line with the free-stream flow from the open jet tunnel.

On the right, complimentary slot azimuthal sections are active to produce force vectoring. Note the yarn tuft is now at an angle indicating the wake deflection brought about by the side force.

In the lower right corner is a panel method solution of the test condition and shows surface pressure distribution and wake deflection.



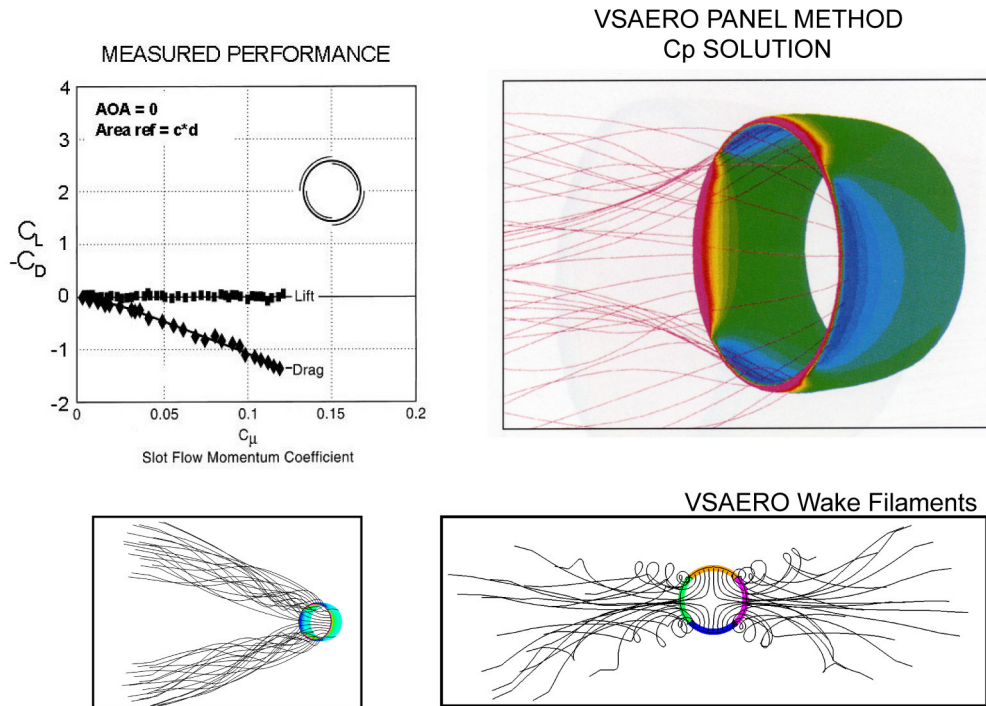
Looking at data from the configuration tested in the previous photo, on the left is a plot of force as a function of  $C_{\mu}$ .

The configuration being used was 180-degrees upper outer and 180-degrees lower inner slots active.

The force developed for these configurations, even at zero pitch angle, was more than twice that available from a passive duct.

The test results conform to expectations, including that the drag is a linear function of  $C_{\mu}$ , as shown in the experiment and derived above on the right. It is linear because  $C_L$  is a function of the square root of  $C_{\mu}$ .

## BRAKING Configuration: Lift Induced Drag Without Net Lift



One of the new findings from this investigation was the ability to produce a “braking,” or drag force, on demand without development of lift.

Alternating the active inside/outside slots every 90-degrees creates two pairs of counter-rotating vortices.

The measured performance, using a reference area of the chord times the diameter, is shown in the upper left. The drag is about the same as it was when lift was being developed.

The VSAERO surface pressure solution and wake filaments are instructive.

## Circular Wing

**Investigators:** Robin Imber, Ernie Rogers

**1995-1996**

**Sponsor:** In-house Research

**Facility:** NSWC 8x10 wind tunnel

**Documentation:**

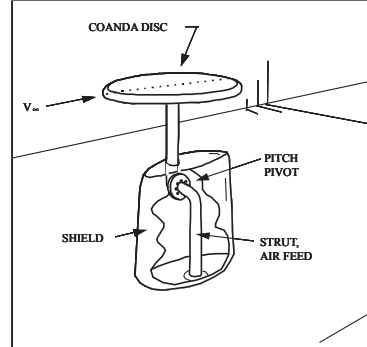
AIAA 96-0558 for first tunnel entry (AoA = 0 deg),  
Subsequent AOA tests await documentation

### Key Findings

- ✘ CC is effective on very low aspect ratio wings and provides an omni-directional capability when full perimeter blowing is applied
- ✘ Lift available is more than double that of unblown when blowing at least  $225j$  around perimeter.
- ✘ Lift limit believed to be from excessive jet turning.
- ✘ Drag from  $\Delta CL$  matches wing theory
- ✘ Roll control is available using asymmetric blowing.
- ✘ When blowing only the lateral edges, lift increases with no change in pitching moment.
- ✘ Sensitivity to a 4:1 change in slot gap is minimal.



Sketch of 2-ft diameter Disc in 8x10-ft wind tunnel



**Objective:** Research low-aspect ratio elliptic wing, lateral blowing, and omni-directional capability.

In 1995, the Coanda disc was created to investigate the effectiveness of CC on very low aspect ratio wings, and to explore the attributes of an omni-directional type of control surface or vehicle.

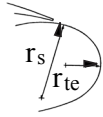
The photo shows the anodized aluminum 2-ft diameter model with a CC slot around the full perimeter of the circular wing.

The disc was tested in the NSWCCD 8x10-foot wind tunnel. The sketch shows the centerline upper and lower surface pressure taps. The model was axi-symmetric and designed to be incrementally rotated in-plane so that full surface pressure maps could be obtained. Also, there was a pitch pivot mechanism to configure from  $-10$  up to  $45$ -degrees angle of attack.

# Wind Tunnel Model

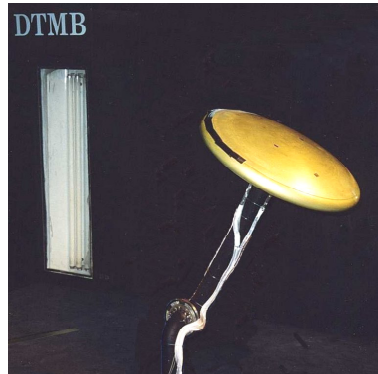
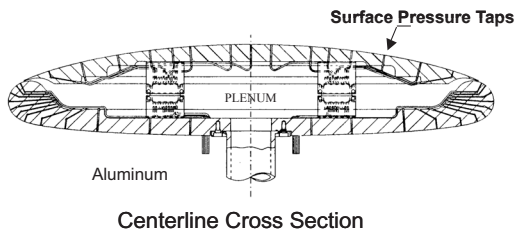
## Specifications

Diameter (Chord):	2 ft
Reference Area (S):	3.14 ft <sup>2</sup>
Aspect Ratio (AR):	1.27
Thickness (t/c):	19%
Camber:	2.4%
Coanda Radius:	$r_s/c = 0.050$ $r_{te}/c = 0.040$
Slot Position:	3.2%c from edge
Slot Lip Thickness:	0.026 inch
Slot Height (h):	0.032 inch
h/c:	0.0013
h/r <sub>s</sub> :	0.027
pressure tap diameter:	0.040 inch



## Test Conditions

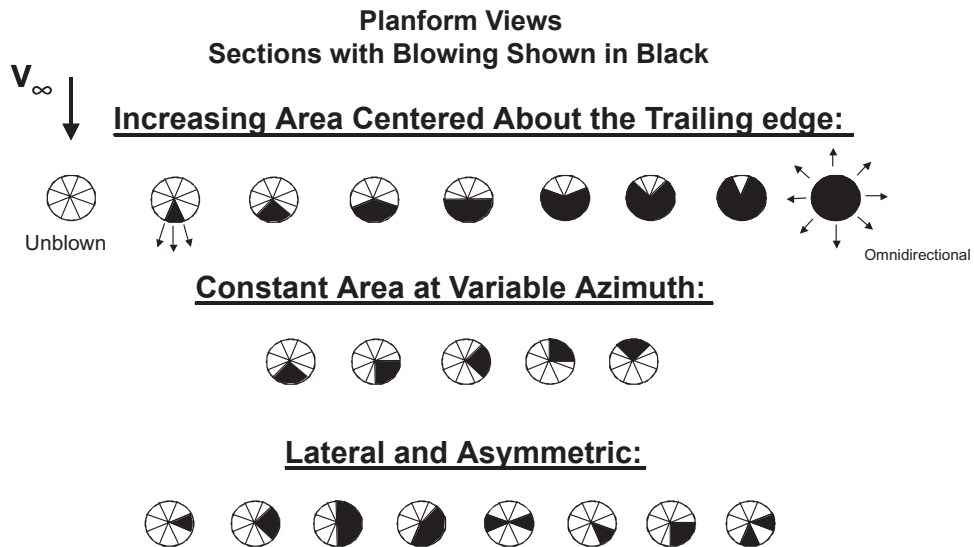
Dynamic Pressure: 0 to 60 psf  
 Angle of Attack: -10 to 45°  
 Six component measurements  
 Full surface pressure maps



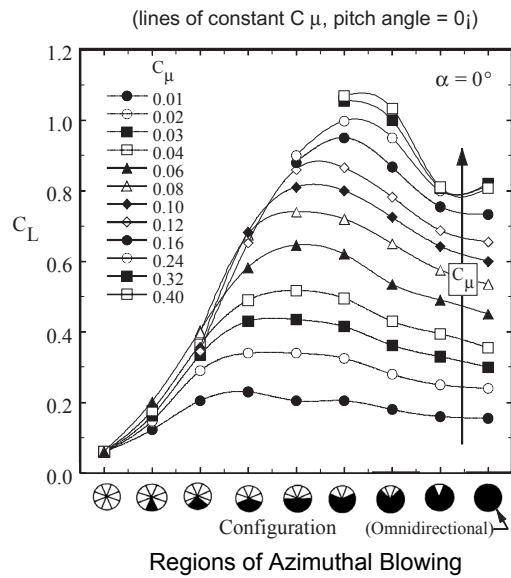
Disc in wind tunnel at angle of attack

Six-component force and moment data from an external balance system, and surface pressure data, were collected. The photo shows the metal foil tape used to block off portions of the slot for many different perimeter blowing configurations (shown below).

## TEST CONFIGURATIONS: Blowing Distributions



## Lift as Function of Azimuthal Mass Ejection Coverage



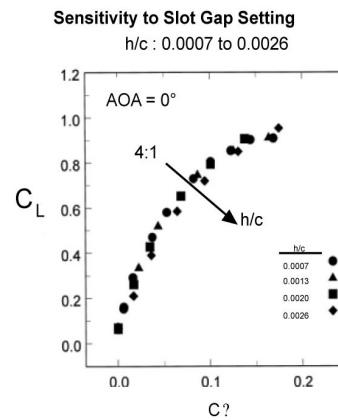
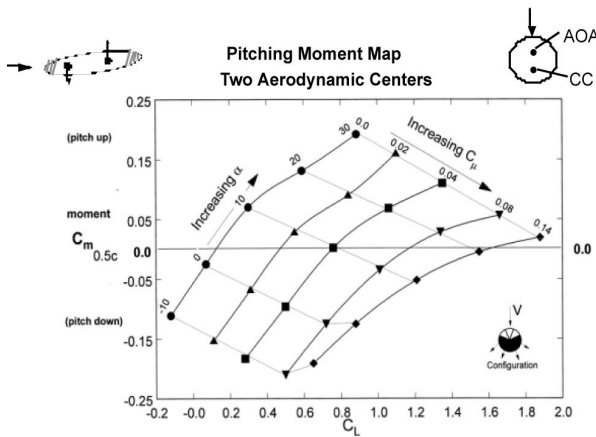
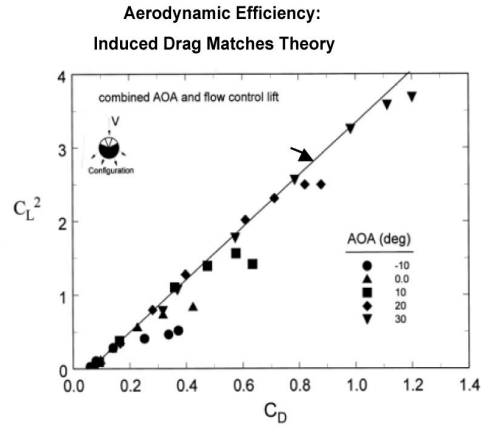
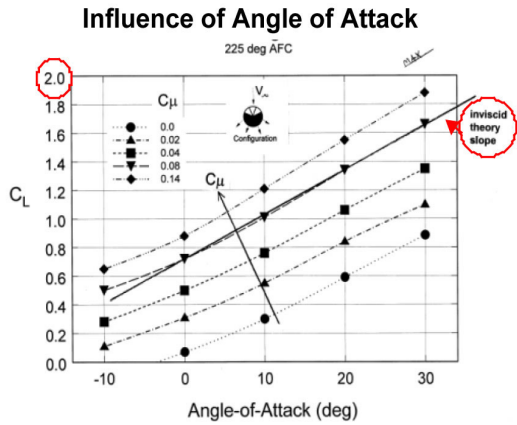
This plot shows lift as a function of azimuthal coverage, for constant  $C_{\mu}$ , with the model set to zero pitch.

Lift is presented as a function of the region of blowing, starting with unblown and then, centered around the trailing edge, increasing the perimeter region blown until full 360-degree blowing.

The lines are for constant blowing coefficient.

The optimum configuration varied somewhat with the  $C_{\mu}$  level. The highest lift was obtained using 225-degree perimeter of fluid ejection.

Notable is that good performance was obtained for full perimeter blowing, meaning that an omni-directional configuration is viable.



The top left plot shows that the maximum  $C_L$  was more than twice that available from an unblown disc at angle of attack. The lift curve slope matches inviscid theory.

Top right: Same configurations, the induced drag trends match lifting surface theory.

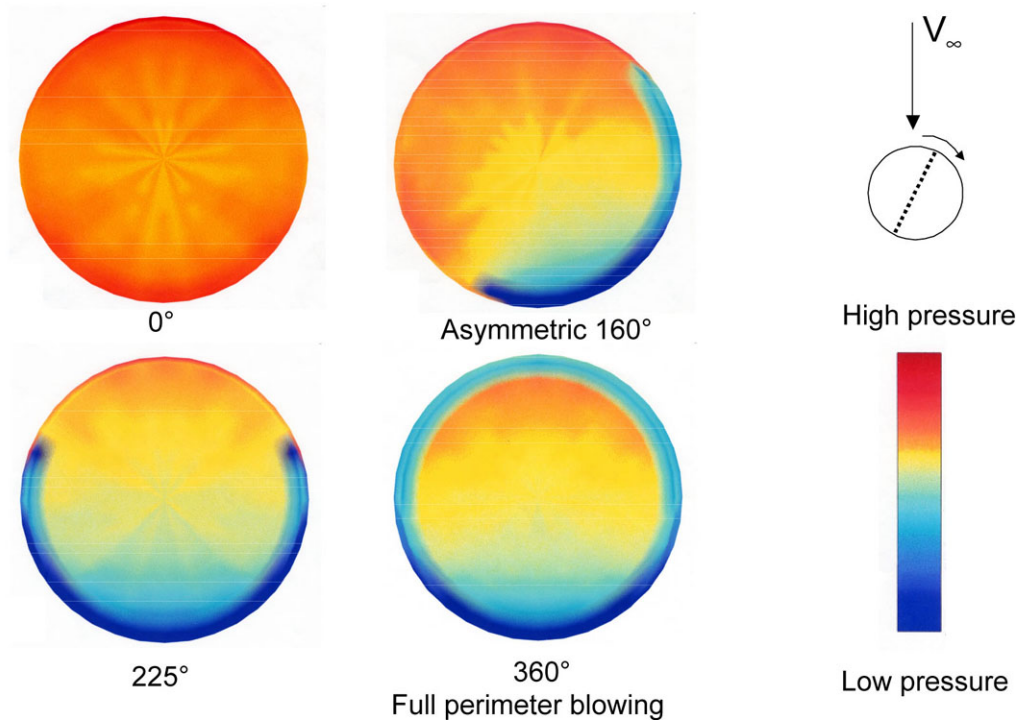
Bottom left: Pitching moment vs. lift coefficient for lines of angle of attack and momentum coefficient. There are two aerodynamic centers – one for lift due to angle of attack, the other for lift due to CC.

Bottom right: Slot height variations of 4 to 1 show that lift performance was nearly independent of slot height for the values tested.



## SURFACE PRESSURE DATA

Upper surface (slotted side) shown



Representative surface pressure data is shown above for various extents of blowing coverage at zero pitch. The configurations are for increasing blowing coverage, all the way to the fully blown omni-directional configuration.

**Flow Control using Miniature Valve for Alternating Flows Between Two Exit Slots, For Cancellation of Unsteady Loading**

jet-flap implementation  
**“Pneumatic Gurney Flap”**

**Investigators :** Dave Fry, Stuart Jessup, Steve McGuigan , Lisa Louie,

**Sponsor :** Office of Naval Technology, 1993

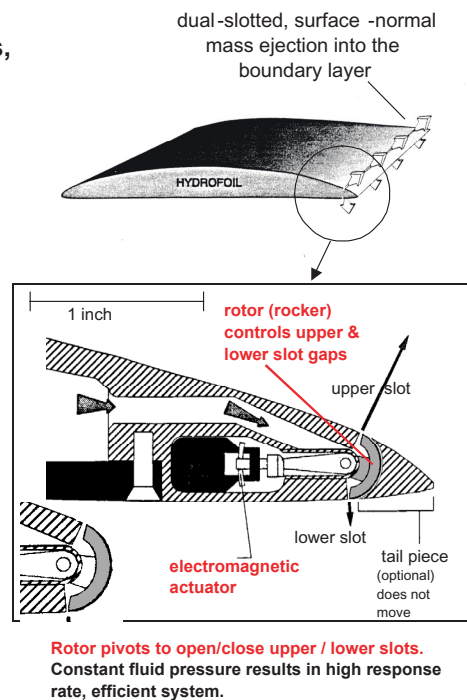
**Facility :** NSWC 24 water tunnel

**Documentation :** NSWC Reports, ASME article\*

**Key Findings**

- ¥ Actuators could follow any steady or time varying input signal up to 500 Hz.
- ¥ Successfully varied hydrofoil forces up to 110 Hz
- ¥ Cancellation of high -frequency periodic hydrofoil load was achieved.

\*Louie, L., Fry, D., and Jessup, S., “An Active Control System to Cancel Unsteady Foil Forces,” Active Control of Vibration and Noise, ASME, DE-Vol. 75, Nov. 1994.



The focus of the flow control actuator investigation was to cancel unsteady foil forces and be adaptive to upstream disturbances.

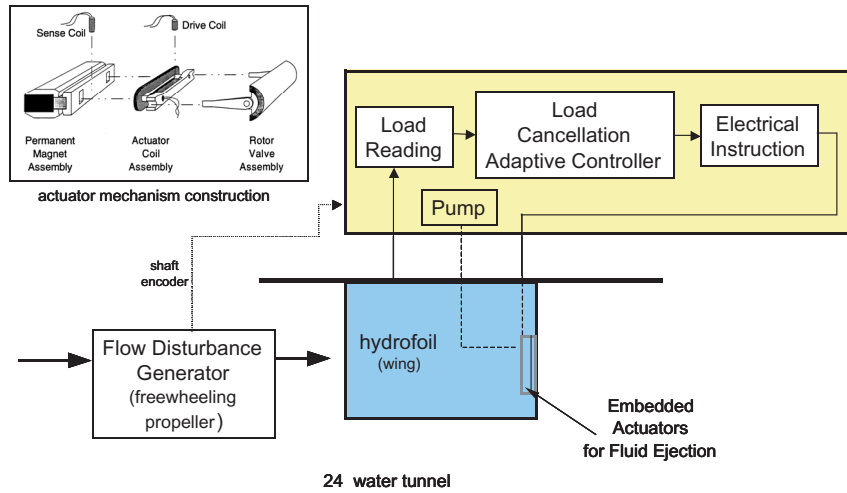
The actuator controlled the slot exit area, not the fluid pressure.

The miniature rocker valve was embedded in the trailing edge of a 15-inch chord hydrofoil.

The section cut of the trailing edge shows the rocker valve, slots, and the optional tail piece.

It should be possible to adapt the actuator concept to production of tangential jets.

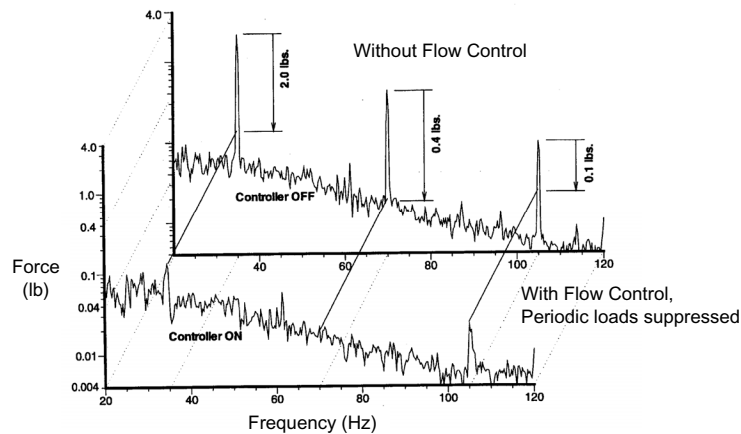
## Operational Schematic of the Test



A schematic of the water tunnel installation is shown with the freestream flow (from the left), a flow disturbance generator upstream of the hydrofoil, trailing edge blowing units, force measuring load cell, and controller. A rotating device upstream of the model was used to produce periodic loading on the hydrofoil (shown in the plot below). The actuator magnet and coil assembly, shown in the upper left, was placed in an oil-filled chamber. Fluid pressure to the trailing edge of the foil is not throttled; it is simply redirected as needed.

## Load Cancellation Effectiveness

3 frequencies of unsteady lift simultaneously reduced to the broadband floor



The targeted hydrofoil load spikes were successfully eliminated by the system. Three frequencies were simultaneously reduced.

## Dual-Slotted Low Aspect Ratio Wing (CC Hydrofoil)

Principle Investigator : Ernie Rogers  
2002

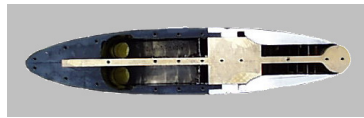
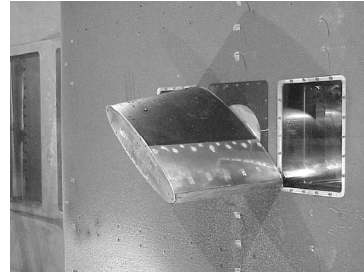
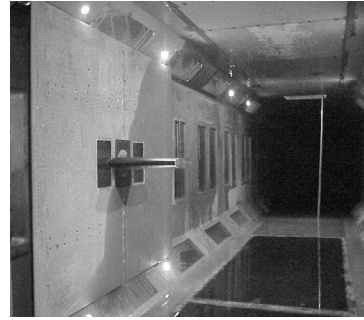
Sponsor : ONR

Facility : NSWC 10-ft x 10-ft water tunnel (LCC)

Documentation : AIAA 2004 -1244

### Key Findings

- ¥ 2nd-slot flow eliminates one form of CC lift limit.
- ¥ Performance meets predictions of Lifting Line theory.
- ¥ Dual slots permit static thrust vectoring 0 -360 deg.
- ¥ Cavitation has benign effect on the Coanda wall jet.
- ¥ Wake Filling is viable with dual slots.
- ¥ Circulatory CL is more than double that of conventional ship appendage.
- ¥ Jet-flap mode appears viable for use at very low speed.

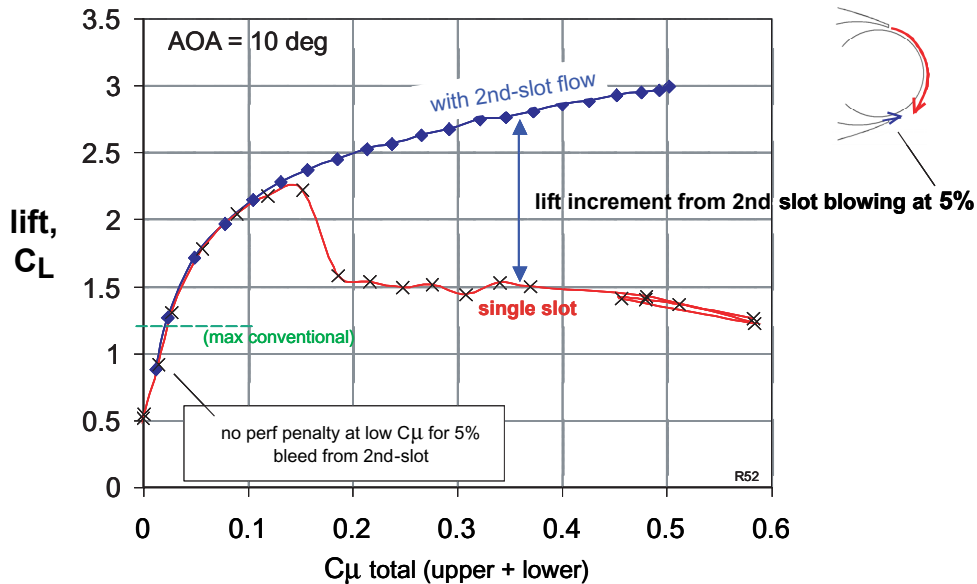


An extremely comprehensive investigation was conducted of a low aspect ratio CC wing in the Navy's 10-foot large cavitation channel in Tennessee, shown above. The intended application is to naval hydrodynamics.

The investigation is extensively documented in the just published in AIAA 2004-1244. Some of the highlights are included in this presentation.

## Lift Benefit of Dual Slot Activation

extreme  $C_{\mu}$  ( $C_L$ ) becomes viable



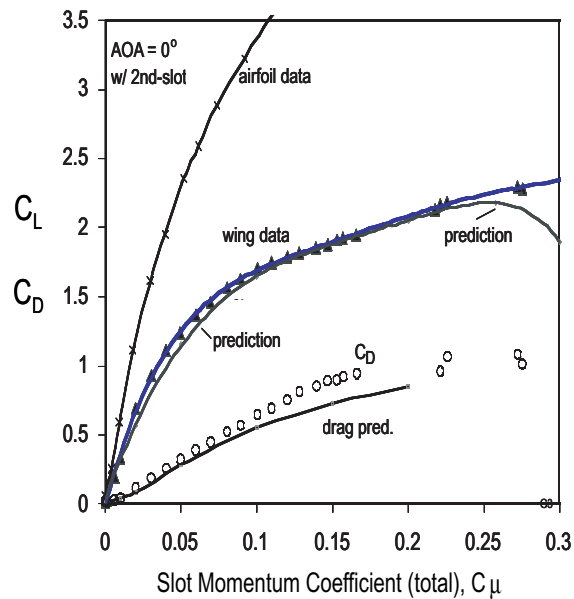
During the initial part of the hydrofoil investigation, with only the upper surface blowing, lift roll-off occurred at a much lower  $C_{\mu}$  than expected – shown as the “single slot” curve in the above plot.

It was concluded that excessive turning of the jet was causing the loss in lift. The lower slot was then employed to produce a very small counter flow to see if it would prevent the excessive turning.

This process allowed the performance as shown in the upper line on the plot. Note that there was no performance penalty at low  $C_{\mu}$  for the dual blowing and that the  $C_{\mu}$  range investigated extended to 0.5.

The slope of the  $C_{\mu}$  curve at the initial linear portion of the curve is 36, which is above average for an uncambered foil. Also the transition from a linear to a square-root like response to  $C_{\mu}$  is as expected.

### Comparison of Actual to Expected Performance



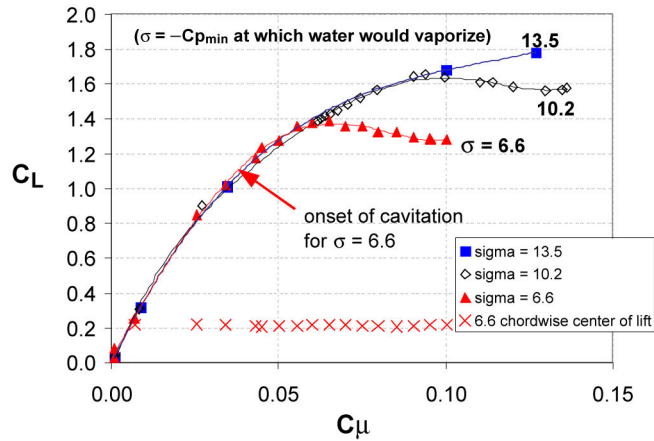
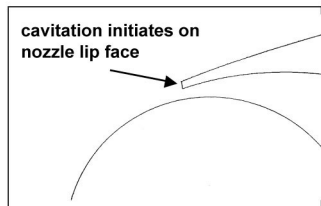
The above comparison of actual to expected performance plot of  $C_L$  vs.  $C_{\mu}$  shows excellent agreement.

For the wing, which has an aspect ratio of two, the response of  $C_L$  to  $C_{\mu}$  is about 50% of that on the corresponding 2-D airfoil. This is the same percentage as the  $C_L$  versus angle of attack change for a conventional wing.

The performance matched the prediction that had been made based on conventional lifting line theory so there is no indication of any basic effects of low aspect ratio that are unique to lift developed by means of the Coanda form of circulation control.

## Lift Response to Coanda Surface Cavitation Development

Tunnel Static Pressure Reduced Below Atmospheric

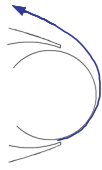


The photograph shows some interesting flow visualization on the CC foil, compliments of cavitation that was produced by decreasing the tunnel static pressure. The white bubbles are vaporized water.

One of the test objectives was to determine where the minimum pressure occurs on the model and what the impact of subsequent cavitation would be on the ability of the jet to induce circulatory lift, or even to remain attached.

The data plot shows that even after the onset of cavitation, as duct pressure increased the lift continued to rise. Eventually the lift began to roll over, but it was not abrupt. At no time did the Coanda jet detach prematurely from the trailing edge due to cavitation. Cavitation is not likely to occur operationally but if it does, it would not be catastrophic.

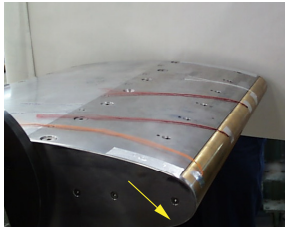
Cavitation occurs when the minimum pressure reaches the value corresponding to the vaporization of water, about 0.5 psia depending on temperature. The cavitation index, sigma, is the term for the absolute value of the pressure coefficient that will result in vaporization and is a function of the test section static and dynamic pressure.



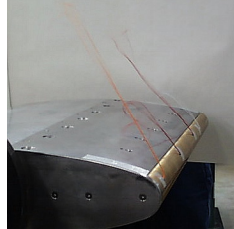
## Dual Slot Operation Checkout in Air no freestream, 0.2 psig



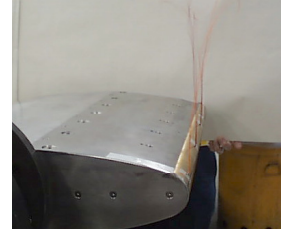
the two wall jets merge to form a steerable free planar jet



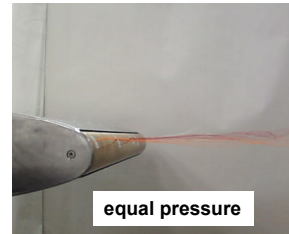
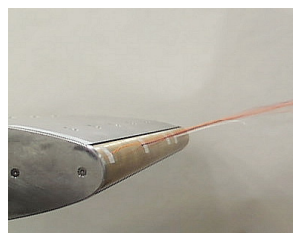
**single slot blowing (lower)**  
180 deg redirection of the wall jet



**initiate dual slot mode**  
very low pressure in upper slot



**upper slot blowing increased**



Load Cell Data in Water tunnel confirmed 0 -360° (70-80% $\eta$ ) Static Thrust Vectoring

Another advantage of dual slots is the ability to vector the jet thrust. In fact, in static conditions, as representative of very low speed operations, the direction of jet thrust can be vectored essentially a full 360-degrees because the two jets merge to form a free planar jet.

These photographs show a sequence of variable relative pressure between the upper and lower slot, using air. The vector directions are visualized using yarn tufts. Quantitative data for the thrust vectoring was obtained in water, revealing a thrust efficiency of 70-80%.

Starting with the photograph at top left, with only the lower slot active, the slot flow follows the curved trailing edge and departs at the leading edge of the upper surface, a 180° redirection.

At center top, a small amount of upper surface flow is introduced, lifting the slot flow off the surface of the wing.

Top right, the upper slot flow is increased resulting in a vertical thrust vector.

The bottom three photographs show increasing the upper surface pressure, until it equals the lower pressure and the thrust vector is now 180 degrees from where we started.



**Why Have Only Two Circulation-Controlled STOL Aircraft  
Been Built And Flown In Years 1974 - 2004.**

by

John L. Loth

Department of Mechanical and Aerospace Engineering

West Virginia University

Morgantown WV 26506

**Abstract:**

Circulation Control (CC) by Coanda blowing over a rounded trailing edge is by far the most blowing power efficient method for high lift generation. Only two CC aircraft have ever been build and flight-tested in the past 30 years. Why was one of the questions posed at the end of the 2004 ONR-NASA Circulation Control Workshop. Other high lift systems, such as the jet flap, upper surface blowing, augmenter wing and flap type thrust deflectors have found many applications on STOL aircraft. The two Circulation Control aircraft were the WVU CC Technology Demonstrator STOL flight-tested in 1974 and the Grumman A-6A flight-tested in 1979. This paper aims to provide some answers to that question. The design and construction of the WVU CC Technology Demonstrator STOL aircraft was completed in the period from 1971 to 1973. Starting on April 10, 1974, professional test pilot Shawn Roberts started 25 hours of flight-testing. Design features incorporated in the WVU CC aircraft include:

a) assuring uniform blowing air distribution; b) by designing the primary nozzle slot for choked flow with precise gap control; c) actively cooling of the fibre-glass wing; d) allowing for thermal expansion of the 3" rounded trailing edge which carries the hot high pressure air; e) pilot actuated Direct Lift Control (DLC); f) developing an airfoil capable of high  $C_{Lmax}$  and high  $C_L/\sqrt{C_\mu}$  ratio; g) by in-flight folding out a CC flap for slow flight and stowing said flap within the wing for high speed performance at low drag.

Flight test results showed that minimum level flight can be achieved at an indicated airspeed of  $V_i = 23.5$  knots equal to a corrected airspeed of  $V_e = 33.2$  knots. This occurred at angle of attack  $\alpha \cong 0^\circ$  with good pilot visibility, and full throttle at 180 HP. The Circulation Control blowing air was supplied at 13 psig producing  $C_{Ltrim} = 5.2$ ,  $C_{Lwing\ av} = 5.6$  at  $C_\mu = 0.17$ .

Flying level at slow speed and high  $C_L$ , required all the available 180 HP propeller thrust, which means flying on the backside of the power curve. This leaves no power to spare to assist in wing stall recovery. With CC, all lift is provided by the wings and no power remains to assist in stall recovery. Stall produces rapid wing roll over and 500 ft altitude was needed for recovery. Other high lift systems, using blowing air, do not have such a severe problem as much of their lift is provided by deflected engine thrust! Pilots need some excess power to help recovering from a stall. This may explain why no more than two such airplanes have build in the past 30 years.

## **Historical Development of Circulation Control:**

The first use of circulation control by blowing over a rounded Coanda surface was disclosed in a 1960 patent<sup>1</sup> application. In 1966 R.J. Kind<sup>2</sup> finished his PhD at Cambridge University and provided the world with a proof of high  $C_L = 6$  capability of an elliptical wing section with circulation control by blowing at very low  $C_{\mu}$ . In the sixties the US deployed several large navy aircraft carriers operating with VTOL helicopters and CTOL aircraft. The tensions worldwide made the Navy look for a new dispersed fleet of smaller carriers operating with Heavy Lift Helicopters and STOL aircraft. Reducing the landing speed from 130 knots to 65 knots reduces the risk of a serious landing accident by a factor of four. Although not as power efficient as boundary layer control by suction through distributed small holes, CC blowing was capable of doubling  $C_{Lmax}$  and was not effected by weather.

R.M. Williams, a young engineer at NSRDC learned about Kind's research on the high  $C_L$  capability of a Circulation Controlled Elliptical Wing Section at low blowing power. Williams started testing 2-D wind tunnel models at NSRDC and promoting the Navy Heavy Lift Helicopter research program. This was about the same time that Dr. Cheeseman, at the University of Southampton, experimented with a four bladed cylindrical rotor rig with CC blowing.

In 1968 WVU received a multi-year research contract from ONR to perform theoretical and experimental research on the elliptical CC rotor section. In particular to provide high Reynold's number test data, free from wind-tunnel wall effects. WVU owned several small aircraft, which were considered for the

possibility of mounting an elliptical rotor section vertically up through the cockpit of one of these. Simple calculations showed that the Cessna 150 did not have enough aileron control to counter the kind of rolling moments generated in such a flight test configuration.

The WVU team decided that the safest way to flight-test a Circulation Controlled airfoil at full Reynolds number for the NAVY Heavy Lift helicopter was to test it as a fixed wing on an airplane. The most economical test bed would be a BD-4 airframe. Its fiberglass wing could readily be converted to a rounded trailing edge by rotating a flap  $166^\circ$  forward into a cavity provided for it. To prevent leading edge stall, a drooped leading edge was designed by Dr. Norio Inumaru from Japan's National Aerospace Laboratory and developer of the Japanese QSTOL. The 1<sup>st</sup> version of a WVU CC Retractable Rounded Trailing Edge wing was designated Model A, see Fig. 1. It was tested full scale in 1970 in the NSRDC 8x10 ft wind tunnel under the direction of Dr. Inumaru, with  $C_L$ - $C_\mu$  performance results also shown in Fig. 1. The  $C_L$  values were based on the sharp trailing edge cruise chord length. In the CC mode, the model A wing, had its chord length reduced by 12%, which lowered its  $C_{Lmax}$ . Results were:  $C_{Lmax} = 5$  could be obtained at only  $\alpha = 8^\circ$ , promising good pilot visibility during landing. The drooped leading edge worked well to prevent L.E. stall. A most interesting observation was that airfoil drag did not appear to be effected by leaving a cavity on the wing bottom surface, into which the flap was stowed in the CC mode. Its performance made it clear that the wing chord must be increased in the CC mode rather than decreased as in the Model A. Walters<sup>3</sup> at all. at WVU tested

the performance of pulsed blowing as would be required for a helicopter blade. They found the same  $C_L$  could be obtained by pulsing and that would save a small amount of blowing air.

### **The WVU CC Technology Demonstrator STOL Aircraft**

For flight testing, the high C.C. airflow requirements would best be met, at a reasonable weight, by installing a small GTC-85 gas-turbine designed to provide 2 lbs/sec of bleed air at up to 25 psig and 300 degree F. Based on such an available blowing air supply the Model B wing was designed, as shown in Fig. 2 and wind tunnel tested<sup>4</sup> at WVU. The available high-pressure air supply can be ducted without much pressure loss through its 3" diameter rounded trailing edge. A choked flow nozzle, made of in-line 1 foot long segments was bolted to the 3" diameter by 10 foot long wing CC round trailing edge. This primary supersonic nozzle had a gap of 0.012" and assured blowing uniformity along its span. The blowing velocity reached up to 1500 ft/s. Such a high blowing velocity at flight speeds down to 33 knots is totally unsuitable for Circulation Control. Therefore an ejector was designed to provide boundary layer suction at the flap hinge. By ducting this suction air through a hollow flap, the fiberglass wings were kept cool. The ejector air reduced the blowing jet temperature down to about 180 degree F. Although the ejector doubled the blowing mass flow rate, its blowing velocity reduced down to about 650 ft/s and the CC blowing slot gap increased to 0.050". Although a 10 times ratio between CC blowing velocity and flight velocity is not the most power efficient ratio, it did produce a large increase  $\Delta C_L$  on the CC

blown wing portion of the wing. Its rounded trailing edge had  $r/c = 0.0275$ . Using an ejector to provide boundary layer removal by suction just upstream of the CC blowing slot, allowed flap deflection up to 30 degree without flow separation. The ten-foot long by 3 inch diameter aluminum CC rounded T.E would expand  $\frac{3}{8}$  of an inch due to the 300°F blowing air from the gas turbine. This was facilitated by anchoring the 3 inch tube inside the fuselage and supporting the ends with a of an inch diameter pin inside a sliding bushing. The wing trailing edge piano hinge connected rigidly to a hollow 9" flap, which guided the BLC suction air to the ejector. The stowable CC rounded surface with flap was actuated by a bell-crank welded in the 3 inch air supply tube. The flap had a sliding connection to the air supply tube to allow for thermal expansion.

The next challenge was to convert the C.C. rounded trailing edge wing, from a slow STOL speed configuration to a low drag, sharp trailing edge CTOL configuration for cruise speeds up to 140 knot. This was accomplished as shown in Fig. 2, the WVU model B configuration. It again used a forward folding flap, which now increased in chord length by 20% in the CC configuration. This design of the WVU type B CC configuration is shown installed in Fig. 3 and compared to the model A geometry, provides a 30% improvement in lift capability! To provide the torque required to rotate the flap in or out within ten seconds was a 2 HP DC motor with a drive worm wheel attached to the 3 inch diameter blowing air supply tube located inside the cockpit. Its centerline was positioned in line with the wing flap hinge. A pair of 90° welded elbows provided the bell crank to transmit the air and torque to the folding CC flap. A cavity was made inside the wing to embed

the 3 inch diameter by 10 ft long CC rounded trailing edge. As this cavity cuts through all the wing ribs, additional structure in the form of external ribs were needed. This is visible in Fig. 3, where they connect the flap hinge to the wing spar. Note also the location of the pilot controlled air dump valve for Direct Lift Control (DLC). The performance of both Model A wing and Model B wing were compared in Fig. 4 taken from Ref. 4, to those of other high lift systems by blowing.

The 1<sup>st</sup> "Circulation Controlled Technology Demonstrator" STOL aircraft, was build by Lee Metheney and his assistants between 1971 and 1973.

### **WVU Flight test results**

On April 14 1974, former NASA VSTOL test pilot Shawn Roberts started 25 hours of scheduled flight-testing. Early tests included position error calibration by tower fly-by. This is probably the most accurate method. The position error, see Fig. 5, is almost 10 knots, at the minimum level flight speed of  $V_i = 23.5$  knots indicated airspeed. The aircraft in flight, with the CC flaps deployed, is shown in Fig. 6. The dimensional drawing included, indicates where the blowing air gas turbine has its air intake and exhaust pipe. Note the exhaust had to be turned up to prevent igniting the runway asphalt. The performance improvement with blowing at an air pressure of 13 psig versus no blowing is shown on Fig. 7, for the level flight condition and the power off glide condition. Three values of  $C_L$  are shown where  $C_{L_{trim}} = \text{weight}$ ,  $C_{L_{wing}} = (\text{weight} + \text{tail download}) / (q_{\infty} S_w)$  and also  $C_{L_{flap}}$  only. The flap folding in-or-out produces a change in stick force less than

17 pounds and takes only 4 seconds to deploy and 10 seconds to retract. The stick forces are shown as a function of flap angle in Fig. 8.

Interesting aspects of the test flights are shown in Fig. 9. Deploying the flap, even without blowing air at 80 knot, increases the required propeller shaft power from 60 to 100 HP. Indicating that it is essential to be able to fold the rounded CC trailing edge out of the way for cruise. Without blowing the minimum speed is limited to about 50 knot at 84 HP. However to go very slow, at minimum level speed of 33.2 knot, all available 180 HP where required. This is a clear indication of flying on the backside of the power curve.

Shawn Roberts provided WVU in 1974, with a detailed report on his flight tests results, see Ref. 5. That same year the WVU team<sup>6</sup> presented the results at AIAA 6<sup>th</sup> Aircraft Design, Flight Test and Operations meeting, Aug,1974. This report was also published<sup>7</sup> in the Journal of Aircraft in 1976.

### **Landing with CC on the backside of the power curve**

In level flight, thrust required is the sum of the viscous parasite drag  $D_{para}$  and the induced drag  $D_i$ . Then the thrust required  $T = D_{para} + D_i =$

$\rho V^2 S_w (C_{Dpara} + C_{Di})$ . The optimum flight speed  $V_{opt}$  is defined when D is minimum or L/D is maximum, which occurs when  $C_{Dpara} = C_{Di}$  or at  $C_{Lopt}$ . For a propeller driven aircraft with constant propeller efficiency the shaft power required remains proportional to the thrust power  $T \cdot V_{\infty}$ . Then the increase in power required flying on the backside of the power curve, at minimum level flight



speed  $V_{\min}$ , corresponding to maximum lift coefficient  $C_{L\max}$  and maximum  $C_{Di}$ , is calculated as follows:

$$\frac{T_{\max} V_{\min} = P_{\max}}{T_{\min} V_{\text{opt}} = P_{\text{opt}}} = \frac{0.5\rho V_{\min}^3 S_w * (C_{Dpara} + C_{Di\max})}{0.5\rho V_{\text{opt}}^3 S_w * (2C_{Dpara})} = \left(\frac{V_{\min}}{V_{\text{opt}}}\right)^3 * 0.5 * \left(1 + \frac{C_{Di\max}}{C_{Dpara}}\right)$$

Defining  $C_{Di\max} = \frac{C_{L\max}^2}{\pi eAR}$  and from  $L = C_{L\max} 0.5\rho V_{\min}^2 S_w = C_{L\text{opt}} 0.5\rho V_{\text{opt}}^2 S_w$  find:

$$\frac{P_{\max}}{P_{\text{opt}}} = \left(\frac{C_{L\text{opt}}}{C_{L\max}}\right)^{3/2} * 0.5 * \left(1 + \frac{C_{L\max}^2}{\pi eAR * C_{Dpara}}\right)$$

For the WVU Circulation Control Demonstrator the increase in power is calculated with the following input parameters with CC flap deployed:

$C_{L\max} = 5.6$  at 33.2 knot and  $C_{L\text{opt}} = 2.5$  at 50 knot and 84 HP. Inserted above gives  $\frac{P_{\max}}{P_{\text{opt}}} = 2.13$  or  $P_{\max} = 180$  HP or full throttle

### **The Grumman CC high lift conversion of an A-6A**

In 1973 Bob Englar, then at NSRDC visited WVU and liked the concept of flight-testing CC of a real airplane. He contracted with Grumman to design a conversion to CC blowing for the A-6A bomber. The planning for this five year project was quite involved and has been described by Englar in many publications for example: 1974<sup>8</sup>, 1975<sup>9</sup> and in 1976<sup>10</sup>. In 1979 the airplane conversion was completed as shown in Fig. 11. This aircraft and WVU aircraft are the only two Circulation Controlled aircraft ever build and flight tested in the past thirty years. In the WVU<sup>11</sup> paper “Circulation Control STOL Design Aspects” presented at the 1986 NASA Ames CC workshop, the WVU 1974 CC Technology Demonstrator results were compared with the 1979 Grumman A6-A

CC Technology Demonstrator. They show excellent agreement. Both aircraft performed as had been predicted from wind tunnel tests. Circulation Control was

shown to fit the model: 
$$C_L = \left( \frac{\partial C_L}{\partial \alpha} \right) \alpha + \left( \frac{\Delta C_L}{\sqrt{C_\mu}} \right) \sqrt{C_\mu}$$

The quantities in brackets, were evaluated from the flight test results:

Grumman 1979 test results: 
$$\left( \frac{\partial C_L}{\partial \alpha} \right)_{Grumman} = 4.74 \quad \text{and} \quad \left( \frac{\Delta C_L}{\sqrt{C_\mu}} \right) = 6.6_{Grumman}$$

WVU 1974 test results: 
$$\left( \frac{\partial C_L}{\partial \alpha} \right)_{WVU} = 5 \quad \text{and} \quad \left( \frac{\Delta C_L}{\sqrt{C_\mu}} \right)_{WVU} = 6.6$$

Boasson<sup>12</sup> addressed the problem of finding the optimum velocity ratio between blowing slot velocity and flight velocity. The take-off thrust loss by using compressor bleed air for CC blowing air has been presented by Funk<sup>13</sup> in Ref. 12. The torque required to fold the CC flap in-or-out can be greatly reduced, as explained in patent<sup>14</sup> and shown in Fig 11.

## **Conclusions**

- a) The ability of the WVU wing to convert in flight, from slow flight with a rounded Coanda trailing edge to high speed cruise with a sharp trailing edge, appears to be essential for practical applications.
- b) Pitching moments associated with flap stowing were acceptable, and would be reduced when incorporating the technology shown in Fig. 11.
- c) Supplying CC air at a pressure of at least 15 psig, reduced duct pressure losses, allowed using an ejector to double the CC blowing air and also provide

BLC by suction just upstream of the blowing slot for CC on a wide range of flap angles.

d) Direct Lift Control (DLC) by dumping air with a bypass valve proved to be very effective, without causing pitch problems.

e) Flying slow, on the backside of the power curve, is not recommended because no power is then left over to assist in stall recovery. This is not so severe when using conventional STOL devices such as: thrust deflection, the blown flap, upper surface blowing and the augments wing. These techniques get only part of the lift from the wing and the rest from the deflected thrust. Then wing stall recovery is not so difficult. With Circulation Control all the lift comes from the wing, when it stalls, the loss in altitude is high and the pilot experiences a high wing roll rate.

f) Until one discovers a new technology which prevents having to land on the backside of the power curve, circulation control may not become popular with pilots for take-off and landings.

g) The drooped leading edge nose design by Dr. Norio Inumaru from Japan on both WVU model A and Model B wing were very effective in protecting the wings from leading edge stall.

## **References:**

1. Davidson, I.M., "Aerofoil Boundary Layer Control System", British Patent No. 913754, 1960.
2. Kind, R.J. and Maull, D.J. , "An Experimental Investigation of a Low-Speed Circulation Controlled Airfoil", May 1968, pp. 170-182
3. Walters, R.E., Myer, D.P., and Holt, D.J., "Circulation Control by Steady and Pulsed Blowing for a Cambered Elliptical Airfoil"TR-32, July 1972 (AD 751045), Dept of Aerospace Eng. at WVU, Morgantown WV.
4. Loth, J. L. ,"Some Aspects of STOL Aircraft Aerodynamics", Business Aircraft Meeting, Wichita Kansas, April 3-6 1973, SAE Paper 730328
5. Roberts, S.C., "WVU Circulation Controlled STL Aircraft Flight Tests", WVU TR 42, July 1974.
6. Loth, J. L. , Fanucci, J. B., Roberts, S.C. ,"Flight Performance of a Circulation Controlled STOL" AIAA 6th Aircraft Design, Flight Test and Operations Meeting. Los Angeles, California August 12-14, 1974.
7. Loth, J. L. , Fanucci, J. B., Roberts, S.C. ," Flight Performance of a Circulation Controlled STOL", Journal of Aircraft, Vol 13 No 3, March 1976, p 169-173.
8. Englar, R.J. , "Investigation into and Application of the High Velocity Circulation Control Wall Jet for High Lift and Drag Generation on a STOL Aircraft", AIAA Paper 74-502, Palo Alto, Calif, June 1974.
9. Englar, R.J., "Circulation Control for High Lift and Drag Generation on a STOL Aircraft", Journal of Aircraft, Vol. 12, No. 5, May 1975, pp. 457-463.

10. Englar, R.J., "Circulation Control for High Lift and Drag Generation on a STOL Aircraft", *Journal of Aircraft*, Vol. 12, No. 5, March 1978, pp. 175-181.
11. Loth, J.L. , Boasson M. "Circulation Controlled Wing Optimization", *Journal of Aircraft*, Vol. 21 No 2, February 1984.
12. Loth, J. L., "Circulation Control STOL Aircraft Design Aspects", NASA Ames Circulation Control Workshop, Feb 19-21 1986. NASA CP-2432.
13. Loth, J. L. , Funk M. S., "Thrust Efficiency of Powered Lift Systems", Paper 872327, *Proceedings of the International Powered Lift Conference*, pp 253-262, Dec 7-10 1987.
14. Loth, J. L. , "Retractable Rounded Trailing Edge for Circulation Control Wing", U.S. Patent 4,600,172, issued July 15, 1986

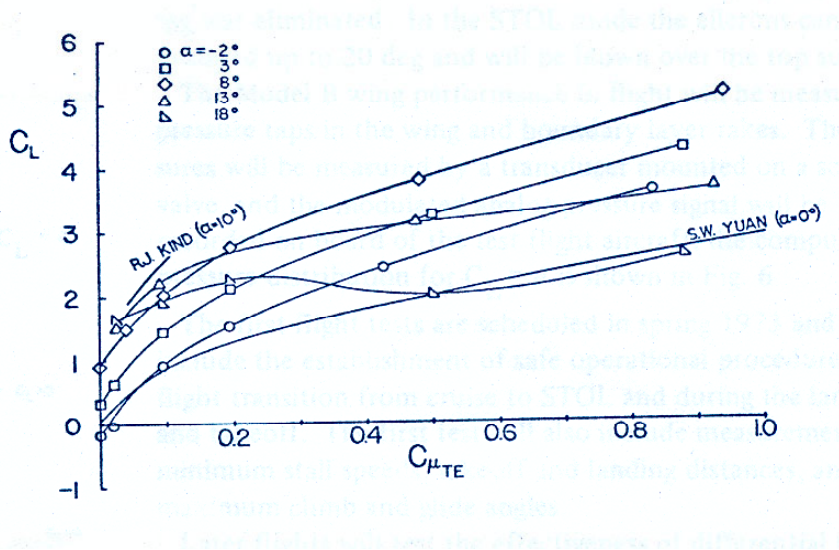
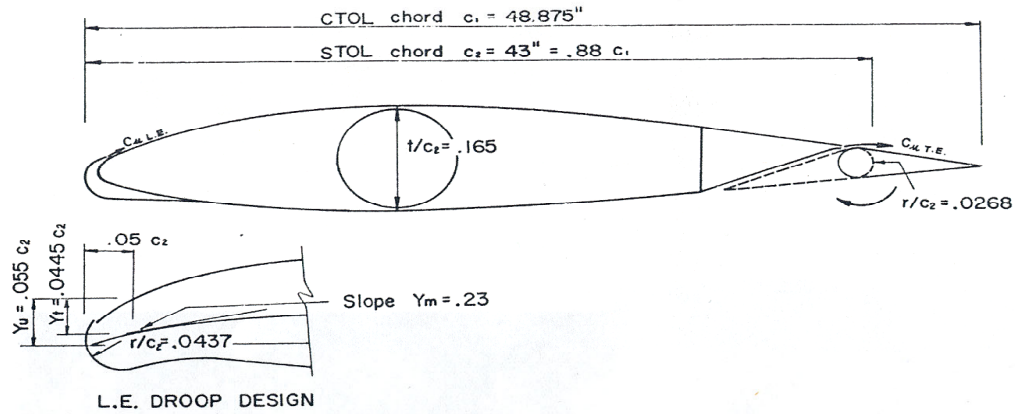


Fig 1. WVU Model A Circulation Controlled wing with folding flap to get rounded trailing edge. Performance curves are from the 8x10ft tunnel at NSRDC tests conducted in 1970.

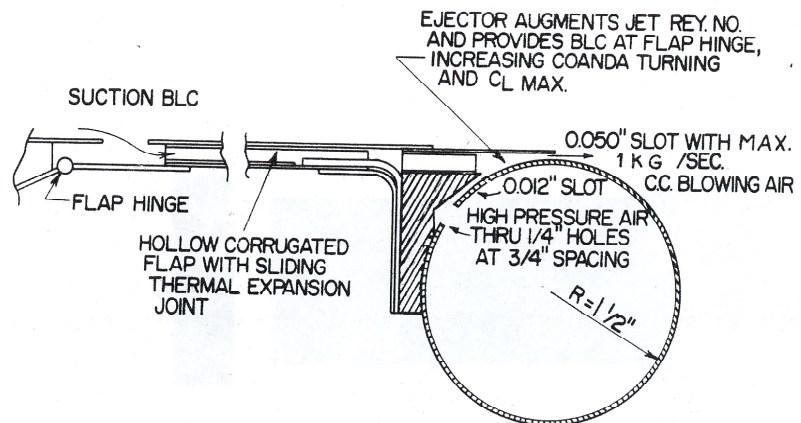
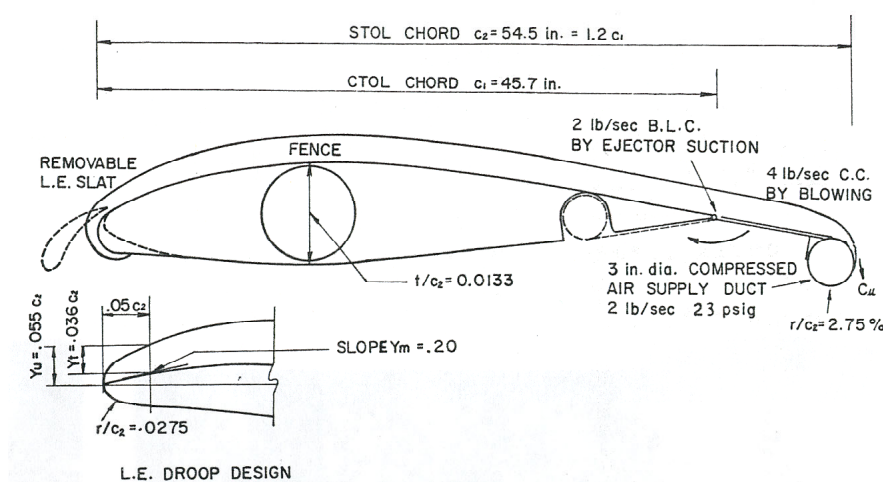


Fig. 2 WVU Model B Circulation Controlled wing performance based on the 20% shorter chord cruise configuration.

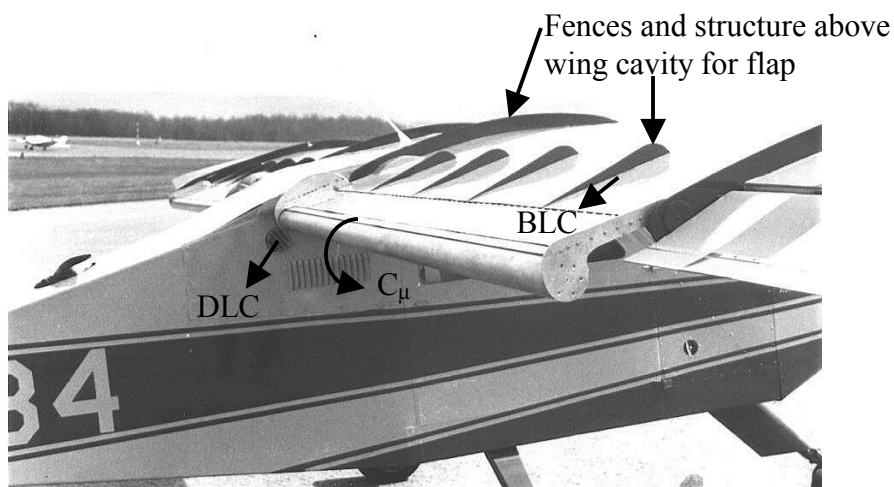


Fig. 3 The Model B wing installed on the CC Technology Demonstrator with arrows used to show location of: DLC,  $C_\mu$  blowing slot, BLC flap hinge suction slot and structure

**Model B wing is more blowing efficient than most other methods of high lift generation.**

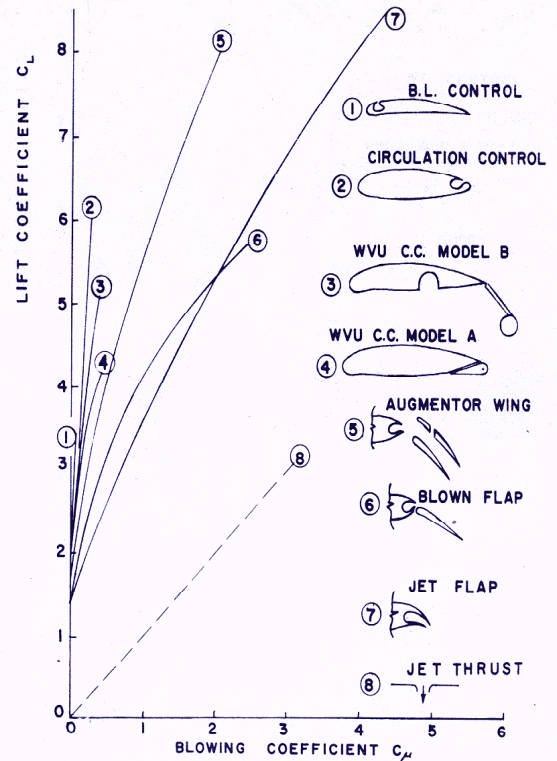
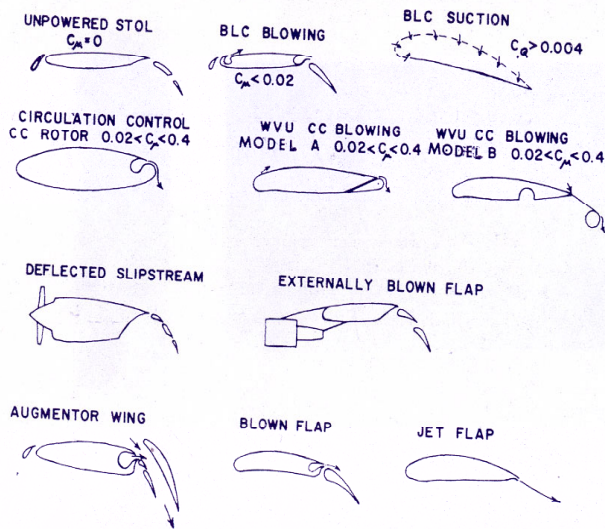


Fig. 4 Comparison of performance between various high lift devices. The circulation controlled elliptical geometry performs better than all others, but without blowing, its performance is very poor.

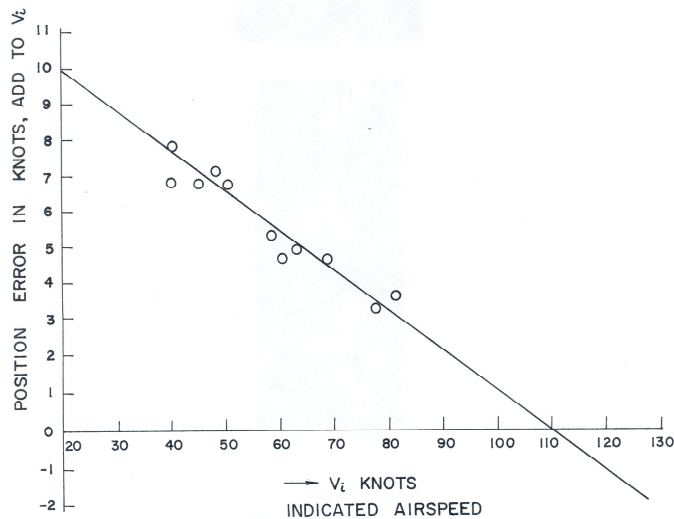


Fig. 5 Position error calibrated during flight testing by tower fly-by



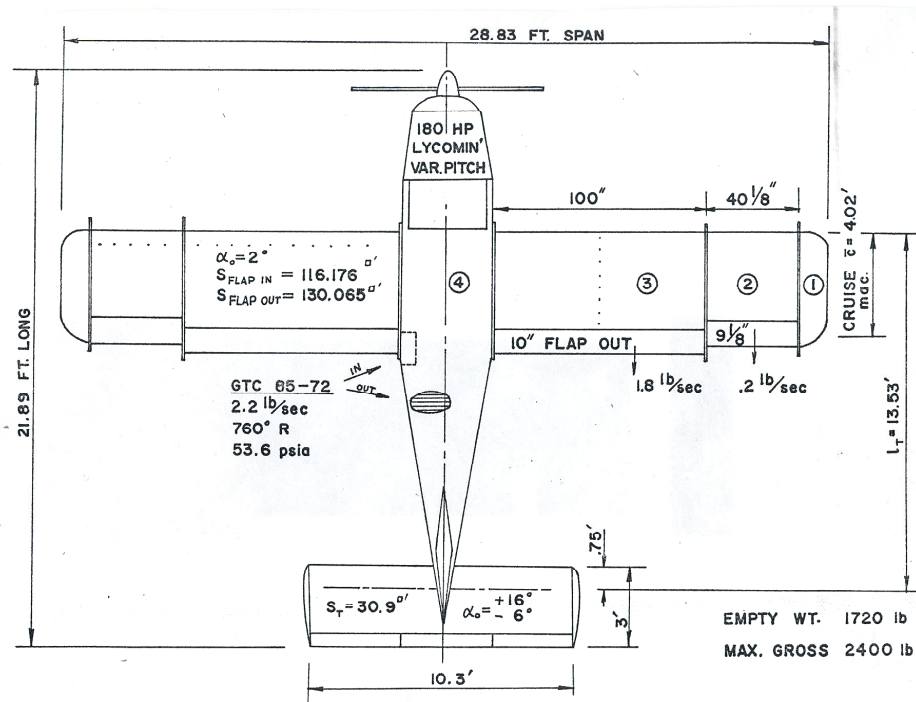


Fig. 6 The WVU Circulation Control Technology Demonstrator, undergoing flight tests April 1974 with its 3" diameter CC rounded trailing edge flaps deployed. Shown below are the dimensions of the Circulation Control Technology Demonstrator.

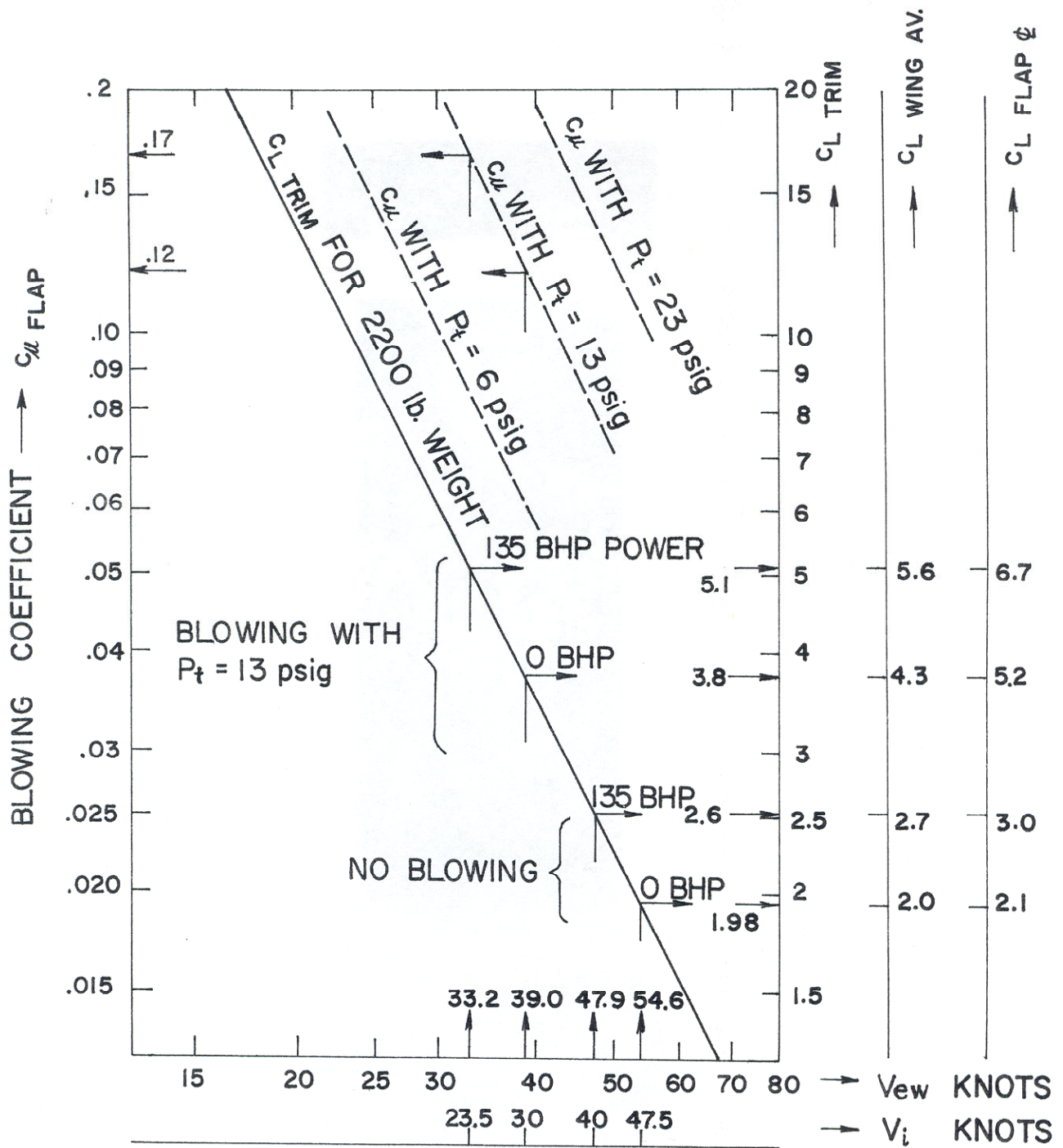


Fig. 7 Flight test results showing differences with blowing power on and off as well as propeller power on and off.

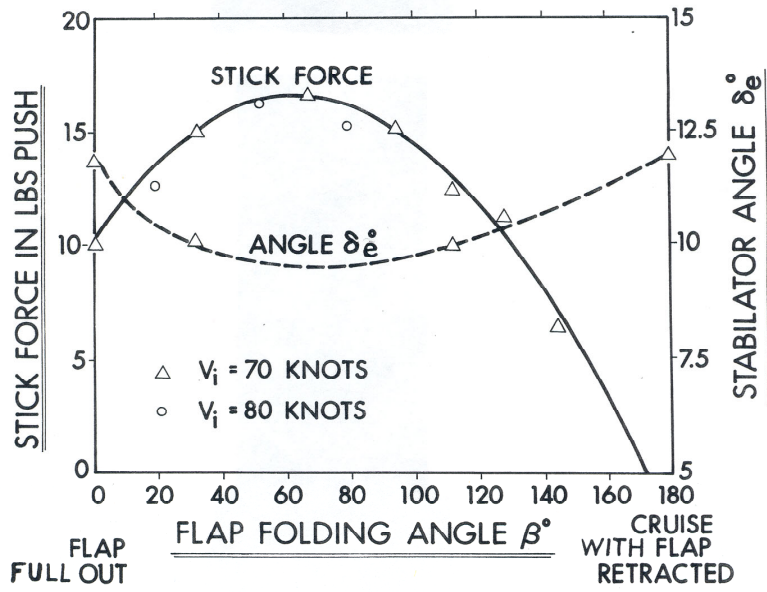


Fig. 8 Flap folds-out in 4 seconds and folds-in within 10 seconds, all with acceptable stick force divergence.

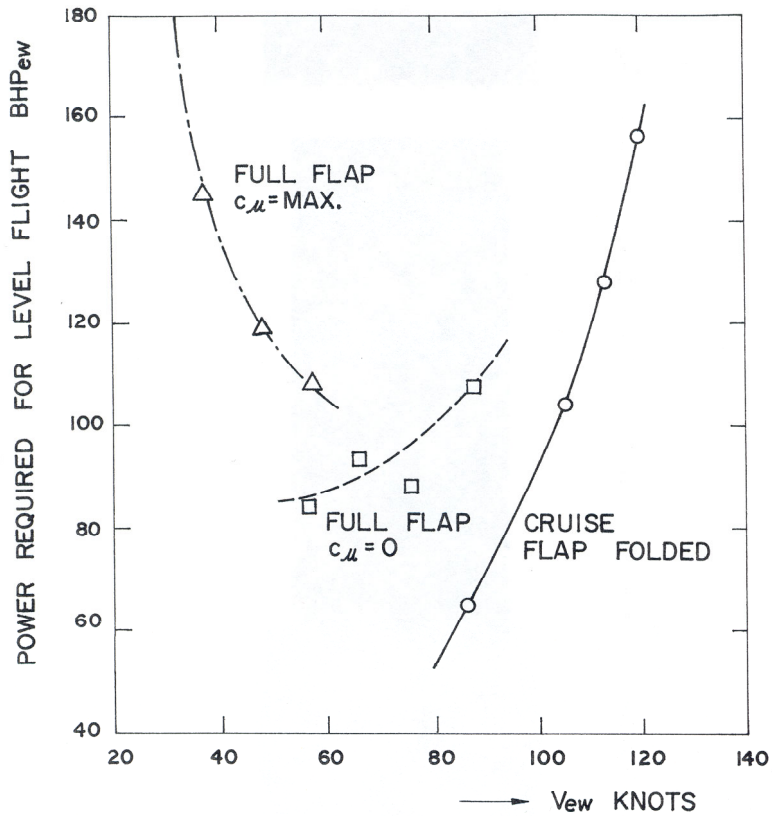


Fig. 9 Power required for level flight. With flap stowed away and with it deployed. Note on the backside of power curve, one must double the power to fly at half speed.





Fig. 10 Circulation Controlled Navy Grumman A-6A, with a fixed rounded CC trailing edge, converted under the direction of Bob Englar, then at NSRDC.

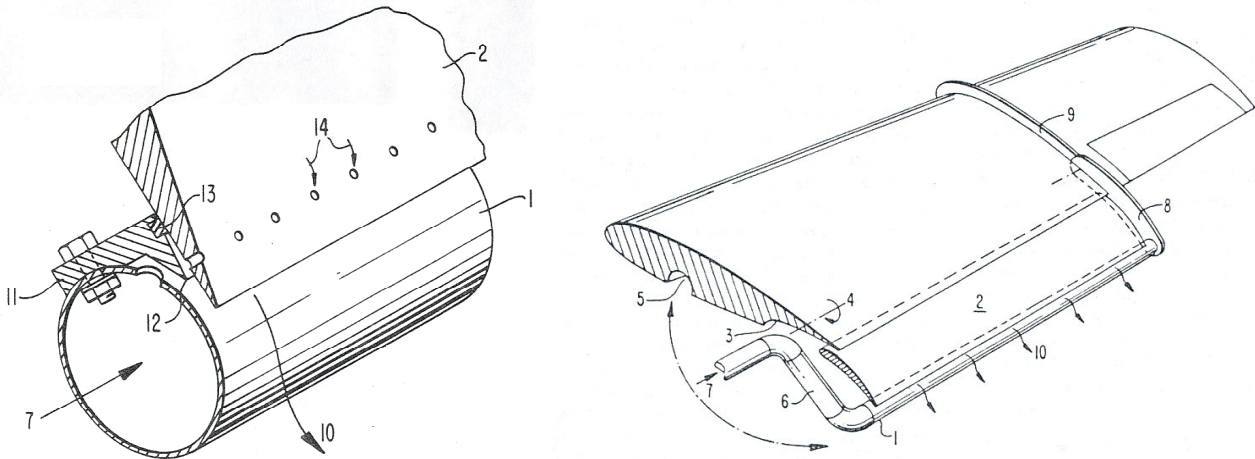


Fig. 11 Minimizing the torque required to retract a rounded CC trailing edge by separating the flap from rounded trailing edge. U.S. Patent 4,600,172.

2004 Circulation Control Workshop, 16-17 March 2004

## **In-Flight Retractable Rounded CC Trailing Edge Configurations with 1974 CC Flight Test Data**

By John L. Loth

Department of Mechanical and Aerospace Engineering  
West Virginia University, Morgantown WV



1

## **Presentation Sequence**

- 1. Reasons for ONR to contract research to WVU on a Circulation Controlled (CC) Rotor for a Heavy Lift Helicopter.**
- 2. Reasons for WVU to flight test a fixed wing CC aircraft instead of a CC helicopter rotor.**
- 3. Reasons for WVU CC wing models A, B and C, to be all in-flight convertible to sharp T.E.**
- 4. 1974 flight test data for the CC Technology Demonstrator STOL aircraft at WVU.**

2

## **Why a CC Heavy Lift Helicopter?**

- In the 60's, U.S. Navy recognized the need for small carriers, with STOL aircraft and helicopters.
- In '67 when Dr. R.J. Kind published his work at Cambridge U. on " CC Powered High Lift Elliptic Wing Sections", a young engineer at NSRDC: Bob Williams, promoted the "Navy High Lift Helicopter with a Dual Plenum CC Rotor".
- In '68, available Project Themis funding was used by ONR, to contract WVU to do theoretical and experimental research on their CC Rotor.
- Note: decades later this same Bob Williams, an engineer with a vision, convinced President Reagan to fund the "National Aero-Space Plane" (NASP).<sub>3</sub>

## **Flight Test an Elliptic CC Blade?**

- NSRDC wind-tunnel test results on CC elliptic rotor blade sections did not match those done at WVU, due to differences in wall interference.
- This is why WVU considered flight testing at full Reynolds number, avoiding wall interference.
- A CC rotor blade sticking out of a Cessna cabin ceiling creates uncontrollable roll moments.
- Therefore a fixed CC wing was considered. For safety, in case of blower failure, a CC wing with in-flight conversion to a sharp T.E. was needed!

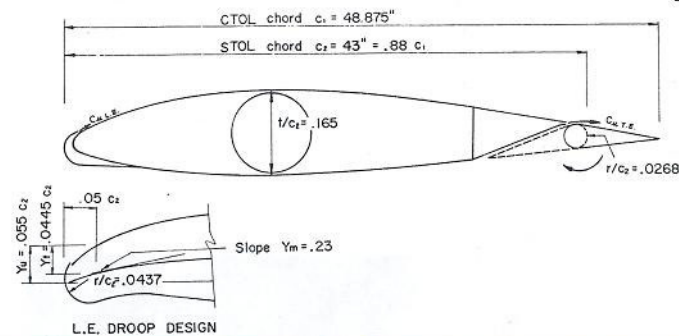
4

## Model A Circulation Control Wing

- First a Bede-4 wing was converted, using its rounded flap hinge as a CC blowing surface, with the flap tucked forward into a cavity.
- Dr. Norio Inumaru (who later built the Japanese QSTOL aircraft), designed a drooped leading edge for the Model A wing.
- In April of 1971, Dr. Inumaru planned and monitored the 2-D Model A wing tests at NSRDC, in their 8x10 ft wind-tunnel.

5

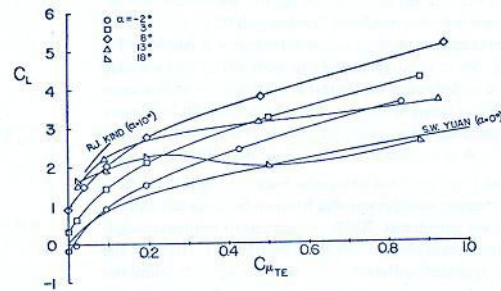
## Model A Circulation Control Wing



6

## Model A Circulation Control Wing

- At  $C_{\mu} = 0.95$  find  $C_{Lmax} = 4.2$  at  $\alpha = 8^{\circ}$ , based on the 12% longer sharp T.E. chord
- Rotating the flap in or out of its cavity did not generate any severe pitching moments.



7

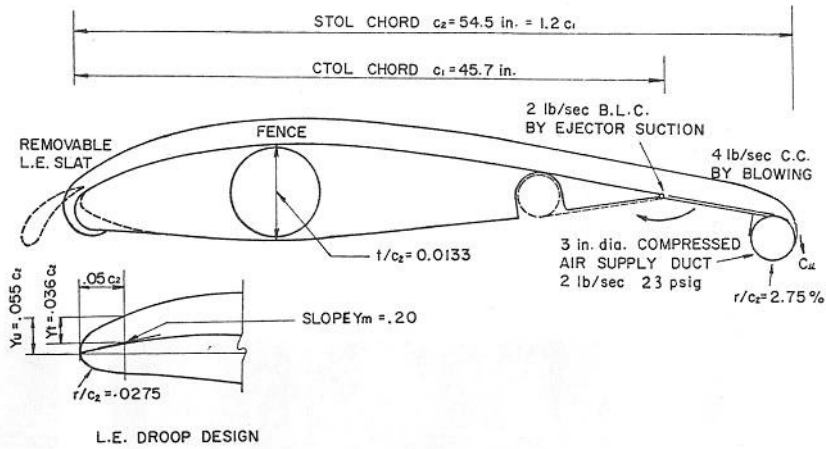
## Model B Circulation Control Wing

- To improve CC wing performance, the flap was made to increase the chord by 20% in CC mode.
- 2 lb/s of hot 300°F at 23 psi compressor bleed-air from GTC 85 gas-turbine was used for CC blowing.
- The fuel containing fiberglass wing must be cooled. This was accomplished by a supersonic ejector which provided 2 lb/s of boundary layer suction air entering the hollow corrugated flap at hinge line.
- The ejector entrained cold air doubled CC blowing flow rate to 4lb/s, and increased the blowing slot gap from 0.012" to 0.048", which improved the Coanda turning of the flow.

8

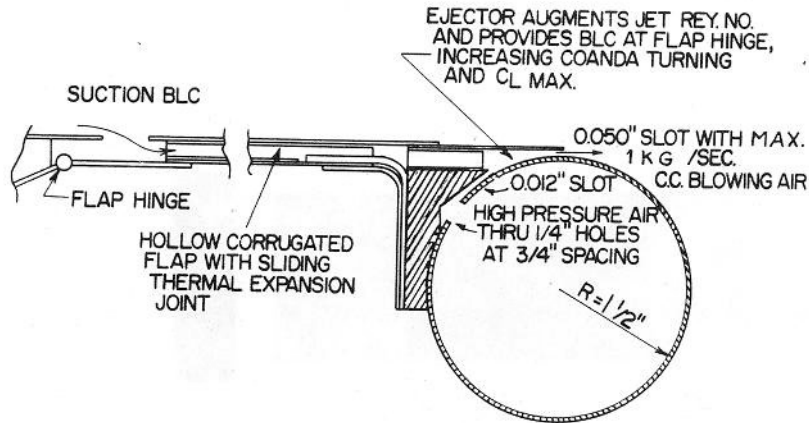


# Model B Circulation Control Wing



9

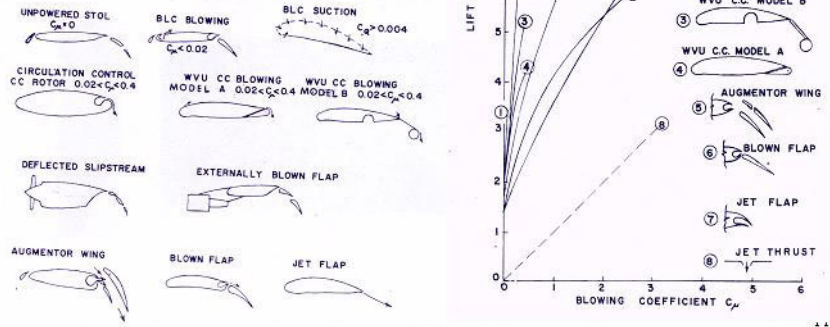
# Model B Circulation Control Wing



10

# Model B Circulation Control Wing

Model B required less blowing momentum  $C_{\mu}$  than most other methods of high lift generation shown.

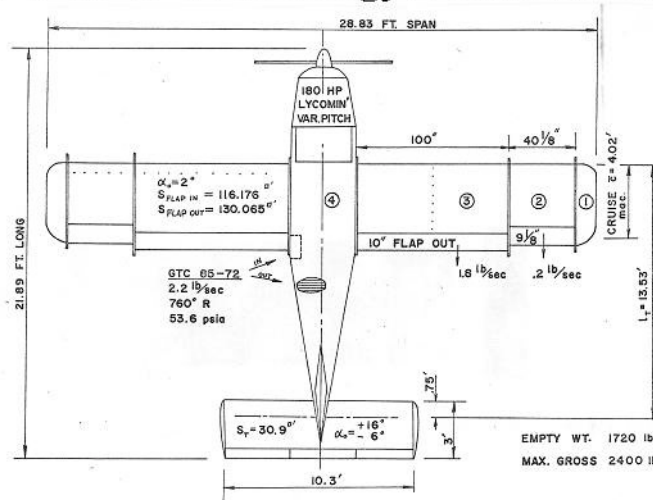


WVU C. C. Technology Demonstrator built on saw horses by Lee Metheny in back .



12

## WVU C. C. Technology Demonstrator



13

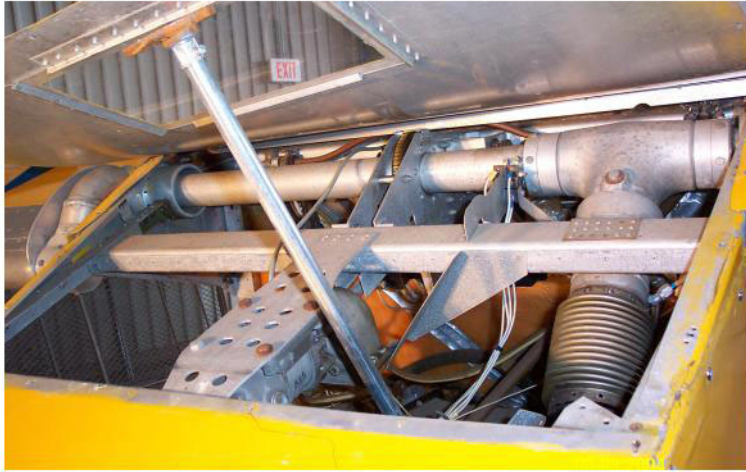
## WVU C. C. Technology Demonstrator

Cockpit shows black handle for throttle. Red knob on handle is for direct lift control (DLC), accomplished by dumping blowing air. Note red handle on left door is to pull its hinge pins out, for easy bail-out. Black panel on dash houses the gas turbine controls.



14

## WVU C. C. Technology Demonstrator



How CC rounded trailing edge folds out, and blowing air gets in

15

## WVU C. C. Technology Demonstrator



The WVU CC Technology Demonstrator is still in good shape

16



## WVU C. C. Technology Demonstrator



Flap in process of retracting, by folding forward into cavity 17

## WVU C. C. Technology Demonstrator



18

## WVU C. C. Aircraft Flight Testing

1<sup>st</sup> Flight by Sean Roberts, Flight Research Inc. April 10, 1974



Note spin chute below tail and parachute on his back

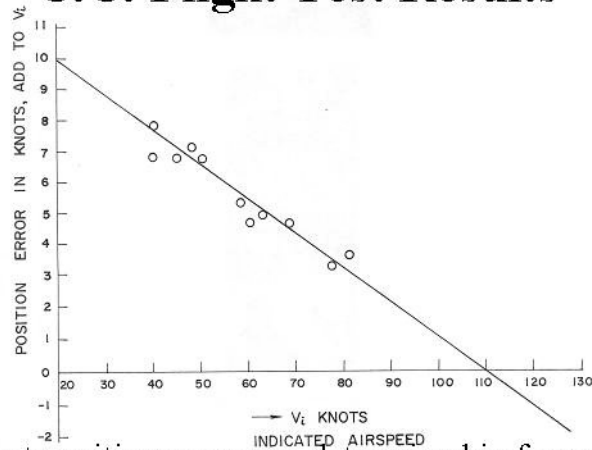
19

## WVU C. C. Aircraft Flight Testing



20

## C.C. Flight Test Results



First position error was determined in formation flight with a calibrated Cessna 150, see above

21

## C.C. Flight Test Results

- **The C.C. flap could be deployed by 173° within 2.5 seconds and retracted in 4.5 seconds. At 70 knots the maximum stick force excursion was 17 lb with a 10 lb out of trim after deployment.**
- **The drooped and blown ailerons forces were heavy, but could be reduced by attaching to the flow dividing valve inside the tee splitting the flow to each wing.**

22

## C.C. Flight Test Results

- At max. C.C. blowing and level flight, the indicated airspeed was 23.5 knots corresponding to 33.2 knots calibrated airspeed with 135 HP shaft-power.
- Circulation Control in STOL mode increases the power required in level flight. Below 60 knots aircraft operates on backside of power curve.
- Angle of attack sensitivity  $\delta CL/\delta\alpha = 5.1$

23

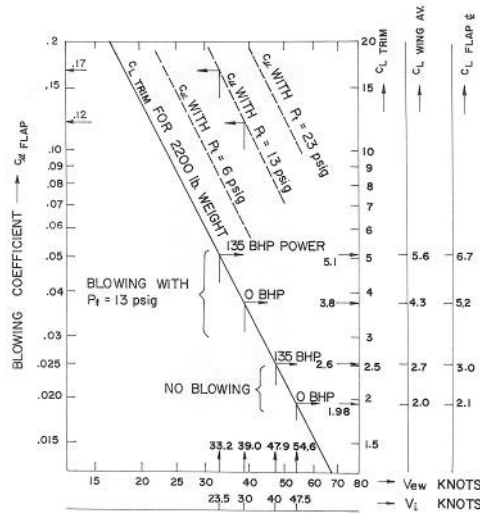
## C.C. Flight Test Results

- Linearize CL with the following equation  $CL = CL_0 + \alpha(\delta CL/\delta\alpha) + C\mu(\delta CL/\delta\mu)$
- With prop at idle, stall speed  $V_{cal} = 39$  knots at  $C\mu = 0.12$ ,  $CL_{trim} = 3.8$  and  $CL_{wing} = 4.3$ ,  $Cl_{flap} = 5.2$
- Without C.C. blowing, stall speed  $V_{cal} = 54.6$  knots at  $C\mu = 0$ ,  $CL_{trim} = 1.98$  with  $CL_{wing} = 2.0$ ,  $Cl_{flap} = 2.1$
- C.C. augmentation:  $\Delta CL_{wing}/C\mu = 2.3/0.12 = 19$ .
- Note  $(\delta CL/\delta C\mu) = \Delta CL_{wing}/\sqrt{C\mu} = 2.3/\sqrt{0.12} = 6.6$
- A-6A tests also had  $\Delta CL_{wing}/\sqrt{C\mu} = 2.1/\sqrt{0.1} = 6.6$

24



## C.C. Flight Test Results



25

## C.C. Flight Test Results

- During 1<sup>st</sup> flight the flap motor stalled with flap half way deployed. Replaced motor with 2 HP.
- Due to higher  $Re$ , the  $C_L$  versus  $C_{\mu}$  performance was better than wind tunnel model data showed.
- Low angle of attack effectiveness with CC blowing provided good visibility for take-off and landing.
- Stall speed was low and stick forces were reasonable.
- Stalling with CC blowing produces a large rolling moment with at least a 200 foot drop.

26

## Conclusions

- **Excellent Direct Lift Control (DLC) using air dump valve to stay on glide slope.**
- **Use safe stall margins when operating in STOL mode**
- **ONR contract monitor and all involved were satisfied with its design and performance.**
- **ONR commissioned Bob Engler, then at NSRDC, to have Grumman modify an A-6A for circulation control flight testing by 1979.**

27

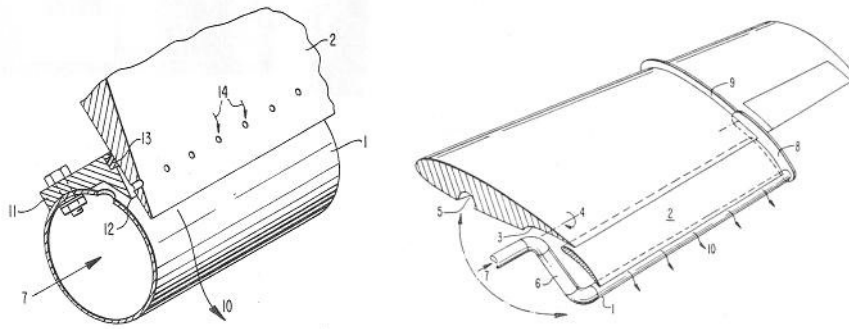
## Conclusions



**Navy Grumman A-6A Intruder All Weather Bomber, modified to demonstrate Circulation Control High Lift Wing Concept flew in 1979.**

28

## Model C Circulation Control Wing



U.S. Patent No: 4,600,172 "Retractable Rounded Trailing Edge for Circulation Control Wing". Issued July 15, 1986

29



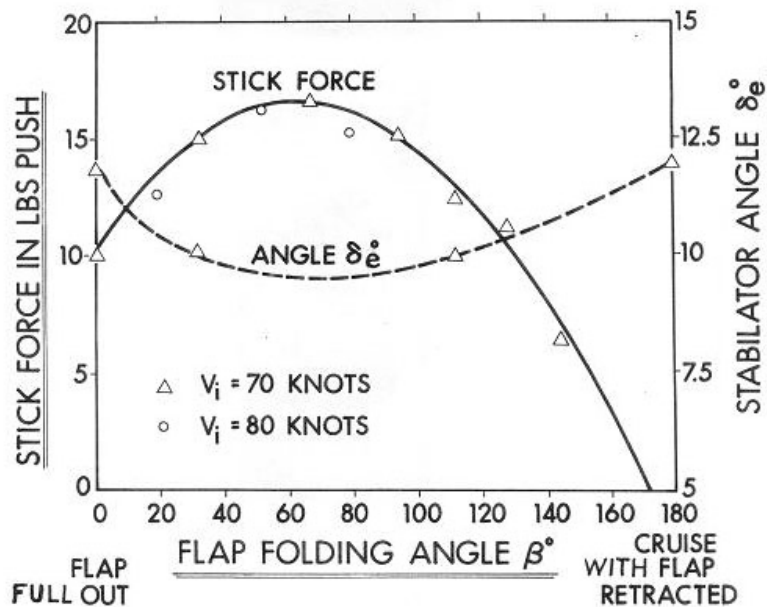
The late Dr. Jerome B. Fanucci, WVU Chairman of Aerospace Engineering, 1964-1980, on left. His vision got WVU involved in Circulation Control research. The Circulation Control Technology Demonstrator designer, John L. Loth, on right.

30

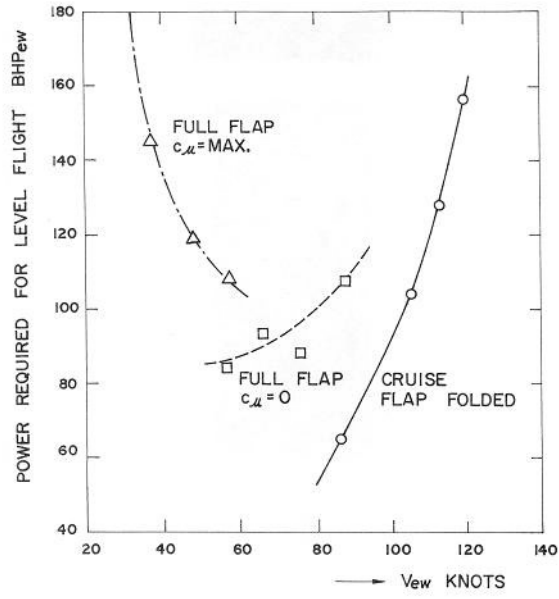
# Flight Test Data

- Taken from the following references:
- 1) Some Aspects of STOL Aircraft Aerodynamics, John Loth Business Aircraft Meeting, Wichita Kansas, April 3-6 1973
- SAE Paper 730328
- Flight Performance of a Circulation Controlled STOL, By John Loth, Jerome B. Fanucci and S.C.Roberts. AIAA 6<sup>th</sup> Aircraft Design, Flight Test and Operations Meeting. Los Angeles, California August 12-14, 1974.
- Flight Performance of a Circulation Controlled STOL, By John Loth, Jerome B. Fanucci and S.C.Roberts. J. Aircraft, Vol 13 No 3, March 1976 p 169-173
- Circulation Controlled Wing Optimization, John L. Loth and Michael Boasson. J. of Aircraft Vol. 21 No 2, February 1984
- Circulation Control STOL Aircraft Design Aspects. By John L Loth, presented at the Feb 19-21 1986 NASA Ames Circulation Control Workshop
- Thrust Efficiency of Powered Lift Systems, John L. Loth and Matthew Funk. Dec 7-10 1987 International Powered Lift Conference

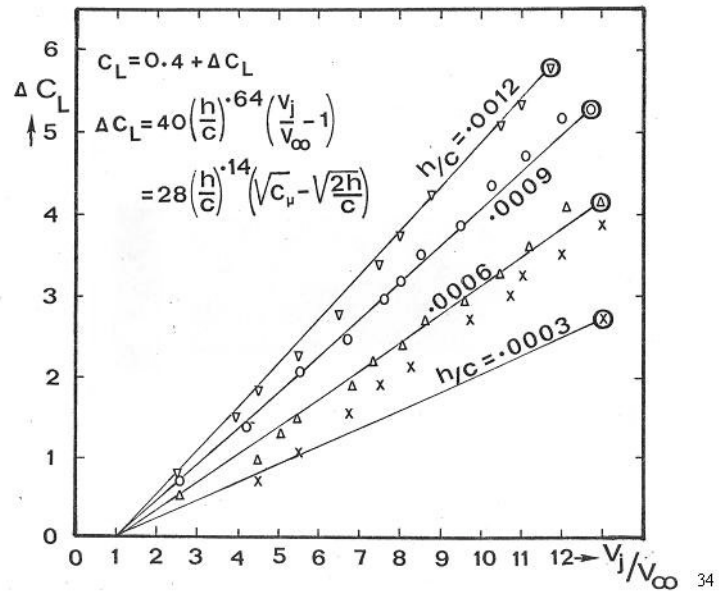
31



32



33



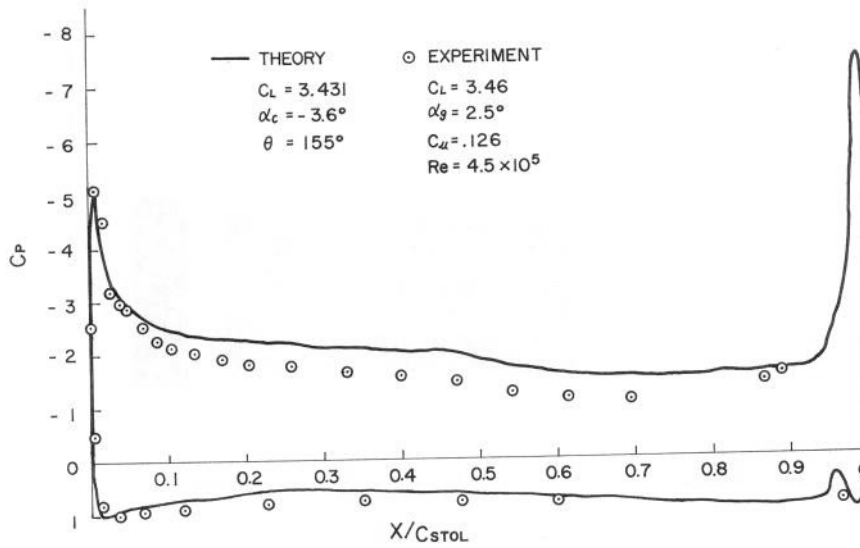


Fig. 4. Type B STOL Wing Model Pressure Distribution Matching to Determine

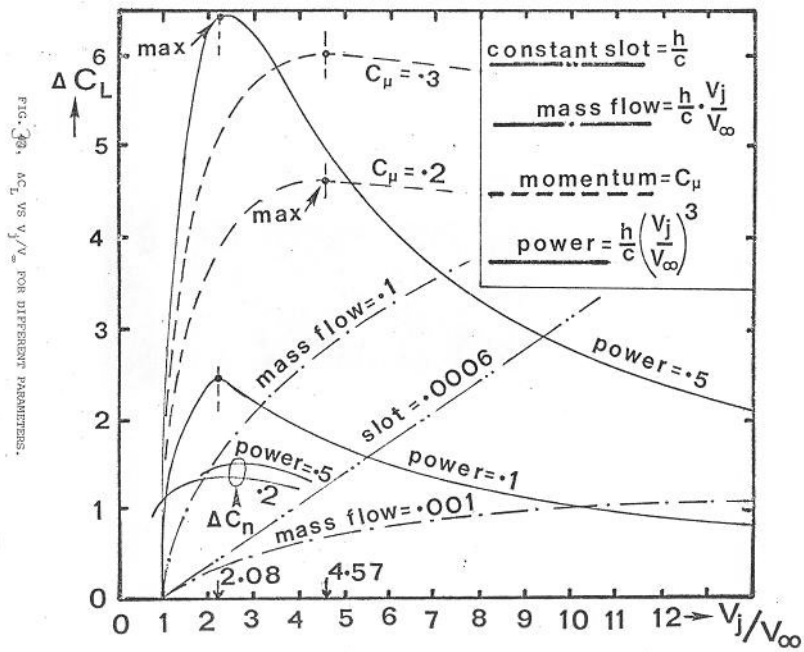


FIG. 3a.  $\Delta C_L$  vs  $V_j/V_\infty$  FOR DIFFERENT PARAMETERS.

# WAKE VORTEX WINTIP-TURBINE POWERED CIRCULATION CONTROL HIGH-LIFT SYSTEM

Mark D. Moore

Personal Air Vehicle Sector Manager, Vehicle Systems Program  
NASA Langley Research Center  
Hampton, VA 23681-2199

## ABSTRACT

NASA's Vehicle Systems Program is investing in aeronautics technology development across six vehicle sectors, in order to improve future air travel. These vehicle sectors include subsonic commercial transports, supersonic vehicles, Uninhabited Aerial Vehicles (UAVs), Extreme Short Takeoff and Landing (ESTOL) vehicles, Rotorcraft, and Personal Air Vehicles (PAVs). While the subsonic transport is firmly established in U.S. markets, the other vehicle sectors have not developed a sufficient technology or regulatory state to permit widespread, practical use. The PAV sector has legacy products in the General Aviation (GA) market, but currently only accounts for negligible revenue miles, sales, or market share of personal travel. In order for PAV's to ever capture a significant market, these small aircraft require technologies that permit them to be less costly, environmentally acceptable, safer, easier to operate, more efficient, and less dependent on large support infrastructures.

A synergistic technology set is proposed that would use Circulation Control (CC) trailing edge blowing coupled to a wake vortex powered wingtip-turbine air compressor. This technology would provide small aircraft with the ability to takeoff and land in shorter distances, while achieving greater efficiency at the cruise condition; or takeoff and land at equivalent speeds and distances as today with a smaller wing and higher wing loading. Circulation Control has been investigated for over 30 years and shown to be very effective in increasing the wing  $C_{Lmax}$  in tests of commercial transport and fighter aircraft vehicles. However, one of the significant penalties associated with CC systems is the power required to supply the source blowing air. Another part of this problem is that the CC mass flow required per pound of aircraft, and therefore the pneumatic power required, is proportional to the square of the takeoff velocity. Applying CC systems to aircraft that takeoff and land at relatively high speeds, such as commercial transports and fighters that are on the order of 120 knots, requires significant blowing power. Applying a CC system to GA aircraft that takeoff and land at speeds of about 60 knots, would require lower mass flows and are potentially a better fit for this technology. GA aircraft currently suffer from

poor cruise efficiencies because the wing areas are sized by the takeoff and landing condition, making the wing approximately twice as large as required for efficient cruise. In addition over sizing the wing to meet takeoff and landing results in low wing loading which is much more susceptible to turbulence, resulting in poor ride quality compared to higher wing loadings. Applying a CC system to a GA aircraft would achieve a higher  $C_{Lmax}$  than current solutions, which are typically on the order of 2.0. Obviously a more sophisticated high-lift system could be applied other than simple, single element flaps; however, GA operations and pilot skills require a system that is less prone to external hanger-rash damage, inspections, and high cost manufacturing and maintenance than those used by other aircraft to achieve a higher  $C_{Lmax}$ . A CC highlift system offers the potential of a no external moving parts, and relatively few internal parts. Development of a CC system for GA aircraft would permit either reduced wing areas for takeoff and landing at equivalent airspeeds and runway lengths as today, with improved gust handling qualities, or reduced field length operation for smaller infrastructure requirements.

Utilizing a wake vortex tip-turbine as a compressor for the CC air mass flow provides a relatively failsafe method that is not coupled to the engine. In addition, the power is pulled from the wing tip vortex during the high-lift condition when the vortex strength is the greatest, and doesn't require additional power. The vehicle is however encumbered with two additional systems, a tip-turbine compressor and a pneumatic trailing edge with internal actuators. The additional weight and cost of these systems is therefore balanced against the benefits to determine if these technologies can sufficiently buy their way onto the vehicle. If a variable pitch wing tip-turbine is utilized, a reduction in cruise induced drag is possible by optimizing the blade pitch, which effectively varies the endplate loading if the blades are locked in place and not permitted to rotate. A systems study is outlined in this paper to determine quantifiable benefits of a GA-CC system, with initial investigation suggesting a potential for favorable tradeoff, although this is highly dependent on the weight and cost of the wing tip-turbine and CC system.



## INTRODUCTION

Personal Air Vehicles (PAVs) are envisioned as the next logical step in the natural progression in the nation's history of disruptive transportation system innovations. As the automobile improved quality of life and standards of living in the 20<sup>th</sup> century, PAVs are envisioned to do likewise in the 21<sup>st</sup> century. PAVs are defined as self-operated aircraft, capable of use and affordable by a large portion of the general public. The goal of these vehicles is to provide a breakthrough in personal air mobility, through dramatic time-savings and increased reach, and therefore a greatly improved quality of life. There are two key questions involving the future of PAVs; first, is there a significant potential benefit developing such a capability, and second, is such a transportation system affordable and technically possible. An understanding of the current state of mobility is required prior to proposing any improvements, or understanding comparative benefits between systems.

Mobility studies<sup>1</sup> have shown that over the last 100 years, while travel speeds have increased ten-fold, the average amount of time traveled per day has remained relatively constant at about 1.25 hours per day. This statistic also holds true for other countries at different effective technology levels. Over the last 30 years average ground speed has increased slightly to the current value of 35 miles/hour, with 1995 and 2000 data showing the first decreases for ground mobility in many of the most productive regions of the country. Therefore the daily radius of action (or reach) has improved from about 3 miles per day in 1900, to about 25 miles per day (each way) in 2000 for intra-urban travel. While autos serve the travel market well for trips under 50 miles, and commercial transports achieve improved block speeds for trips over 500 miles; neither method provides door-to-door speeds between 50 and 500 miles that PAVs could provide. Considering that this trip distance accounts for approximately half of all trips for distances greater than 50 miles, there is the potential for a significant impact to how people travel. The objective of PAVs is to further increase the daily reach another factor of 4 to 8 times, to permit a similar expansion of society into underutilized land resources.

The vision of providing on-demand personal air mobility is tightly aligned with NASA's Aeronautical Research Theme of enhancing mobility, and providing faster, further travel, anywhere, at anytime. NASA's aeronautics blueprint defines the areas of responsibility of increasing national security, improving quality of life, and expanding economic growth. A robust aviation system, providing increased daily mobility, and a new growth market for industry products meets these

goals. The key discriminator to determine if NASA should be involved is whether there is a substantial public benefit, and if NASA is the only entity capable of bringing about this benefit. The most telling answer to this question is the fact that with the many 25 year plans that exist across federal and local government planning, the focus is on trying to maintain current mobility, not provide a radical improvement.

NASA has already made investments in small aircraft through AGATE (Advanced General Aviation Transportation Experiments), GAP (General Aviation Propulsion), and SATS (Small Aircraft Transportation System)<sup>17</sup>. Combined, these programs have established advanced cockpit systems, crashworthiness and lightning strike standards, an advanced small turbofan engine, automatic takeoff and landing vehicle control, prototype efforts for a Highway in the Sky airspace control system, and many other elements of the total required system.

Achieving focused research objectives requires that there is a clear understanding of the vehicle class being proposed, as well as the concept of operations. PAVs would operate in the near-term from the current base of 5300+ public and 5000+ private general aviation airports<sup>17</sup>. Many more airfields are in use than people suspect, with a recent survey of operations showing over 18,000 airfields in use. This number excludes the nearly 10,000 additional heliports that are available, with many of these locations coincident to hospitals. PAVs would not operate out of the busiest 100 public airports, which comprises the hub and spoke system. Essentially, the infrastructure already exists today to support a distributed PAV transportation system, at least in terms of land use. Typically one of the largest hurdles in developing a radical improvement in society is the development of the new infrastructure. In the case of PAVs, the infrastructure is essentially already in place, and is simply a drastically underutilized resource.

However, the availability of existing infrastructure raises a critical issue in terms of the window of opportunity for when a PAV transportation system could be operational. One argument would be to wait until the current ground and air systems reach a level of service that requires market forces to demand a new solution. This is not realistic for two reasons. First, establishing the changes required in the airspace system will almost certainly take over 20 years, just as it took local governments 20 years from the introduction of the automobile to provide sufficient infrastructure for autos to be considered useful. Certainly local governments are not going to build the air highways, and federal implementation of a national system is required. There is the need to plan at least 20 years ahead, which puts



the U.S. squarely up against the wall of 20-year congestion projections that appear unmanageable for many of the most productive regions of the country. The second reason for near-term development of an on-demand transportation system is that the required infrastructure is disappearing at a rapid rate. Currently small, public use airports are being dismantled at an averaged rate of one airport every several days as neighborhoods encroach upon rural areas, and populated regions petition them out of existence because they are viewed as irrelevant and an annoyance. These small airports provide an untapped transportation resource that will not be able to be replaced in later years.

### VEHICLE CAPABILITIES AND REQUIREMENTS

The question arises, what are the mission requirement differences between PAVs of the future and current GA aircraft that are available in the market today. The future PAV on-demand market will certainly evolve from the current GA market as technologies and capabilities are developed to affect a larger market share. A shift to point-to-point operation models has already occurred with some airlines, though still only at larger airports. As the on-demand market evolves, it is likely to first exist as professionally piloted air-taxi operations from the smaller airports as an intermediate step towards personal on-demand service. As costs decrease, through such factors as lower acquisition costs and single-pilot operations, more pervasive air-taxi operations of higher utilization vehicles will establish the initial on-demand market. The self-operated on-demand market will follow with the addition of ease of use technologies that permit low cost licensing, and modern certification practices that permit manufacturers to utilize current quality assurance manufacturing processes (instead of the current quality control processes) to achieve both safer and lower cost, high quantity products. The self-operated market will likely evolve into missions that align themselves to the transportation needs of two very different mission classes, rural/regional and intra-urban travel. There will not be a single optimum configuration for these missions, but instead a spread of future potential missions and vehicles that is very broad, just as the automobile market involves from sports cars to SUVs. Therefore it is difficult to select one or two representative missions that can accurately convey the vision of their future capabilities; however representative concepts put the missions into context and provide the ability to understand the vehicle sensitivity to technology investments.

The technology challenges of providing a common place, safe, affordable, comfortable, and acceptable method of self-operated air travel are significant. This list includes developing aircraft ease of use on par with autos, involving uniform displays and controls, along with ease of pilot licensing. At the same time, these vehicles must be able to operate in near all weather capability to achieve high mission completion rates, requiring weather avoidance, and icing awareness systems, with no visibility restriction for landing. In order to provide access to many more operators, licensing and training must become far more easy, requiring a high degree of vehicle automation for systems involving self-diagnosis, pre-flight checklists, emergency procedures, and health monitoring. The combination of all these ease of use characteristics must combine into safety statistics that are on par with commercial airlines, requiring a reduction of almost ten times to the current GA accident rate. Good neighbor operations must be achieved that include noise levels that are on par to motorcycle standards, along with emissions that are equivalent to current autos. Comfort must also be significantly improved, with interior noise levels, and ride quality that are comparable to automobiles. Unless both manufacturing and operating costs are reduced dramatically, personal air travel cannot support a rational selection, even based on value of time and travel time savings for the vast majority of the public. Small aircraft major cost elements are the engine and avionics subsystems, and assembly labor; this necessitates new propulsion system solutions that are based on higher volume production such as auto engines, standardization of avionics and data transfer systems, and lean structural design concepts that can achieve drastically reduced touch labor.

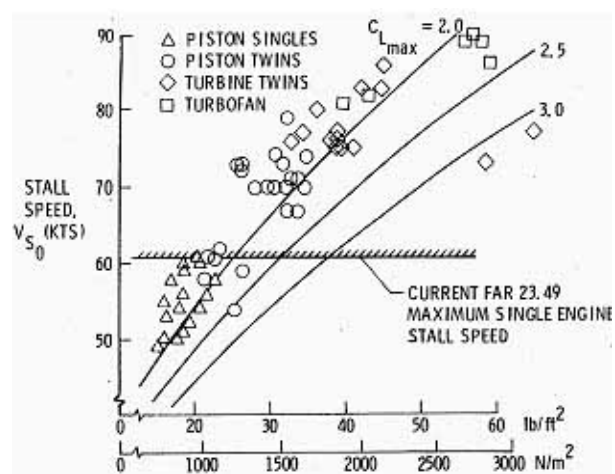


Figure 1: Stall speed of GA aircraft that results in low wing loading and relatively poor gust handling qualities.

The required capabilities that this paper focuses on are the need for improved efficiency, and reduced takeoff and landing field lengths. Currently a 4 passenger, 160 knot GA aircraft achieves about 13 miles per gallon at cruise, about the same as large SUVs. If PAVs are to be an environmentally responsible alternative mode of travel, at least a doubling of efficiency is required. Small aircraft typically achieve only a cruise  $L/D$  of about 11, while their  $L/D_{max}$  is typically 16 or higher. Obviously another alternative would be to decrease the cruise speed until the vehicle is cruising at the  $C_L$  for  $L/D_{max}$ , however, this drastically reduces the block speed benefit that is being pursued. Therefore, development of a highlift system that could provide an improvement in usable  $C_{Lmax}$  would assist towards improving the efficiency.

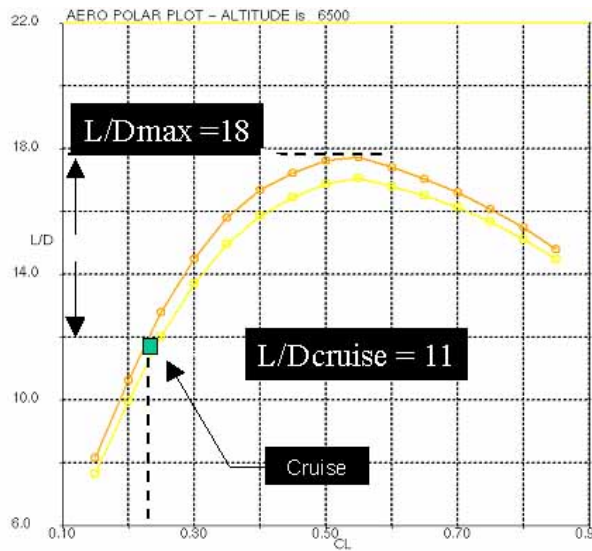


Figure 2: Drag polar of a GA aircraft similar in performance to the Cirrus SR-22, demonstrating the low cruise efficiency due to takeoff and landing wing sizing, instead of cruise wing sizing.

Achieving a  $C_{Lmax}$  of 3.75 compared to conventional GA aircraft that achieve about 2.0, would yield a 50% improvement in  $L/D$  through cruise wing sizing alone. Development of a simple, effective highlift system becomes an attractive method of achieving a substantial benefit when compared to other efficiency candidate technologies such as laminar flow, riblets, cooling drag reduction devices, retractable landing gear, etc. Alternatively, the improved  $C_{Lmax}$  can provide a reduction in the takeoff and landing field length required, and therefore the infrastructure acreage size and cost. Implicitly there is an additional safety benefit as vehicles perform Short Takeoff and Landing (STOL) operations as the effective ground speed is reduced and the potential impact speeds are decreased. However,

accompanying this potential improvement in crash survivability is the increased risk of gust upset since the ratio of gust speed to vehicle speed has increased. Obviously to empower missions such as the Gridlock Commuter (Figure 4), which depend on highly accessible and widely distributed small STOLports, the infrastructure will need to be minimized.

Required Capability	SOA	5-Years	15-Years
	General Aviation	Next Gen GA	Gridlock Commuters
Ease of Use	No	Auto-like	Autonomous
Acquisition Cost (\$K)	330	75	150
Community Acceptable (dba Flyover)	74	55	50
Emissions (HC/NOx/Lead grams/mile)	.5/1.0/.2	.05/.10/0	.03/.06/0
Reliability (accidents/100K hr)	6.5	2.0	.5
Efficiency (mpg)	13	16	28
Field Length (balanced - feet)	2500	1000	250
Block Speed (mph)	35 Auto <sub>50 GA</sub>	100	200

Table 1: PAV Sector Capability Goals

The combination of these challenges lead to the PAV sector capabilities and goals as shown in Table 1. In order to investigate the potential technology impacts towards these goals, advanced reference concepts have been developed. Reference concepts for the 5-year, 10-year, and 15-year timeframes are shown in Figures 4 through 6, with each using a different suite of technologies to address the goals. While these vehicle concepts are not developed as a product, they do perform the valuable function of evaluating system trade-offs as a candidate technology is quantified through analysis and experimental data. The technologies listed under each of these concepts are only the initial candidate technologies that are being investigated at NASA to address the goals, many more technologies will be evaluated as they become known from other contributors. Essentially this list of capability challenges is the problem statement bounding the box of PAV technology investigations, and any proposed technology effort should be able to show significant improvements towards these goals, without causing other system penalties that negate their benefit.

The efficiency and field length goals span the entire 15-year period, and can be traded off from each other depending on the design priority. These two goals are effectively expressed by the speed range of the vehicle. The speed range is a measure of the speeds that an aircraft can effectively fly at with sufficient power and control, and is shown by the drag polar of the aircraft. The ratio of the highest achievable flight speed to the lowest is the speed range, typically on the order of 3 to 4 for most aircraft. The stall or maximum cruise speeds are not a good measure of the aircraft performance independently, because the drag polar can be shifted left or right by simply changing the wing area; however, the speed range remains the same. Thus the goal of the combination of the efficiency and field

length performance goals are to maximize the speed range of the vehicle, permitting efficient flight at both the lowest and highest possible speeds.

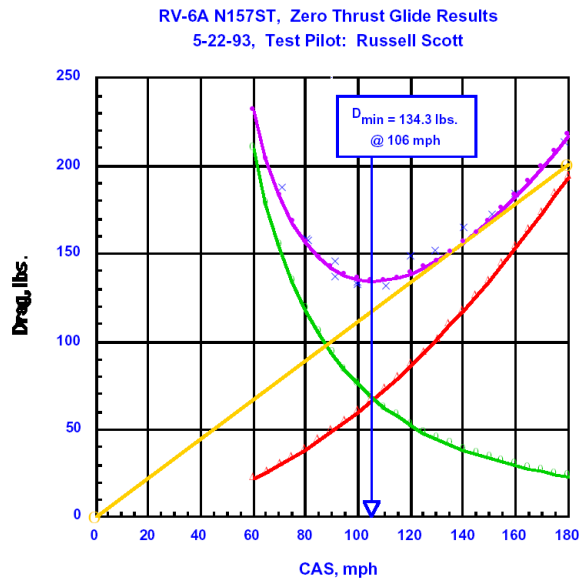


Figure 3: Drag versus airspeed graph demonstrating the effective speed range of an RV-6A 2-seat aircraft of approximately 60 to 200 mph. From CAFÉ flight test report with x indicating flight data, red line is parasite drag, green line induced drag, and the purple the combined drag polar. The yellow line intercept of the drag polar indicates Carson's speed, which is the velocity for best speed to drag ratio, or maximum speed per unit of fuel burned. The speed for the maximum L/D, or minimum power, is the lowest point on the drag polar.

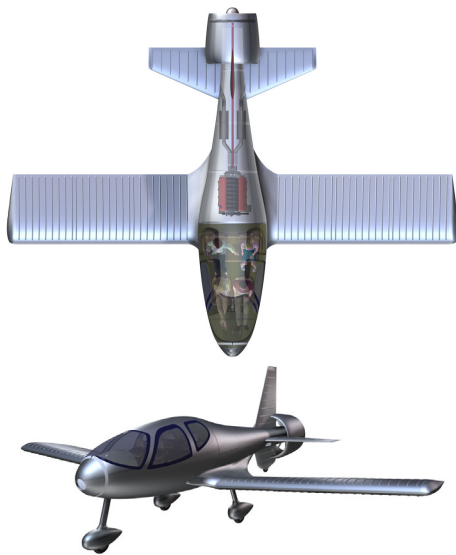


Figure 4: Near-term 5-year advanced Tailfan concept that utilizes a Haptic avionics suite, skin-stiffened low assembly labor/part count structural design, and a low

tip-speed, quiet ducted propeller. This is a next generation General Aviation design for use from existing GA airports with a 2500 ft field length.

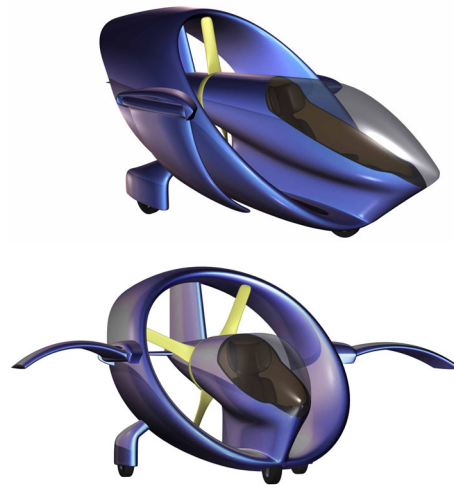


Figure 5: Mid-term 10-year advanced Spiral Duct concept that utilizes a no externally moving part deflected slipstream design based on the Custer Channel Wing and Lippisch Aerodyne to achieve a  $C_{Lmax}$  of 8-12 and achieve field lengths of approximately 250 ft. The mission for this vehicle is envisioned as a Gridlock Commuter, enabling 1 to 2 persons to travel very close to their final destination and then complete the door-to-door trip through limited speed, side-street road use.



Figure 6: Far-term 15-year advanced Tilt Nacelle Vertical Takeoff and Landing (VTOL) concept that utilizes a Multi-Gas Generator Fan propulsion system to reduce engine-out sizing penalties, and a Circulation Control Nacelle to externally expand the ducted propeller flow pneumatically to reduce the ground plane velocities and permit matching of the cruise and hover disloadings. This mission is envisioned as a Air-Taxi that accomplishes very high utilization to

amortize the significantly higher cost of achieving a VTOL aircraft.

### CIRCULATION CONTROL SYSTEM

Circulation Control has been shown to be very effective in generating highlift in analysis, wind tunnel testing, and flight experiments over the past 30 years. The method of CC discussed in this paper involves blowing air from a rounded trailing edge coanda surface of the wing. This trailing edge blowing is fed from a plenum of compressed air inside the wing which is regulated with internal valves. The compressed air is typically provided by bleed from a turbine engine, or from an APU. The effectiveness of the CC system is a function of the velocity of the jet squared, therefore, to achieve the best  $C_{Lmax}$  possible, the highest jet velocities are required. Sonic jet nozzles have been shown to be substantial noise sources (a function of  $V_{jet}^5$ ), and since noise is one of the primary goals of the PAV research, any CC system under investigation has been limited to less than 700 ft/s jet velocities. The same  $C_{Lmax}$  can be achieved by raising the mass flow through larger nozzle areas, however the power requirement for the compressor will rise proportionally. One of the principle reasons CC systems have not achieved transition to operational aircraft is because of the blowing power. The power required for the pneumatic system is also aggravated by the engine-out climb requirement during takeoff; this is the principle engine sizing condition so any bleed taken at this critical sizing point results in even larger engines. Recent research into CC systems have centered on unsteady or pulsed blowing since this has the potential to reduce the mass flow required by up to one half while achieving the same  $C_{Lmax}$ .

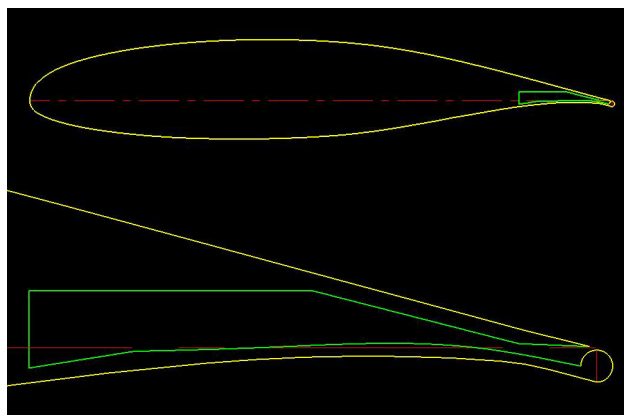


Figure 7: A GA airfoil section with a Circulation Control plenum and trailing edge.

The CC wing concept involves a jet of high-speed air blown over a circular or semi-circular trailing edge that,

due to the Coanda effect, clings to the trailing edge. This allows active control of the stagnation points and, consequently, control over the circulation of the wing. A 17% supercritical airfoil designed for circulation control is shown in figure 7. The shape of the supercritical airfoil section is very close to that of the GAW-1. With this type of CC airfoil, it is possible to achieve a  $C_{Lmax}$  of 5 to 6 with sonic flow. Using data from reference 2, an approximate 3-D drag polar for a GA aircraft was developed over the full range of  $C_{\mu}$ .  $C_{\mu}$  is the measure of merit, defined as the mass flow rate multiplied by the jet velocity at the slot divided by the multiplication of the dynamic pressure and the reference wing area, or:

$$C_{\mu} = \frac{\dot{m}V_j}{qS_{ref}}$$

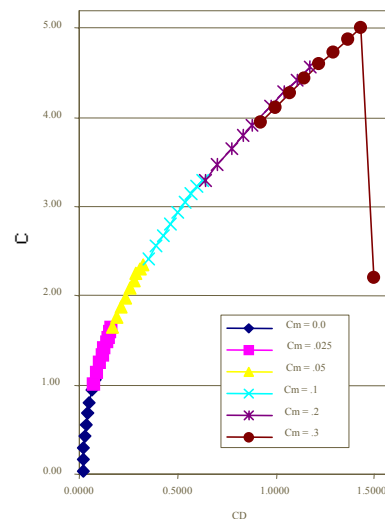


Figure 8: 3-D Drag Polar of a GA-CC Wing System

The wing system is assumed to have full span blowing from the fuselage to the tip, thus necessitating spoilers as roll control surfaces. One of the system impacts of utilizing a CC system, or any high performance highlift system, is the need for additional tail surfaces to trim the larger pitching moments, resulting in lower performance of the 3D system when compared to 2D wind tunnel results.



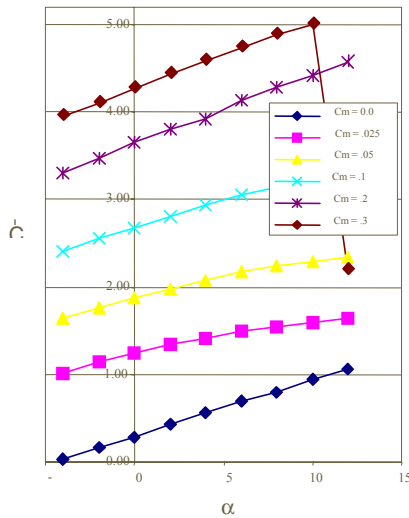


Figure 9: 3-D Lift Curve Slopes of a GA-CC Wing System

Initially an engine turbocharger was investigated for the supply of compressed air for the CC highlift system. This arrangement appeared to have promise since aircraft turbocharging is only used for altitude compensation, and not for increasing power at takeoff. Therefore, with the pressurized turbocharger air going out the wastegate at takeoff and landing, 100% of the turbocharger air mass flow is available for bleed to the CC system. However, use of the turbocharger as the air source is complicated by the problem of engine failure and the need to still achieve the same highlift with or without the engine running. A slow burn rocket gas generator was investigated as a backup system since only a limited 1 to 2 minute air plenum supply would suffice for an emergency landing flare while still achieving the CC system highlift performance during the approach. However, this added complexity plus the need for the engine to remain at high power during landing to supply the air while decelerating under normal conditions would impose an additional thrust reversing system. As the complexity of such a system continued to rise, alternate methods of providing an air source that were not dependent on the propulsion system were investigated.

In prior CC application studies, it has been argued that since the CC blowing results in a thrust component (since the air mass is injected at the trailing edge), using bleed air does not result in a thrust loss. However, this is not accurate since the bleed air is pulled prior to use in a combustion process, so that pulling 1 hp of bleed air results in robbing many times that power amount from the engine. In addition, the amount of thrust generated from a small, high-speed jet area is

considerably less than the thrust generated by an equal amount of power put into a lower speed flow in a larger area. This is especially true for small propeller aircraft that takeoff and land at low speed; this can easily be visualized by looking at a curve of horsepower required versus thrust disloading, with a typical propeller providing about 6 lbs of thrust per hp, while a high speed jet nozzle providing less than 2 lbs of thrust per hp. The key problem remains however, that the CC system power must be provided at the propulsion sizing critical condition of low-speed engine failure, so that any blowing power extraction is magnified by the ratio of total power to engine-out power. Clearly CC systems will have a difficult time buying their way unto an aircraft system when propulsion system scaling is required.

### WAKE VORTEX WINGTIP TURBINE SYSTEM

An ideal source of air for a CC system would provide a pressurized air source without power required during the takeoff and landing phases of flight, while providing some additional benefit during the other phases of flight to cover the additional CC system cost and weight. A wake vortex wingtip turbine system offers exactly this potential.

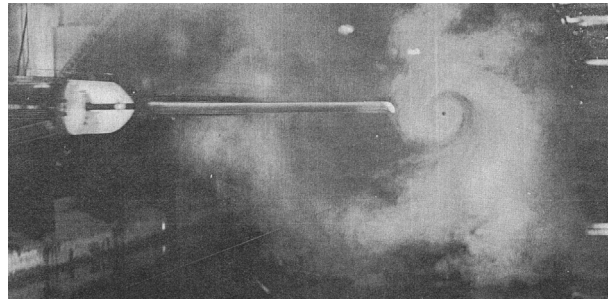


Figure 10: A wing tip vortex demonstrated in forward airspeed wind tunnel tests.

As shown in Figure 10, vortices are shed when any change in lift occurs along a wing span. These vortices roll up where the vortices are strongest, which is at the tip location where the lift becomes zero. The resulting rolled-up core vortex has energy associated with it, which is equivalent to the induced drag of the vehicle. Returning to Figure 3, it can be seen that the induced drag, or vortex energy, is greatest at the lowest speed when the vehicle is flying at the highest  $C_L$ , which is at the takeoff and landing portion of flight. Therefore the vortex velocity component is a maximum at the condition where we need to extract the most energy for a CC compressed air source. Figure 11 shows a representation of a wingtip turbine and the velocity components that provide power to the turbine blades; namely that there is a vortex velocity component, and a

free stream velocity component, and the resulting velocity component is the vector sum of the two. Again, the easiest way to visualize the magnitude of the resulting velocity vector, which is directly proportional to the vortex energy available to use for turbine work, is to look at the total drag at any given vehicle flight speed as in Figure 3.

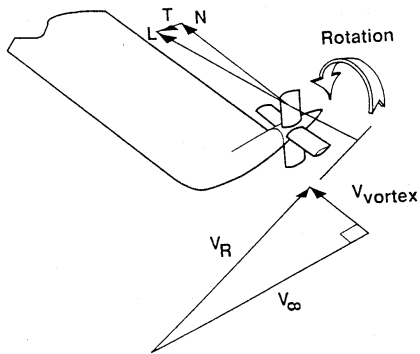


Figure 11: A wingtip vortex turbine system and the velocity components seen by the blades.

Prior research has been conducted on wake vortex wingtip turbines at NASA in the 1980's. However, the focus of this research activity was to provide an APU-like energy source for transport aircraft during cruise to increase efficiency. Analysis, wind tunnel, and flight test investigations resulted which demonstrated that the vortex turbine could successfully remove energy from the vortex and free stream velocities. The flight tests were conducted on a GA aircraft not because this was the intended application vehicle class, but because this was the lowest cost practical testing method. Figure 12 shows of a picture of the modified Piper Arrow GA aircraft in flight with the tip turbines active, and a close-up of the turbines blades after conducting oil flow visualization tests. The oil flow on the wingtip pod in front of the blades clearly shows the vertical flow direction, even at the efficient cruise condition. All analysis and flight test data was performed at the efficient cruise condition, since this was the area of application for the study. However, this speed point also corresponds to the weakest energy state of the vortex turbine, so only marginal amounts of power were shown. Figure 13 shows the amount of horsepower extracted from the 4 bladed system at various blade angle settings, but only at the 122 knot flight speed. The twist distribution was also not ideal, but simply a first principles approximation of an elliptical load distribution across the blade at one flight speed. The turbine blades for this test were fixed, but ground adjustable for simplicity of manufacture, though

this resulted in each data point along the Figure 13 curve being a different flight test. While valuable research, the prior effort into vortex wingtip turbines offers only a glimpse of the required data for application to the power source of a CC system.



Figure 12: Piper Arrow GA aircraft modified with a wingtip turbine system in 1988 to investigate the potential for extracting power during cruise for replacement or elimination of APUs and improved cruise efficiency.

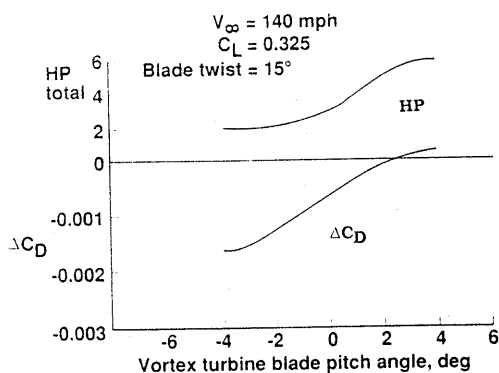


Figure 13: Horsepower extracted or drag reduction versus the blade pitch angle setting, demonstrated from cruise speed flight tests of a GA aircraft wingtip turbine system. Additional power extraction was possible, but no testing was performed of blade angles involving an increase in the vehicle drag since the investigation was for cruise drag applications.

As mentioned previously, a desirable attribute of a CC power source is that it also serves some purpose during the other phases of the mission besides at takeoff and landing. Figure 13 shows that depending on the blade angle, a vortex turbine can be used to either extract power, or provide a reduction in the induced drag. To derive the maximum benefit both for the CC air source power and cruise drag reduction, a variable pitch system would be required to vary the turbine blades. For each of these blade angles, a different turbine rpm results, with optimum power extraction occurring at approximately 400 rpm. The induced drag is reduced as the rpm is decreased, with the minimum induced drag occurring with the blades fixed in a stationary position acting effectively as wing endplates.

A first principles sizing effort was performed to see if a vortex wingtip turbine has sufficient energy to power a CC system. A full span blowing system was sized to yield a 30 ft trailing edge nozzle with a height of .06 inches. A constraint of Mach .70 was imposed on the CC blowing jet for noise reasons, yielding a plenum pressure of 20 psi, or a 1.4 pressure ratio. The CC system provided an improved lift curve slope as shown in Figure 8 and 9 previously, with the mass flow required at a  $C_{mu}$  of .20 being approximately 9.2 lbm/sec. This system yields a 3-D  $C_{Lmax}$  of about 4.0, yielding a  $C_{Llanding}$  of about 2.6 and  $C_{Ltakeoff}$  of 2.1 when stall margins are taken into account. The net effect on the vehicle is a reduction in wing area from 174 to 104 square feet, and an improvement in  $L/D_{cruise}$  from 11.8 to 15.1. However, the power required to drive the CC system with a 75% efficient compressor is about 40 hp per side at the peak condition to achieve a  $C_{Lmax}$  of

4.0. While this amount of blowing would not be used (due to the stall margin), it does raise the interesting dilemma that in order to maintain a sufficient stall margin the sizing condition for the CC system needs to have a significant excess capacity. In order to maintain a stall margin of 1.3, the CC system would require the ability to quickly vary the  $C_{mu}$ , thus imposing a gust alleviation/stall response time on the CC system in order to be certifiable. Looking at Figure 9 it can be seen that it is not possible to achieve an adequate stall margin at a constant  $C_{mu}$  unless the approach angle of attack is very low, for this example -10 degrees at landing!

The question remains whether there is sufficient energy in the vortex flow to power a CC system. A less aggressive  $C_{Lmax}$  could have been selected to achieve a lower mass flow requirement. Also, the mass flow estimate is artificially high due to the assumption of a constant thickness slot and constant spanwise blowing. Tailoring of the spanwise blowing to achieve a minimum induced drag would reduce the mass flow at outboard wing sections. Increased turbine power could be extracted by increasing the blade diameter and number of blades. While it is possible to extract this amount of energy from the wingtip vortex, it will be a significant challenge to do so with a compact system that can permit use near ground proximity, and with a lightweight turbine system. An estimate was performed of the weight of a CC wake vortex system, with the results indicating a 130 lbs total system weight (which is about half the weight of the wing), distributed over the following weights per side: 30 lbs centrifugal compressor, 12 lbs gear reduction from 40,000 rpm to 400 rpm, 8 lbs 4 bladed 3.5 ft diameter turbine, 5 lbs housing, and 10 lbs in internal valving and ducting. From a mission and sizing perspective, for this GA application effort, there was a net savings in fuel weight of 77 lbs from the baseline of 404 lbs. In addition the wing weight was reduced by a marginal 8 lbs from the 276 baseline wing weight. The reason the wing weight reduction is so low, considering the wing area was reduced by 40%, is that the reduction in wing skin weight is taken up by increased wing spar weight due to the decreased thickness of the beam. This is a result of the chord decreasing and keeping a constant thickness to chord ratio of the airfoil. Obviously the ability to go to thickness sections would permit an additional benefit, if the circulation control system also had some method of achieving a boundary control system to avoid separation due to the increased thickness. So, from a first principles analysis, a CC vortex turbine system sized for equivalent takeoff field length, but with a smaller wing, yields a slightly heavier aircraft. However, a more detailed analysis, and the incorporation of alternate integration schemes or blowing systems (such as pulsed blowing to reduce the

mass flow) could dramatically change this result. In order to really understand the potential of such a system, a detailed system study needs to be performed.

### **PROPOSED SYSTEM STUDY**

While the first principles study was useful for determination of application potential, a much higher-order analysis is required to make a determination of the exact performance differences. It is proposed that the following study is conducted to develop a more complete understanding of this synergistic technology suite, and justify scale or flight testing.

- 1) Perform a wake vortex energy balance for a determination of vortex energy available, and the required capture area and turbine/compressor efficiencies.
- 2) Vortex lattice static blade force and torque modeling and analysis in proximity to wing for a determination of turbine loads at the takeoff and landing conditions.
- 3) Transient takeoff time step analysis to show sufficient takeoff power and turbine blowing availability, as well as the CC/Tip-turbine responsiveness at landing at an assumed maximum gust response condition.
- 4) Wingtip-turbine number of blade, diameter, chord, twist, taper, axial location optimization for maximum power extraction and minimum cruise drag.
- 5) Sensitivity studies of a cruise-sized wing, varying the  $C_{mu}$ ,  $C_{L,max}$ , and compressor power available.
- 6) Optimization of the wing aspect ratio and CC system in combination, incorporating the vortex blade endplate effectiveness at cruise.
- 7) A detailed CC system weight and cost estimation with feedback into aircraft system in order to yield a cost to benefit ratio.
- 8) Estimation of the wake vortex dissipation with vortex energy removal for highlift to understand if this is another potential benefit as this type of system is applied to very large span constrained transports that cause significant takeoff and landing vortex hazards that yield operations timing delays.
- 9) Investigation of turbine failure modes (ie locking in non-optimum positions) to determine system robustness.
- 10) A repeat of steps 5 and 6 for a STOL wing application.

### **SUMMARY**

The use of Circulation Control and a Wake Vortex Tip-Turbine are suggested for investigation in order to provide a simple, effective highlift system for General

Aviation aircraft. This synergistic use technologies offer the potential to achieve on the order of a 50% increase in cruise efficiency, or a reduction in field length for STOL performance. A first principles assessment of considerations has been laid out in this paper, along with the steps required in order to conduct a complete system study. Initial results suggest that use of a wake vortex wing-tip turbine could provide sufficient power for a modest CC system that could achieve a  $C_{L,max}$  on the order of 3.5. However, prior test results of a wingtip turbine was extrapolated from cruise data points to the landing condition and therefore deserves significantly more systems investigation prior to large-scale testing. This use of a wingtip turbine provides a unique method of providing an air source for a CC system that is not associated with the vehicle propulsion system. In addition the tip turbine may be locked in place during cruise, when compressed air is not required, to provide an endplate effect, and therefore a reduction in induced drag. While the combination of these systems could provide a relatively simple highlift system that is fault tolerant, it does have the possibility of adding on the order of 130 lbs of weight to the wing, which is less than the 85 lbs of fuel and wing weight savings due to reduced wing area and the improvement in efficiency. Therefore, a GA aircraft with a CC and tip-turbine system would be somewhat heavier than a conventional GA aircraft, thus reducing some of the efficiency improvement. It is suggested that an in-depth system study be conducted to determine improved estimates of the CC and tip-turbine systems, including higher-order analysis at the landing condition, and that a full systems analysis of the concept be completed.

### **REFERENCES**

1. Moore, Mark, D., Personal Air Vehicles: A Rural/Regional and Intra-Urban On-Demand Transportation System, AIAA Paper 2003-2646.
2. Englar, Robert J.: Low-Speed Aerodynamic Characteristics of a Small Fixed-Trailing-Edge Circulation Control Wing Configuration Fitted to a Supercritical Airfoil. David Taylor Naval Ship R&D Center Report DTNSRDC/ASED-81/08, 1981.
3. Turnbull, Andy: Fixed Wing PAV Sizing Study, SWALES, Memorandum AACG 02001.
4. Flow Control Research at NASA Langley in Support of High Lift Augmentation, Sellers, W.L, Jones, G.S., and Moore, M.D., AIAA Paper 2002-6006, Nov 2002.
5. Abeqounis, William K. and Patterson, J. C., Wingtip Vortex Turbine Investigation for



- Vortex Energy Recovery, SAE 90-2936. Oct 1990, Aerotech Long Beach, CA.
6. Patterson, J. C., Effect of a Wing-tip Mounted Pusher Turboprop on the Aerodynamic Characteristic of a Semi-span Wing, AIAA Paper 85-1286.
  7. Patterson, J. C. and Flechner S. G., Exploratory Wind Tunnel Investigation of a Wingtip-Mounted Vortex Turbine for Vortex Energy Recovery, NASA TP 2468, 1985.
  8. Miranda, L.R. and Brennan J.E., Aerodynamic Effects of Wingtip-Mounted Propellers and Turbines, SAE 86-1802, Lockheed-California Company.
  9. Lin, Wen-Fan, Analysis of Wingtip Vortex Energy, Aerodynamics Technology Research Boeing Commercial Airplane Company, Feb 6, 1987.
  10. Bilanin, Alan J., Integral Analysis of the Performance of a Vortex Turbine in a Vortex Flow, Continuum Dynamics Inc, Jan 1988.

## Wake Vortex Wingtip-Turbine Powered Circulation Control High-Lift System



**EQUIPT**  
Easy-to-Use, Quiet Personal Transportation

Mark D. Moore  
Personal Air Vehicle Sector Manager  
NASA Langley Research Center

Circulation Control Workshop  
Hampton, VA  
March 17<sup>th</sup>, 2004

## EQUIPT Vehicle Technology Capabilities

On-Demand Access to 10,000 airports in the near-term, with point-to-point community accessibility in the long-term; providing reduced travel times compared to auto and airlines for ranges of 25 to 500 miles.



Required Capability	SOA General Aviation	5-Years Next Gen GA	15-Years Gridlock Commuters
Ease of Use	No	Auto-like	Autonomous
Acquisition Cost (\$K)	330	75	150
Community Acceptable (dbA Flyover)	74	55	50
Emissions (HC/NOx/Lead grams/mile)	.5/1.0/.2	.05/.10/0	.03/.06/0
Reliability (accidents/100Khr)	6.5	2.0	.5
Efficiency (mpg)	13	16	28
Field Length (balanced - feet)	2500	1000	250
Block Speed (mph)	35 Auto / 50 GA	100	200

Mission: Range = 600 miles, Payload = 4 passengers, Gross Weight ~ 3600 lbs, IFR capable

FY04

FY09

FY14

FY19



## EQuiPT Efficiency Technologies

### Initially a 20% improvement in sfc is achieved by utilizing automotive engine technologies

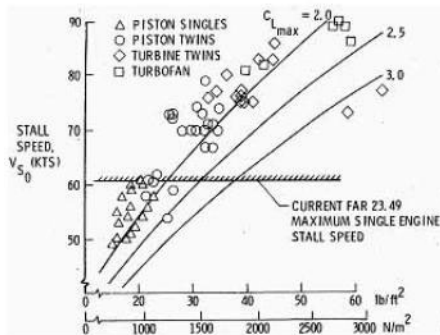
- Near-term elimination of 100LL fuel; replaced with slightly reformulated auto grade fuel
- Auto engines have higher compression ratios, digital control, improved combustion, etc...
- Auto engines are potentially certifiable with complete airframe/propulsion redesign (with a slight weight penalty but huge cost reduction), but are not retrofittable to existing airframe/propulsion

### An additional 50 to 60% improvement in mpg is required to achieve automobile efficiency levels

- Engine technologies can offer an additional 20% reduction in sfc (with a weight penalty)
- Small aircraft currently achieve cruise L/D's of 10 to 12, although they have L/D<sub>max</sub>'s of 16 to 18
- Combination of FAR Part 23 low takeoff and landing speeds (achieving 2500' field length operation and operational safety) and relatively low cruise altitudes result in wing sizing that is 3 times larger than cruise sizing (C<sub>Lcruise</sub> of .18 vs .54)
- Current small aircraft achieve a C<sub>Lmax</sub> of 2 to 2.2, and personal use will continue to require simple highlift systems that are not complex or expensive, maintenance prone, or hanger-rash vulnerable.
- Achieving a simple, effective highlift system could yield a 60 to 80% improvement in aero efficiency.

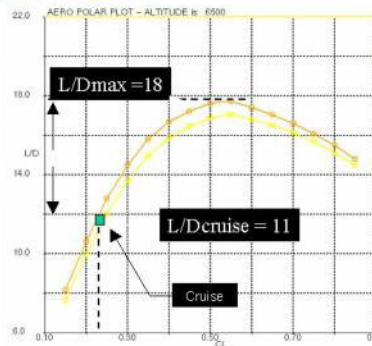


## EQuiPT Aero Efficiency Technologies



FAR Part 23 requires a stall speed of 61 knots, resulting in low wing loading and relatively low takeoff and landing speeds.

Higher wing loading would provide improved ride quality.  
(lower gust and cross-wind sensitivity)



Small aircraft have significantly oversized wings for cruise, with a 60% increase in L/D possible with a cruise-sized wing.

Re-sizing the wing with a C<sub>Lmax</sub> = 4.0 yields an L/D<sub>max</sub> ~ 20.  
(assuming no additional drag ie blunt TE)

## EQuiPT Short Takeoff/Landing Technologies

### **In the near-term a 1000' field length enables reduced approach speeds for improved safety and reduced community noise signatures**

- The ultimate objective in reducing the balanced field length is to reduce the infrastructure investment and runway protection zone required for highly distributed airfields.
- Safety (in terms of accident avoidance reaction time and survivability) is proportional to the approach speed (if equivalent control margins and gust sensitivity can be achieved).
- Takeoff and approach community noise footprint can be reduced through field length reduction.
- However, a 1000' field is not significant enough of a reduction to justify a new infrastructure, but it does permit an evolution in capability towards the 250' long-term objective.

### **The long-term 250' field length is a near VTOL capability that enables point-to-point.**

- Permits highly distributed, community-based point-to-point operation with maximum potential block speed, productivity, and mobility.
- Vehicles become cross-wind insensitive due to 100' roll distances and omni-directional landing.
- Powered-lift systems are required, with high TAW and engine-out tolerance, but not nearly the penalties of a hoverable VTOL (typically VTOL capable aircraft are operated this way for overload).

## Circulation Control (CC) Application

### **CC provides maximum effectiveness for small aircraft**

- CC effectiveness is based on  $(V_{jet}/V_{inf})^2$  velocity ratio, yielding either greater effectiveness or reduced mass flow given the same lift requirement.
- A Boeing 737 has an approach and rotation speed of approximately 135 knots, while a Cessna 182 is only about 65 knots, yielding a 4 x improvement in effectiveness
- A CC highlift system is potentially relatively simple, with no external moving parts.
- CC could be used to solve either the efficiency or short field problem, or possibly both through integration with additional technologies (combining higher altitude cruise, gust alleviation, limited powered-lift, etc.)

### **Low penalty integrated air source possible for small aircraft**

- High performance small aircraft are turbocharged for altitude compensation, not increased power at takeoff, so that considerable compressed air is thrown out the wastegate at takeoff (2 lbm/sec)
- However, linking the highlift system to the propulsion system is problematic since the same field length performance must be achievable after engine failure, and the need for high power approaches.
- An emergency air source backup is possible (ie slow-burn, solid gas generator for 1-2 min), however it adds unwanted complexity and only single pass approaches.
- Another alternative is using the wake vortex energy to power a wingtip-turbine.

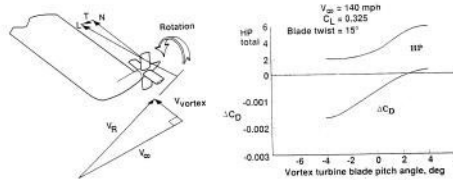
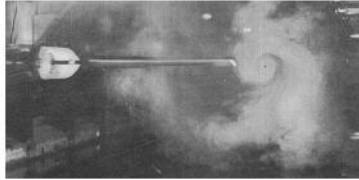




## Vortex Wingtip-Turbine Application

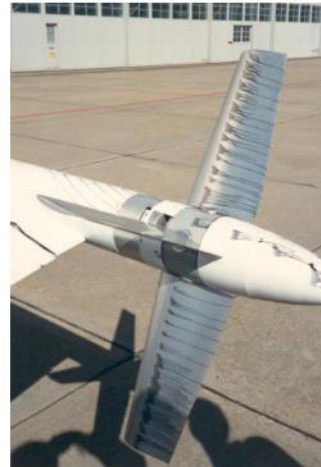
### Wake vortex could provide energy for air source

- Rotational velocity source that is proportional to the  $C_L$ , providing more energy at highlift conditions.
- Independent of propulsion; auto-gyro like in terms of engine-out and safety.
- Wingtip-turbine can provide either energy source or induced drag reduction.



### Experimentation already performed on small aircraft

- Flight validation experiment in 1988 on a Piper to verify cruise power extraction and drag reduction, (research was directed at use as cruise APU power substitute).
- Ability to extract 6 hp at cruise with no drag increase, or a reduction of 16 drag counts with 2 hp power extraction, while reducing the vortex strength.
- If increased drag is acceptable (such as at landing), there was the potential to extract 20-40 hp at low speed flight conditions.



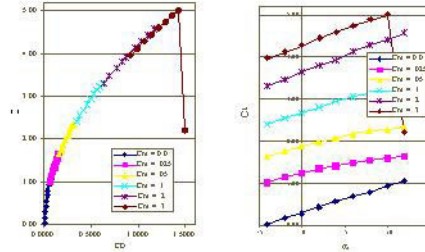
Wingtip Turbine Wake Vortex Experiment, Paterson et al, 1988, NASA Langley



## Baseline EQuIPT CC System

### Baseline CC system (limit turbine power, close to cruise-sized wing)

- Constant wing span,  $span_{with\ blowing} = 30\ ft$ ,  $s_{ref} = 104/174\ ft^2$ ,  $height_{slot} = .06\ in$
- $C_{mu} = .2$ ,  $P_{plenum} = 20.25$  (1.39 pressure ratio),  $m_{dot} = 9.18\ lbm/sec$ ,  $M_{inf} = .09$ ,  $M_{jet} = .70$ ,
- $C_{Lmax\ landing} = 4.0$ ,  $C_{Landing} = 2.6$ ,  $C_{Lmax\ takeoff} = 3.0$ ,  $C_{Ltakeoff} = 2.1$
- $L/D_{baseline\ avg} = 11.8$ ,  $L/D_{cruise-sized\ avg} = 15.1$
- Power<sub>Landing</sub> ~ 40 hp required per side peak, not operationally (with 75% comp<sub>eff</sub>)
- 30 lb (40K rpm centrifugal compressor)
- 12 lb (100:1 gearbox)
- 8 lb (4 bladed, 400 rpm, 3.5' turbine)
- 5 lb (housing)
- 10 lb (valving and ducting)
- 65 lb CC system weight per side
- 77 lbs mission fuel savings / 404 lbs
- 8 lbs / 276 lbs wing weight savings
- Initial starting point, non optimal solution
- Variable pitch required to achieve both highlift air source and cruise induced drag reduction



## Conclusions

### Only initial results from system study are present and premature to determine system merits; considerable additional effort is ongoing

- Wake vortex energy balance
- Vortex lattice static blade force and torque modeling in proximity to wing
- Transient takeoff time step analysis to show takeoff power availability, CC/Tip-turbine responsiveness at landing
- Wingtip-turbine number of blade, diameter, chord, twist, taper, axial location optimization for maximum power extraction and minimum cruise drag
- Cruise-sized wing  $C_{mu}$ ,  $C_{Lmax}$ , Compressor power sensitivity studies
- Optimization of wing AR and CC system combined
- Detailed CC system weight and cost estimation with feedback into aircraft system and cost to benefit
- Estimation of wake vortex dissipation with vortex energy removal for highlift
- Investigation into turbine failure modes (ie locking in non-optimum positions)
- Repeat for Short field CC system sizing and extrapolate into 737 transport class

**Geometry problems are present: rpm mismatch, compressor diameter, area reduction causes spar depth decrease, blade locking and variability for cruise**

**Use for short field performance is more likely than to achieve cruise-sized wing**

# THE USE OF CIRCULATION CONTROL FOR FLIGHT CONTROL

Steven P. Frith\* and Norman J. Wood†

School of Engineering, University of Manchester, Manchester, United  
Kingdom.

## Abstract

An experimental investigation into the application of circulation control on a 50° swept delta wing has been performed in a closed return wind tunnel at 25m/s. This was then extended to a sting-mounted circulation control demonstrator with two control surfaces, in order to determine whether the technique could be use for roll control whilst maintaining high lift coefficients within the limits of pitch trim. A lift augmentation of approximately 20 was achieved with all configurations. Roll of the aircraft was possible with differential blowing of the circulation control systems.

## Nomenclature

$b$	span
$\bar{c}$	Mean aerodynamic chord (m)
$c_o$	Chord (m)
$C_D$	Drag coefficient
$C_L$	Lift coefficient

---

\*Postgraduate Research Student, Fluid Mechanics Research Group, Aerospace Engineering, University of Manchester, Manchester, UK.

†Professor, Head of Department, Aerospace Engineering, University of Manchester, Manchester, UK.

$C_m$	Pitching coefficient
$C_p$	Pressure coefficient, $(p-p_\infty)/q_\infty$
$C_\mu$	Blowing coefficient
$\left(\frac{\partial C_l}{\partial C_\mu}\right)$	Lift augmentation
$h$	Slot height (mm)
$\dot{m}$	Jet mass flow rate (kg/s)
$M$	Jet Mach number
$p$	Static pressure on aerofoil (Pa)
$p_p$	Pressure inside plenum (Pa)
$p_\infty$	Ambient static pressure (Pa)
$q_\infty$	Freestream dynamic pressure (Pa)
$r$	Trailing edge radius (mm)
$s$	Semi-span (mm)
$S$	Wing reference area (m <sup>2</sup> )
$V_J$	Jet blowing velocity (m/s)
$\alpha$	Angle of attack (degrees)

## **1. Introduction**

Circulation control has been recognised as a technique by which very high lift coefficients can be achieved. It exploits the Coanda effect by blowing a high velocity jet over a curved surface, usually a rounded or near-rounded trailing edge, causing the rear stagnation point to move. In turn, the upper surface boundary layer is energised, resulting in a delay in separation. As the circulation for the entire wing is modified, there is an increase in overall lift,



often much greater when compared to more conventional mechanical lift devices.

Earlier research<sup>1,2</sup> has mainly concentrated on two-dimensional unswept wings, where the flow is predominantly attached to the airfoil. However, in this work the performance benefits of the application of circulation control for delta wings, with massive regions of separated flow, were investigated. Although more recent work<sup>3</sup> uses pulsed jets in a bid to reduce the total jet mass flow rate required, a steady jet was used in this investigation for model simplicity. With a system with few or no moving parts, the Circulation Control Wing (CCW) has provided considerable interest, as it is mechanically simpler, and therefore cheaper to manufacture, and less prone to mechanical failure in comparison with conventional high lift devices. Also, lift increments can be similar to those with conventional high lift control surfaces, but pitch increments can be lower, leading to improved aircraft control.

The initial aim of the study was to investigate the effect of various trailing edge configurations with a view to eliminate the cruise drag penalty attributed to large trailing edges, whilst still obtaining high lift augmentation. This was then extended to an investigation into the interaction of two circulation surfaces on a delta-wing planform with trailing edge sweep to determine whether there would be an interaction between the two jets and also whether circulation control could be used for roll control, within the limits of pitch trim and maintaining previous lift augmentation.

## 2. Experimental Procedure 1

The model used for the preliminary studies<sup>4</sup> is shown in figure 1. The CCW consisted of a generic delta wing leading edge section and a plenum/trailing edge section. The leading edge section comprised of a sharp leading edge profile with a  $50^\circ$  sweep, incorporating strengthening sections to reduce flexing when under aerodynamic load. The trailing edge consisted of a 6mm diameter brass rod, giving a trailing edge radius to mean aerodynamic chord ratio of  $0.005\bar{c}$ , over which a narrow convergent slot provided the jet blowing. A series of push-pull screws allowed the slot height to be adjusted to 0.15mm and to 0.3mm ( $0.00025\bar{c} \leq h \leq 0.0005\bar{c}$ ).

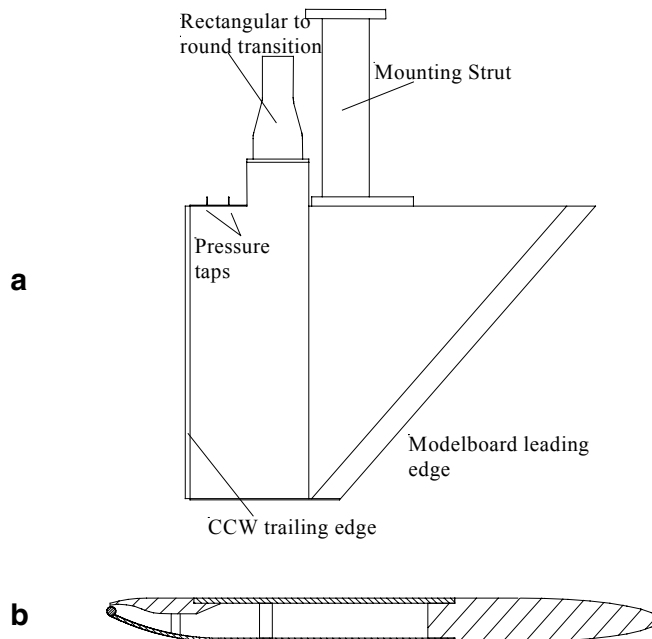


**Figure 1: Model Geometry**

**(a). Upper surface view (b). Cross-sectional view**

The model was mounted from the overhead balance in the Avro 2.74m x 2.13m (9' x 7') wind tunnel at the Goldstein Laboratory, Manchester, U.K., as shown in figure 2. A splitter board was mounted to ensure that the wind tunnel boundary layer did not interfere with measurements and the Coanda jet. Force and moment data was measured using the 6-component balance. The freestream velocity was set at 25m/s, corresponding to a freestream Reynolds number of approximately  $8.5 \times 10^5$ , and maximum jet velocities were approximately 180m/s.

The air supply was from pressurised receiver tanks fed by an Atlas-Copco compressor, delivered to the plenum by a flexible hoses, such that tare effects out of the plane of measurement were avoided. The mass flow rate was determined using an orifice plate rig and pressure and flow temperature data was transferred to the computer via an A-to-D card.

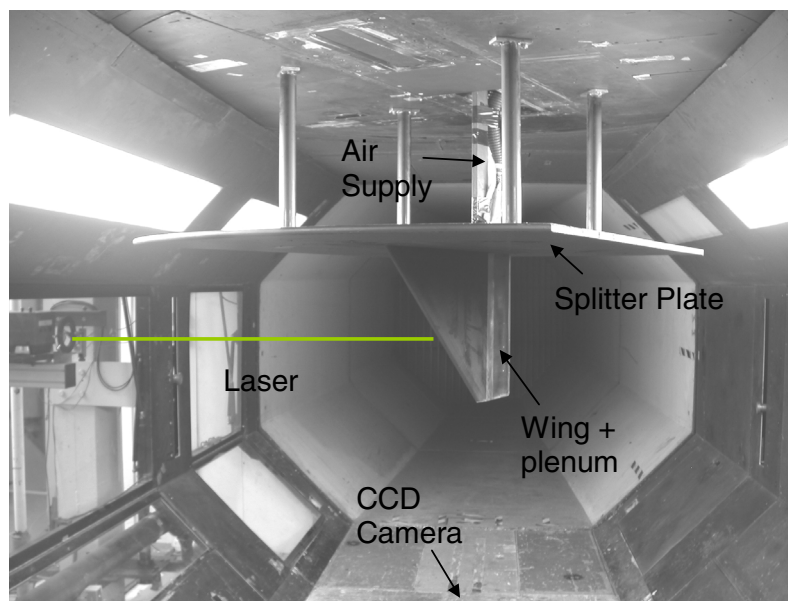


**Figure 2: Model mounted in wind tunnel**

A computer program was written to accumulate data and calculate the flow rate. From this the blowing momentum coefficient,  $C_{\mu}$ , could be calculated. This was calculated using,

$$C_{\mu} = \frac{V_J \dot{m}}{qS},$$

where  $V_J$  is the velocity of the Coanda Jet,  $\dot{m}$  is the jet mass flow rate,  $q$  is the freestream dynamic pressure and  $S$  is the model surface area. The jet velocity was calculated using the isentropic pressure distribution,

$$\frac{p_p}{p_{\infty}} = \left(1 + \frac{M^2}{5}\right)^{\frac{\gamma}{2}},$$

to avoid errors that can occur using the jet area as a variable. As interest was at the low blowing rates, data was recorded at increments of  $C_{\mu}$  of 0.0005 up to 0.01 and then using increments of 0.005 up to 0.03 to obtain general force or moment curves.

Particle Image Velocimetry (PIV) was also performed to obtain more information on the interaction of the jet with the freestream flow<sup>5</sup>. A horizontal lightsheet was fired at the trailing edge of the CCW and a CCD camera, positioned under the wind tunnel floor, captured pairs of images of the seeded freestream flow over the wing, as shown in figure 2. These were then

analysed using TSI Insight and Tecplot 9 software to obtain velocity and vorticity data.

As part of a joint project, BAE Systems<sup>6</sup> calculated CFD data to compare with the experimental data.

### **3. Results 1**

The results given in figure 5 show the effect of circulation control on the lift characteristics with a variation in slot height. There is an increase in lift with an increase in blowing coefficient,  $C_{\mu}$ , although the greatest lift increments were found at lower blowing rates. The level of lift augmentation  $\left(\frac{\partial C_L}{\partial C_{\mu}}\right)$  is of the order of 10-20. Also, it was found that the smaller slot height yields a stronger lift augmentation at smaller values of  $C_{\mu}$ . It is anticipated, though, that a minimum slot height will be reached, where the jet no longer attaches to the Coanda surface. This requires further research.

The drag coefficient was also found to increase as the blowing rate is increased although the drag augmentation is significantly less than the equivalent value for lift, suggesting an overall increase in L/D. However, drag measurements are not presented in this paper due to an inconsistency in the data, which may be due to fluctuations in the Coanda jet or the accuracy range of the balance.

Figure 6 shows the calculated velocity vectors obtained using PIV in the form of a contour plot using the TSI Insight and Tecplot softwares. It can be seen that the external flow visibly changes at higher blowing rates, indicated by a downward deflection of the velocity vectors. The data also demonstrates the downstream extent of the wake was reduced. Due to restrictions with apparatus it was not possible to seed the jet and investigate the interaction with the freestream flow.

#### **4. Experimental Procedure 2**

A full span model was designed and constructed at the Goldstein Laboratory, Manchester, to investigate any interaction of the Coanda jets and examine the possibility of roll control, as well as lift enhancement (figure 3).

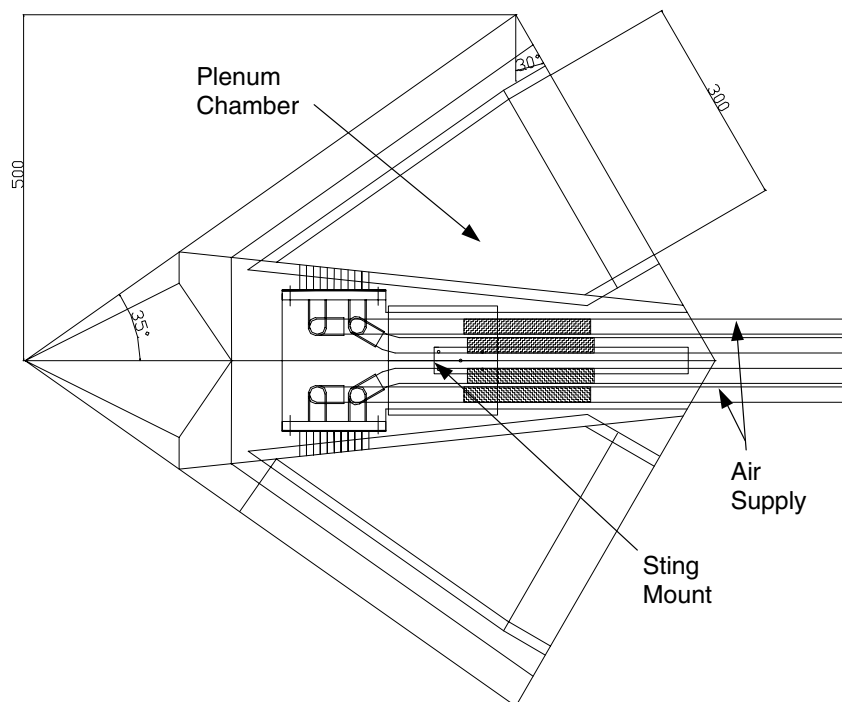


**Figure 3: Schematic of full span model**

The main body was constructed using modelboard, with the fuselage made from aluminium sheet. The plenum sections, made from aluminium for the upper surface and brass for the lower surface, incorporated similar trailing edge dimensions as the previous model: trailing edge diameter of 6mm and slot height adjustment from 0.05mm to 0.30mm (this was set at 0.15mm to compare with previous results). The blowing rate was again controlled using an orifice plate rig for each plenum, such that the plenum sections could be controlled independently. The air supply was controlled by the use of two valves for each plenum, allowing finer and more accurate control.

The model was mounted on a sting in the 9' x 7' wind tunnel as shown in figure 4, incorporating an internal 6-component strain-gauge sting balance to measure forces and moments.

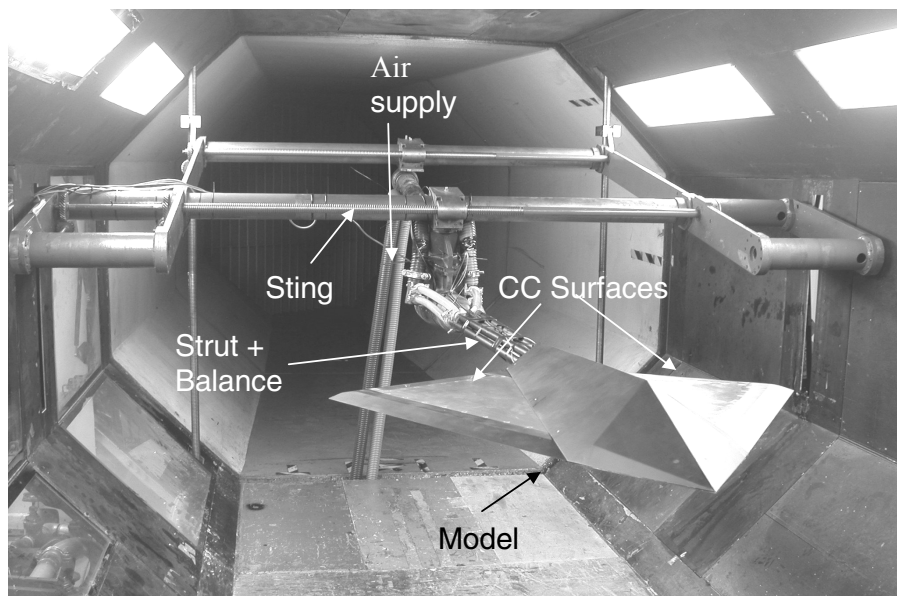


**Figure 4: Sting-mounted model in wind tunnel**

The air supply was again taken from pressurised tanks and passed through a series of flexible hose. Tare effects due to flexing of the hoses when under pressure were minimised by incorporating highly flexible hose within the model, adjacent to the calibration centre of the balance. Any tare effects due to any flexing of hoses were measured wind-off.

Preliminary tests were performed prior to data collection to determine efficiency of both Coanda surfaces, check for any leakages and uniformity of both slots. Test runs were made in the wind tunnel to examine model integrity and performance.

Tests were accomplished at 25m/s (a freestream Reynolds number of approximately  $1.3 \times 10^6$ ) and the angle of attack was varied from  $0^\circ$  to  $15^\circ$  in  $5^\circ$  increments. The blowing was varied from zero to 0.004 at increments of 0.0005. Data was taken for various test parameters; symmetric blowing, in which the jet momentum from both plenums was identical, and asymmetric (or differential) blowing, in which only one side of the model would use the jet blowing.

## **5. Results 2**

In quiescent conditions, both Coanda jets performed as expected, with the jets fully attaching to the Coanda surfaces. Figures 7 to 12 show the effectiveness of the full span model, in the form of carpet plots with contours of constant  $C_\mu$  and angles of attack. A lift augmentation,  $\left(\frac{\partial C_L}{\partial C_\mu}\right)$ , of 10-25 was



achieved, as demonstrated in figure 7, in which data is shown for both Coanda jets at the same mass flow rate, and therefore the same  $C_{\mu}$  (symmetric blowing). Although the lift augmentation achieved is not as great as those achieved in other studies<sup>7</sup>, it is believed that this can be attributed to the small radius of the Coanda surface. The trade-off of a lower lift augmentation is that the drag for such a surface is reduced when compared to traditionally large CC Coanda surfaces.

Assuming the centre of gravity to be at the quarter-chord position, the pitching moment about this point is nose-down (figure 8), which is as expected as the centre of lift is located aft of the quarter chord. It is encouraging to see that the circulation control device could be used to trim the aircraft, whilst maintaining high values of lift augmentation, as the variation in  $C_{\mu}$  required at various angles of attack is approximately linear, as shown in figure 9. This suggests that the control of this parameter could be simply transferred to stick control in a real-flight situation.

The investigation in using circulation control for roll control revealed some interesting characteristics. The variation of lift with asymmetric blowing (zero blowing from the right Coanda jet) is shown in figure 10. Again, a lift augmentation of approximately 20-25 is achieved and it was demonstrated that the jet momentum is additive, that is, if the left jet was used at the maximum value of  $C_{\mu}$ , the activation of the right jet would result in a similar lift curve to that obtained with symmetric blowing.

The control of rolling moment by circulation control is demonstrated in figures 11 and 12. It can be seen that a particular rolling moment can be achieved with a particular value of  $C_{\mu}$  independent of the angle of attack, although the leading edge vortex, particularly effective at angles of attack from approximately  $7.5^{\circ}$ , produces an additional pro-roll moment. This pro-roll moment results from a secondary effect of the blowing that enhances the vortex suction signature ahead of the blowing slot. This can be seen by the kink in the rolling moment curves. The data shows that, for example, a blowing coefficient of 0.0015 would be equivalent to an aileron deflection of approximately  $5^{\circ}$ . The slight negative rolling moment present at an angle of attack of  $0^{\circ}$  and  $C_{\mu} = 0$  indicates that there is a slight model asymmetry, although this only equates to approximately 1 Nm of rolling moment.

## **6. Conclusions**

An experimental investigation of circulation control, initially on a single delta wing configuration with varying trailing edge geometry and then on a full-span model, has been successfully completed.

The variation of slot height indicated that a smaller slot height yielded a higher lift augmentation,  $\left(\frac{\partial C_L}{\partial C_{\mu}}\right)$ . However, it is anticipated that there is a limiting height, requiring further work. Lift augmentations of approximately 10-25 for low blowing rates were obtained with both models. This suggests that useful lift increments can be obtained with  $C_{\mu}$ 's of the order 0.005, equivalent to those achieved using existing flap systems ( $\Delta C_L \sim 0.1$ ). As the CC system is

considerably less complex mechanically than other high lift devices, this may be significantly beneficial when contemplating maintenance, production costs and reliability.

Importantly, the production of roll moments can be superimposed on the lift generation, suggesting minimised interaction and simple control development.

More detailed work at even smaller increments of  $C_{\mu}$ , especially in the lower blowing regions, will enable greater understanding of the physics involved in circulation control and the areas of higher lift augmentation. Further experimental work using the full-span model will continue to investigate the application of circulation control to roll control and pitch trim. The implementation of pulsed jets will also reduce the required mass flow bleed yet provide similar lift augmentations<sup>3</sup>.

## **7. References**

1. Wood, N.J. and Nielsen, J.N., *Circulation control airfoils – Past, present, future*, AIAA, 23<sup>rd</sup> Aerospace Sciences Meeting, Reno, Jan 1985.
2. Englar, R.J. and Applegate, C.A., *Circulation Control – A Bibliography of DTNSRDC Research and Selected Outside References (Jan 1969 through Dec 1983)*, DTNSRDC – 84/052, September 1984.
3. Jones G.S. and Englar R.J., *Advances in Pneumatic-Controlled High-Lift Systems Through Pulsed Blowing*, 21<sup>st</sup> AIAA Applied Aerodynamics Conference, Orlando, Florida, June 2003.

4. Frith, S.P. and Wood, N.J., *Effect of Trailing Edge Geometry on a Circulation Control Delta Wing*, 21<sup>st</sup> AIAA Applied Aerodynamics Conference, Orlando, Florida, June 2003.
5. Raffel, M. et al., *Particle Image Velocimetry – A Practical Guide*, Springer 1998.
6. Sellars, N.D., Wood, N.J. and Kennaugh, A., *Delta Wing Circulation Control Using The Coanda Effect*, AIAA 1<sup>st</sup> Flow Control Conference, St. Louis, June 2002.
7. Englar, R.J., *Circulation Control Pneumatic Aerodynamics: Blown Force and Moment Augmentation and Modification – Past, Present and Future*, AIAA Fluids 2000 Conference and Exhibit, 2000.

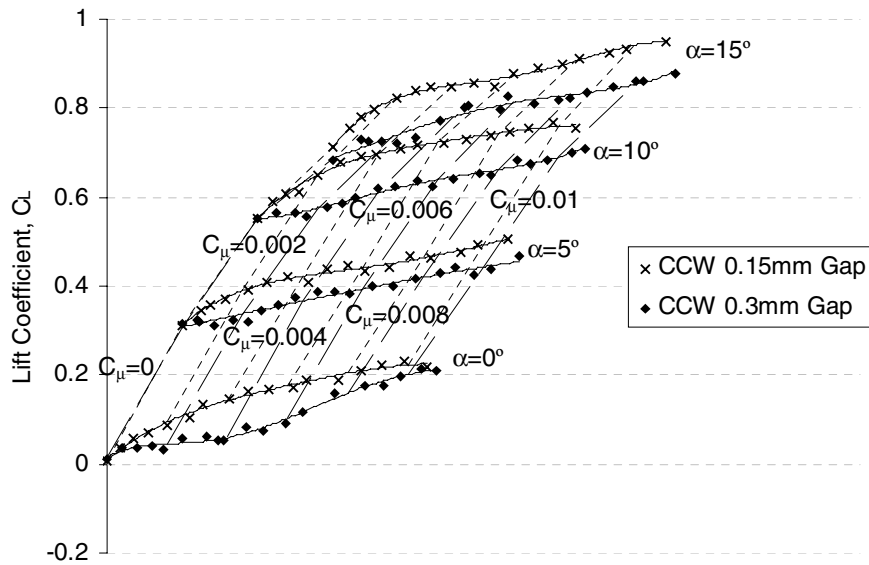


Figure 5:  $C_L$  v  $C_\mu$  - Effect of slot height on circulation control

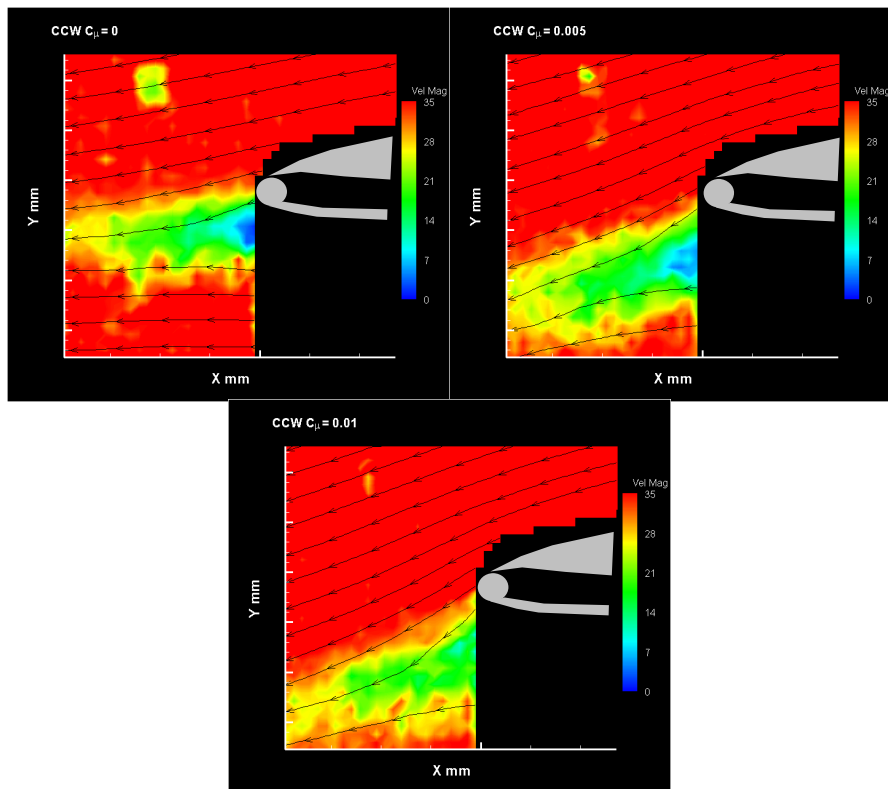
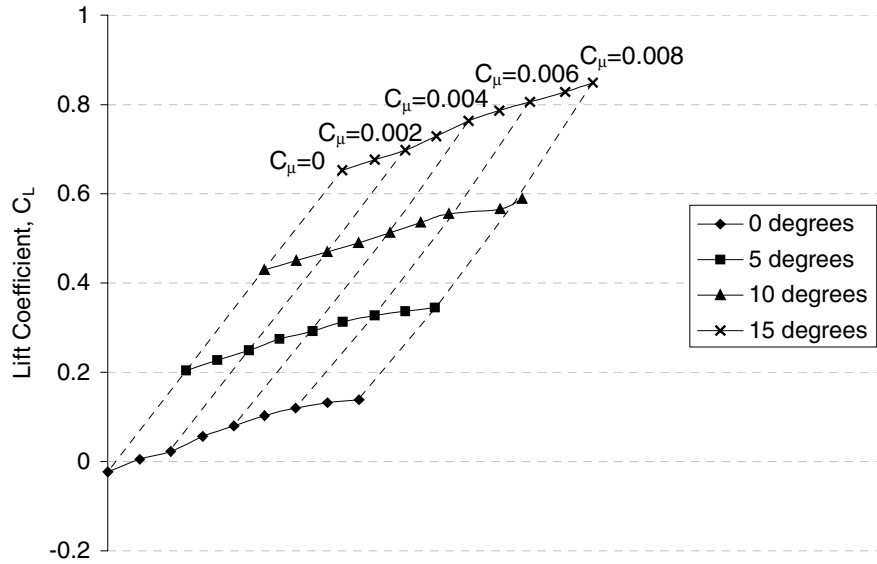
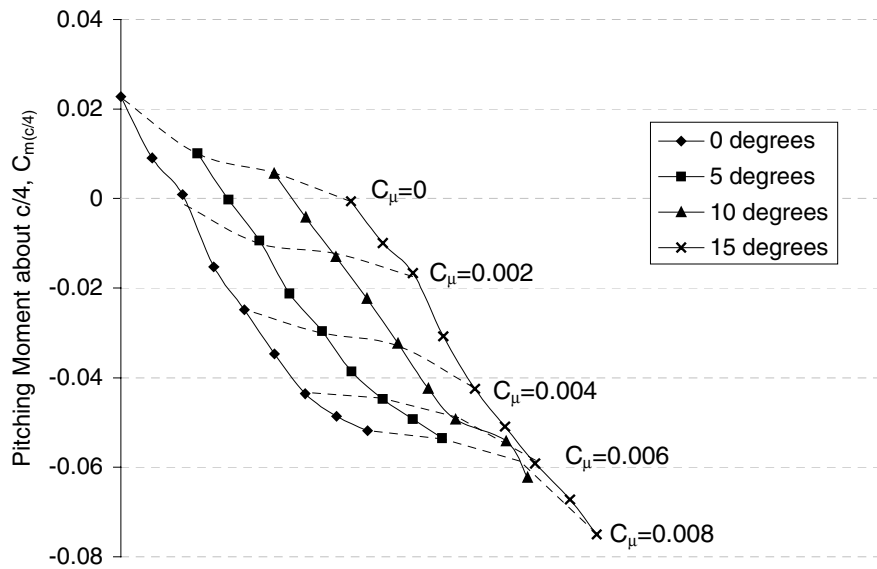


Figure 6: PIV velocity contour plots with streamlines obtained for angle of attack  $10^\circ$  at following blowing coefficients: a)  $C_\mu = 0$ , b)  $C_\mu = 0.005$ , c)  $C_\mu = 0.01$ .



**Figure 7: Variation of lift with both circulation control systems blowing with same mass flow rate (symmetric blowing).**



**Figure 8: Variation of pitching moment about the quarter-chord position with both circulation control systems blowing with same mass flow rate (symmetric blowing).**

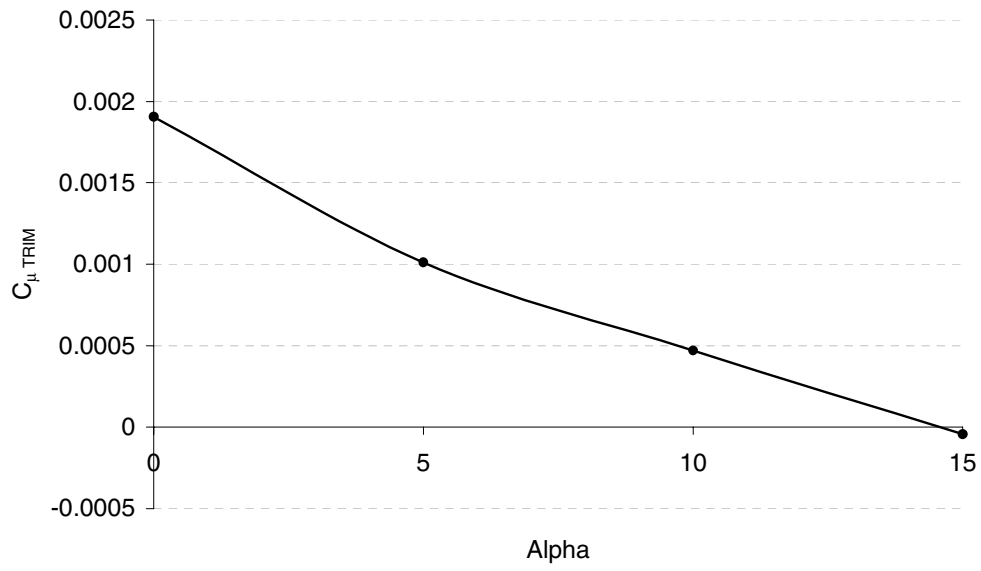


**Figure 9: Blowing required for pitch trim at varying angles of attack with both circulation control systems blowing with same mass flow rate (symmetric blowing).**

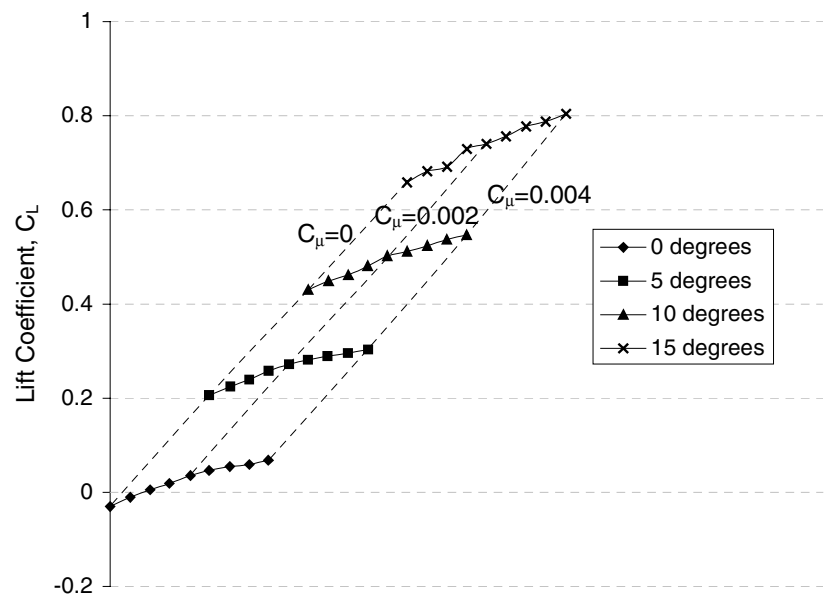


**Figure 10: Variation of lift with only one circulation control system blowing (asymmetric blowing).**

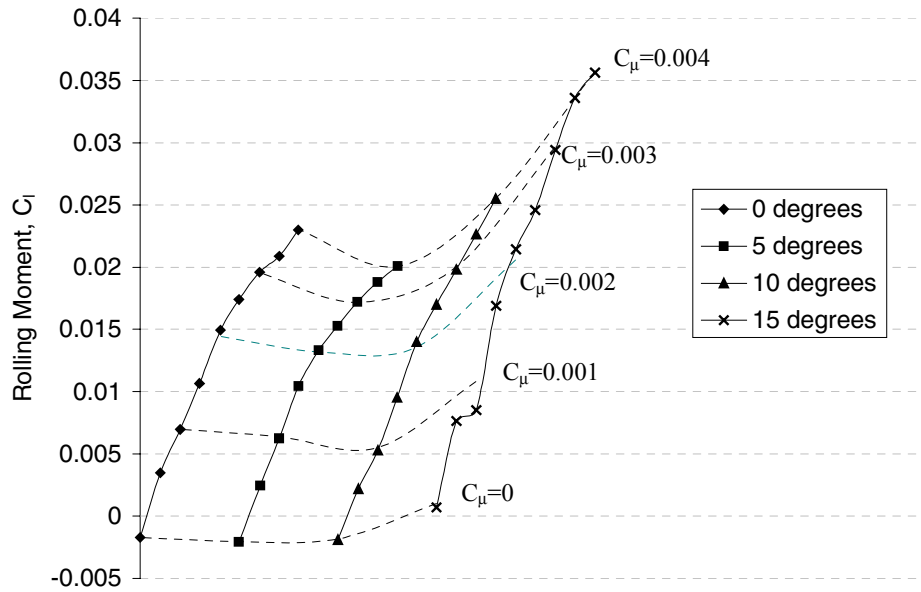


**Figure 11: Variation of roll with only left circulation control system blowing (asymmetric blowing).**

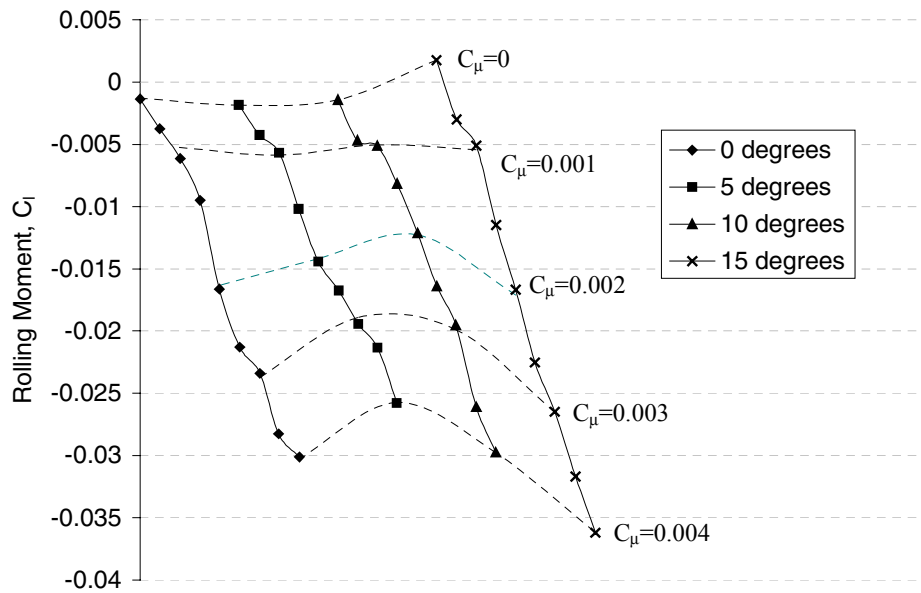


**Figure 12: Variation of roll with only right circulation control system blowing (asymmetric blowing).**





## The Use of Circulation Control for Flight Control

---



THE UNIVERSITY  
of MANCHESTER



Steven Frith and Norman Wood

## Contents

---



THE UNIVERSITY  
of MANCHESTER

- Aims and Objectives
- Circulation Control Concept
- Experimental Set-up and Configurations
- Preliminary Tests
  - Force Measurements
  - Particle Image Velocimetry
- Recent Work
  - Manufacture and Set-up
  - Results
- Conclusions and Further Work

## Objectives of the project

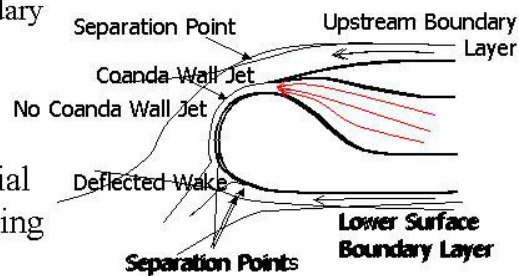


- To investigate various trailing edge configurations with a view to optimising the circulation control system on a delta wing.
- To determine whether the leading edge vortex contributes to the circulation control characteristics.
- To extend circulation control as a flight control device as well as providing high lift.

## Introduction - 1



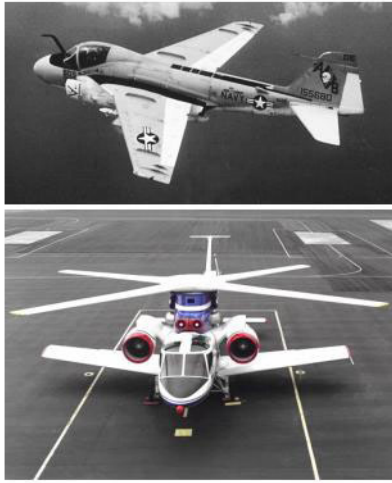
- Use of Coanda Effect
  - re-energise boundary layer to delay separation.
- Rearward tangential blowing over trailing edge
  - causes increase in lift.



## Introduction - 1



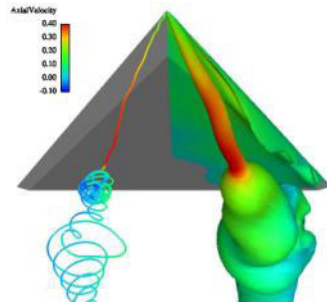
THE UNIVERSITY  
of MANCHESTER



## Introduction - 2



THE UNIVERSITY  
of MANCHESTER



- Delta Wings
  - Leading edge vortex.
  - Variation due to wing geometry.
  - Primarily used on military aircraft.
  - High lift at high angles of attack.

## Introduction - 3

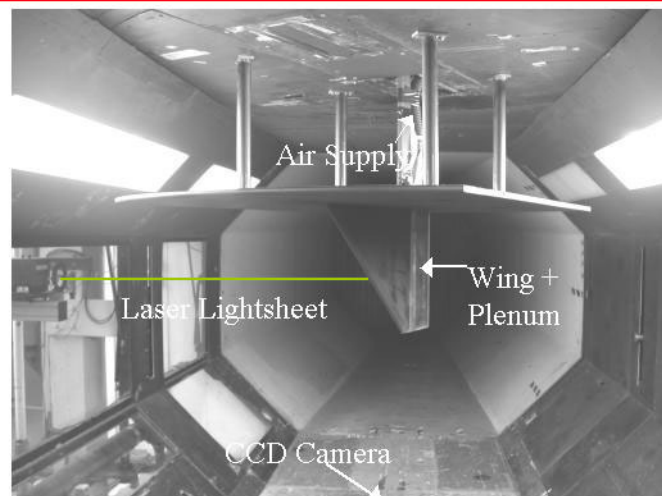
---



- Benefits of circulation control applied to delta wings?
  1. Enhance the lift capabilities with minimum energy input.
  2. To have an impact on the pitch trim case.
  3. To replace conventional control surfaces.

## Test Configuration - Half-Span

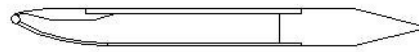
---



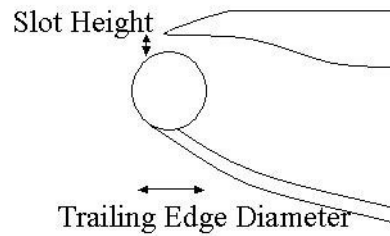
## Trailing Edge Geometry



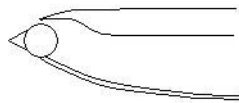
- 6mm diameter trailing edge, sharp leading edge profile



- 0.3mm slot height
- 0.15mm slot height



## Hybrid Trailing Edge



## Blowing Parameters



- Blowing coefficient:

$$C_{\mu} = \frac{\dot{m}V_j}{qS}$$

- Lift augmentation:

$$\frac{\partial C_L}{\partial C_{\mu}}$$

- Scaling Information:

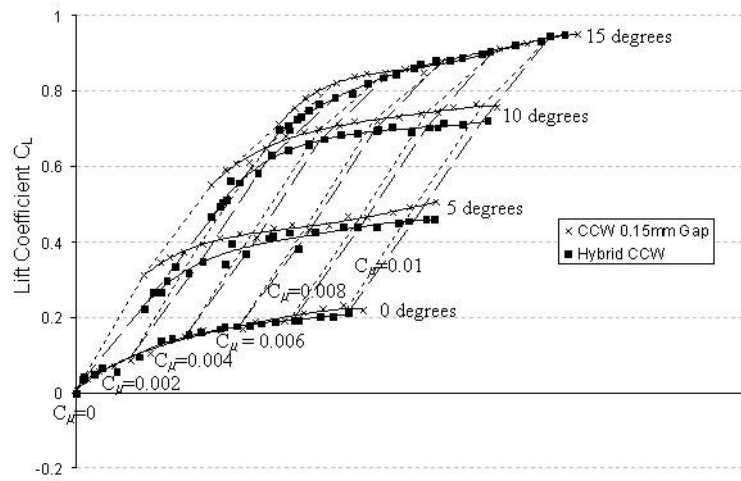
### **Eurofighter Typhoon**

Engine Mass Flow = 75kg/s,  
S = 50m<sup>2</sup>, M=0.3 @ sea level

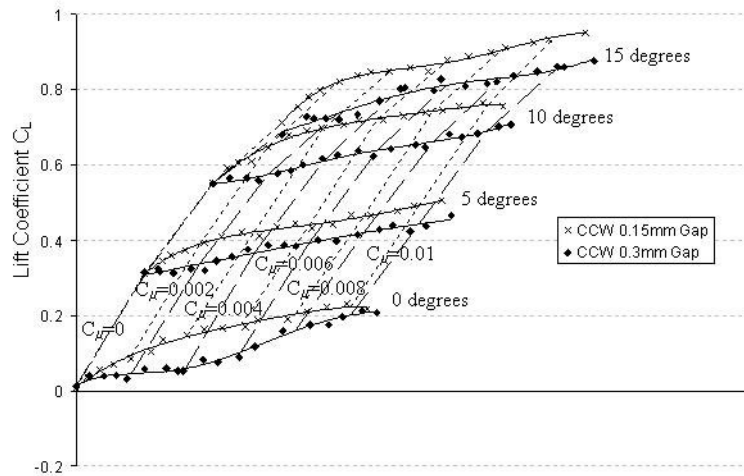
For 5% engine mass flow

$$C_{\mu} = 0.008$$

## Force Measurements



## Force Measurements

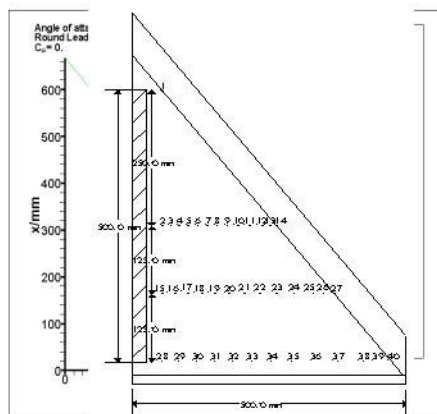


## Force Measurements



- Lift augmentation of 10-20 obtained (cf. Jet flaps  $\approx$  1-2).
- Similar trends obtained with all trailing edge configurations.
- Variation in leading edge vortex showed that circulation control properties unaffected.

## Pressure Measurements

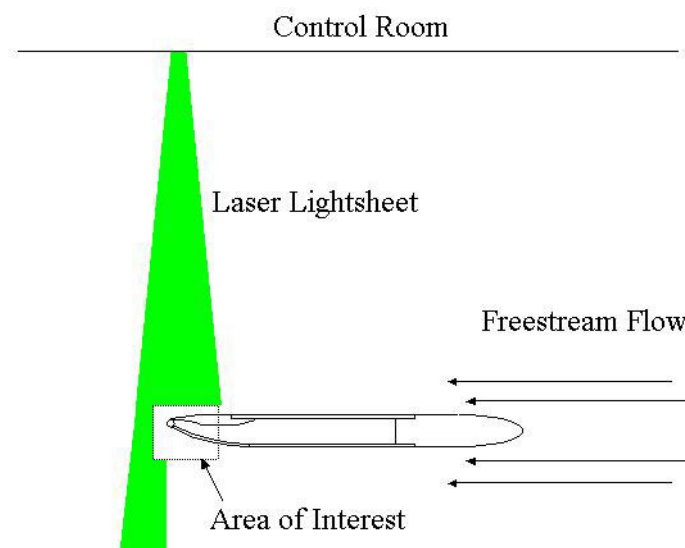


- Pressure readings taken using Scanivalves and series of pressure tappings along rounded leading edge.
- Demonstrate presence of leading edge vortex.
- Shows that higher lift obtained at lower  $\alpha$  where burst exists further aft.

## Particle Image Velocimetry

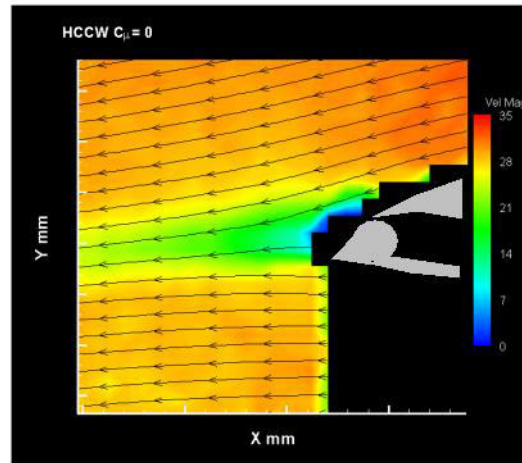


- Non-intrusive flow visualisation technique.
- Used to obtain more data about flow structures around the wing.
- Laser light sheet illuminates seeding particles, CCD camera captures images.
- Velocity and vorticity plots obtained using software.





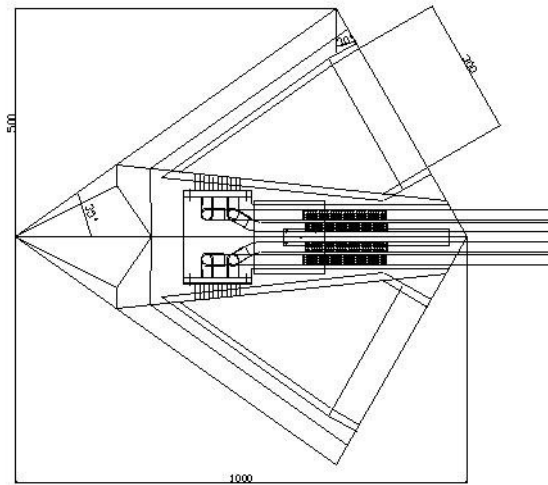
## PIV Velocity Contours



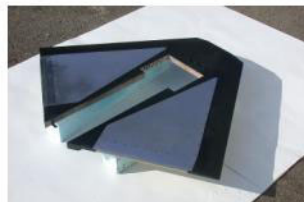
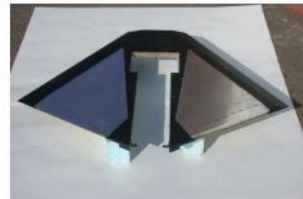
## Test Configuration - Full-Span

- Application to full span model.
  - Interaction of Coanda jets
  - Possibility of roll control
  - Use as high lift control device with pitch trim control.
  - Investigate any superposition of control forces.

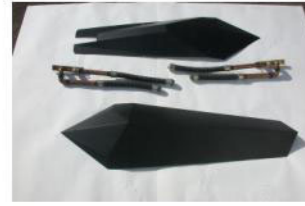
## Test Configuration - Full-Span



## Manufacture



## Air Supply Linkage

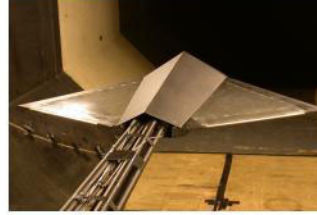


## Experimental Set-up

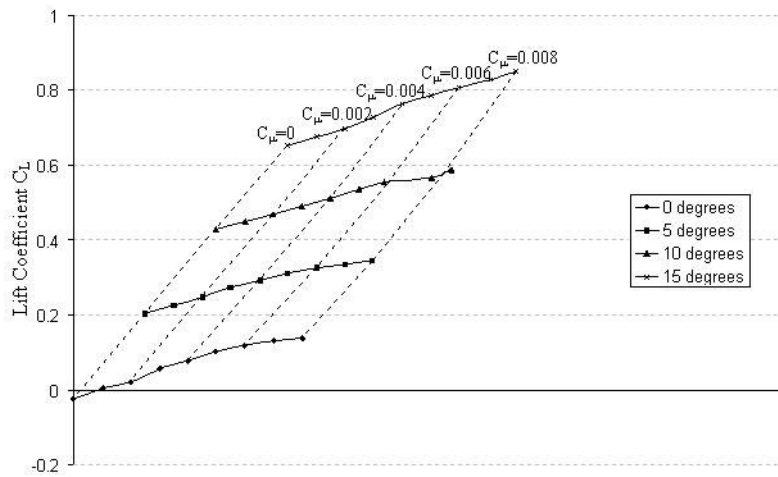


- Sting-mounted model in Avro 9' x 7' wind tunnel at Goldstein Laboratory, Manchester.
- Used internal 6-component strain gauge sting balance.
- Independent air supplies.
  - Symmetric blowing.
  - Asymmetric blowing.

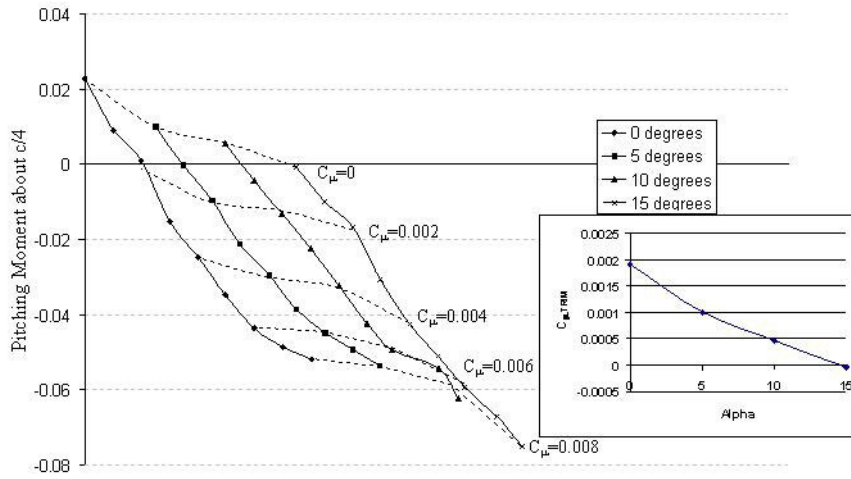
## Sting-mounted Model



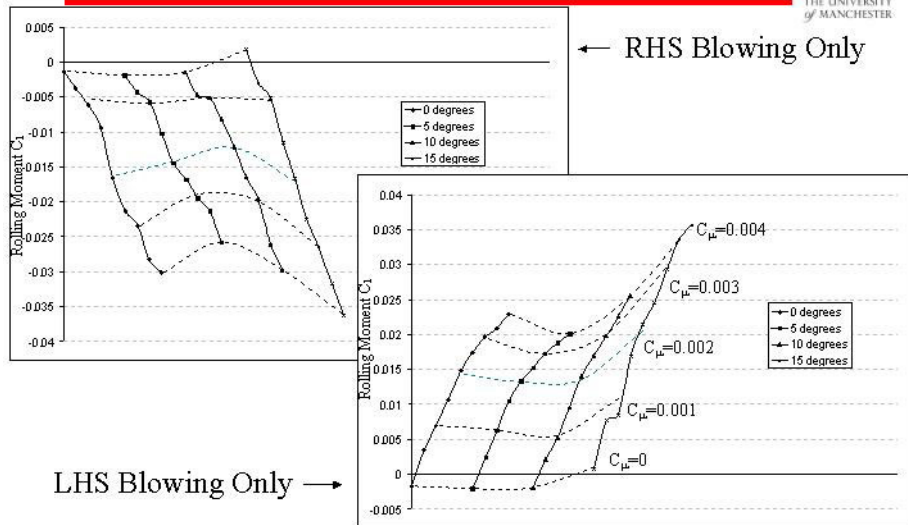
## Symmetric Load Measurements



# Symmetric Load Measurements



# Asymmetric Rolling Moment Measurements



## Conclusions

---



- Load measurements indicate that smaller slot heights produce similar trends to larger slot heights.
- Pressure measurements indicate presence of leading edge vortex and that circulation control leads to an increase in lift on wing.
- Benefits from circulation control appear to be independent of the state or position of the leading edge vortex.
- With circulation control active, vortex burst moves further aft.
- Hybrid Circulation Control Wing yields similar lift characteristics to CCW
- PIV effectively shows deflection of the wake due to Coanda Jet.
- Pitch Trim potential with CC, as well as roll control.

# TIME-ACCURATE SIMULATIONS OF SYNTHETIC JET-BASED FLOW CONTROL FOR A SPINNING AXISYMMETRIC BODY

**Dr. Jubaraj Sahu**

U.S. Army Research Laboratory  
Aberdeen Proving Ground, MD 21005, USA

## ABSTRACT

This paper describes a computational study undertaken to determine the aerodynamic effect of tiny unsteady synthetic jets as a means to provide the control authority needed to maneuver a spinning projectile at low subsonic speeds. Advanced Navier-Stokes computational techniques have been developed and used to obtain numerical solutions for the unsteady jet-interaction flow field at subsonic speeds and small angles of attack. Unsteady numerical results show the effect of the jet on the flow field and on the aerodynamic coefficients. The unsteady jet is shown to substantially alter the flow field both near the jet and the base region of the projectile that in turn affects the forces and moments even at zero degree angle of attack. The results have shown the potential of computational fluid dynamics to provide insight into the jet interaction flow fields and provided guidance as to the locations and sizes of the jets to generate the maximum control authority to maneuver a projectile to hit its target with precision.

## INTRODUCTION

Accurate determination of aerodynamics is critical to the low-cost development of new advanced munitions [1,2]. Competent smart munitions that can more accurately hit a target can greatly increase lethality and enhance survivability. Desert storm convincingly demonstrated the value of large-scale precision-guided munitions. A similar capability for small-scale munitions would increase the effectiveness of the infantry units, reduce collateral damage, and reduce the weight of munitions that must be carried by individual soldiers. The Army is therefore, seeking a new generation of autonomous, course-correcting, gun-launched projectiles for infantry soldiers. Due to small projectile diameter (20 to 40mm), maneuvers by canards and fins seem very unlikely. *An alternate and new evolving technology* is the **micro-adaptive flow control** through synthetic jets. These very

tiny (of the order of 0.3mm) synthetic micro-jet actuators have been shown to successfully to modify subsonic flow characteristics and pressure distributions for simple airfoils and cylinders [3,4]. The synthetic jets (fluid being pumped in and out of the jet cavity at a high frequency of the order of 1000 Hz) are control devices (Figure 1) with zero net mass flux and are intended to produce the desired control of the flow field through momentum effects. Many parameters such as jet location, jet velocity, and jet actuator frequency can affect the flow control phenomenon. Up to now, the physics of this phenomenon has not been well understood and advanced numerical predictive capabilities or high fidelity computational fluid dynamics (CFD) design tools did not exist for simulation of these unsteady jets. However, the research effort described here has advanced the aerodynamic numerical capability to accurately predict and provide a crucial understanding of the complex flow physics associated the unsteady aerodynamics of this new class of tiny synthetic micro-jets for control of modern projectile configurations. High performance CFD techniques were developed and applied for the design and analysis of these Micro-Adaptive Flow Control systems for steering a spinning projectile for infantry operations.

The control of the trajectory of a 40mm spinning projectile is achieved by altering the pressure distribution on the projectile through *forced* asymmetric flow separation. Unsteady or time-accurate CFD modeling capabilities were developed and used to assist in the design of the projectile shape, the placement of the synthetic actuators and the prediction of the aerodynamic force and moments for these actuator configurations. Additionally, the advanced CFD capabilities provided a simpler way to explore various firing sequences of the actuator elements. Time-accurate unsteady CFD computations were performed to predict and characterize the unsteady nature of the synthetic jet interaction flow field produced on the M203 grenade launched projectile for various yaw and spin rates for fully viscous turbulent flow conditions. Turbulence was initially modeled using a traditional Reynolds-Averaged Navier-Stokes (RANS) approach. Although, this approach provided some detailed flow physics, it was found to be less accurate for this new class of unsteady flows associated with synthetic jets. In order to improve the accuracy of the numerical simulation, the predictive capability was extended to include a higher order hybrid RANS/LES (Large Eddy Simulation) approach [5,6]. This new approach computes the large eddies present in the turbulent flow structure and allowed the simulation to capture with high fidelity additional flow structures associated the synthetic jet interactions in a time-dependent fashion. Modeling of azimuthally placed synthetic micro-jets required tremendous grid resolution, highly specialized boundary conditions for the jet activation, and the use of advanced hybrid LES approach permitting local resolution of the unsteady



turbulent flow with high fidelity. The addition of yaw and spin while the projectile is subjected to the pulsating micro-jets rendered predicting forces and moments a major challenge. The Department of Defense high performance computing modernization office selected this research as a *grand challenge project* and provided the massive computational resources required by these unsteady time-accurate simulations. The new capability has been demonstrated and this technology has recently been successfully applied to the self-correcting projectile for infantry operations (SCORPION) program.

## COMPUTATIONAL METHODOLOGY

The complete set of three-dimensional (3-D) time-dependent Navier-Stokes equations [7] is solved in a time-accurate manner for simulations of unsteady synthetic jet interaction flow field on the M203 grenade launched projectile with spin. The 3-D time-dependent Reynolds-averaged Navier-Stokes (RANS) equations are solved using the finite volume method [8]:

$$\frac{\partial}{\partial t} \int_V \mathbf{W} dV + \oint [\mathbf{F} - \mathbf{G}] \cdot d\mathbf{A} = \int_V \mathbf{H} dV \quad (1)$$

where  $\mathbf{W}$  is the vector of conservative variables,  $\mathbf{F}$  and  $\mathbf{G}$  are the inviscid and viscous flux vectors, respectively,  $\mathbf{H}$  is the vector of source terms,  $V$  is the cell volume, and  $A$  is the surface area of the cell face.

Second-order discretization was used for the flow variables and the turbulent viscosity equations. Two-equation [9] and higher order hybrid RANS/LES [6] turbulence models were used for the computation of turbulent flows. The hybrid RANS/LES approach based on Limited Numerical Scales (LNS) is well suited to the simulation of unsteady flows and contains no additional empirical constants beyond those appearing in the original RANS and LES sub-grid models. With this method a regular RANS-type grid is used except in isolated flow regions where denser, LES-type mesh is used to resolve critical unsteady flow features. The hybrid model transitions smoothly between an LES calculation and a cubic k- $\epsilon$  model, depending on grid fineness. A somewhat finer grid was placed around the body, and near the jet, the rest of the flow field being occupied by a coarser, RANS-like mesh. Dual time-stepping was used to achieve the desired time-accuracy. In addition, special jet boundary conditions were developed and used for numerical modeling

of synthetic jets. Grid was actually moved to take into account the spinning motion of the projectile.

## PROJECTILE GEOMETRY AND COMPUTATIONAL GRID

The projectile used in this study is a 1.8-caliber ogive-cylinder configuration (see Figure 2). Here, the primary interest is in the development and application of CFD techniques for accurate simulation of projectile flow field in the presence of unsteady jets. The first step here was to obtain converged solution for the projectile without the jet. Converged jet-off solution was then used as the starting condition for the computation of time-accurate unsteady flow field for the projectile with synthetic jets. The jet locations on the projectile are shown in Figure 3. The jet conditions were specified at the exit of the jet for the unsteady (sinusoidal variation in jet velocity) jets. The jet conditions specified include the jet pressure, density and velocity components. Numerical computations have been made for these jet cases at subsonic Mach numbers,  $M = 0.11$  and  $0.24$  and at angles of attack,  $\alpha = 0^\circ$  to  $4^\circ$ . The jet width was  $0.32$  mm, the jet slot half-angle was  $18^\circ$ , and the peak jet velocities used were  $31$  and  $69$  m/s operating at a frequency of  $1000$  Hz.

A computational grid expanded near the vicinity of the projectile is shown in Figure 4. Grid points are clustered near the jet as well as the boundary layer regions to capture the high gradients flow regions. The computational grid has  $211$  points in the streamwise direction,  $241$  in the circumferential direction, and  $80$  in the normal direction. The unsteady simulation took thousands of hours of CPU time on Silicon Graphics Origin and IBM SP3 computers running with  $16$ – $24$  processors.

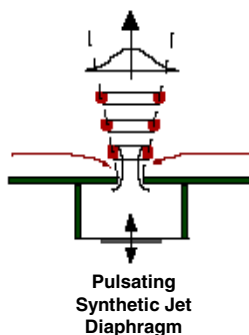


Figure 1. Schematic of a synthetic jet.

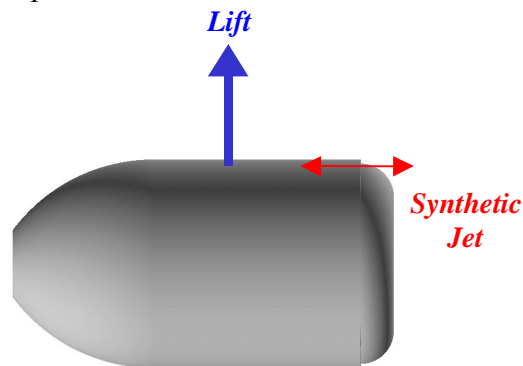


Figure 2. Projectile geometry.

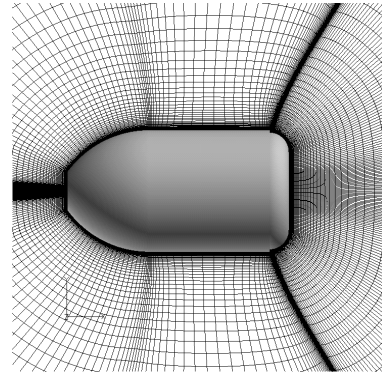
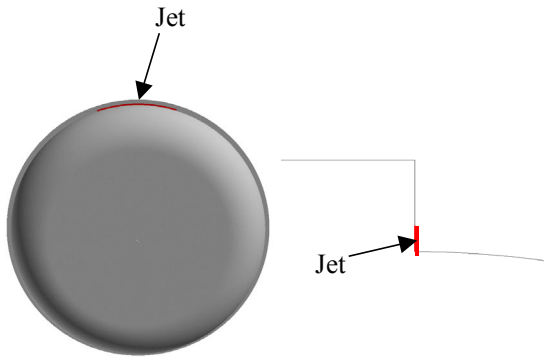


Figure 3. Aft-end geometry showing the jet location.

Figure 4. Computational grid near the projectile.

## RESULTS

Time-accurate unsteady numerical computations using advanced viscous Navier-Stokes methods were performed to predict the flow field and aerodynamic coefficients on both a non-spinning and a spinning projectile. Limited experimental data [11,12] exists only for the non-spinning case and was used to validate the unsteady CFD results.

### Non-spinning Projectile Case

3-D unsteady CFD results were obtained at a subsonic Mach number of 0.11 and several angles of attack from  $0^\circ$  to  $4^\circ$  using both RANS and the hybrid RANS/LES approaches. These 3-D unsteady CFD results have provided fundamental understanding of fluid dynamics mechanisms associated with the interaction of the unsteady synthetic jets and the projectile flow fields. Many flow field solutions resulting from the simulation of multiple spin cycles and, hence, a large number of synthetic jet operations, were saved at regular intermittent time-intervals to produce movies to gain insight into the physical phenomenon resulting from the synthetic jet interactions. The unsteady jets were discovered to break up the shear layer coming over the step in front of the base of the projectile. It is this insight that was found to substantially alter the flow field (making it unsteady) both near the jet and in the wake region that in turn produced the required forces and moments even at zero degree angle-of-attack (level flight). Time-accurate velocity magnitude contours (Figures 5 and 6) confirm the unsteady wake flow fields arising from the interaction of the synthetic jet with the incoming free stream flow at Mach = .11.

Figure 7 shows the particles emanating from the jet and interacting with the wake flow making it highly unsteady. More importantly, the break up of the shear layer is clearly evidenced by the particles clustered in regions of flow gradients or vorticity (evident in computed pressure contours, Figure 8). Verification of this conclusion is provided by the excellent agreement between the predicted (solid line) and measured [11] (solid symbols) values of the net lift force due to the jet (Figure 9). The net lift force ( $F_y$ ) was determined from the actual time histories of the highly unsteady lift force (an example shown in Figure 10 for various angles of attack) resulting from the jet interaction at zero degree angle of attack and computed with the new hybrid RANS/LES turbulence approach.

### Spinning Projectile Case

In this case, the projectile (40mm grenade) spins clockwise at a rate of 67 Hz looking from the front (see Figure 11). The jet actuation corresponds to one-fourth of the spin cycle from  $-45^\circ$  to  $+45^\circ$  with zero degree being the positive y-axis. The jet is off during the remaining three-fourths of the spin cycle. The unsteady CFD modeling

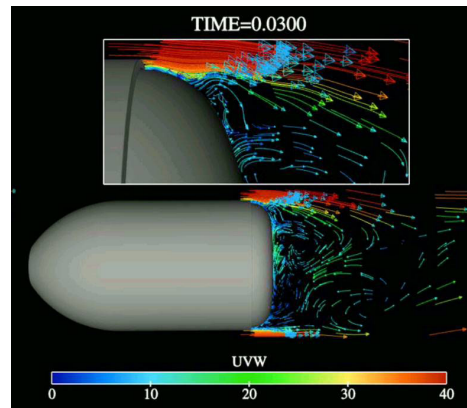
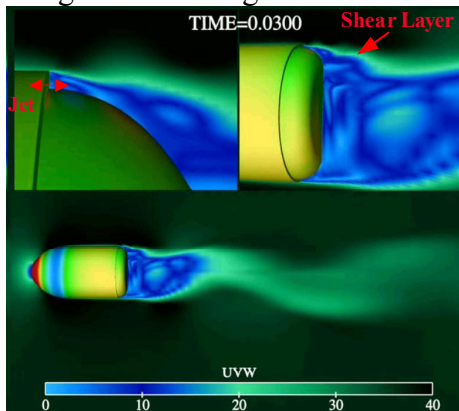


Figure 5. Velocity magnitudes,  $M=0.11$ ,  $\alpha = 0^\circ$ . Figure 6. Velocity vectors,  $M = 0.11$ ,  $\alpha = 0^\circ$ .

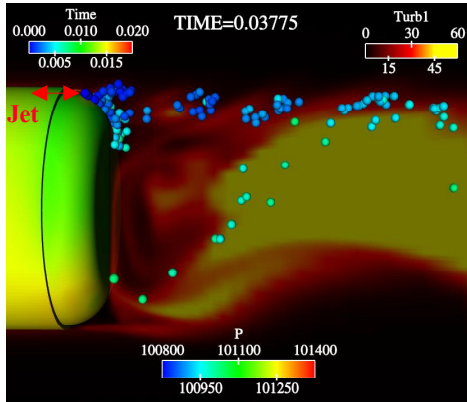


Figure 7. Particle Traces,  $M = 0.11$ ,  $\alpha = 0^\circ$ .

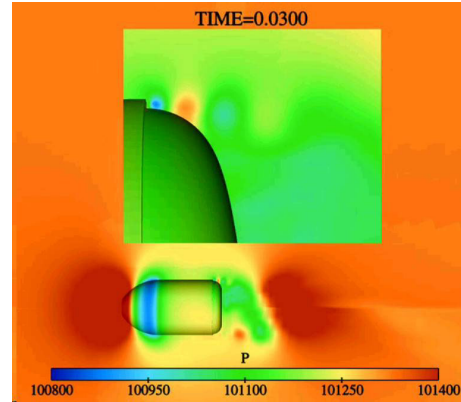


Figure 8. Computed Pressures,  $M = 0.11$ ,  $\alpha = 0^\circ$ .

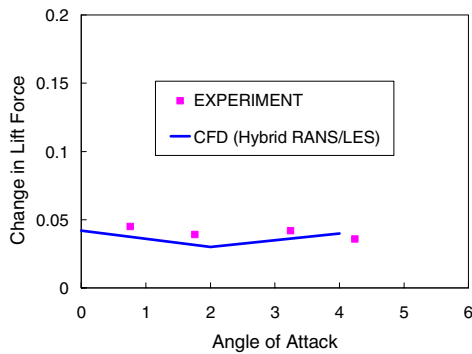


Figure 9. Computed change in lift force due to jet at various angles of attack,  $M = 0.11$ .

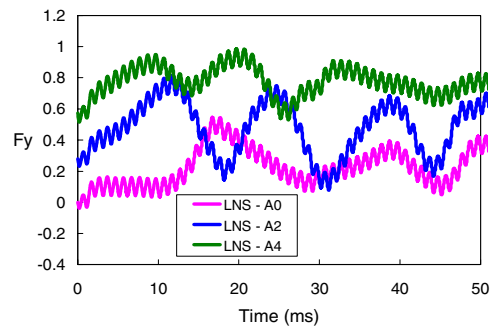


Figure 10. Computed lift force for various angles of attack,  $M = 0.11$ .

required about 600 time steps to resolve a full spin cycle. For the part of the spin cycle when the jet is on, the 1000 Hz jet operated for approximately for four cycles. The actual computing time for one full spin cycle of the projectile was about 50 hours using 16 processors (ie. 800 processor-hours) on an IBM SP3 system for a mesh size about four million grid points. Multiple spin cycles and, hence, a large number of synthetic jet operations were required to reach the desired periodic time-accurate unsteady result. As will be seen later, some cases were run for as many as 60 spin cycles requiring over 48,000 processor hours of computer time. Computed particle traces (colored by velocity) emanating from the jet into the wake are shown in Figure 12 at a given instant in time for  $M = 0.24$  and  $\alpha = 0^\circ$ . The particle traces emanating from the jet interact with the wake

flow making it highly unsteady. It shows the flow in the base region to be asymmetric due to the interaction of the unsteady jet.

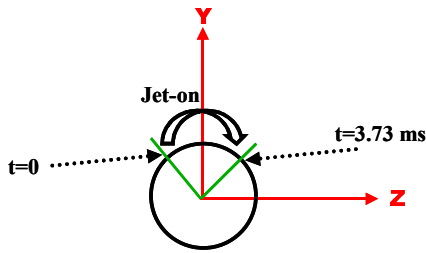


Figure 11. Schematic showing the jet actuation in One spin cycle (view from the front or the nose).

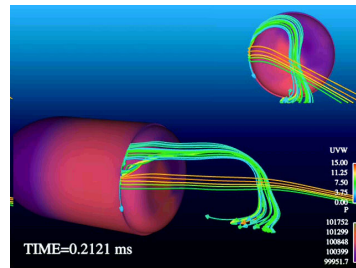


Figure 12. Computed particle traces colored by velocity, jet-on,  $M = 0.24$ ,  $\alpha = 0^\circ$ .

The computed surface pressures from the unsteady flow fields were integrated to obtain the aerodynamic forces and moments [13] from both unsteady RANS (URANS) as well as the hybrid RANS/LES approach referred here as the LNS. The jet-off unsteady RANS calculations were first obtained and the jets were activated beginning at time,  $t = 28$  ms. Computed normal or lift force ( $F_Y$ ) and side force ( $F_Z$ ) were obtained for two different jet velocities,  $V_j = 31$  and  $69$  m/s and are shown here in Figure 13 for the bigger jet as a function of time. These computed results clearly indicate the unsteady nature of the flow field. When the jet is turned off, the levels of these forces drop to the same levels prior to the jet activation corresponding to the jet-off wake flow. Figure 14 shows the comparison of the predicted lift force using URANS and LNS models. The URANS result clearly shows when the jet is on and when it is off during the spin cycle.

As described earlier, the comparisons for the non-spinning cases showed that the level of lift force predicted by LNS closely matched the data. Here, the addition of spin as well as the jet actuation for part of the spin cycle, further complicates the analysis of the CFD results with LNS. The level of oscillations seen is quite large and the effect of the jet cannot be easily seen in the instantaneous time histories of the unsteady forces and moments. To get the net effect of the jet, unsteady computations were run for many spin cycles of the projectile with the synthetic jets. The CFD results are plotted over only one spin cycle, each subsequent spin cycle was superimposed and a time-averaged result was then obtained over one spin cycle. In all these cases, the jet is on for one-fourth of the spin cycle (time,  $t=0$  to  $3.73$  ms) and is off for the remainder (three-fourths) of the spin cycle.

Figures 15 through 16 show the time-averaged results over a spin cycle. Figure 15 shows the computed lift force again averaged over many spin cycles for the peak jet velocity of 69 m/s. The jet effect can clearly be seen when the jet is on ( $t=0$  to 3.73 ms) even after 5 or 10 spin cycles. The net lift is about 0.17 Newton due to the jet actuation and seems to have converged after 20 spin cycles. For the remainder of the spin cycle, the jet is off; however, the effect of the jet on the wake still persists and this figure shows that lift force (mean value .07 Newton) is still available. Figure 16 shows the computed averaged lift force after 50 and 60 spin cycles for jet velocities 31 and 69 m/s, respectively. It clearly shows that the larger jet producing larger lift force than the smaller jet when the jet is activated. The lift force can be integrated over time to obtain the impulse. Figure 17 shows the impulse obtained from the lift force as a function of the spin cycles for both jets. As seen here, in both cases it takes about 30 to 40 spin cycles before the impulse asymptotes to a fixed value.

The computed lift force along with other aerodynamic forces and moments, directly resulting from the pulsating jet, were then used in a trajectory analysis [14] and the synthetic micro-jet produced a substantial change in the cross range and thus, provided the desired course correction for the projectile to hit its target.

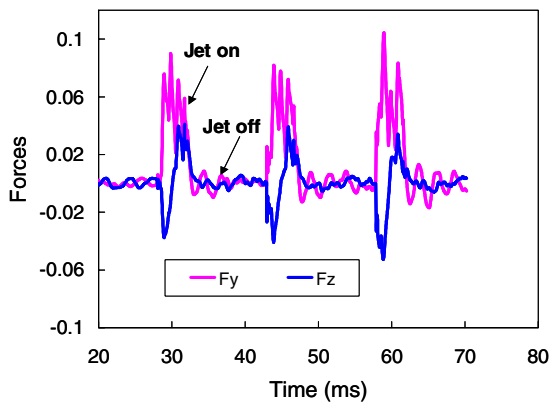


Figure 13. Computed lift and side forces, URANS,  $M = 0.24$ ,  $V_j = 69$  m/s,  $\alpha = 0^\circ$ .

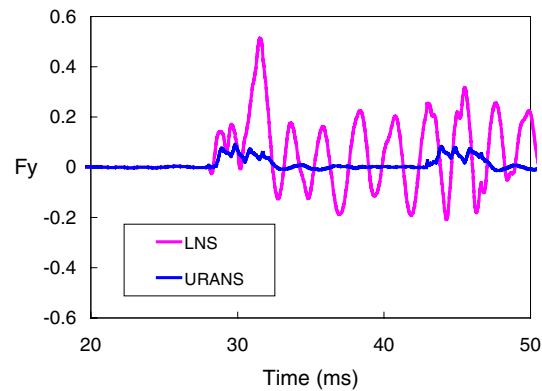


Figure 14. Computed lift forces, URANS and LNS  $M = 0.24$ ,  $V_j = 69$  m/s,  $\alpha = 0^\circ$ .

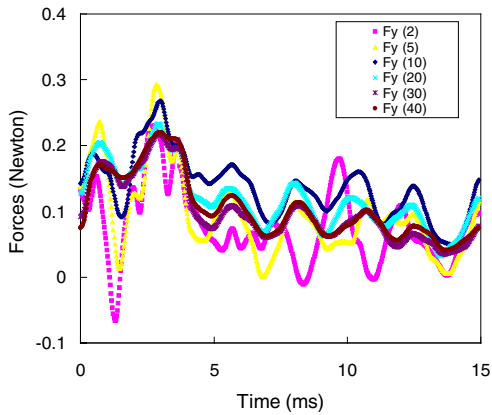


Figure 15. Computed lift force over many spin cycles, LNS,  $V_j = 69$  m/s,  $M = 0.24$ ,  $\alpha = 0^\circ$ , Spin = 67 Hz.

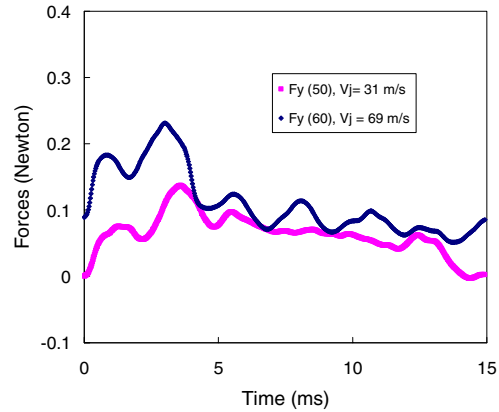


Figure 16. Computed lift force over many spin cycles for different jet velocities, LNS,  $M = 0.24$ ,  $\alpha = 0^\circ$ , Spin = 67 Hz.

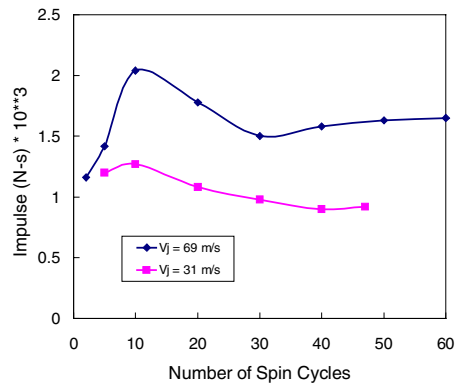


Figure 17. Impulse from the lift force vs. spin cycles for two jet velocities,  $M = 0.24$ ,  $\alpha = 0^\circ$ , Spin = 67 Hz

## CONCLUDING REMARKS

This paper describes a computational study undertaken to determine the aerodynamic effect of tiny synthetic jets as a means to provide the control authority needed to maneuver a projectile at low subsonic speeds. Computed results have been obtained for a subsonic projectile for both non-spinning and spinning cases using time-accurate Navier-Stokes computational technique and advanced turbulence models. The unsteady jet in the case of the subsonic projectile is shown to substantially alter the flow field both near the jet



and the base region that in turn affects the forces and moments even at zero degree angle of attack. The predicted changes in lift force due to the jet match well with the experimental data for various angles of attack from  $0^\circ$  to  $4^\circ$  in the hybrid RANS/LES computations. For the spinning projectile cases, the net *time-averaged* results obtained over the time period corresponding to one spin cycle clearly showed the effect of the synthetic jets on the lift as well as the side forces. The jet interaction effect is clearly seen when the jet is on during the spin cycle. However, these results show that there is an effect on the lift force (although reduced) for the remainder of the spin cycle *even* when the jet is off. This is a result of the wake effects that persist from one spin cycle to another. The impulse obtained from the predicted forces for both jets seem to asymptote after 30 spin cycles.

The results have shown the potential of CFD to provide insight into the jet interaction flow fields and provided guidance as to the locations and sizes of the jets to generate the control authority required to maneuver a spinning munition to its target with precision. This research represents a major increase in capability for determining the unsteady aerodynamics of munitions in a *new area of flow control* and has shown that micro-adaptive flow control with tiny synthetic jets can provide an *affordable* route to *lethal* precision-guided infantry weapons.

## REFERENCES

1. J. Sahu, K. R. Heavey, and E. N. Ferry, "Computational Fluid Dynamics for Multiple Projectile Configurations", *Proceedings of the 3<sup>rd</sup> Overset Composite Grid and Solution Technology Symposium*, Los Alamos, NM, October 1996
2. J. Sahu, K. R. Heavey, and C. J. Nietubicz, "Time-Dependent Navier-Stokes Computations for Submunitions in Relative Motion", *6<sup>th</sup> International Symposium on Computational Fluid Dynamics*, Lake Tahoe, NV, September 1995
3. B. L. Smith and A. Glezer, "The Formation and Evolution of Synthetic Jets." *Journal of Physics of Fluids*, vol. 10, No. 9, September 1998
4. M. Amitay, V. Kibens, D. Parekh, and A. Glezer, "The Dynamics of Flow Reattachment over a Thick Airfoil Controlled by Synthetic Jet Actuators", AIAA Paper No. 99-1001, January 1999
5. S. Arunajatesan and N. Sinha, "Towards Hybrid LES-RANS Computations of Cavity Flowfields", AIAA Paper No. 2000-0401, January 2000
6. P. Batten, U. Goldberg and S. Chakravarthy, "Sub-grid Turbulence Modeling for Unsteady Flow with Acoustic Resonance", AIAA Paper 00-0473, *38th AIAA Aerospace Sciences Meeting*, Reno, NV, January 2000
7. T. H. Pulliam and J. L. Steger, "On Implicit Finite-Difference Simulations of Three- Dimensional Flow" *AIAA Journal*, vol. 18, no. 2, pp. 159–167, February 1982

8. O. Peroomian, S. Chakravarthy, S. Palaniswamy, and U. Goldberg, "Convergence Acceleration for Unified-Grid Formulation Using Preconditioned Implicit Relaxation." AIAA Paper 98-0116, 1998
9. U. Goldberg, O. Peroomian, and S. Chakravarthy, "A Wall-Distance-Free K-E Model With Enhanced Near-Wall Treatment" *ASME Journal of Fluids Engineering*, Vol. 120, 457-462, 1998
10. P. Batten, P., U. Goldberg and S. Chakravarthy, "Sub-grid Turbulence Modeling for Unsteady Flow with Acoustic Resonance", AIAA Paper 00-0473, 38th AIAA Aerospace Sciences Meeting, Reno, NV, January 2000.
11. C. Rinehart, J. M. McMichael, and A. Glezer, "Synthetic Jet-Based Lift Generation and Circulation Control on Axisymmetric Bodies." AIAA Paper No. 2002-3168
12. McMichael, J., GTRI, Private Communications.
13. J. Sahu, "Unsteady Numerical Simulations of Subsonic Flow over a Projectile with Jet Interaction" AIAA Paper 2003-1352, Reno, NV, 6-9 January 2003
14. M. Costello, Oregon State University, Private Communications.



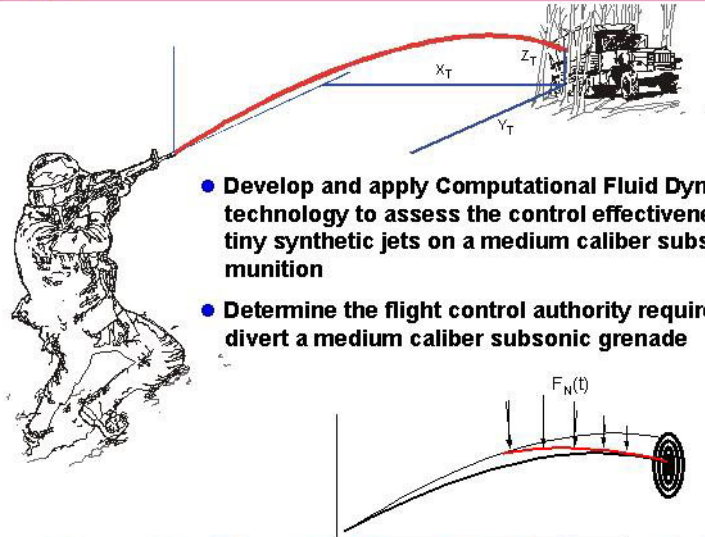
## OUTLINE



- INTRODUCTION
- COMPUTATIONAL TECHNIQUES
  - ◆ FULL 3D UNSTEADY NAVIER-STOKES
  - ◆ RANS
  - ◆ HYBRID RANS/LES TURBULENCE MODELING
- RESULTS
  - ◆ UNSTEADY SYNTHETIC JETS
    - 3-D (non-spinning)
    - 3-D (spinning)
- CONCLUDING REMARKS



# Objectives

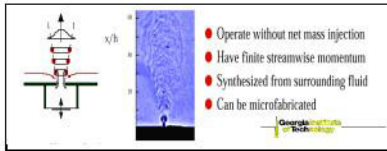


- Develop and apply Computational Fluid Dynamics technology to assess the control effectiveness of tiny synthetic jets on a medium caliber subsonic munition
- Determine the flight control authority required to divert a medium caliber subsonic grenade

*Demonstrate Adequate Aerodynamic Steering Forces using Flow Control*



# Synthetic Jets for Subsonic Projectile Control



- Operate without net mass injection
- Have finite streamwise momentum
- Synthesized from surrounding fluid
- Can be microfabricated

- Predict and characterize the unsteady nature of the synthetic jet interaction flow field produced on spinning projectiles for infantry operations by time accurate CFD computations
- Modeling of azimuthally placed synthetic jets require increased grid resolution coupled with large demands of special boundary conditions and hybrid RANS/LES CFD approach.

### Issues

- Examine the utility of synthetic jets
- Can synthetic jets be used to provide control authority ?
- Identify critical flow features
- Jet interaction with free stream flow
- Unsteady turbulent computations
- Time accuracy



Flow Solver: CFD++ by Metacomp  
 Freestream Velocity: 37, 82 m/s  
 Angle of Attack: 0 to 4 degrees

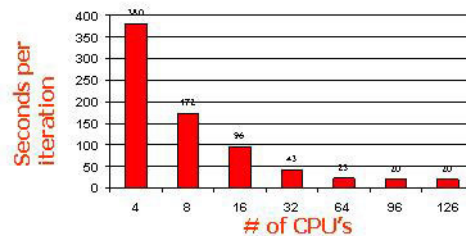


## CFD++ CODE



- Unified Grid (structured, unstructured, overset)
- Unified Physics (incompressible to hypersonic, advanced topology-free higher-order turbulence models including LES and hybrid RANS/LES)
- Up to second order spatial accuracy and up to fourth order accuracy in time
- Finite-Volume Framework
- Fast convergence to steady state
- Fast computation of unsteady flows
- Dual time-stepping

- 2.65 Million Hexahedral Grid
- 7 Equations, k- $\epsilon$  Turbulence model
- Multigrid turned on



SGI is Configured with 128x300Mhz R.12K CPUS



## Hybrid RANS/LES Model (LNS)



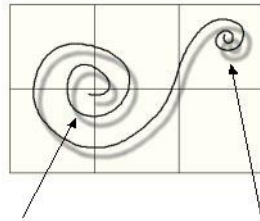
- RANS:
  - High level of empiricism
  - Additional resolution does not aid fidelity
  - Unsteady behavior may be suppressed altogether
- LES:
  - Expensive
  - Uncertainties in near-wall modelling
  - More suitable for unsteady flows
- LNS: Limited Numerical Scales
  - Combines best features of RANS and LES according to the local mesh resolution



## Hybrid RANS/LES Model (LNS)



- Small (unresolvable) scales are modelled via sub-grid stress model
- Large (resolvable) scales are computed directly



**Resolvable eddy**

**Unresolvable eddy**

$$L^{\Delta} = 2\max(\Delta x, \Delta y, \Delta z)$$

$$\text{DNS} \Rightarrow L^{\Delta} = O(\text{Kolmogorov})$$

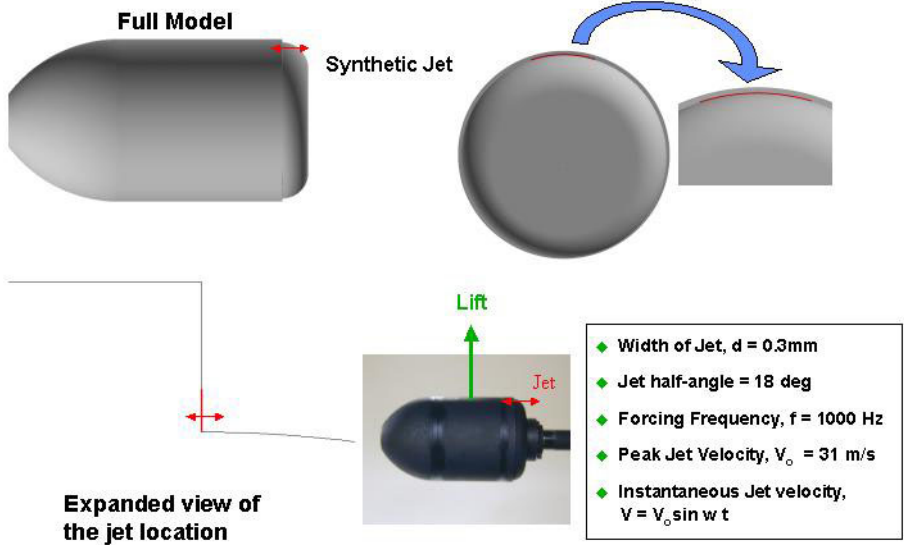
$$\text{LES} \Rightarrow L^{\Delta} = 10 \times O(\text{Kolmogorov})$$



**RESULTS**  
**Non-Spinning Case**



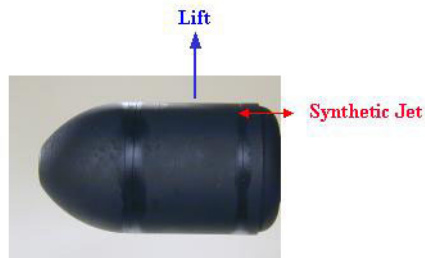
**Projectile Model and Jet details**  
**Non-Spinning Case**



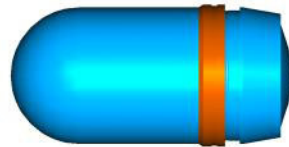




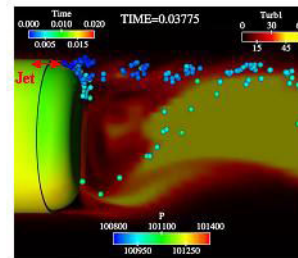
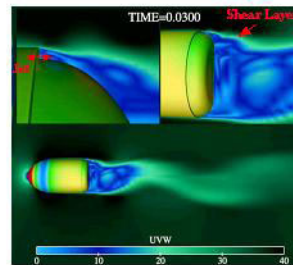
## Synthetic Jets for Subsonic Projectile Control



40mm HE/PD M203

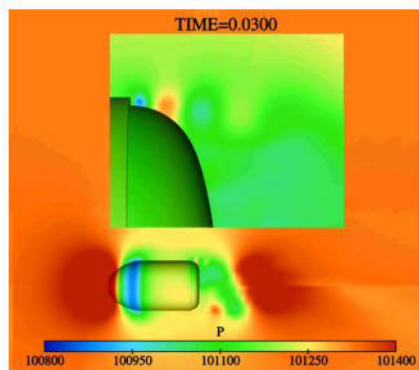


- Investigate "placement" of jets for
  - lift control to improve accuracy
  - drag reduction to extend range

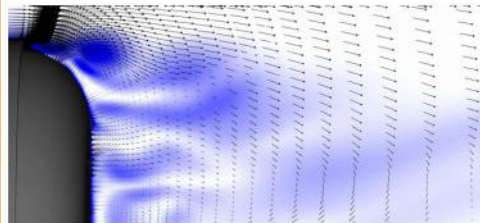


## Computed Pressure and Vorticity Contours

$U = 37 \text{ m/s}$ ,  $\alpha = 0^\circ$ ,  $U_{jet} = 31 \text{ m/s}$ ,  $f = 1000 \text{ Hz}$



Pressure Contours



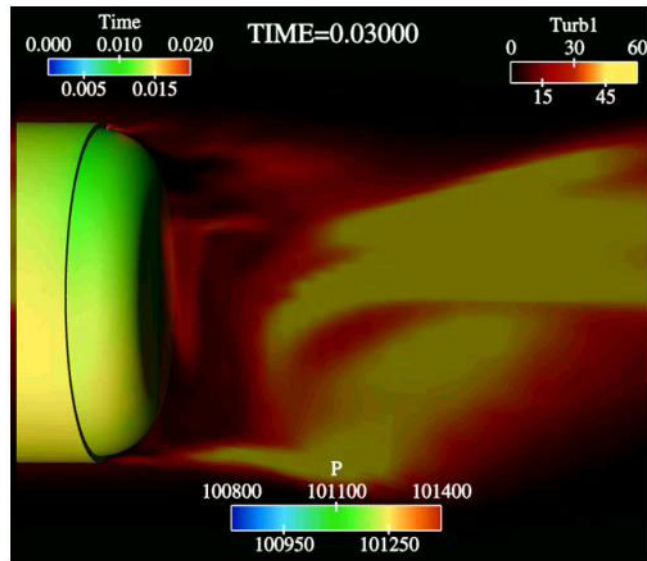
Vorticity Contours





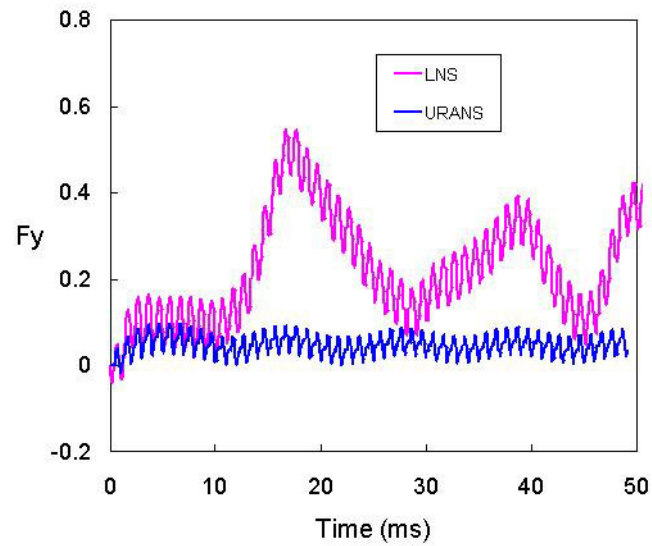
## Computed Particle Traces

$U = 37 \text{ m/s}$ ,  $\alpha = 0^\circ$ ,  $U_{\text{jet}} = 31 \text{ m/s}$ ,  $f = 1000 \text{ Hz}$



## LIFT FORCE

$U = 37 \text{ m/s}$ ,  $\alpha = 0^\circ$ ,  $U_{\text{jet}} = 31 \text{ m/s}$ ,  $f = 1000 \text{ Hz}$

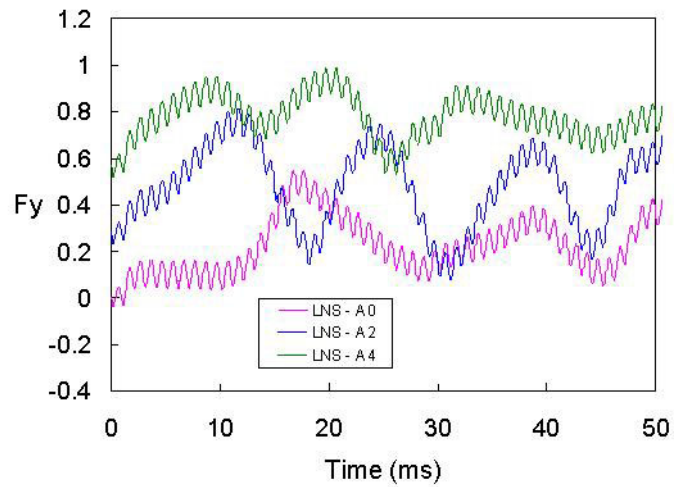




## LIFT FORCE Synthetic Jet Unsteady CFD



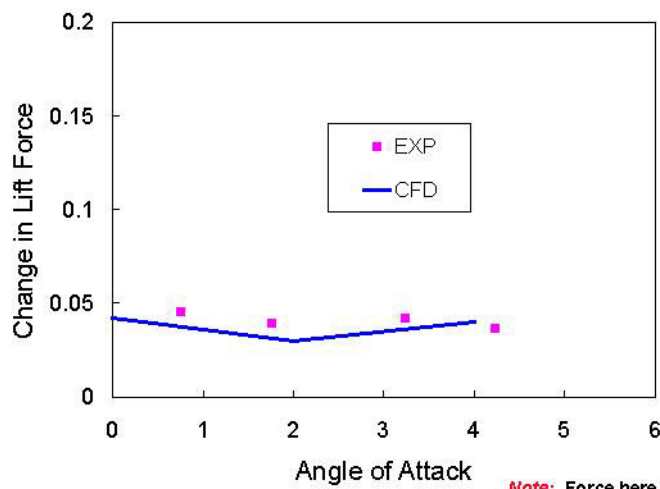
$U = 37\text{m/s}$ ,  $U_{\text{jet}} = 31\text{ m/s}$ ,  $f = 1000\text{ Hz}$



## CHANGE IN LIFT FORCE DUE TO JET Non-Spinning Case



$U = 37\text{m/s}$ ,  $U_{\text{jet}} = 31\text{ m/s}$ ,  $f = 1000\text{ Hz}$



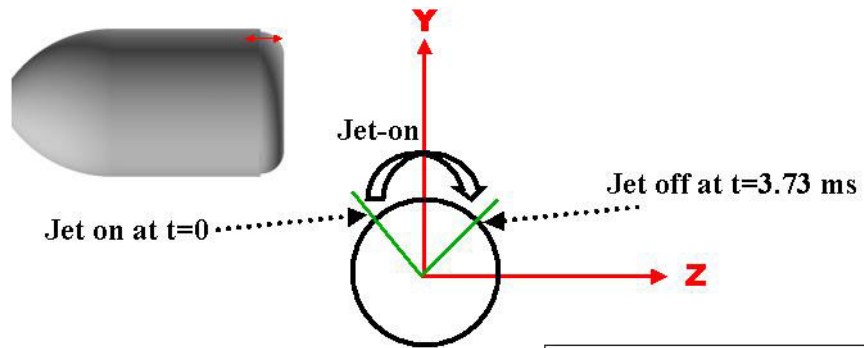
**Note:** Force here is in lbf  
Experiment conducted at GTRI



## RESULTS Spinning Case



### Coordinate System and Schematic Spinning Case (Spin = 67 Hz)



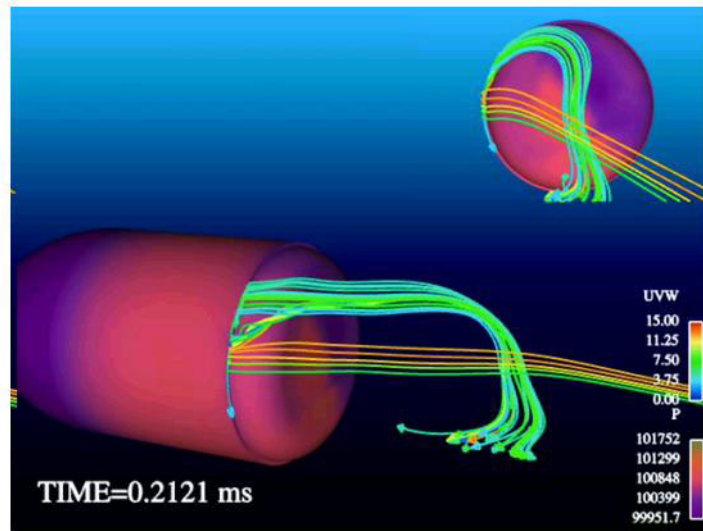
Looking from the nose

- ◆ Width of Jet,  $d = 0.3\text{mm}$
- ◆ Jet half-angle = 18 deg
- ◆ Forcing Frequency,  $f = 1000\text{ Hz}$
- ◆ Peak Jet Velocity,  $V_o = 31,69\text{ m/s}$
- ◆ Instantaneous Jet velocity,  
 $V = V_o \sin \omega t$



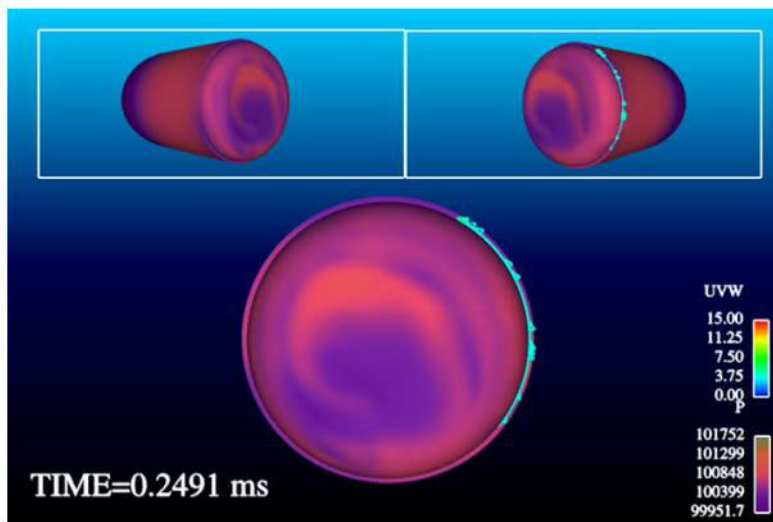
### Instantaneous Velocity Vectors

$U = 82 \text{ m/s}$ ,  $\alpha = 0^\circ$ ,  $U_{jet} = 31 \text{ m/s}$ ,  $f = 1000 \text{ Hz}$ ,  $\text{Spin} = 67 \text{ Hz}$



### Velocity Vector Visualization

$U = 82 \text{ m/s}$ ,  $\alpha = 0^\circ$ ,  $U_{jet} = 31 \text{ m/s}$ ,  $f = 1000 \text{ Hz}$ ,  $\text{Spin} = 67 \text{ Hz}$



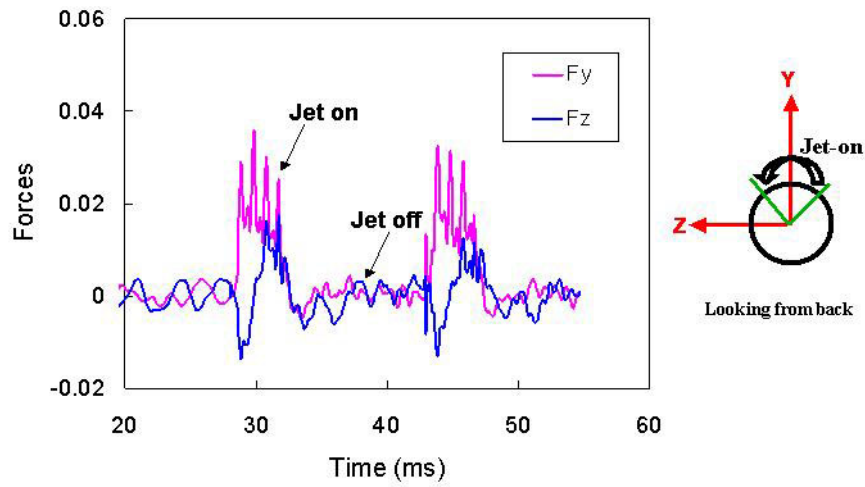
AoA=0



## AERODYNAMIC FORCES Synthetic Jet Unsteady CFD Using RANS



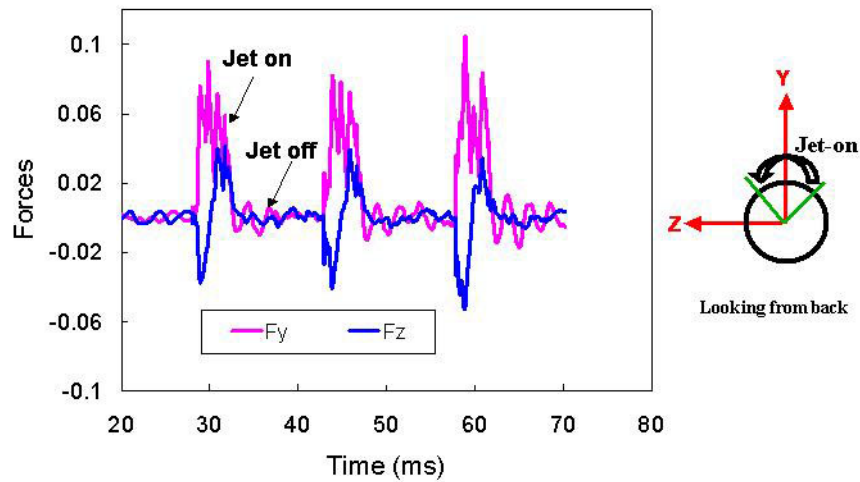
40mm shell,  $U = 82\text{m/s}$ , Jet velocity =  $31\text{ m/s}$ ,  $f=1000\text{ Hz}$ , Spin =  $67\text{ Hz}$



## AERODYNAMIC FORCES Synthetic Jet Unsteady CFD Using RANS



40mm shell,  $U = 82\text{m/s}$ , Jet velocity =  $69\text{ m/s}$ ,  $f=1000\text{ Hz}$ , Spin =  $67\text{ Hz}$

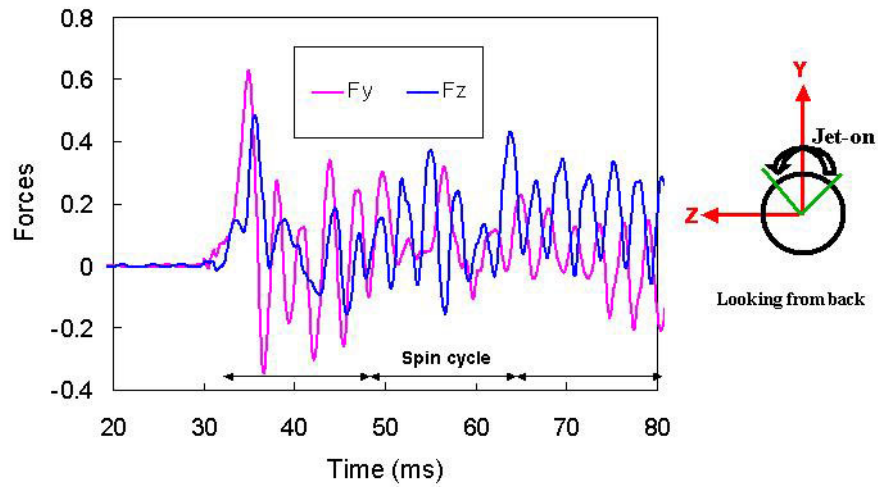




## AERODYNAMIC FORCES Synthetic Jet Unsteady CFD using LNS



40mm shell,  $U = 82\text{m/s}$ , Jet velocity =  $31\text{ m/s}$ ,  $f=1000\text{ Hz}$ , Spin =  $67\text{ Hz}$

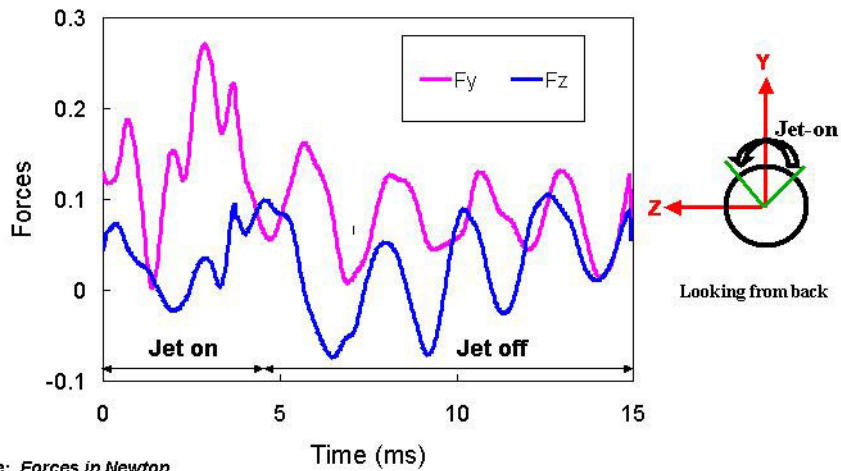


## Aerodynamic Forces Synthetic Jet Unsteady CFD, Spinning Case



Unsteady LNS Computations (superimposed over 4 spin cycles)

40mm,  $U = 82\text{ m/s}$ ,  $\alpha = 0$ ,  $V_j = 69\text{ m/s}$ , Spin =  $67\text{ Hz}$



Note: Forces in Newton



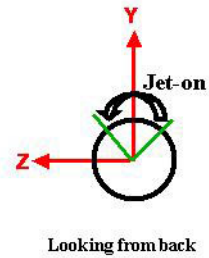
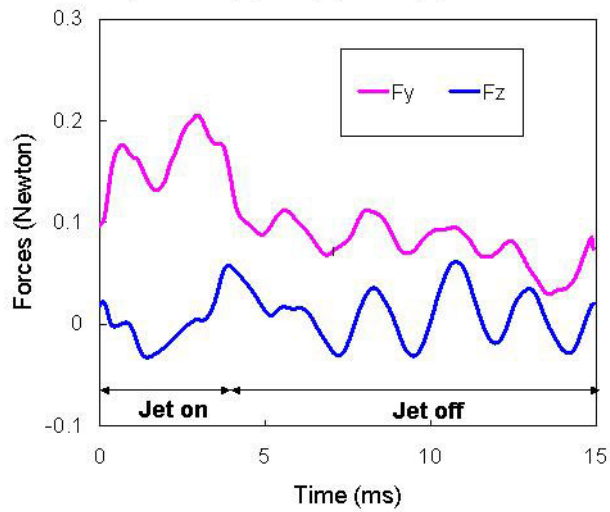


# AERODYNAMIC FORCES

## Synthetic Jet Unsteady CFD using LNS

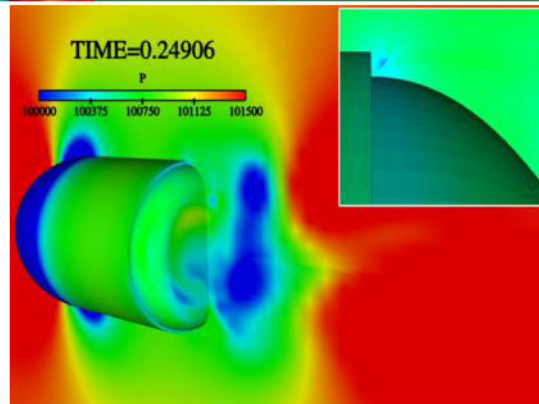
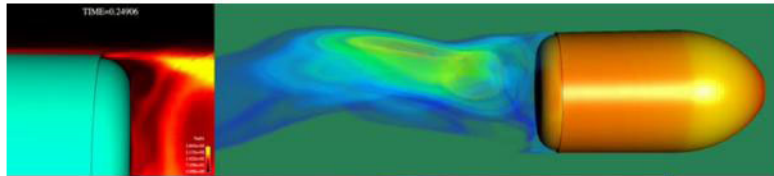


Unsteady LNS Computations (superimposed over 24 spin cycles)  
40mm,  $U = 82$  m/s,  $\alpha = 0^\circ$ ,  $V_j = 69$  m/s, Spin = 67 Hz



## Flow Visualization

$U = 82$  m/s,  $\alpha = 0^\circ$ ,  $U_{jet} = 31$  m/s,  $f = 1000$  Hz, Spin = 67 Hz



Pressure  
Contours

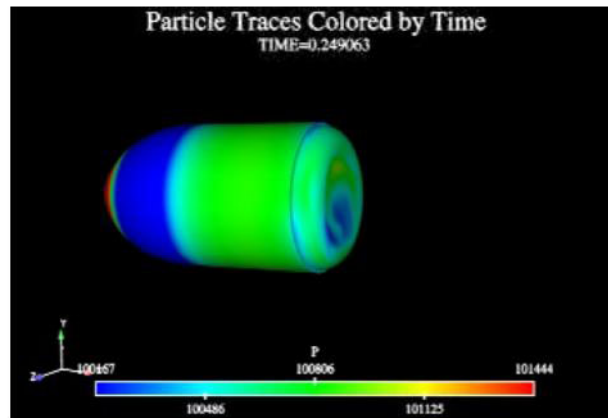
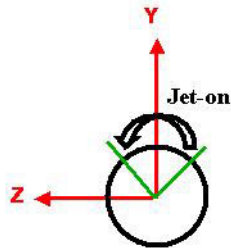


## Particle Traces Visualization

$U = 82 \text{ m/s}$ ,  $\alpha = 0^\circ$ ,  $U_{jet} = 31 \text{ m/s}$ ,  $f = 1000 \text{ Hz}$ ,  $\text{Spin} = 67 \text{ Hz}$



For one Spin Cycle



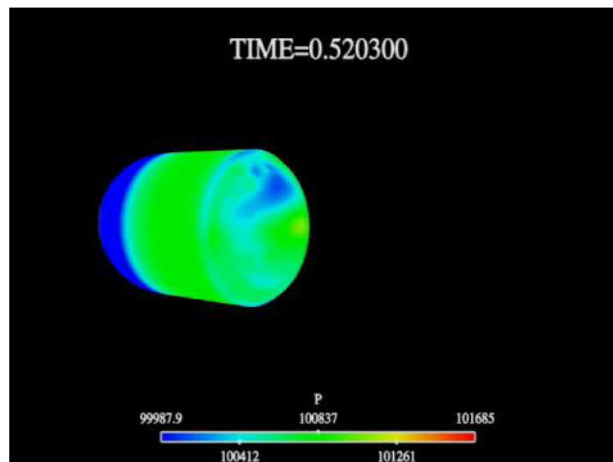
## Particle Traces Visualization

$U = 82 \text{ m/s}$ ,  $\alpha = 0^\circ$ ,  $U_{jet} = 31 \text{ m/s}$ ,  $f = 1000 \text{ Hz}$ ,  $\text{Spin} = 67 \text{ Hz}$



For Two Spin Cycles

1<sup>st</sup> cycle: **Red**, 2<sup>nd</sup> cycle: **Blue**

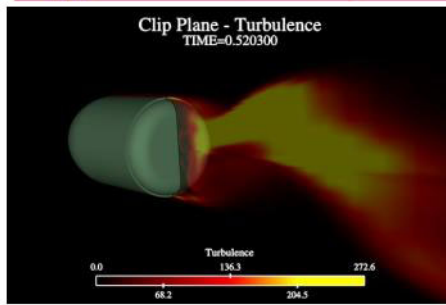






## Particle Traces Visualization

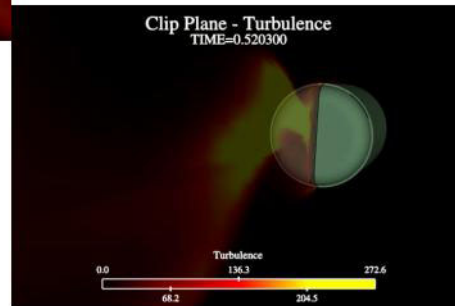
$U = 82 \text{ m/s}$ ,  $\alpha = 0^\circ$ ,  $U_{jet} = 31 \text{ m/s}$ ,  $f = 1000 \text{ Hz}$ ,  $\text{Spin} = 67 \text{ Hz}$



For Two Spin Cycles

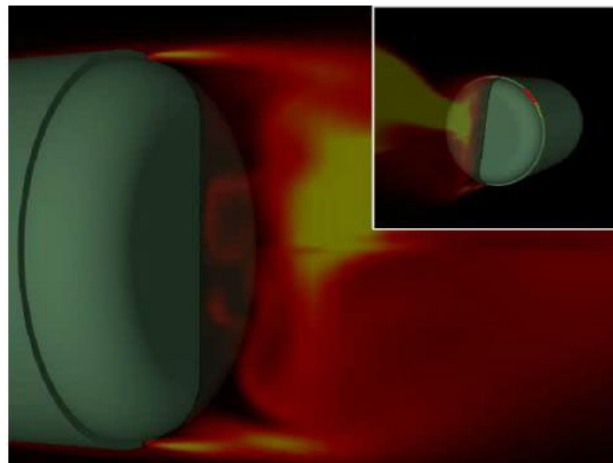
1<sup>st</sup> cycle: **Red**

2<sup>nd</sup> cycle: **Blue**



## Particle Traces Visualization

$U = 82 \text{ m/s}$ ,  $\alpha = 0^\circ$ ,  $U_{jet} = 31 \text{ m/s}$ ,  $f = 1000 \text{ Hz}$ ,  $\text{Spin} = 67 \text{ Hz}$





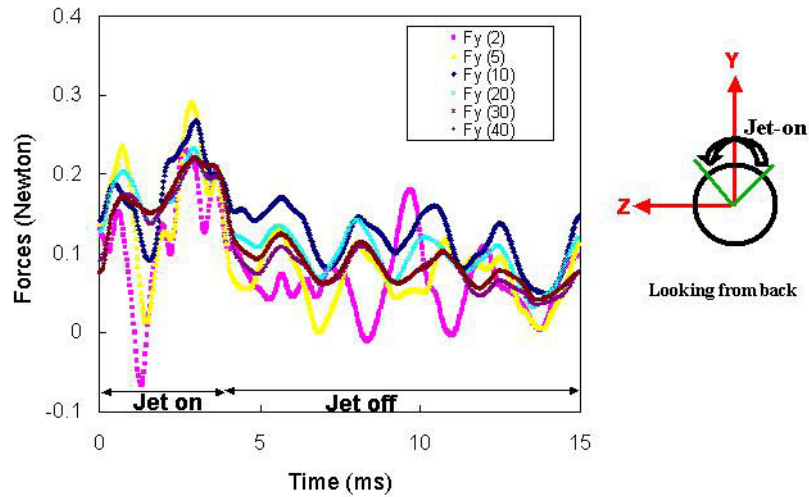
# AERODYNAMIC FORCES

## Synthetic Jet Unsteady CFD using LNS



Unsteady LNS results superimposed over many spin cycles

$U = 82 \text{ m/s}$ ,  $\text{Alpha} = 0$ ,  $V_j = 69 \text{ m/s}$ ,  $\text{Spin} = 67 \text{ Hz}$



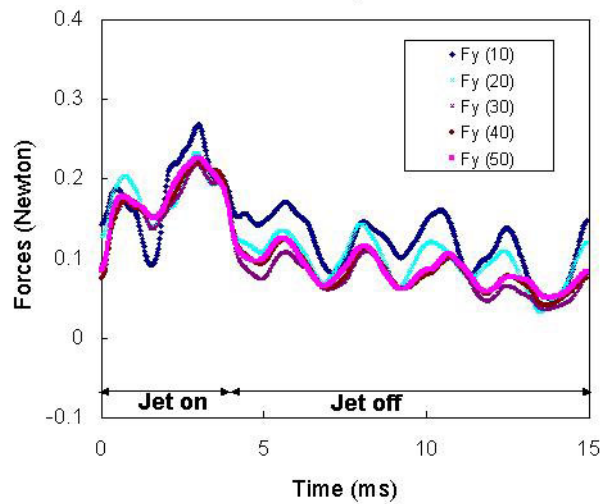
# AERODYNAMIC FORCES

## Synthetic Jet Unsteady CFD using LNS



Unsteady LNS results superimposed over many spin cycles

$U = 82 \text{ m/s}$ ,  $\text{Alpha} = 0$ ,  $V_j = 69 \text{ m/s}$ ,  $\text{Spin} = 67 \text{ Hz}$



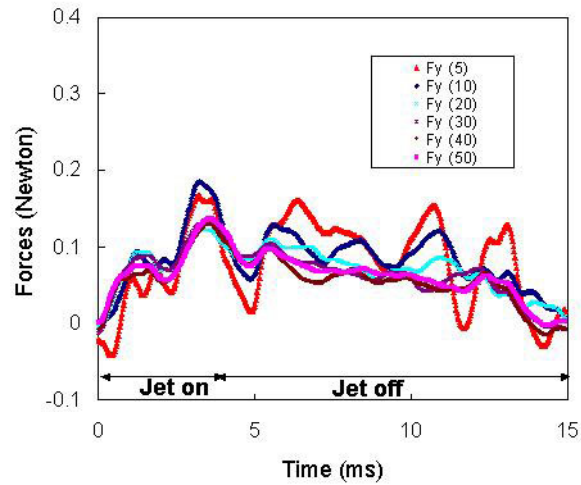


## AERODYNAMIC FORCES Synthetic Jet Unsteady CFD using LNS



Unsteady LNS results superimposed over many spin cycles

$U = 82 \text{ m/s}$ ,  $\text{Alpha} = 0$ ,  $V_j = 31 \text{ m/s}$ ,  $\text{Spin} = 67 \text{ Hz}$

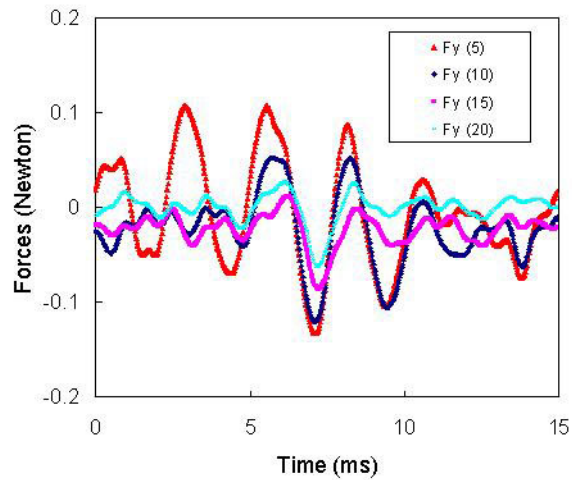


## AERODYNAMIC LIFT FORCES Unsteady Jet-Off CFD using LNS



Unsteady LNS jet-off results superimposed over many spin cycles

$U = 82 \text{ m/s}$ ,  $\text{Alpha} = 0$ ,  $\text{Spin} = 67 \text{ Hz}$



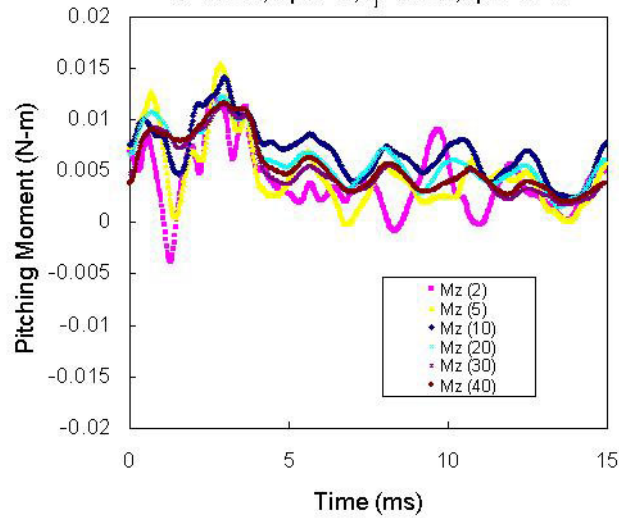


## AERODYNAMIC PITCHING MOMENT Synthetic Jet Unsteady CFD using LNS



Unsteady LNS results superimposed over many spin cycles

$U = 82 \text{ m/s}$ ,  $\alpha = 0$ ,  $V_j = 69 \text{ m/s}$ , Spin = 67 Hz

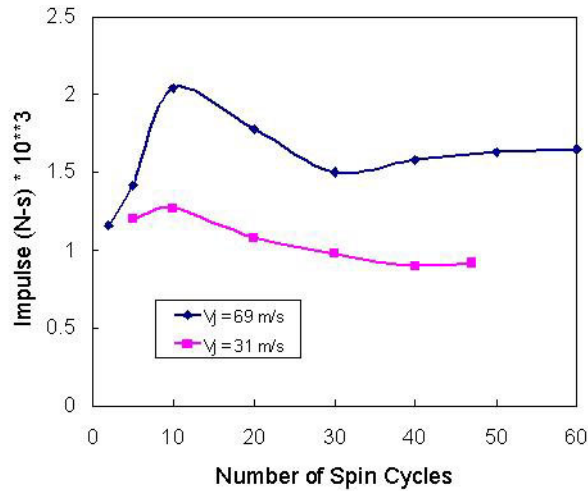


## AERODYNAMIC IMPULSE Synthetic Jet Unsteady CFD using LNS



Unsteady LNS Jet-On CFD, Impulse (from  $F_y$ ) Vs. Spin cycles

40 mm,  $U = 82 \text{ m/s}$ ,  $\alpha = 0$ , Spin = 67 Hz

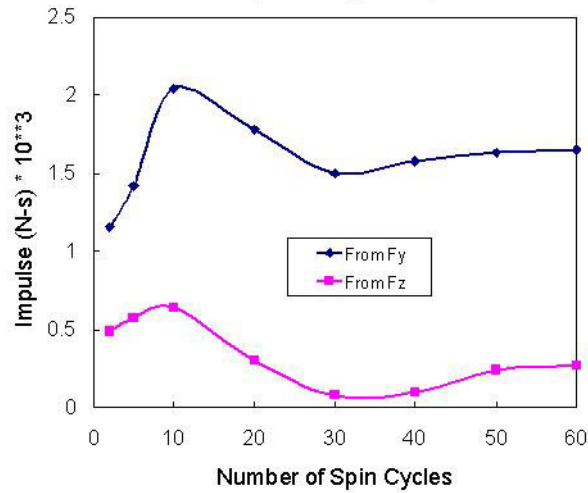




## AERODYNAMIC IMPULSE Synthetic Jet Unsteady CFD using LNS



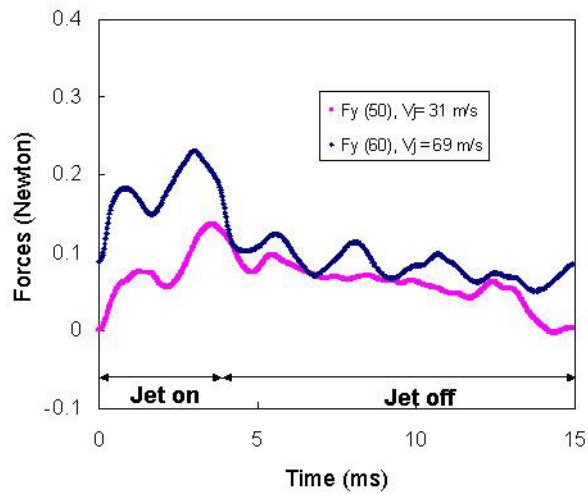
Unsteady LNS Jet-On CFD, Impulse Vs. Spin cycles  
40mm,  $U = 82$  m/s,  $V_j = 69$  m/s,  $\alpha = 0$ , Spin = 67 Hz



## AERODYNAMIC LIFT FORCES Synthetic Jet Unsteady CFD using LNS



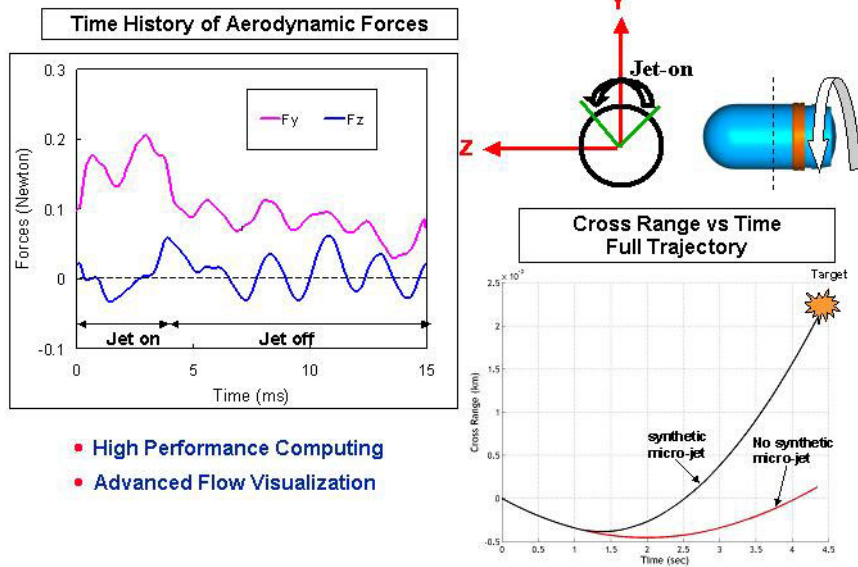
Unsteady LNS jet-on results superimposed over many spin cycles  
 $U = 82$  m/s,  $\alpha = 0$ , Spin = 67 Hz





# Synthetic Jets for Subsonic Projectile Control

## Spinning Case



## CURRENT AND FUTURE EFFORTS



- Couple CFD with 6-DOF and Controls
- Compute jet divert authority with the coupled method
- Different Base Configurations
- Other Applications
- Supersonic Flows





## CONCLUDING REMARKS



- **Development and application of advanced CFD predictive technologies are critical for synthetic jet subsonic flow control.**
- **Synthetic jets involve new issues such as time accuracy, turbulence modeling, and jet interaction associated with unsteady aerodynamics.**
- **RANS/LES Hybrid model predictions are better than RANS.**
- **Predicted change in lift force due to the jet match well with limited data (non-spinning cases). For the spinning case, some lift force is produced even when the jet is off during the spin cycle.**
- **Time-accurate CFD modeling of synthetic jets can provide critical flow field information and physical insight for control of maneuvering munitions at low subsonic speeds.**



## Acknowledgments



- Sukumar Chakravarthy, METACOMP Technologies, Thousand Oaks, CA.
- Rick Angelini, U. S. Army Research Laboratory Major Shared Resource Center (ARL MSRC) Scientific Visualization Team Leader.
- This work was partially supported by DARPA. Also, thanks to the ARL MSRC, Aberdeen Proving Ground, Maryland and DoD High Performance Computing Modernization Office (HPCMO) for providing the computer resources critical to the success of this grand challenge project.





# DESIGN AND FABRICATION OF CIRCULATION CONTROL TEST ARTICLES

*Kenneth P. Burdges*

Novatek, Inc.

## ABSTRACT

This paper is an overview of a decade of experience in Computer Aided Design (CAD) and Computer Aided Machining (CAM) of test articles for wind tunnel and road testing of Circulation Control (CC) vehicles. Internal flow design features, such as sub-plenums and instrumentation are discussed. Techniques for slot adjustment mechanisms are described as well as difficulties in machining thin edges for blowing slots. Test articles include low speed and transonic wind tunnel models, racecar models and wings. Application of CC for drag reduction of heavy trucks and sport utility vehicles is included to illustrate some current design problems.

## **Informal Integrated Design approach-- cost, timing, control**

Design of a test article is driven by a number of conflicting requirements. Cost to design and build the test article is usually very important, second only to timing. The project must be completed in time to meet a test schedule. The approach used at Novatek, Inc. is to integrate the design and fabrication in an informal shop environment, where the designer may program and machine parts. Drawings are informal, with additional information easily available from the CAD system. The CAD system model is the documentation for the model if any future design information is needed. Of course, traditional engineering drawings can be made from the CAD model if required.

Another feature of the design approach used at Novatek, Inc. is total control of the design details. The design can be tailored to the available machines, tooling and fixtures. This has several advantages; no time is lost in approval of a design change by the customer, unless it impacts the test plan objectives. Time and money is not expended in ordering special cutters or other tooling.

## **CAD System is the Key**

Novatek, Inc uses the CAD program CADKEY for design and CNC programming. This program is one of the mid priced systems that have CNC machining included. This program uses solids, surfaces and entity construction. The wind tunnel model can be built using any of these methods of construction. Utilities are included to convert the model to surfaces for CNC programming. This cad system is base on the ACIS computational engine, so importation of customer files usually goes smoothly if they can provide a SAT format configuration. Other formats can be imported, such as IGES, STEP, and STL.

## **Design to build**

It is important to design a test apparatus with careful consideration of how it will be built. Rarely is the customer not driven by cost considerations. Use of CNC machines reduces machining time dramatically, but requires more engineering time. Surface finish requirements can make a large difference in model cost. A good example is finish of internal passages. Polishing an internal passage can be a very time consuming process that improves airflow. However, most testing setups have more than enough air pressure. Total pressure must be measured just ahead of the blowing slot so internal losses due to not polishing internal passages are of no consequence.

## **Material Selection**

Choice of material is important. Novatek uses aluminum for critical aerodynamic surfaces, but mahogany works fine for non-critical aerodynamic surfaces, reducing material and labor cost significantly. Steel is not required for most low speed models unless thin sections or welding is required.

## **Radius choices**

Choice of radius for internal passages can make a significant difference in machining time. If a small radius is chosen that requires a tool change and cutting with a small cutter that is prone to deflection, the machining and programming cost rise quickly, usually for a very small increase in passage area. Additionally, using radius values available with standard cutters avoids ordering special tools or making multiple passes. Concave radius cuts made with common radius tools can be finished in one pass of the cutter. Convex surfaces are the place to use a non standard radius because hand finishing a convex surface is much easier than a concave. This choice often occurs in designing convergent slots where a good surface is required.

## **Three Axis Model**

It is very desirable to keep the model so that parts can be machined on a 3-axis machine, since most machines are three axis. A simple choice of tilting the direction of a group of screws can require a new setup with considerable increase in time to build the parts. This does not mean that curved surfaces have to be avoided. Extra setups should be avoided.

## **Internal instrumentation**

Models with blowing slots require the total pressure be measured at the slot exit. Since the accelerating flow at the slot does not suffer any total pressure losses from the plenum chamber ahead of the slot, Measuring the total pressure with a "U" shaped total pressure tube in the plenum ahead of the exit slot is a very

satisfactory method. Only a few pressure tubes are required to make this measurement, so it has been found that the tubes can be routed through the air supply ducts, avoiding a lot of machine time to cut separate passages. The tubes must be attached in a secure manner using a suitable epoxy. Often a hand-drilled hole through the dividing partition between the primary plenum and secondary plenum will provide a very stable holder.

### Internal Model Design

Design of air passages in a model must consider two somewhat opposing aerodynamic effects. The air must not lose too much energy because of undesirable internal flow paths, but the air must be evenly distributed to the blowing slots. It is necessary to force uniform distribution of the air by restricting the flow area so that the primary air plenum is uniformly pressurized and the velocity reduced. The air then flows through the restriction in a uniform manner into a secondary plenum, where additional uniformity is achieved.

The primary air passage must be larger in cross-section than the maximum exit slot area to prevent choking of the internal flow. The internal passages should have twice the cross-sectional area as the maximum exit slot area. Internal flow passages for blowing are machined into the models, by dividing the area where the air passages are located into upper and lower surfaces, so that each part can be machined on the inside and outside. This normally poses a registration requirement so some feature must be included in the design to allow the part to be correctly located back on the mill to machine the other surface.

Figure 1 shows a 2-D airfoil with leading edge and trailing edge blowing plus a central passage for pressure tap tubing. Air for the aft blowing slot enters through

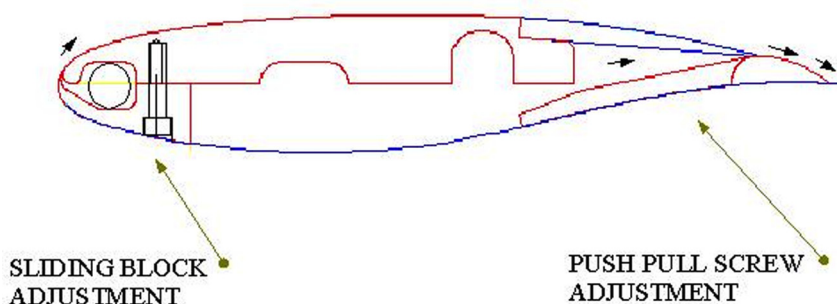


Figure 1 Two-dimensional airfoil with leading edge and trailing edge blowing

the oval shaped channel. A series of fore to aft passages allow the air to turn and enter the aft secondary plenum before exiting the blowing slot. Adjustment of the slot height is accomplished by a series of push pull screws. In this case, the push pull screws were a span-wise row of screws alternating between setscrews to push the slot open and flat head screws for pull to hold the slot closed.

The leading edge blowing shown in this figure illustrates an alternative to the push pull slot adjustment. The lip on the leading edge blowing is nearly vertical, so sliding the lower surface block fore and aft makes the adjustment. The hold down bolt is in an elongated slot. Placing a feeler gage between the sliding block and the body of the airfoil made adjustment of the slot fairly easy. An O-ring strip controlled leakage of the plenum. The original design had large variations in exit jet velocity. A tube with numerous holes in the aft wall was added to provide even distribution of the air to the slot.

### Design for Success

A successful test requires an understanding of the overall objectives and aerodynamic flow field to integrate blowing and the air supply into the model. Figure 2 shows a Formula 1 style car model where blowing was applied to several areas of the car. This type car is very close to the ground and that part of the flow field was under study, so it was necessary to mount the car upside down against the top of the wind tunnel to provide undisturbed flow between the model and the “ground.” The model was mounted to a balance by a tube inside of a non-metric fairing. This tube also provided the external compressed air for the blowing.



Figure 2 Formula 1 car with CC blowing on bottom plate

A similar mount was used on the heavy truck model shown in Figure 3. This model has the unusual use of blowing to reduce the drag due to separated flow of the basic box shape. Blowing slots were provided on the leading edge of the trailer to reduce separation on the blunt corners. Adjustment of the blowing slots used a row of alternating push pull screws.

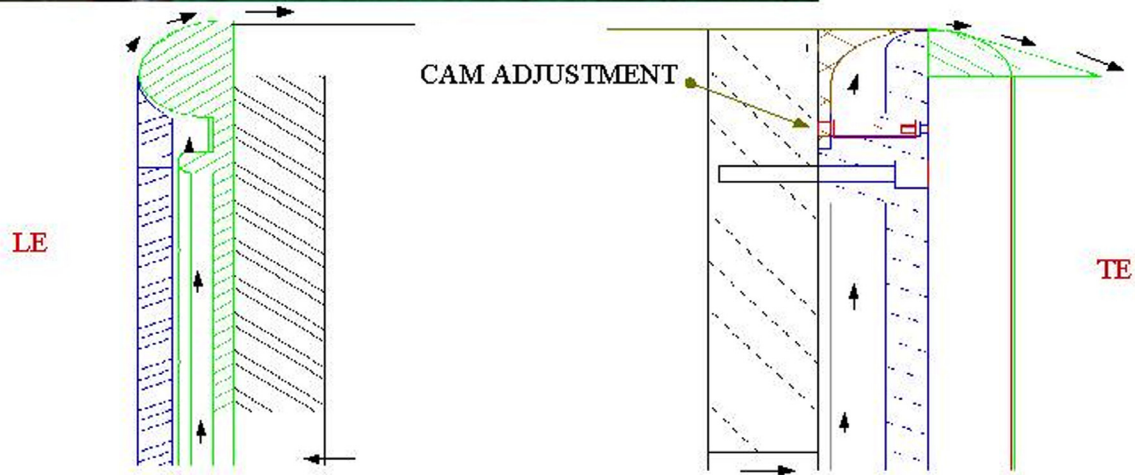
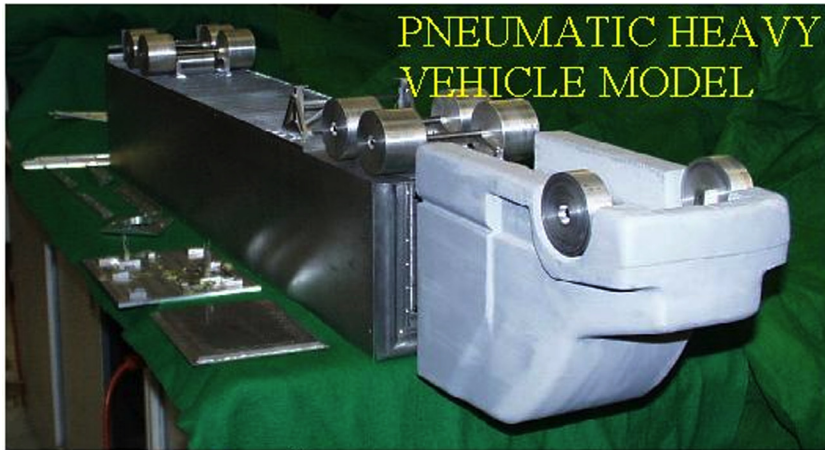


Figure 3 CC application to heavy truck

Blowing slots were used on the trailing edge of the box by providing rounded corners for the Coanda turning of the air from the slots to reduce the vehicle drag. In this case, a cam type adjustment was used. The cams were made by eccentric turning of aircraft bolts that had hex key in the end of the bolt.

Figure 4 shows the model in the wind tunnel mounted on the air supply pipe with a non-metric fairing. The complex flow field between the truck and the ground was an important part of the flow field under study. The wind tunnel boundary layer was re-energized by a blowing slot ahead of the truck model. The CAD model shown in the figure illustrates the complexity of the model.



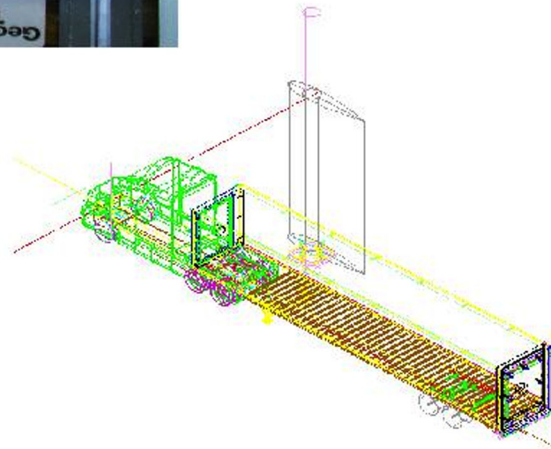
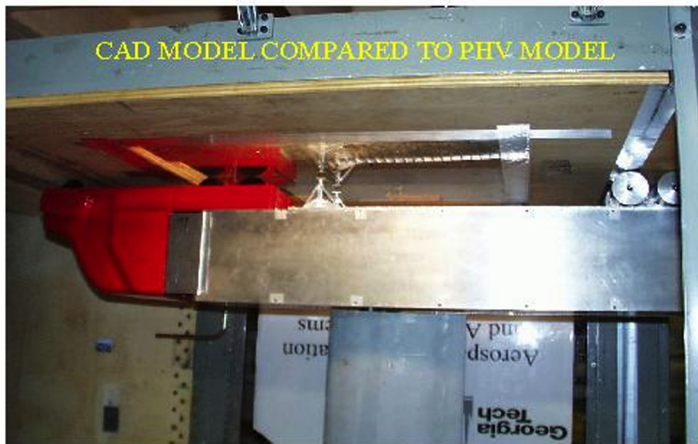


Figure 4 Comparison of CAD and PHV model

### Exit Slots on Compound Curved Surfaces

Figure 5 shows an application of blowing to reduce separated flow on a future car with all rounded surfaces. In this case, the blowing slot was achieved by the sliding block adjustment method. The Coanda turning was so effective that the flow would turn 180 degrees around the aft end of the car and blow all the way to the front of the car.



Figure 5 Futuristic Car with Aft CC (Sliding Block Adjustment)

## Thin Wings May Require Blowing Slots

Blowing for lift and pitching moment control was applied to a high-speed civil transport shown in Figure 6. This model has canards with trailing edge blowing. The canards could also vary pitch angle by matching the mount as a round tube with an o-ring seal. The wing has trailing edge blowing for increased lift with variations in flap angle. The leading edge has blowing at the hinge line of the leading edge droop. All of these blowing features were included in a wing that is only 1/4 an inch thick.



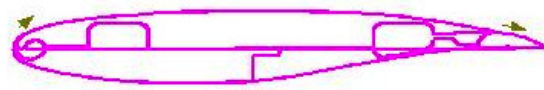
Figure 6 High-speed civil transport with CC blowing on canard TE, Wing TE, and Wing LE

## Propellers May Work With Blowing Jets

Figure 7 shows a model with the additional complexity of an electric motor and propeller. This model is a channel wing powered lift configuration. The propeller and nacelle can be mounted in longitudinal positions from  $X/C = 0.6$  to  $0.95$ . High amperage wires were routed inside of the 0.25-inch thick struts. The wing is a transonic design with constant chord in the channel. Trailing edge blowing is incorporated to enhance lift and slipstream deflection. Air channels for independent leading edge and trailing edge blowing of the outboard wing are provided. The outboard wing a blowing slot with push pull screw adjustment on the trailing edge. The trailing edge flap deflections are accomplished by machining a separate lower surface with the deflected flap. The leading edge blowing is adjusted using the sliding block method.



DUCT SECTION



OUTER WING SECTION

Figure 7 Channel wing with CC blowing on Channel TE, Outer Wing LE and TE

### Adjustable Slots on Cylindrical Shapes Require Segment

The adjustment of the trailing edge blowing in the channel is done with push pull screws. However, since the channel is a circle, the adjustment required segmenting the outer part (lower surface) into 8 pieces to accommodate circumferential growth as the slot was opened. A shim was placed in a slot on each segment to bridge the segment breaks and keep the plenum from leaking at the segment breaks.

### Full Scale Truck Requires Larger Plenum Chamber

Application of Coanda blowing to a full size heavy vehicle is illustrated in Figure 8. Some of the internal flow procedures developed for wind tunnel models could not be used on the full-scale vehicle, because the available air pressure is limited. In this case, aluminum sheet metal was used to build the ducts. The ducts were sized to provide plenty of flow area. The slots were adjusted by push pull screws in the adjustment blocks, shown in Figure 9. Total pressure was measured near the slot exit as shown in Figure 9. The supply air was provided by two 4650 CFM fans at 14.0 HG.





Figure 8 Pneumatic heavy vehicle (PHV) with TE blowing

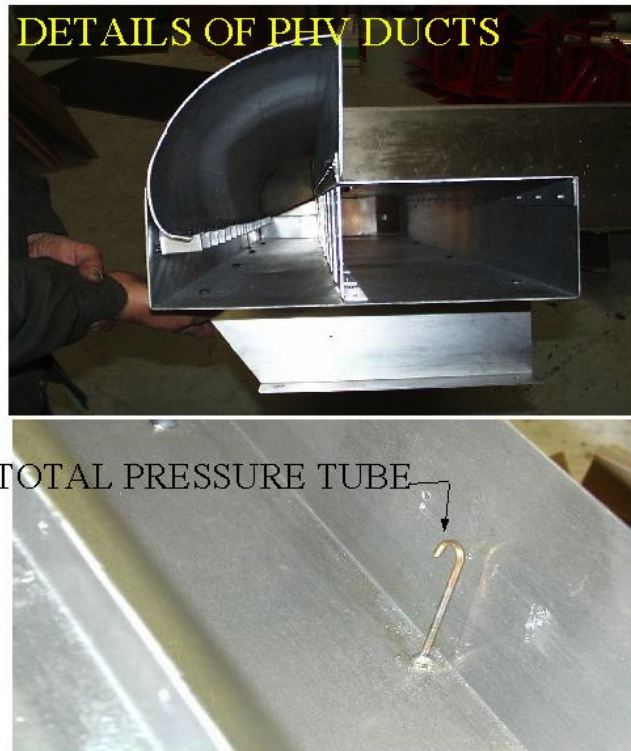


Figure 9 Details of ducts for PHV

## Effect of Plenum Pressure May Change Slot Geometry

Another unusual application of Coanda blowing is shown in Figure 10. This patented design used the pressure difference between the upper and lower surfaces of a wing to force air through a dense radiator. Since over 10 times the pressure differential is available for this configuration as compared to a conventional radiator system, a radiator with much more surface area can be used to increase the heat transfer. This was applied to a racecar that used the lift for down-force. The blowing plenum and slot was built from extrusions. The concept of dual plenum was used in this arrangement. Air entered through the round tube, flowed through the slot near the bottom into the secondary plenum ahead of the slot. Adjustment of the slot was made by pull only screws. However, the air pressure caused round tube to deflect aft. Horizontal screws had to be added to eliminate this unacceptable deflection.

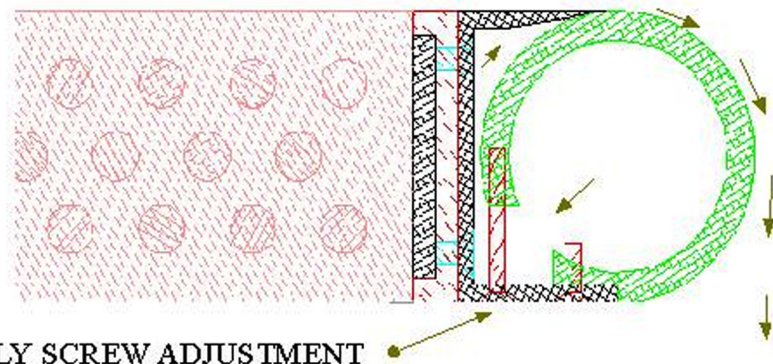
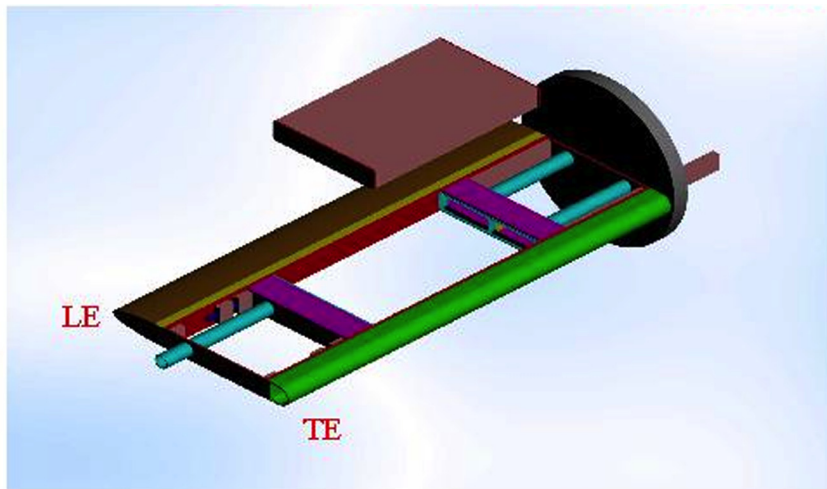


Figure 10 CC radiator

## Pulsed Blowing at Transonic Speeds

Proprietary pulsed blowing techniques were used on the weapons bay shown in Figure 11. The weapons bay is part of a new floor for the high Reynolds number

transonic/supersonic wind tunnel at GTRI. Model weapons were mounted in the weapons bay and automatically traversed out through the shear layer. The proprietary blowing system reduced the turbulence and noise in the weapons bay.

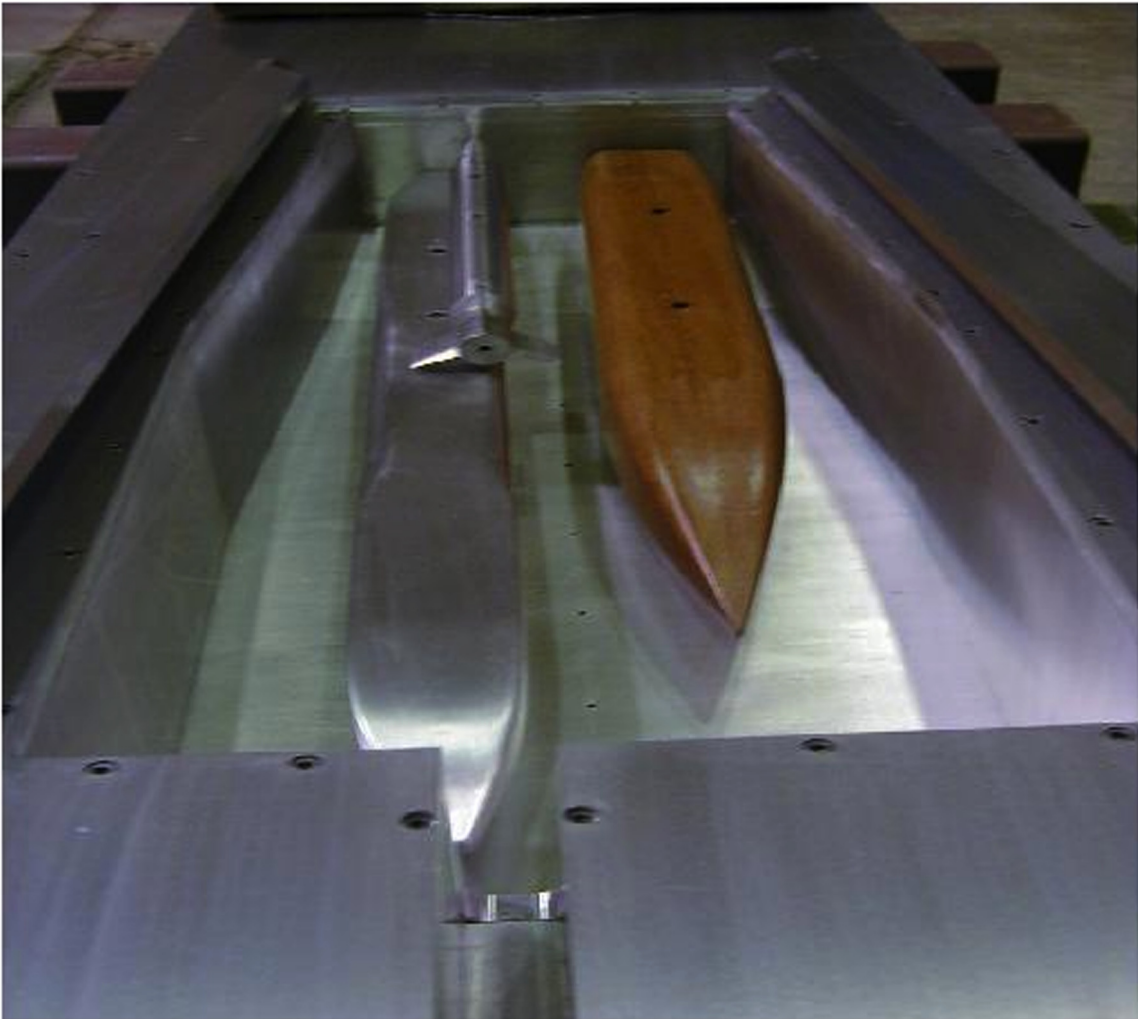


Figure 11 Transonic weapons bay with pulsed blowing (not shown)

### **Separation Control of Laser Portal**

Distortion of the view through a laser port at transonic and supersonic speeds is the subject of the test article shown in Figure 12. The test article is designed to inject a jet of air across the flat window in a manner that will reduce separation on the downwind side of the hemispherical shape. Since there is no curved surface, it was decided to inject the jet an angle half way between tangent to the sphere and the angle of the optical flat. This model was built using a CNC lathe to turn the complex internal shapes. Slot adjustment on this model is done by the sliding block technique. The central wall of the plenum can be moved by adding shim washers. The design slot gap was 0.005 for this model.



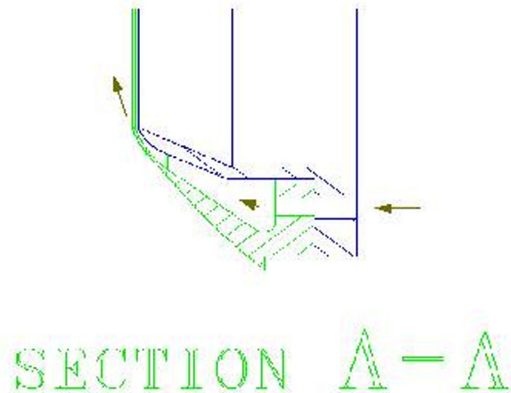


Figure 12 Laser portal with pneumatic separation control

## CONCLUSIONS

- Blowing jets have been applied to a wide variety of air and land vehicle configurations.
- Dual plenum air supply has been the most reliable method of establishing uniform flow at the blowing jet.
- Total pressure in the jet must be measured as close to the exit slot as possible, using a “U” shaped tube.
- Routing of jet instrumentation inside of the air supply channels is practical.
- Deflection of the slot geometry under pressure load can be significant.
- Push pull screws for slot adjustment is the best method.

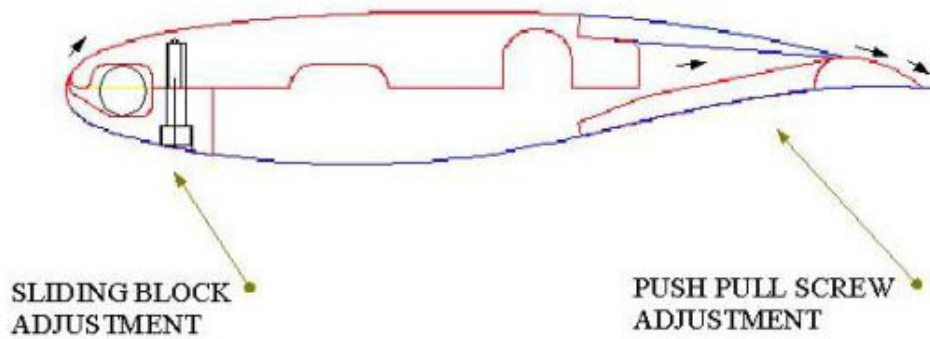
# DESIGN AND FABRICATION OF CIRCULATION CONTROL TEST ARTICLES

**KENNETH P. BURDGES**

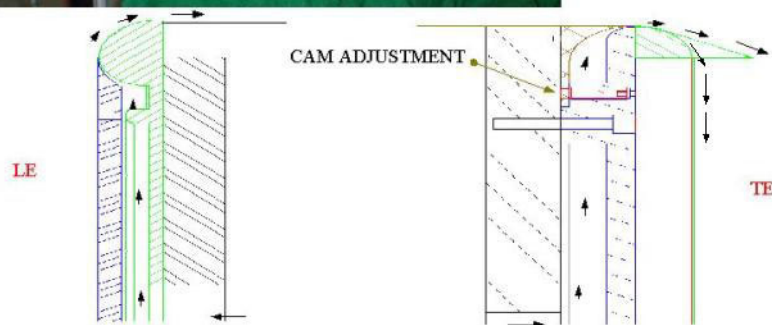


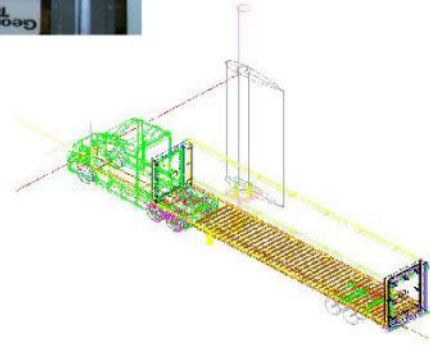
NOVATEK, INC.  
1850 ATLANTA RD.  
SMYRNA, GA. 30080  
770.801.8899

## TWO DIMENSIONAL AIRFOIL WITH LE AND TE BLOWING



FORMULA 1 CAR WITH CC BLOWING  
ON BOTTOM PLATE





## FUTURE CAR WITH AFT CC BLOWING

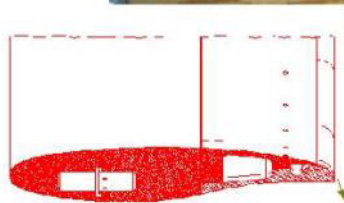


SLIDING BLOCK ADJUSTMENT

HIGH SPEED CIVIL TRANSPORT WITH CC BLOWING ON CANARD TE, WING TE, AND WING LE.



CHANNEL WING WITH CC BLOWING ON CHANNEL TE, OUTER WING LE AND TE



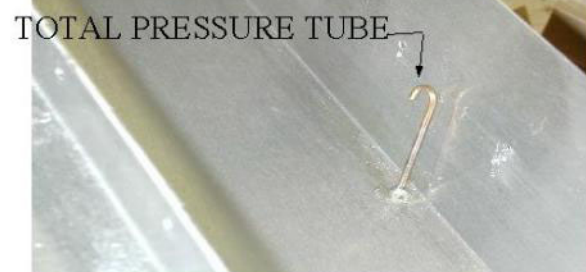
DUCT SECTION



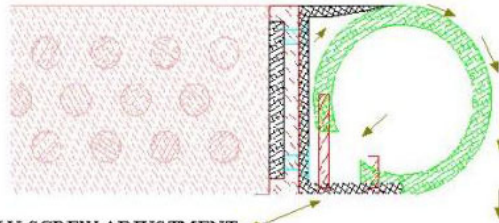
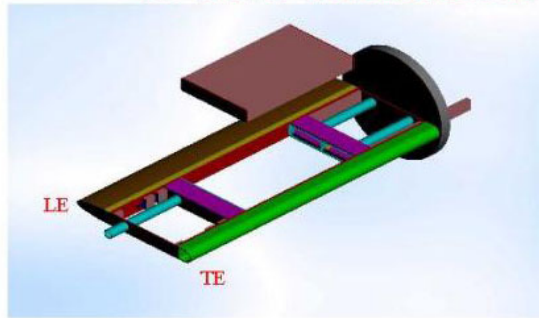
OUTER WING SECTION



PNEUMATIC HEAVY VEHICLE (PHV) WITH TE BLOWING

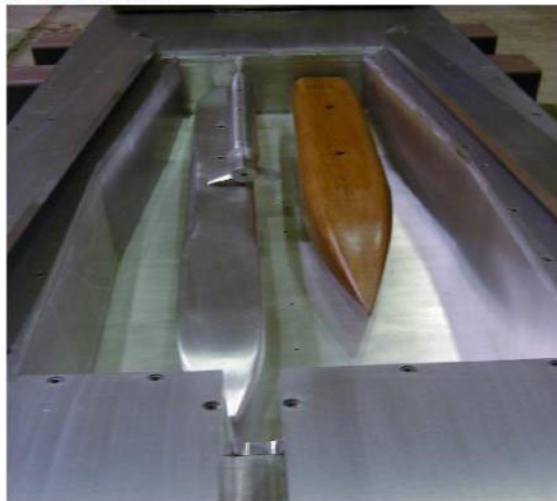


## CC WING WITH RADIATOR



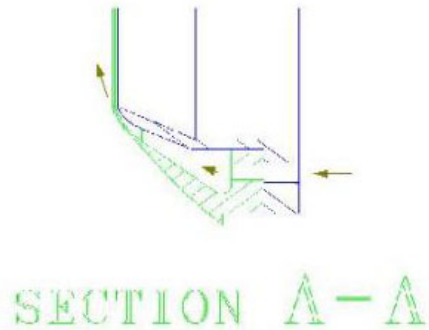
PULL ONLY SCREW ADJUSTMENT

## HIGH SPEED WIND TUNNEL FLOOR WITH WEAPONS BAY



PULSED BLOWING (NOT SHOWN) TO REDUCE CAVITY NOISE

## LASER WINDOW WITH PNEUMATIC SEPARATION CONTROL



### CONCLUSIONS

COANDA TURNING JETS HAVE BEEN APPLIED TO A WIDE VARIETY OF AIR AND LAND VEHICLE CONFIGURATIONS.

DUAL PLENUM AIR SUPPLY PROVIDES UNIFORM EXIT JET

U SHAPED TOTAL PRESSURE TUBE NEAR THE EXIT IS NECESSARY

ROUTING OF INSTRUMENTATION IN AIR SUPPLY IS PRACTICAL

DEFLECTION OF SLOT GEOMETRY UNDER PRESSURE LOAD CAN BE SIGNIFICANT

PUSH PULL SCREWS FOR SLOT ADJUSTMET IS BEST.



---

## **Selected Topics Related to Operational Applications of Circulation Control**

Ernest O. Rogers  
Jane Abramson

Naval Surface Warfare Center, Carderock Division  
Bethesda, MD

Circulation Control Workshop, March 2004

---

Approved for public release; distribution is unlimited.

1

### **TOPICS**

- Techniques for exploring new CC application ideas
  - 3D panel-methods (inviscid), usage and validation
  - modeling of rotary devices
  - Checklists: initial concept examination; slot flow power accounting
- Assorted items:
  - Lift: behavior under conditions of very low or negative  $V_{jet}$
  - Drag: the airfoil measurement 'correction' term
- Recommendations of tasks to support future applications

## 3D Panel-Methods

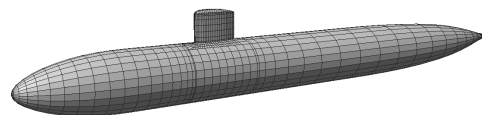
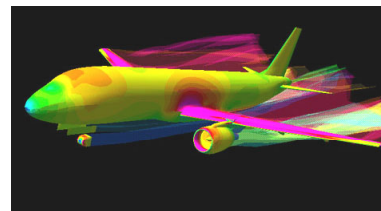
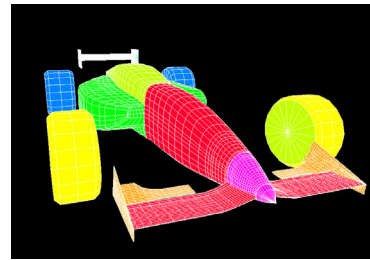
no flow field gridding;  
suitable for end-users;  
quick and prolific results;  
existing paneled vehicles can  
be converted to simulate CC

VSAERO

PANAIR

PMARC

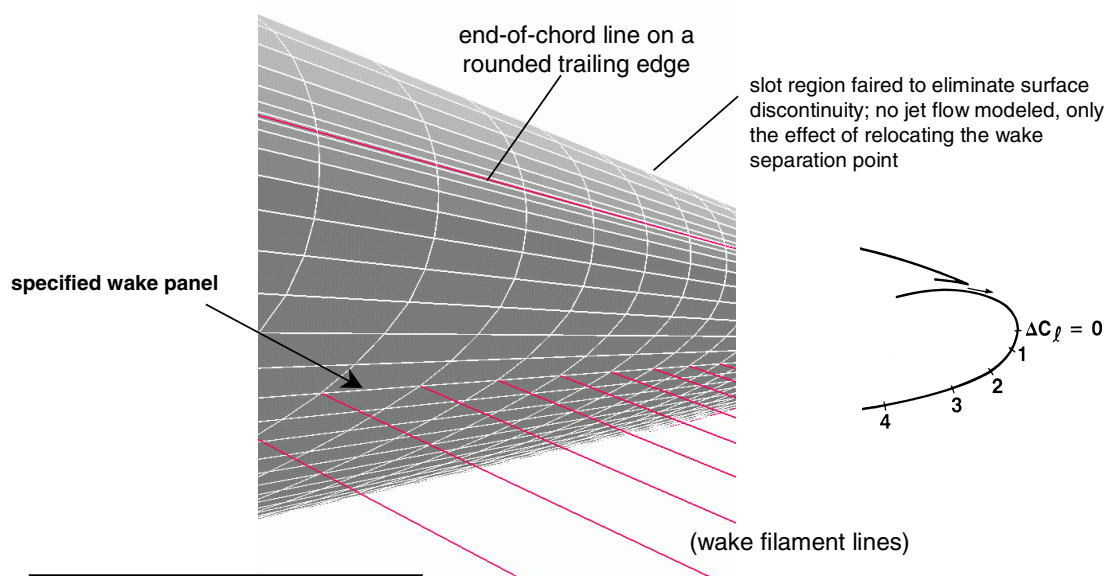
VSAERO application examples (conventional)



3

Some inviscid 3D computational panel codes other than VSAERO are PANAIR and PMARC. In many cases, existing paneled vehicle configurations can be readily converted to simulate CC for what-if assessments.

Assessment of New CC Concepts using 3D Panel-Method Codes\* (Inviscid):  
Relocation of the Wake Shedding Panel Mimics Effect of CC

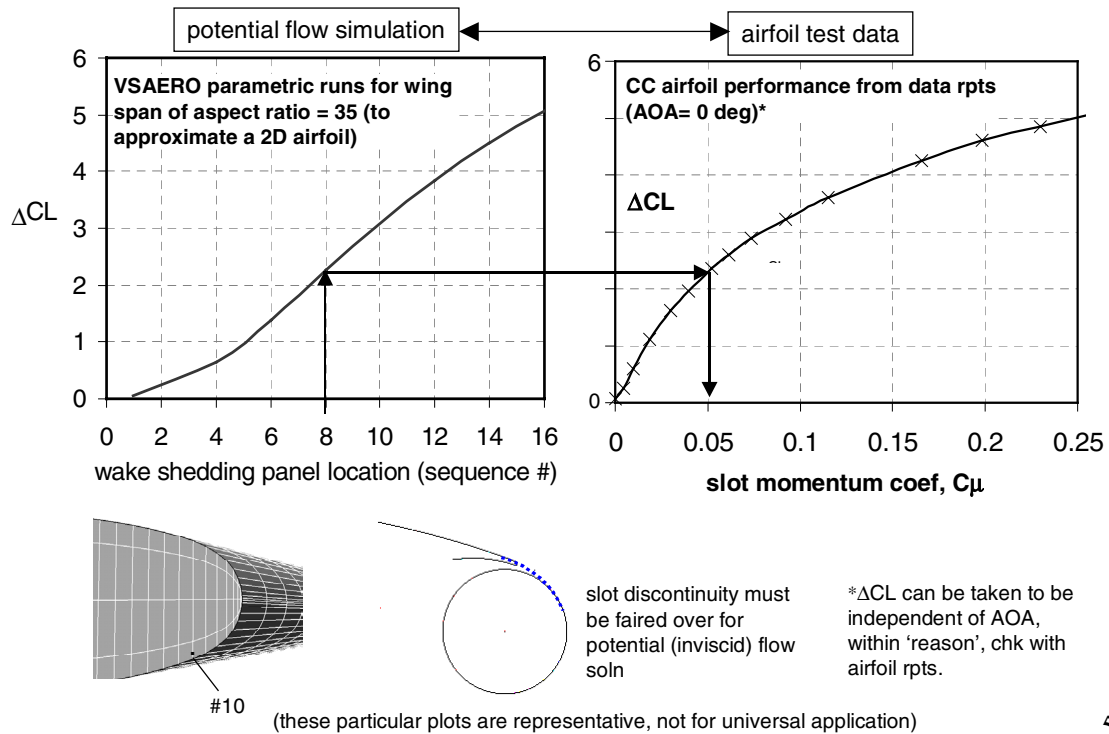


\*examples will use VSAERO (AMI) with Omni3d for post-processing

4

A shedding panel is where the upper and lower surface flows merge and depart into the wake. Relocation of the wake shedding panel mimics the desired effect of circulation control.

Panel-Method Technique for CC: Associate Wake Shedding Panel Location with Airfoil incremental CL and Hence  $C_{\mu}$

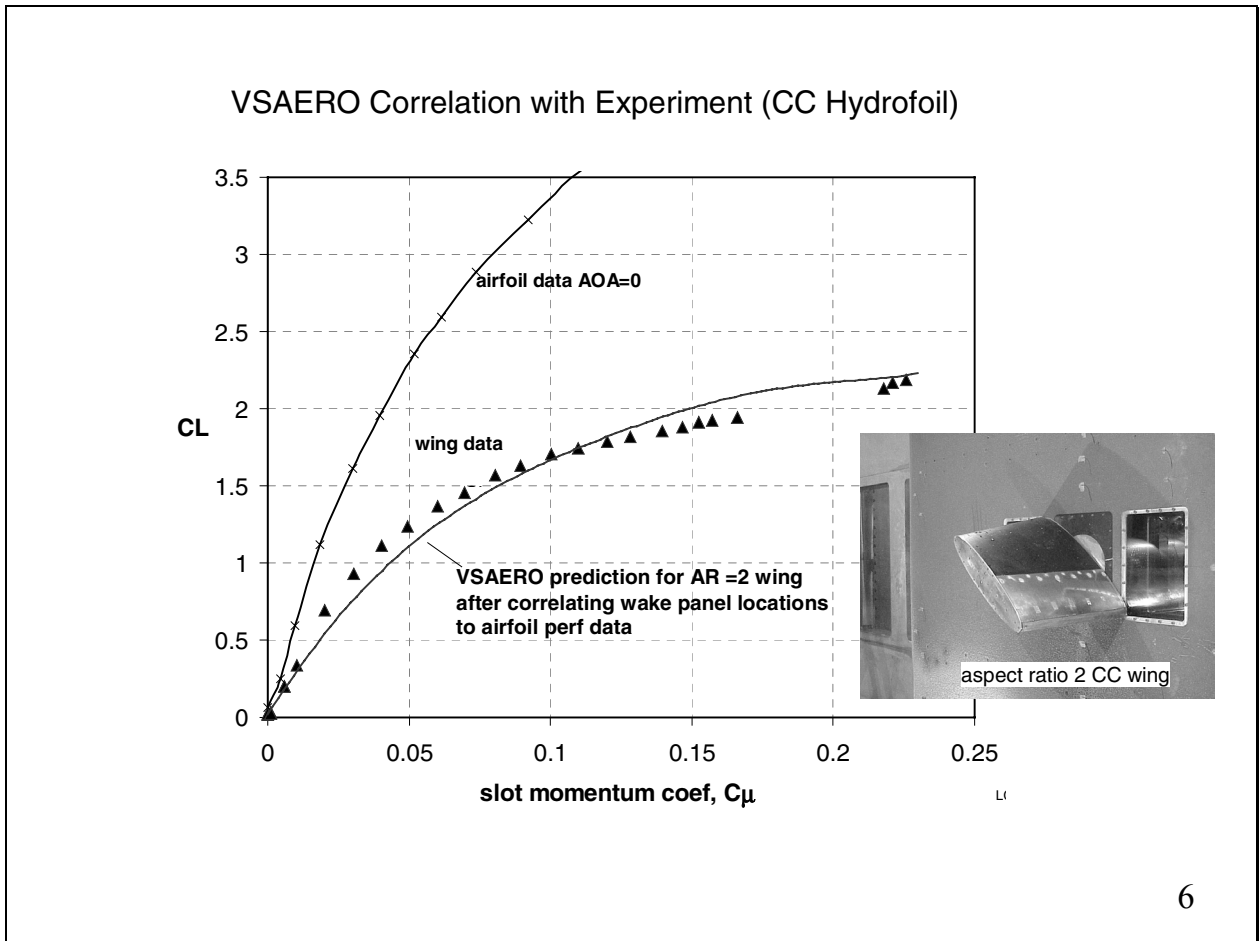


5

By setting a very large wing aspect ratio to approximate a 2D airfoil, the incremental lift arising from changing the wake departure location is determined as a function of panel location for purposes of subsequent 3D CC application analysis. Plots of experimental airfoil  $\Delta CL$  as a function of  $C_{\mu}$  provide the connection between the 3D inviscid lifting surface solution--with its specified wake panel location--and the required blowing. (A variation on this approach is to use wing performance data to correlate panel location on the VSAERO modeled wing planform.)

The wake panel technique will provide useful insights even if there is no pre-existing airfoil or wing  $C_{\mu}$  data that is closely relevant to the intended new airfoil design. Chordwise and spanwise pressure distributions will still be obtained for a specified wake shedding panel, however, the estimated required slot momentum coefficient will not be known, or even if the desired lift can be achieved using the proposed foil cross-section. The historical CC airfoil database can be used as a general feasibility guide.

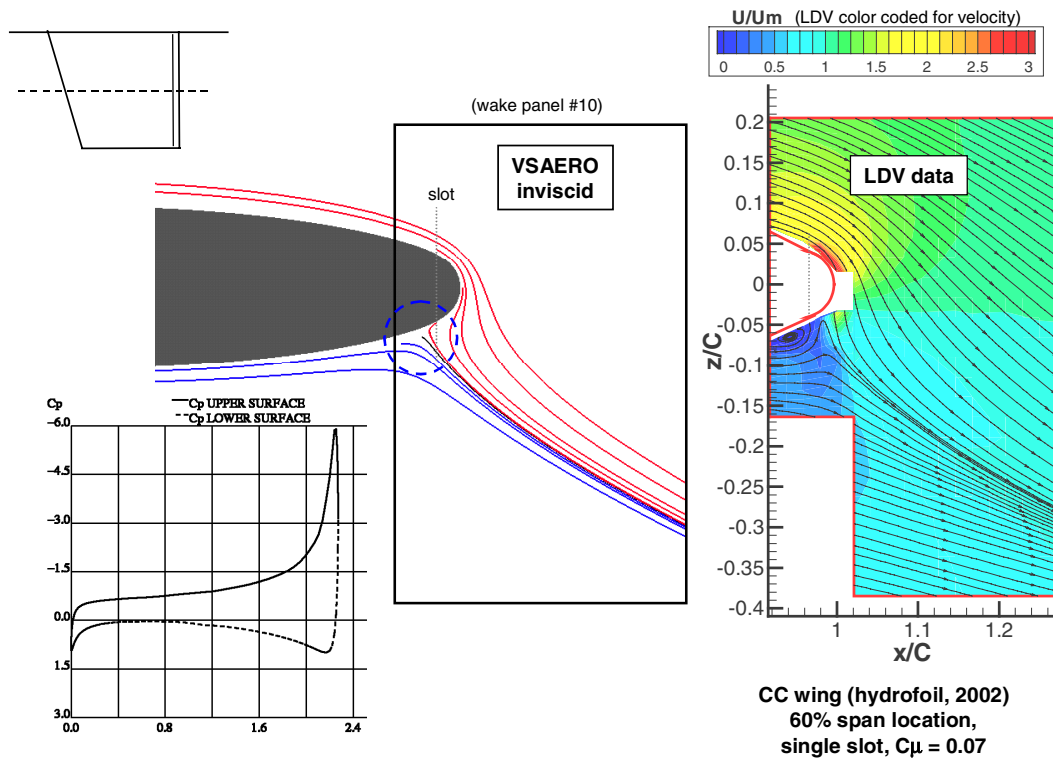




As a check of the panel-method approach, there is satisfactory agreement with experimental data for a simple CC wing. This method relies on using a small portion of the airfoil data for the  $C_\mu$  tie-in between 2D and 3D. In contrast, lifting line theory allows use of the full airfoil performance map, which gives an even better correlation than shown here through the use of the concept of an equivalent 2D angle-of-attack based on lift induced downwash.

## Inviscid Solution Streamlines: Comparison to LDV for same CL

$CL = 1.4$ ,  $AOA = 0$ ,  $C_{\mu} = 0.07$  (2D equivalent AOA is approx -13 deg)

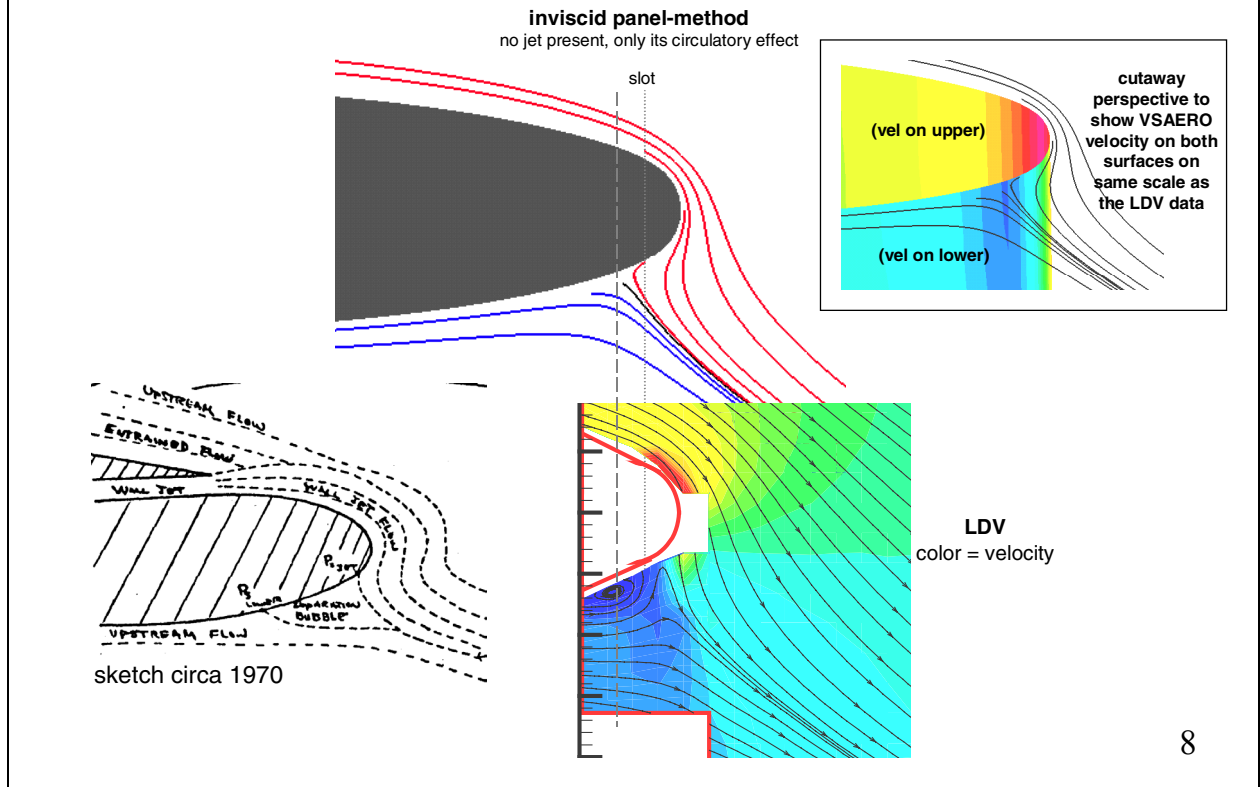


7

Note how well the VSAERO solution compares to LDV flow field survey data for this wing. There is a very similar wake profile, except as expected, for details in the zone near where the lower and upper surface flows merge. Experimentally, the lower surface flow has a separated region exactly where the inviscid solution shows stagnation pressure, followed by a reattachment just before a final separation. (It is not expected that the surface pressure in this region would fully approach stagnation pressure, due to viscous losses.)

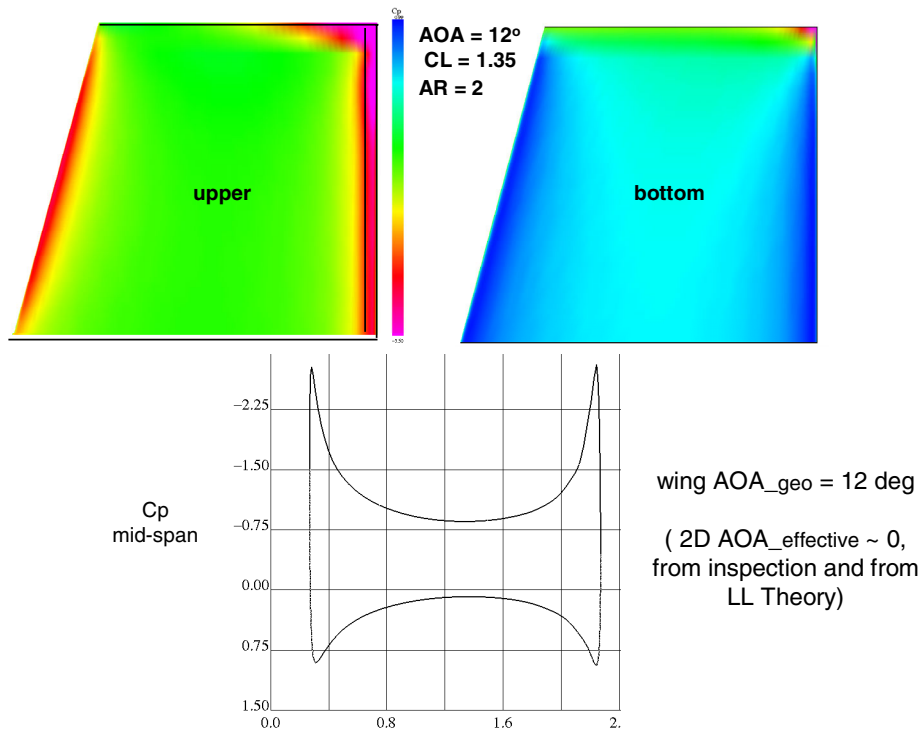
## Inviscid Solution Streamlines: Comparison to LDV for same CL

CC Hydrofoil Wing:  $CL = 1.4$ ,  $AOA = 0$ ,  $C_{\mu} = 0.07$  (2D equivalent AOA is approx -13 deg)



This is a rearrangement of the previous Slide. The LDV results are interpreted as showing that the lower surface flow continues well past that of the inviscid stagnation point location--where a separation bubble is seen--before a final departure from the surface as it merges with the upper flow. There is a good match with the surface velocity distribution data, the velocity color scales are the same to assist comparison.

## Example of a Panel Code Computation of Pressure Loading

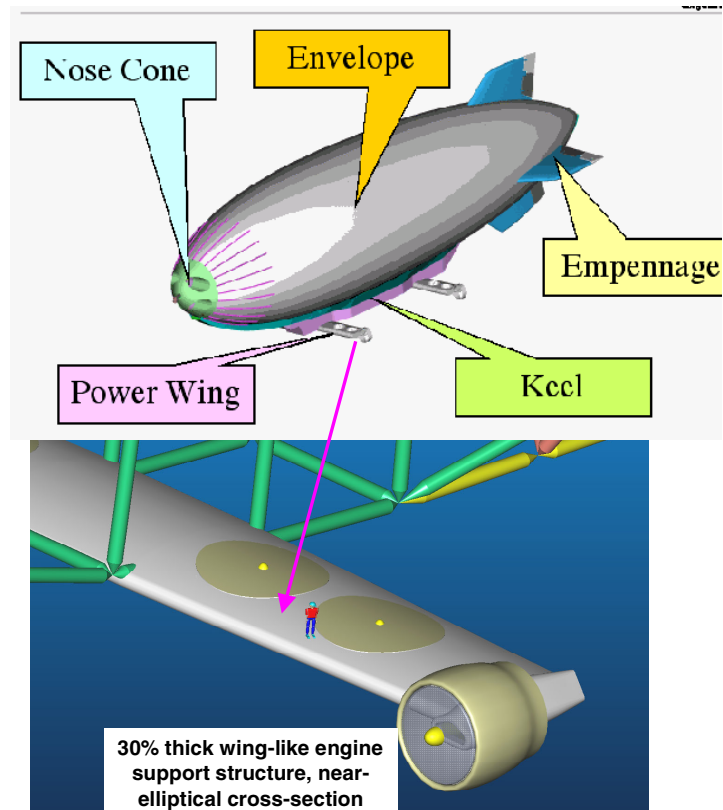


9

Having established confidence in panel methods, this illustrates a typical use, for wing pressure loading. Inviscid solutions for application studies require inspection for likelihood that the flow will separate at either the leading edge or in the aft region ahead of the proposed slot position; refer to CC airfoil test reports for general indications of resulting impact on performance.

Panel-Method  
Application Example:  
Examination of CC  
Wings for a Large  
Airship

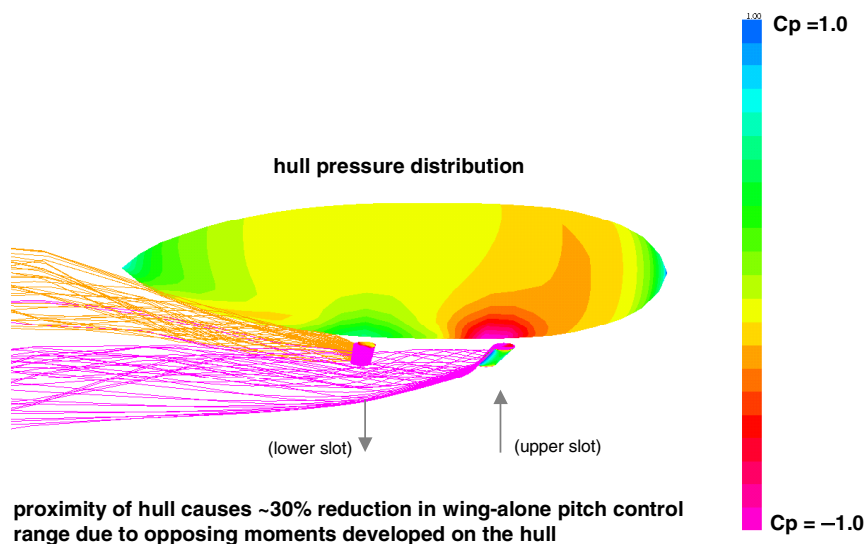
high-lift technical questions:  
--tandem wing effect  
--wing-body interaction  
--lift penalty from the somewhat  
low aspect ratio of 4



10

A commercial airship design had included tandem wing-like engine support structures. The 'power wing' cross-section profile resembled that of a 30% thick ellipse, a profile for which a CC airfoil database existed. Of interest was the benefit of using CC on these wing structures to generate vehicle pitch control moments at low speed. Tandem wing effects and wing-body interaction were the high-lift technical issues investigated using VSAERO.

## Airship in Proximity to Tandem Wings at Very High Lift



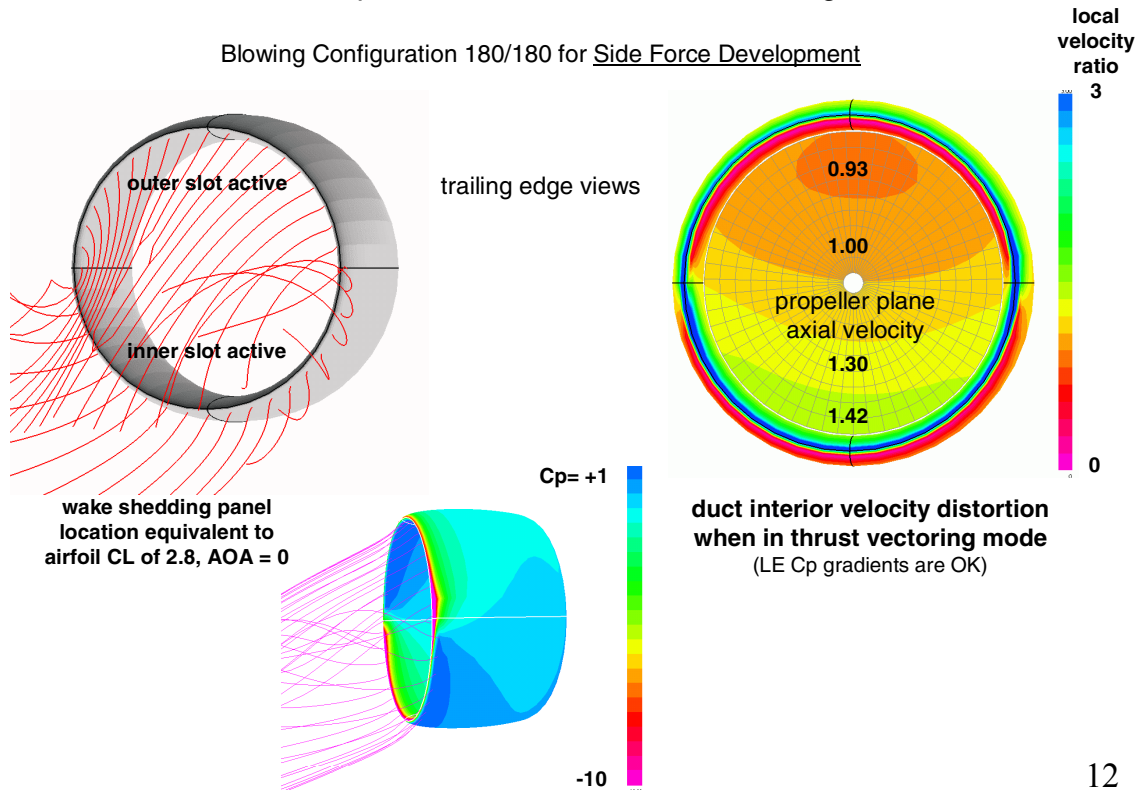
VSAERO, wake shedding panel selected to give isolated wing  $CL = 4.8$  for aspect ratio = 100, to match Englar's 30% t/c airfoil test results at high  $C_{\mu}$

11

Wing 'blowing slots' in this solution are set to produce a vehicle pitch-up moment. Wing  $CL$  is about 3, corresponding to an estimated  $C_{\mu}$  of about 0.16. The high lift wings impose a pressure field on the hull that causes a pitch-down effect, resulting in a 30% decrease in overall control effectiveness versus the isolated tandem wing capability (this was acceptable). This was one of a number of parametric variations on the CC-wing airship configuration that were readily conducted with VSAERO.

## Application of VSAERO to CC Duct Studies Example of a Dual-Slotted Annular Wing

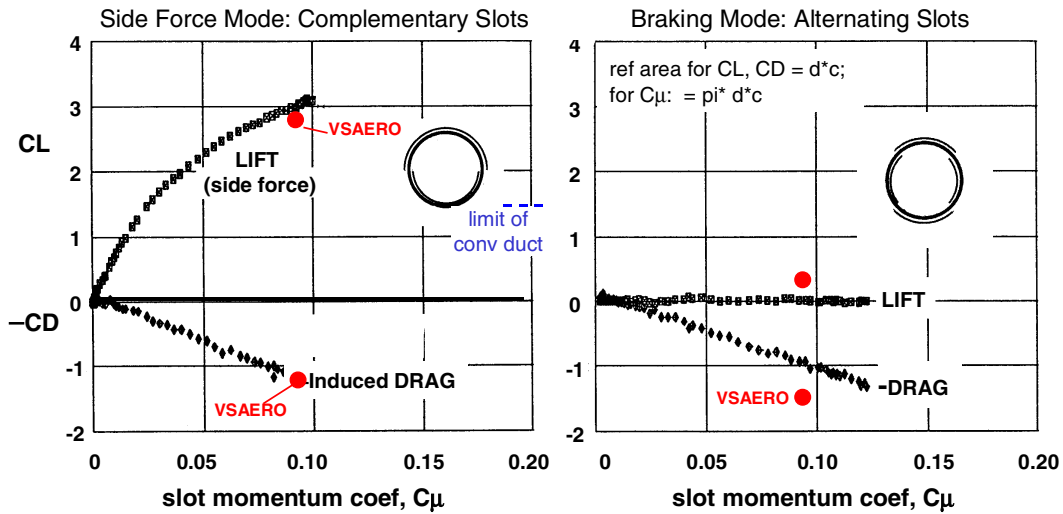
Blowing Configuration 180/180 for Side Force Development



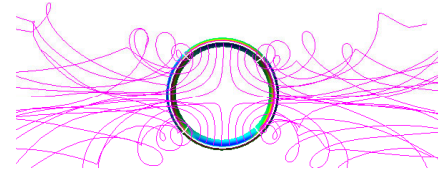
12

An easily generated shape for exploratory studies is that of an annular wing for which one operational application would be as a propeller shroud. Asymmetric trailing edge blowing enables development of steering forces (thrust vectoring). Essentially, half of the duct becomes a diffuser, with the other portion becoming an accelerator of flow. This figure illustrates a study of how non-symmetrical blowing would distort the uniformity of the interior flow velocity, as related to propeller blade cyclic stress loading.

## Comparison of VSAERO with CC Duct Data



Data taken in the AARC Acoustic Wind Tunnel, 1994. Propeller absent.



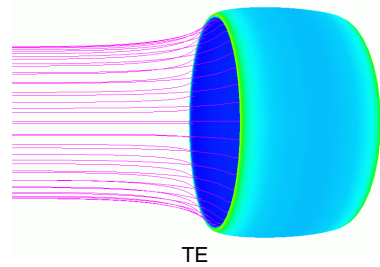
13

The VSAERO solution compares well to experimental data on this CC duct. (No propeller was present, the test is covered in the presentation/paper by Imber). In the image of the alternating quadrant slot 'braking' mode, the 4 vortices formed at the changeovers between inner/outer slots merge into 2 pair. There is no net lift but there is an induced drag arising from the wake vorticity effects.

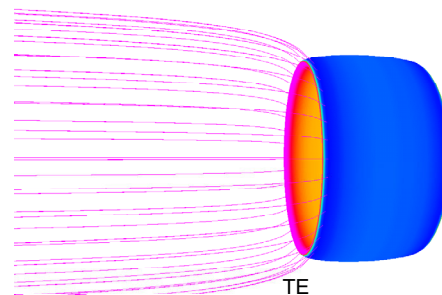


Panel-Method Exploration of 3D Configurations:  
Example of a Dual-Slotted Annular Wing (Duct)

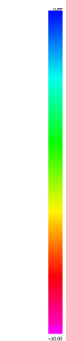
Decelerating: Outer Slot Active  
centerline Vel = 0.5



Accelerating: Inner Slot Active  
centerline Vel = 2.5



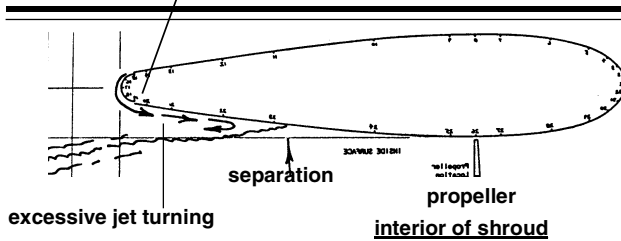
Cp = 1



Cp = -10

(LE gradients OK; would need a bleed from the inner slot to control diffuser stall due to jet)

(as seen on the color scale, this level of acceleration has excessive Cp gradient at LE, which is same as shown here on the TE)

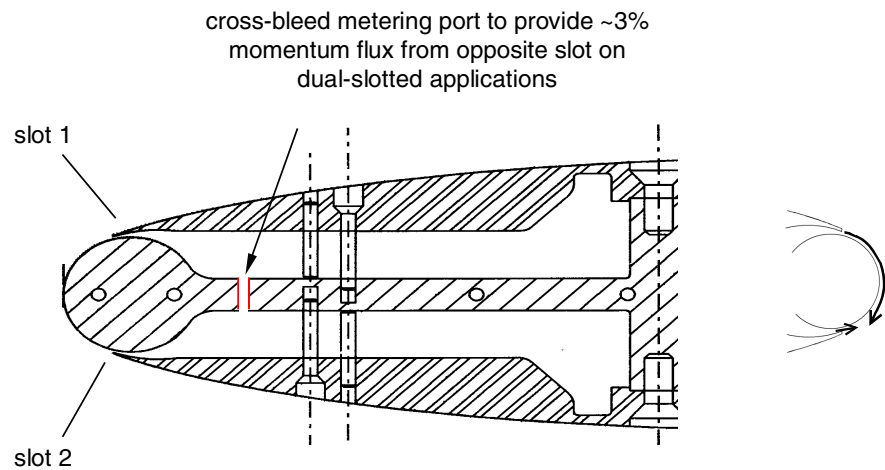


experiment with propeller operating,  
no freestream, WVU observations of  
interior separation, 1993

14

Inviscid solutions can indicate operating limits, such as probability of leading edge inlet separation on the accelerating duct. For the decelerating mode, it calls attention to ‘diffuser stall’, which can be aggravated by excessive turning of the wall jet at high blowing. It has recently been demonstrated that a very low level of bleed from the 2nd-slot will influence the primary slot flow in a manner which will alleviate the negative effects that a (primary) Coanda jet can directly produce on the high pressure side of a lifting surface.<sup>5</sup> The sketch is from a propeller/duct checkout (single active slot) at WVU prior to a tunnel test at AARC, which was without a propeller. The inherent dual-slot provision in a CC duct concept provides capability to control excessive wall-jet turning.

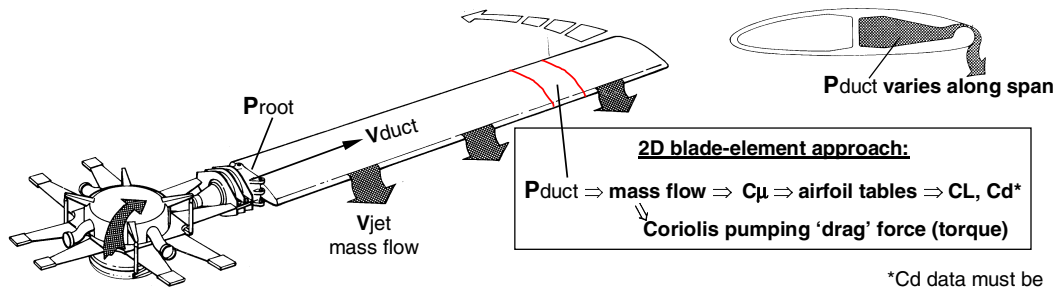
## Provision (conceptual) for Simultaneous 2nd-slot Flow to Preclude Excessive\* Jet Turning



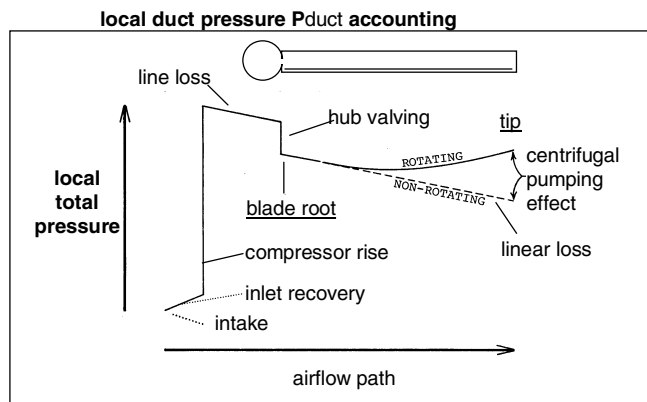
Conceptually, a small cross-feed port could be used on a dual-slot configuration to eliminate a possible lift limit associated with excessive jet turning at the higher blowing levels.

## Modeling of Rotary Applications

duct pressure and Coriolis effects, with airfoil data table look-up



\* $C_d$  data must be without penalty of intake ram drag, and as would be read by an airfoil drag load cell.



16

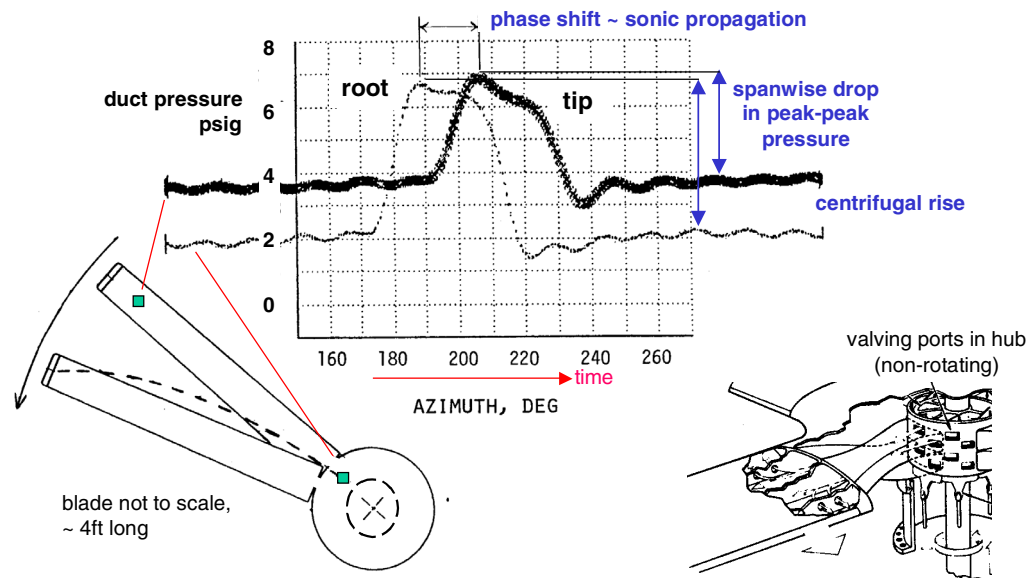
There is no requirement for lifting surface panel methods on long slender blades. Airfoil 2D strip theory is used in combination with careful modeling of local duct pressure and the Coriolis pumping power effect on shaft drive torque. Centrifugal pressure rise often offsets spanwise flow losses. A suggested numerical model: 20% linear loss in  $P_{duct}$  (gage, non-rotating) from root to tip, with 10% reduction in the theoretical centrifugal pressure rise.



6.7 ft diameter RBCCR rotor model, NSWC 1975

## Propagation of Duct Pressure Control Inputs in a CC Rotor Blade ~ sonic lag

**Impulsive pressure input to rotor blade duct, rotational tip speed = 470 fps**

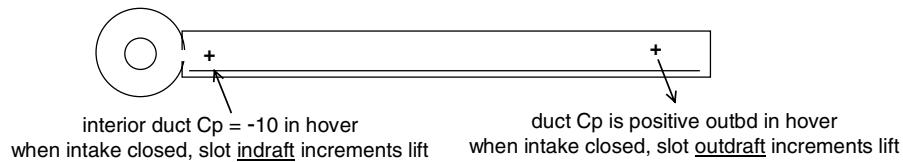
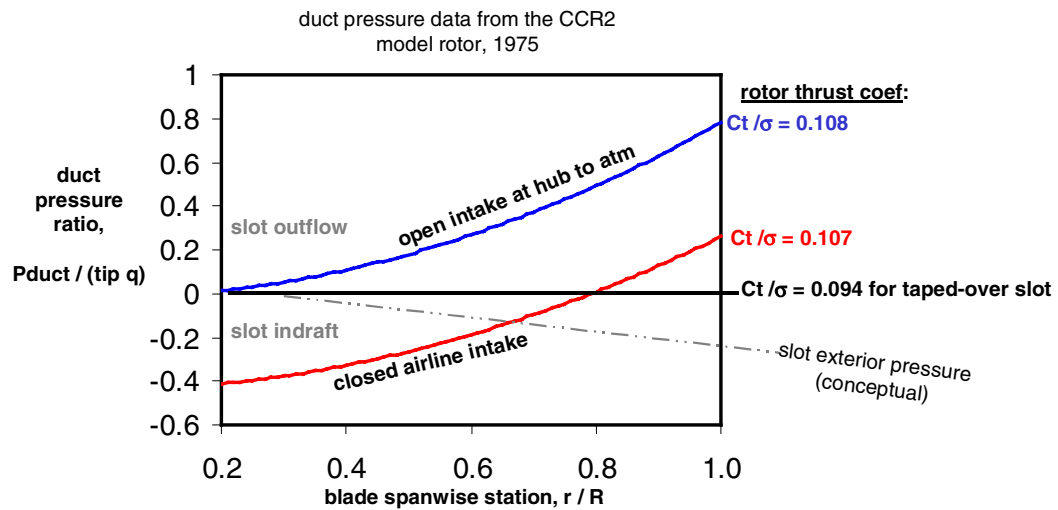


17

This time history recording of blade duct pressures from a blown rotor test illustrates several factors: centrifugal pressure rise, spanwise loss in pressure (manifest here as a decline in peak-to-peak range), and a propagation time delay corresponding to the approximate speed of sound that results in a spanwise azimuthal phase shift. These are easily modeled effects, empirically. This was a checkout of the cyclic pressure valving system, the waveform is not representative of flight operation. The rotor is described in citation 4 on Slide 29.

## Self-Pumping Lift Augmentation Characteristics of a Blown Rotor

special considerations for CC: can't be turned-off (unless slot gap area is controlled)



18

The rotor is a significant centrifugal pump that contributes to the required mass flow rate for a blown rotor. This plot is from special tests for a model rotor blade in which the slots were sealed with tape to obtain a baseline thrust coefficient. Then with the slot unsealed, two situations were examined: 1) air line disconnected from the compressor so that the rotor could draw intake air, and 2) air line blocked. It is seen that the lift augmentation due to self pumping cannot be turned-off, because the blade draws either from the hub inlet or from the inboard portion of the spanwise slot. Similar situation of self-augmentation could arise on non-rotating wings, due to spanwise changes in slot exit conditions.

## Suggested Procedures for Initial Analysis of CC Concepts

- Use airfoil potential flow code to examine the surface velocities corresponding to the CL being demanded from the CC action; reasonable surface Mach Number and  $C_p$  gradient?
  - Explore response of  $C_p$  to different Coanda radii, foil thickness, camber.
  - Acceptability of estimated pressure, flow rates, unblown drag, and pitching moment.
- Rotary blades. Convert any generic rotor perf code. High aspect ratio permits use of CC airfoil data directly (with correct choice of Cd defn and a local  $C_{\mu}$  calc). Account for local duct pressure and Coriolis torque effects; identify average mass flow and peak blade entrance pressure. Flight control valving: specify Pduct at root as a variable in accordance with operational objectives.
- Simple wings and planar control surfaces: hand calculations with airfoil perf map and Lifting Line theory to give AOA\_eff (Ref. AIAA 2004-1244)
- Non-simple wings and complex shapes: inviscid lifting surface code (3D panel-method)
- Other situations: model test, based on guidance in the Ref. All test articles need to have at least some surface pressure taps.

Ref : Englar, RJ, "Test Techniques for High Lift Two-Dimensional Airfoils with Boundary Layer and Circulation Control for Application to Rotary Wing Aircraft", NSRDC Report 4645, AD015-623.

19

A 2D potential flow code where the end-of-chord Kutta condition can be released and replaced by an input specified circulatory lift and angle-of-attack is the first essential step in looking at a new CC airfoil design or application. An early code that has supported CC development is described in citation 7 on Slide 29. Development of a Kutta-released variant of XFOIL wherein CL (and AOA) is the input specification would be useful.

## Slot Flow Power Accounting for Design Applications

- Use a wing or blade element  $C_d$  that has no air-source ram drag or power penalty
- System perspective:
  - sum required mass flows,
  - identify peak duct pressure (excluding any centrifugal pressure rise)
  - derive ideal pneumatic power ( $\sim$ peak pressure x mass flow)
  - account for estimated pressure losses from source to duct,
  - identify air intake ram drag and any intake pressure recovery.
  - compressor pressure rise and efficiency
  - pumping power is thereby identified
  - refinement: vary slot gap setting to trade-off pressure vs flow rate to minimize the plumbing losses

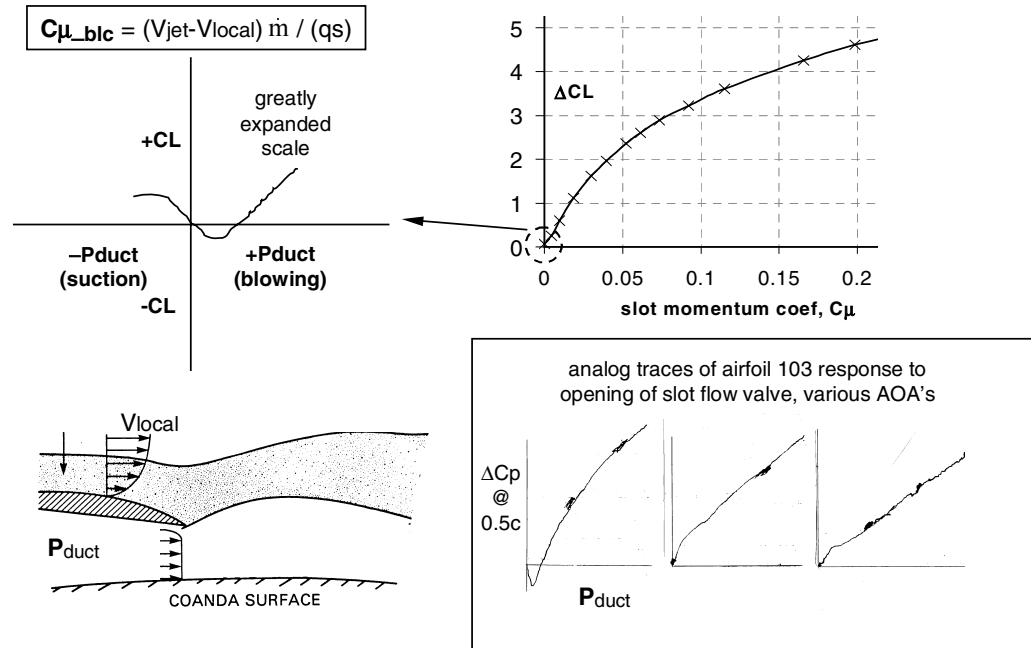
Checklist: intake location static pressure, inlet pressure recovery into face of compressor, fuel flow or hp used for compressor pressure rise, temperature of output, flow losses to slot, throttling losses, ability of slot to recover duct total pressure (duct velocity and interior design factor).

20

An assessment of slot flow power requires that a number of factors be considered, after the local  $C_{\mu}$ 's have been determined from the required augmented force performance. Part of this process should include the practical question of the slot height-to-chord ratio ( $h/c$ ). For a given  $C_{\mu}$ , the theoretical compressor or pump power declines as  $h/c$  is increased. However, the  $C_{\mu}$  required to produce a given  $CL$  can increase with increasing  $h/c$ . Experimental data for  $h/c$  effects is needed to identify the overall best slot gap setting for minimizing slot flow power requirements.

## Lift Characteristics at Very Low Flow Rates

reversed response to slot flow at low  $V_{jet}$  in certain AOA ranges



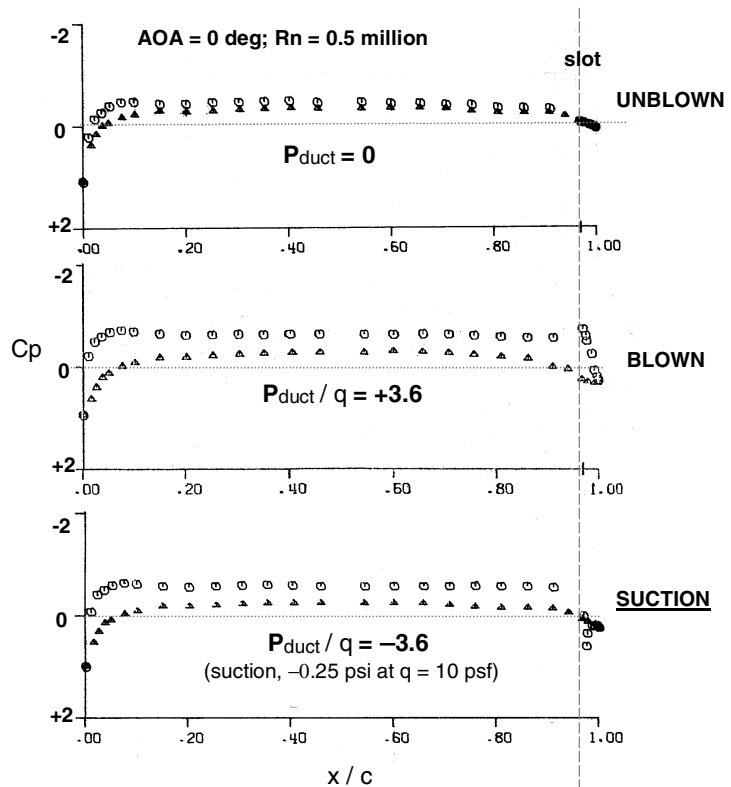
21

For some applications, there may be a significance to the reversed lift response when  $V_{jet}$  is much less than  $V_{local}$ . The reverse is because the momentum of the slot flow is less than that within the local flow, hence a retarding effect. This condition is illustrated by the definition of  $C_{\mu\_blc}$ , a parameter used in boundary layer control research. Phenomena shown here would be relevant to unintentional slot valve leakage conditions, or spanwise flow originating within the duct on a fixed wing when the slot valve is closed (with an open slot). The reaction to duct suction is addressed in the next Slide.



## Augmented Lift via Slot Suction

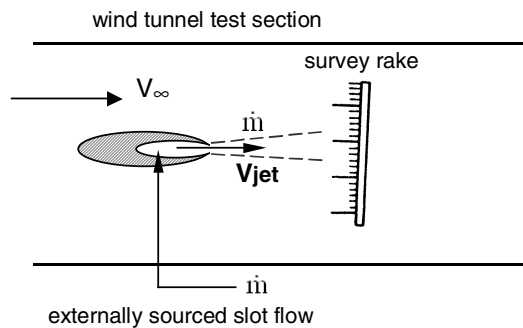
Special experiments on the 20/0 airfoil (1975, Abramson); relevant to certain applications, such as rotor blades.



22

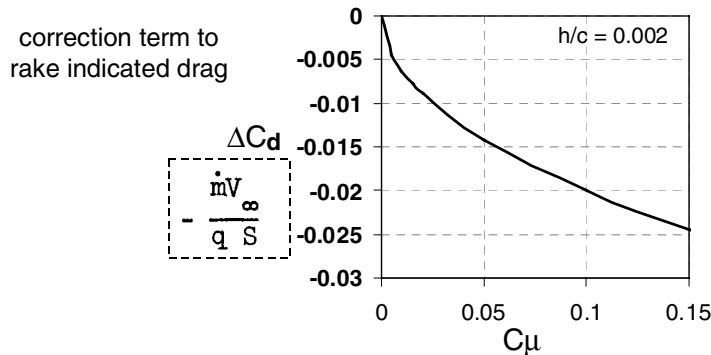
Slot flow intake, as obtained using a duct suction pump, will also increment circulatory lift, to a limited extent. The lift augmentation is a result of the upper surface flow momentum level being raised by extracting a portion of the low energy boundary layer flow. Note that the mid-chord  $C_p$  differential is same in both the blown and suction data, therefore the identical circulatory lift is obtained for the same absolute duct pressure (with respect to free stream static). Suction does not enable attachment to end of chord, in contrast to blowing. Has implications for rotary blades (centrifugal pump-down), and perhaps for fixed-wing applications where there could be spanwise gradients of slot exit pressure when unblown.

## Blown Model Test Procedures: Necessary Correction to Airfoil Drag if Determined by Wake Survey



$$C_d = C_{d\_rake} - \frac{\dot{m}V_\infty}{qS}$$

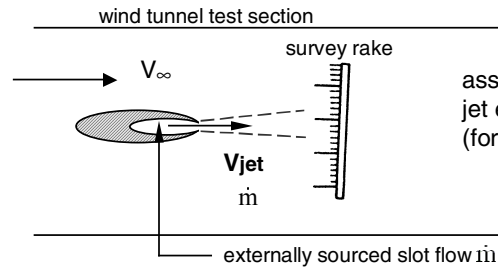
$$= C_{d\_rake} - C_\mu \frac{V_\infty}{V_j}$$



23

For a blown airfoil, there are a number of definitions of drag, depending on what force contributions and slot flow power components are included. For vehicle application studies, intake ram drag and pumping power are best handled on a system basis, not as part of the wing or airfoil  $C_d$ . Therefore, the desired definition of  $C_d$  for the airfoil data set is simply the force that would be measured by a load cell in a test setup where the slot flow is sourced remotely. Most blown airfoil tests do not use a load cell for a number of reasons, including pressure line tares, but rather use a survey of wake momentum, most commonly employing a wake rake. For the blown model, to arrive at a drag which corresponds to that from a load cell requires a modification to the drag indicated by the wake rake survey ( $C_{d\_rake}$ ). The modification or 'correction' is large, resulting in the  $C_d$  of a typical CC airfoil becoming negative; historically, this adjustment to the rake reading has been a source of contention. Attempts to independently derive the drag correction term seem to often result in arriving at the conclusion that the sign of the term should be opposite to that given in the literature, hence the following numerical demonstration is offered.

## Numerical Demonstration of Need for Drag Correction



assume a frictionless model and no jet entrainment induced losses\* (for unity mass flow)

Scenario Table

$V_{jet} / V_\infty$	drag, if by a load cell	<u>uncorrected</u> drag <sub>rake</sub>	corrected drag <sub>rake</sub>
0	0	0	0
1.0	-1.0	0	-1.0
0.3	-0.3	+0.7	-0.3
2.5	-2.5	-1.5	-2.5

sink

source

$$C_d = C_{d_{rake}} - \frac{\dot{m} V_j}{\rho S V_\infty}$$

$$= C_{d_{rake}} - C_\mu \frac{V_\infty}{V_j}$$

\*In real use, corrected drag<sub>rake</sub> will inherently include all effects of friction, form drag, jet thrust recovery, jet entrainment effects on the model,...

A simple numerical experiment on paper will illustrate the need for the drag correction term. Only the corrected drag matches what would intuitively be the reading from a load cell (most CC airfoils tests do not use a load balance because of pressure line tares and other factors).

### Drag and Slot Thrust Recovery for the Typical CC Airfoil with correction to $C_{d_{rake}}$

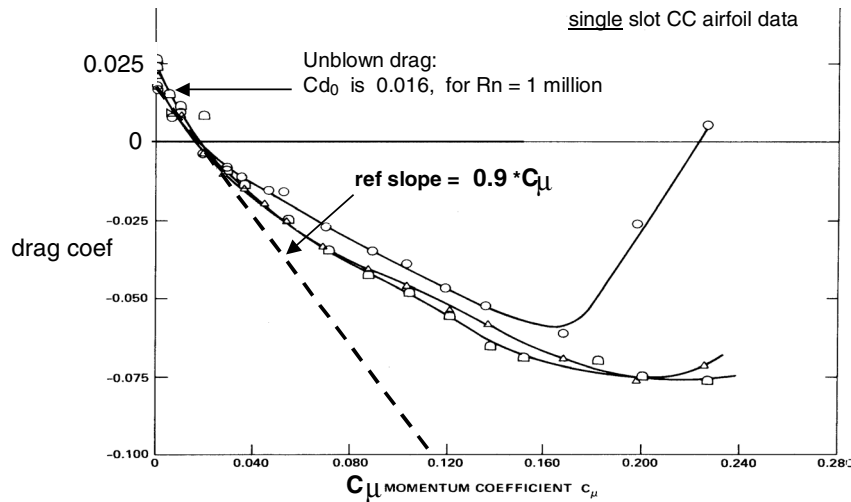


Figure 17 - Model NCCR 1510-7067N Drag Coefficient Variation with Momentum Coefficient,  $h/c = 0.0022$

The corrected drag coefficient of a typical CC airfoil corresponds to about a 90% recovery of the slot momentum thrust. Depending on the intended use of the coefficient, other definitions of  $C_d$  can include the equivalent drag associated with air intake and compression; with those definitions the coefficient would not go negative.

## Drag Correction Explanations in the Literature

### “The Effect of Base Bleed on a Periodic Wake”

C. J. Wood

Journal of the Royal Aeronautical Society, July 1964, pp 477-482.

$$C_d = C_{d_{\text{rake}}} - C_{\mu} (V_{\infty} / V_{\text{jet}}) + C_{\mu}$$

simulates an air intake on the model

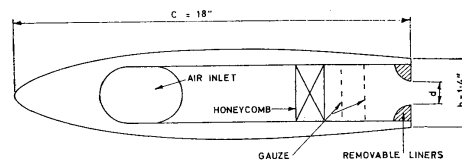


Figure 1. Diagram of aerofoil section (not to scale).

#### Other sources of explanation:

R. Kind:

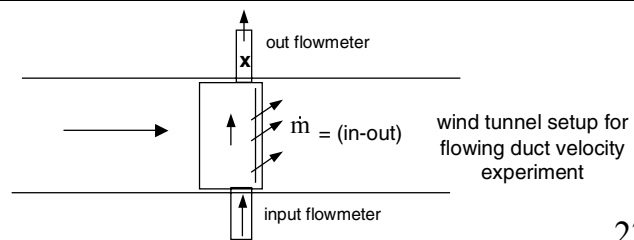
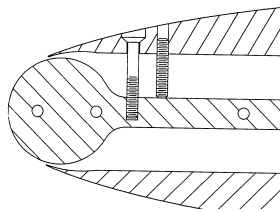
--Dissertation, University of Cambridge, June 1967;

--“An Experimental Investigation of a Low-Speed Circulation-Controlled Airfoil,” The Aeronautical Quarterly, Vol. 19, May 1968, pp. 170-182.

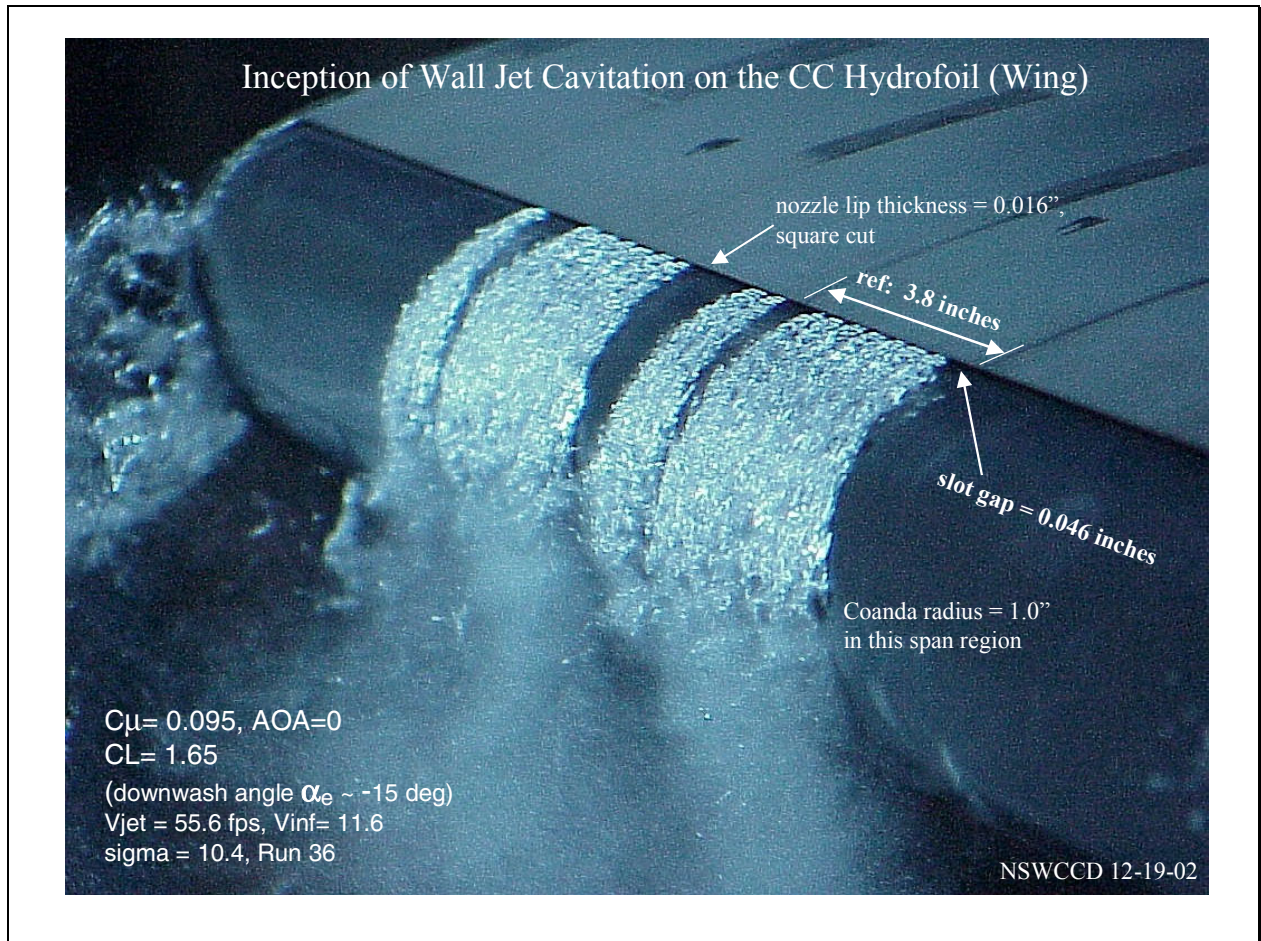
Drag correction explanations in the literature--although sparsely worded--can be found in these publications.

## Recommendations of Tasks to Support Commercial Applications

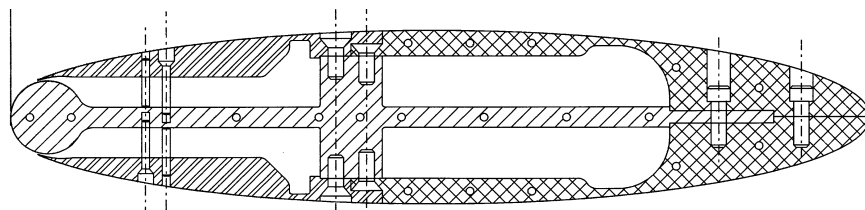
- **Design Guide (working) for certain engineering details and fabrication tolerances**
  - slot nozzle details, lip thickness
  - interior structures in the flow path; slot gap adj approaches, see sketch
  - materials for lip and Coanda
  - fabrication specs for surface smoothness, tolerance, surface and gap waviness
  - summary of design resources for the feeding of a long slot from a duct
- **Airfoil experiment to examine duct spanwise velocity effects (“flowing plenum”), skewed Vjet vector (see sketch)**
- **Airfoil analysis code for chordwise loads, insight, and initial feasibility examination**
  - develop a released-Kutta variant of XFOIL, plus a rounded TE cambered ellipse profile generator
  - or a modified Euler code
- **Establish the ability of a public domain panel-method code to simulate CC action**



These recommendations represent experiences with a number of CC projects.



As a concluding slide, this image provides a close-up visualization of the Coanda wall jet on a 24-inch chord model. In the water tunnel, the test section static pressure was decreased until first occurrence of cavitation, which for these test conditions corresponds to a minimum  $C_p$  on the model of -10. See citation 5 on Slide 29 for details. The cavitation originates on the nozzle lip face, not within the slot itself. The dimensions are provided for any future endeavor to computationally correlate with the flow structures revealed in this visualization. (The non-uniform spanwise distribution is because the duct pressure is at exactly the first appearance of any cavitation and there are presumably minor slot gap variations, etc. along the span.)



## Representative Bibliographic Selections

1. Abramson, J., "Two-Dimensional Subsonic Wind Tunnel Evaluation of a 20-percent-thick Circulation Control Airfoil," DTNSRDC ASED 311, June 1975
2. Englar, R. J. and R.M. Williams. "Test Techniques for High Lift Two-Dimensional Airfoils with Boundary Layer and Circulation Control for Application to Rotary Wing Aircraft," Canadian Aeronautics and Space Journal, Vol 19, No.3, pp. 93-108, Mar 1973; also published as NSRDC Report 4645, AD015-623.
3. Englar, R.J. "Low-Speed Aerodynamic Characteristics of a Small, Fixed-Trailing-Edge Circulation Control Wing Configuration Fitted to a Supercritical Airfoil," DTNSRDC/ASED-81/08, 1981.
4. Reader, K.R. (DTNSRDC) and W.J. Dixon, Jr. (Boeing Vertol Co.) "Evaluation of a 10-Foot Diameter X-Wing Rotor," AHS Forum May 1984
5. Rogers, E. O. and M. J. Donnelly "Characteristics of a Dual-Slotted Circulation Control Wing of Low Aspect Ratio Intended for Naval Hydrodynamic Applications," 42<sup>nd</sup> Aerospace Sciences Mtg, AIAA paper 2004-1244
6. Schwartz, A. and E. Rogers. "Hover Investigation of an Integrated Pneumatic Lift / Reaction-Drive Rotor System," AIAA 30<sup>th</sup> Aerospace Sciences Mtg, paper 93-0630
7. Rogers, E.O., "Numerical Solution of Subcritical Flow Past Airfoils", NSRDC Report 4112, May 1973





## From Concept to Production of the Coanda Driven Exhaust Deflector for the V-22

NASA/ONR 2004 Circulation Control Workshop

Hampton, VA

T. Wood

March 16, 2004



210407-1

## Outline

- Introduction
- Need
- Concept
- Trade Study
- Ground Testing
- Production

200407-3

The contents of this document are the direct subject matter of the Bell Helicopter's business.

## Introduction



Henri Coanda



Circulation Control Tail Boom on NOTAR



V-22 Coanda Exhaust Deflector

*"These airplanes we have today are no more than a perfection of a toy made of paper children use to play with. My opinion is we should search for a completely different flying machine, based on other flying principles. I consider the aircraft of the future, that which will take off vertically, fly as usual and land vertically. This flying machine should have no parts in movement. The idea came from the huge power of the cyclones."*

*Coanda's comments from 1967 symposium organized by the Romanian Academy*

200407-4

The contents of this document are the direct subject matter of the Bell Helicopter's business.

# Acknowledgements

*Larry Jenkins, Co-Inventor*  
*Albert Brand, Co-Inventor*

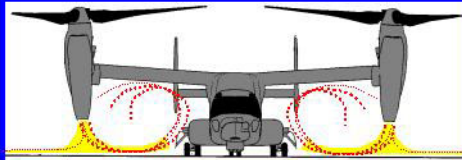
**Bell Team:**  
*Martin Peryea*  
*Dale Sowers*  
*Brent Achttien*  
*Ralph Rockett*  
*David Snyder*

**Navy Team:**  
*Captain Tom Curtis*  
*Ray Slacker*  
*Ernie Rogers*

200407-5

The contents of this document are the direct subject matter of the Bell Helicopter's business.

# Need



**GROUND OPERATIONS SHOWED  
NEED TO REDUCE HEAT ON  
COMPOSITE STRUCTURE**



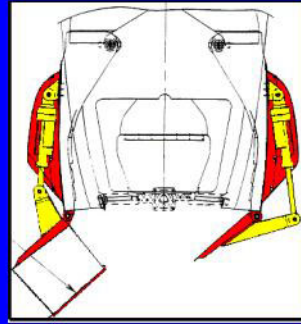
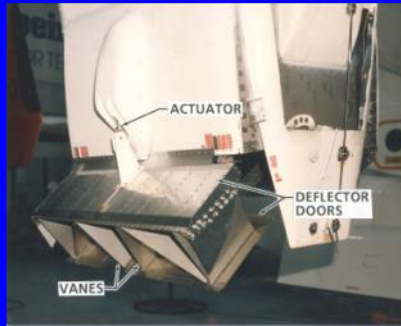
**NEED TO DEFLECT ENGINE  
EXHAUST OUTBOARD WHEN  
SETTING ON DECK TO PROTECT  
EQUIPMENT ON SIDE OF SHIP**

**INITIAL SOLUTION WAS A MECHANICAL DEFLECTOR  
TO BE ACTIVATED WHEN SETTING ON GROUND TO  
DEFLECT EXHAUST OUTBOARD**

200407-5

The contents of this document are the direct subject matter of the Bell Helicopter's business.

## Mechanical Deflector Provided a Solution



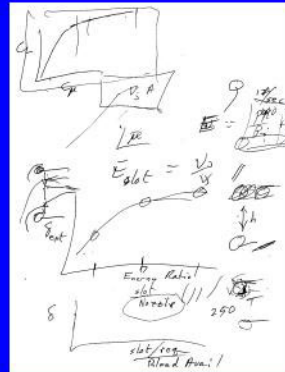
*Issues: Weight, Cost, Reliability, Drag, Impact on IR Signature, Effectiveness on Reducing Temperatures*

200407-7

The or (Bell) of this document is the direct subject of the work done on the Bell's side of the discussion

## Is There an Alternative Solution?

- Jenkins challenged to see if Coanda effect could deflect channel flow
- Literature search did not locate any uses of Coanda effect for this purpose
- Only needed on ground where bleed air losses are acceptable

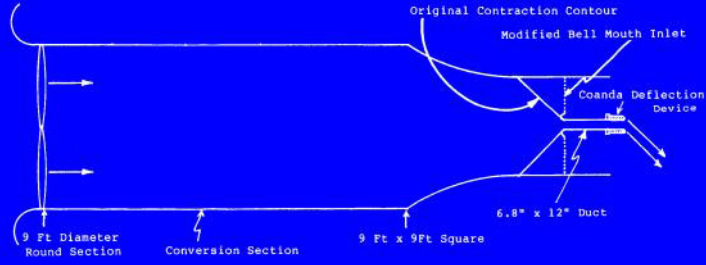


**MANY GOOD IDEAS START AS SKETCHES DURING DISCUSSIONS**

200407-9

The or (Bell) of this document is the direct subject of the work done on the Bell's side of the discussion

# Test Set Up

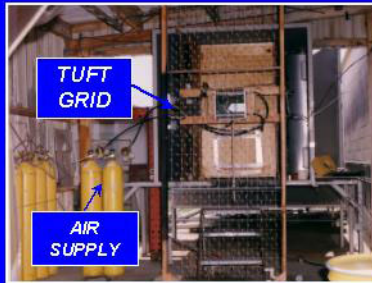


**ESTABLISHING CHANNEL FLOW**

200407-9

The use of Bell Helicopter is restricted to this specific subject unless permission is obtained from Bell Helicopter.

# Small Scale Testing Initiated



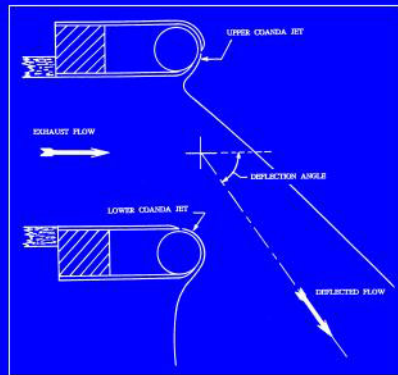
**BALANCE SLOT MOMENTUM WITH EXHAUST MOMENTUM  
VERIFY BLEED MASS FLOW IS ADEQUATE**

200407-10

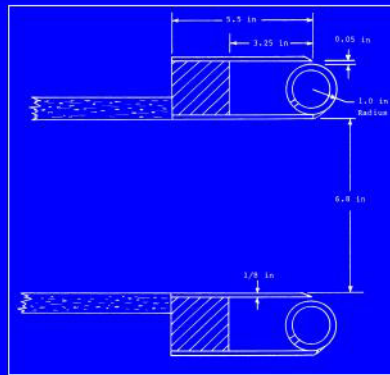
The use of Bell Helicopter is restricted to this specific subject unless permission is obtained from Bell Helicopter.



# Test Configurations



**CONFIG #1: RELEASE FLOW  
AT 90 DEG ON TOP**

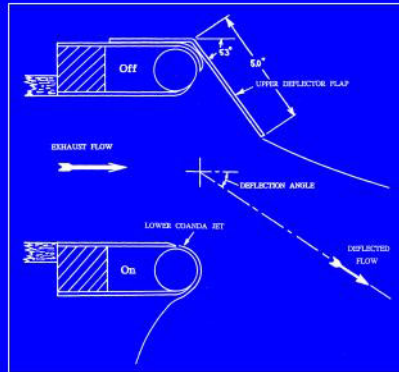


**CONFIG #2: HARDWARE  
IDENTICAL ON BOTH SIDES**

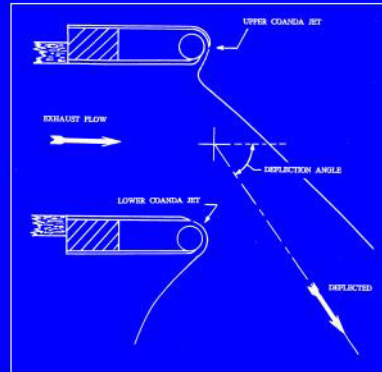
200407-11

Use or disclosure of this content on any media subject to the restriction on the disclosure made in this document

# Test Configurations



**CONFIG #3: RISK REDUCTION  
WITH MECHANICAL ON ONE SIDE**



**CONFIG #4: SMALLER  
DIAMETER COANDA TUBE**

200407-12

Use or disclosure of this content on any media subject to the restriction on the disclosure made in this document

## Test Results



COANDA OFF

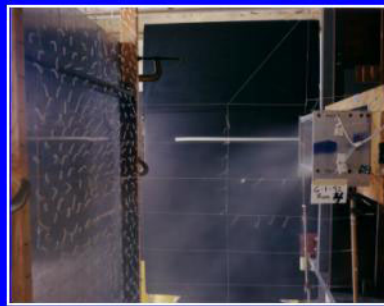


COANDA ON

200407-13

The air flowlines of this model are the result of the interaction of the air flowlines of the air flowlines.

## Investigating Ground Plane Effects

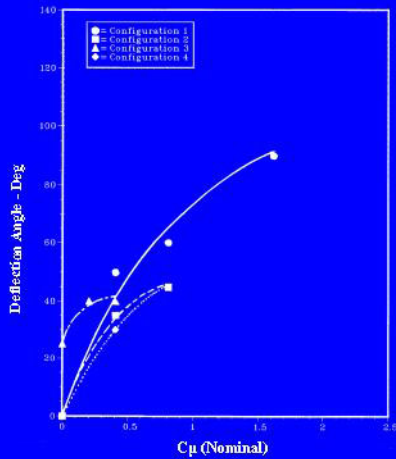


NO CHANGE IN DEFLECTION DUE TO  
GROUND PLANE

200407-14

The air flowlines of this model are the result of the interaction of the air flowlines of the air flowlines.

## Achieved Deflection Angles Greater Than 40 Degrees

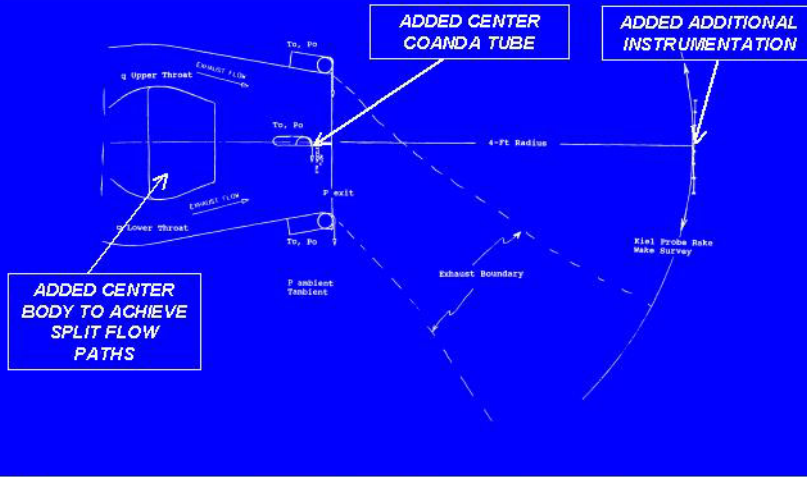


**BASED ON CONCEPT TEST RESULTS, NAVY FUNDED TRADE STUDY BETWEEN COANDA AND MECHANICAL DESIGN**

200407-15

Use or disclosure of this content on any media subject to the restriction on the disclosure of this document

## Upgraded Model to V-22 Representative Cross-Section

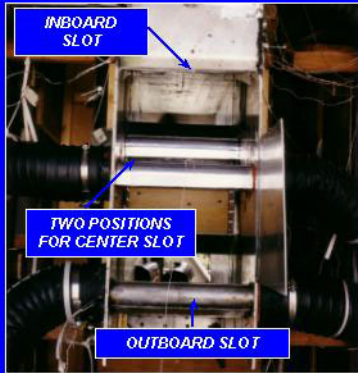


200407-15

Use or disclosure of this content on any media subject to the restriction on the disclosure of this document



## New Set Up



MATCHED V-22 EXHAUST WIDTH WITH 12 INCH LENGTH

200407-17

Use or disclosure of this material is strictly subject to the restrictions of this document

## Instrumentation



KIEL PROBE RAKE FOR DEFLECTION ANGLE

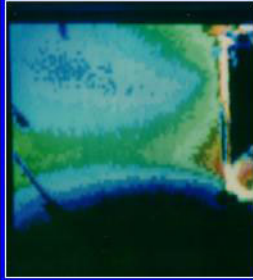


PITOT TUBE FOR FLOW VELOCITIES

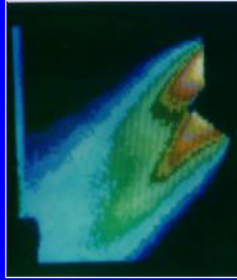
200407-18

Use or disclosure of this material is strictly subject to the restrictions of this document

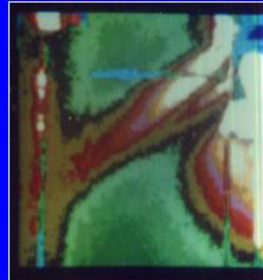
## Imaging Results



NO DEFLECTOR



MECHANICAL  
DEFLECTOR

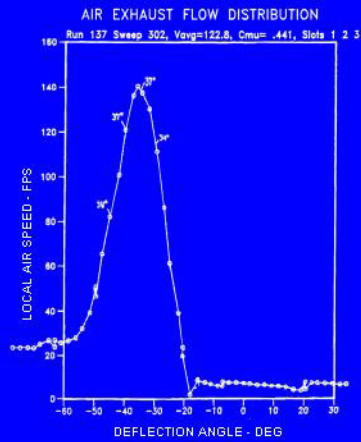


COANDA  
DEFLECTOR

200407-19

The air deflection of this model is not directly subject to the restriction on the deflection angle of the deflector.

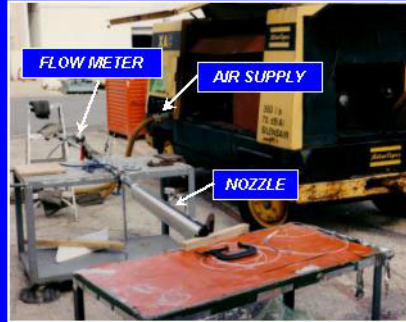
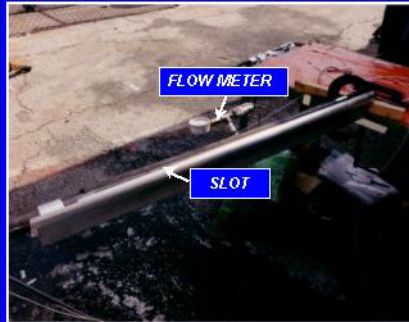
## Achieved 37 Degree Deflection With Coanda Configuration



200407-20

The air deflection of this model is not directly subject to the restriction on the deflection angle of the deflector.

## Full Scale Nozzle Testing



GENERATE UNIFORM FLOW ALONG ENTIRE SLOT WITH SINGLE INLET

200407-21

The use of Bell Helicopter is the subject of this document on the Bell Helicopter website.

## Checking Uniformity of Slot Flow



200407-22

The use of Bell Helicopter is the subject of this document on the Bell Helicopter website.

## Slot Flow Validation



CHECKING UNIFORMITY OF  
SLOT FLOW

ACHIEVED UNIFORM FLOW  
WITH SINGLE INLET AT ONE  
END OF TUBE

200407-23

Use or disclosure of this content to any third party is strictly prohibited on the disclosure date of this document.

## Trade Study Conclusions

- Model tests and analysis indicate Coanda deflector provides same deflection as mechanical door
- Three nozzle configuration which uses 7% engine bleed from 14<sup>th</sup> stage is required
- Full Scale nozzle test showed uniform slot velocities can be achieved using single air supply line
- Estimated weight savings is 64 pounds with a cost savings of \$38,400 per aircraft

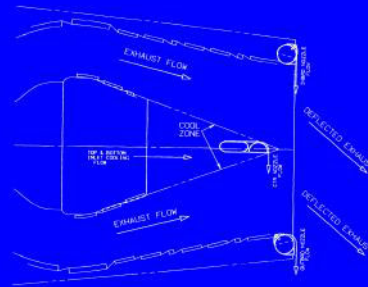
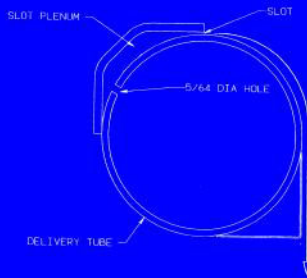
**RECOMMENDED FULL SCALE GROUND TEST**

200407-24

Use or disclosure of this content to any third party is strictly prohibited on the disclosure date of this document.



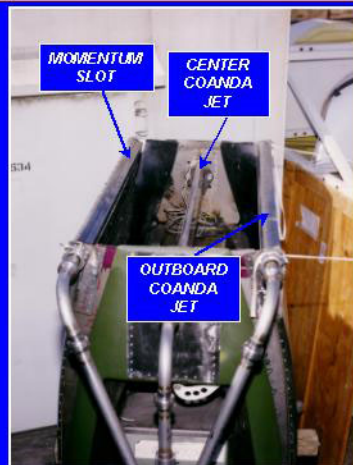
## Coanda Tube Construction and Prototype Installation



200407-26

The use of Bell Helicopter is the subject of this document on the Bell Helicopter website.

## Prototype System Calibration



200407-26

The use of Bell Helicopter is the subject of this document on the Bell Helicopter website.

## Mechanical Deflector Installed on Aircraft



200407-27

The use of Bell Helicopter's mechanical deflector is subject to the restrictions of the applicable FARs.

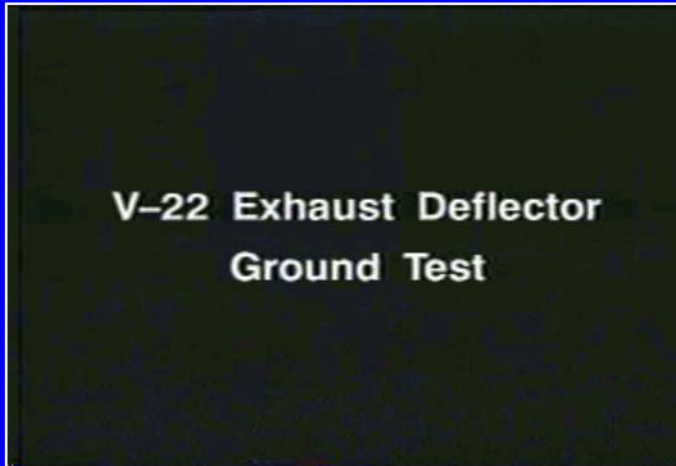
## Prototype Coanda Deflector Installed on Aircraft



200407-28

The use of Bell Helicopter's prototype Coanda deflector is subject to the restrictions of the applicable FARs.

## Moment of Truth Two Nozzle Coanda



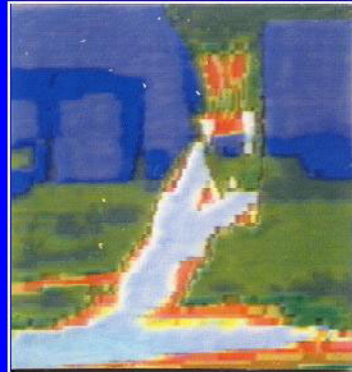
200407-29

The or disclosure of this content to any third party is the responsibility of the disclosure holder of this document

## Deflection Angle is Comparable Between Configurations



TWO NOZZLE COANDA



MECHANICAL DEFLECTOR

200407-30

The or disclosure of this content to any third party is the responsibility of the disclosure holder of this document

## Ground Test Results

- Both mechanical and Coanda deflectors provided equal or lower fuselage temperatures compared to original mechanical deflector
- Three Nozzle Coanda configuration deflected flow 45 degrees or greater
- Two Nozzle Coanda configuration deflected flow 40 degrees

**TWO NOZZLE COANDA CONFIGURATION SELECTED  
FOR PRODUCTION**

200407-31

The contents of this document are the property of Bell Helicopter and are not to be distributed outside the Bell Helicopter organization.

## Sand Evaluation on Coanda Deflector



**TESTING DEMONSTRATED  
COANDA SLOT WOULD  
EXPEL ALL OF SAND  
INGESTED BY ENGINE THAT  
WOULD BE PASSED  
THROUGH BLEED AIR  
SYSTEM**

200407-32

The contents of this document are the property of Bell Helicopter and are not to be distributed outside the Bell Helicopter organization.



## Effectiveness of Coanda Surface if Contaminated With Oil and Dirt

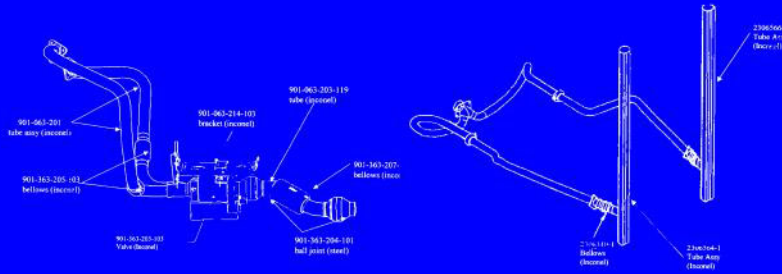


**COANDA BLOWING IS NOT ADVERSELY AFFECTED AND NO FLOW SEPARATION OCCURRED**

200407-33

Use or disclosure of this document is strictly subject to the restrictions of this document.

## Production Configuration



**COANDA TUBING LEADING TO IR SUPPRESSOR**

**COANDA TUBING INSIDE IR SUPPRESSOR**

200407-34

Use or disclosure of this document is strictly subject to the restrictions of this document.

## Coanda System Operation

- Shut off valve controls Coanda deflector bleed air supply
- Operation is controlled by Integrated Avionics System
- Manual override to turn off deflector is provided to pilot
- Pressure switch monitors health of shut off valve
- To operate following criteria must be met
  - Weight on Wheel
  - Nacelle > 52 degrees
  - Ng > 65%

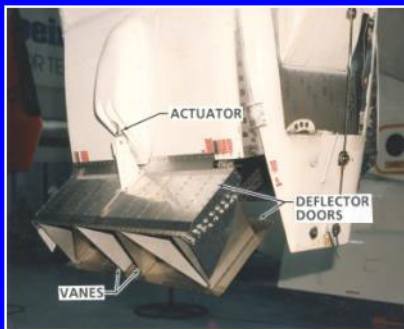
**NOT ALLOWED TO OPERATE IN FLIGHT**

200407-36

Use or disclosure of this content is strictly subject to the restrictions on the disclosure of this document

## Coanda Effect Solution

REPLACE THIS SYSTEM



WITH THIS SYSTEM



200407-36

Use or disclosure of this content is strictly subject to the restrictions on the disclosure of this document

# Today



**OVER 5350 FLIGHT HOURS WITH COANDA DEFLECTOR INSTALLED  
PERFORMS AS EXPECTED  
INSTALLED ON 44 AIRCRAFT TO DATE**



# Simulation of Steady Circulation Control for the General Aviation Circulation Control (GACC) Wing

Warren J. Baker\* and Eric G. Paterson†

Computational Mechanics Division, Applied Research Laboratory  
The Pennsylvania State University, State College, PA, 16803

The aerodynamic characteristics of the General Aviation Circulation Control (GACC) airfoil have been investigated using non time-accurate, 2D, Reynolds-averaged Navier-Stokes simulations with a blended  $k-\omega/k-\varepsilon$  turbulence model. An initial study has been completed to determine the most efficient and accurate method to model the jet flow introduction. Convergence histories show that modeling the jet at the jet orifice, instead of including a plenum decreases computational runtime by a factor of 4, while obtaining accurate results as compared to experiment. A 3-point grid study with  $\sqrt{2}$  refinement was completed for the computational domain without the plenum. Monotonic convergence was not achieved for the grid study, as the convergence rate of  $(\Delta x)^2$  was not consistent with a second order scheme. Results for the fine grid show good agreement of surface pressure over the leading 95% of the foil for a given blowing coefficient. Along the aft 5% of the airfoil, CFDSHIP under predicts the magnitude of both the maxima and minima of surface pressure, located at the two jet-slot exits. Mean lift values agree very well with experiment and previous RANS simulations, but RANS results predict a source of unsteadiness not seen in experiment. This source of unsteadiness may be related to using a large domain approach instead of including the tunnel walls in the computational domain. At larger values of  $C_\mu$ , where no experimental data has been obtained, CFDSHIP simulations differ from previous RANS efforts. The near wall spacing for the coarse and medium grids was insufficient to properly capture the physics of the coanda jet, more specifically, the location of the jet separation. Results for the fine grid RANS simulations are encouraging, and as more data from experiment is obtained, more definitive conclusions may be made.

## Nomenclature

$C_d$	Section drag coefficient = $\frac{F_d}{1/2 \rho U_\infty^2 S}$
$C_l$	Section lift coefficient = $\frac{F_l}{1/2 \rho U_\infty^2 S}$
$C_p$	Pressure coefficient = $\frac{p - p_\infty}{1/2 \rho U_\infty^2}$
$C_\mu$	Jet momentum coefficient = $\frac{\dot{m} U_j}{1/2 \rho U_\infty^2 S}$
$c$	Chord length
$h$	Slot height
$k$	Turbulent kinetic energy (TKE)
$\dot{m}$	Mass flow rate

M	Mach number = $\frac{U}{A}$
P	pressure
Re	Reynolds number = $\frac{\rho U_\infty c}{\mu}$
S	Plan form area
x,y,z	Cartesian Coordinates

## Subscripts

$\infty$	Freestream
j	At jet-slot exit

## Introduction

The concept of circulation control using the Coanda effect is a phenomenon involving a 2D wall bounded jet passing along a curved surface. The jet itself is introduced via a slot, which expels the jet,

\* Graduate Research Assistant, Department of Aerospace Engineering

† Department Head and Senior Research Associate, Computational Methods Development Department

typically, tangential to the curved surface. This jet adds momentum to the boundary layer close to the curved surface, yet still retains properties of a free jet farther away from the curved surface. With the curved surface, the Kutta condition is not held, and the rear stagnation point is free to move. The resultant is a net change in the circulation, and the flow turning and separation location are altered based on the rate of mass addition. Accompanying the change in circulation are changes in certain aerodynamic values such as lift, total drag, and local skin friction coefficient. Figure 1 shows an example of coanda jet circulation control setup with a single slot geometry.

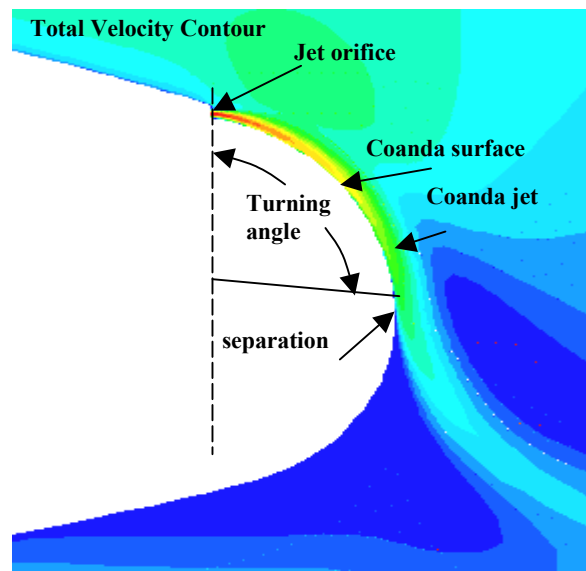


**Figure 1: Trailing edge coanda jet**

The performance benefits of circulation control have been shown in many experiments since the early 1970's.<sup>1-3</sup> Increases in lift of as much as 10 times the typical flap system have been reported. Other possible benefits of the use of circulation control include elimination of moving parts, part/cord decrease, significant weight decrease, and a less complex high lift systems.

Circulation control is very attractive for certain naval applications, in particular, the replacement of current actuation techniques on surface ship and submarine control surfaces with that of circulation control schemes. Circulation control schemes would provide very high lift at very low speeds, i.e., in littoral operation or for evasive maneuvering, where the current control surface technologies are insufficient. The placement of a fixed control surface would increase shock resistance, allow placement of sensors or payload on the control

surface, or even allow for the placement of the control surface in non-traditional areas previously restricted by the need for moving surfaces, such as on the outside of the propulsor duct. Even with the potential for increased performance, other issues need to be addressed before circulation control can become reality on a full-scale production vehicle. Some of these issues include acoustic signature, cavitation, and fouling.

The long term objective of our research is to develop validated simulation tools using multiple data sets. These data sets include a two-dimensional CC experiment using the NCCR 1510-7067N,<sup>2</sup> a low-aspect-ratio, tapered, control surface for marine applications, CCFOIL,<sup>3</sup> and the General Aviation Circulation Control (GACC) wing,<sup>4</sup> the latter two of which are three-dimensional configurations. The work presented herein is the initial effort to investigate steady blowing circulation control of the GACC wing using the Reynolds-Averaged Navier-Stokes (RANS) equations, and knowledge gained here will be combined with that from previous studies of the NCCR foil<sup>5</sup> to continue to develop, validate, and verify our simulation tools for circulation control.

The GACC was selected as a validation benchmark because it provides a modern experiment with Computational Fluid Dynamics (CFD) validation in mind. Also, other CFD efforts have been initiated for the GACC, and both steady and pulsed actuation were used in experiment. The geometry itself has 2 slots (upper and lower) and has multiple trailing edge variants. Our progress is reported in the following sections: Geometry, conditions, and data; Computational methods; Grid generation; Initial and boundary conditions; Results; and Conclusions.

### **Geometry, Conditions, and Data**

The GACC continues to be tested in the Basic Aerodynamics Research Tunnel (BART) at NASA Langley Research Center (LaRC). The GACC section is a modified General Aviation Wing (GAW(1)), and is a supercritical 17% thick airfoil, with two slots. The upper slot is located at  $x/c = 0.985$  and the lower slot is located at  $x/c = 0.975$ . The chord length is 9.4 inches and the free stream velocity for experimentation is 110 ft/sec giving a chord Reynolds number of  $5.33 \times 10^5$  and a free stream mach number,  $M_\infty$ , of approximately 0.10. The slot height-to-cord ratio,  $h/c$ , is 0.0011. The circular trailing edge has a radius-to-chord ratio,  $r/c$ , of 2%. A cross-section of the model is shown in figure 2.

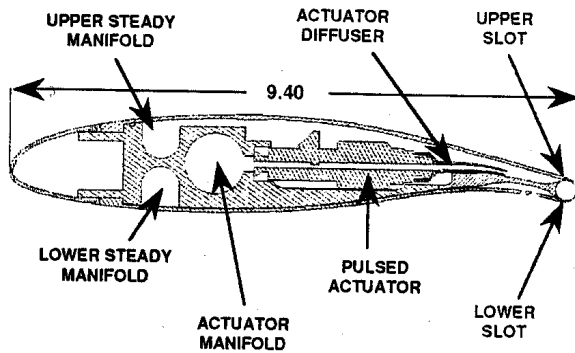


Figure 2: Cross-section of the GACC wing

A range of blowing coefficients,  $C_{\mu}$ , were investigated, with the highest being 0.162. Assuming that the jet is incompressible, the maximum non-dimensional jet velocity, corresponding to a blowing coefficient of 0.162, can be calculated using equation 1, and is 8.33.

$$\frac{U_j}{U_\infty} = \sqrt{\frac{1}{2} \frac{\rho_j}{\rho_\infty} \frac{c}{h} C_\mu} \quad (1)$$

For all cases studied, the angle of attack was  $0^\circ$ .

Available experimental data to this point is mostly for baseline (no blowing), upper slot steady blowing, and dual assist blowing.<sup>3</sup> Present experimentation is focusing on pulsed actuation and initial data from pulsed testing has been released.<sup>6</sup> Table 1 summarizes the data currently available. Experimental uncertainty has not yet been provided.

CFD simulations from Jones et. al., show comparisons to experiment of lift and drag data for a range of steady blowing coefficients. Two slot heights were used in simulations,  $h/c = 0.010$  and  $0.020$ , and results showed good trend agreement for the smaller of the two heights. Figures 3 and 4 show the lift vs. blowing coefficient curve and the drag polar for simulation and experiment, respectively.

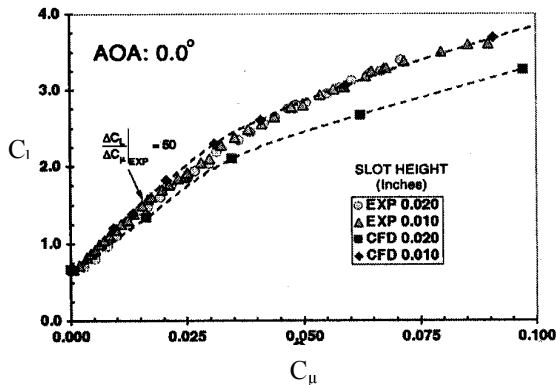


Figure 3:  $C_l$  vs.  $C_\mu$  for previous CFD simulations and experiment

BASELINE (NO JET ACTUATION)	1. SURFACE PRESSURE DISTRIBUTION 2. LIFT-CURVE SLOPE 3. DRAG POLAR
Steady upper slot blowing	1. Surface pressure distribution ( $c_\mu = 0.059$ and $0.162$ ) 2. Lift-curve slope ( $C_\mu = 0.007, 0.015, 0.025, 0.041,$ and $0.060$ ) 3. Lift vs. blowing coefficient (slot height = $0.01''$ and $0.02''$ ) 4. Drag polar 5. Jet exit Mach number profiles ( $c_\mu =$ range from $0 - 0.162$ ) 6. Lift vs. mass flow rate
Pulsed, upper slot blowing	1. Surface pressure distribution ( $C_l = 1.2$ ) 2. Lift vs. mass flow rate
Steady, lower slot blowing	1. "Negative lift configuration" Lift vs. blowing coefficient 2. "Negative lift configuration" drag polar
Dual slot assist steady blowing	1. Drag polar (slot height = $0.01''$ and $0.02''$ ) 2. Drag Polar (matched slot $C_\mu = 0.0, 0.004, 0.005, 0.009, 0.021,$ and $0.0041$ ) 3. drag vs. angle of attack 4. Angle of attack vs. L/D

Table 1: Available data from GACC experiment

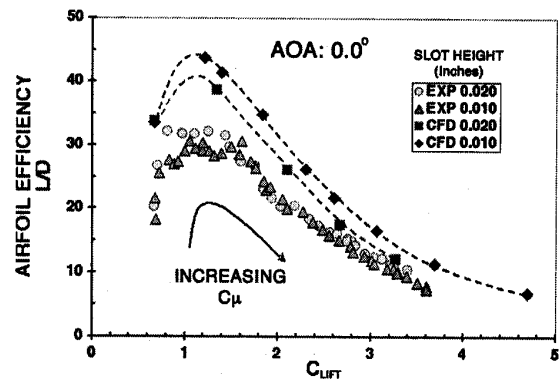


Figure 4: Drag polar for previous CFD simulations and experiment



## Computational Methods

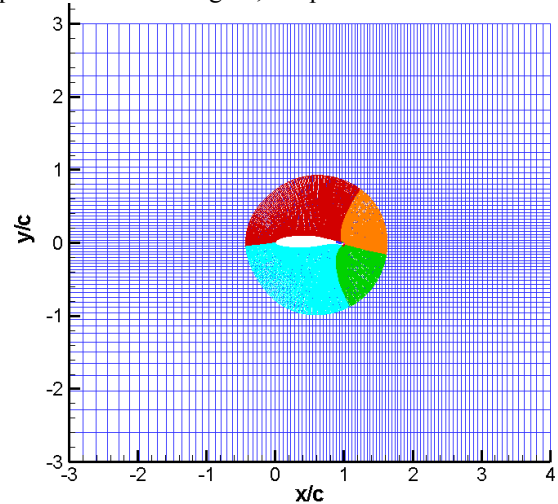
CFDSHIP-IOWA is a general-purpose, parallel, unsteady, incompressible, Reynolds-averaged Navier-Stokes CFD code. The computational approach is based upon structured, overset-grid, higher-order finite-difference, and pressure-implicit split-operator (PISO) numerical methods. Production turbulence model uses a linear closure and the blended  $k-\omega/k-\varepsilon$  SST 2-equation model.<sup>7</sup> Efficient parallel computing is achieved using coarse-grain parallelism via MPI distributed computing. For time-accurate unsteady simulations, global solution of the pressure-Poisson equation is achieved using pre-conditioned GMRES and the PETSc libraries.

## Grid Generation

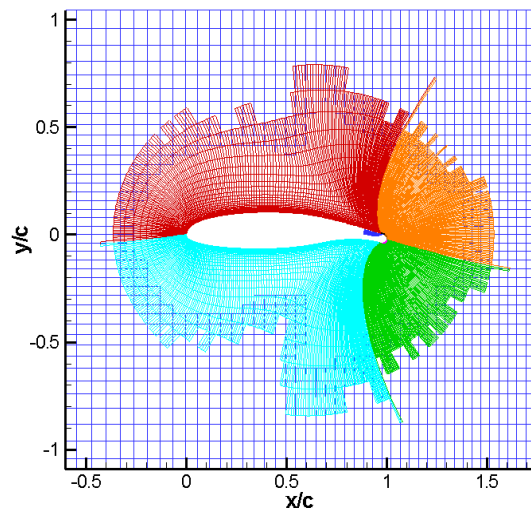
Overset grids are generated primarily using hyperbolic extrusion and orthogonal box grids, although transfinite interpolation and elliptic smoothing of blocks can be used when needed. Overset interpolation coefficients are calculated and holes are cut using Pegasus 5.1.<sup>8</sup> CFDSHIP-IOWA employs double-fringe outer and hole boundaries so that the 5-point discretization stencil (i.e., in each curvilinear coordinate direction) and order-of-accuracy does not have to be reproduced near overset boundaries. The level-2 interpolation capability of PEGASUS 5.1 is used to achieve an optimal match between donor and interpolated meshes.

Two grids were created initially for simulations. One grid included the plenums for modeling of the jet at the diffuser nozzle, whereas the second grid did not contain the plenum grid and modeled the jet at the orifice. The former of the grids is shown in Figure 5. The domain size, as marked by the outermost boundaries of a nested orthogonal box grid, ranges from  $-3 < x/c < 4$ ,  $-3 < y/c < 3$ , and  $0 < z/c < 0.1$ . Near-wall spacing ranged between  $2e^{-5}$ - $2e^{-6}$ . The finer spacing was applied to the circular trailing edge to assure a proper  $y^+ = 1$ , or proper resolution of the sub-layer region of the turbulent boundary layer. Two elliptically smoothed blocks span along the trailing edge from upper to lower slot. Then, a hyperbolically extruded O-grid was used around the body. A plenum block was created and finally, an overset grid was placed along the knife edge of the upper slot, for investigation of the slot-lip interaction. The RANS simulations were performed in a pseudo-2D fashion which requires 5-points in the spanwise direction. The grid contains a total of 9 blocks consisting of 394,665 points. Block

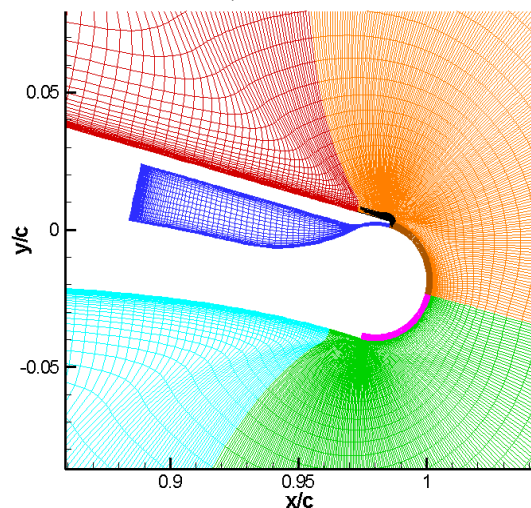
sizes ranged from 31,000 to 61,000 points, with the plenum block having 33,000 points.



a) Overall view



b) Foil view



c) Plenum view

Figure 5: Overset system for grid with plenum



The second grid, shown in Figure 6, which does not include the plenum, totals 8 blocks with 381,810 points. At a few locations slightly larger near wall spacing was used coupled with the 33,000 less points from not including the plenum block accounts for the difference in grid sizes between the grids with and without the plenum block.

A 3-point grid study was completed for uncertainty assessment. The previous grid without the plenum was used as the fine grid for the study. A  $\sqrt{2}$  refinement process was completed to create a medium and coarse grid. This process was completed by decreasing the number of grid points by  $\sqrt{2}$  in each of the x and y directions of the finest grid to create the medium grid. The result is a reduction of grid points by a factor of approximately 1/2 from fine to medium grids. The same process is done to create the coarse grid from the medium. The coarse grid has approximately 1/2 the total grid points as the medium grid and approximately 1/4 the total points of the fine grid. Thus from the fine to coarse grid, we have what is called “grid halving.” Table 1 shows the total number of grid points for the fine, medium, and coarse values. Also to be noted is that from the fine to coarse mesh, all spacing, including near wall spacing is twice as large

Total Grid Points	
Fine	381,810
Medium	193,980
Coarse	97,575

Table 2: Total grid points for the fine, medium, and coarse grids

### Initial and Boundary Conditions

Initial conditions for the steady-state RANS simulations are prescribed to be equal to the free stream velocity, turbulence, and pressure:

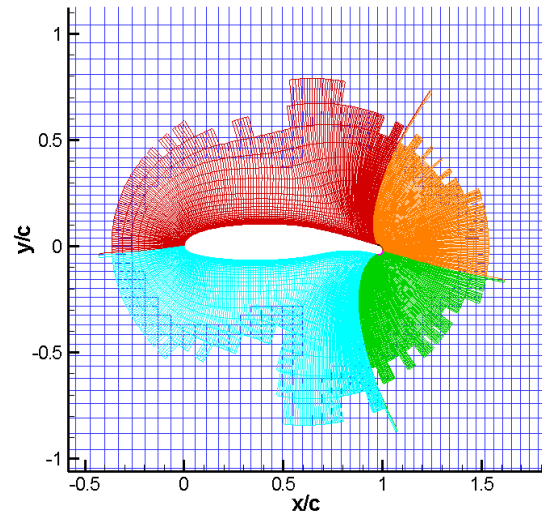
$$\begin{aligned} U &= U_{\infty} & V &= V_{\infty} \\ k &= k_{\infty} & \omega &= \omega_{\infty} \end{aligned} \quad (2)$$

where the subscript  $\infty$  refers to freestream conditions.

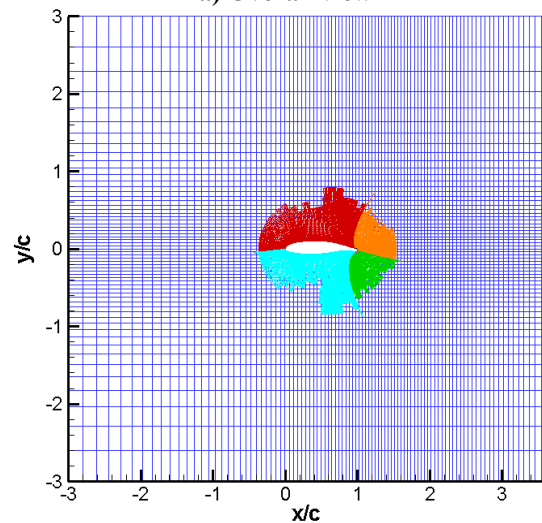
No-slip boundary conditions were applied to the upper and lower surface of the airfoil, the round trailing edge region, and the upper and lower surfaces of the plenum. For each grid, a different boundary condition was specified for the steady blowing.

Figure 7 shows the location of the steady blowing boundary condition for the grid without the plenum. This occurs on the bottom portion of the jet

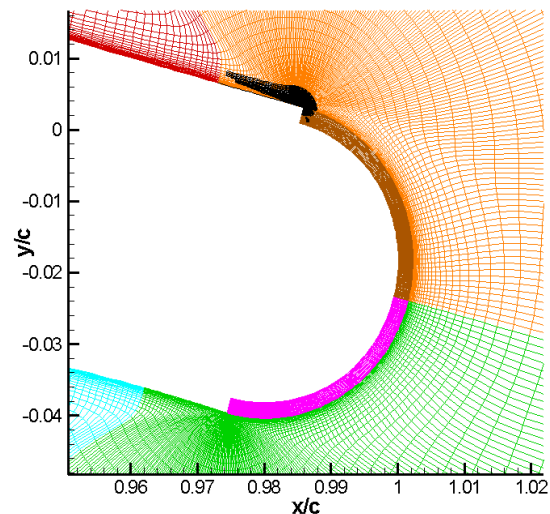
slot. A no-slip condition is prescribed along the top portion of the jet slot. A velocity boundary



a) Overall view



b) Foil view



c) Trailing edge view

Figure 6: Overset system for grid without plenum

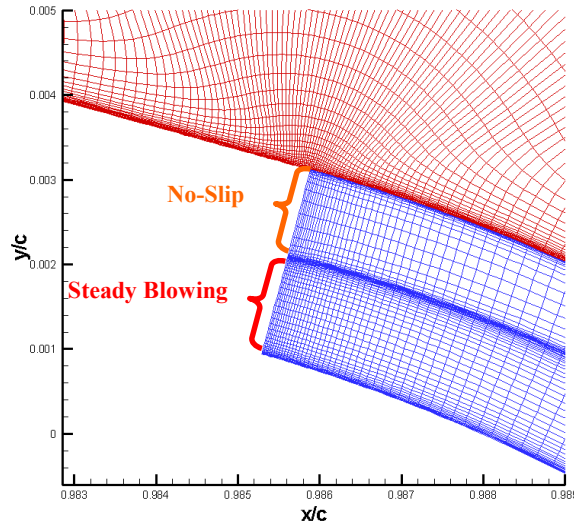


Figure 7: Boundary condition for grid without the plenum

condition is prescribed, and the velocity profile is a 10<sup>th</sup> order polynomial curve fit of a typical CC jet profile seen in previous work<sup>5</sup> and is given by Equation 3.

$$\begin{aligned}
 Upoly = & ((-1.2222 \times 10^2 * y/l^{10}) - (1.7043 \times 10^2 * y/l^9) \\
 & + (1.8036 \times 10^3 * y/l^8) - (3.4603 \times 10^3 * y/l^7) \\
 & + (2.9482 \times 10^3 * y/l^6) - (1.0602 \times 10^3 * y/l^5) \\
 & - (9.7236 \times 10^1 * y/l^4) + (2.2944 \times 10^2 * y/l^3) \\
 & - (8.5386 \times 10^1 * y/l^2) + (1.4472 \times 10^1 * y/l) + 0.0036
 \end{aligned}
 \tag{3}$$

where  $y/l$  is the non-dimensional distance along the boundary. To acquire tangential flow to the round trailing edge, an initial angle of  $\theta = 18^\circ$  was enforced. The velocity boundary condition for the grid without the plenum is given as:

$$U = vjet * ramp * \cos(\theta) * Upoly \tag{4}$$

$$V = vjet * ramp * \sin(\theta) * Upoly \tag{5}$$

where  $vjet$  is the velocity amplitude based on the blowing coefficient and Equation 1, and  $ramp$  is a cubic polynomial used to accelerate the velocity amplitude from 0 to the final value after a non-dimensional time of 1.0. The velocity profile for the boundary condition is shown in Figure 8.

The boundary condition for the grid with the plenum is less complex. Figure 9 shows the

upstream face of the plenum where the steady blowing boundary condition is applied. In this case, the velocity profile prescribed is just a top-hat

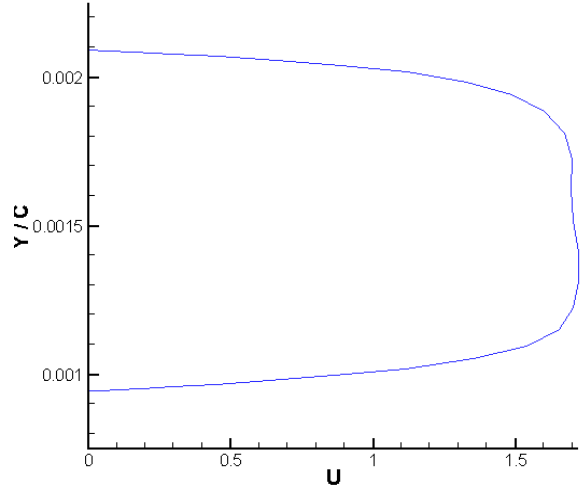


Figure 8: Velocity profile at steady blowing boundary condition

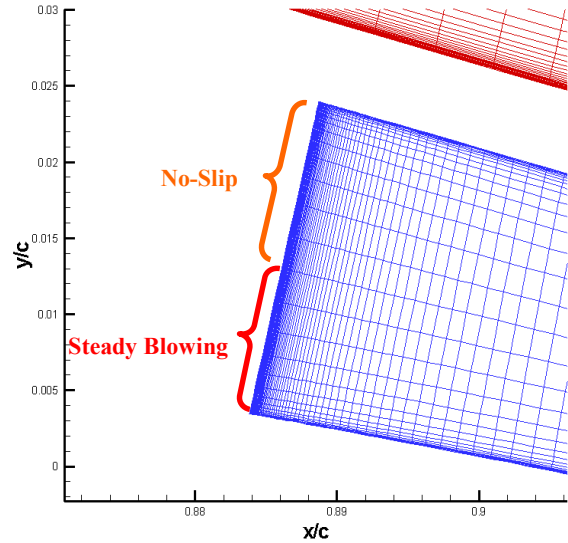


Figure 9: Boundary condition for grid with plenum

distribution. Also, no additional flow angle is required to obtain tangential flow. The velocity boundary condition for steady blowing with the grid including the plenum is given in Equation 6.

$$U = vjet * ramp \tag{6}$$

## Results

All simulations were executed on an IBM SP Power 3 machine with 64 nodes. Each node

contains 16, 375 MHz Power 3 processors. Each cpu has 64 KB level-1 cache and 8 MB level-2 cache memory along with 1 GB RAM. Each processor has a maximum sustainable performance of 1.5 GFLOPS, giving each node 24 GFLOPS peak performance. 3.2 TB of scratch space is available to users.<sup>9</sup> As a reference point, a fine grid without the plenum completed 10,000 iterations (well past convergence for most simulations completed) in 16.7 wall-clock hours or 133.7 cpu hours.

### Plenum vs. No Plenum

Steady RANS simulations of a baseline case at 0° angle of attack and a low blowing coefficient,  $C_{\mu} = 0.031$ , at 0° angle of attack were initially completed for the two grids, with and without plenum. The goal was to determine which technique for modeling the jet would be the most efficient and accurate. When both simulations were run to convergence, results showed good agreement to each other as can be seen in Figure 10, which shows the drag vs. time step number.

Although both grids converge to a similar value, what is of importance is the total time to reach convergence. The case without the grid obtained a converged solution around 5,000 iterations, while the grid with the plenum is not yet completely converged at 20,000 iterations. Both grids had similar runtimes per iteration, thus when calculating the computational costs, one sees at least 4 times the cpu runtime, and one extra cpu per simulation due to the added plenum block. The long time to reach convergence for the grid with the plenum is caused by a lengthy pressure transient inside the plenum along with continued slow pressure convergence throughout the simulation, even after the initial transients.

### $C_{\mu}$ Study

The fine grid without the plenum was chosen for further simulations. A wide range of blowing coefficients was studied, and results were compared to experiment and previous RANS CFD simulations. Experimental data included the surface pressure distribution for one case,  $C_{\mu} = 0.059$ . The corresponding results from CFDSHIP are compared to experiment, and are shown in Figure 11. The simulation compares well to experiment over the leading 95% of the airfoil. Simulation under predicts the magnitudes of the maximum positive pressure by a factor of 2 and over predicts the maximum negative pressure by a factor of 1.5. These locations correspond to the two slot locations at  $x/c = 0.975$  and  $0.985$ , respectively. More investigation needs to be done to further understand the discrepancy, and it must be noted that experimental uncertainty is high

in these regions because of slow pressure leaks during experimentation.

The mean lift coefficient vs. blowing coefficient is shown in Figure 12. The plot shows very good agreement with experiment and previous CFD simulations (FUN2D) for  $C_{\mu} \leq 0.091$ . At higher values of  $C_{\mu}$ , no experimental data has been recorded, but the results vary from FUN2D solutions. Although it does appear that the experimental results are beginning to roll over, similar to the trend CFDSHIP shows, conclusions for larger blowing coefficients are inconclusive until more experimental data is obtained.

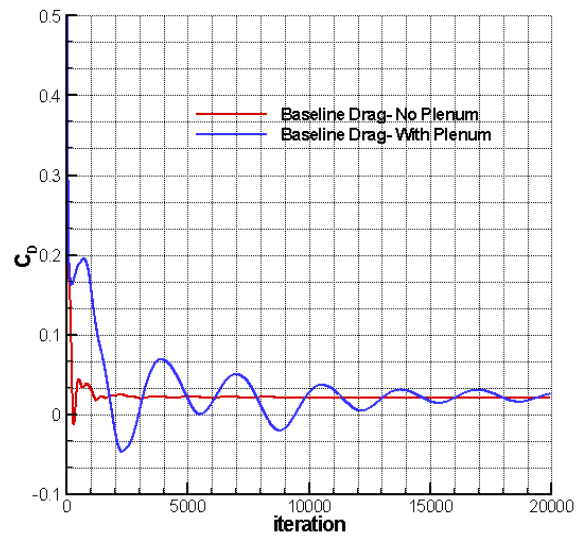


Figure 10: Convergence comparison of drag coefficient for grids with and without plenum

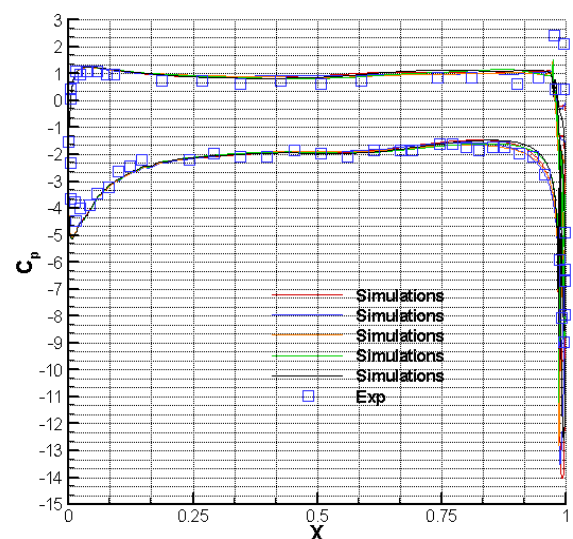


Figure 11: Surface pressure distribution for experiment and simulation-  $C_{\mu} = 0.059$

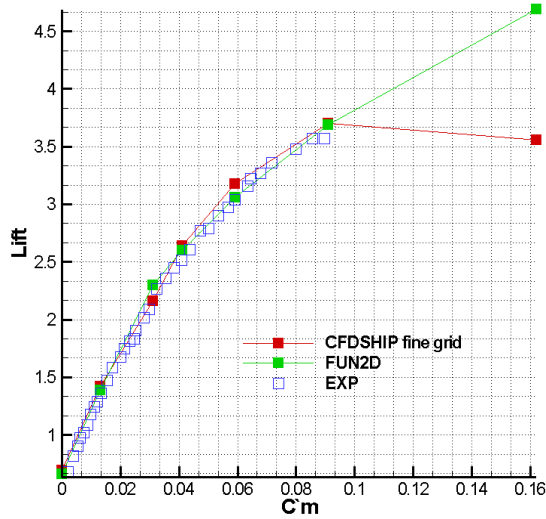


Figure 12: Lift vs.  $C_\mu$  for experiment and simulations

Results show that the difference between the FUN2D and CFDSHIP solutions at the highest blowing coefficient is caused by the prediction of the location of separation of the coanda jet. FUN2D simulations predict the separation at the lower slot as shown in Figure 13, while CFDSHIP predicts the location of separation on the bottom side of the airfoil back upstream about 50% chord (shown by the streamtraces), as shown in Figure 14. Until more experimental data is obtained, it is hard to decide which is more accurate, the FUN2D or CFDSHIP simulation.

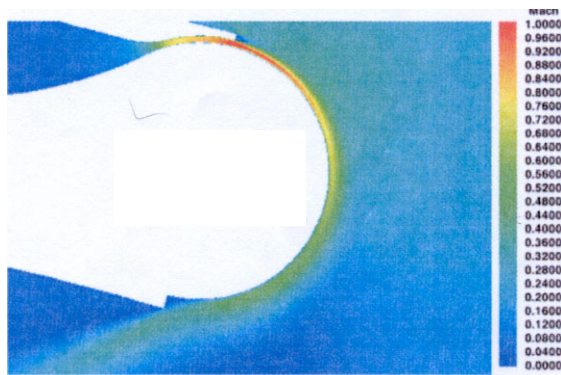


Figure 13: Mach contours for FUN2D simulations  $C_\mu = 0.162$

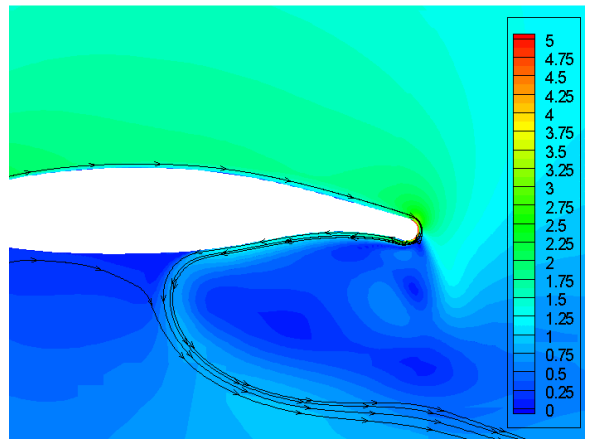
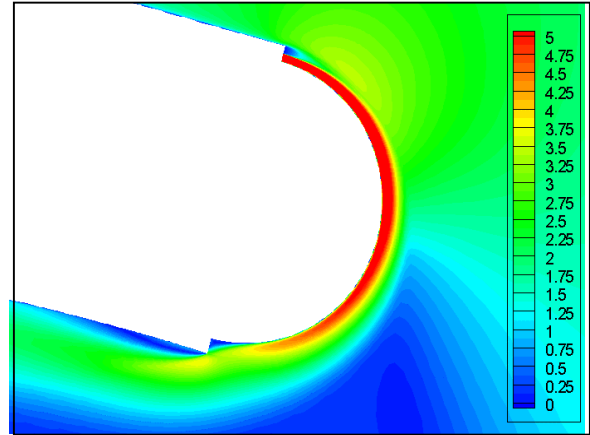


Figure 14: Total velocity contours for CFDSHIP simulations  $C_\mu = 0.162$

Figure 15 shows the time history of the lift and drag coefficient for a wide range of  $C_\mu$ . For  $C_\mu \leq 0.031$ , forces are steady. For larger  $C_\mu$ , forces begin to show unsteadiness. As the blowing coefficient increases, the amplitude of the unsteadiness increases, and the frequency decreases. It can be seen in Figure 16 that the surface pressure changes quite a bit, especially at the trailing edge, across one period of unsteadiness, corresponding with the significant changes in the forces. Experimental data obtained thus far does not show the unsteadiness as predicted by simulations.

The turbulent kinetic energy is shown in figure 17, for a low, moderate, and high blowing coefficient. For the lowest blowing coefficient,  $C_\mu = 0.021$ , there exists two definitive regions of increased turbulent kinetic energy (TKE).



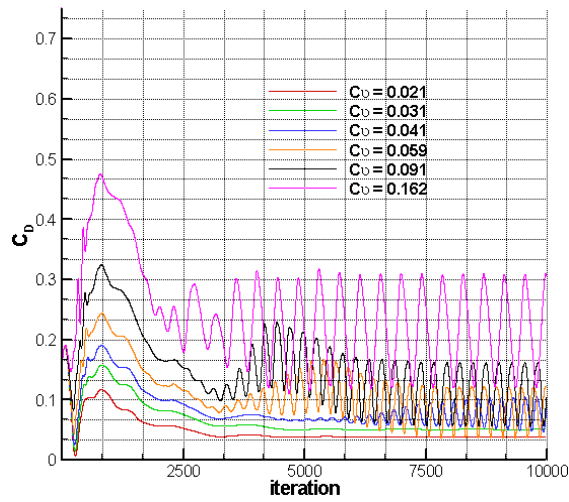
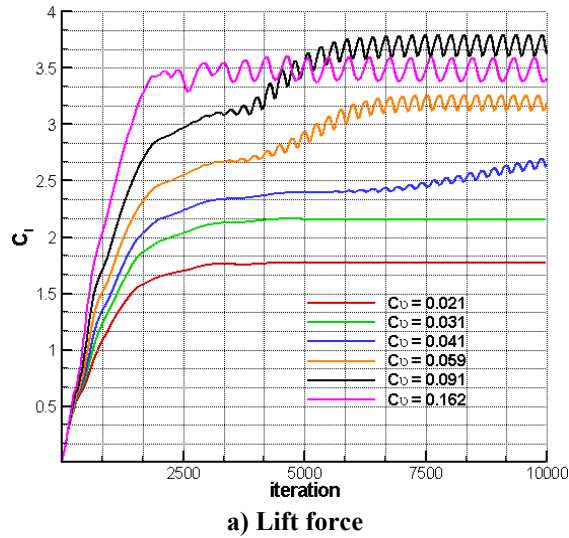


Figure 15: Force histories for a wide range of  $C_\mu$

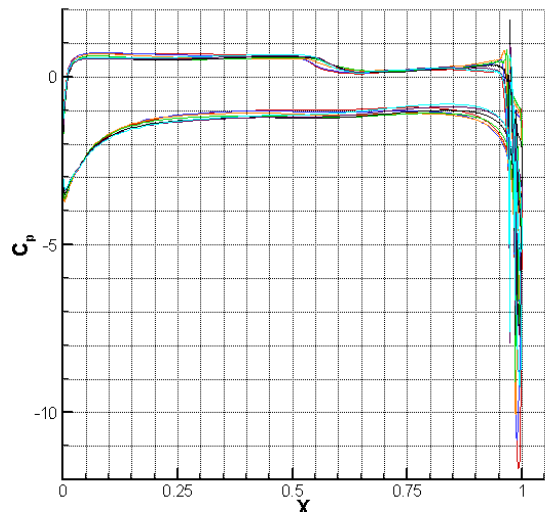


Figure 16: Surface pressure at different intervals along 1 period of unsteadiness-  $C_\mu = 0.162$

The first, denoted as (a), is the interaction of the jet shear layer and layer from the top half of the foil beginning just aft of the jet orifice and terminating at the jet separation. The second region of high TKE, (b), originates near the jet slot separation and protrudes into the wake. At the moderate blowing coefficient,  $C_\mu = 0.059$ , we see the same interaction of the jet shear layer and layer from the top half of the foil, (a). The second region of high TKE comes from the interaction of the jet passing around the bottom corner of the slot, and the small recirculation zone in the inside corner of the slot and round trailing edge, (b). For the highest blowing coefficient,  $C_\mu = 0.162$ , (a) is the same as the previous 2 blowing coefficients, and the second region of high TKE originates at the location of jet reattachment after the jet has wrapped back around the lower slot, (b).

### Grid Study

A 3-point grid study was completed for verification of results, as detailed in a previous section. Table 2 shows grid size and runtimes for each of the 3 grids used in the study. These values coincide with a non-time-accurate RANS simulation of 10,000 iterations for each grid.

	Coarse	Medium	Fine
Grid Points	97,575	193,980	381,810
Seconds/time step	1.0	2.8	6.5
Wall-clock hours	3.6	9.9	16.7
Cpu hours	29.1	79.1	133.7

Table 3: Grid size and runtime characteristics for grid study

A wide range of blowing coefficients was investigated, and results were compared to each other and experiment. Figure 18 shows a plot of mean lift coefficient vs. blowing coefficient for all three grids compared to experiment. All three grids show agreement to experiment for the baseline case. It was determined that coarse and medium grids were of inadequate fidelity to capture the coanda jet physics properly, in particular, the location of separation of the coanda jet (not shown here) due to insufficient near wall spacing, which caused inaccuracies in the prediction of the turbulent kinetic energy in the buffer layer. To correct this

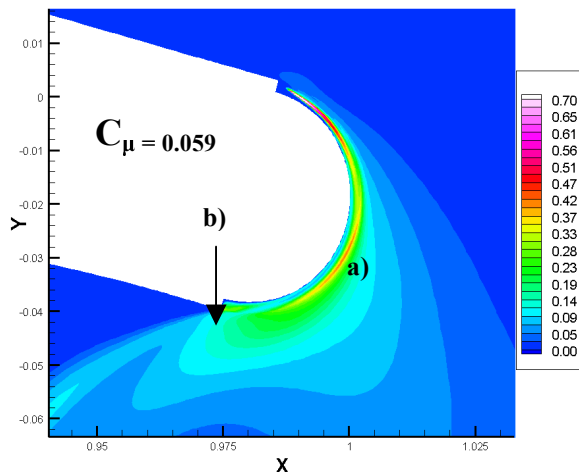
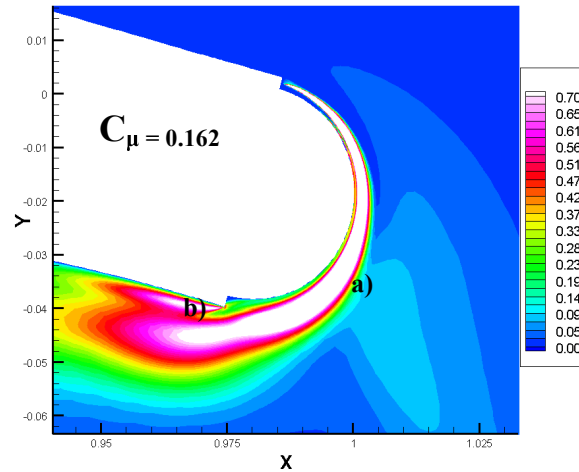
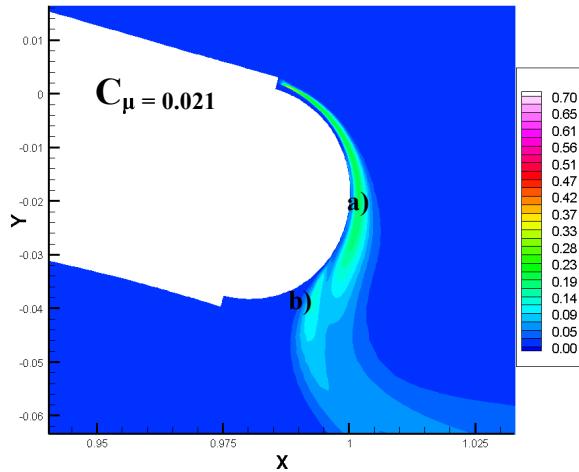


Figure 17: Turbulent kinetic energy for selected  $C_{\mu}$

problem we need to assure that the finest grid has a near wall spacing less than or equal to 0.5 to assure that the coarse grid has near wall spacing less than or equal to 1.0. The coarse, medium, and fine solutions show monotonic divergence, and to properly complete the grid study, it would require including a grid with more nodes than the current fine grid, perhaps a  $\sqrt{2}$  increase.

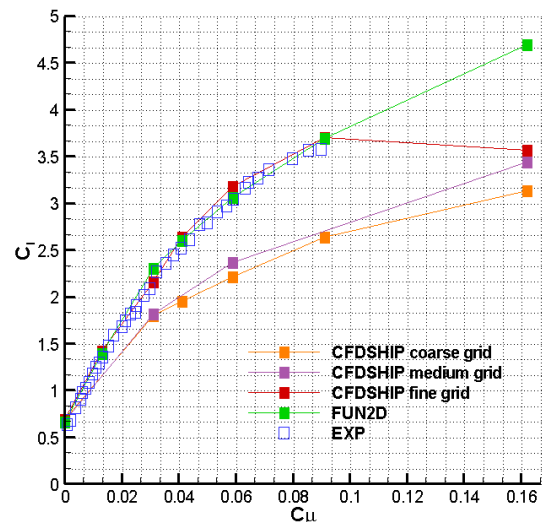


Figure 18: Lift vs.  $C_{\mu}$  for experiment and simulations

### Conclusions

The General Aviation Circulation Control wing was studied using non time-accurate, RANS CFD. It

was shown that by careful consideration, computational runtime could be decreased by modeling the jet at the orifice instead of including the plenum and modeling the jet at the diffuser nozzle exit, shown in figures 7 and 9, respectively.

After choosing the most efficient grid, a study of the mean forces on the airfoil for a wide range of blowing coefficients showed good agreement with experiment and previous RANS efforts for blowing coefficients  $C_\mu \leq 0.091$ . For higher coefficients, no experimental data is provided and CFDSHIP results differ from previous RANS results. CFDSHIP simulations showed the presence of unsteady flow due to the jet separation and interaction with the wake. Initial indications are that experiment did not show these details, but further clarification is needed. A grid study was performed to verify results, but showed monotonic divergence from the coarse to fine grid solutions. Both the medium and coarse grids had insufficient near wall spacing along the coanda surface, which effected the modeling of the buffer layer turbulent kinetic energy.

Future work includes recreating the grid to add in the tunnel walls and optimizing the near wall spacing. This will determine what effects the interaction between the wake and the tunnel walls have on the source of unsteadiness. Some early indication from experiment is that there was interaction between the wake and tunnel walls, but no quantitative value could be given yet. Other means to address this include using time-accurate RANS to investigate whether the oscillations shown are a product of the computational model, i.e. the large domain, or a result of non time-accurate simulations. Finally, a finer grid, with  $\sqrt{2}$  more points compared to the current fine grid in the x and y direction, needs to be investigated to properly verify results.

### **Acknowledgements**

The authors acknowledge NAVSEA SUB-RT (Program Manager: Ms. Meg Stout) for support in the form of a graduate student fellowship for the first author, and to the Office of Naval Research for support through Grant Number N00014-03-1-0122 (Program Officer: Dr. Ron Joslin) for the second author. Also, the authors would like to acknowledge the DoD High Performance Computing Modernization Office (HPCMO) and Army Research Laboratory- Major Shared Resource Center for providing computing resources through a DoD HPCMO Challenge Project.

### **References**

- 1) Englar, R.J., Stone, M.B., and Hall, M., "Circulation Control-An Updated Bibliography of DTNSRDC Research and Selected outside references," DTNSRDC Report 77-0076, September 1977.
- 2) Abramson, J., "Two-Dimensional Subsonic Wind Tunnel Evaluation of Two Related Cambered 15-Percent Circulation Control Airfoils," DTNSRDC ASED-373, September 1977.
- 3) Rogers, E.O., and Donnelly, M.J., "Characteristics of a Dual-Slotted Circulation Control Wing of Low Aspect Ratio Intended for Naval Hydrodynamic Applications," 42<sup>nd</sup> AIAA Aerospace Sciences Meeting & Exhibit, Reno, NV, January 5-8, 2004, AIAA Paper 2004-1244, 2004.
- 4) Jones, G.S., Viken, S.A., Washburn, L.N., Jenkins, L.N., and Cagle, C.M., "An Active Flow Circulation Controlled Flap Concept for General Aviation Aircraft Applications," AIAA Paper No. 2002-3157, 2002.
- 5) Paterson, E.G., and Baker, W.J., "Simulation of Steady Circulation Control for Marine-Vehicle Control Surfaces," 42<sup>nd</sup> AIAA Aerospace Sciences Meeting and Exhibit, Reno, NV, January 5-8, 2004, AIAA Paper 2004-0748, 2004.
- 6) Jones, G.S., and Engle, R.J., "Advances in Pneumatic-Controlled High-Lift Systems Through Pulsed Blowing," 21<sup>st</sup> Applied Aerodynamics Conference, Orlando, FL, June 23-26, 2003, AIAA Paper 2003-3411, 2003.
- 7) Menter, F., "Two-Equation Eddy Viscosity Model for Engineering Applications," *AIAA Journal*, Vol. 32, No. 8, 1994.
- 8) Suhs, N., Dietz, W., Rogers, S., Nash, S., and Onufer, J.T., "PEGASUS User's Guide Version 5.1e," Technical Report., NASA 2000.
- 9) ARL MSRC IBM SP Information, "<http://www.arl.hpc.mil/userservices/ibm.html>"

## Simulation of Steady Circulation Control for the General Aviation Circulation Control (GACC) Wing

Presented by Warren Baker and Eric Paterson

NASA Langley  
March 16-17, 2004

- Introduction
- Objectives
- GACC Experiment
  - ◆ Geometry
  - ◆ Flow conditions
  - ◆ Experimental data
  - ◆ Related CFD efforts
- Approach
  - ◆ Flow code
  - ◆ Grid generation
  - ◆ Boundary conditions
- Results
- Future Work

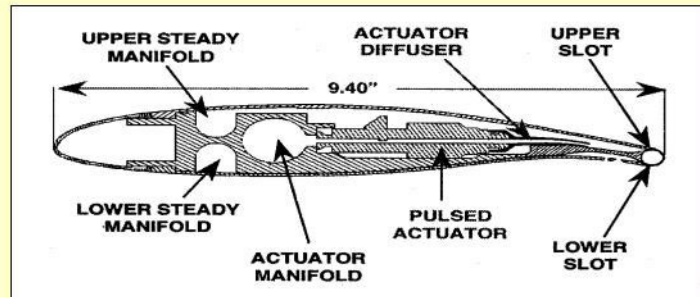


- Naval need: effective and safe low-speed littoral operations without degrading traditionally good open-water performance
  - ◆ Traditional control surfaces lose control authority at low speeds
  
- Circulation control (CC) provides a method for achieving increased maneuvering forces necessary at low speeds or for high-lift events such as evasive maneuvers
  
- CC offers other potential benefits
  - ◆ fixed control surfaces
    - ◆ improved shock resistance
    - ◆ placement of sensors and payloads on control surfaces
  - ◆ placement of control surfaces on the propulsor duct and other non-traditional locations precluded by actuation constraints.

3

- Develop validated simulation tools using:
  - ◆ Wind-tunnel data for a pulsed CC configuration (Jones et al., 2002)
  - ◆ Incompressible water-tunnel data for a low aspect-ratio tapered control surface (Rogers and Abramson, 2003)
  - ◆ NCCR foil (Abramson 1977)
    - ◆ Demonstrated that standard 2-equation models could resolve coanda effect lift increment
    - ◆ DES may provide a route to hydro-acoustics but requires development of "grey-region" models
  
- This work represents the initial efforts to apply RANS to the pulsed GACC airfoil (Jones et al.)
  - ◆ 2D geometry
  - ◆ Modern experiment (with CFD validation in mind)
  - ◆ Dual slot configuratin
  - ◆ Steady and pulsed actuation
  - ◆ Multiple trailing edge variants
  - ◆ Other RANS CFD efforts

4



- NASA LaRC GACC
  - ◆ Modified GAW-1
  - ◆ 17% supercritical airfoil- provides ample interior volume for CC hardware
  - ◆ 2% r/C trailing edge
  - ◆ Dual slot configuration

5

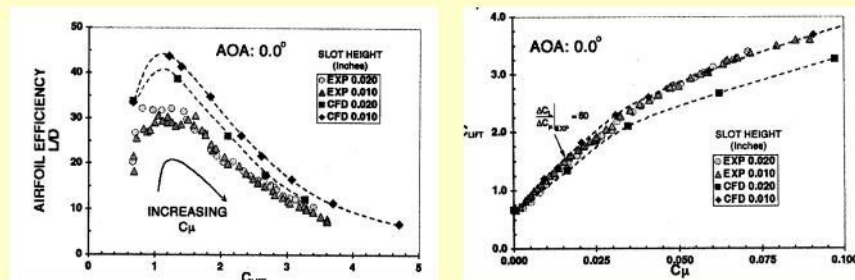
$Re_c$	$5.33e^5$
$U_\infty$	110 ft/sec
Chord (in)	9.4
Tunnel Medium	Air
Slot height	0.01" and 0.02"
$V_{jet} / V_\infty$	0 - 9
$Re_{jet}$	$\sim 1.02e^4$ (0.01" slot)
$M_{jet}$	$\sim 0.8$

6

- NASA Langley, 2002-present
- Baseline (no blowing)
  - ◆ Surface pressure distribution
  - ◆ Lift-curve slope
  - ◆ Drag polars
- Steady blowing
  - ◆ Surface pressure distribution ( $c_{\mu} = 0.059$ )
  - ◆ Lift-curve slope ( $c_{\mu} = 0.007, 0.015, 0.025, 0.041, 0.060$ )
  - ◆ Lift vs. blowing coefficient (slot height = 0.01" and 0.02")
  - ◆ Drag polars for single slot and dual assist blowing
- Pulsed blowing
  - ◆ Surface pressures for full airfoil and detailed coanda surface
  - ◆ Lift vs. mass flow
- Data Uncertainty – ?

7

- Jones et al 2002
  - ◆ Fun2D- unstructured, compressible simulations
  - ◆ Presented data matching experiment
  - ◆ Trend agreement- better performance for slot height of 0.010



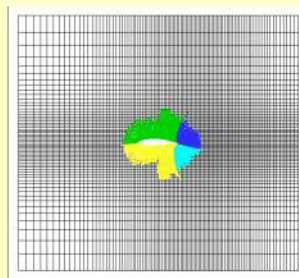
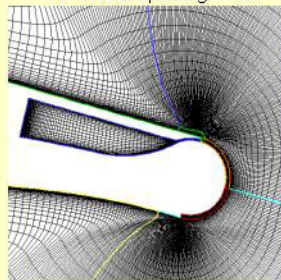
8

- CFDSHIP-IOWA (Paterson et al., 2003) is a general-purpose, parallel, unsteady, incompressible, Reynolds-averaged Navier-Stokes (RANS) CFD code
  - ◆ Structured overset grids- CHIMERA overset gridding via interface with PEGASUS (NASA Ames)
  - ◆ Higher order finite-difference schemes
  - ◆ Pressure-implicit split-operator (PISO) algorithm
  - ◆ Blended  $k-\omega$  /  $k-\epsilon$  SST 2-equation model
  - ◆ Coarse-grain parallelism via MPI distributed computing
  - ◆ Pre-conditioned GMRES solver for pressure-Poisson equation

9

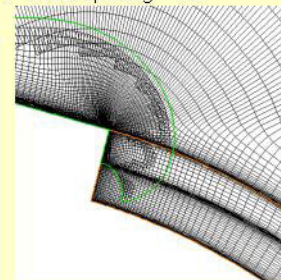
■ **Option 1- With plenum**

- ◆ 9 blocks
- ◆ 394,665
- ◆ Initial spacing =  $2e^{-6}$



■ **Option 2 - Without plenum**

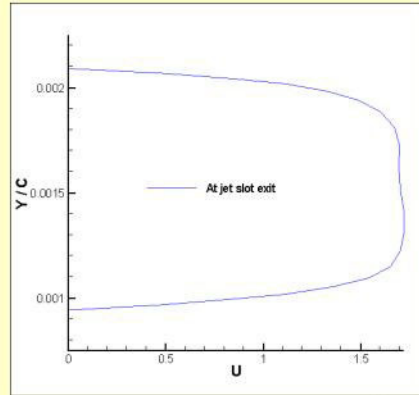
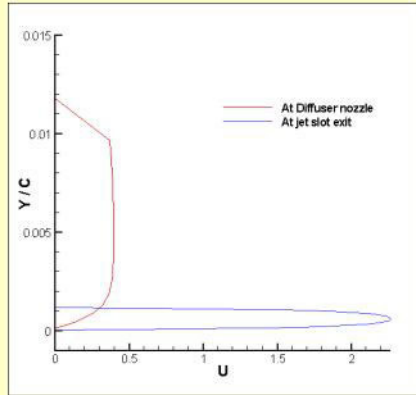
- ◆ 8 blocks
- ◆ 381,810 nodes (fine mesh)
- ◆ Initial spacing =  $2e^{-6}$



- Rectangular far field boundary
- O-grid around the body
- Higher fidelity along coanda surface
- Refinement around the upper slot

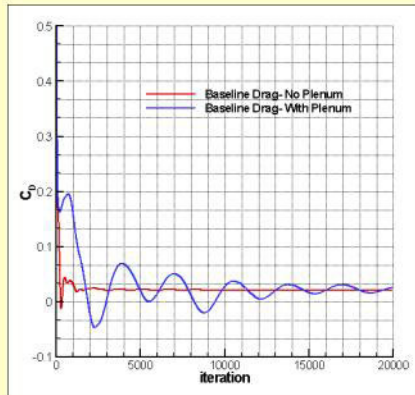
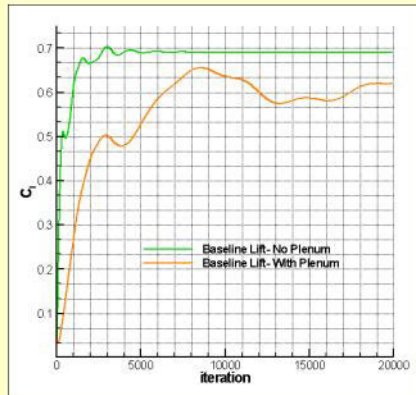
10

- Jet velocity profiles with plenum
- Jet velocity profiles without plenum



11

- Time step history of the forces shows much higher computational costs per simulation
- Note that the plenum forces were not removed in the figures
- Chose the grid without the plenum for further simulations



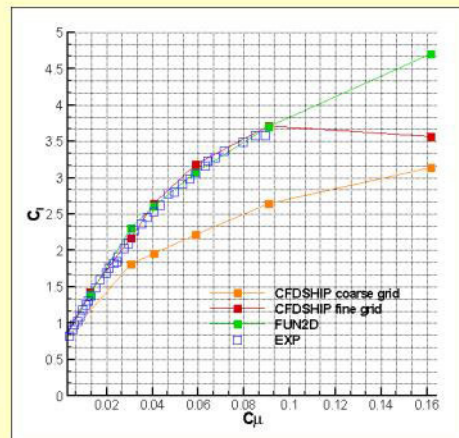
12



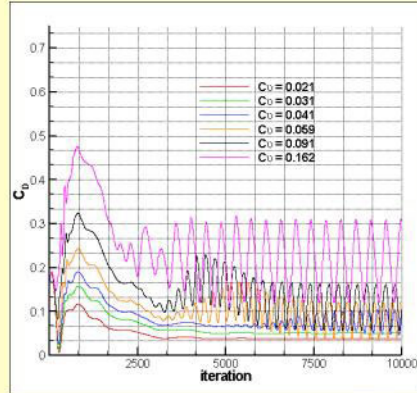
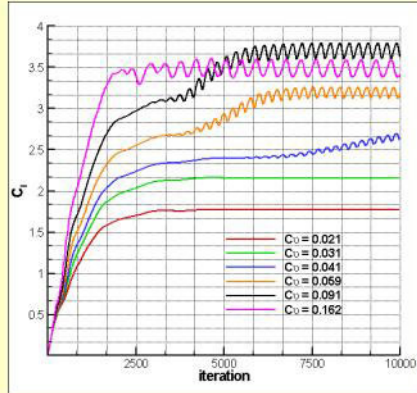
- 3 point grid study using grid refinement ratio of  $\sqrt{2}$   
(Fine → Coarse is grid halving)
- Simulations were completed on an IBM P3

	COARSE	MEDIUM	FINE
Nodes	74,700	150,342	381,810
Seconds/time step	1.0	2.8	6.5
Wall-clock hours	3.6	9.9	16.7
Total cpu hours	29.1	79.1	133.7

- $0 \leq C_{\mu} \leq 0.091$ 
  - ◆ Simulations show agreement with experimental data
- $C_{\mu} > 0.091$ 
  - ◆ No experimental data
  - ◆ CFDSHIP  $C_l$  levels off
  - ◆ FUN2D  $C_l$  shows linear increase
- Large grid dependence shown. Medium-grid simulations in progress.
- Relate  $C_l$  results to force time histories, surface pressure, and flow-field animations.

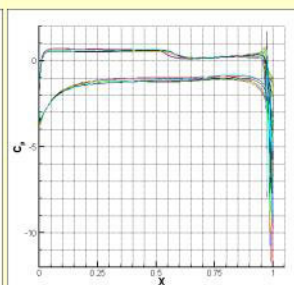
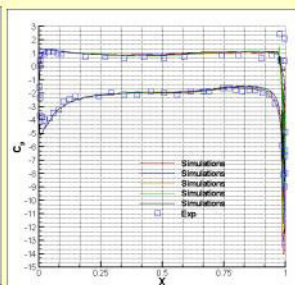
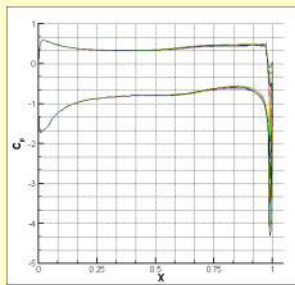


- Forces begin to show unsteadiness for  $C_{\mu} \geq 0.041$
- Amplitude of unsteadiness increases with increasing  $C_{\mu}$
- Frequency decreases for increasing  $C_{\mu}$



15

- Surface pressure for  $C_{\mu} = 0.041$
- Surface pressure for  $C_{\mu} = 0.059$  with experimental data
- Surface pressure for  $C_{\mu} = 0.162$

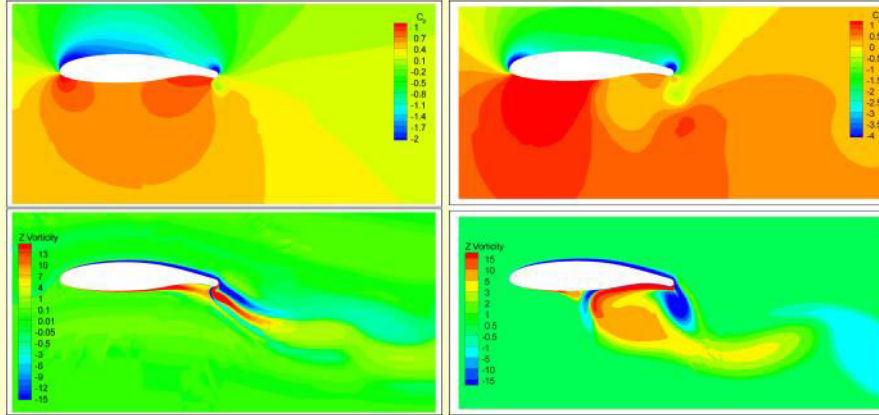


16

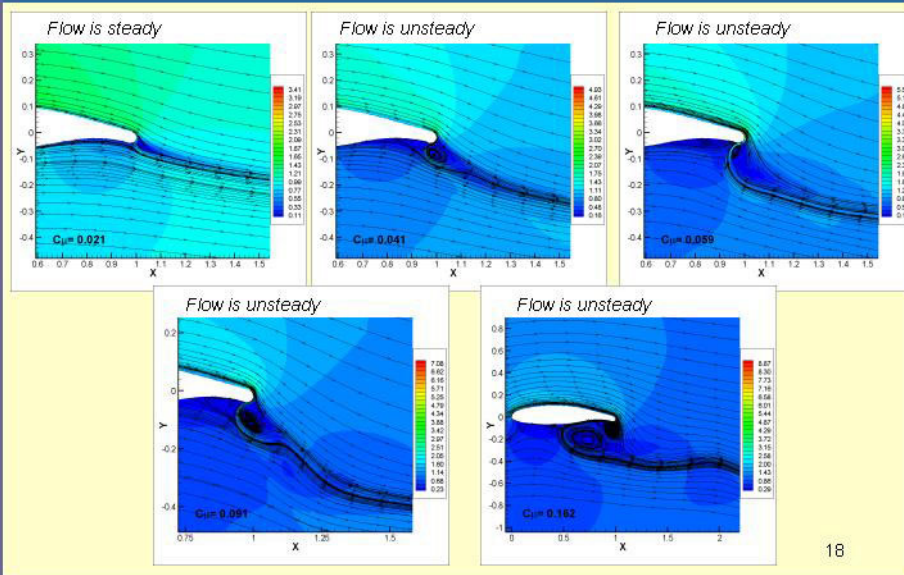


■ Pressure and Vorticity contours for  $C_{\mu}=0.041$

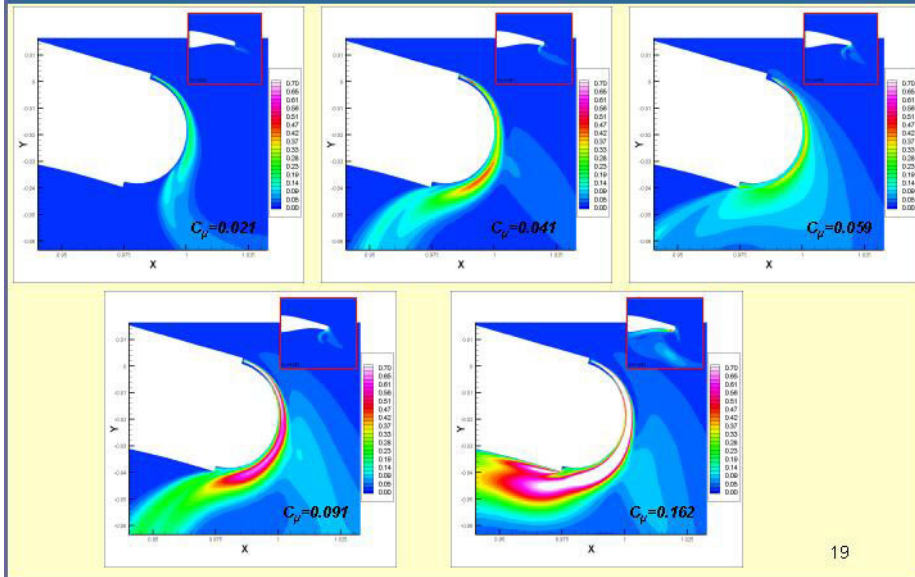
■ Pressure and Vorticity contours for  $C_{\mu}=0.162$



17



18



19

- Complete Medium-Grid Simulations
- DES for steady blowing
- URANS and DES for pulsed blowing
  - ◆ Interaction between forces and natural unsteadiness
- Application of ARL CHAMP (Combined Hydro-acoustic Modeling Program)
- Complete M.S. Thesis Aug 2004

20



# CFD Analysis of a Circulation Control Airfoil Using Fluent

Gregory McGowan\* and Ashok Gopalarathnam<sup>†</sup>  
*North Carolina State University, Raleigh, NC 27695-7910*

## Abstract

In an effort to validate computational fluid dynamics procedures for calculating flows around circulation control airfoils, the commercial flow solver FLUENT was utilized to study the flow around a general aviation circulation control airfoil. The results were compared to experimental and computational fluid dynamics results conducted at the NASA Langley Research Center. The current effort was conducted in three stages: (i) a comparison of the results for free-air conditions to those from experiments, (ii) a study of wind-tunnel wall effects, and (iii) a study of the stagnation-point behavior. In general the trends in the results from the current work agree well with those from experiment, some differences in magnitude are present between computations and experiment. For the cases examined, FLUENT computations showed no noticeable effect on the results due to the presence of wind-tunnel walls. The study also shows that the leading-edge stagnation point moves in a systematic manner with changes to the jet blowing coefficient and angle of attack, indicating that this location can be sensed for use in closed-loop control of such airfoil flows.

## Nomenclature

$A$	area
$b$	wing span
$c$	chord
$C_d$	drag coefficient
$C_l$	lift coefficient
$C_m$	pitching moment coefficient about quarter chord
$C_\mu$	momentum coefficient
$h$	slot height
$\dot{m}$	mass flow rate
$M$	Mach number
$P$	pressure
$q$	dynamic pressure

---

\*Graduate Research Assistant, Department of Mechanical and Aerospace Engineering, Box 7910. e-mail: gzmcgowa@ncsu.edu.

<sup>†</sup>Assistant Professor, Department of Mechanical and Aerospace Engineering, Box 7910, (919) 515-5669. e-mail: ashok\_g@ncsu.edu.

$R$	gas constant for air
$r$	radius of coanda surface
$Re$	Reynolds number
$T$	temperature
$U$	velocity magnitude
$w$	slot width
$\alpha$	angle of attack
$\gamma$	ratio of specific heats
$\mu$	viscosity
$\rho$	density

### Subscripts

$duct$	stagnation conditions inside plenum
$fc$	conditions at flow-control boundary
$\infty$	freestream conditions
$J$	slot-exit conditions

## 1 Introduction

Recent research in the Applied Aerodynamics Group at NCSU has led to the development of an automated cruise-flap system.<sup>1,2</sup> The cruise flap, introduced by Pfenninger,<sup>3,4</sup> is a small trailing-edge flap which can be used to increase the size of the low-drag range of natural-laminar-flow (NLF) airfoils. The automation is achieved by indirectly sensing the leading-edge stagnation-point location using surface pressure measurements and deflecting the flap so that the stagnation-point location is maintained at the optimum location near the leading-edge of the airfoil. Maintaining the stagnation point at the optimum location results in favorable pressure gradients on both the upper and lower surfaces of the airfoil. With such a cruise-flap system, the airfoil is automatically adapted for a wide speed range. This automated cruise-flap system was successfully tested in the subsonic wind tunnel at NCSU.<sup>2</sup>

While the use of a cruise flap on an NLF airfoil results in low drag over a large range of speeds, there is a need for a revolutionary approach that integrates the achievement of significantly lower drag over a large range of operating speeds with the capability for generating very high lift at takeoff and landing conditions. Toward this objective, it is of interest to study an approach that integrates aerodynamic adaptation with the well-established high-lift capability of circulation control (CC) aerodynamics. This aerodynamic adaptation carries with it the possibility for significant skin-friction drag reductions through extensive laminar flow in addition to the high-lift benefits of CC aerodynamics. Figure 1 illustrates the overall concept. In a manner similar to a cruise flap, it is believed that by utilizing this stagnation-point sensing scheme, an adaptive CC airfoil can achieve extensive laminar flow over a large lift-coefficient range.

As a first step toward the long-term goal of studying an adaptive CC airfoil, the current effort was undertaken for establishing and validating computational fluid dynamics (CFD) analysis procedures for blown-trailing-edge airfoils. The CFD package used for this work was the FLUENT flow solver. The results are compared to CFD and experimental data obtained from a recent study by Jones et al.<sup>5</sup> of a General Aviation CC (GACC) airfoil conducted at the NASA Langley Research Center. Since previous CFD studies on this airfoil did not include tunnel walls, the current CFD



study also includes an investigation of the effect of tunnel walls on the solution. In order to provide a foundation for the adaptive CC airfoil concept, the effects of CC on the leading-edge stagnation-point location was also examined in the current work.

## 2 Approach

### 2.1 CFD study

The commercial flow-solver code FLUENT version 6.1 was used in the current research. Grid generation was performed using GAMBIT, which is the preprocessor packaged with the FLUENT code. These codes were used to study two separate cases. The first case involves the examination of the GACC airfoil in free air with the objective of comparing the FLUENT results to CFD and wind-tunnel results presented in Ref. 5. The second case involves simulations of the GACC airfoil in the Basic Aerodynamic Research Tunnel (BART) to examine the influence of tunnel walls on this particular airfoil. Results from FLUENT were obtained for a matrix of 15 data points for both the cases.

#### 2.1.1 Geometry and grid details

The geometry chosen for the current research was the General Aviation Circulation Control (GACC) airfoil, designed by Jones.<sup>5</sup> The GACC airfoil was derived from a 17% GAW(1) airfoil by modifying the trailing edge to incorporate a 2%  $r/c$  coanda surface and is shown in Fig. 2.

For the first study, a circular computational domain (Fig. 3) was generated that extends to approximately 20 chord lengths in all directions and is comprised of 132,762 cells. For the study of wall effects, a second grid was generated to include the wind-tunnel geometry and is shown in Fig. 4. The experiments were conducted by Jones et al.<sup>5</sup> in the BART wind-tunnel which is located at the NASA Langley Research Center in Hampton, Va. The BART tunnel has a physical test-section size of 28"  $\times$  40"  $\times$  120". The GACC model chord length was 9.4" with angle of attack changes made about the half-chord location. The details of the experimental setup are given in Ref. 6. For the computation with walls, a separate grid was generated for each angle of attack, each of which is comprised of 123,602 cells and extends to 20 chord lengths upstream and downstream of the airfoil.

The grids for all of the analyses are hybrid unstructured grids. The domains consist of an unstructured grid far from the airfoil in order to reduce the number of cells and structured grid near the airfoil in order to maintain good resolution through the boundary and shear layers.

#### 2.1.2 Solver settings

For the current study, the steady, coupled, and implicit solver settings with node-based discretization scheme were selected. The coupled solver was chosen for two reasons. First compressibility effects need to be modeled, as the Mach number at the slot exit can often approach the sonic condition as the blowing rate is increased. Secondly, the FUN2D code has a compressible solver and because the results from the current study were compared with FUN2D results, a compressible solver was also used for the

FLUENT analysis. There was an attempt to run these problems with the segregated (decoupled) solver using very low relaxation factors, however it was found that for the cases with larger blowing rates the solution began to exhibit an unsteady effect after a few thousand iterations. In order to compare with the FUN2D<sup>5</sup> results, the one-equation Spalart-Allmaras turbulence model was chosen.

### 2.1.3 Boundary conditions

FLUENT does not allow the user to input freestream Mach number and Reynolds number directly. Instead, the freestream velocity and operating pressure were calculated using Eqs. 1–3 and provided as inputs for the analyses. The Mach and Reynolds numbers were set to 0.1 and 533,000, respectively, to match those used in Ref. 5

$$U_\infty = M_\infty \sqrt{\gamma RT_\infty} \quad (1)$$

$$\rho_\infty = \frac{Re\mu_\infty}{U_\infty c} \quad (2)$$

$$P_\infty = \rho_\infty RT_\infty \quad (3)$$

An approximate method was developed to estimate the required velocity at the flow control boundary ( $U_{fc}$ ) to achieve a desired  $C_\mu$ ,  $C_{\mu_{desired}}$ . This method assumes incompressible flow throughout the duct, and was derived by solving the continuity equation. The equation for  $U_{fc}$  from this approximate method is given in Eq. 4.

$$U_{fc} = U_\infty \sqrt{\frac{C_\mu A_J c b}{2A_{fc}^2}} \quad (4)$$

Once FLUENT converged, an integration was performed across the slot exit as shown in Eq. 5 to obtain the actual  $C_\mu$  of the jet at the slot. This  $C_\mu$ , however, is different from  $C_{\mu_{desired}}$  because the  $U_{fc}$  for the latter is set using an approximate method.

$$C_{\mu_{integrated}} = \frac{\int_{slot} \rho V^2 dy}{\frac{1}{2} \rho_\infty V_\infty^2 c b} \quad (5)$$

Furthermore, in order to be consistent with the methods used for calculating  $C_\mu$  in Ref. 5, all of the  $C_\mu$  values presented in this paper were calculated using isentropic flow relations.<sup>5</sup> The equations for this procedure are given in Eqs. 6–8. In order to determine how close the isentropic  $C_\mu$  is to the integrated  $C_\mu$ , the two values are compared in Fig. 5 for several cases. The  $C_\mu$  values indicated along the x-axis are values calculated using the isentropic relations. Values for  $C_\mu$  on the y-axis were computed by integrating the flow across the slot exit. The solid line in Fig. 5 indicates where the data points would lie if the two methods generated the same values for  $C_\mu$ . The symbols are representative of the actual values calculated using FLUENT and isentropic relations. Although the differences are very small, care must be taken to ensure consistency in the CFD solutions and experiments.

$$\dot{m} = \rho_J U_J A_J \quad (6)$$



$$U_J = \sqrt{\frac{2\gamma RT_{duct}}{\gamma - 1} \left(1 - \left(\frac{P_\infty}{P_{duct}}\right)^{\frac{\gamma-1}{\gamma}}\right)} \quad (7)$$

$$C_\mu = \frac{\dot{m}U_J}{q_\infty cb} = 2 \left(\frac{hw}{cb}\right) \left(\frac{\rho_J}{\rho_\infty}\right) \left(\frac{U_J}{U_\infty}\right)^2 \quad (8)$$

### 3 Results

The results from FLUENT predictions for the GACC airfoil are presented in three parts. In the first part, the prediction for the GACC airfoil in free-air conditions are compared with the results presented in Ref. 5. In the second part, the predicted results for the GACC airfoil with tunnel walls are presented and compared with the free-air results. In the third part, the effect of  $\alpha$  and  $C_\mu$  on the leading-edge stagnation-point location are presented and discussed.

#### 3.1 Results for free-air conditions

In this part of the study, FLUENT results for free-air conditions are compared with CFD and experimental results from Ref. 5. The comparison is illustrated using  $C_l$ - $\alpha$  curves in Fig. 6. The results from FLUENT analyses consist of a matrix of 15 data points for  $\alpha = -5, 0,$  and  $5$  deg and  $C_\mu = 0, 0.008, 0.024, 0.047,$  and  $0.078$  and are presented in Fig. 6 using red dashed lines and square markers. The wind-tunnel results from Ref. 5 are presented as blue markers with best-fit lines in Fig. 6 for several angles of attack and for  $C_\mu = 0, 0.007, 0.015, 0.025, 0.041,$  and  $0.060$ . The values of  $C_\mu$  for the FLUENT results differ from those for the results of Ref. 5 because of the difference between the actual  $C_\mu$  and the desired  $C_\mu$  when using the approximate method in Eq. 4 for estimating the  $U_{fc}$  using incompressible-flow equations.

Although the values of  $C_\mu$  for the FLUENT results do not match those for the results of Ref. 5, it is clear that the trends and most of the predictions for the  $C_l$  are close to those from Ref. 5. In particular, the FLUENT predictions for  $C_\mu = 0, 0.008,$  and  $0.047$  agree quite well with the results for similar values of  $C_\mu$  from Ref. 5. Two discrepancies between the FLUENT predictions and those from Ref. 5 are apparent: (i) for the  $C_\mu = 0.024$  and (ii) for  $C_\mu = 0.078$ . The reason for the first discrepancy in the results is attributed to the incorrect prediction of the jet-separation location on the Coanda surface for  $C_\mu = 0.024$ . The apparent discrepancy in the results for  $C_\mu = 0.078$  is attributed to nonlinear effects at the high blowing rates and the fact that the highest blowing rate in the results of Ref. 5 is for  $C_\mu = 0.060$ .

The flow-field data for the FLUENT results are presented in two separate parts. In the first part, the effects of increasing  $C_\mu$  for a constant angle of attack is presented. The second part examines the effect of angle-of-attack changes and their influence on the CC airfoil for a constant  $C_\mu$ . The flow-field data is presented as pressure contours and streamline plots; these aid in the understanding of the effects of CC on the flow over the airfoil.

The first part of the flow-field data is shown in Figs. 7(a)–(c). It can be seen that as the blowing rate is increased the streamlines become more curved — an indication of increased circulation. The second part of the flow-field data is shown in Figs. 8(a)–(c) and Figs. 9(a)–(c) to illustrate the effects of changing the angle of attack while

holding blowing rates constant. The results are presented for two blowing rates: the mild blowing case  $C_\mu = 0.047$  and the highest blowing rate  $C_\mu = 0.078$ . The results show that changes to  $C_\mu$  have a significant effect on the jet-separation location and the resulting  $C_l$ . In comparison, changes to  $\alpha$  have a much smaller effect on the jet-separation location.

### 3.2 Wind-tunnel wall effects

In this sub-section, the FLUENT results for the GACC airfoil with the effect of wind-tunnel walls are presented. Figures 10–12 show the influence of the wall on the CFD solution. These figures present the predicted  $C_l$  as a function of  $C_\mu$  for  $\alpha = 0, 5,$  and  $-5$  deg respectively. Figure 10 also includes a comparison to results for the FUN2D study<sup>5</sup> for  $\alpha = 0$  deg, the only angle of attack for which the FUN2D results were presented in Ref. 5. Figures 10–12 indicate that the presence of walls has very little influence on the CFD solution. The solution, including tunnel walls, consistently show that for low blowing coefficients, the  $C_l$  values are predicted to be lower than those without walls. However, at the largest blowing coefficients, the trend reverses and  $C_l$  values with walls are predicted to be higher than those without walls.

### 3.3 Stagnation-point location

The motivation for examining the stagnation-point behavior is that the stagnation-point location was used successfully in earlier research<sup>1,2</sup> for closed-loop control of a trailing-edge flap. It was, therefore, desirable to examine the CFD solutions for the CC airfoils to see if there was any evidence that would suggest that a similar approach could be extended for use with CC airfoils.

Stagnation-point location, measured as an arc length from the jet exit around the upper surface of the airfoil, as a function of  $C_l$  is presented in Fig. 13. Each line in Fig. 13 represents a different blowing rate and for each blowing coefficient there are three points that correspond to three different angles of attack ( $-5, 0,$  and  $5$  deg). From Fig. 13 it can be seen that the stagnation point moves in a predictable manner, both with angle of attack and with changing blowing rate. This behavior provides an indication that the stagnation-point location can be used as a means to develop closed-loop control of the jet  $C_\mu$  on CC airfoils.

## 4 Conclusions

The results from a two-part CFD study using the FLUENT flow solver have been presented. Results of the first study show that while the FLUENT predictions do not match the CFD and experimental results of Ref. 5 exactly, the overall trends are followed very closely. Throughout the range of blowing coefficients, FLUENT consistently predicted a slightly lower overall lift coefficient.

In addition, a study was performed on the influence of wind tunnel walls on the CFD solution. For low blowing coefficients, it was found that the lift is predicted to be lower for the cases with walls. The trends are reversed for the higher blowing coefficients, for which the cases with walls yield a higher predicted lift. Although the

solutions are different, the differences are small, and could as well be attributed to differences in the grids rather than the actual presence of walls.

The influence of circulation control on the leading-edge stagnation point location was examined. It was shown that changes in blowing rate and angle of attack result in systematic changes to the stagnation-point location. This observation indicates that it is possible to use a closed-loop control system by sensing the stagnation-point location.

## 5 Acknowledgments

The authors would like to acknowledge the funding for this research through a grant from the NASA Langley Research Center and the National Institute of Aerospace. The technical monitor, Dr. Greg Jones of NASA Langley, is thanked for many valuable discussions and for the geometry of the GACC airfoil and the wind-tunnel test results. In addition Dr. Greg Stuckert from FLUENT Inc. and Dr. Hassan Hassan of NCSU are thanked for their advice regarding the CFD simulations.

## References

- [1] McAvoy, C. W. and Gopalarathnam, A., “Automated Cruise Flap for Airfoil Drag Reduction over a Large Lift Range,” *Journal of Aircraft*, Vol. 39, No. 6, 2002, pp. 981–988.
- [2] McAvoy, C. W. and Gopalarathnam, A., “Automated Trailing-Edge Flap for Airfoil Drag Reduction Over a Large Lift-Coefficient Range,” AIAA Paper 2002–2927, June 2002.
- [3] Pfenninger, W., “Investigation on Reductions of Friction on Wings, in Particular by Means of Boundary Layer Suction,” NACA TM 1181, August 1947.
- [4] Pfenninger, W., “Experiments on a Laminar Suction Airfoil of 17 Per Cent Thickness,” *Journal of the Aeronautical Sciences*, April 1949, pp. 227–236.
- [5] Jones, G. S., Viken, S. A., Washburn, A. E., Jenkins, L. N., and Cagle, C. M., “An Active Flow Circulation Controlled Flap Concept for General Aviation Aircraft Applications,” AIAA Paper 2002–3157, 2002.
- [6] Cagle, C. M. and Jones, G. S., “A Wind Tunnel Model to Explore Unsteady Circulation Control for General Aviation Applications,” AIAA Paper 2002–3240, 2002.

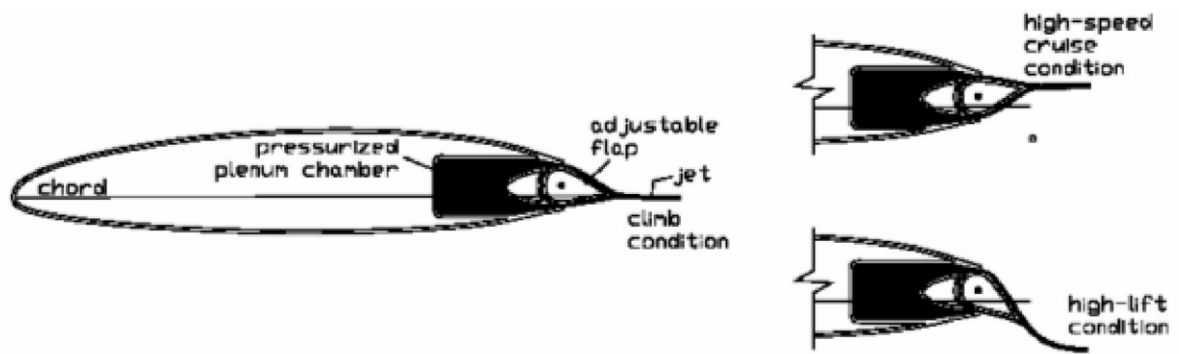


Figure 1: Illustration of the NCSU concept of an adaptive circulation control airfoil.

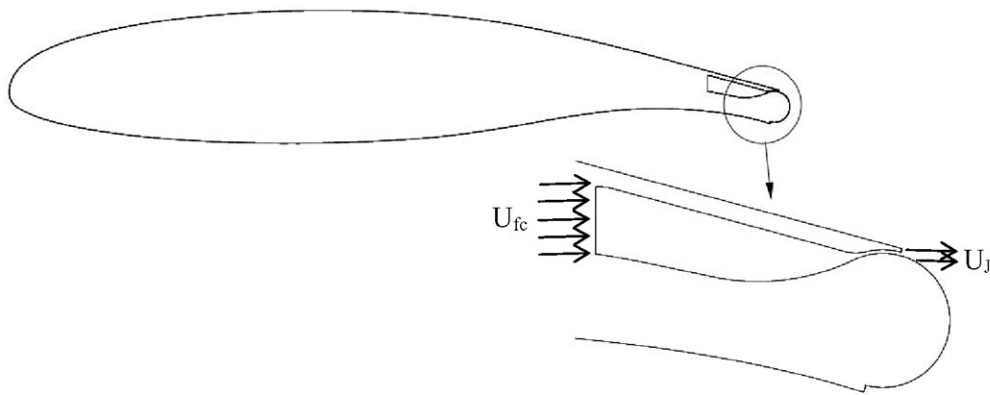


Figure 2: General Aviation Circulation Control (GACC) airfoil geometry used in the current research.

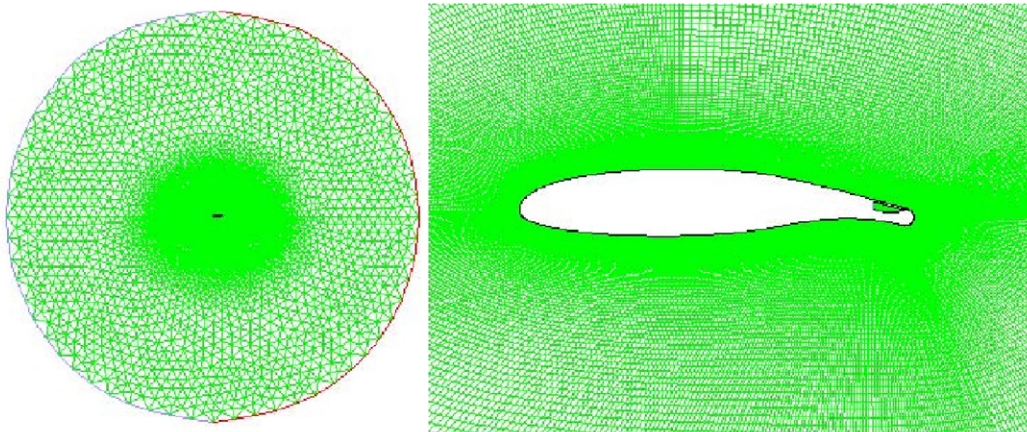


Figure 3: Grid generated for FLUENT comparison to FUN2D.



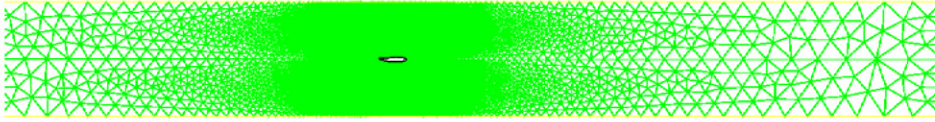


Figure 4: Grid generated for FLUENT study of wall effects.

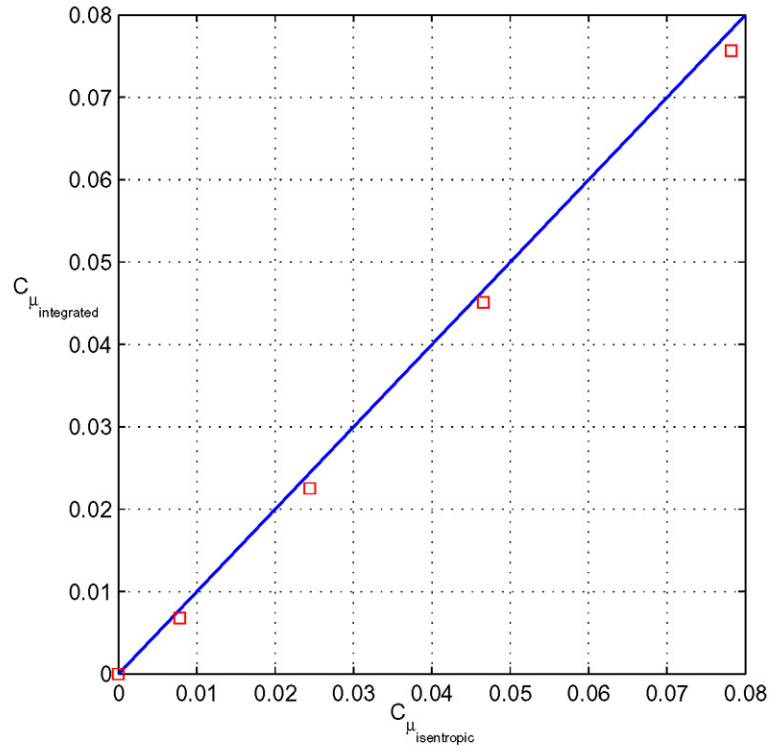


Figure 5: Comparison of  $C_{\mu_{integrated}}$  with  $C_{\mu_{isentropic}}$  for  $\alpha = 0$ ; the straight line is included to indicate deviation from a perfect correlation.

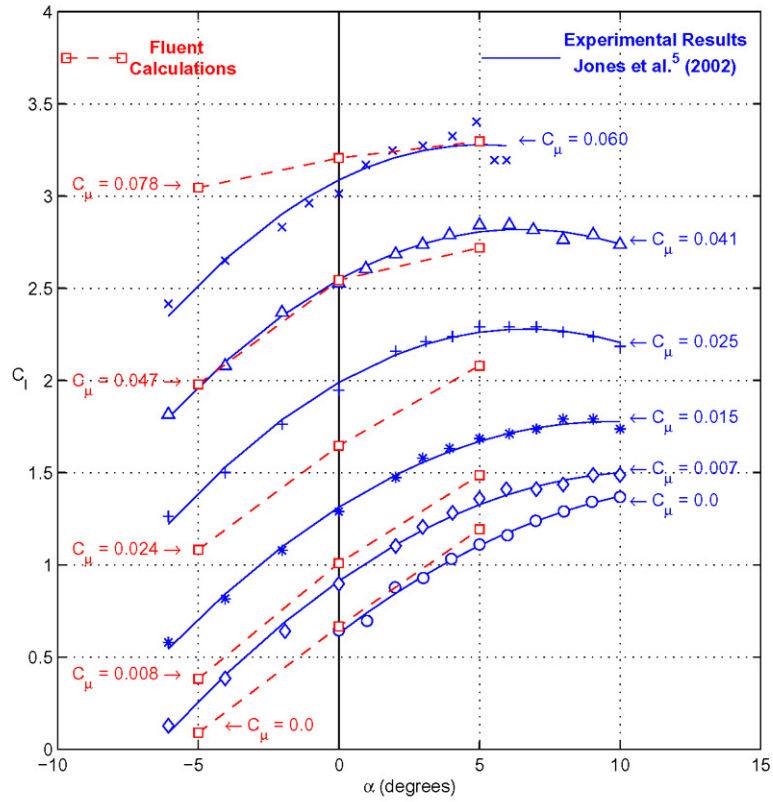
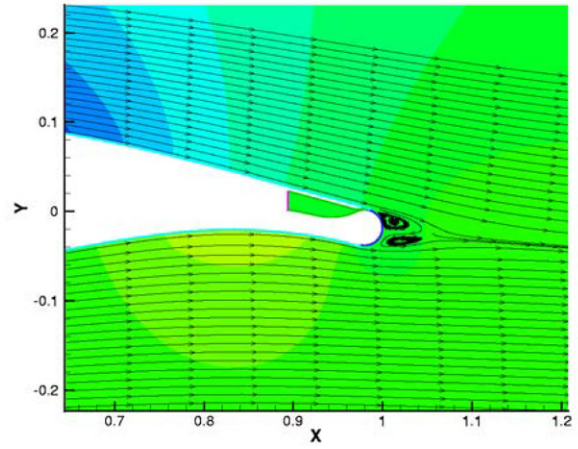
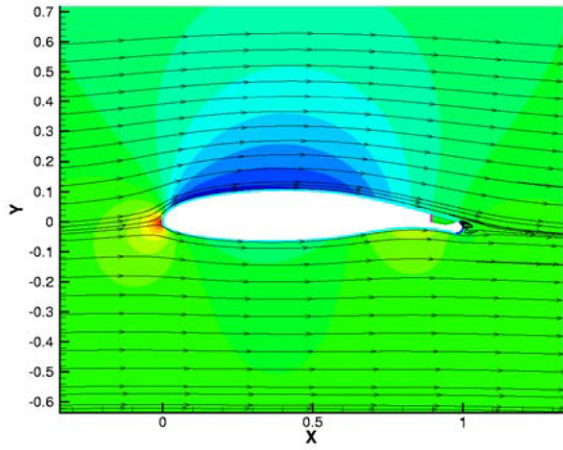
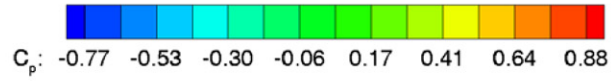
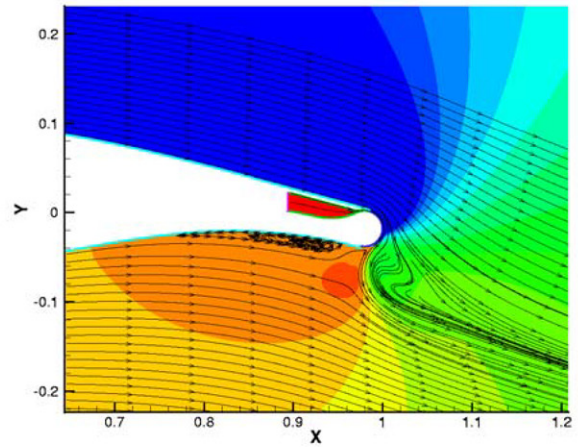
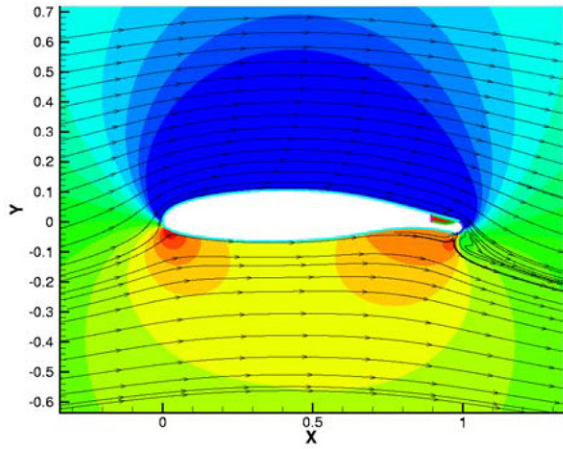


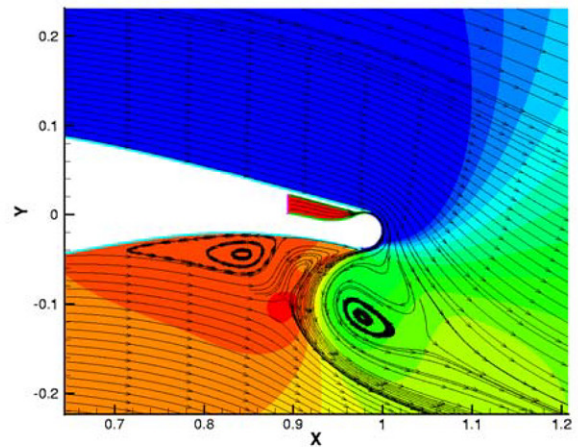
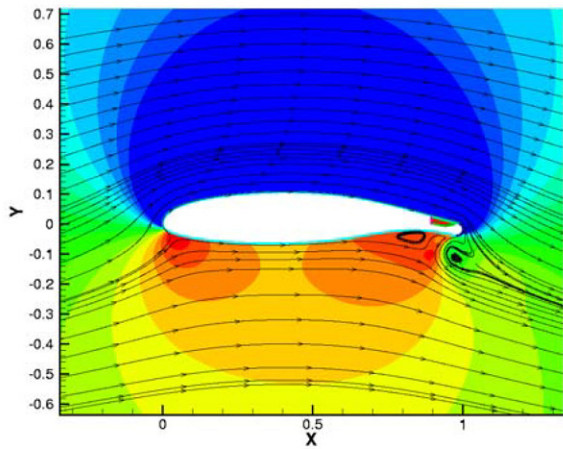
Figure 6: Comparison of Langley experimental and FUN2D analysis with the NCSU FLUENT analysis.



(a)  $C_\mu = 0.000$



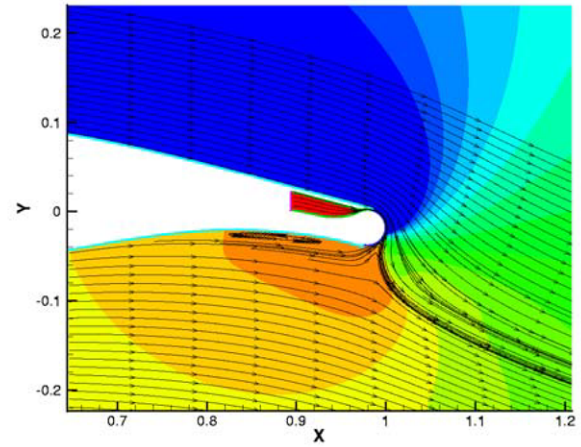
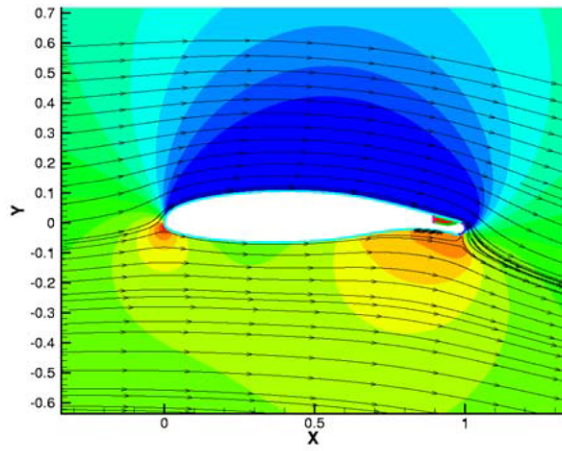
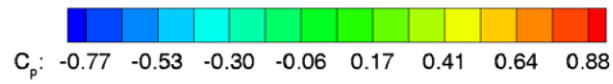
(b)  $C_\mu = 0.047$



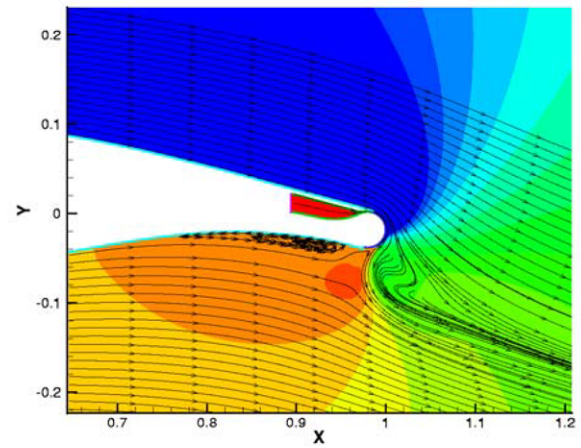
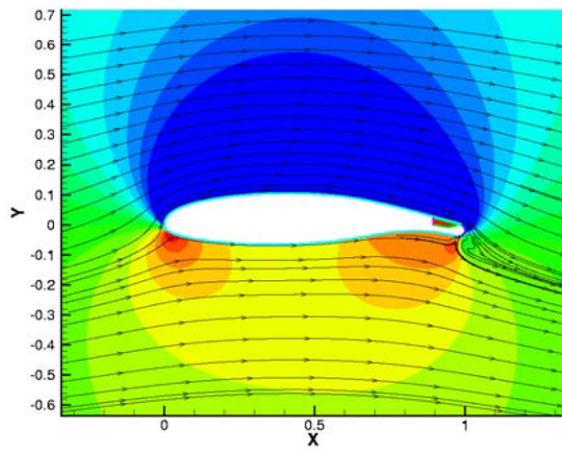
(c)  $C_\mu = 0.078$

Figure 7: CC effects on the flow field at  $\alpha = 0$  for various values of  $C_\mu$ .

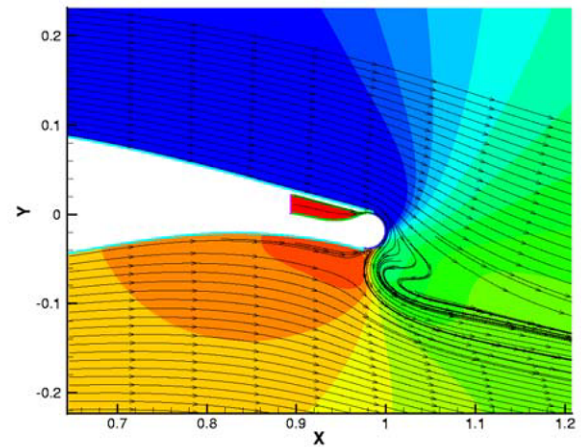
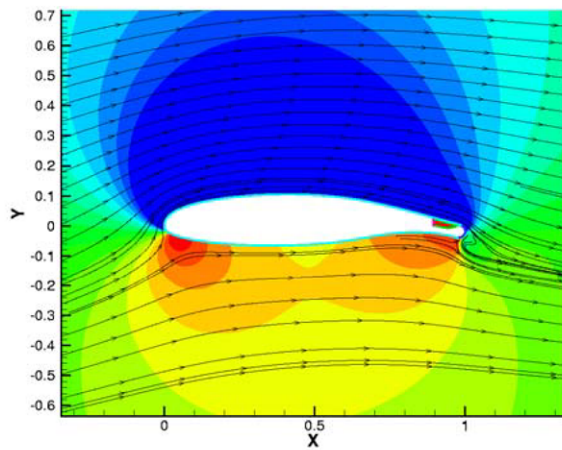




(a)  $\alpha = -5$  deg

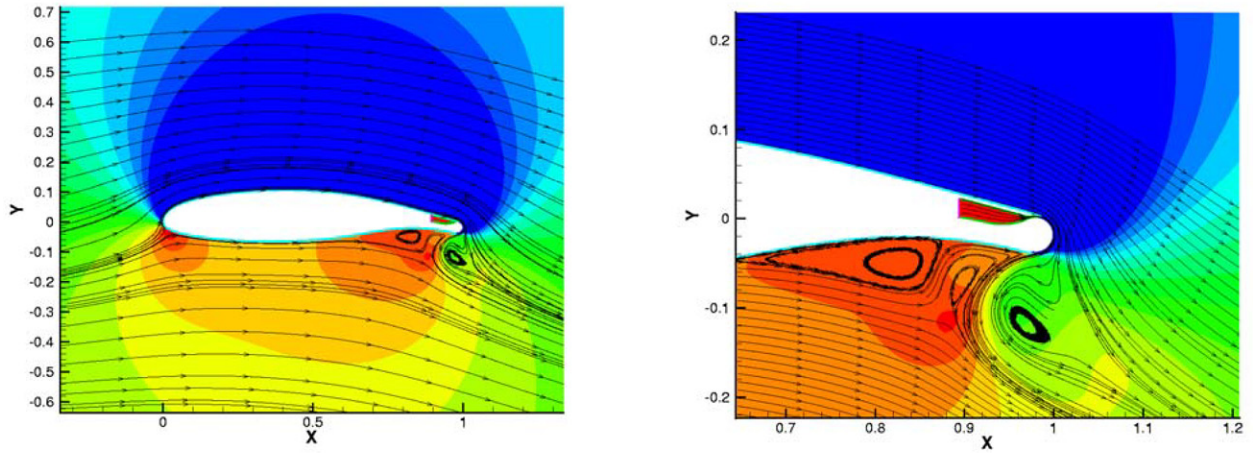
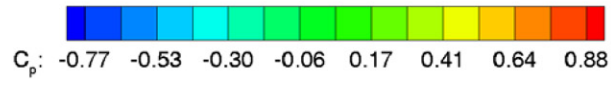


(b)  $\alpha = 0$  deg

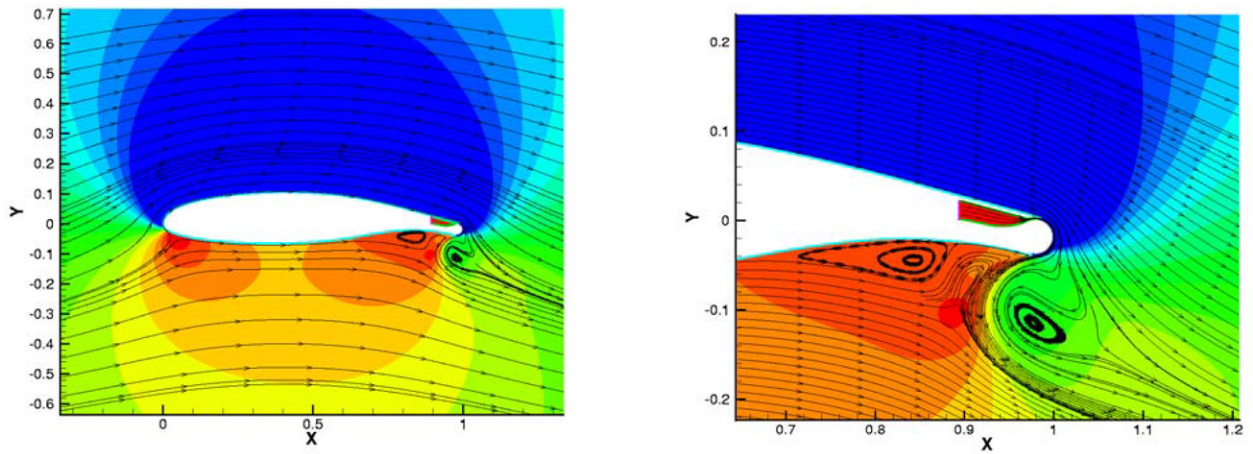


(c)  $\alpha = 5$  deg

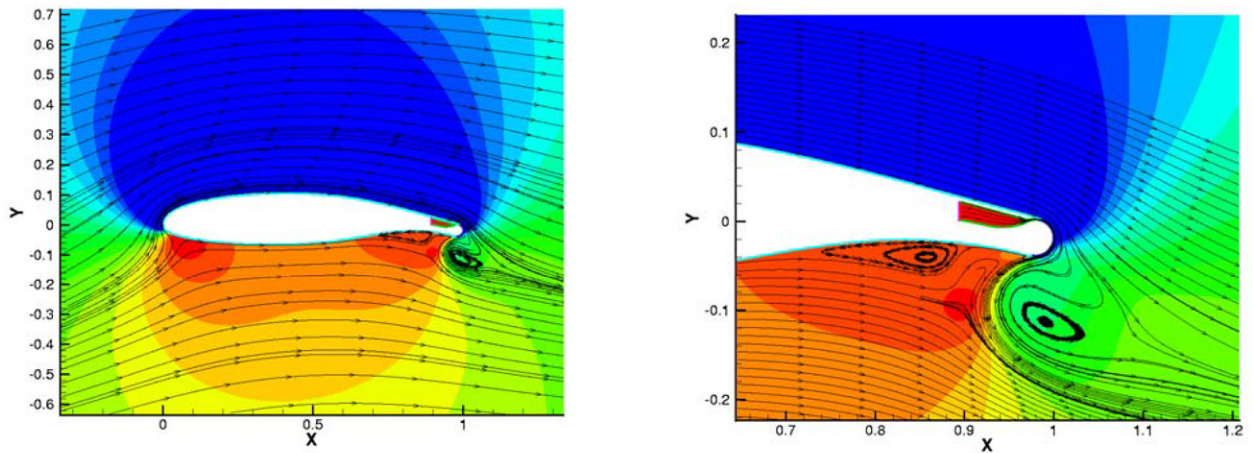
Figure 8: CC effects on flow field at  $C_{\mu} = 0.047$  for various values of  $\alpha$ .



(a)  $\alpha = -5$  deg



(b)  $\alpha = 0$  deg



(c)  $\alpha = 5$  deg

Figure 9: CC effects on flow field at  $C_{\mu} = 0.078$  for various values of  $\alpha$ .



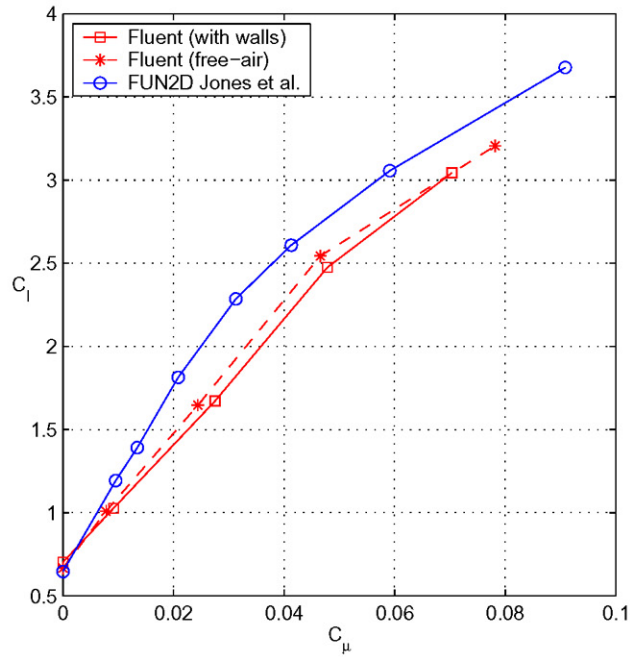


Figure 10: FLUENT prediction of wind-tunnel wall effects for varying values of  $C_\mu$  at  $\alpha = 0$  deg.

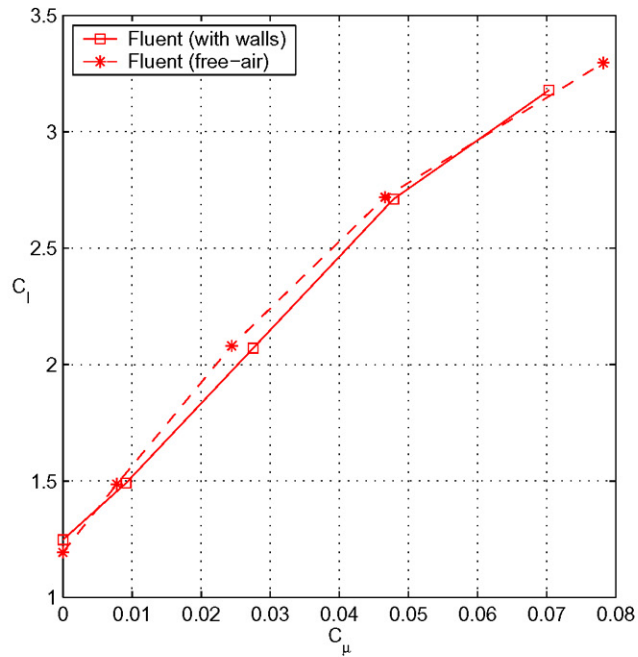


Figure 11: FLUENT prediction of wind-tunnel wall effects for varying values of  $C_\mu$  at  $\alpha = 5$  deg.

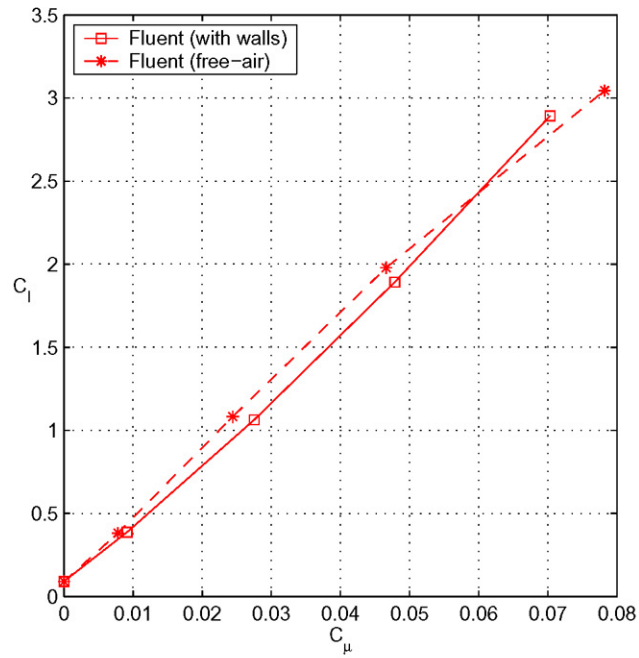


Figure 12: FLUENT prediction of wind-tunnel wall effects for varying values of  $C_\mu$  at  $\alpha = -5$  deg.

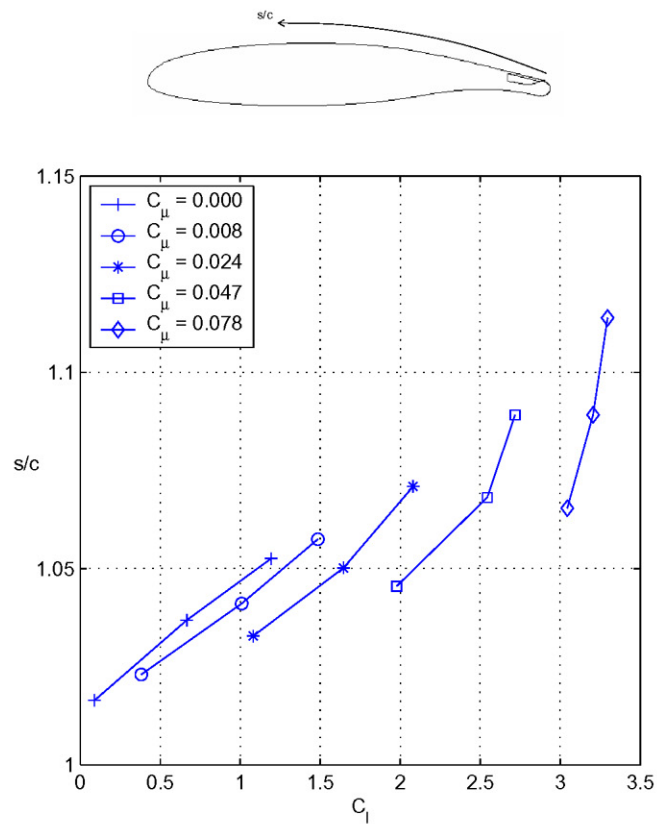


Figure 13: CC effects on stagnation-point location.

# CFD Analysis of a Circulation Control Airfoil Using Fluent

Greg McGowan  
M.S. Candidate  
gzmcgowa@ncsu.edu

Ashok Gopalarathnam  
Assistant Professor  
ashok\_g@ncsu.edu

NCSU Applied Aerodynamics Group  
Mechanical and Aerospace Engineering  
North Carolina State University, Raleigh, NC

*NASA/ONR 2004 Circulation Control Workshop  
Hampton, VA  
16-17 March, 2004*



## Outline

- Background & Motivation
- Geometry
- Grid Details
- Solver Details
- Results
- Conclusions



# Background & Motivation

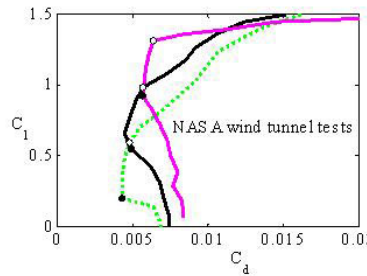
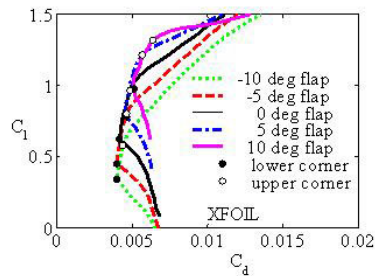
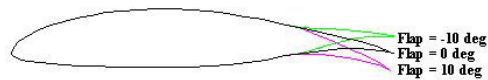
- A recent NCSU Applied Aero Group (APA) accomplishment in adaptive aerodynamics
- NCSU APA long-term goal in CC
- Current CC project in collaboration with Dr. Greg Jones, NASA LaRC



## Recent NCSU APA Accomplishment

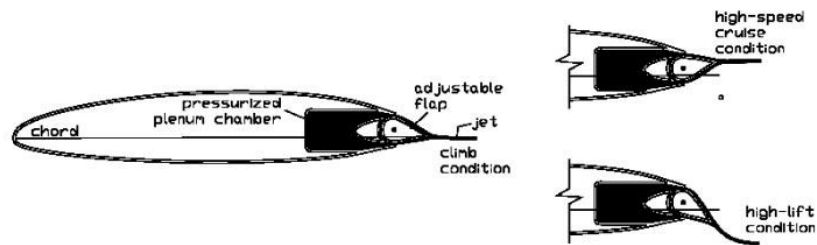
- Aerodynamics for adaptive aircraft
- Recent successful work on auto-adaptive airfoil (TE flap)

Example:  
 NASA NLF(1)-0215F at  $Re = 6$  million



## Long-term NCSU APA Goal in CC

- Adaptive jet-flap/CC concept



## Current CC Research Project

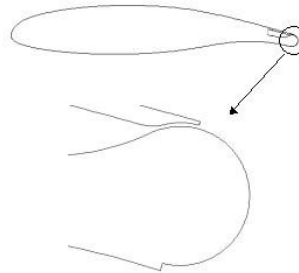
- In collaboration with Dr. Greg Jones (LaRC)
- Use Fluent code to analyze the GACC airfoil
- Compare results with LaRC experiments and FUN2D computations
- Build CFD expertise in CC for follow-on adaptive jet flap research





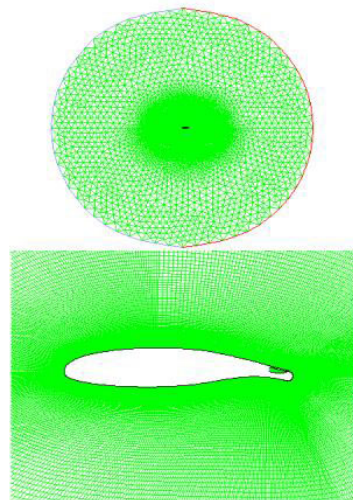
# Geometry

- General Aviation Circulation Control (GACC) Airfoil (Supplied by Dr. Greg Jones)
- Designed for upper and lower blowing
- Conditions for landing/take-off conditions
  - $Re_{\infty} = 533,000$
  - $M_{\infty} = 0.1$



# Grid Details

- Generated using Gambit
- Hybrid unstructured grid
- Structured near airfoil
- Unstructured in far-field
- ~ 20 chord lengths
- 132762 elements



## Solver Details

- Fluent version 6.1
- Steady
- Coupled-Implicit
- Node-based discretization
- Spalart-Allmaras turbulence model

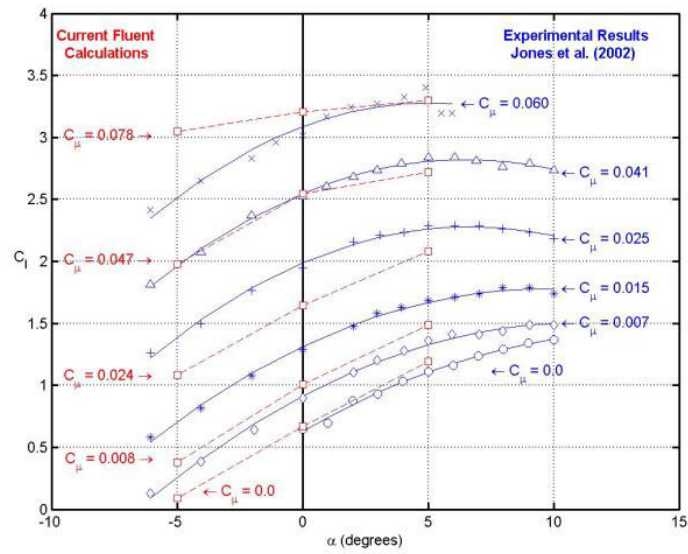


## Results

- Current Fluent work compared to Jones et al. (2002)
  - Experiment
  - FUN2D CFD analysis
- Parametric study of  $\alpha$  and  $C_\mu$  variations



## Comparison of Lift Characteristics

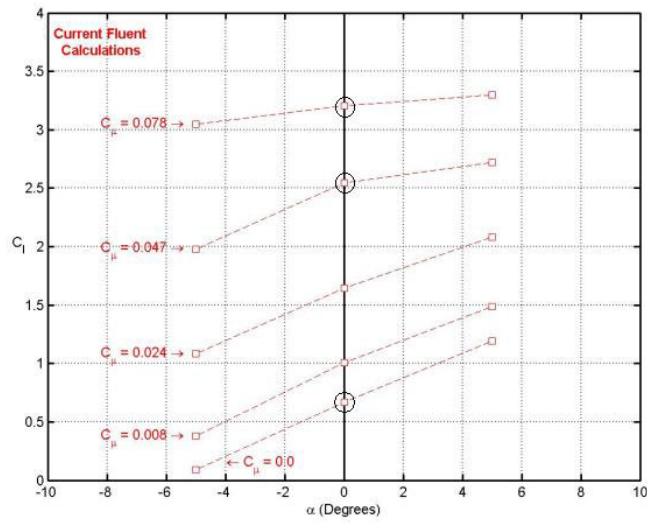


## Parametric Studies

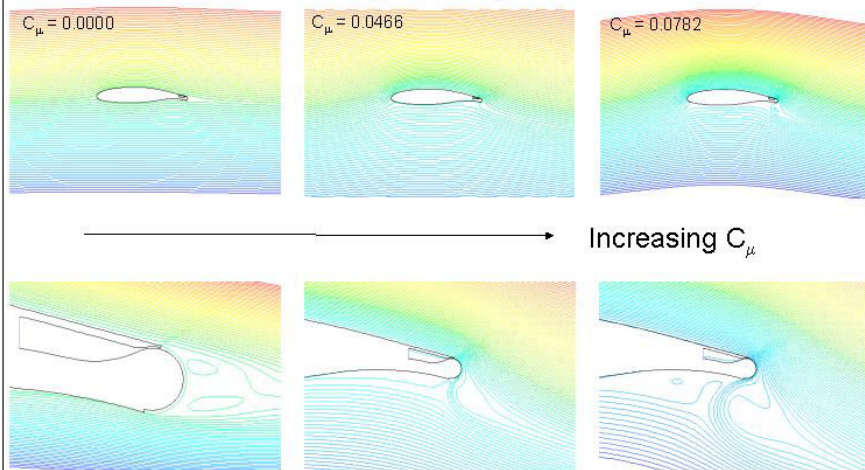
- Increasing  $C_\mu$  at  $\alpha = 0^\circ$
- Increasing  $\alpha$  at  $C_\mu = 0.047$
- Increasing  $\alpha$  at  $C_\mu = 0.078$



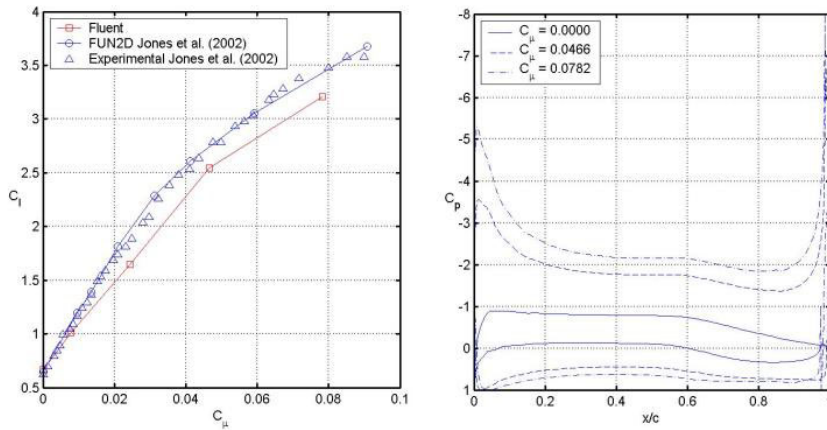
### Increasing $C_{\mu}$ $\alpha = 0^{\circ}$



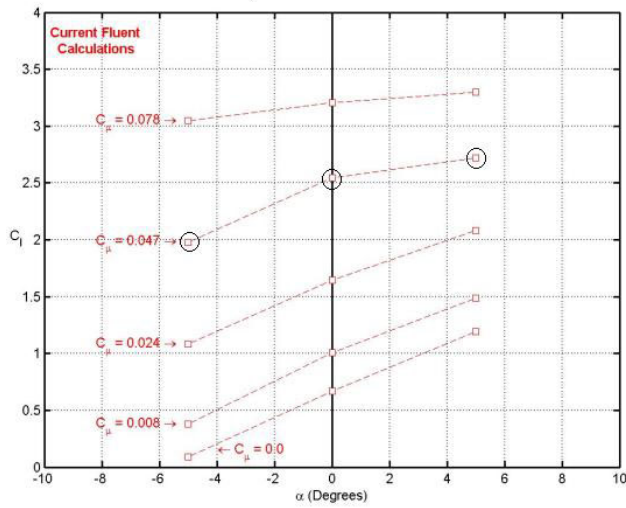
### CC Effects on Streamlines ( $\alpha = 0^{\circ}$ )



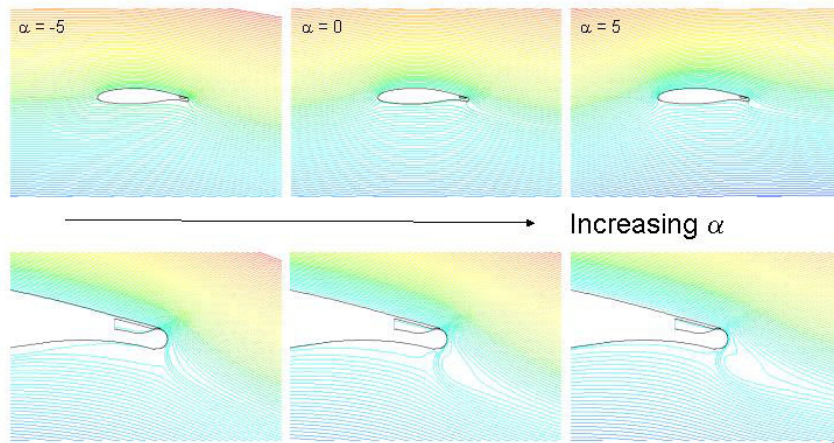
## Trends in Lift and Pressure Coefficient ( $\alpha = 0^\circ$ )



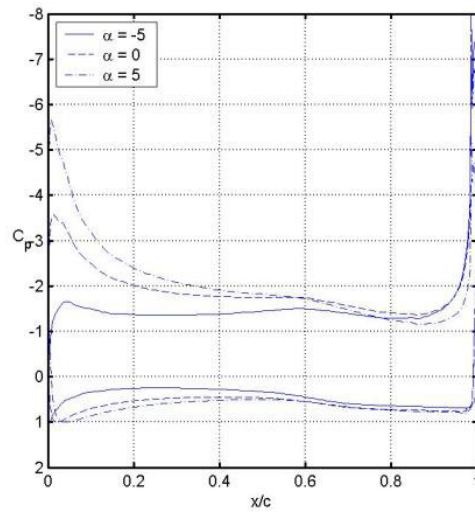
## Increasing $\alpha$ $C_\mu = 0.047$



Increasing  $\alpha$   
 $C_{\mu} = 0.047$

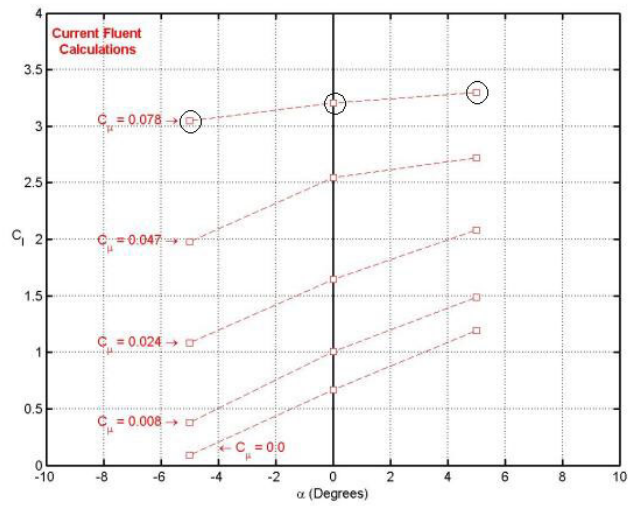


Airfoil Surface Pressure Coefficient  
 $C_{\mu} = 0.047$

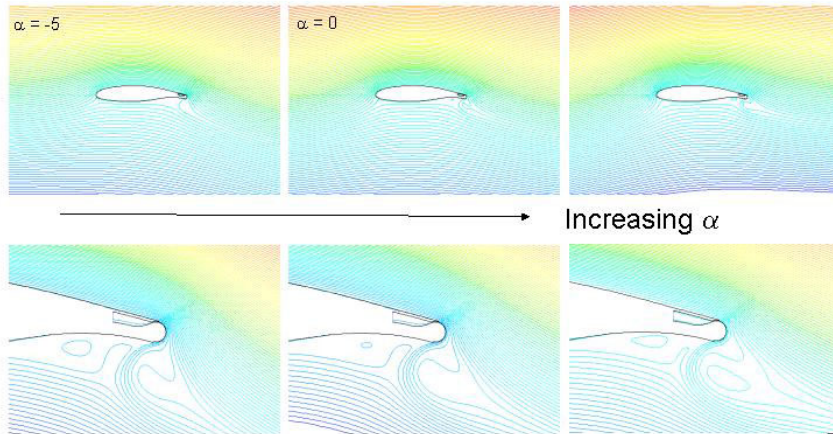




Increasing  $\alpha$   
 $C_{\mu} = 0.078$



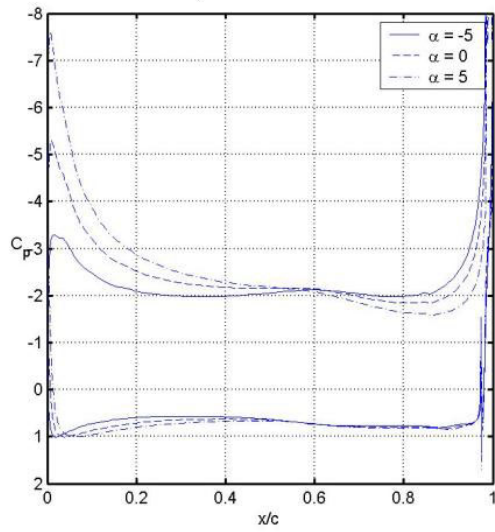
Increasing  $\alpha$   
 $C_{\mu} = 0.078$



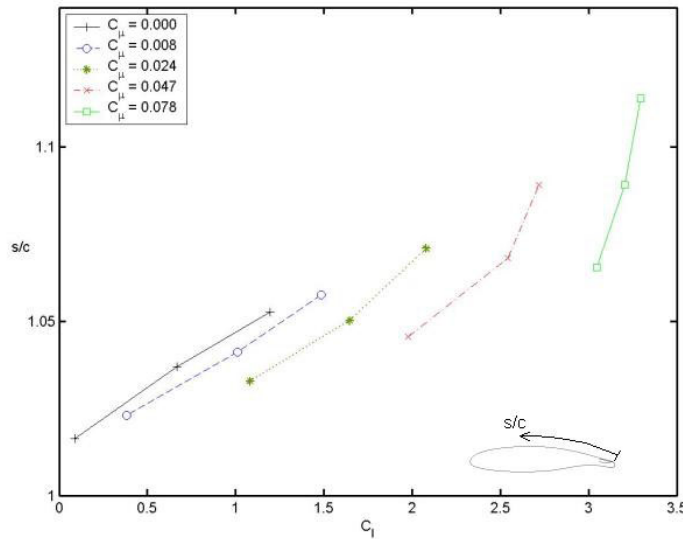


### Airfoil Surface Pressure Coefficient

$C_{\mu} = 0.078$



### CC Effect on LE Stagnation Point



## Conclusions

- CFD computations performed for GACC with Fluent
- Trends and much of data compare well with LaRC experiments and FUN2D
- Typical run time of 1.5-2.5 days per case (Pentium Xeon 3.0 GHz)
- Systematic movement of LE stagnation point can be used for sensing and closed-loop control
- Provides foundation for adaptive jet flap/CC research



## Acknowledgements

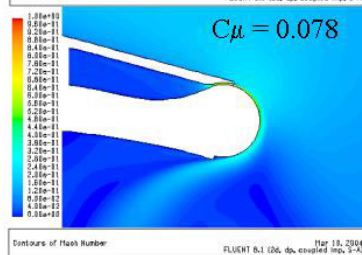
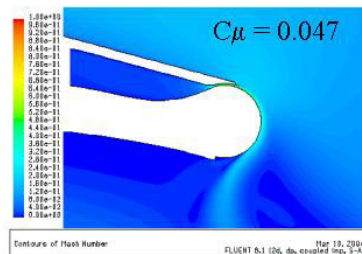
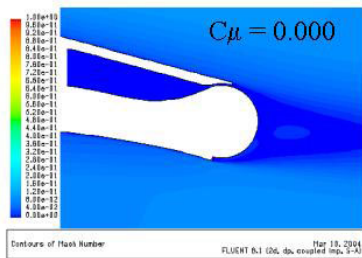
- Dr. Gregory S. Jones for geometry, data, and helpful discussions



# Supplemental Slides

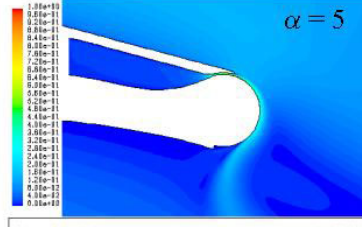
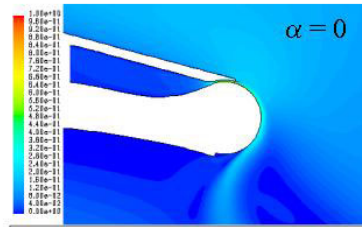
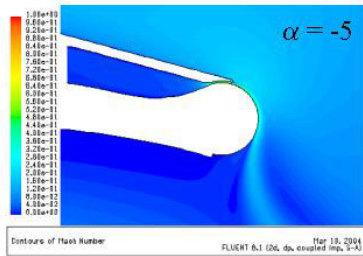


## Mach contours for increasing $C_{\mu}$ $\alpha = 0$



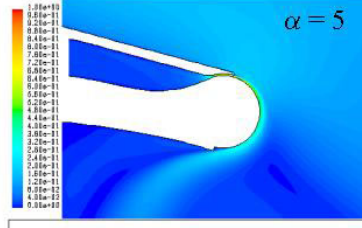
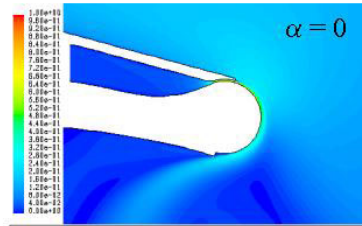
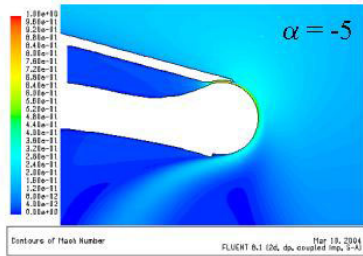
# Mach contours for increasing $\alpha$

$C_{\mu} = 0.047$

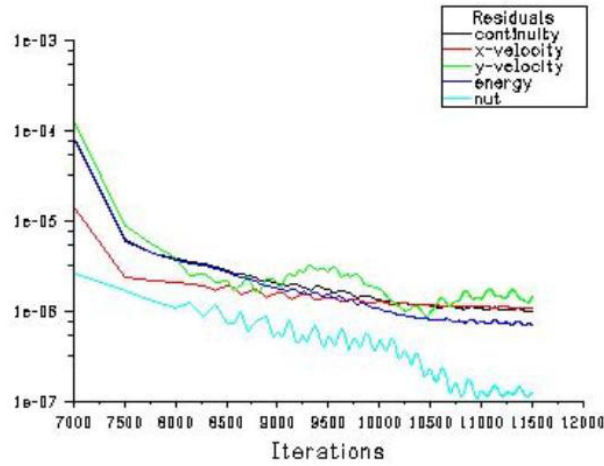


# Mach contours for increasing $\alpha$

$C_{\mu} = 0.078$



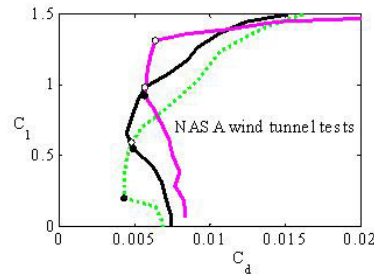
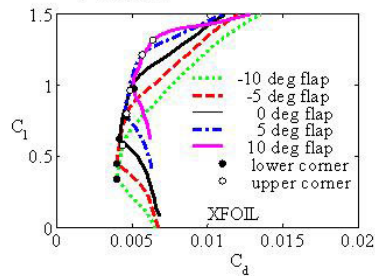
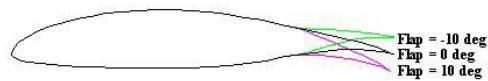
## Typical Residual Plot



## Cruise Flaps for NLF Airfoils

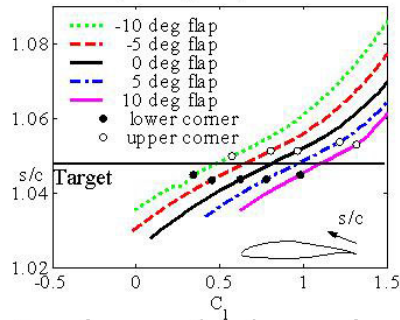
- Trailing-edge flaps or “cruise flaps” can be used to shift the drag bucket of an airfoil.
- Originally conceived by Pfenninger (1947)

Example:  
 NASA NLF(1)-0215F at  $Re = 6$  million

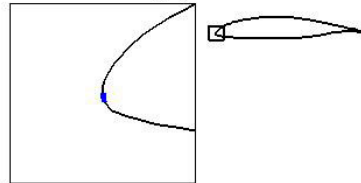


# Stagnation-point Sensing

- Cruise flaps work by maintaining the stagnation point within a small desirable region near the leading edge (well known)



Example:  
NASA NLF(1)-0215F



- Sensing can be done using surface hot-film array







# *Pneumatic Flap Performance for a 2D Circulation Control Airfoil, Steady & Pulsed*

Gregory S. Jones

NASA LaRC

## Abstract

Circulation Control technologies have been around for 65 years, and have been successfully demonstrated in laboratories and flight vehicles alike, yet there are few production aircraft flying today that implement these advances. Circulation Control techniques may have been overlooked due to perceived unfavorable trade offs of mass flow, pitching moment, cruise drag, noise, etc. Improvements in certain aspects of Circulation Control technology are the focus of this paper. This report will describe airfoil and blown high lift concepts that also address cruise drag reduction and reductions in mass flow through the use of pulsed pneumatic blowing on a Coanda surface. Pulsed concepts demonstrate significant reductions in mass flow requirements for Circulation Control, as well as cruise drag concepts that equal or exceed conventional airfoil systems.

## Symbols

<p>Ao effective cross-sectional area of 2d model</p> <p>b airfoil 2-D span, (inches)</p> <p>CC circulation control</p> <p>Cp pressure coefficient</p> <p>C airfoil chord, (inches)</p> <p>C<sub>d</sub> section profile-drag coefficient</p> <p>C<sub>l</sub> section lift coefficient c<sub>n</sub> cos(α) – c<sub>n</sub> sin(α)</p> <p>C<sub>m</sub> moment coefficient</p> <p>C<sub>n</sub> normal force coefficient</p> <p>C<sub>T</sub> thrust coefficient = C<sub>μ</sub></p> <p>C<sub>μ</sub> momentum coefficient = <math>\frac{\dot{m}U_j}{q(bC)}</math></p> <p>CCW circulation controlled wing</p> <p>DC duty cycle (time on/total time)</p> <p>D drag (lbf)</p> <p>h slot height of Coanda jet (inches)</p> <p>H tunnel height (inches)</p> <p>I,J,K pressure tare coefficients for balance</p> <p>LE leading edge</p> <p>L lift (lbf)</p> <p>M mach number</p> <p><math>\dot{m}</math> mass flow (lbm/sec)</p> <p>NPR nozzle pressure ratio = P<sub>DUCT</sub>/P<sub>∞</sub></p> <p>P<sub>f</sub> fluid power (ft-lb/sec)</p> <p>P pressure (lbf/in<sup>2</sup> or lbf/ft<sup>2</sup>)</p> <p>p' fluctuating pressure (lbf/in<sup>2</sup> or lbf/ft<sup>2</sup>)</p>	<p>r trailing edge radius (inches)</p> <p>S airfoil reference area (ft<sup>2</sup>)</p> <p>t airfoil thickness (inches)</p> <p>U velocity (ft/sec)</p> <p>u' fluctuating velocity (ft/sec)</p> <p>q dynamic pressure (lbf/ft<sup>2</sup>) = <math>\frac{1}{2}\rho U^2</math></p> <p>S wing plan form area (ft<sup>2</sup>)</p> <p>SCFM standard mass flow (ft<sup>3</sup>/min) (expanded to 14.7 psia &amp; 72°F)</p> <p>SPL sound pressure level (dB)</p> <p>TE trailing edge</p> <p>T static temperature (°R)</p> <p>w slot width (inches)</p> <p>α angle of attack (degrees)</p> <p>δ<sub>jet</sub> Reactionary force angle (degrees)</p> <p>β Prandtl-Glauert Compressibility <math>\sqrt{1-M^2}</math></p> <p>θ<sub>jet</sub> Coanda jet separation angle (degrees)</p> <p>ε blockage interference ratio u/U</p> <p>ρ density (lbm/ft<sup>3</sup>)</p> <p><u>Γ</u> circulation</p>
---	---

## Introduction

Recent interest in circulation control (CC) aerodynamics has increased for both military and civil applications with emphasis on providing better vehicle performance and prediction capability<sup>1</sup>. The history of Coanda driven circulation control has met with varying degrees of enthusiasm as the requirements for improved high lift systems continue to increase. Current lift coefficient goals for Extremely Short Take Off and Landing (ESTOL) vehicles are approaching 10 and lift to drag ratios greater than 25<sup>2</sup>. Personal Air Vehicles (PAV) has a field length goal of 250 feet<sup>3</sup>. To achieve these goals require more than what a conventional high lift system can provide. In addition to high lift and cruise drag requirements, the next generation of aircraft will need to address other issues that include weight and noise. Conventional high lift systems that use flaps and leading edge slats can be associated with significant weight and volume penalties of a typical wing assembly. These assemblies are also complex (up to 3 and 4 sub-elements) and very sensitive to location relative to the main element of the wing. The need to simplify and reduce the weight of these systems without sacrificing performance is the focus of this effort.

Coanda driven circulation control techniques generally offer high levels of lift for small amounts of blowing<sup>4, 5</sup>. These systems are perceived to be simpler and less weighty than conventional high lift systems. However advanced system studies of circulation control systems being applied to a modern aircraft have been limited or non-existent. So the ability to buy it's way onto an aircraft is generally unproven. Nevertheless several roadblocks to real aircraft applications reappear in every discussion of circulation control. These include, source of air (typically bleed or bypass air from the engine or added auxiliary power unit), unknown weight penalties related to the internal air delivery system, engine out conditions, drag penalty associated with blunt trailing edge, and large pitching moments associated with aircraft trim. While this is not a comprehensive list, these

issues will be used as a guide in developing a CC wing for general aviation applications.

A primary objective of this effort is to evaluate the benefits of pulsed circulation control and to reduce the mass flow requirements for a given lift performances as well as reduce the cruise drag penalty associated with a large circulation control trailing edge. Secondary objectives of this study were to evaluate the dual blown pneumatic concept as a control device and to determine potential benefits of returned thrust, (i.e. thrust is lost at the engine due to bleeding mass from the engine, so how much thrust is returned to the aircraft through the wing).

## NASA CC Requirements

Application of circulation control to different aircraft platforms is driven by requirements that are dictated by mission.<sup>6</sup> NASA's Vehicle Integration, Strategy and Technology Assessment (VISTA) office describe many of these missions. Each of the vehicle sectors within the VISTA program could benefit from circulation control technologies, but Personal Air Vehicles (PAV) and ESTOL vehicles seem to benefit the most.

Personal Air Vehicles shown in Figure 1 have characteristics that resemble general aviation vehicles but meet stiffer requirements for field length (i.e. high lift), noise signatures, and cruise efficiency (L/D). With a fresh look at point-to-point travel, NASA's PAV program will address airport infrastructure, ease of use, and reductions in the cost of travel.



Figure 1 Notional concepts of NASA Personal Air vehicles

Today's small aircraft utilize significantly oversized wings for cruise and simple hinged flaps for high lift. These systems are adequate for the current airport infrastructure. However as

these airport requirements become more stringent, high lift and cruise efficiency must be improved. The PAV goals used for this effort included a 250' field length that will require re-sizing the wing with a  $C_{Lmax} = 4.0$  that yields an  $L/D_{max}$  of 20.

In the near-term reduced approach speeds enables a 1000' field length and can improve safety in addition to reducing community noise signatures. If equivalent control margins and gust sensitivity are achieved, safety (in terms of accident avoidance reaction time and survivability) is proportional to the approach speed. These reduced speeds require more efficient high lift systems. Circulation control technologies have been identified as a candidate simplified high lift system. It may be necessary to integrate this system with other active flow control technologies (combining higher altitude cruise, gust alleviation, limited powered-lift, etc.)

Air sources for circulation control systems for small aircraft may have a low penalty. Current high performance small aircraft are turbocharged for altitude compensation. At landing and takeoff conditions, compressed air is thrown out the waste-gate of the turbocharger (~2 lbf/sec). This is a potential source for air augmentation to a CC system. Since engine out conditions are an issue for CC applications, another air source alternative is using the wake vortex energy to power a wingtip-turbine. Regardless of the air source it is important to optimize the efficiency of the CC system for minimizing mass flow at a given lift requirement.

The NASA ESTOL vehicle sector requirements are directed to a 100-passenger class vehicle that would include the following elements:

- $\leq 2000'$  balanced field length (related goal of  $C_{Lmax} = 10$ )
- Cruise at  $M=0.8$
- Noise footprint contained within the airport boundary
- Landing speed ~50 knots

The current state of the art aircraft systems can only achieve 2 or 3 of these elements

simultaneously. Circulation control has the potential of enabling the achievement of all the elements of the desired capability set and could be integrated to the high lift, flight controls, and propulsion systems as shown in Figure 2.

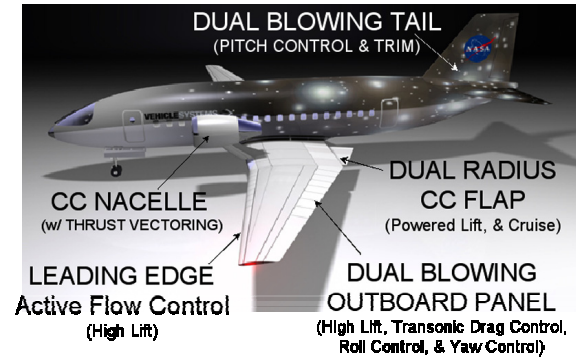


Figure 2 Notional concept of NASA ESTOL 100 passenger vehicle showing potential CC applications

It is recognized that the integration of the propulsion system and the wing is paramount to the success of either of these vehicle concepts. The focus of this paper will be targeted at a 2D baseline CC airfoil proposal that could be applied to the outer wing panel of either concept.

## Theoretical Considerations

2D aerodynamic performance is traditionally categorized into lift, drag, and pitching moment. Most fluid mechanic devices that alter the forces on a body are characterized in two force categories:

- Induced forces due to circulation
- Reaction forces due to jet momentum

This section will focus on lift and drag forces associated with active flow control systems that utilize pneumatic flow control. Pneumatic or blown active flow control systems can be related to boundary layer control and/or supercirculation modes. These modes are often characterized by the fluidic power required to achieve the performance augmentation.

To achieve the maximum performance on body, it is desired to drive the stagnation streamlines toward the equivalent inviscid solution.<sup>7</sup> Practically this is achieved by moving the

boundary layer separation to the trailing edge. This is the performance limit for boundary layer control techniques. To achieve supercirculation it is necessary to extend the effective trailing edge beyond the physical trailing edge location with a virtual or pneumatic flap as simulated in Figure 3

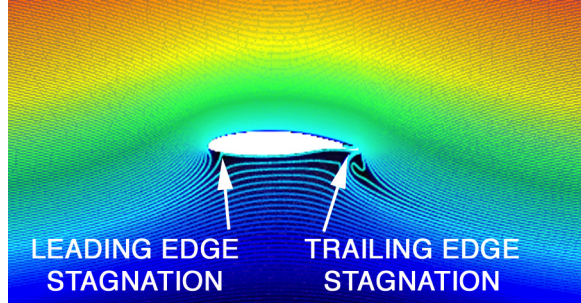


Figure 3 CFD simulation of pneumatic flap and streamline tuning using a Coanda jet

To understand the limits of airfoil performance, it is necessary to be aware of the inviscid characteristics of lift. The influence of the airfoil thickness on the maximum theoretical inviscid lift coefficient (not including jet thrust or camber effects) can be described as:

$$C_{LMAX} = 2\pi \left(1 + \frac{t}{C}\right) \quad \text{Equation 1}$$

For a limiting case of  $t/C$  of 100% (i.e., circular cylinder) the maximum lift coefficient is  $4\pi$  and can be related to classic un-blown circulation ( $\Gamma_C$ ) around the body<sup>8</sup>.

$$L = \rho U \Gamma_C \quad \text{Equation 2}$$

The magnitude of the circulation ( $\Gamma_C$ ) is a function of geometry alone and will be referred to as induced lift and can be related to the modified pressure on the integrated boundary of the body.

$$L = - \int_0^{2\pi} p r (\sin\theta) d\theta \quad \text{Equation 3}$$

Recall for an inviscid solution (circular cylinder) the normal force is solely directed in the vertical plane and that drag is zero. As seen in **Figure 4** the streamlines are significantly influenced by the magnitude of the circulation  $\Gamma_C$ . In practice, the inviscid limit is never reached because of flow separation. However for an airfoil employing a boundary layer control or a circulation control device, the maximum inviscid lift is possible.

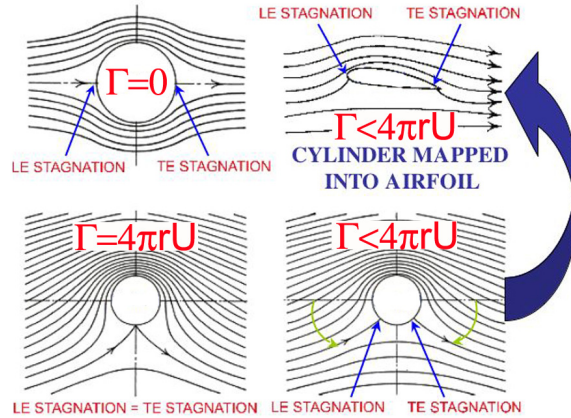


Figure 4 Classic lift due to circulation for a circular cylinder and mapped into airfoil profile

When a pneumatic system that adds mass is used, an additional circulation term is added to the induced circulation to account for the reactionary forces produced by the jet as describe in equation 4.

$$L = \rho U (\Gamma_C + \Gamma_{jet}) \quad \text{Equation 4}$$

where  $\Gamma_{jet} = \frac{\dot{m} U_{jet}}{\rho U_{\infty}} (\alpha + \delta)$  Equation 5

and can be related to lift and drag as:

$$C_{Ljet} = C_T \sin(\alpha + \delta) \quad \text{Equation 6}$$

$$C_{djet} = C_T \cos(\alpha + \delta) \quad \text{Equation 7}$$

This reactionary force term can affect lift or drag depending on the orientation of the jet exit angle ( $\delta_{jet}$ ) at the boundary of the body. For pneumatic systems this reactionary force should not be confused with thrust vectoring that an articulating nozzle generates on an engine nacelle. The reactionary force that is characteristic of a pure jet flaps is at a fixed jet angle as shown in Figure 5.

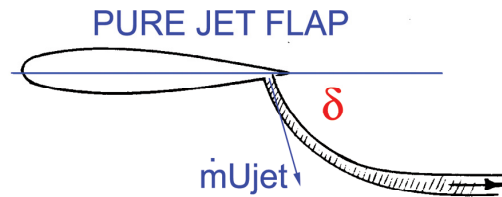


Figure 5 Thrust vectoring using a classic pure jet flap



The efficiency of a pure jet flap (vectored vertical), compared to typical CC airfoils (vectored tangential to the upper surface) is realized in the airfoil profile and the associated induced effects that accompany the Coanda geometry and the leading edge shape. It is recognized that both of these airfoil techniques benefit from induced forces and reaction forces that can be correlated to jet position and orientation. Nominally the jet flap airfoils depend largely on the reaction force of the jet momentum. Coanda type CC systems capture the induced forces more efficiently and typically deliver larger lift gains that a pure jet flap.

The combined induced circulation and reactionary forces are generally captured experimentally with a balance, integrated surface pressures, and/or wind tunnel wall pressure signatures combined with wake rake pressures. The force balance is a direct measure of both induced circulation and reaction forces. Because these forces are integrated and summed at the balance the ability to decompose the induced and reactionary components is dependant on knowing the vectored force associated with the jet.

Integrated surface pressures are representative of induced circulation forces alone. To obtain the total forces along the boundary of the body, reactionary forces must be added at the appropriate  $\delta_{jet}$  angle. The integrated wind tunnel wall signature and wake rake must also account for the reaction forces generated by the jet.

For typical CC systems, the jet exit is nominally directed aft, resulting in a reactionary thrust force that contributes very little to lift (except when a aft camber causes the a small  $\delta_{jet}$ ) as shown in Figure 6. It should be recognized that the benefit of turning the flow with the wall bounded jet along the Coanda surface is reflected in the 2D induced circulation found in the modified surface pressure field.

The reactionary force of the CC system augments the thrust produced by the primary propulsion system, Figure 7. Returning a portion of the thrust that was bled from the engine to supply the CC sub-system, reduces the overall system penalty associated with CC. The recovery of this

thrust will be dependant on the efficiency of the Coanda nozzle and internal losses of the CC air delivery system, etc.

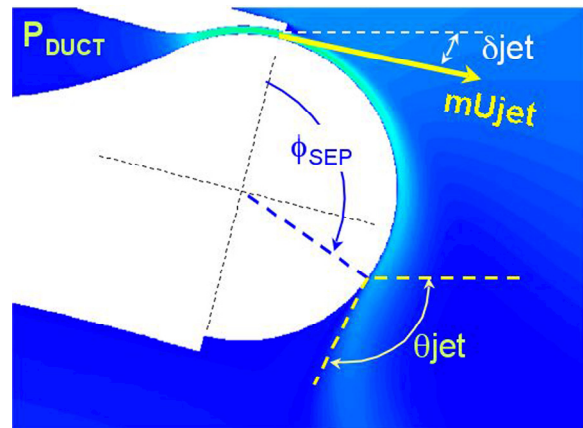
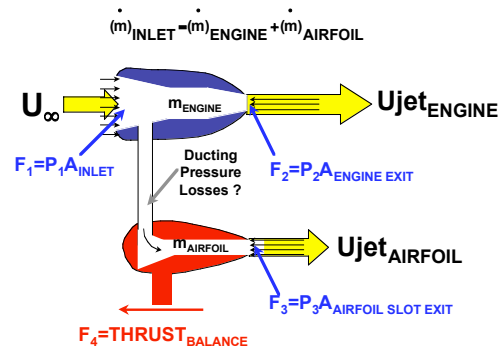


Figure 6 Schematic of flow angles associated with typical Coanda driven flow



$$\Sigma F_{REACTION} = \left[ (\dot{m}U_{JET})_{ENGINE} + (\dot{m}U_{JET})_{AIRFOIL} \right] - (\dot{m}U_{\infty})_{INLET} + THRUST$$

Figure 7 Block diagram of reactionary forces for an integrated wing and propulsion system

It is known that nozzle efficiency is very dependant on nozzle aspect ratio. Propulsion system studies of rectangular nozzle losses are generally limited to aspect ratios less than 10. Since there is not a data base for large aspect ratio nozzles ( $h/b > 1300$  similar to those used in CC airfoils), it would not be practical to extrapolate to obtain thrust recovery. However for this 2D study, (where nozzle aspect ratio is meaningless) it is appropriate to neglect the nozzle efficiency and assume no losses.

For 2D CC studies the thrust can be described at the jet exit of the airfoil by the momentum or

thrust coefficient:

$$C_{\mu} = \frac{\text{THRUST}}{qS} = \frac{mU_{\text{JET}}}{qS} = \frac{2hw}{C_b} \frac{\rho_J}{\rho_{\infty}} \frac{U_{\text{JET}}^2}{U_{\infty}^2} \quad \text{Equation 8}$$

where

$$m = \rho_J U_J(C)(w) \quad \text{Equation 9}$$

and

$$U_J = \sqrt{\frac{2\gamma R(T_{\text{DUCT}})}{\gamma - 1} \left[ 1 - \left( \frac{P_{\infty}}{P_{\text{DUCT}}} \right)^{\frac{\gamma - 1}{\gamma}} \right]} \quad \text{Equation 10}$$

The trade offs of engine thrust verses reduced engine thrust augmented with CC thrust will involve detailed specifications of the geometry of the airfoil, the intake lip, internal diffusers, ducting, compressor, and jet-nozzle designs. Obviously the results would be applicable for that design only. In the absence of these details some general estimates of the benefits or penalties of CC systems can be formulated by estimating the power requirements of CC.

For a crude estimate of fluid power ( $P_f$ ), it is assumed that the jet is taken from a large reservoir. Then the total power expended will be at least equal to the power required to supply the jet velocity head plus the power lost at the intake as the fluid is drawn into the large reservoir. This ideal power can be described as<sup>9</sup>:

$$P_f = P_{\text{Jet}} + P_{\text{ram}} \quad \text{Equation 11}$$

where

$$P_{\text{jet}} = \rho g(\Delta H)Q \approx \frac{1}{2} \rho U_J^2 \frac{m}{\rho} \quad \text{Equation 12}$$

and

$$P_{\text{ram}} = (\rho Q U_{\infty}) U_{\infty} = m U_{\infty}^2 \quad \text{Equation 13}$$

Hence, the power (ft-lb/sec) required to supply a flow with a total momentum coefficient  $C_{\mu}$  is:

$$P_f = C_{\mu} \frac{U_J}{2U_{\infty}} \left[ 1 + 2 \left( \frac{U_{\infty}}{U_J} \right)^2 \right] (q_{\infty} U_{\infty} S) \quad \text{Equation 14}$$

and non-dimensionally

$$C_{P_f} = \frac{P_f}{q_{\infty} U_{\infty} S} = C_{\mu} \frac{U_J}{2U_{\infty}} + C_{\mu} \frac{U_{\infty}}{U_J} \quad \text{Equation 15}$$

If the jet slot height ( $h$ ) is constant and is known for a rectangular wing, the fluid power can be expressed in terms of just the parameters  $C_{\mu}$  and height to cord ratio ( $h/C$ ):

$$C_{P_f} = \frac{C_{\mu}^{(3/2)}}{2\sqrt{2(h/C)}} \left[ 1 + \frac{4(h/C)}{C_{\mu}} \right] \quad \text{Equation 16}$$

Figure 8 shows the non-dimensional ideal power for a typical CC jet orifice.

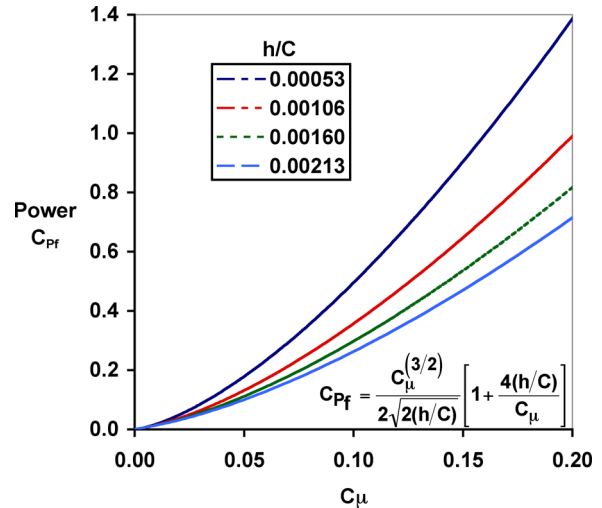


Figure 8 Ideal Power requirements for typical Coanda jets

### 2D Drag with Blown systems

2D drag characteristics for blown airfoils are often complicated by the juncture flow created by the wind tunnel and airfoil model. To avoid these issues the most reliable measurement technique for experimentally determining the drag of a blown airfoil is the momentum-loss method that employs a wake rake and described in detail by Betz and Jones<sup>10</sup>. The profile drag can be determined by integrating the wake profile<sup>11</sup> measured 1 to 3 chords downstream of the trailing edge.

$$C_{DRAKE} = \frac{2}{c} \int \sqrt{\frac{q}{q_0}} - \frac{q}{q_0} dy \text{ Equation 17}$$

For blown airfoils, it is important to note that the measured profile drag from a wake rake must be corrected by subtracting the momentum that was added by the CC system<sup>12</sup>. The total horizontal forces on a 2D model do indeed exceed that indicated by conventional wake rake calculations

by the quantity  $\dot{m}U_0$ . Considering a frictionless hypothetical case where the jet is exhausted at a total head equal to free stream total head easily confirms this principle. Here, the wake will indicate zero drag, but the model will experience a thrust of  $\dot{m}U_0$ . The way the net forces are book kept results in:

$$C_D = C_{DRAKE} - \frac{\dot{m}U_\infty}{\rho c} = C_{DRAKE} - C_\mu \frac{U_\infty}{U_J} \text{ Equation 18}$$

Equation 18

This is equivalent to what a force balance would measure, assuming that the air source is considered to be internal to the model.

### Equivalent Drag

To make direct comparisons of different blown systems such as traditional circulation control airfoils, jet flaps, blown flaps, engine augmented powered lift systems, etc. it is necessary to define an equivalent lift-to-drag ratio. For powered airfoil systems, the system efficiency should contain the effects of the energy that is required to obtain the airfoil performance. This also avoids the infinite efficiency that would occur when the drag goes zero due to blowing. A correction can be made through an equivalent "kinetic energy" drag coefficient that is related to the power described above. This equivalent drag can be described as:

$$D_{EQUIV} = D_{PROFILE} + D_{POWER} + D_{RAM} + D_{INDUCED}$$

where

$D_{PROFILE}$  is the profile drag

$D_{POWER}$  is fluid power

$D_{RAM}$  is momentum drag force required to ingest the blowing flow rate

$D_{INDUCED}$  is induced drag (equal to zero for 2D)

For 2D flows the equivalent drag becomes:

$$D_{EQUIV} = DRAG + \frac{\dot{m}U_J^2}{2U_\infty} + \rho U_\infty \frac{\dot{m}}{\rho} \text{ Equation 19}$$

$$C_{DEQUIV} = C_D + C_\mu \frac{U_J}{2U_\infty} + C_\mu \frac{U_\infty}{U_J} \text{ Equation 20}$$

The practical implementation of the Betz or Jones wake integration techniques for blown systems are described in reference 13. When the rake drag coefficient is applied to the equivalent drag, it becomes

$$C_{DEQUIV} = C_{DRAKE} + C_\mu \frac{U_J}{2U_\infty} \text{ Equation 21}$$

It should be noted that the kinetic energy or power that is added to the equivalent drag, dominates the equation and leads to drag values that are not practical (10,000 counts, see Figure 8) and hides the thrust generated by a typical CC airfoil..

### Mass Flow Requirements

To optimize the performance of a CC system at the lowest mass flow, it is necessary to recognize the relationships between mass flow,  $C_\mu$ , and slot geometry. Figure 9 highlights this relationship for a given free stream condition and geometry that is consistent with experiments described in this report. Assuming that the performance is dominated by the jet velocity ratio, reducing the slot height would result in a lower mass flow requirement.

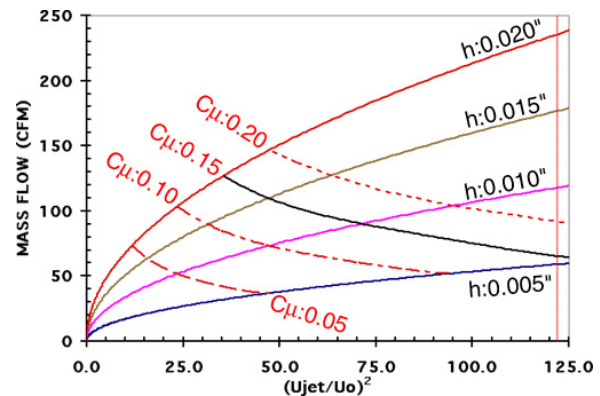


Figure 9 Mass flow requirements  $q=10$  psf  $T_0=75^\circ F$



## GACC Airfoil Design

The General Aviation Circulation Control (GACC) wing concept was initially developed for PAV<sup>14</sup> and is now being considered for the ESTOL concept described above. To address the requirements of PAV, the airfoil design and initial performance goals of this wing concept were to achieve:

- 2-D  $C_L = 3$  using a simplified Coanda driven circulation control trailing edge.
- Provide a pneumatic flap capability that will minimize cruise drag and provide potential roll and yaw control (Dual blowing is defined as upper and lower Coanda surface blowing). This is based on closing the wake of the bluff trailing edge associated with typical blunt Coanda surfaces.
- Provide the capability to change the Coanda surface shape (e.g. Circular, Elliptical, and Bi-convex).
- Provide pulsed pneumatic control to minimize the mass flow requirements for high lift.
- Provide distributed flow control to customize the span-wise loading on the airfoil.

To establish a relevant circulation control airfoil geometry that is readily available to the aerodynamic community (not restricted due to proprietary issues) and that has the potential to be modified for the flight applications described above, several geometries were considered. From the late 1950's and into the 1970's, NASA has engaged in designing supercritical airfoils for transonic transport and fighter applications. These 6-series supercritical airfoils were developed to improve the cruise performance by increasing the drag rise to Mach numbers that approached 0.8<sup>15</sup>.

The selection of the airfoil profile for this study was largely driven by the high lift requirements and with a secondary influence of cruise drag requirements. The baseline airfoil shape was initially based on un-blown wing performance. Nominally the thickness ratio has a direct effect on maximum lift, drag, stall characteristics, and structural weight<sup>16</sup>.

The effect of airfoil thickness on lift and drag are

typically counter-demanding and result in tradeoffs. For un-blown and typical CC wings the thickness ratio primarily affects the maximum lift and stall characteristics by its effect on the nose shape. For a wing of fairly high aspect ratio and moderate sweep, a larger nose radius provides a higher stall angle and a greater maximum lift coefficient.<sup>17</sup> However, without blowing or active flow control the drag increases with increasing thickness due to increased separation.

Wing thickness also affects the structural weight of the wing. "Statistical equations for wing weight show that the wing structural weight varies approximately inversely with the square root of the thickness ratio. Halving the thickness ratio will increase wing weight by about 41%. The wing is typically 15% of the total empty weight, so halving the thickness ratio would increase empty weight by about 6%<sup>17</sup>." Another benefit of a thick airfoil is the increase volume for fuel. The tradeoffs of thickness ratios will not be discussed in this paper, but the larger thickness ratio will be pursued based on the trends of maximum lift and the ability of the CC system to manage the separation issues related to large streamline turning at high lift conditions.

Therefore it was desired to combine a typical supercritical section with Coanda type CC trailing edges. Several key design for a CC airfoil are:

1. A large leading-edge radius is used to alleviate the large negative peak pressure coefficients and can be used as a substitute for a mechanical leading edge device by delaying leading edge separation and airfoil stall to high angles of attack.
2. The airfoil was contoured to provide an approximate uniform chord-wise load distribution near the design lift coefficient of 0.4.
3. A blunt trailing edge was provided with the upper and lower surface slopes approximately equal to moderate the upper surface boundary layer separation and pressure recovery and thus postpones the stall.

The NASA LS(1)-0417 airfoil is popularly known as the GA(W)-1 airfoil. Test results for the GA(W)-1 show that  $C_{l_{max}}$  for this type airfoil is approximately 30% greater than a typical NACA 6-series airfoil and a L/D at  $C_l=0.9$  was about 50% greater. This 17-percent-thick supercritical airfoil<sup>18</sup> was chosen as a baseline geometry for the general aviation circulation control airfoil (GACC)<sup>19</sup> because of its blunt leading edge, large thickness ratio, and potential to be easy to apply active flow control for transonic speeds as shown in Figure 10. It is recognized that leading

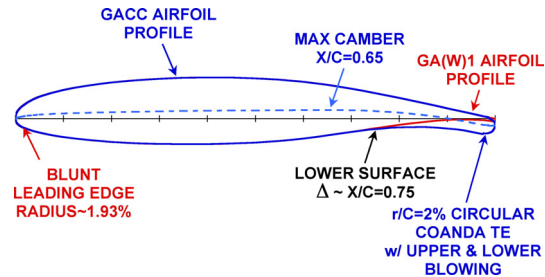


Figure 10 17 percent Thick General Aviation Circulation Control (GACC) profile with circular trailing edge

edge separation will become a problem as the leading edge stagnation moves aft. For large leading edge radius airfoils this problem occurs beyond the target lift coefficients of 3 so leading edge control will not be addressed for this study.

It was decided to modify the GA(W)-1 with Coanda type trailing edges by altering only the aft lower section of the original airfoil. The original GA(W)-1 chord line was used as the reference for AOA on the GACC airfoil design as shown in Figure 10.

The tradeoffs of sizing the Coanda surface can be related to optimizing the lift and drag for high lift or cruise conditions<sup>20,21</sup>. Nominally a larger trailing edge Coanda radius of curvature would lead to a higher CC lift coefficient as well as a higher cruise drag due to an increase in the trailing edge diameter. The shaded area shown in Figure 11 highlights the region of effective Coanda turning and proven lift performance highlighted by the A-6/CCW flight demonstrator<sup>7</sup>. The A-6/CCW airfoil<sup>22</sup> was a 6% thick supercritical wing section that incorporated a state-of-the-art large circular trailing edge radius of 3.67 percent chord. This large trailing edge was to guarantee a successful flight demonstration

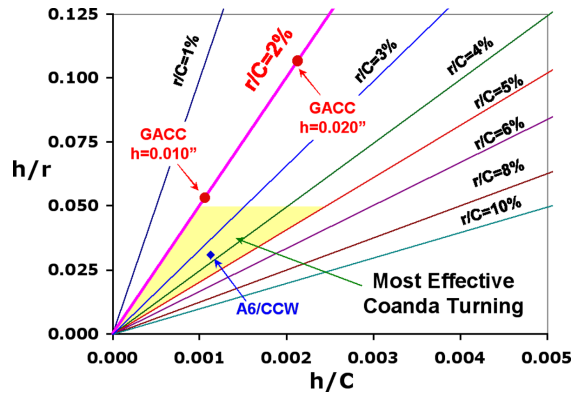


Figure 11 Effective Coanda performance for different radius and jet slot heights

of the high lift system<sup>23</sup> only. Any operational use of this design would require a mechanical retraction of the CC system into the wing to avoid a large cruise drag penalty.

To minimize the GACC airfoil drag performance without the use of a mechanical system a dual blowing pneumatic concept with a small radius trailing edge was designed. A baseline circular r/C of 2% was chosen for the GACC.

Three different trailing edge shapes were designed to be interchangeable and integrate with the GACC model as shown in. Figure 12 The distance between the slots remained fixed and

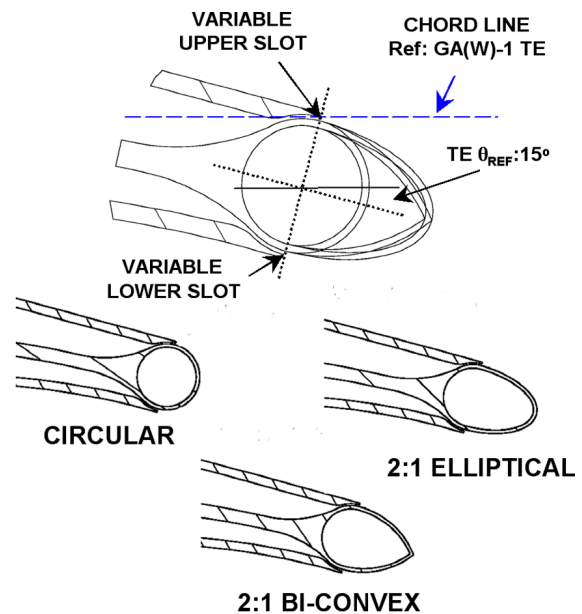


Figure 12 Sketch of interchangeable trailing edge shapes for the GACC airfoil

used the circular shape as a baseline. Both the elliptic and bi-convex shapes extended the chord by 1% (0.174"). The 2:1 elliptic shape reduced the  $r/C$  to 1% and the bi-convex shape had an  $r/C$  of 0.

To compare steady, pulsed, and dual blowing using a common model required careful design of the internal flow path as shown in Figure 13. The

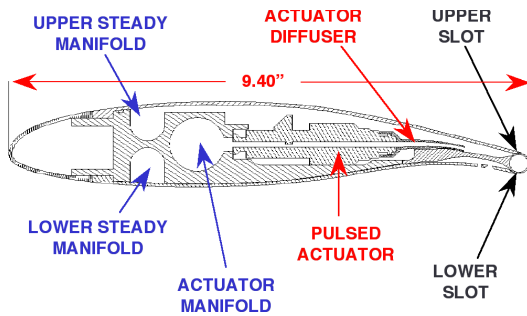


Figure 13 Sketch of internal flow path of the GACC airfoil

ability to independently control the upper and lower slot flow enables the investigation of both positive and negative lift as well as drag and thrust for both high lift and cruise conditions. A pulsed actuator system was integrated into the upper plenum of the model for investigation of unsteady circulation control.

To obtain a uniform flow path and create a 2D flow environment at the Coanda surface it was necessary to carefully design the internal flow path of all three air sources in the model as shown in Figure 14. 20 actuators were distributed in the upper plenum along the span to optimize the

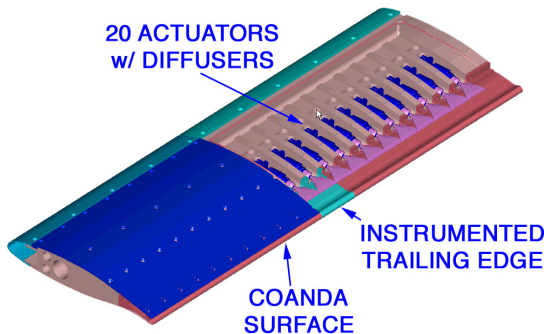


Figure 14 Sketch of GACC model with upper skin removed to highlight the flow path and instrumentation of the upper plenum.

pulsed authority to the upper Coanda jet for the high lift mode. Air for all three sources was fed from one end of the model and was expanded into large plenums then channeled to the trailing edge jet exit. Both the upper and lower slots were adjustable ( $0.005 < h < 0.025$ ) and were fed from a smooth contraction that had a minimum area ratio of 10.

It is difficult to create an infinite or 2D environment with a fixed wall wind tunnel for blown airfoil systems. One must consider the relative size of the model to the size of the test section and the expected trajectory of the jet created by the blown system. To minimize the impact of the wind tunnel interference for CC systems, several experimental design considerations were considered:

- Solid Blockage (physical chord and span related to wind tunnel cross section)
- Wake Blockage (how much streamline turning will be achieved with blown system)
- Juncture flow regions (aspect ratio of model)

The GACC model was sized and built for the NASA LaRC Basic Aerodynamic Research Tunnel (BART) and had a chord to test section height ratio of 0.23, an aspect ratio of 3 based on a chord of 9.4 inches and a 2D wall-to-wall span of 28 inches. These values are conservative for the unblown configuration<sup>24</sup>, however once blowing is applied the influence of the Coanda jet on streamline turning could be significant. A 2D RANS code (FUN2D) was used to evaluate the streamline turning related to Coanda blowing and super-circulation high lift conditions<sup>19</sup>. The free air results of this preliminary CFD evaluation indicated streamline turning and wake deflection would not impact the tunnel walls for the BART test conditions but would be influenced by the presence of the solid tunnel walls. The study of wall interference is ongoing for this experiment.

## Experimental Setup

Experimental results have been obtained for a General Aviation Circulation Control (GACC) airfoil in the open return Langley Basic Aerodynamic Research Tunnel as seen in figure 15. The tests were conducted over a Mach

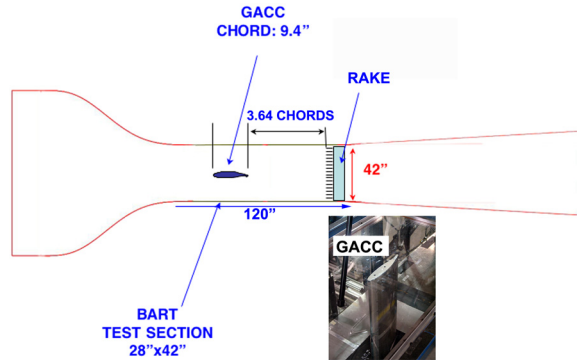


Figure 15 Sketch of the GACC setup in the Basic Aerodynamic Research Tunnel

number range of 0.082 to 0.116 corresponding to dynamic pressures of 10 psf and 20 psf respectively. Lift, drag, pitching moment, yawing moment, and rolling moment measurements were obtained from a 5-component strain gage balance. Drag data were also obtained from a wake rake. Airfoil surface pressure measurements (steady and unsteady) were used to highlight boundary layer transition and separation.

A block diagram of the BART data acquisition is shown in Figure 16. To capture the transients and time dependent characteristics of the pulsed flow field two approaches were developed, arrayed thin films and miniature pressure transducers. This report will focus only on the miniature pressure transducers. The small scale of the model did not lend itself to using off the shelf pressure transducers. Custom differential pressure gages were designed and fabricated using MEMS sensors attached directly to the skins of the model leading and trailing edges. These transducers were not temperature compensated making real time calibration necessary. To keep the measured errors from exceeding 0.05% of the full scale (2 psid) a reference pressure was monitored and calibrations were performed when necessary. This was also the case with the ESP system for 10

32-port modules with ranges of 10" H<sub>2</sub>O, 1 psid, and 2.5 psid.

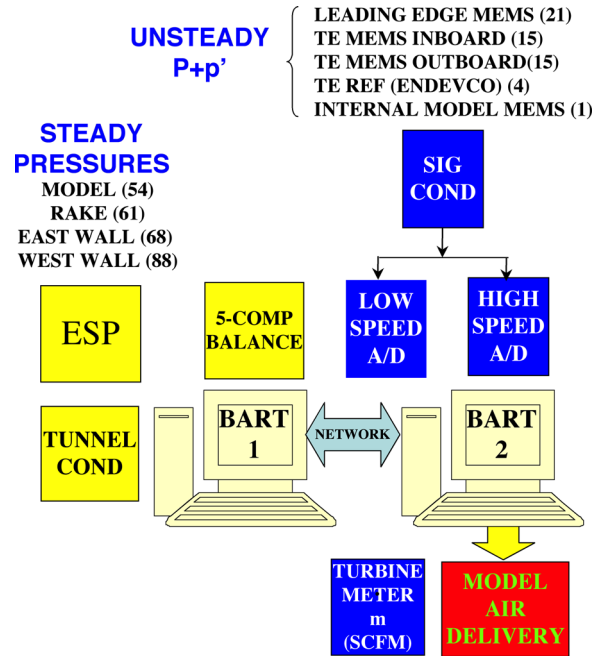


Figure 16 Block diagram of BART data acquisition for GACC setup

The 5-component strain gage balance was also custom designed and fabricated for the GACC model. Normal, axial, pitching moment (ref 50% chord), rolling moment, and yawing moment limits are shown in table 1. A drawback to the GACC balance was that the axial resonance of the balance/model system was too close to the dynamics of the loaded airfoil resulting in vibration of the model. This vibration did not always exist but led to larger than expected errors in the axial force measurement. Therefore the drag data will be reported only from the wake rake results.

Normal (lbf)	Axial (lbf)	Pitching Moment (in. lbf)	Rolling Moment (in lbf)	Yawing Moment (in. lbf)
100	10	1600	400	40

Table 1 GACC balance limits

The GACC model has three plenums that are required for use in different modes of operations, (e.g. high lift, cruise, pulsed, etc.). Each plenum

is supplied with air that is independently regulated as shown in Figure 17. To achieve the potential mass flow requirements for the largest slot area, a 2000 psia high-pressure external air source (3000 psia max) was used. The air is pre-heated to compensate for Joule Thompson effects and temperatures are maintained to within 1°R.

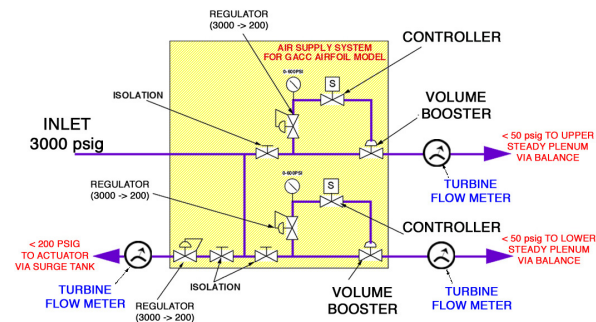


Figure 17 GACC Air delivery system

The mass flow was measured with three independent turbine meters. These flow meters are pre-calibrated and compensated for density variation at the point of measurement (accuracy=1% reading). The high-pressure plenum that supplies the pulsed actuation system is buffered with a 7.1 cubic foot air tank to eliminate the pulsed backpressure flow at the control and flow measurement station. The pressure limits of each of these systems were driven by the pressure ratio at the slot exit. Due to pressure losses in the system the upper and lower plenums were limited to 50 psid and the actuator pressure limited was 200 psid. These limits enabled sonic capability at the slot exit.

A trapeze system was used to couple the air delivery system to the model as shown in Figure 18. Special attention was given to the calibration of the balance due to the number of airlines that cross the balance. Un-pressurized calibration results are applied to a 6 x 21 calibration matrix that account for the linear interactions (1<sup>st</sup> order) and the second-degree nonlinear interactions of the balance.<sup>25 26</sup> Each pressure line was then independently loaded and characterized with no flow (see appendix).

With the model mounted vertically in the tunnel

the only loads experienced by the model as a result of the air delivery system were thrust loads along the span of the model. This is the same as the side-force that is not gauged or measured. The flexible hoses maintain a vertical orientation to the model and eliminate horizontal forces being applied to the balance.

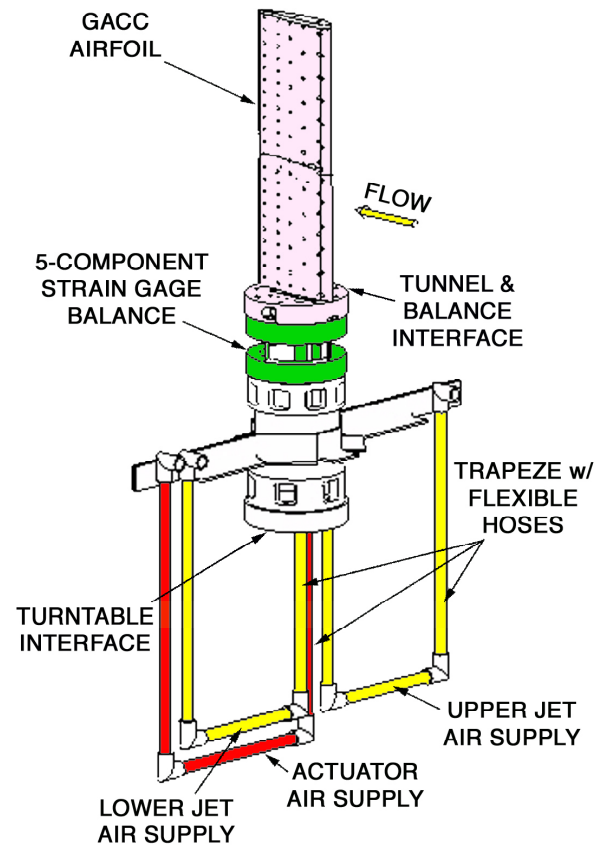


Figure 18 GACC Balance and Model interface with air delivery through trapeze system

Measurement of the drag was initially obtained with the balance and reported in reference 14. However upon careful inspection of the issues related to juncture flow interference and balance vibration, it was determined that the drag information from the balance was unreliable. A total head wake rake was designed and fabricated for the BART. The stream wise location of the rake was determined based on a balance of streamline turning (flow angle at the rake face) and the sensitivity of the pressure transducers. CFD and wind tunnel wall pressure signatures were used to identify that the jet wake was



aligned with the free stream streamlines at  $X/C$  greater than 3.5 from the trailing edge of the model. An example of the wall pressure signature is shown in **Figure 19** for typical high lift conditions.

The magnitude of the wall pressure signatures shown in Figure 19 indicates that a correction may be warranted for the dynamic pressure and angle of attack. Several wall correction techniques are described in the 1998 AGARD “Wind Tunnel Wall Corrections” report.<sup>27</sup> Corrections of 2-D experiments for wall effects are compounded by the 2D aspect ratio and the juncture flow of the model and wind tunnel wall interface. As a first approximation of the wall interference characteristics, corrections for 2D lift interference are made using a classic approach described in the appendix. It is recognized that these corrections

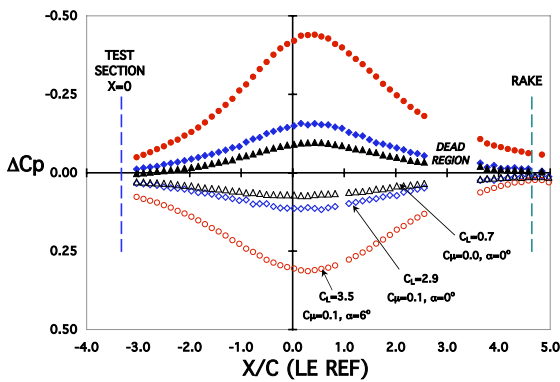


Figure 19 Wind tunnel wall pressure signatures for different lift coefficients (solid symbols for upper wall, open symbols for lower wall),  $h=0.020$ ,  $q=10$  psf, circular trailing edge

are inadequate and that wall signature method may be more appropriate. Evaluations<sup>28</sup> of the wall signature method are ongoing and are not applied to the data presented in this report.

The wall signature pressure distribution is also used to locate the streamwise wake rake position for this experiment. The criteria for the rake measurements are based on a tradeoff of transducer sensitivity and flow angularity of the flow at the probe tip. Based on these criteria, the wake rake was located 3.6 chords downstream of the trailing edge of the model at an angle of attack of 0 degrees. The wake profiles shown in **Figure**

**20** are representative of the effectiveness of the streamline turning created by the circular CC airfoil configuration. The errors associated with the integration of the wake to determine measured drag are related to the non-zero pressures outside the wake region. Even though the rake spans the entire test section only 86% is used for the wake integration, thus eliminating the influence of the floor and ceiling boundary layers. The measured drag was determined to have a repeatability of  $C_d=\pm 0.0005$ .

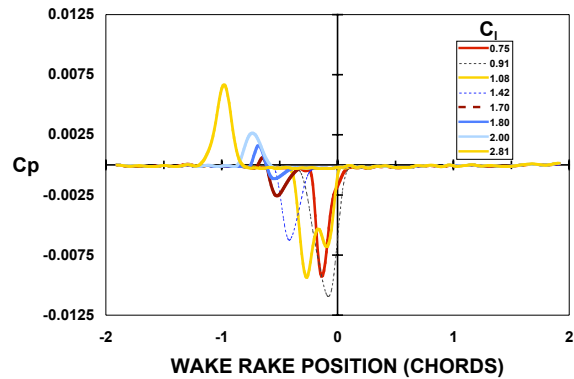


Figure 20 Wake profile of GACC with circular trailing edge,  $AOA=0$

For the momentum sweep at  $AOA=0$ , the wake moved approximately one chord below the centerline. An example of an  $AOA$  sweep at a fixed blowing rate is shown in Figure 21. The wake moved approximately 1.5 chords below the centerline prior to stalling.

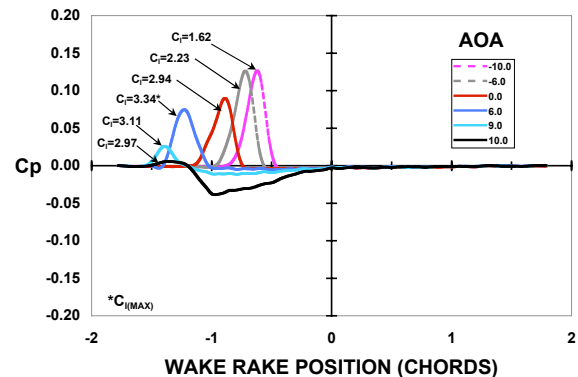


Figure 21 Wake profile of GACC with circular trailing edge,  $-10 < AOA < 10$ ,  $C_{\mu}=0.075$

### Errors associated with Coanda slot setup

The measurement of the non-dimensional momentum coefficient can be obtained from parameters described in Equation 8. Using mass flow and measured pressure ratios ( $U_{jet}$ ) the momentum coefficient can be calculated without any knowledge of slot height. This is the preferred method due to the potential errors in measuring the slot height of the small-scale model used in this test. However post test evaluation of the mass flow data revealed problems with the turbine meters, requiring the use of slot height to determine the momentum coefficient.

Slot height is a critical parameter for correlation to airfoil performance and was given careful attention. Nominally the slot height was set with a digital height gage (accuracy: 0.0001") under no flow conditions. The height was then readjusted to obtain a uniform velocity along the span of the slot. The slot height was locked into place with a push-pull set of screws located approximately one inch from the slot exit inside the settling region of the jet plenum. The 0.010" trailing edge of the stainless steel skin was observed under load with a micro-telescope and did not appear to move. However, post-test span-wise jet velocities measured at the slot exit with a hot wire probe, shown in Figure 22, indicate variations of 20%

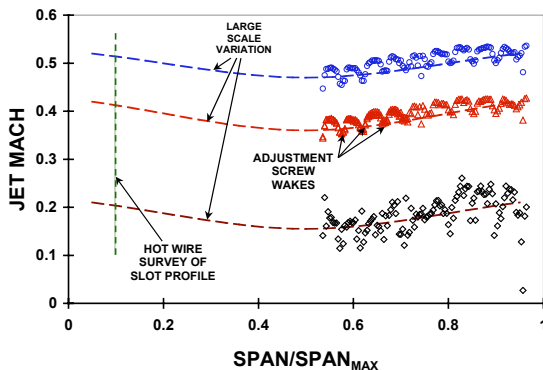


Figure 22 Example of span-wise velocity deviation for different jet exit Mach numbers (biconvex TE configuration,  $h=0.020''$ )

relative to the reference jet velocity determined from pressure ratio. Most of these variations are can be identified with the wake of the internal

push-pull screws used for setting slot height. The variations of the low jet velocities are larger than the higher jet velocities. It was also discovered that the extreme inboard and outboard slot velocity (not shown) was significantly lower than the core region of the span. This is attributed to internal flow separation at the inlet and exit of the flow manifold internal to the model. While affecting only the extreme 0.5" sections of the span, it does effectively reduce the length of the blowing section of the jet.

The large-scale span-wise variation is thought to be due to internal flow variations and/or errors in setting the slot height under loaded conditions. Setting the final slot height was done onsite with the model mounted in the tunnel and mass flow being added. The confined space of the small wind tunnel made setting the slot height difficult due to accessibility and noise. Pressurizing the model for maximum conditions created a jet noise and flow environment that was uncomfortable for the operator setting the slot height. Therefore a low jet velocity was chosen for the slot height adjustment process. As seen in Figure 22 there is a large scatter in the low speed jet data. This gives rise to a greater sensitivity and data scatter to the location of the measurement while setting the slot height. To compound this problem, a hand held 0.010" OD flattened pitot-probe sized to fit just inside the slot was used to make the span-wise velocity profile of the jet exit. The errors in probe location and angularity led to additional data scatter that contributed to the errors in setting slot height.





## Airfoil performance

Airfoil performance will be discussed for two modes of the GACC airfoil; the high lift mode with upper slot blowing and the cruise mode with upper and lower slot (dual) blowing. The efficiency of pulsed blowing will be discussed as part of the high lift mode.

### High Lift Mode

#### Baseline (No Blowing)

Lift, drag, and pitching moment will be used to establish the 2D baseline performance of the GACC airfoil with different trailing edges. The original GACC airfoil was designed around the circular trailing edge having an  $r/c$  of 2%. Therefore the circular trailing edge will be used as the reference for the elliptic and biconvex trailing edges. Comparing the lift performance of the three trailing edges with no blowing in Figure 26, the circular trailing edge has a lift enhancement of  $\Delta C_l = 0.16$  at a zero degree angle of attack

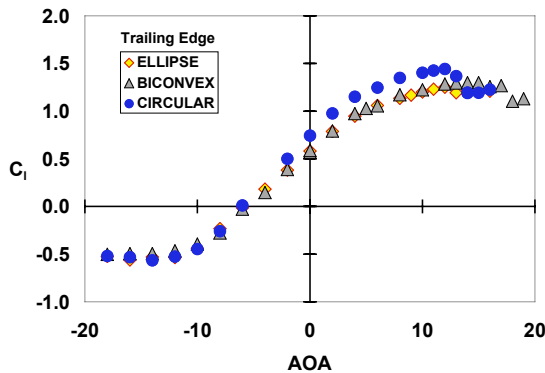


Figure 26 Baseline lift coefficient with no blowing (Balance Data)

relative to the biconvex and elliptic trailing edges. This is also reflected in the trailing edge pressures shown in Figure 27.

Comparisons of the drag performance for the three trailing edges are shown in Figure 28. There are little differences in the indicated drag. This can be related to boundary layer transition fixed at 5% chord and the fixed trailing height

established by the steps created by the upper and lower slots. Minimum drag occurs at zero lift and  $AOA = -6$ .

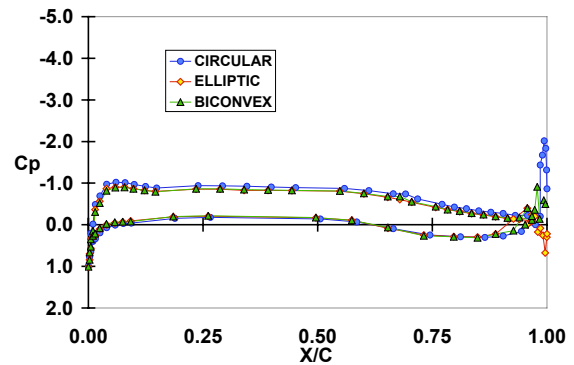


Figure 27 Pressure distribution for GACC airfoil no blowing  $AOA = 0$

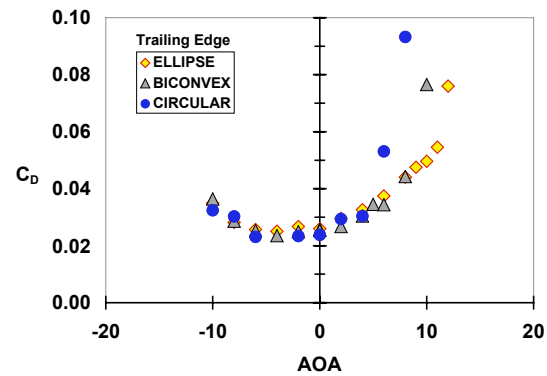


Figure 28 Baseline drag coefficient with no blowing (wake rake)

The airfoil efficiency is shown in Figure 29 indicates that the circular trailing edge is more efficient than the elliptic or biconvex trailing

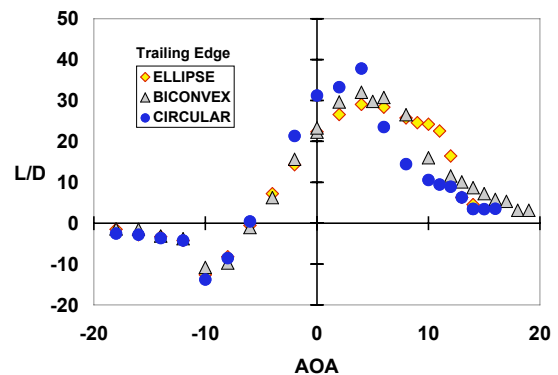


Figure 29 Baseline GACC airfoil efficiency with no blowing

edges with no blowing. The peak efficiency occurs at AOA of 6 degrees and is consistent with the differences in lift. The drag polar shown Figure 30 illustrates a relatively flat drag characteristic for the region of lift that is consistent with cruise conditions (e.g.  $C_l=0.5$ ).

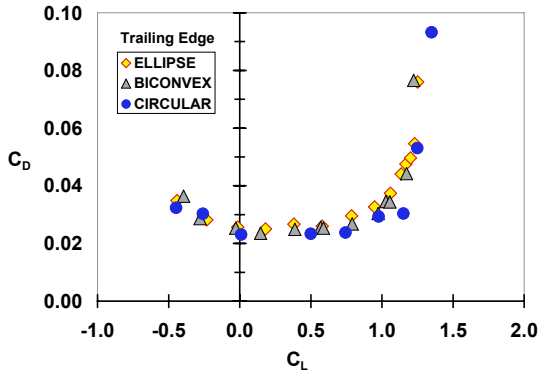


Figure 30 Baseline drag polar for GACC airfoil with no blowing

### Circular Trailing Edge

The circular Coanda trailing edge will be used as a reference for comparisons of performance throughout the rest of this paper. This section will highlight the circular trailing edge performance for high lift conditions. While somewhat arbitrary, the initial goal of this effort was to generate a lift coefficient of 3 at an AOA of 0 degrees. Figure 31 illustrates that using

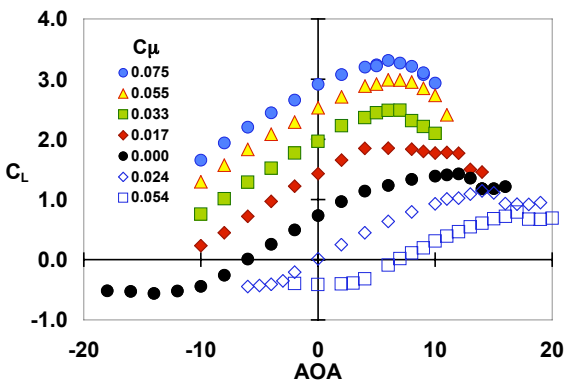


Figure 31 Airfoil lift performance with circular TE &  $h/C=0.0022$  (Open symbols represent lower blowing)

upper Coanda blowing the target lift coefficient of 3.0 was achieved. The maximum lift that this airfoil can achieve is still undetermined, but will be limited by the leading edge performance of the airfoil. The leading edge stall characteristics of this CC airfoil are highlighted in Figure 31. These data are consistent with other supercritical CC airfoils with large leading edges.

Lower Coanda blowing gives this airfoil configuration a unique ability to manage lift and drag by generating a negative lift capability. The open symbols shown in Figure 31 highlight the lower Coanda blowing. The pneumatic flap effect of lower blowing compensates for the trailing edge camber as demonstrated by zero lift at AOA of zero ( $C_{\mu, \text{LOWER}}=0.024$ ). These effects are more related to cruise drag and will be discussed later in this paper.

The efficiency of the Coanda blowing can be related to the slot height and the radius of the Coanda surface. For a fixed Coanda surface radius of  $r/C=2\%$ , an  $h/C$  of 1.4% performed better than an  $h/C$  of 2.2% as shown in Figure 32.

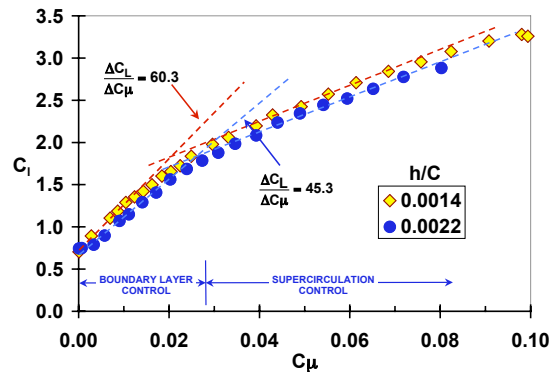


Figure 32 Lift performance of Circular TE, AOA=0

The lift augmentation for the small slot was 60.3 in the separation control regime compared to the 45.3 augmentation for the larger slot. To extend into the supercirculation regime it is necessary to push the rear stagnation beyond the physical trailing edge forming a pneumatic flap. A shift in the lift augmentation efficiency highlights this effect as shown in Figure 32. The limit of the separation region for this airfoil occurs at a  $C_{\mu}$  of approximately 0.03 and a lift coefficient of 1.8. To predict the mass flow requirements and lift

performance in the supercirculation region, it is possible to extend the supercirculation lift augmentation line.

The drag characteristics corresponding to Equation 18 are shown in Figure 33. Thrust is generated for low blowing rates that are characteristic of most CC airfoils including GACC. Combinations of Coanda blowing and AOA allow for variable drag at a fixed lift condition. As an example, the drag can be varied by  $\Delta C_d=0.060$  at a lift coefficient of 2.0, This would include both a thrust and drag capability...The limitations of this capability are related to the leading edge stall characteristics and may be augmented with leading edge active flow control.

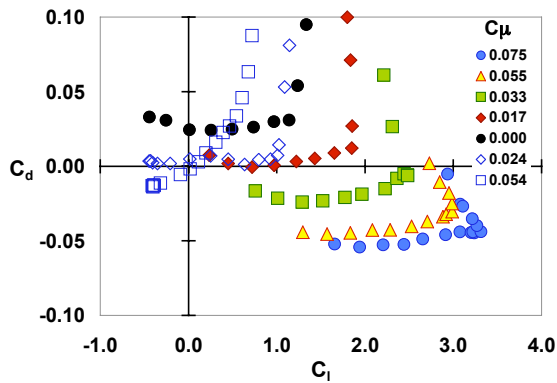
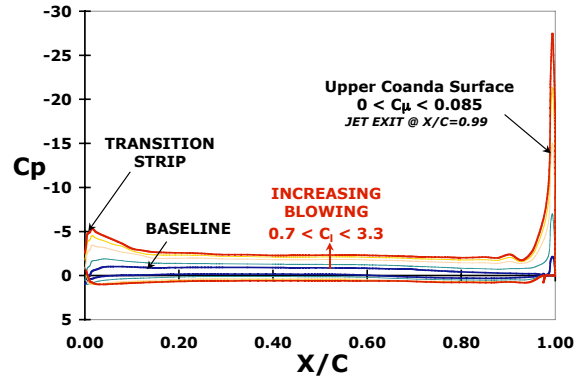


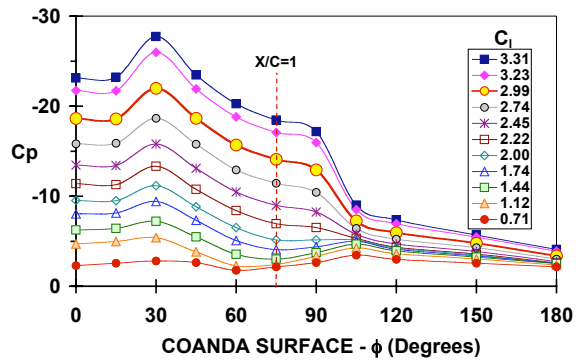
Figure 33 Airfoil drag polar for circular TE  $h/C=0.0022$ , Wake rake data (Open symbols represent lower blowing)

To gain a greater understanding of drag characteristics for this airfoil, the total drag measured in the wake can be decomposed into a 2D circulation induced force represented by the pressure distribution on the airfoil (shown in Figure 34) and the reactionary force created by the Coanda jet evaluated at the jet exit. The reactionary force and the induced force can be combined to create the total force measured. Since the total drag force is known from the wake rake data and the reactionary force  $C_r$  is equivalent to  $C_\mu$ , then the 2D circulation induced force will become:

$$C_{d_{2D-INDUCED}} = C_{d_{TOTAL}} - C_\mu [\cos(\alpha + \delta)]$$



(a) Airfoil pressure distribution



(b) Expanded view of circular trailing edge pressure distribution

Figure 34 GACC pressure distribution with circular trailing edge,  $AOA=0$ ,  $h/C=0.00106$

An example of the 2D circulation induced drag force is shown in Figure 35. This data corresponds to the lift data in Figure 32. An observation that the slope change that is related to the supercirculation region in the lift data is also evident in the drag data, occurring at a momentum coefficient of approximately 0.03.

The efficiency of a blown airfoil has traditionally been related to an equivalent drag as described earlier in the text. The equivalent drag shown in Figure 36 highlights the conversion of measured thrust to equivalent drag for two slot configurations. While this enables the one to compare one blown system to another, it is dangerous for the designer to use these values as seen by comparing figures Figure 35 and Figure 36.

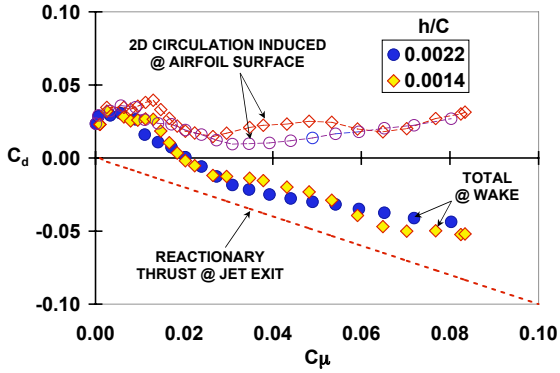


Figure 35 Drag performance of Circular TE, AOA=0

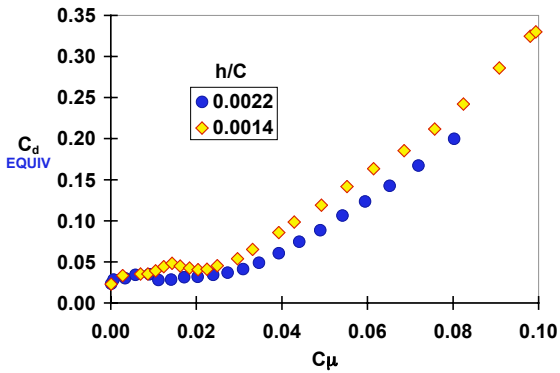


Figure 36 Equivalent drag of Circular TE, AOA=0

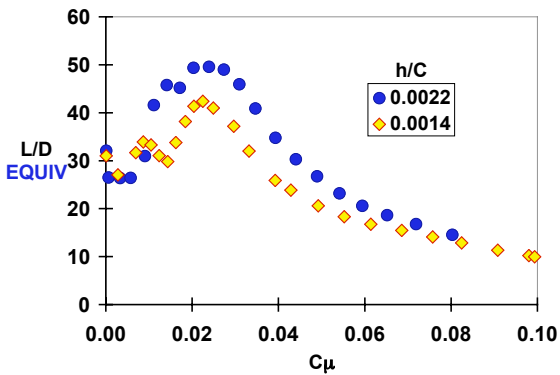


Figure 37 Efficiency of Circular TE, AOA=0

The efficiency of the airfoil can be represented by the lift to equivalent drag ratio shown in Figure 37. Comparison of the two slot configurations

indicates a greater efficiency of the larger slot. This is a result of the drag benefits of the larger slot and is believed to be related to the turbulence characteristics of the Coanda jet. The peak efficiency occurs in the vicinity of the transition from boundary layer control to supercirculation (refer to Figure 35).

The 2D L/D equivalent efficiency of the airfoil can also be related to the fluidic power required of the high lift system as shown in Figure 38. The corresponding equivalent drag data are shown in Figure 39. The fluidic power can be related to the reactionary thrust component described in Figure 35. The dashed line represents the contribution of the fluidic power to the equivalent drag. Any values that deviate above or below this line can be related to the 2D circulation induced effects described above and highlight the magnitude of the dominating contribution of the fluidic power to the equivalent drag.

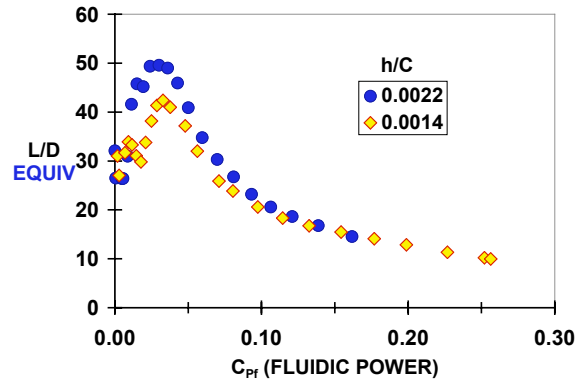


Figure 38 Pumping power required to achieve equivalent GACC airfoil efficiency for circular TE, AOA=0

Evaluating the measured drag per fluidic power reveals that the most efficient use of the fluidic power occurs in the boundary control region. This is shown in Figure 40 where  $\Delta C_d/C_{pf}$  is a minimum. The magnitude of the incremental thrust for the larger slot height is 0.9324 at a fluidic power of 0.03873 shown in Figure 41. This corresponds to a thrust of 0.0295 (reference Figure 35).

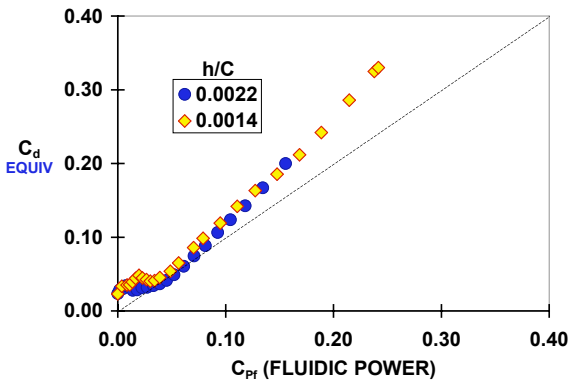


Figure 39 Fluidic power required to achieve equivalent drag for circular TE, AOA=0

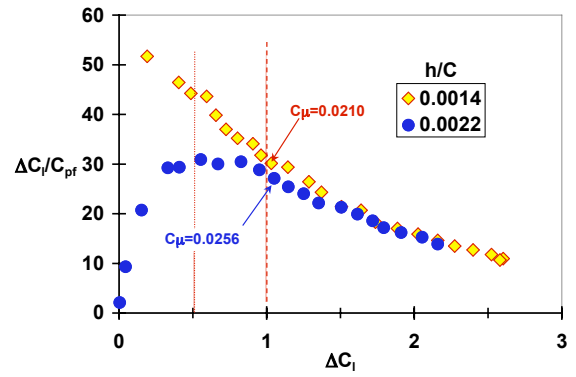


Figure 42 Lift per power ratio for GACC airfoil with circular TE, AOA=0

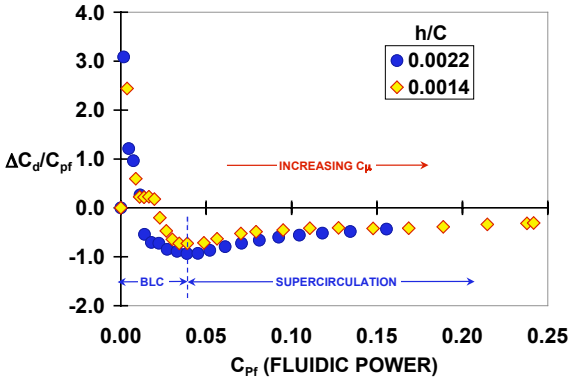


Figure 40 Drag efficiency per fluidic power for GACC airfoil with circular TE, AOA=0

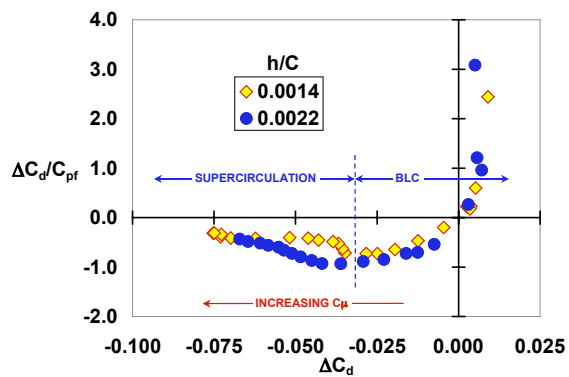


Figure 41 Drag per power ratio for GACC airfoil with circular TE, AOA=0

This also illustrates a benefit of a blown system compared to other active flow control techniques such as synthetic jets and suction systems.

Without the benefit of the reactionary force of the jet, the best performance a traditional active flow control system could achieve would be related to moving or attaching the boundary layer to the

the most aft portion of the airfoil. This would result in a theoretical zero drag. For a tangentially blown system typical of CC airfoils, the reactionary forces enable thrust to the system that is not available to unblown systems. To make a direct comparison of these different active flow control systems it would be necessary to equate the relevant power (watts, horsepower, etc.) to achieve a comparable drag performance.

Another performance parameter of interest is the lift-increment-per-power ratio,  $\Delta C_l/C_{pf}$  shown in Figure 42. This parameter is occasionally used for direct comparisons of similar power-augmented devices<sup>9</sup>. The comparisons are made at  $\Delta C_l$  of 0.5 and 1.0, which are consistent with the boundary control region, and the initial stage of supercirculation. For the GACC airfoil the smaller slot develops more lift for a given power setting than the larger slot in the boundary layer control region. As the power (or momentum) is increased into the supercirculation region, the influence of slot height on lift-to-power augmentation decreases.

Comparing the power requirements for the GACC to other similar airfoils are shown in Table 1. The GACC airfoil performance is comparable to that of a similar CC airfoil and blown flaps with active flow control.

ITEM	$\Delta C_l / C_{Pf}$ ( $\Delta C_l = 0.5$ )	$\Delta C_l / C_{Pf}$ ( $\Delta C_l = 1.0$ )
GACC ( $h/C=0.0014$ )	44.3	31
ELLIPTIC CC <sup>29</sup>	40.4	28.6
TE BLOWN FLAP <sup>30</sup>	42.6	33.2
FLAP KNEE <sup>31</sup> (BLC Mode)	26.8	7.48

Table 1 Comparison of GACC lift increment-per-power to similar powered systems<sup>9</sup>

The pitching moment characteristics of the GACC airfoil are shown in Figure 43. These values are consistent with other CC airfoils.

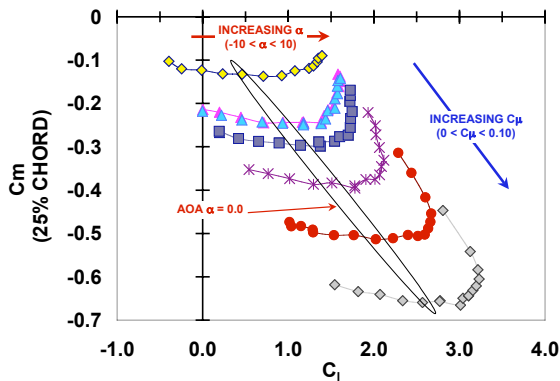


Figure 43 25% chord pitching moment characteristics of GACC,  $h/C=0.0022$

### Performance Comparisons of Trailing Edges

The following section will focus on comparisons of the different shape trailing edges with a fixed slot height of  $h/C=0.0022$ . The shapes include circular, elliptic, and biconvex profiles having effective trailing edge radius of  $r/C=2\%$ ,  $1\%$ , and  $0\%$  respectively. The lift performance of the larger radius configuration is higher than the other configurations as seen in Figure 44.

A comparison of the drag performance, shown in Figure 45, highlights the improvement of the drag as a function of the smaller  $r/C$ . The elliptic trailing edge ( $r/C=1\%$ ) has less drag than the circular trailing edge ( $r/C=2\%$ ) throughout the boundary layer and supercirculation region. Transitioning from the boundary layer region to the supercirculation region the total thrust of the elliptic trailing edge exceeds the reactionary thrust, implying a net 2D circulation induced thrust. The drag performance of the biconvex shape mimics the circular trailing edge performance in the boundary layer control region. The thrust for the biconvex configuration extends beyond the reactionary thrust throughout the supercirculation region.

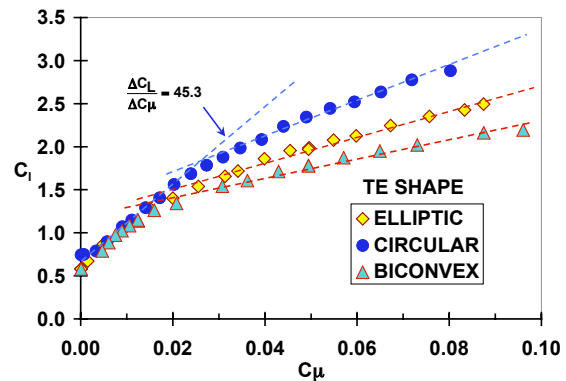


Figure 44 Comparison of lift performance for the GACC airfoil for different trailing edge shapes,  $h/C=0.0022$

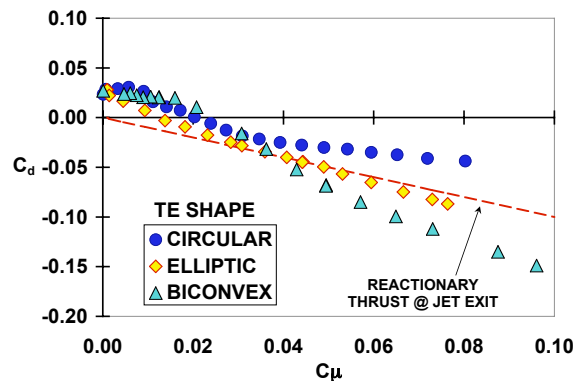


Figure 45 Comparison of the thrust performance of the GACC having three different trailing edge shapes.



Comparisons of drag polars for the three different trailing edges are shown in Figure 46. The effectiveness of the sharp trailing edge is reflected in the increased thrust for the biconvex trailing edge.

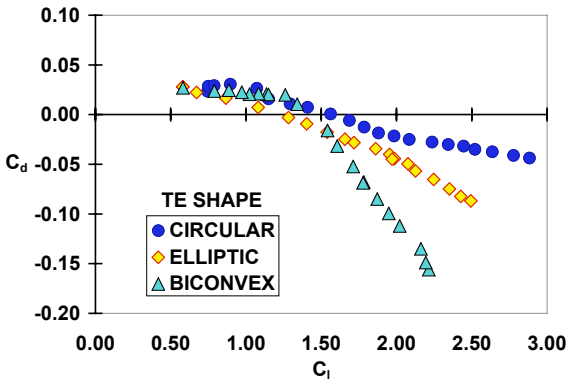


Figure 46 Comparison of drag polars for three different trailing edge shapes,  $h/C=0.0022$

Comparisons of pitching moments for the three trailing edges are shown in Figure 47. The biconvex trailing edge has the lowest pitching moment for any given lift. The benefits of high thrust and low pitching moment comes at the price of momentum coefficient, e.g. for a lift coefficient of 2 the thrust of the biconvex is 110 counts larger and the moment is 50 counts smaller than the circular trailing edge performance. However the momentum coefficient increased by a factor of 2.

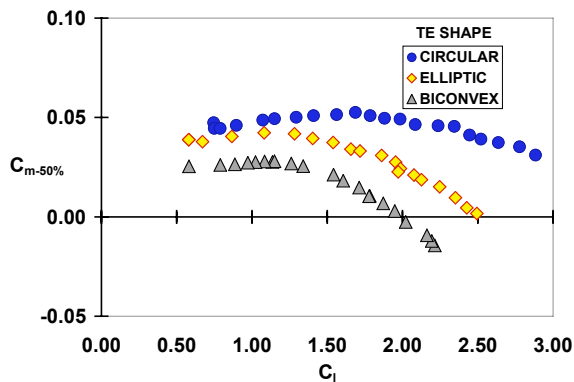


Figure 47 Comparison of pitching moments (referenced to 50% chord) for three different trailing edge shapes,  $h/C=0.0022$

## Cruise Configuration

To address the issue of a blunt trailing edge for typical CC configurations at cruise, the GACC was designed with a dual blowing capability, i.e. upper and/or lower blowing on the Coanda surface<sup>32, 33</sup>. This enables the operator to augment the system thrust while providing roll and/or yaw control. The following section will address only the dual blown circular trailing edge performance.

### Dual Blowing for Circular Coanda surface

It should be recognized that the cruise condition for this airfoil would be operated at a substantially higher Mach number and higher dynamic pressure, thereby reducing the momentum coefficient. These low speed data do not account for the airfoil compressibility and potential shock manipulation that typical CC configurations may provide. For cruise conditions the CC performance characteristics are limited to the boundary layer control region. Nominally lift coefficients that are the order of 0.5 are desired during cruise operations.

To characterize the lift performance of the dual blown configuration of the GACC airfoil, the upper blowing condition was fixed and the lower blowing was swept as shown in Figure 48. As expected the upper blowing performance remains proportional to the lift. Combining this upper blowing with lower blowing will result in a lift reduction. However, this reduction does not

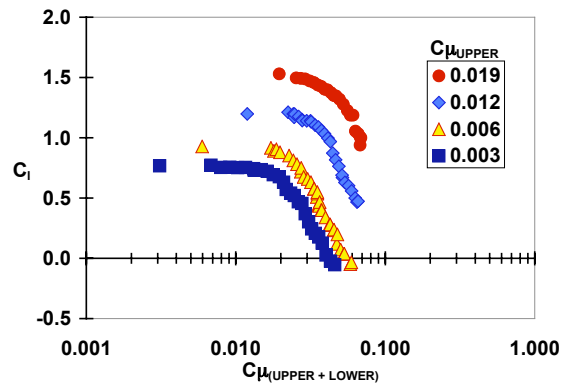


Figure 48 Lift performance for dual blowing  $h/C=0.0022$  occur until the initial stages of thrust.

The effectiveness of the dual blown configuration is realized in the drag performance. The drag characteristics associated with Figure 48 are shown in Figure 49. The drag performance seems to be independent of upper blowing in the

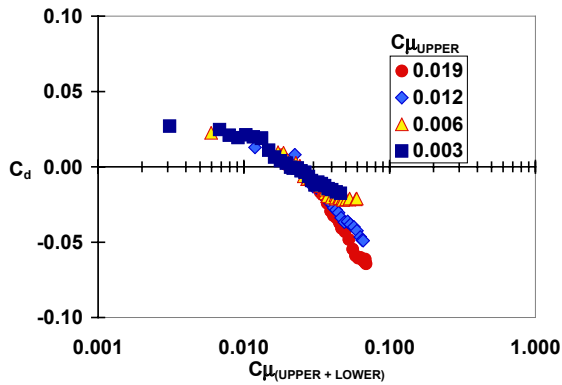


Figure 49 Drag characteristics of the circular dual blown configuration,  $h/C=0.0022$

boundary layer control region. The drag polar, shown in Figure 50, indicates that thrust can be adjusted for a given lift. (e.g. for a fixed  $C_l=0.5$  a  $\Delta C_d=-0.043$  can be adjusted using dual blowing).

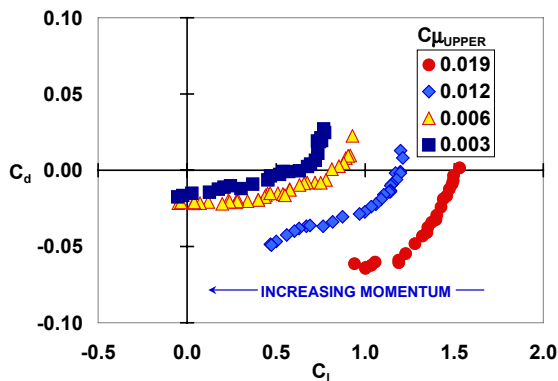


Figure 50 Drag polar for the dual blowing cruise configuration of the GACC airfoil, circular trailing edge,  $h/C=0.0022$  (upper and lower)

The wake profile shown in Figure 51 corresponds to the fixed upper blowing of  $C\mu=0.003$ . As the blowing rate increases, the profile goes from a single peak to a double peak, then returns to a single peak. This indicates that the upper and lower jets are independent and do not mix efficiently for the blunt circular trailing edge.

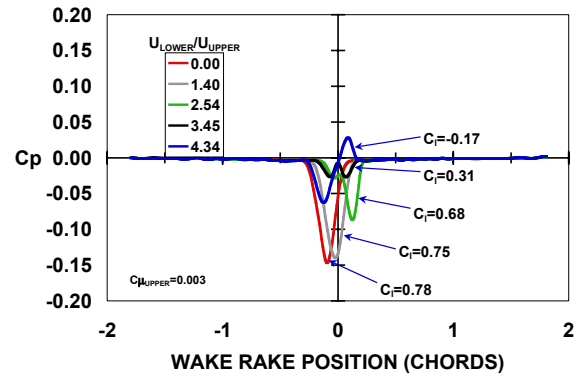


Figure 51 Wake profiles for the dual blowing cruise configuration of the GACC airfoil, circular trailing edge, reference  $C\mu_{upper}=0.003$ ,  $h/C=0.0022$  (upper and lower)

The equivalent drag for the circular dual blown configuration is shown in Figure 52. The minimum equivalent drag occurs at a combined momentum coefficient of 0.03 and a fixed upper momentum coefficient of 0.003. This is

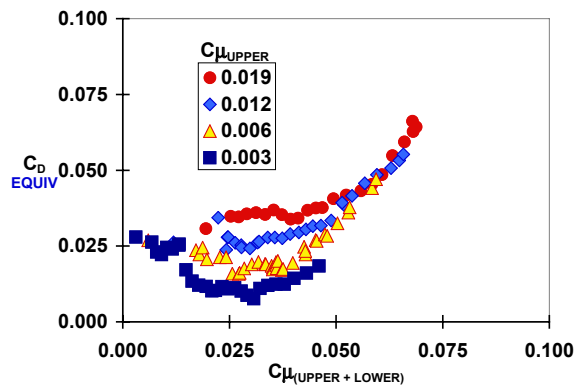


Figure 52 Equivalent drag for the GACC dual blown circular trailing edge

consistent with a measured total drag of  $-0.012$ .

The peak efficiency shown in Figure 53 occurs at a total momentum coefficient of 0.021. This is consistent with the measured drag transitioning from drag to thrust.

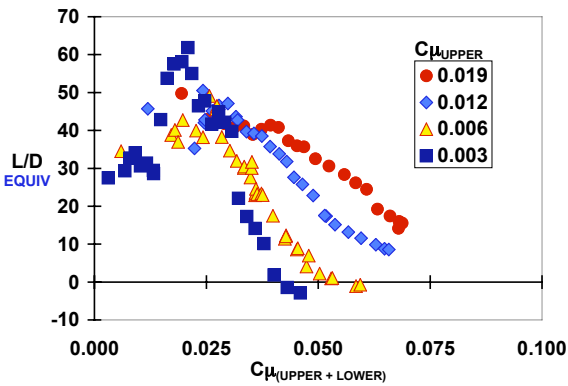


Figure 53 Airfoil efficiency for the GACC dual blown circular trailing edge

### Pulsed Blowing

As will be shown in this section, pulsed blowing from the upper slot is intended to reduce the mass flow requirements for a comparable steady blowing performance.<sup>34, 35</sup> The GACC pulsed blowing system<sup>19</sup> is based on a high-speed valve that delivers a high volumetric flow to the upper jet exit. The actuator is close coupled (internally located  $x/C=0.90$ ) to the jet exit through a rapid diffuser to deliver a pulse of air that can be varied in magnitude, frequency, and duty cycle. An example of the pulse train is shown in Figure 54.

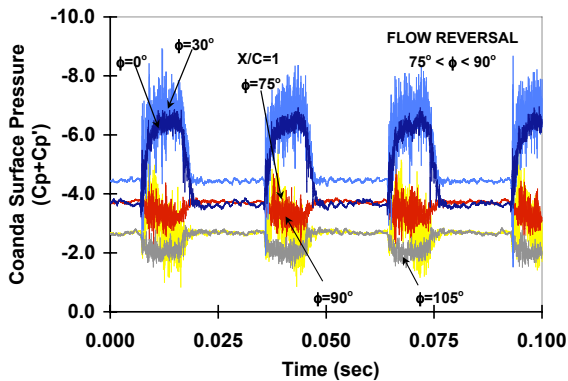


Figure 54 Time record of circular Coanda surface pressures with pulsed upper blowing, 35 Hz, 40% duty cycle, circular trailing edge  $h/C=0.00106$ .

The quality of the rise time and decay of the pulse train is related to the overall actuator authority. The rise and decay time of the pulse train is dependent on the internal volume located

internally just upstream of the jet exit. This includes the 10:1 contraction and the settling area downstream of the rapid diffuser exits.

The time dependant pulse train is referenced to the jet exit or  $\phi=0$  of the Coanda surface. The averaged pressure field is compared to a comparable steady blowing condition, shown in Figure 55. The separation associated with this condition was identified to occur  $75^\circ < \phi < 90^\circ$ , whereas steady blowing produced a separation

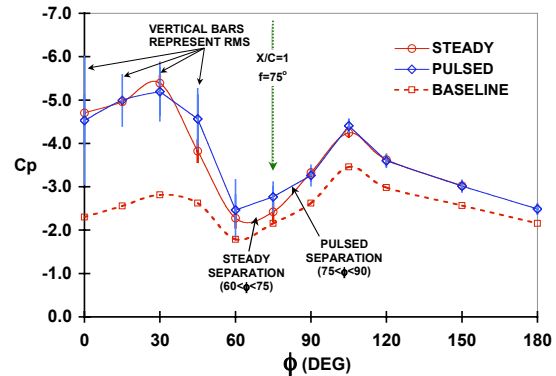


Figure 55 Comparison of steady and pulsed pressure distribution for the circular trailing edge,  $h/C=0.00106$

$60^\circ < \phi < 75^\circ$ . This corresponds to a lift performance shown in Figure 56. The mass flow reduction of 55% corresponds to the 40% duty cycle shown in Figure 54. It should be emphasized that this reduction is limited to the boundary layer control region due to current limits in actuator authority.

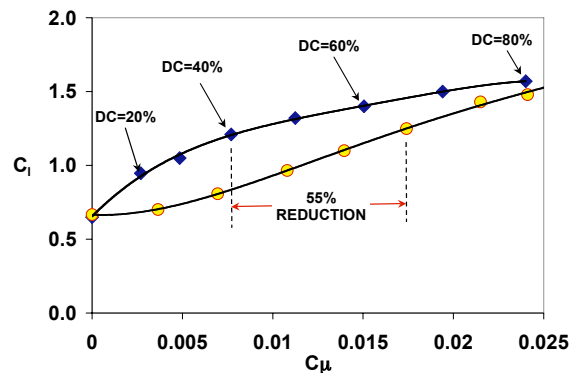
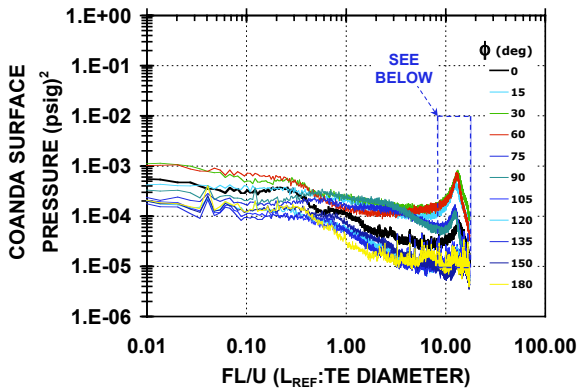
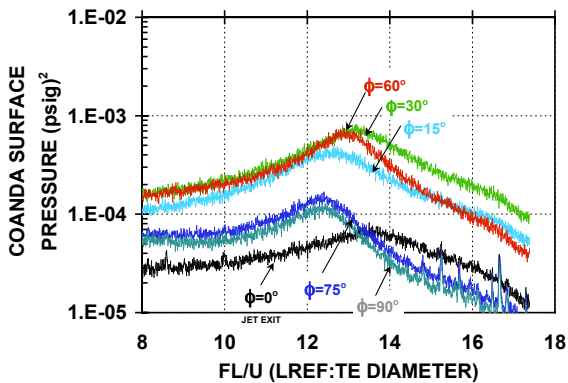


Figure 56 Comparison of lift performance for steady and pulsed blowing on the circular trailing edge,  $h/C=0.00106$

The turbulence magnitude and frequency of the steady jet, shown in Figure 57, increases just downstream of the jet exit, then increases along the Coanda surface to peak at  $\phi=30^\circ$ . The magnitude and frequency then decays until the jet separates from the Coanda surface between



(a) Non-dimensional Spectra for steady jet



(b) Expanded view of frequency content for the influence of the shear and entrained flow

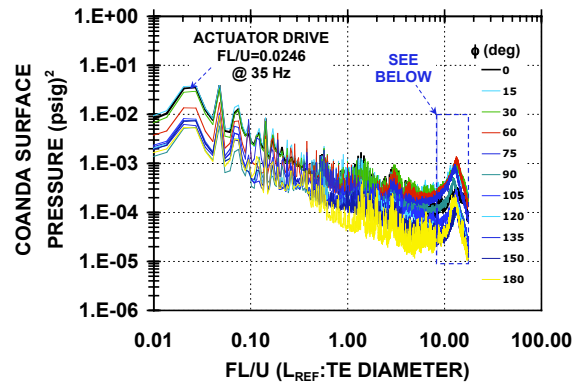
Figure 57 Frequency content of the pressure field on Coanda surface, steady jet, circular TE,  $h/C=0.00106$

$60 < \phi < 75$ .

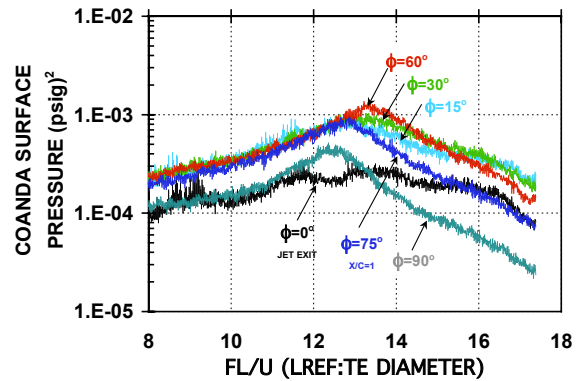
The turbulence magnitude and frequency of the jet-on portion of the pulse train increases just downstream of the jet exit, then increases along the Coanda surface to peak at  $\phi=60^\circ$  shown in Figure 58. The magnitude and frequency then decays until the jet separates from the Coanda surface between  $75 < \phi < 90$ .

The performance benefit of the pulsed elliptic trailing edge is significantly less than that of the

circular trailing edge, shown in Figure 59. For a lift coefficient of 1.0 there is a 29% reduction of mass flow for the pulsed elliptic trailing edge compared to the 55% reduction of the circular trailing edge. There was no measurable benefit in mass flow reduction for the pulsed biconvex



(a) Non-dimensional Spectra for pulsed jet



(b) Expanded view of frequency content for the pulse-on portion of pulse train

Figure 58 Frequency content of the pressure field on Coanda surface, actuator drive: 35 Hz, 40% duty cycle, circular TE,  $h/C=0.00106$

trailing edge.

The effectiveness of the pulsed blowing can be related to radius of curvature of the Coanda surface and jet separation. The pulsed effectiveness for larger  $r/C$  that is represented by the 2% circular trailing edge, moved the time averaged separation beyond the maximum trailing edge location of  $x/C=1.0$ , i.e. from the upper Coanda surface to the lower Coanda surface.

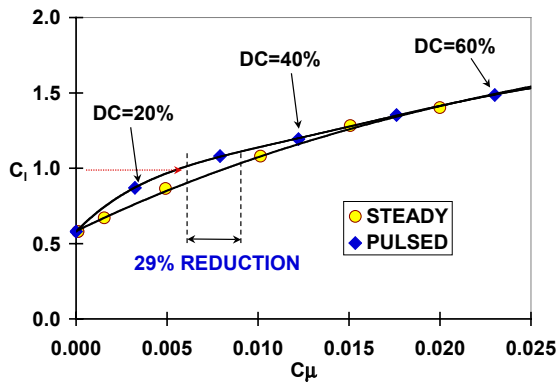


Figure 59 Mass flow reduction for pulsed elliptic trailing edge,  $h/C=0.0022$ , boundary layer control region

Several factors contribute to the effectiveness of the pulsed jet, that include a larger instantaneous velocity, the increased turbulence (for mixing), pulse frequency, pulse duty cycle, and the limitation of a steady jet to remain attached to a small radius of curvature. Further research is needed to isolate these parameters.

### Concluding Remarks

The efficiency of the GACC airfoil is compared to other CC airfoils in Figure 60. The details of the other CC airfoil data are described in reference 9 and shown here to capture the range of possibilities for the GACC configuration.

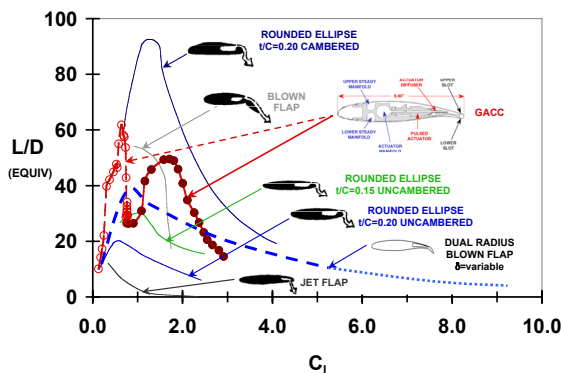


Figure 60 Comparison of GACC efficiency with similar CC airfoils,  $AOA=0$  unless otherwise noted, (curves do not necessarily represent the envelope of maximum efficiency  $C_L/C_{dEQUIVALENT}$ )

Comparing the improved efficiency of the cambered rounded ellipse airfoil<sup>21</sup> is believed to be a function of the larger radius of the circular trailing edge used in the elliptical airfoil. The increased efficiency of the camber for the elliptical airfoil is also shown for the  $t/C=0.20$  configuration<sup>21</sup>. The camber effects of the GACC airfoil are demonstrated in the generation of higher lift for comparable momentum coefficients. Comparing the GACC efficiency to a typical blown flap<sup>36</sup> reveals the lift benefit of attaching the jet through Coanda turning. It is speculated that the blown flap prematurely separates, limiting its lift performance to  $C_L < 2$ . Reshaping the blown flap to the dual radius CC flap profile, enables the jet to remain attached to the trailing edge of the flap, extending its lift performance to  $C_L \approx 5$ . It should be noted that leading edge blowing was required to extend the lift coefficient beyond  $C_L \approx 5$  for the dual radius flap<sup>37</sup>. The poor efficiency of the jet flap<sup>38</sup> is generally related to the large blowing requirements associated with the reactionary force, and the minimal effect on the 2D induced pressure field.

The efficiency of the GACC's dual blown configuration highlights the low speed cruise conditions. Nominally the lift requirements for cruise are  $C_L \approx 0.5$ . Recall from Figure 50 that most of the real drag is in the form of thrust. It is also unclear what  $U_{jet}$  to use in the  $C_\mu$  equation since the upper and lower are controlled independently.

The general performance of the GACC airfoil is good, but has not been tested to its limits. It is recommended that leading edge active flow control be added to extend the limits of lift. It is also important to extend the pulsed performance benefits into the supercirculation region.

Selecting the GACC airfoil section for use on an ESTOL or PAV vehicle may be premature. It does seem to be an excellent candidate for the outboard portion of the wing, having good lift augmentation capability and good roll and yaw potential.

## Appendix

### Wall Interference

As a first approximation of the wall interference characteristics, corrections for 2D lift interference can be made using a classic approach described by Krynytzky<sup>39</sup> and Allan and Vincenti<sup>40</sup>. For a small model centrally located between two closed parallel walls, corrections for angle of attack, lift, and pitching moment can be estimated using the following:

$$\Delta\alpha = \frac{\pi c^2}{96\beta H^2} (C_L + 4C_M) \quad \text{Equation 23}$$

$$\Delta C_L = -\frac{\pi^2}{48} \left(\frac{c}{\beta H}\right)^2 C_L \quad \text{Equation 24}$$

$$\Delta C_m = \frac{\pi^2}{192} \left(\frac{c}{\beta H}\right)^2 C_L \quad \text{Equation 25}$$

$$q_{\text{CORR}} = \left[1 + (2 - M^2)\varepsilon\right] q_{\text{UNCORR}} \quad \text{Equation 26}$$

where

$$\varepsilon = \varepsilon_{\text{SOLID}} + \varepsilon_{\text{WAKE}} \quad \text{Equation 27}$$

and

$$\varepsilon_{\text{SOLID}} = \frac{\pi}{6} \left[1 + 1.2\beta \left(\frac{t}{c}\right)\right] \left[1 + 1.1 \left(\frac{c}{t}\right) \alpha^2\right] \frac{A_0}{\beta^3 H^2}$$

$$\text{Equation 28}$$

and

$$\varepsilon_{\text{WAKE}} = \frac{C_D}{4\beta^2} \left(\frac{c}{H}\right) \quad \text{Equation 29}$$

Example of the wall interference corrections described by equations 22, 23, and 24 are small as seen in Figure 60, 61, 62, and 63.

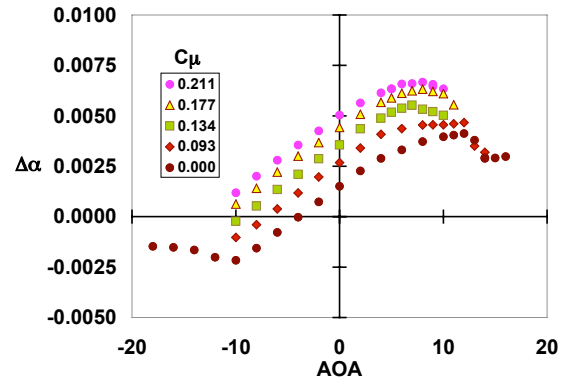


Figure 61 Angle of attack correction from wall interference (circular TE)

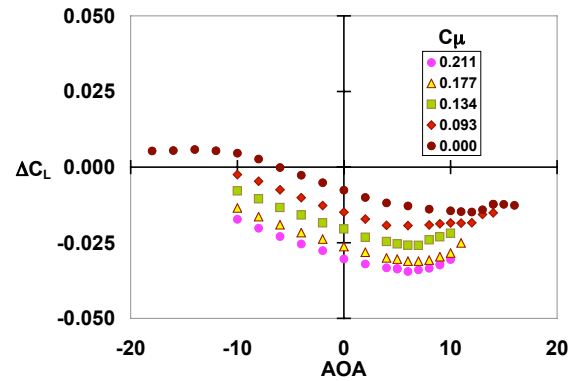


Figure 62 Lift corrections from wall interference (circular TE)

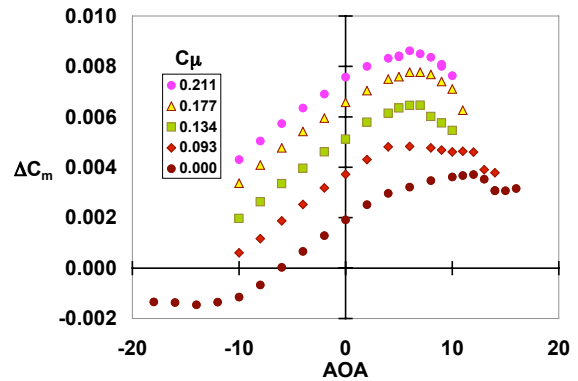


Figure 63 Moment correction from wall interference (circular TE)

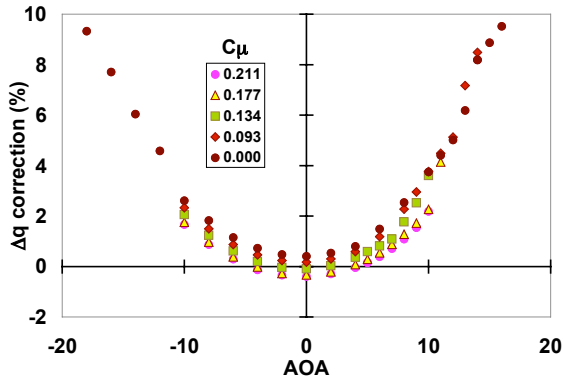


Figure 64 Dynamic pressure correction from wall interference (circular TE)

$$PM_{LOAD} = (PM_{LOAD})_{CALCULATED} + \sum(PRESSURE\ TARE_{CORRECTION})$$

where

$$PRESSURE\ TARE_{CORRECTION} = K_1 P_{ACT} + K_2 P_{UPPER} + K_3 P_{LOWER} + K_4 P_{ACT} P_{UPPER} + K_5 P_{ACT} P_{LOWER}$$

$$YM_{LOAD} = (YM_{LOAD})_{CALCULATED} + \sum(PRESSURE\ TARE_{CORRECTION})$$

where

$$PRESSURE\ TARE_{CORRECTION} = I_1 P_{ACT} + I_2 P_{UPPER} + I_3 P_{LOWER} + I_4 P_{ACT} P_{UPPER} + I_5 P_{ACT} P_{LOWER}$$

The accuracy of the balance is highlighted in table 2. The rolling moment and yawing moments are meaningless for 2-D testing and will be ignored except in when calculating the interactions to obtain corrected Normal, Axial, and Pitching moments.

Normal (%FS)	Axial (%FS)	Pitching Moment (%FS)	Rolling Moment (%FS)	Yawing Moment (%FS)
0.04	0.39	0.12	0.07	1.64

Table 2 GACC Strain gage balance accuracy (95% confidence level)

### Balance Corrections

Data reduction equations and tare corrections for pressure lines across balance:

$$NF = \theta_{NF}(NF_{SC}) - \sum(NF_{INTERACTIONS})$$

$$AF = \theta_{AF}(AF_{SC}) - \sum(AF_{INTERACTIONS} + PressureCorrection)$$

$$PM = \theta_{PM}(PM_{SC}) - \sum(PM_{INTERACTIONS} + PressureCorrection)$$

$$YM = \theta_{YM}(YM_{SC}) - \sum(YM_{INTERACTIONS} + PressureCorrection)$$

$$RM = \theta_{RM}(RM_{SC}) - \sum(RM_{INTERACTIONS})$$

Pressure tare correction for axial, pitching moment, and yawing moment forces:

$$AF_{LOAD} = (AF_{LOAD})_{CALCULATED} + \sum(PRESSURE\ TARE_{CORRECTION})$$

where

$$PRESSURE\ TARE_{CORRECTION} = J_1 P_{ACT} + J_2 P_{UPPER} + J_3 P_{LOWER} + J_4 P_{ACT} P_{UPPER} + J_5 P_{ACT} P_{LOWER}$$



## References

- 
- <sup>1</sup> Jones, G.S., Joslin, R.D., "NASA/ONR 2004 Circulation Control Workshop", Oral presentation, Hampton, VA. March 2004.
- <sup>2</sup> McKinley, R.J., "Future Vehicle Capabilities & the Potential Contribution of Circulation Control", NASA CP xxxx, pg x-x, March 2004.
- <sup>3</sup> Moore, M.D., "Wake Vortex Wingtip-Turbine Powered Circulation Control High-Lift System", NASA CP xxxx, pg x-x, March 2004.
- <sup>4</sup> Wood, N., and J. Nielson, "Circulation Control Airfoils Past, Present, and Future," AIAA Paper 850204, January, 1985.
- <sup>5</sup> Englar, R.J., Circulation control Pneumatic Aerodynamics: blown force and Moment Augmentation and Modifications; Past, Present, & Future", AIAA 2000-2541, June 2000
- <sup>6</sup> Jones, G.S., Bangert, L.S., Garber, D.P., Huebner, L.D., McKinley, R.E., Sutton, K., Swanson, R.C., Weinstein, L., "Research Opportunities in Advanced Aerospace Concepts", NASA TM-2000-210547, December 2000
- <sup>7</sup> Davenport, F. J., "A Further Discussion of the Limiting Circulatory Lift of a Finite-Span Wing," J. of the Aerospace Sciences, Dec. 1960, pp. 959-960.
- <sup>8</sup> Smith, A.M.O., "High-Lift Aerodynamics," J. Aircraft, Vol. 12, No. 6, June 1975
- <sup>9</sup> Wilson, M.B., von Kerczek, C., "An Inventory of Some Force Producers for use in Marine Vehicle Control", DTNSRDC-79/097, November 1979
- <sup>10</sup> Schlichting, H., "Boundary Layer Theory", 6<sup>th</sup> ed. N.Y., McGraw-Hill, 1968
- <sup>11</sup> Rae, W.H., Pope, A., "Low-Speed Wind Tunnel Testing", 2<sup>nd</sup> Edition, John Wiley & Sons, 1984
- <sup>12</sup> Kind, R.J., "A Proposed Method of Circulation Control", University of Cambridge Ph.D. Thesis, June 1967
- <sup>13</sup> Englar, R. J., Williams, R.M., "Test Techniques for High Lift, Two-Dimensional Airfoils with Boundary Layer and Circulation Control for Application to Rotary Wing Aircraft", Canadian Aeronautics and Space Journal, vol. 19, no. 3, March 1973
- <sup>14</sup> Jones, G.S., Viken, S.A., Washburn, A.E., Jenkins, L.N., & Cagle, C.M., "An Active Flow Circulation Controlled Flap Concept for General Aviation Applications", AIAA 2002-3157, June 2002
- <sup>15</sup> Lan, C.E. and Roskam, J., "Airplane Aerodynamics and Performance," Published by Roskam Aviation and Engineering, 1981
- <sup>16</sup> Horner, "Aerodynamic Lift",
- <sup>17</sup> Raymer, D.P., "Aircraft Design: A Conceptual Approach," AIAA Education Series, 3<sup>rd</sup> Edition, 1999
- <sup>18</sup> McGhee, R.H. and Bingham, G.H., "Low-Speed Aerodynamic Characteristics of a 17-Percent Thick Supercritical Airfoil Section, Including a Comparison Between Wind-Tunnel and Flight Data," NASA TM X-2571, July 1972
- <sup>19</sup> Cagle, C.M., Jones, G.S., "A Wind Tunnel Model to Explore Unsteady Circulation Control for General Aviation Applications", AIAA 2002-3240, June 2002
- <sup>20</sup> Englar, R.J., "Low Speed Aerodynamic Characteristics of a Small Fixed Trailing Edge Circulation Control Wing Configuration Fitted to a Supercritical Airfoil", Report number DTNSRDC/ASED-81/08, March 1981
- <sup>21</sup> Englar, R.J., and Williams, R.M., "Design of Circulation Controlled Stern Plane for Submarine Applications," David Taylor Naval Ship R&D Center Report NSRDC/AL-200 (AD901-198), March 1971

- 
- <sup>22</sup> Englar, R.J., et.al., "Design of the Circulation Control Wing STOL Demonstrator Aircraft," AIAA Paper No. 79-1842 presented at the AIAA Aircraft Systems and Technology Meeting, New York (Aug 1979). Republished in AIAA Journal of Aircraft, Vol. 18, No.1, pp. 51-58 (Jan 1981)
- <sup>23</sup> Pugliese, A.J. and Englar, R.J., "Flight Testing the Circulation Control Wing," AIAA Paper No 79-1791 presented at AIAA Aircraft Systems and Technology Meeting, New York (Aug 1979)
- <sup>24</sup> Rae, W.H., Jr., Pope, A. "Low-Speed Wind Tunnel Testing", 2<sup>nd</sup> Edition, John Wiley & Sons, 1984
- <sup>25</sup> Preller, R.F., Rose, O.J., "Langley Wind Tunnel Force Reduction Program," NASA CR-165650, November 1980
- <sup>26</sup> Smith, D.L., "An Efficient Algorithm using Matrix Methods to Solve Wind Tunnel Force-Balance Equations," NASA-TN-D-6860, August 1972
- <sup>27</sup> Ewald, B.F.R. (editor), Wind Tunnel Wall Correction, AGARDograph 336, October 1998
- <sup>28</sup> Iyer, V., Kuhl, D.D., and Walker, E.L., "Improvements to Wall Corrections at the NASA Langley 14X22-FT Subsonic Tunnel", AIAA 2003-3950, June 2003
- <sup>29</sup> Englar, R.J., NSRDC Technical Note AL-211 (1971)
- <sup>30</sup> Lawford, J.A. and Foster, D.N., "Low-Speed Wind-Tunnel Tests on a Wing Section with Plain Leading and Trailing-Edge Flaps Having Boundary-Layer Control by Blowing", British aeronautical Research Council R&M 3639 (1970)
- <sup>31</sup> Alvarez-Calderon, A., and Arnold, F.R., "A study of the Aerodynamic Characteristics of a High-Lift Device Based on a Rotating Cylinder and Flap," Stanford-University, Department of Mechanical engineering Technical Report RCF-1 (1961)
- 
- <sup>32</sup> Rose, R.E., Hammer, J.M., & Kizilos, A.P., "Feasibility Study of a Bi-directional Jet Flap Device for Application to Helicopter Rotor Blades," Honeywell Document No. 12081-FR1, July 1971
- <sup>33</sup> Rogers, E.O., Donnelly, M.J., "Characteristics of a Dual-Slotted Circulation Control Wing of Low Aspect Ratio Intended for Naval Hydrodynamic Applications," AIAA 42nd Aerospace Sciences Meeting, Reno, NV, 5-8 Jan 2004 AIAA 2004-1244
- <sup>34</sup> Oyler, T.E., Palmer, W.E., "Exploratory Investigation of Pulse Blowing for Boundary Layer Control", North American Rockwell Report NR72H-12, January 15, 1972
- <sup>35</sup> Walters, R.E., Myer, D.P., & Holt, D.J., "Circulation Control by Steady and Pulsed Blowing for a Cambered Elliptical Airfoil", West Virginia University, Aerospace Engineering TR-32, July 1972
- <sup>36</sup> Lawford, J.A., and Foster, D.N., "Low-Speed Wind Tunnel Tests on a Wing Section with Plain Leading- and Trailing-Edge Flaps Having Boundary-Layer Control by blowing," British Aeronautical Research Council R&M 3639 (1970)
- <sup>37</sup> Englar, R.J., Huson, G.G., "Development of Advanced Circulation Control Using High-Lift Airfoils," AIAA Paper No. 83-1847, July 13-15, 1983
- <sup>38</sup> Williams, J. and Alexander, "Some Exploratory Three-Dimensional Jet-Flap Experiments," Aeronautical Quarterly, Vol. 8, pp 21-30 (1957)
- <sup>39</sup> Krynytzky, A., & Hackett, J.E., "Choice of Correction Method", Section 1.4, AGARDograph 336, October 1998
- <sup>40</sup> Allan, H.J., and Vincenti, W.G., "Wall Interference in a Two-Dimensional-Flow Wind Tunnel with Consideration of the Effect of Compressibility, NACA Report 782, 1944



## Pneumatic Flap Performance for a 2D Circulation Control Airfoil

*Greg Jones, Ph.D.*

*Flow Physics and Control Branch*

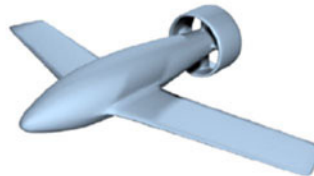
*NASA Langley Research Center*

2004 NASA & ONR FLOW CONTROL WORKSHOP



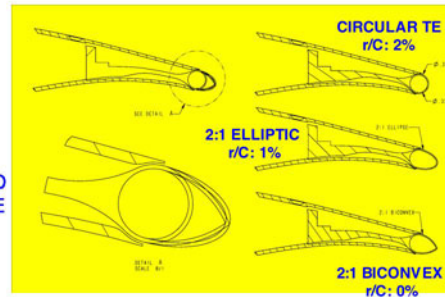
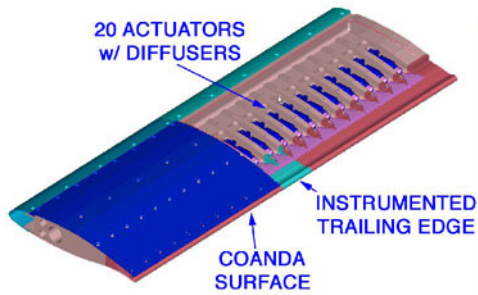
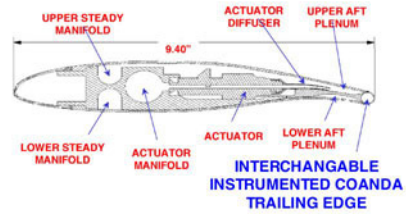
## OBJECTIVES

- Establish Baseline Performance of GACC (Steady blowing)
  - HIGH LIFT (upper Coanda blowing - TARGET  $C_{LIFT} = 3$ )
  - CRUISE (pneumatic flap - dual blowing to Reduce Cruise Drag associated with blunt trailing edge)
- Determine the Performance benefits of Pulsed CC
  - Actuator Performance
  - Model Performance
- Evaluate Trailing Edge Shape
  - Circular
  - 2:1 Elliptic
  - 2:1 Biconvex



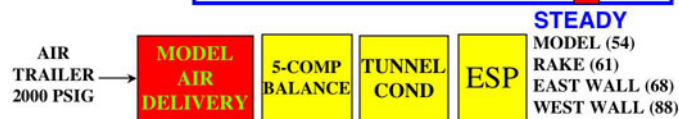
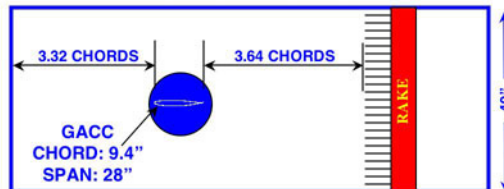
2004 NASA & ONR FLOW CONTROL WORKSHOP

**Multi-Functional Configurations**  
 Upper Blowing : High Lift  
 Lower Blowing : Flight Control  
 Dual Blowing : Cruise  
 Pulsed Blowing : Economic Control  
 Distributed Blowing: Load Control

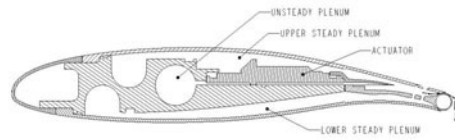


2004 NASA & ONR FLOW CONTROL WORKSHOP

**BART TEST SECTION 28"X40"**



2004 NASA & ONR FLOW CONTROL WORKSHOP

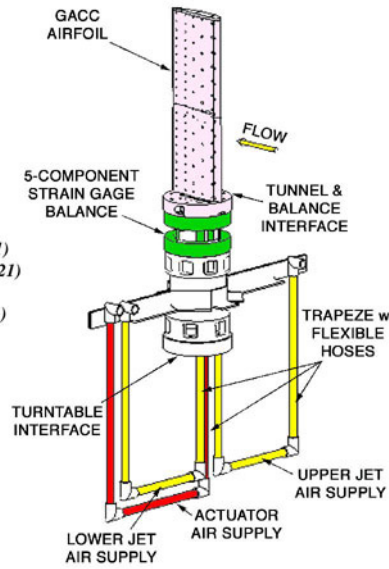
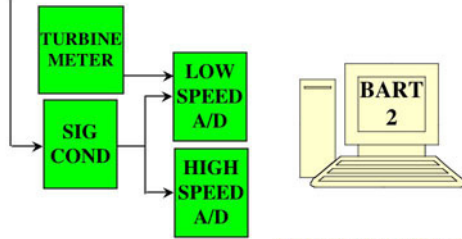


**UNSTEADY**  
**P+p'**

- LEADING EDGE MEMS (21)
- TE MEMS INBOARD (15)
- TE MEMS OUTBOARD (15)
- TE REF (ENDEVCO) (4)
- INTERNAL MODEL MEMS (1)

**UNSTEADY**  
**E+e'**

- TE HOT FILMS INBOARD (21)
- TE HOT FILMS OUTBOARD (21)
- TE REF (ENDEVCO) (4)
- INTERNAL MODEL MEMS (1)



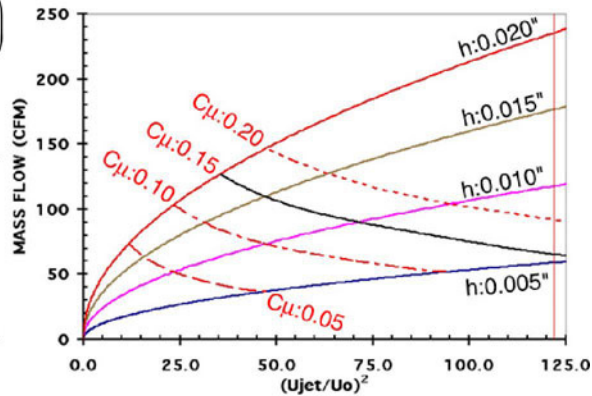
2004 NASA & ONR FLOW CONTROL WORKSHOP

$$C_{\mu} = \frac{\text{Thrust}}{qS} = \frac{\dot{m}(U_J)}{q(C)(b)} \quad U_J = \sqrt{\frac{2\gamma R (T_{\text{DUCT}})}{\gamma - 1} \left( 1 - \left( \frac{P_{\infty}}{P_{\text{DUCT}}} \right)^{\frac{\gamma-1}{\gamma}} \right)}$$

$$C_{\mu} = 2 \left[ \frac{(h)(w)}{(C)(b)} \right] \left( \frac{\rho_J}{\rho_{\infty}} \right) \left( \frac{U_J}{U_{\infty}} \right)^2$$

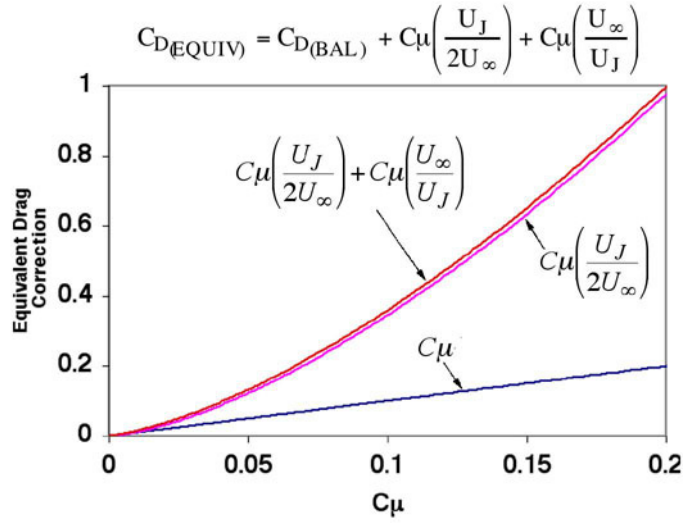
$$c_d = c_{d_{\text{rake}}} - \frac{\dot{m}}{q S_b}$$

$$= c_{d_{\text{rake}}} - c_{\mu} \frac{V_{\infty}}{V_J}$$



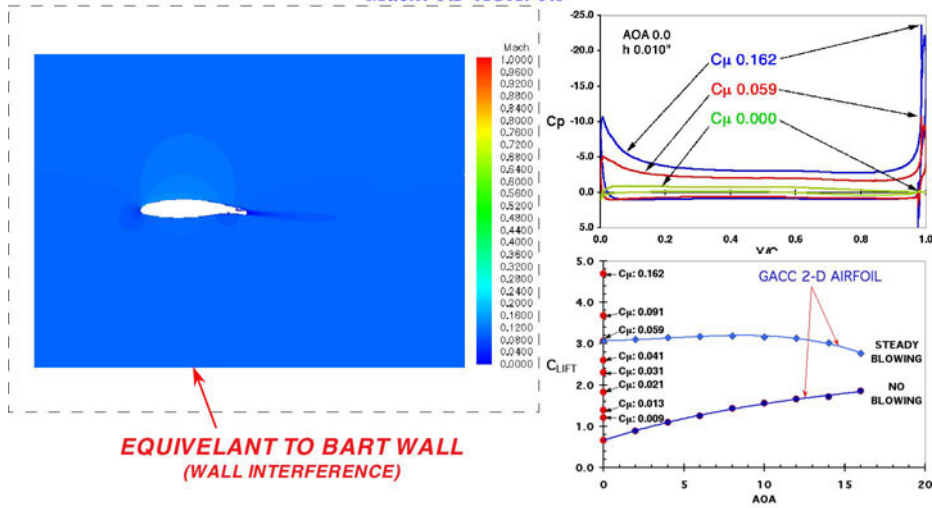
2004 NASA & ONR FLOW CONTROL WORKSHOP

### MOMENTUM INFLUENCE ON DRAG



2004 NASA & ONR FLOW CONTROL WORKSHOP

### CFD - FUN(2D) Mach: 0.1 AOA: 0.0°

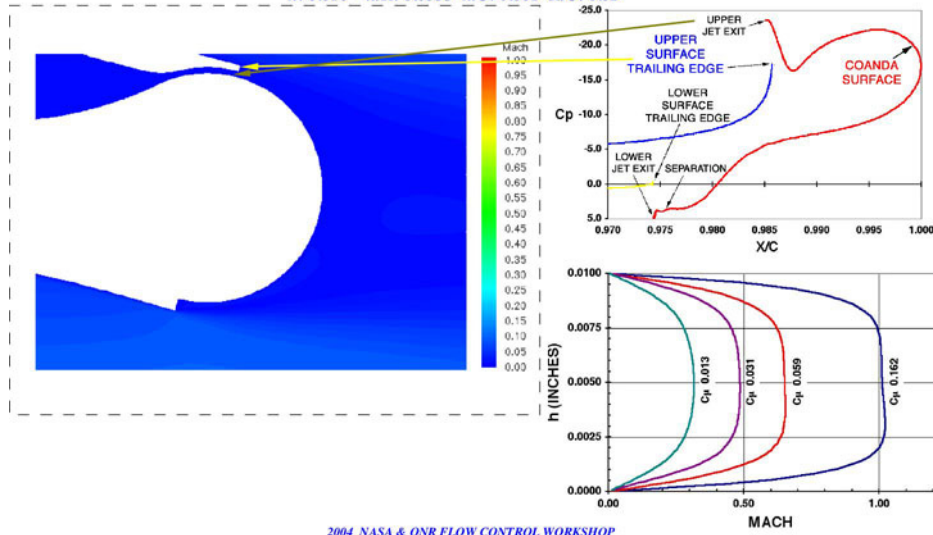


2004 NASA & ONR FLOW CONTROL WORKSHOP



*Trailing Edge & Slot Data*

$h: 0.010''$   $h/R: 0.0533$   $h/C: 0.001$   $R/C: 0.02$

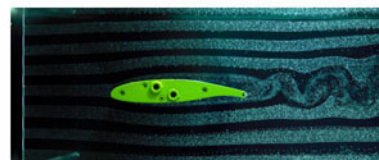
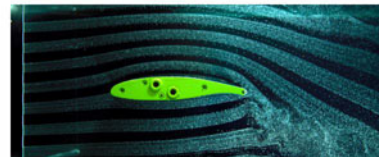
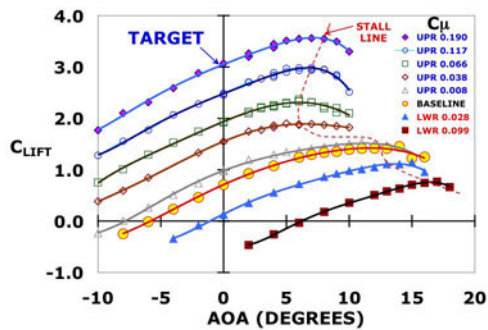


2004 NASA & ONR FLOW CONTROL WORKSHOP

**LIFT PERFORMANCE**

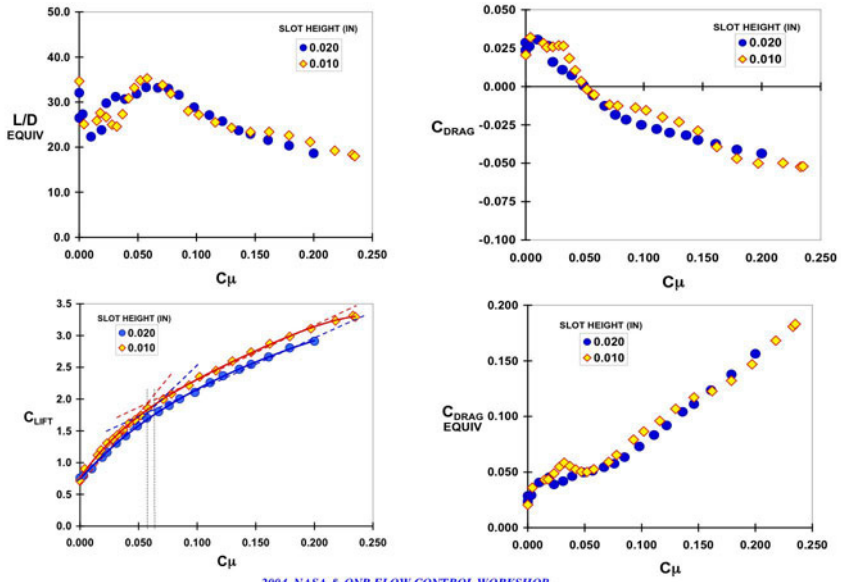
**GACC**  
**W/ CIRCULAR TE**

$h/C=0.00106$   $h/r=0.0533$

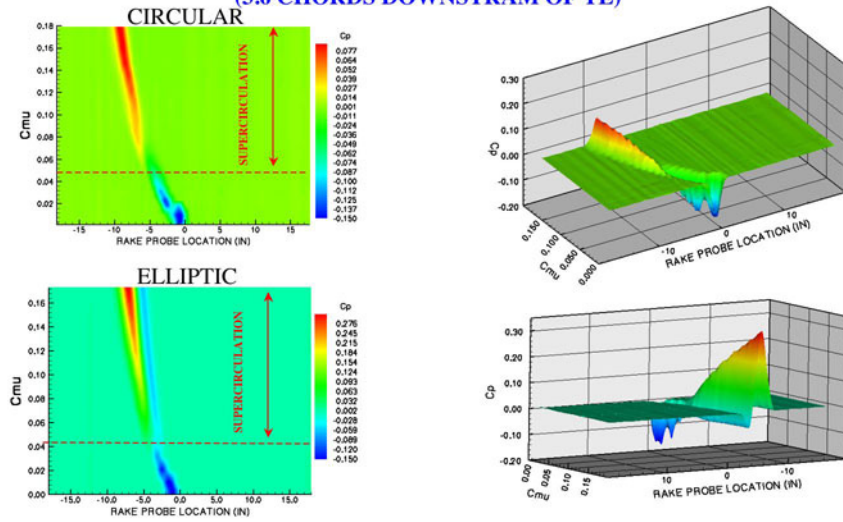


2004 NASA & ONR FLOW CONTROL WORKSHOP

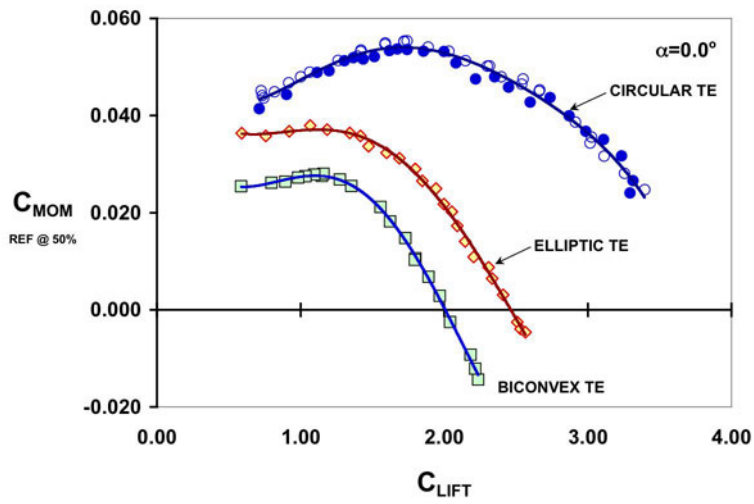




PRESSURE PROFILES  
(3.6 CHORDS DOWNSTREAM OF TE)



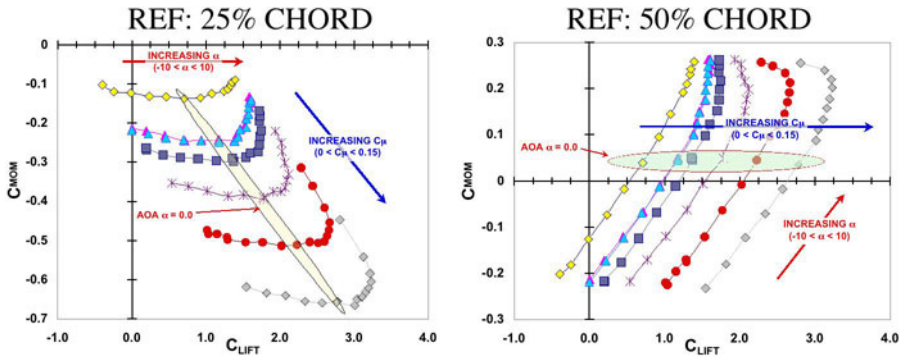
### NOSE UP PITCHING MOMENT



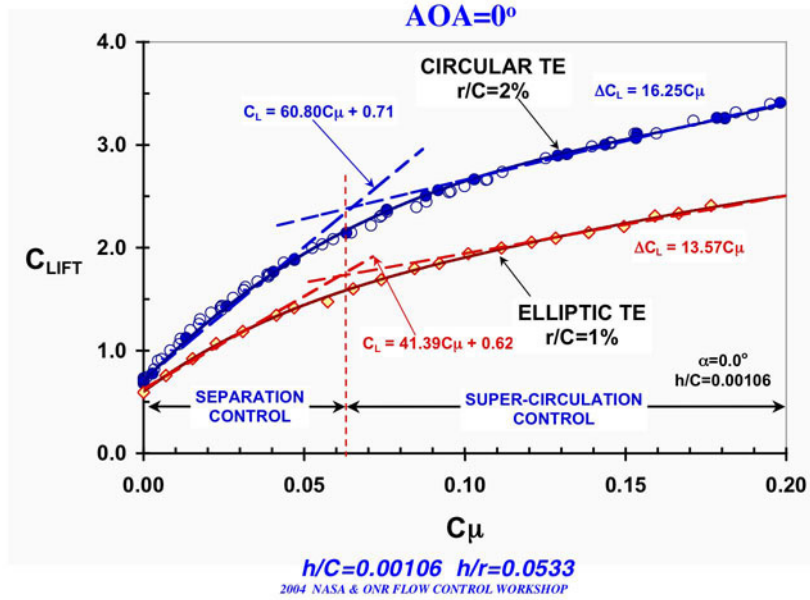
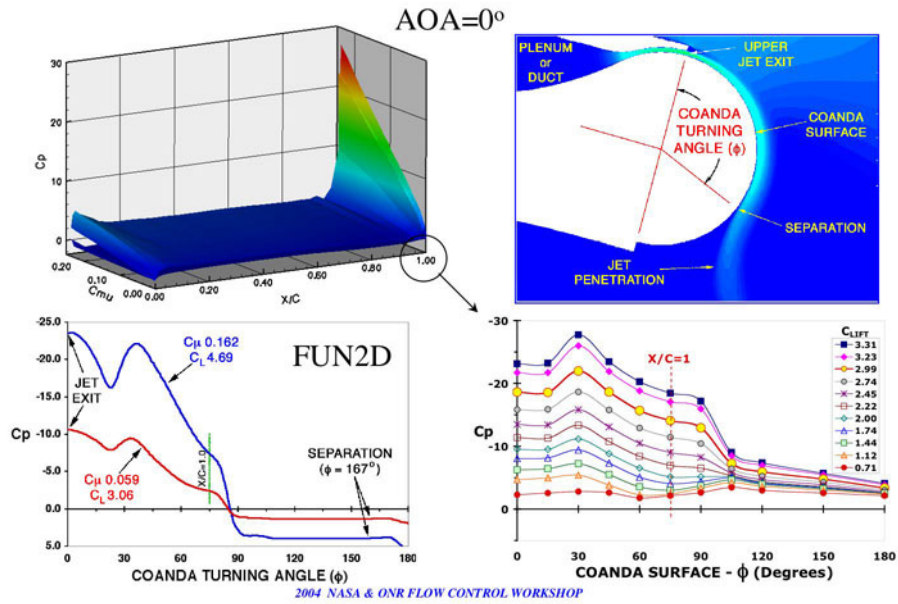
2004 NASA & ONR FLOW CONTROL WORKSHOP

### Pitching Moment

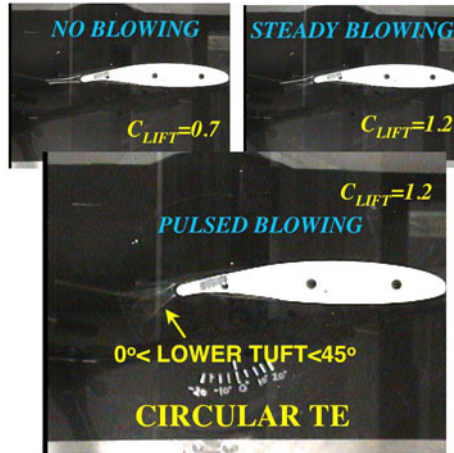
#### BALANCE DATA for CIRCULAR COANDA TE



2004 NASA & ONR FLOW CONTROL WORKSHOP



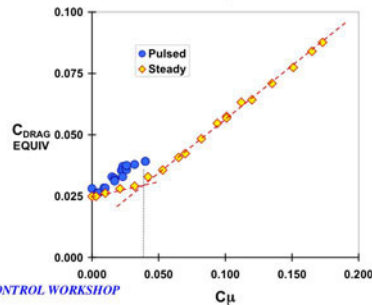
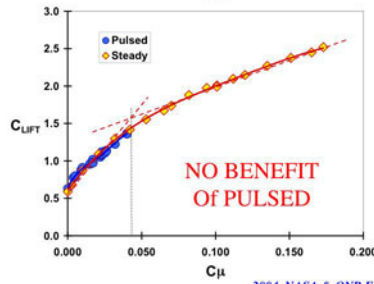
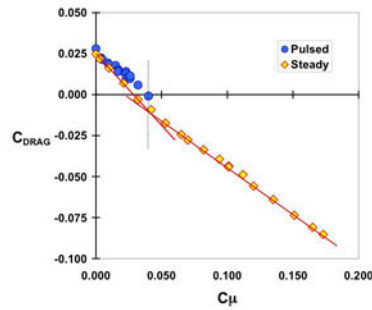
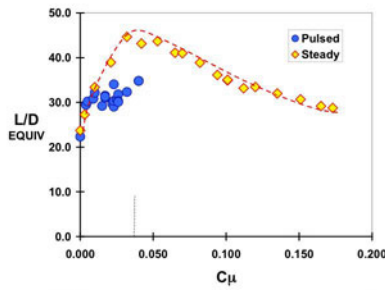
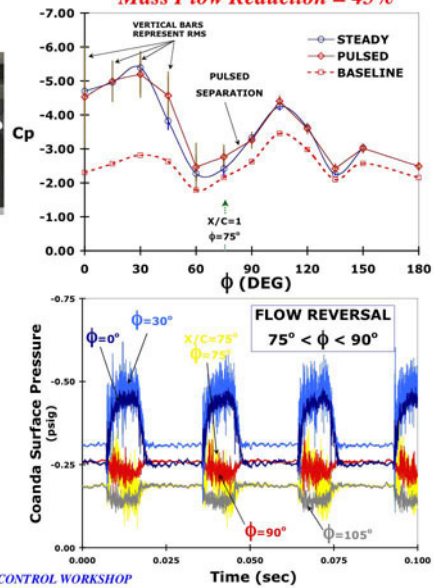
GACC w/ Tufts



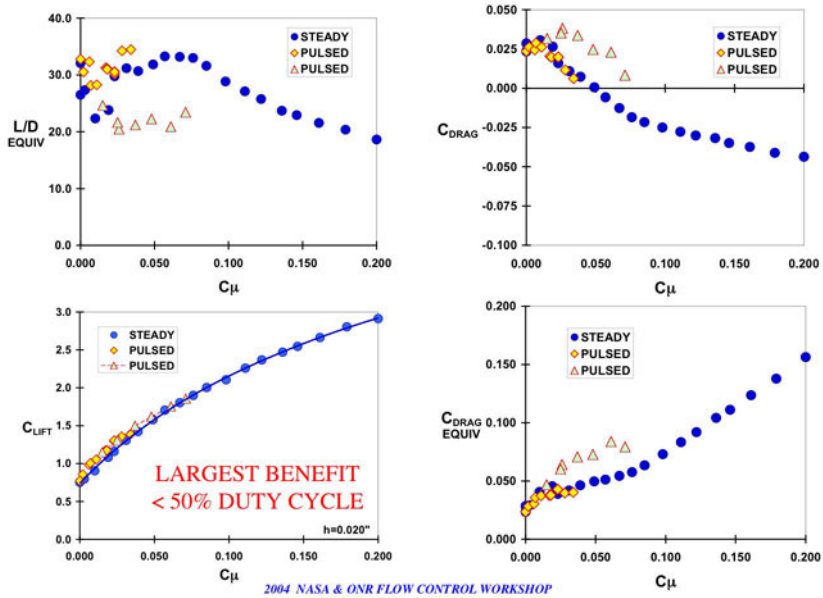
35 Hz & 40% DUTY CYCLE

2004 NASA & ONR FLOW CONTROL WORKSHOP

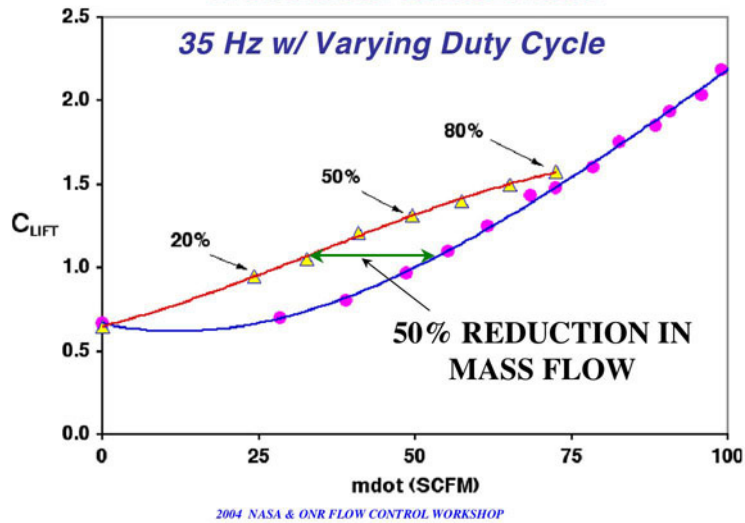
Mass Flow Reduction = 45%



2004 NASA & ONR FLOW CONTROL WORKSHOP



**CIRCULAR TE PERFORMANCE BENEFIT**  
*IN SEPARATION CONTROL REGION*

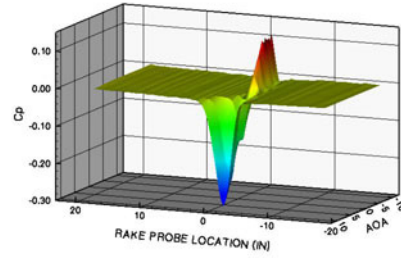
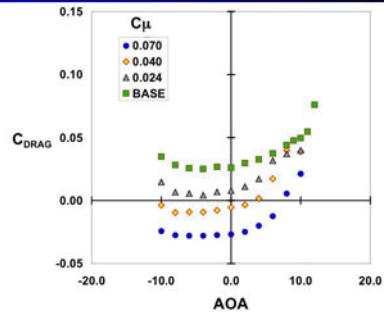
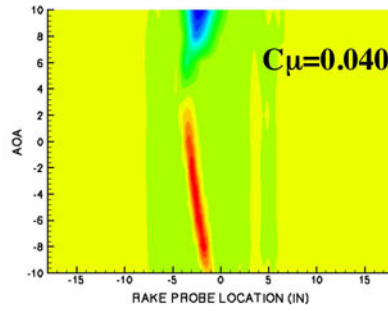




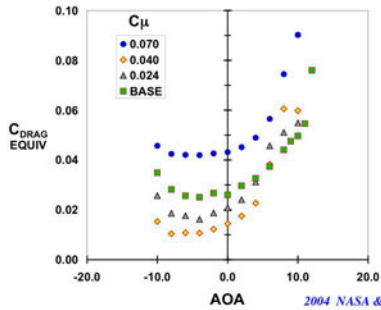
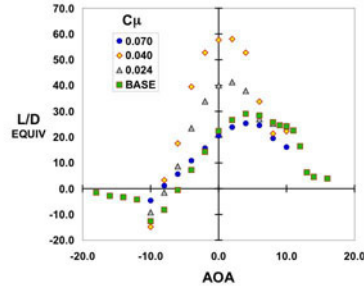
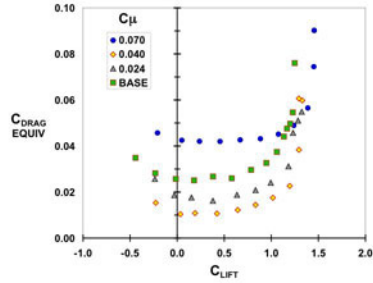


$$C_{\mu} = C_{\mu_{UPPER}} + C_{\mu_{LOWER}}$$

$$C_{\mu_{UPPER}} = C_{\mu_{LOWER}}$$



2004 NASA & ONR FLOW CONTROL WORKSHOP



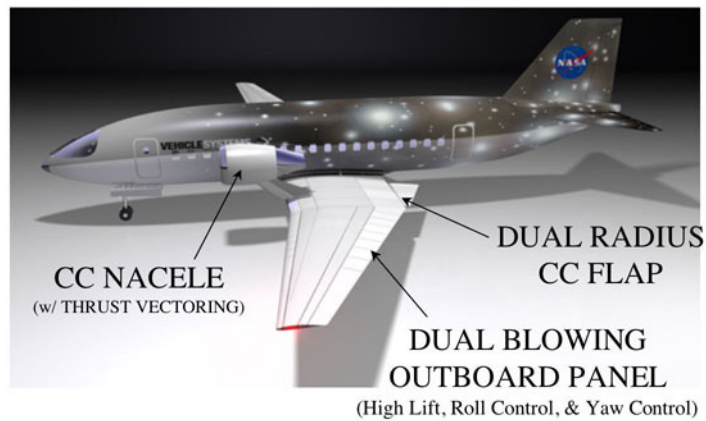
Over Blowing Results  
In Increased Equivalent  
Drag but Increased Thrust

2004 NASA & ONR FLOW CONTROL WORKSHOP



- CIRCULAR TE PRODUCED MORE LIFT THAN ELLIPTIC OR BICONVEX TE
  - r/C EFFECT
- ELLIPTIC TE PRODUCED LESS DRAG THAN CIRCULAR TE
- WAKE RAKE WAS MORE RELIABLE THAN FORCE BALANCE IN DETERMINING DRAG
  - JUNCTURE FLOW INFLUENCE (NO SIDEWALL BLOWING)
- PULSED BLOWING WAS EFFECTIVE ON CIRCULAR TE BUT NOT ELLIPTIC OR BICONVEX TE
  - ACTUATOR AUTHORITY NOT ENOUGH TO ACHIEVE SUPERCIRCULATION
- ERRORS IN SETTING SLOT HEIGHT PROPOGATE THRU  $C_{\mu}$  THEN  $C_{\text{DRAG(EQUIV)}}$

2004 NASA & ONR FLOW CONTROL WORKSHOP



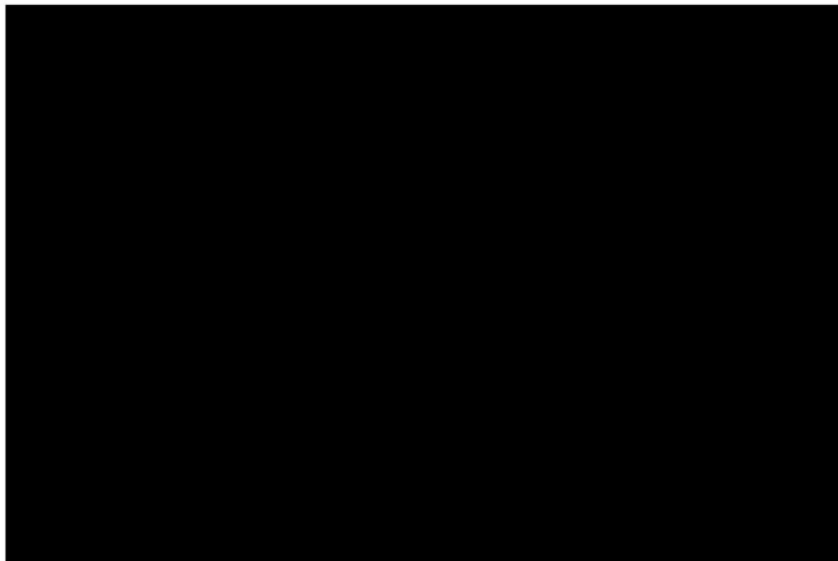
2004 NASA & ONR FLOW CONTROL WORKSHOP



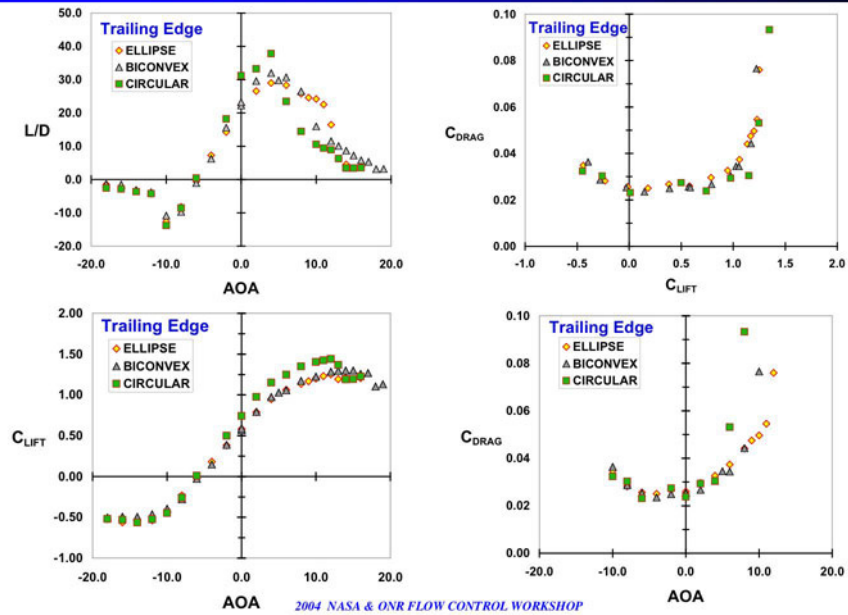


## BACKUP SLIDES

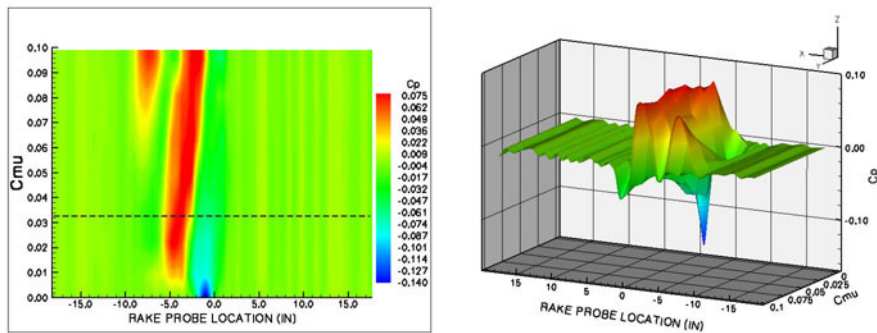
2004 NASA & ONR FLOW CONTROL WORKSHOP



2004 NASA & ONR FLOW CONTROL WORKSHOP



2004 NASA & ONR FLOW CONTROL WORKSHOP



2004 NASA & ONR FLOW CONTROL WORKSHOP

# **Experimental and Computational Investigation into the use of the Coanda Effect on the Bell A821201 Airfoil.**

Gerald M. Angle II  
Wade W. Huebsch  
James E. Smith  
West Virginia University

## **Abstract**

Tilt-rotor aircraft, e.g. the V-22 “Osprey”, experience a unique flow scenario in the vertical flight / hover mode. While hovering, this aircraft impinges its rotor wash upon the main wing, limiting the available lift performance. Circulation control (CC) techniques, such as blowing slots using the Coanda effect, can reduce the downforce felt on the main wing, thus recovering part of the lost lift. Leading and trailing edge blowing slots have been added to experimental and computational models of the V-22 main wing to induce the Coanda effect over the curved leading edge and to align the flow with the trailing-edge flap, in the operationally deployed position of 67 degrees. The overall goal is to reduce the size of the wake region below the main wing and thus reduce the downwash force. Initial experimental results show approximately a 10% reduction in download, while the computational fluid dynamics (CFD) analysis indicates a potential 35% reduction could be achieved. Optimal conditions are currently under investigation.

## **Introduction**

The Coanda effect can be described as the balance between the normal and pressure gradient forces in a near-surface jet of a fluid. The simple case to describe this phenomenon is a two dimensional wall jet, which entrains the surrounding fluid. As the boundary layer is entrained the local pressure in the boundary layer is reduced creating a pressure gradient which pushes the jet towards the surface.

From the conservation of momentum, as fluid is entrained, the jet velocity is reduced. Eventually the jet velocity is low enough that the fluid viscosity creates an adverse pressure gradient, again separating the flow. Expanding this concept to a

convexly-curved surface, a pressure gradient is created forcing the jet to bend around the surface, until the adverse pressure gradient is reached.

Newman (1961) determined that the flow in a curved wall jet is relatively insensitive to Reynolds number,  $Re$ , as defined below, provided it is in excess of a threshold value of 9000. Thus

$$Re = \left[ \frac{(P - p_{\infty})ba}{\rho v^2} \right]^{1/2} \quad (1)$$

where  $P$  is the local pressure,  $P_{\infty}$  is atmospheric pressure,  $a$  and  $b$  are the jet and freestream velocities, and  $\rho$  and  $\nu$  are the density and viscosity of air.

An approximation of a Coanda jet is a constrained jet, where the streamlines of the free stream act as a restricting surface. Early experimentation into constrained jets determined that the inflow velocities of the jet flow do not differ from the constrained and unconstrained cases, provided that the momentum of the jet is sufficiently higher than that of the free stream.

Looking in more detail at the boundary layer of the confined jet as the Reynolds number increases, the flow tends to compress slightly which inhibits its boundary layer development. This delay in boundary layer growth hinders the entrainment of the flow, maintaining the composition of the jet and increasing the bulk jet velocity. The goal of this work is to use blowing slots to induce the Coanda effect in the leading and trailing edges of the airfoil.

Parameters other than the free stream velocity that affect the ability for flow to remain attached to a curved surface include the four primary variables, radius of curvature, slot location, slot size (height and span), and blowing pressure, which is characterized by the coefficient  $C_{\mu}$  as defined in Equation 2;

$$C_{\mu} = \frac{\rho_j V_j^2 h b}{\frac{1}{2} \rho_{\infty} V_{\infty}^2 c b} \quad (2)$$

where  $\rho$  is the density,  $V$  is velocity,  $h$  is the slot height,  $b$  is the span,  $c$  is the airfoil chord and the subscripts  $j$  and  $\infty$  represent the jet and freestream values respectively. General trends exist for these parameters. For instance, as the slot size is reduced, the separation of the flow is delayed because less mass flow can be added to the boundary layer. For a given slot location, an increase in the radius of curvature, or the blown pressure, results in a delay of the onset of flow separation. This delay in separation, controlled by the interaction of all three of the variables experiences an upper limit at approximately 240 degrees, measured from the slot opening

These Coanda jets, placed on the leading and trailing edge of the main wing of the V-22 “Osprey”, can be used to reduce the downforce caused by the rotorwash. Experimental tests conducted by Angle et al (2003), and expanded upon in this paper have shown reductions in the downforce. Computational methods have also been developed and results are compared to the experimental results. These methods can eventually be used to reduce the number of test cases needed to determine the optimal placement and jet blowing coefficient for this circulation control application.

### **Experimental Apparatus and Procedure**

A model of the Bell A821201 airfoil with a 19 inch chord length and an 18 inch span (see Figure 1) was constructed and tested at the West Virginia University Aerodynamic Wind Tunnel Facility. The reader is referred to Angle, et al (2003) for additional information on the model geometry and wind tunnel facility. This model produced a test section blockage of 15 percent, which is relatively high for wind tunnel testing. However, this size was needed for the desired instrumentation for the two dimensional preliminary testing of this concept.

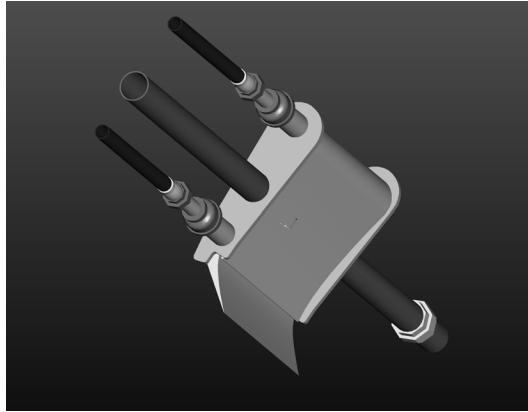


**Figure 1: CAD Drawing of the Experimental Model.**

Surface pressure readings were taken on this model using multiple static pressure ports, as discussed in Angle<sup>1</sup>. The aerodynamic forces were measured using a three load cell (0-25 pounds each) system, two in the download direction to provide force and moment and the third in the normal direction to measure force as shown in Figure 2. The structure supporting the model in the test section produced a measurable drag that had to be accounted for when calculating the drag on the wing.

The drag on the support apparatus was determined from the standard drag coefficient for a cylinder, from Young, Munson and Okiishi (1997). The resulting moments about the pivot point, above the test section, were removed from the recorded moments resulting in Equation 3 for the determination of download force on the model:

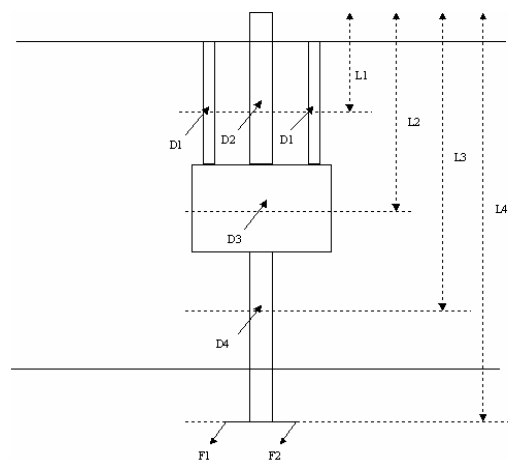


**Figure 2: Force Measuring Configuration for the Experimental Testing.**

$$D_3 = \frac{L_4(F_1 + F_2) - L_1D_1 - L_3D_2}{L_2}, \quad (3)$$

where D represents the resulting forces, L denotes the corresponding moment arms and the subscripts are as shown in Figure 2. This figure shows the attachment points for the two load cells used to determine the drag on the system, as in Angle<sup>1</sup>, and a third load cell was added to measure the force normal to the drag. Surface pressure taps were also provided on the model but not repeated for the tests associated with this phase of the project.

The large test section, 4ft x 6ft, of the Closed Loop Wind Tunnel at West Virginia University was used for this testing. The maximum airspeed of this test section is just above 60 ft/s, however due to blockage effects only 59 ft/s could be achieved during testing. The resulting Reynolds Number was  $6 \times 10^5$ , based on airfoil chord length.

Once the model was installed in the test section and the load cells calibrated, testing was conducted with the results shown in Figure 3. To perform a test the wind tunnel was brought to the desired airspeed and data was collected from the load cells. Data was collected for each test point for a four minute test sample, with repeats of the baseline after every five tests. Use of the term baseline refers to testing with zero pressure on both the leading and trailing edge blowing slots. After collection of the data the following procedure was used to reduce the raw voltage data from the load cells.



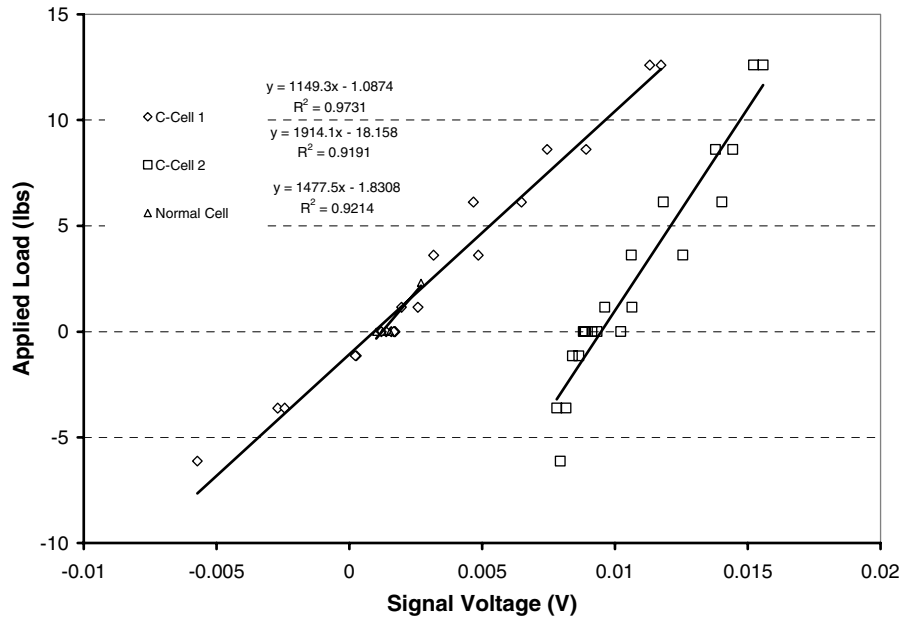


**Figure 3: Calibration Curves for the Three Load Cells.**

The voltage values were taken through the calibration curves shown in Figure 3. A baseline average was computed from the three baseline runs to be used as the reference force as well as the zero pressure force value. A simple percent reduction was calculated between the time average data for each run and the baseline average.

### **Computational Model and Procedure**

A digital replica of the wind tunnel model was created in GAMBIT (the preprocessor for the CFD code Fluent) using the geometrical data from the experimental model construction for slot locations. This computational model was then placed in two scenarios: one to simulate the wind tunnel test section walls and one with a large computational domain an “open-air” test. For the open-air case, the boundaries of the domain were placed at a large distance from the model to minimize boundary effects.

Several meshed grid configurations were modeled to find an appropriate representation of the experimental results. A triangular paved mesh was attempted though it was determined that this mesh was not adequate. Therefore a series of

segmented grids was developed, of which an 11 region grid, shown in Figure 4 was selected.

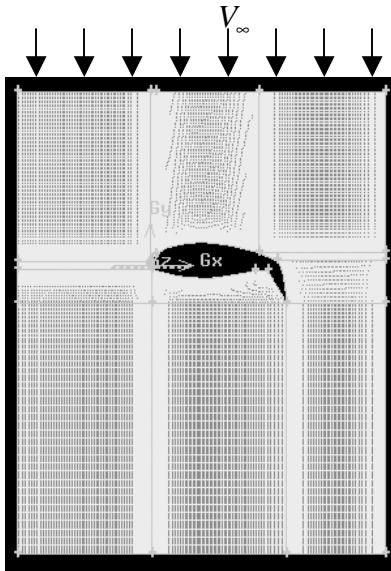
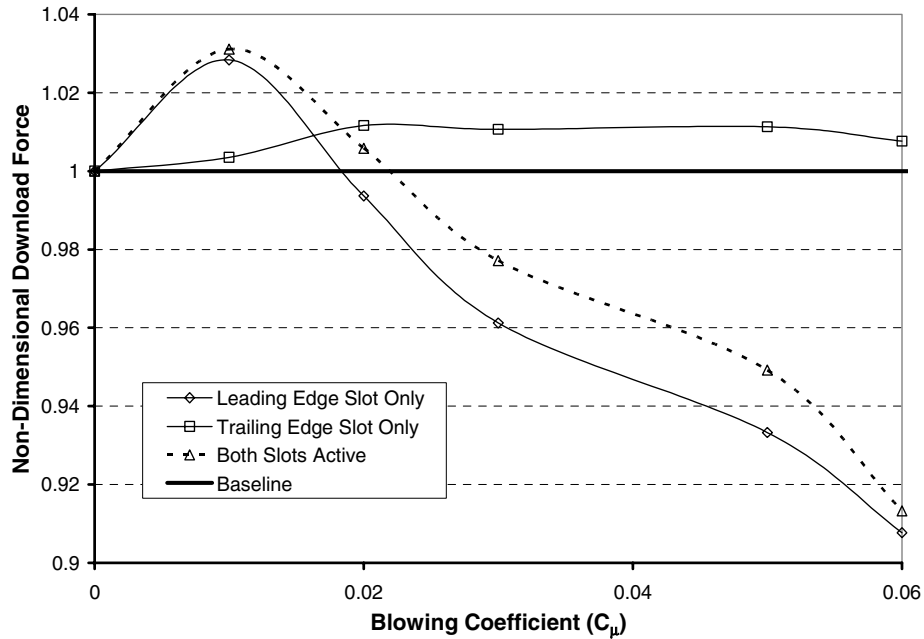


Figure 4: Segmented Mesh of Wind Tunnel Scenario.

### **Results: Experimental**

Data from the normal load cell was found to be negligible since it was on the order of less than 1 pound. This corresponds to a deflection of less than five thousandths of an inch, indicating an error on the order of the resolution of the load cells in the download direction. The baseline test case (non-active blowing) experienced a total download force of 18.75 lbs, measured from the two load cells, at the test Reynolds number of  $5.94 \times 10^5$ . As seen in Figure 5, which is non-dimensionalized by dividing out the no blowing download force, for lower blowing coefficients there is an increase in the download force with the leading edge slot active and smaller increase when the trailing edge is activated. As the blowing coefficient is increased, the leading edge slot decreases the non-dimensional download force, while the trailing edge slot produces a fairly constant increase in download above the baseline value as the blowing coefficient is increased. The curve showing data for both slots active demonstrates the combined effects of the individual blowing slots.



**Figure 5: Download Force Variation with Blowing Coefficient.**

This data is summarized in Table 1, where a positive value indicates a reduction in the download on the A821201 airfoil model. These results show that with the current configuration the leading edge is more effective at reducing the download force. However, when using both slots there is still an 8 percent reduction in the force. It should be noted that no effort has yet been made to optimize slot placement and that the trailing edge flap is deflected according to current V-22 operating practices. These results do show the overall viability of the blowing slot mechanism as a means of reducing the downwash force.

There is also the potential to use a variant of the technique discussed in this paper to assist in the control of the pitching moment of the airfoil. By adjusting the blowing pressures separately, the pitching moment can be altered. With further testing this potential benefit can be better defined. Additional experimental data can be found in Angle, et al<sup>1</sup>.

**Table 1: Experimental Reductions in Download Force**

Internal Pressure (psig)	$C_{\mu}$	Percent Reduction		
		L.E. Only	T.E. Only	Both
0	0	0	0	0
5	0.01	-2.84	-0.35	-3.12
10	0.02	0.63	-1.16	-0.59
15	0.03	3.88	-1.07	2.29
20	0.05	6.67	-1.13	5.08
25	0.06	9.23	-0.77	8.68

**Results: Computational**

The CFD simulations of the Bell A821201 wind tunnel model produced a slightly increased baseline download force, approximately 25 lbs, compared to the experimental result of 18.75 lbs. However, a similar trend with respect to the blowing coefficient was present between the experimental and computational models. As seen in Figure 6, there is little change in download force using the trailing edge blowing slot and approximately a 20 percent reduction with the use of the leading edge slot. The combined effect of both slots active produced almost a 40 % reduction.

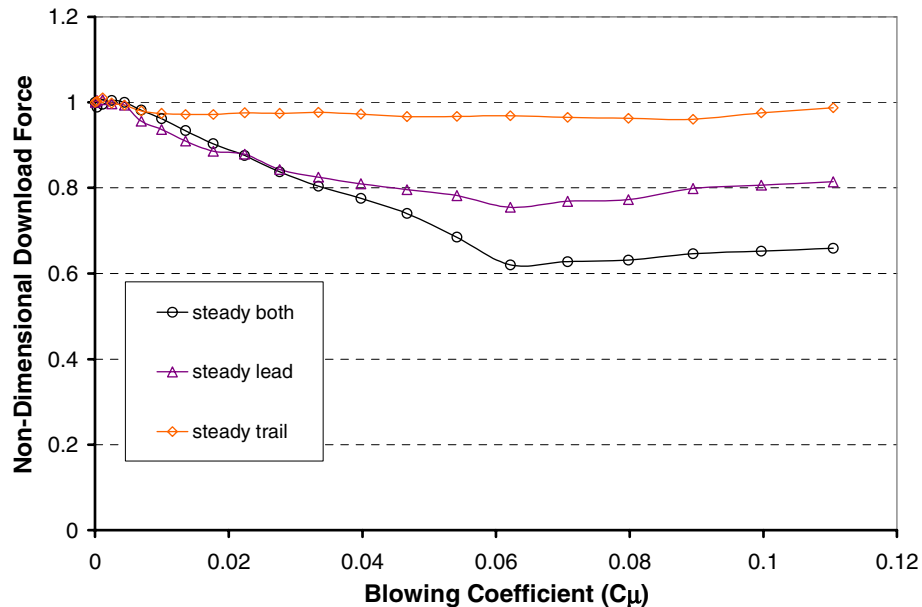


**Figure 6: Computational results of non-dimensional download as dependent upon blowing coefficient.**

A computational model of the airfoil was also tested with the walls of the wind tunnel moved away from the model to investigate the influence of the walls on the aerodynamics of the results. As seen in Figure 7 there are minor influences on the non-dimensional download profile with respect to blowing coefficient. The tunnel computational model resulted in a slightly higher peak reduction but the open-air scenario required less blowing coefficient to produce a 30 percent reduction in download. In addition, the open-air case had a greatly reduced baseline download force of approximately 8 lbs.

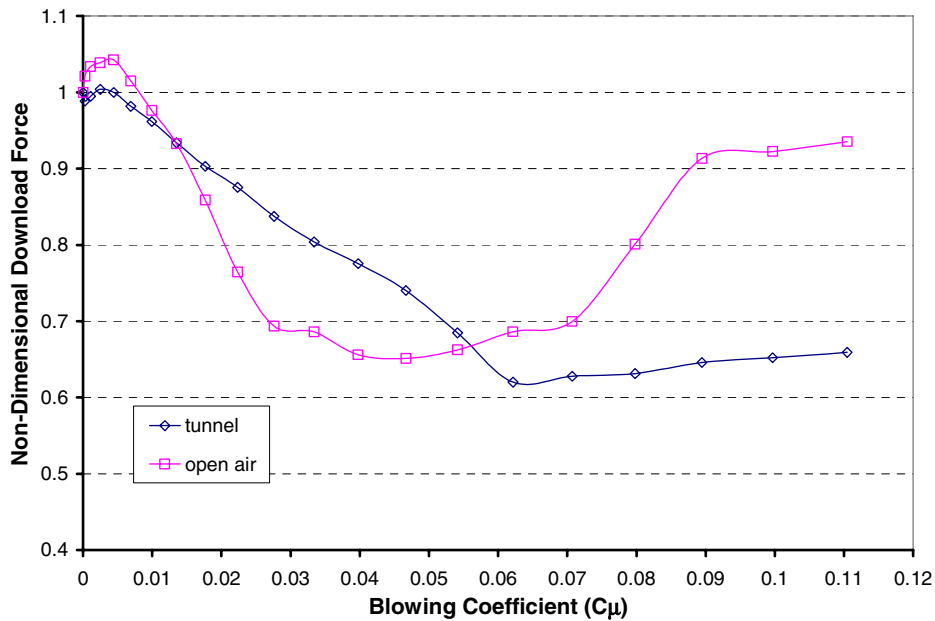


**Figure 7: Comparison of Tunnel and Open-Air Computational Results**

Figure 8 shows a comparison of the experimental and computational results for the download. Ease of adjusting the computational boundary conditions for the blowing coefficient allowed for a greater number of data points to be collected. The associated reduction in download, relative to the baseline value, is shown in Figure 9. The experimental result is a lower reduction in download for the blowing coefficients tested.

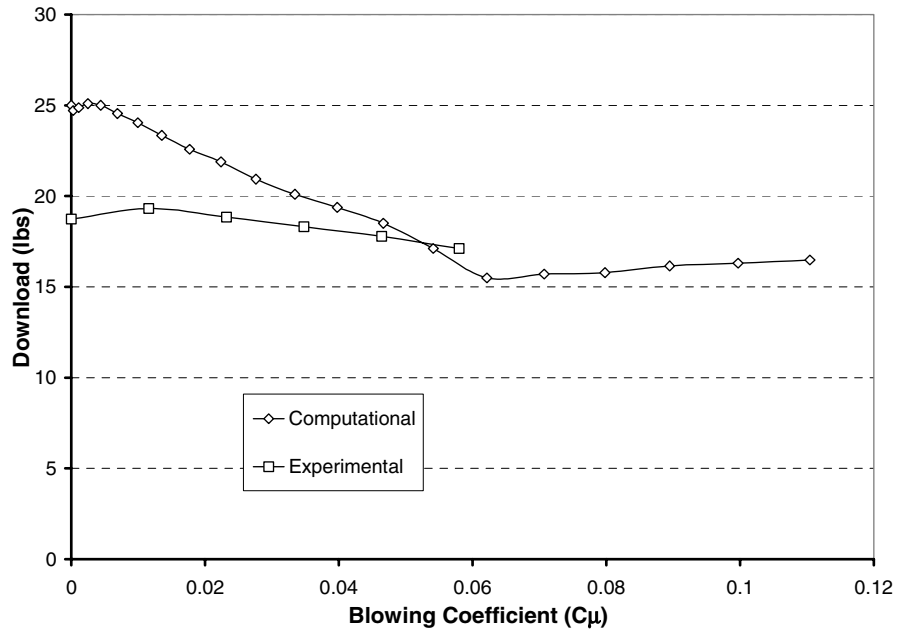


Figure 8: Download force comparison of experimental and computational results.

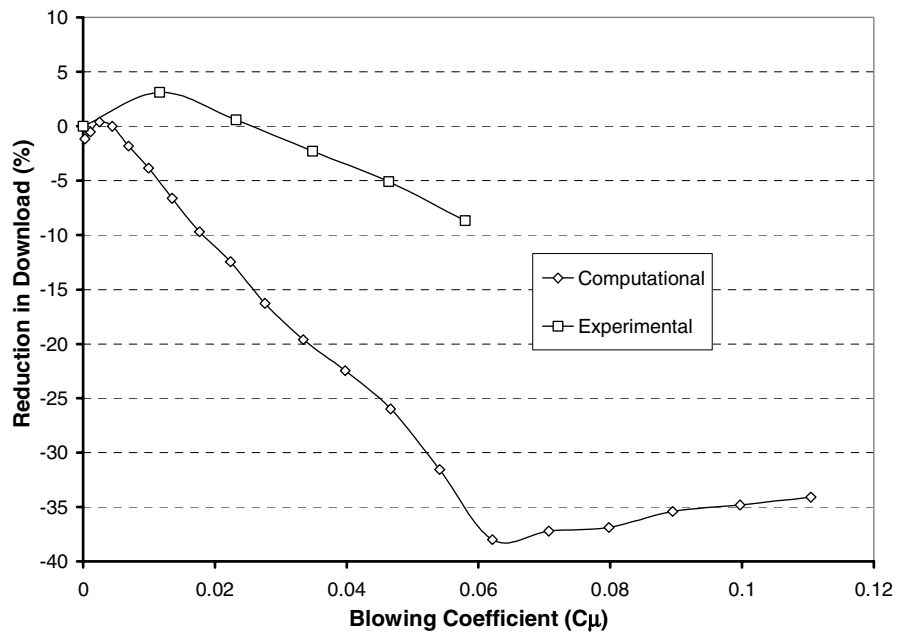


Figure 9: Download reduction comparison of experimental and computational results.

## **Conclusions**

Despite the differences between the experimental and computational tests, the trends show that circulation control, through the use of blowing slots on the leading and trailing edge of the Bell A821201 airfoil, can reduce the download force felt from the rotor wash of a tilt rotor aircraft. Experimental testing had a reduction of approximately 10 % from the baseline 18.7 lbs download. The baseline download of the computational tunnel simulation was found to be 25 lbs and had a maximum reduction of around 37 %. Computational runs with the tunnels walls moved away from the model resulted in a 35 % reduction from the baseline download of 8 lbs. The discrepancies in the different test scenarios require further refinement of the computational model. Investigation into blockage effects of the experimental testing is also being considered.

## **Recommendations**

Many aspects of using circulation control need to be investigated further. Some of these include looking into optimizing the placement of the leading and trailing edge slots, current testing has only studied one location for each of the slots. This could be simplified if better agreement could be made between the computational model and the experimental results. An improved CFD analysis could then be used to test various slot locations to narrow the range of required experimental testing.

Currently new experimental and computational models are under development to address aspects of the current data. The new experimental model will be sized to fit into the small test section of the WVU Closed Loop Wind Tunnel to allow for testing at different Reynolds Numbers and take test section blockage into account.



## References

1. Angle, G., Riba, C., Huebsch, W., Thompson, G., Smith, J., “Download Wake Reduction Investigation for Application on the V-22 ‘Osprey’,” SAE Technical Paper 2003-01-3020, September 2003.
2. Englar, R.J. “Experimental Investigation of the High Velocity Coanda Wall Jet Applied to Bluff Trailing Edge Circulation Control Airfoils,” Masters Thesis, University of Maryland, College Park, MD, 1973.
3. Felker, F. F., “Wing Download Results from a Test of a 0.658-Scale V-22 Rotor and Wing,” *Journal of the American Helicopter Society*, 1992. pp 58-63.
4. Felker, F. F., Shinoda, P. R., Heffernam, R. M., Sheehy, H. F., “Wing Force and surface Pressure Data from a Hover Test of a 0.658-Scale V-22 Rotor and Wing,” NASA, 1990.
5. Felker, F. F., and Light, J. S., “Reduction of Tilt Rotor Download Using Circulation Control,” *Proceedings of the Circulation-Control Workshop*, 1986, pp 429-447.
6. Newman, B.G., *The Deflexion of Plane Jets By Adjacent Boundaries – Coanda Effect*; contained in Boundary Layer and Flow Control, Pergamon Press vol. I, 1961; p. 232.
7. Riba, C. A., “Circulation Control for Download Wake Reduction in the V-22 Aircraft,” Master’s Thesis, West Virginia University, Morgantown, WV, 2003.
8. Young, D.F., Munson, B. R., Okiishi, T. H., *A Brief Introduction to Fluid Mechanics*, John Wiley & Sons, Inc., New York, ny, 1997.



---

## Experimental and Computational Investigation into the use of the Coanda Effect on the Bell A821201 Airfoil.

---



**Gerald M. Angle II, MSAE**  
**Wade W. Huebsch, PhD**  
**James E. Smith, PhD**  
West Virginia University



---

## Outline

---

- Problem statement
- Purpose
- Experimental testing
- Computational testing
- Comparison
- Future work



## Problem Statement

---

Use blowing jets to induce coanda effect on surface normal to the rotor wash of a tilt-rotor aircraft (i.e. V-22 Osprey).

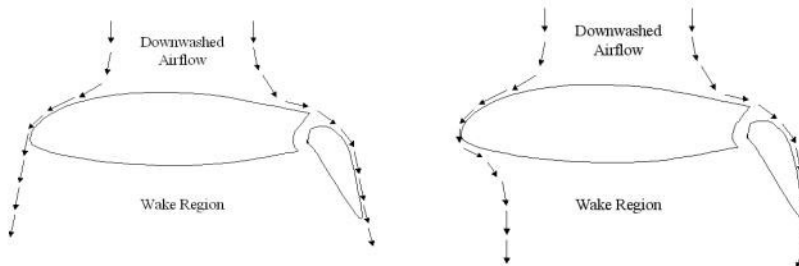
- Decrease rotor downwash effects on wing
- Resulting in increased performance of aircraft



## Purpose

---

- Proof of concept
- Minimize download force by:
  - Wake reduction
  - Induction of coanda effect





## Experimental Investigation

- Model description
- Testing facility
- Results
- Conclusions



## Experimental Model Description



- 24 Surface pressure taps
- Leading and trailing edge blowing slots

Bell A821202 Airfoil

- 19 inch Chord
- 18 inch Span





# Experimental Testing Facility

## WVU's Closed Loop Wind Tunnel

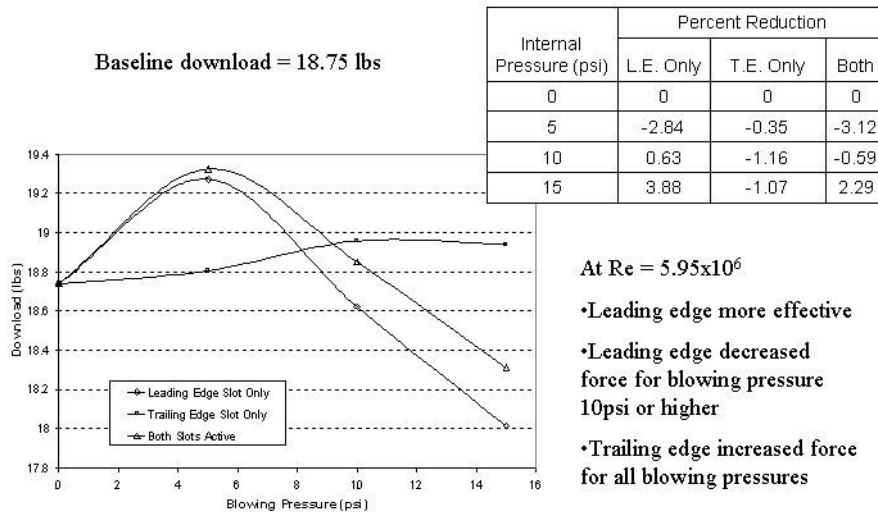
6 ft by 4 ft Test Section

60 ft/s Airspeed

Reynolds Number:  $5.95 \times 10^6$



## Experimental Results:





## Experimental Conclusions

---

- Force reduction
  - Maximum 8%
  - Strategically located blowing slots can reduce download force on the Bell A821202 Airfoil.
- Optimal location under investigation.



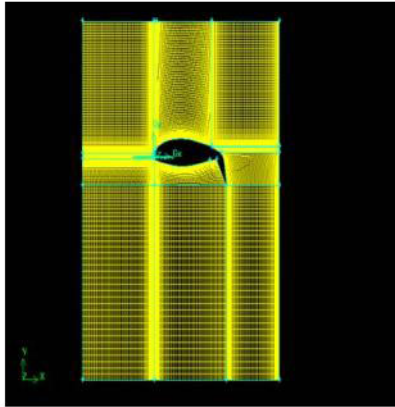
## Computational Investigation

---

- Model description
- Testing parameters
- Results
- Conclusions



## Computational Model Description



### Grid evolution

- Triangular paved mesh
- 8 Region segmented grid
- 11 Region segmented grid



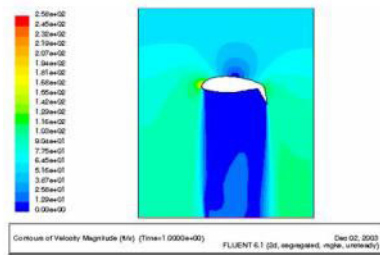
## Computational Testing Parameters

- Steady flow / unsteady flow
- Compressible / incompressible
- Wind tunnel conditions / real world conditions
- K-Epsilon turbulence model

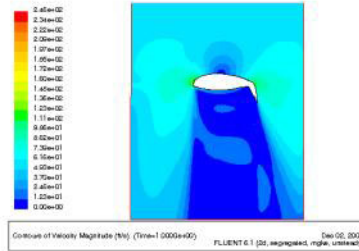




# Computational Results



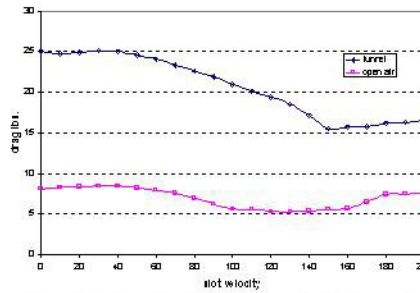
Computed velocity contour for wind tunnel conditions ( $Re=1.8 \times 10^6$ )



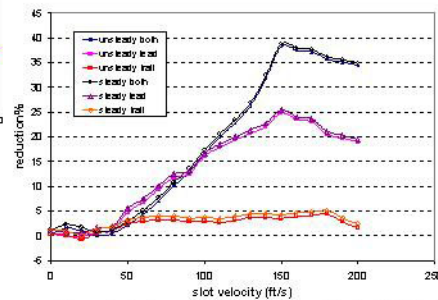
Computed velocity contour for real world conditions ( $Re=1.8 \times 10^6$ )



# Computational Results (cont.)



Computed download force for steady, tunnel conditions  $U_{inf} = 59$  ft/s and a slot velocity of 140 ft/s and both slots active.



Computed download reductions for individual and combined blowing slots



## Computational Conclusions

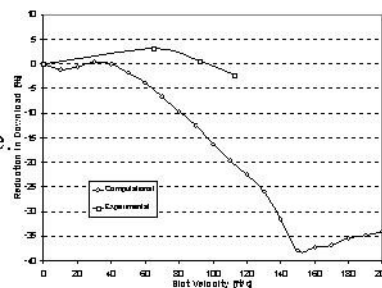
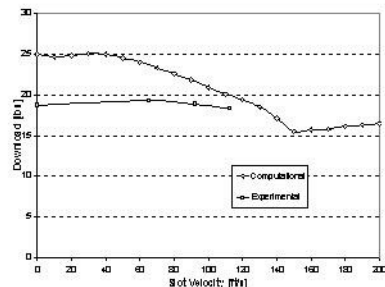
Issues that need resolved in future work:

- Large difference between wind tunnel and real world scenario
  - Larger test volume to minimize wall effects
  - Further look into unsteady effects
  - Investigate different turbulence models



## Experimental & Computational Comparisons

Experimental and computational methods both show that blowing slots can reduce the download force.



Currently developing:

- New experimental models with smaller blockage ratio
- More refined computational models



## Future Work

---

- Reynolds number matched testing
  - $Re_{EXP} = 5.95 \times 10^6$
  - $Re_{CFD} = 1.80 \times 10^6$
  - $Re_{ACTUAL} = 2.30 \times 10^6$
- Use of lower blockage ratio in experimental testing
- Use computational methods to predict possible optimal slot locations
- Investigate power requirements
- Investigate effect of rotational velocity
- Investigate use of coanda effect during transition of tilt rotor

**Low-Cost, High-Quality Wind Tunnel Testing of a  
30% Elliptical Circulation Control Airfoil at Low Blowing  
Levels for Application to Wind Turbines**

Frederick J. Kelso, Kenneth L. Laubsch, Rikard K. Haraldsson  
AdvanTek International, LLC  
7 Creek Parkway, Suite 770  
Boothwyn, PA 19061-3148

March 17, 2004  
NASA/ONR 2004 Circulation Control Workshop

- Motivation for Wind Tunnel Testing
- Expert Team
- Test Matrix
- Design, Fabrication & Instrumentation
- Test Results
- Conclusions
- Path Forward

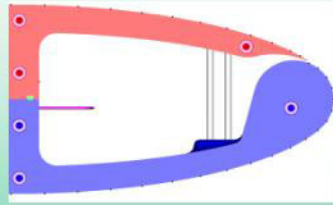
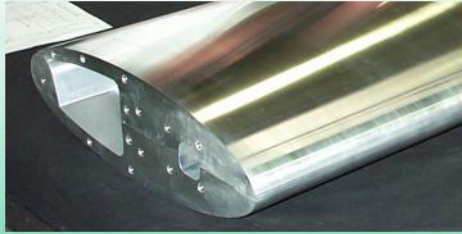
- When we began our project, we needed to determine if CC was economically viable for power production from the wind. We explored the concept using existing NSWC wind tunnel data for a 30% elliptical helicopter blade. The data set was modified to fit our application. This early analysis convinced us we were on the right track
- However, the data set was not complete enough for our final design and analysis efforts:
  - Data was limited to single slot height, other slot heights extrapolated
  - Not enough resolution at low blowing levels
  - It had been conservatively constructed from the available data
- This was also a good opportunity for us to fabricate a working circulation control airfoil using the Coanda surface geometrical constraints which had been given to us, together with an appropriate pressurization system

- Risky to proceed solely with data from helicopter rotor regime
  - Helicopter rotors use a brute-force approach with low concern for blowing power cost
  - A wind turbine rotor requires a finessed approach with minimal blowing power cost
- Needed to understand true effects of slot height and  $C_{\mu}$  variation on lift (with better resolution at lower blowing levels)

<p><b>Wind Turbine Consultant</b> P. Jamieson Garrad Hassan Scotland</p>	<p><b>CC Consultants</b> E. Rogers, J. Abramson NSWC VA</p>	<p><b>Wind Tunnel Consultant</b> D. Somers Airfoils, Inc. PA</p>
<p><b>Test Facility</b> Low Turbulence Wind Tunnel Dr. Mark Maughmer Penn State University</p>	<p><b>Model Fabricator</b> Advanced Technologies, Inc. VA</p>	<p><b>Sys. Designer/Fabricator</b> Accudyne Systems, Inc. DE</p>

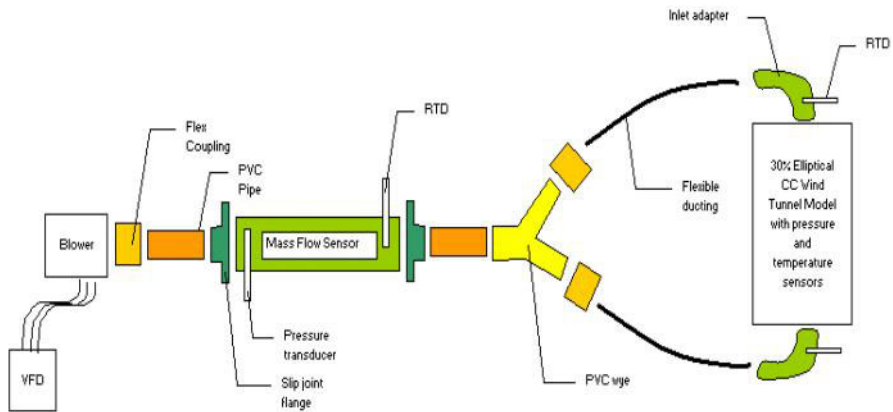
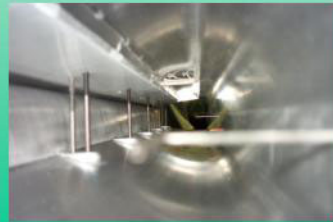
- Defined the operating envelope with regard to Reynolds Number, Slot Height,  $C_{\mu}$  and Angle of Attack for our application
- Constructed a test matrix with prioritized combinations of the above parameters based on cost and schedule (budgeted \$200,000 and 6 months)
  - Most data taken at Reynolds Number of 1 million, with excursions to 0.75 million and 1.25 million for optimum slot height and  $C_{\mu}$
  - Slot height-to-chord ratios of 0.0015 to 0.004
  - Blowing Coefficients of 0.02 to 0.04
  - Blown Angles-of-Attack of  $-10^{\circ}$  to  $+10^{\circ}$
  - Unblown Angles-of-Attack of  $-15^{\circ}$  to  $+20^{\circ}$

Final Assembled Model, Slot Adjusters



Model Span – 40"  
Model Chord – 18"

Slot Adjuster was capable of providing slot height of 0.2 – 2.0 mm in increments of 0.05 mm



Schematic of Pressurization System



Blower and Mass Flow Sensor In-Situ Underneath Wind Tunnel; Bifurcation of Air Supply



Routing of Blower Air Supply to Model Plenum



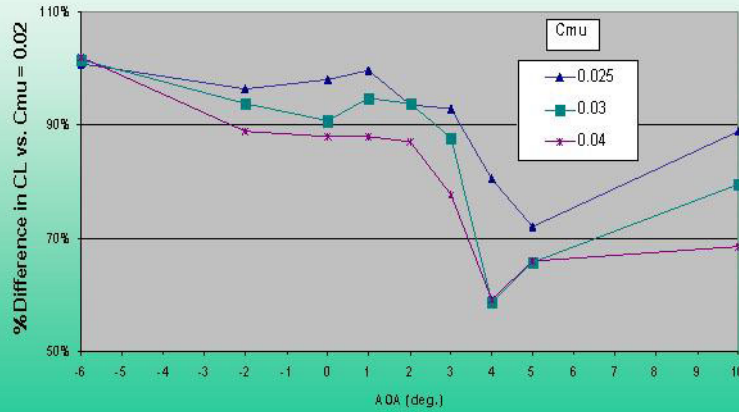
Variable Frequency Drive; Dual Data Acquisition Systems



- Non-Dimensional Comparative Test Results (Absolute data proprietary)
  - Effect of  $C_{\mu}$  on Lift-to-Blower Demand Ratio, with Lowest Practical  $C_{\mu}$  Value Set as Baseline – Determination of Ideal  $C_{\mu}$
  - Effect of Slot Height on Lift, with Lowest  $h/c$  Value Set as Baseline – Determination of Ideal  $h/c$
  - Comparative Lift - PSU vs. NSWCC Data Set, with NSWCC Data as Baseline Data Set
  - Comparative Corrected Drag - PSU vs. NSWCC Data Set, with NSWCC Data as Baseline Data Set

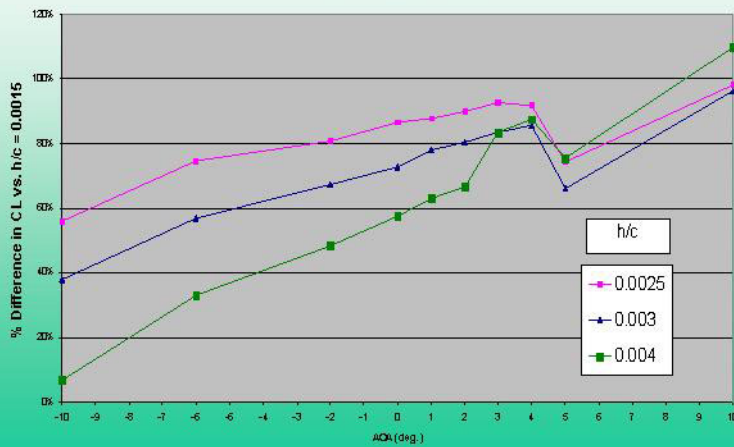
**Effect of  $C_{\mu}$  Variation on  $C_l/C_{\mu}$**

Re = 1 million, h/c = 0.0015, Smooth LE

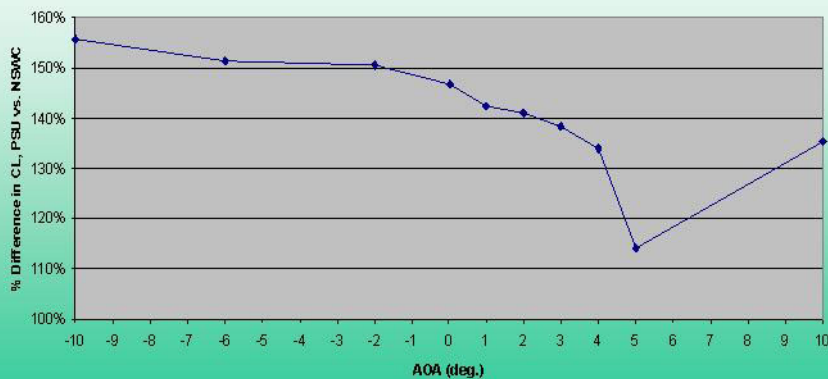


**Effect of Slot Height Variation on Lift**

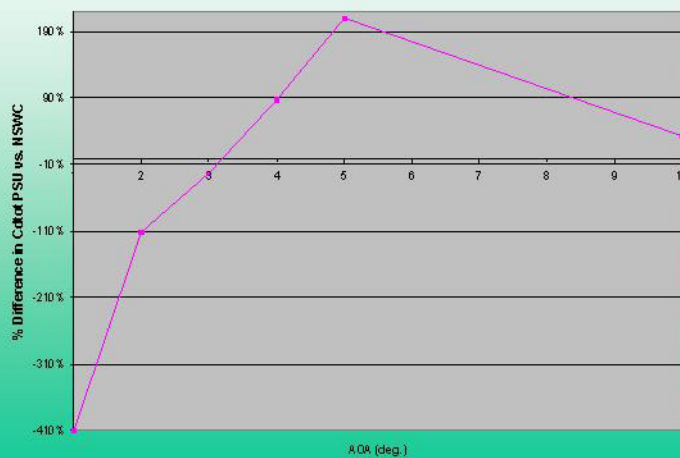
Re = 1 million,  $C_{\mu} = 0.02$



**Comparison of PSU Lift Data To NSWC Data**  
( $Re \sim 1$  million,  $h/c \sim 0.0015$ ,  $Cmu = 0.02$ )



**Comparison of PSU Corrected Drag Data To NSWC Data**  
( $Re \sim 1$  million,  $h/c \sim 0.0015$ ,  $Cmu = 0.02$ )



- It is possible to build a circulation control model and get useful wind tunnel test results from it within 6 months and for under \$250,000
- The Coanda surface geometry which we had been given produced the Coanda effect perfectly
- The pressurization system that we designed and built from scratch also performed its tasks without a hitch
- Our new data set confirmed the NSWCC assumption that the original modified data set we had used was conservative
- This new data set was well-populated and sufficient to plug into our design and analysis tools
- We gained the confidence to proceed with our pursuit of CC technology for our wind turbine application

- Advantek intends to pursue field testing of a circulation control wind turbine to validate the cost-effectiveness of our technology
- We would be interested in discussing any input the CC research community may have with regard to
  - Dynamic stall
  - Alternate CC airfoils for the low blowing regime
  - Resolution of the issue of wake drag corrections



# VORTEX DYNAMICS PTY LTD

ACN 062 634 306

Unit 1/ 1 Distribution Ave  
Molendinar QLD 4214  
Tel: 61 + 7 + 5597 4388  
Web: [www.vortex-dynamics.com.au](http://www.vortex-dynamics.com.au)  
Mobile: 0402-377-254

P.O. Box 312  
Ashmore City Qld 4214  
Fax: 61 + 7 + 5597 3811  
Email: [terry@vortex-dynamics.com.au](mailto:terry@vortex-dynamics.com.au)  
[terryday1@hotmail.com](mailto:terryday1@hotmail.com)

Paper presented at the NASA/ONR 2004 circulation control workshop in Hampton, VA, March 16-17,2004.

## COANDA EFFECT AND CIRCULATION CONTROL FOR NON AERONAUTICAL APPLICATIONS.

By **TERENCE R DAY**  
March 16-17 2004

### A SPECIAL NOTE ABOUT THIS PAPER

The author is a consultant to industry and is in private enterprise himself, therefore because of confidentiality issues, client company names cannot be mentioned nor can certain proprietary information be fully revealed whether of the authors clients or of his own projects.

### ABSTRACT

The author contends that the roadblocks to the further development and success of CC may be due to either past failures to address certain deficiencies or an inability to find solutions even though sought. An example of an operational deficiency is insufficient quantity of CC air, heavy and complicated air pumps including energy wasting plumbing etc. Partly to address some of these issues the author has built and describes here a number of practical non-aeronautical devices employing either the Coanda Effect or Coanda/CC and a High Volume Pump to supply CC air.

### About the Author:

*The author is a member of the International Society of Automotive Engineers and consultant to:  
(1) The entertainment industry producing special effects including on stage tornados (twenty two feet high) and tornados for movies.*



(Click on Photo to enlarge)



(Click photo for Tornado video)



*(2) Also a consultant to industry in fluid movement; Completely re-designing an electric automotive centrifugal water pump and volute with 30% efficiency increase over the clients existing production pump with a more plateau like efficiency curve and now in production; the design of a swimming pool and spa pump with increased mechanical efficiency while reducing noise 9 dba; a consultant to a major US company to develop the Coanda Effect and Ring Vortex technology for air-care, insect control and odour elimination etc.*

## **PURPOSE OF THIS PAPER**

First purpose is to describe a number of examples of the Coanda Effect, including **“Circulation Control,”** often abbreviated to **“CC”**. These examples are very different to each other and are proposed as commercial outcomes for Coanda Effect and CC, and are or have been actual projects. That purpose then is to show that there exist a number of novel applications recently conceived and that some creativity may be beneficial in furthering the cause of the Coanda Effect and CC to gain credibility in a wider arena than only the Coanda Effect/CC scientific community.

The second purpose for this paper is that as the question was posed before and during the two day Coanda Effect/CC workshop (March 16-17, 2004) namely **“What are the roadblocks to further development”?**, the author contends that identifying those roadblocks is necessary to find solutions and so a number of the examples presented in this paper may contribute something positive to solving the problematic issues examined during the workshop.

The available literature ([see Bibliography # 2, 10 and 11](#)) contains adequate history and applications of the Coanda Effect as it relates to CC up to the present and therefore there is no need here to repeat that material given the target audience of this paper. The author will start from this established platform of Coanda Effect and CC knowledge and add to it by applying it to novel non aeronautical situations.

## **PRESENT COANDA PROJECTS**

### **FIRST EXAMPLE**

#### **Oscillating Channel Flow including self oscillating channel flow (Coanda Effect)**

[\(Click for video\)](#)

While this phenomenon has been understood for quite some time (*see bibliography # 12*), it apparently has been little more than a curiosity with little vision for many useful applications. The geometry of a rectangular channel that can allow for self oscillating flow must be relatively precise especially to achieve best efficiency. Gas jets in a channel can be made to oscillate by imposition of a pressure change alternating either side perpendicular to the jet. With precise geometry a round jet will self oscillate. Once the idea is understood it is not difficult to produce either type of oscillating flow if the air supply is conveniently from the lab compressor.

The significant breakthrough here is being able to convert the highly turbulent discharge from a fan into a flow structure that can oscillate in a channel. The author is not aware of any previous work describing this. The aim is to achieve a practical device employing the Coanda Effect (oscillating or self oscillating jet flow), that is efficient and easy to manufacture and has higher efficiency distribution of air throughout a room.

For certain applications including odour elimination, certain chemicals are coated onto surfaces that an airflow must inter-act with. The air flow must be highly turbulent.

If the airflow is laminar, the odour molecules contained in the airflow cannot contact the chemical coated surfaces. Oscillating or self-oscillating channel flow gives the desired turbulence. A second reason for employing oscillating channel flow is because as the jet skips from wall to wall, a particularly formed passageway is able to accept each branch of the flow.

## **SECOND EXAMPLE**

### **RING VORTEX PROJECTION**

[\(Click Video\)](#)

The fan flow of example “1” above is able to be re-formed and to arrive at a particular area as an air slug as would be produced by a piston stroke or the stroke of an acoustic driver. This fan produced flow is far less complex and expensive than a piston or acoustic driver technique. While the particular geometry needed to do this is proprietary it can be said that after formation that slug of air can be tripped over an orifice plate and turned into a ring vortex.

The ring vortex is able to travel ten to twenty times the distance of a normal discharge from a nozzle as the ring stores kinetic energy like a flywheel for a short time. [\(Click for Video 2\)](#) The ambient fluid is entrained from in front of the ring and transported to the rear and so the result is (almost) propulsion by negative drag. The strength of the ring vortex is purpose tuned and the active chemical of the correct density can then be transported over a large distance bound within the vortex.

Another reason that this technique is useful is because as the jet oscillates, one side may be re-routed through labyrinthine pathways which may be treated with suitable surface chemistry and have increased surface area for longer inter-action time and may be then returned to the inflow to the fan. Makeup air is venturied into the main flow and in this way it is possible to have a portion or the largest part of the airflow re-circulating within the system, while only the smaller part is ejected as a ring vortex. This technique has applications for propagation of ring vortices to transport fragrances and insecticides. It may also be applied to transport chemicals to foliage as in orchards due to the turbulence within the ring enabling full wetting of each side of the leaves. The chemical would be vaporised first by: pressure reduction, heating, ultrasound or any suitable means.

It also better promotes whole room circulation because even though the amount of ejected air in a ring vortex is smaller than that ejected through a nozzle when employing the same system power, never the less the nozzle air by not travelling the required distance can re-circulate back through the fan. The ring vortex travelling across a room necessarily displaces air at a distance which air must flow back around the room towards the source of the ring vortex.

### **THIRD EXAMPLE**

#### **THE COANDA VACUUM CLEANER**



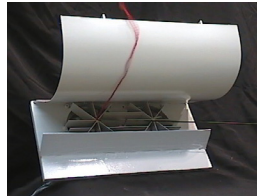
Only one of several versions of this vacuum cleaner is presented here. The accompanying video ([Click video](#)) shows an underside view of the vacuum while operating over glass with flour representing the dirt. Viewing the video from centrally, a ring of small nozzles can be seen. A high pressure fan (a jetfan) drives air through and from these nozzles which stirs the carpet pile. Viewing further out there is seen an annular slot blowing air over a Coanda surface and this air plus entrained dirt enters into an annular suction slot thus augmenting its performance. Once travelling vertically the reduced pressure in the system causes the air to spin while it is forced to travel medially.

This makes it very difficult for any large particles to ascend up through the system as they have to travel inwardly while spiraling. The vortex dumps the remaining dirt into a cheap flexible bag ([Click for video](#)) which does not collapse onto the low pressure vortex because a lower pressure is created between the bag and the bowl that it is contained within. The vortex flows in on itself to form a central vortex which then returns back through the fan to do the circuit over again. This way most of the air can be recirculated minimizing the quantity of air to be filtered.

Some of the other technical features and versions are proprietary. The main emphasis here is that it is the Coanda Effect that is being employed and is the main feature of this type of vacuum cleaner.

#### **FOURTH EXAMPLE**

##### **THE COANDA CHICKEN SHED**



A local government authority gave approval for a housing estate to be built nearby chicken meat producing sheds. 14 x one meter diameter fans at one end of the shed discharge odour laden air and dust (a euphemism) towards the housing estate. The local authority is taken to court by the residents. The company has been established for many years and violently resists any attempts to move them. Local authority explores various ways to solve the problem.

A way suggested by their consultants is to duct the discharge at first horizontally and then vertically to dilute with prevailing winds. In practise the idea doesn't work because of the losses through ducting, especially the right angle turn, no matter how gentle, plus the ducting is expensive. The system resistance causes the fans to overheat, possibly burn out in hot weather and also to draw excessive current resulting in high electricity bills.

The author was asked by the local authority to present a possible solution. That possible solution is presented in the accompanying photo, ([Click for photo](#)) which shows a wool tuft turning 90 degrees around a Coanda surface. The trick was how to get the highly turbulent air from the rotating fans to be captured by the Coanda surface, especially when the air speed is relatively low. Once travelling around and upward over the Coanda surface air is entrained from the direction of the housing estate instead of blowing towards it.

The local authority agrees that this technique is probably a large part of the solution. At present the author is negotiating with private enterprise to build these low cost Coanda surfaces at the ends of chicken meat production sheds where there is the need.  
*(Patents and IP are involved).*

## FIFTH EXAMPLE

### COANDA CEILING FAN.



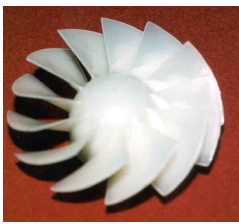
[\(Click for video\)](#)

Video shows smoke filled air pathway from top side to underside of the toroidal body. An annular jet exits at a certain angle over a step with particular geometry. The jet is tripped and three counter rotating ring vortices circle the top side (standing ring vortices). These entrain ambient air and a turbulent flow travels outwardly and circulates to the underside.

The jet is the working fluid and that same amount of air re-enters the underside annular passageway. The ambient air entrained into the jet on top is ejected underneath. By altering underside geometry, discharge can be diffused or a concentrated plume, whatever is desired; body can be translucent with a circular fluorescent tube inside. Excellent mixing enhances air-conditioned air distribution throughout the room.

## SIXTH EXAMPLE

### THE JETFAN



[\(Click to enlarge\)](#)

[\(Click here for University Report\)](#)

A new type of fan and water-pump is presented. These do not employ the Coanda affect but may be useful in producing fan or pump flows of sufficient power for CC. Potential applications are the NOTAR (see Bibliography # 7) and some other high flow but lower velocity CC applications and water applications where high speed water jets may boil. As a fan (air pump), the jet-fan gives a 60% mechanical efficiency in a 5 inch diameter version with a high static efficiency.

It is a fan of moderate flow with moderate pressures and a rough rule of thumb is that its pressures will be somewhere mid way between a good axial flow fan and a centrifugal fan employing a volute. It has a **NO STALL** characteristic. It is an axial inflow and discharge fan.

Significant features of the jet-fan is that to generate a static pressure **it does not employ stators or a volute** unlike virtually any other kind of fan or pump. Static pressure is produced within the blade passageways and this means that by employing no stators and no volute with its tongue or cutwater, wake collisions are eliminated and noise reduced. This may have applications for stealth and even such mundane applications as water pumps for kitchen sinks etc in shipping including submarines.

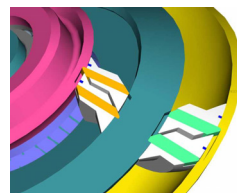
The **Jetfan** including the water pumping version ([click for photo A B](#)) is of complex geometry with overlapping blades. These fans and water pumps are however able to be made at low cost due to the fact that a manufacturing method ([Click for photos A B](#)) has been invented to enable them to auto-rotate from the tooling and can be made for approximately the same price as any low cost injection moulded impeller.

The same manufacturing method enables **axial flow** ([Click for photo A B C](#)) fans with overlapping blades to be made at low cost and also **centrifugal impellers** to be made with high performance geometry and able to be rotationally extracted from the mould instead of employing investment casting and subsequent milling for precision.

The Jetfans pressure/flow features make it ideal for the Coanda Hovercraft/W.I.G, the last subject of this paper. (The **JETFAN** technology and patents are the property of **DBG INVESTMENTS PTY. LTD.**)

## SEVENTH EXAMPLE

### WIND TURBINES AND ORBITAL PUMP



([Click B for video](#))

[B](#)

([Click for additional pictures of pump](#))

[1](#) [2.](#)

The author has patents pending for cc wind turbines. Full span and also tip blowing ([see Bibliography # 3](#) ) is proposed. Wind tunnel testing has indicated that turbine efficiency increases of 30 to 40 % are likely. This is after all parasitic losses including by the Orbitalpump are subtracted. Given the experience with Coanda Effect and CC of the target audience of this paper, it is not necessary to elaborate on the theory any further here as it will be well understood.

There are **2** main points though here:

1. Wind turbine power generation is a potential target for CC, which target could well be revolutionized by a significant increase in efficiency and needs to be explored fully as soon as possible before the world trend towards alternative energy sources including wind-power generation progresses too far, making it difficult later to retro-fit this probable innovation.
2. It is likely the practitioners of CC have discovered that there are few CC applications where adequate air supply can be obtained for control air. The NOTAR is a very successful exception, The V22 tilt rotor exhaust deflection is another good example but CC there is not strictly speaking critical to the aircraft performance. Many proposed applications including some successfully achieved are risky as other aircraft systems may be compromised generally or occasionally. If the only reason that CC development has stagnated is that of insufficient control air, then the application to wind turbines would not be likely to be any more successful!

The author therefore believes that it was necessary that if CC were to be suggested for application to wind turbines that an answer to the problem of control air supply be furnished simultaneously. That potential answer may also apply to many other examples of Coanda effect or CC. So this subject is two in one namely:

1. Circulation Control for Wind Turbines and the air supply pump to provide the CC air.
2. Non Wind Turbine Applications.

*(click for renderings of improved pistons & pins with positive engagement )*

[A](#)   [B](#)   [C](#)   [D](#)   [E](#)   [F](#)

The animation provides the basic idea of the **ORBITALPUMP**. It shows how the pins that support the pistons are activated to allow the pistons to change over, one replacing the other. The main features of the Orbital Pump are that it is high volume relatively low speed, low noise, low wear, fills and exhausts simultaneously and can function as either a compressor or high volume air pump or both.



Patents pending depict the Orbitalpump as the hub of a wind turbine. For most applications the Orbitalpump shell, being a hollow toroidal body would remain stationary while the shaft is turned. However in the case of wind turbines the shaft would be held stationary while the pump body rotates with the blades. The advantage here is that the pressurized air can be fed directly or almost directly into the hollow blades, thus eliminating significant amounts of plumbing and the accompanying losses. It also simplifies air delivery to the slots.

The Orbital Pump is also designed to be or to be attached to the hub of fans, including CC centrifugal fans. A 1975 document by Robert J. Fury & Robert Whitehead ([see item 9 Bibliography](#)) shows the results of applying CC to a centrifugal fan, The abstract is here supplied. “The static characteristics of a circulation control (CC) fan were determined to demonstrate the feasibility of the CC concept as a means of meeting the lift system requirements of a large, open ocean capable, surface effect ship (SES). These requirements being variable performance, at constant RPM, of sufficient range to provide for heave alleviation when operating at high speeds in advanced sea-states. The scope of the program included two solidity ratios within the model centrifugal impeller and, in effect, two volutes. The better performing combination of these variations was the low solidity ( $\sigma=0.65$ ) impeller mated with a reduced internal volume volute. *This fan demonstrated a flow rate increase of 100 percent over that achieved at the design point, through increasing the flow of control air, while maintaining a constant head rise. The peak efficiency of this combination was 83 percent. From this peak efficiency, achieved with a moderate amount of control air, the efficiency dropped to a low of 65 percent when operating with a maximum flow of control air. It is shown that the most likely demands of the heave alleviation system would allow for the fan to operate at the highest efficiency possible for the flow rate required. The high solidity ( $\sigma=1.3$ ) impeller was found to produce an increase in flow rate of 50 percent over that achieved at the design point, through increased control air, and did not achieve as high an efficiency as that of the lower solidity configuration*”. Notice it achieved in some cases a 100% increase in flow over the design point while maintaining head pressure with an 83% efficiency.

The Orbital Pump PCT document is: Patent Application No. PCT/AU03/00635. In addition a recent patent pending (*unpublished yet*) applying the orbital pump to wind turbines shows that via the hollow stationary shaft a reversing gear can drive the pistons in the opposite direction to the rotation of the connected turbine and pump shell and also at a higher RPM, thus increasing the air supply significantly over and above that achievable at low RPM. In addition it has shown that two or more Orbital Pumps may be placed on the same shaft thereby multiplying capacity.

The Author contends that shifting the rear stagnation point and attenuating or eliminating tip vortices in wind turbines and fan blades is as valid as it is for aircraft wings. Applying CC to wind turbines may have other benefits. For example a smaller diameter wind turbine may be able to be employed while achieving the same efficiency. This would reduce manufacturing costs, reduce maintenance and reduce stress on components. It may also enable wind turbines to be efficient in areas of lower wind speed. Wind Turbine and Orbitalpump mix development is being vigorously pursued at present. It should be noted that the Orbitalpump depicted herein is not the only version.

Provided that all the features of the **ORBITALPUMP** are successfully developed, mainly the locking pins and sealing methods, when looked at geometrically, the **ORBITALPUMP** is the highest volume positive displacement pump possible.

This high capacity can be increased by multi-staging on one shaft. Other applications of the **ORBITALPUMP** may include a compressor, a pump, a super charger, a refrigeration compressor and low speed high volume water pumps. For CC applications it can be placed in close proximity to the pre-slot plenum with minimum plumbing.

## **EIGHTH APPLICATION**

### **HOVERCRAFT / W.I.G.**



**Ekranoplan/WIG**



**Amphistar/WIG**



**X- Hovercraft/WIG**

[\(Click for additional photos\)](#)

[1.](#) [2.](#)  
[\(Click here for Video\)](#)

This is a model hovercraft/ wing in ground effect craft (WIG) initially aimed at the hobby market. It employs several methods of blowing generally called the Coanda effect. One form is upper surface blowing (USB) where a large mass of fluid is blown across the upper surface. It also employs CC, which is also the COANDA effect and is achieved by a thin wall jet circulating around a reasonably small radius over a relatively short distance. In “conventional” USB applications, USB gas may be supplied from the engine by having the jet exhaust spread out to scrub the top of a wing. This may be induced to co-flow with the CC jet around the trailing edge.

This model hovercraft was initially designed as a toy and or for the entertainment industry. It is a circular platform and employs two annular blowing slots. One slot found more centrally employs “USB” and the more peripheral CC slot blows a smaller mass, higher speed flow over the rim to entrain the USB flow over to underneath. For small models of two feet in diameter there is not the capacity to carry a compressor, so the peripheral blowing slot is deleted and in its place are employed several suction slots. These suction slots serve to reduce the pressure over the rim and also return air to the internal fan (a **Jetfan** having proved the most ideal).

One of the number of models is shown in the video hovering above a table. The two wires seen underneath are merely restraints in case of instability. That particular version employs a SuperTigre 90 model aircraft engine and a Jetfan. It also employs a tuned pipe. The model lifts onto an air cushion by the following mechanisms. Motor and fan pump a significant amount of air to scrub the top surface (USB). The suction generated is by Bernoulli’s principle.

Ideally a peripheral CC slot would also blow. In the case of this model, as stated, suction slots are employed. This lowers the pressure over the rim and the whole USB flow circulates to underneath. This pressurizes the underside by jet stagnation and lifts the craft onto an air cushion. Suction slots have been employed before for other applications and otherwise have been suggested by many.



[http://www.cousteau.org/en/cousteau\\_world/our\\_ships/alcyone.php?sPlug=1](http://www.cousteau.org/en/cousteau_world/our_ships/alcyone.php?sPlug=1)

Jacques Cousteau’s yacht the “**Halcyon**” (see Bibliography – 8) employed suction slots each side of a metal sail with a reported dramatic increase in thrust. “It is claimed that thereby the **Turbosail** has an efficiency **3.5** to **4** times that of a cloth sail”. The disadvantage of using suction slots in this manner is that inflow to the fan throat is restricted and so efficiency of USB in the case of this hovercraft/WIG suffers somewhat. All the proprietary information regarding this Hovercraft/W.I.G. cannot be presented here as the author obviously does not want to lose a commercial advantage.

Many models have been constructed with varying results and roll, pitch and yaw have been successfully achieved.

It should be noted that with this particular model while roll control was achieved, pitch control was impaired by asymmetric inflow due to the tuned pipe positioned in the inlet duct which distorted the underside plate. This caused the model to droop on that side, so a small stay was placed under the edge of the model. As this video was only originally meant for the entertainment and movie industry to demonstrate other skills that stay was digitally removed. Also digitally removed was a thin wire which prevented counter torque. Pitch control is restored by restored symmetry of inflow and counter-torque and yaw is solved but is proprietary.

The main point here is that a curious result emerged. When weights were placed on the model to test lift it supported a 100% payload. A paper by Robin Imber and Ernest Rogers "*Investigation of a Circular Planform Wing with Tangential Fluid Ejection*" (see Index # 1) shows testing performed on a similar configuration. Robin Imber and Ernie Rogers work was aimed at other applications such as "*air and underwater control surfaces, radome scanning sensors, rotor hub fairings on helicopters, marine propellers and aircraft wings that have parabolic tips, and towed underwater arrays.*" Imber and Rogers showed that by varying positions of azimuthal blowing, they could achieve roll and pitch moments. This was achieved entirely pneumatically. They did not address the issue of counter torque, however the author has addressed that with satisfactory results, also achieved pneumatically without any projecting surfaces.

Imber & Rogers paper reveals achievement of:

- : Roll Control**
- : Pitch Control**
- : Omnidirectional Capability**
- : Lift Augmentation**

In addition the author shows:

- : Upper surface blowing of high mass flow(USB)**
- : Rim blowing slot (CC) or suction slots or both**
- : Co-flow of USB/CC wall jets**
- : Self contained power plant and fan**

The Author has also established propulsion means. This small model then has achieved VTOL into a kind of surface effect or air cushion. It is well understood that to translate from this hovering/loitering mode into a W.I.G mode of ground effect travel will require further work and experimentation on larger models. Indeed if a manned craft is attempted, like any other CC applications a suitable high flow pump will need to be found for adequate CC air. Perhaps the Orbital pump will fill that need.

## CONCLUSIONS

There are many other important applications for the Coanda Effect and CC in addition to aeronautical ones. This fact should stimulate increased interest in solving the very few but important impediments to being able to incorporate the Coanda effect and CC into aeronautical, industrial and domestic applications.

## **BIBLIOGRAPHY**

1. **Investigation of a Circular Planform Wing with Tangential Fluid Ejection** by **Robin D. IMBER** (Aerospace Engineer) and **Ernest O. ROGERS** (Senior Aerospace Engineer, Member AIAA)
2. **Investigation into the Application of the High Velocity Circulation Control Wall Jet for High Lift and Drag Generation on Stol Aircraft** by **Robert J. ENGLAR** (Senior Aerospace Engineer, Aviation and Surface Effects Department, Naval Ship Research and Development Center)
3. **Aerodynamic Surface Tip Vortex Attenuation System** by **Robert M. TAYLOR**
4. **Ekranoplans & Very Fast Craft** by\_ The University of New South Wales –The Institute of Marine Engineers (Sydney Branch) – The University of New South Wales (Dept., of Naval Architecture) – Australian Maritime Safety Authority – Australian Maritime Engineering CRC Ltd. – Russian Australian Advanced Technology Group
5. **WISE up to ekranoplan GEMs** by University of New South Wales – The Institute of Marine Engineers (Sydney Branch) – The University of New South Wales (Dept. of Naval Architecture) – Australian Maritime Engineering CRC Ltd – Dept., of Industry Science and Tourism.
6. **Twenty-First Century Flying Ships** by The Institute of Marine Engineers (Sydney Branch) - The University of New South Wales (Dept. of Naval Architecture – The Australian Chamber of Shipping – Russian Australian Advanced Technology Group – Australian Maritime Engineering CRC Ltd – The Royal Institute of Naval Architects (Australian Division).
7. **AOPA PILOT** (Magazine) March 1992 MD 520 NOTAR
8. [http://www.cousteau.org/en/cousteau\\_world/our\\_ships/alcyone.php?sPlug=1](http://www.cousteau.org/en/cousteau_world/our_ships/alcyone.php?sPlug=1)
9. **Static Evaluation Of A Circulation Control Centrifugal Fan** by **Roger J. Furey** and **Robert E. Whitehead** – David W. Taylor Naval Ship Research and Development Centre, Bethesda, MD 20084
10. **Applied Aerodynamics of Circulation Control Airfoils and Rotors** by **Rogers, E.O., A. W. Schwartz** and **Jane S. Abramson**
11. **Two-Dimensional Subsonic Wind Tunnel Evaluation of Two related Cambered 15-Percent Thick Circulation Control Airfoils:** by **Abramson, J.**
12. **Self Oscillation Phenomena of Turbulent Jets in a Channel:** by **K. Murai, Y. Kawashima, S. Nakanishi, M. Taga**

# Commercial Applications of Circulation Control

by

Terence R Day

Australia

## Commercial Activities

- Entertainment Industry





## On Stage Tornado



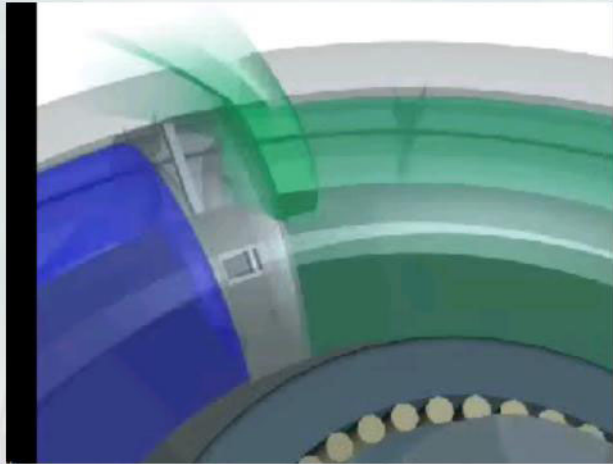
## Wind Turbine Applications

- Wind turbine blade 'lift' can be enhanced by CC. Blowing slot is placed in a similar fashion to 'blown wings' and the slot extends around the tip for tip blowing. Overall efficiency gains of 30 to 40% appear probable.
- **But how do we pump enough air to 'Blow the Slot' ? . .**





## The Orbital Pump



## Orbital Pump

The annular geometry of the Orbital Pump enables a stroke up to ten times longer than a conventional reciprocating compressor. Whilst pumping, the chamber fills simultaneously.

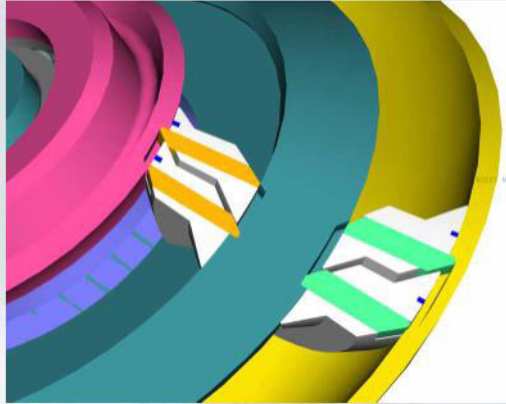
The advantages are: no air receiver required, lightweight, simple construction.

When applied in the hub of wind turbines or CC fans the orbital pump rotates with the fan or turbine whilst its shaft remains stationary avoiding the need for a complicated interface between compressed air supply and hollow blade.



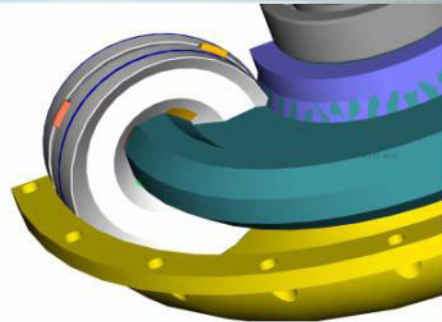
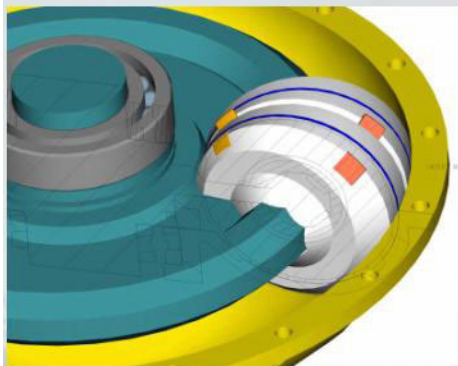
## Orbital Pump Operation

- Piston Latching Mechanism



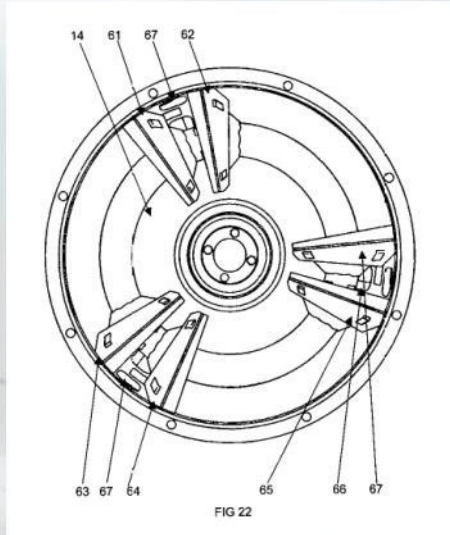
## Orbital Pump Operation

- Piston Changeover



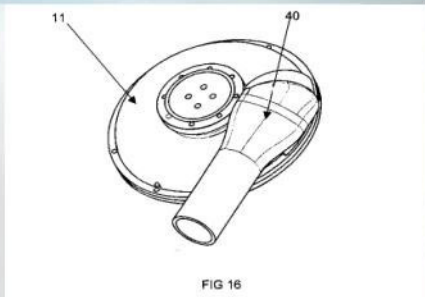
# Orbital Pump

- Plan View

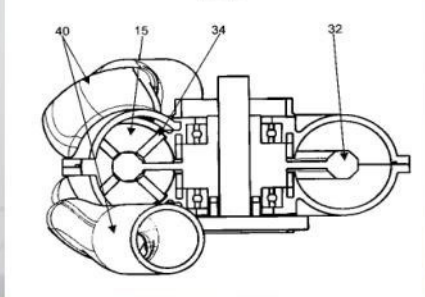


# Orbital Pump

- Manifold Design



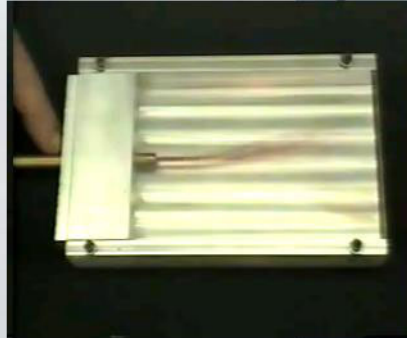
- Pump Cross-section



## Oscillating Channel Flow

Oscillating Channel Flow (Coanda Effect) is employed to eliminate laminar flow so that all air can contact reactive surfaces. This is applied to odour control applications and to generate good mixing.

The second application of oscillating channel flow is that each redirection of the jet can enter into a specially formed passageway so that the flow manifests at the far end of the passageway as a pulse.



## Oscillating Channel Flow

- This pulse can then be tripped over an orifice plate to eject ring vortices. The ring vortices can carry for example: an insecticide or a fragrance which can be carried a far greater distance than if the airflow was from a simple nozzle.
- In addition one side of the oscillating jet can be re-routed for greater surface interaction.



## Oscillating Channel Flow

- Ring Vortex Production



## Jetfan Coanda Vacuum Cleaner

- The Coanda blowing slot adjacent to the carpet allows for both blowing and suction at the same time enhancing dirt agitation and increasing performance.



## Jetfan Coanda Vacuum Cleaner



## Jetfan Coanda Vacuum Cleaner



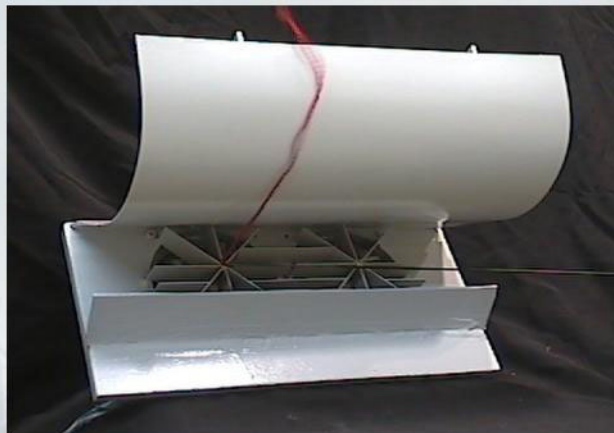
## Jetfan Driven Coanda Ceiling Fan

The annular topside slot and step configuration generates ring vortices, which entrain and circulate over the rim to the underside. Entrained air is projected downwards. Geometry determines underside distribution pattern.



## Coanda Effect for Odour Dilution

Highly turbulent rotating flow is captured by a Coanda Surface for redirection to meet Odour and Government Legislation requirements.





## The Jetfan

These fans with overlapping and convergent blades demonstrate a 'no stall' characteristic, good efficiency without the need for stator rows or diffusers. Noise is reduced due to elimination of 'wake collisions'.

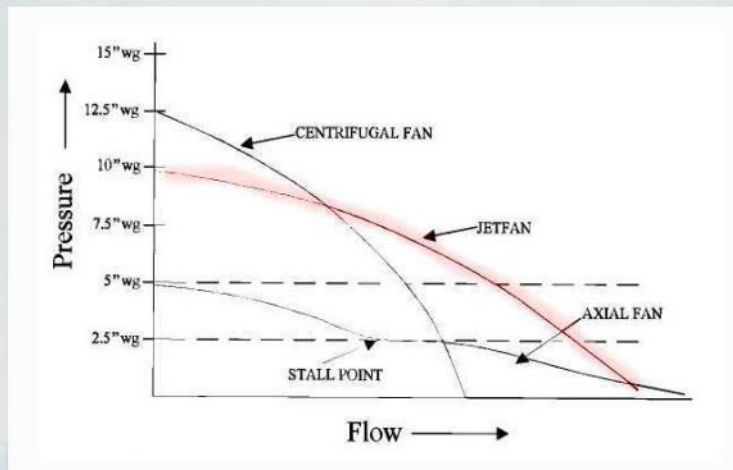


These fans produce flow characteristics suitable for high flow CC applications such as the Notar. A unique manufacturing method makes these fans and water pump impellers at low cost.



## The Jetfan

**Jetfan produces a mix of Axial and Centrifugal fan flow characteristics.**



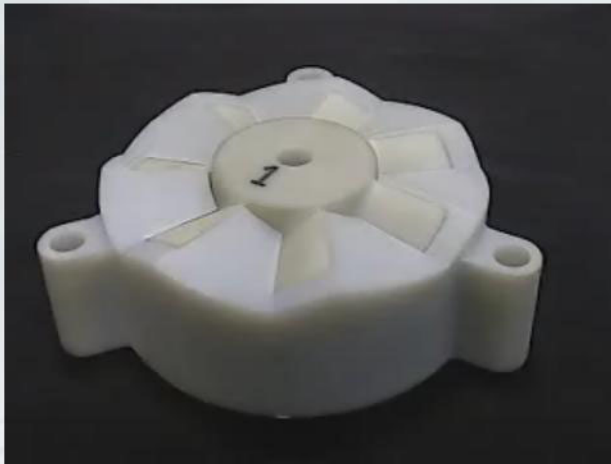
## The Jetfan Manufacturing Method

Injection Moulded with the ease and cost of any other fan



## Jetfan Manufacturing Method

- Fans simply Rotate from the Mould



## Jetfan as a Water Pump

The Jetfan water pump is high flow moderate pressure and 'cavitationless'. This may make it suitable for CC marine applications.

Other applications would be where very low noise is essential.



## Water Pump University Report Extracts

### RESULTS:

The following results were produced from tests on the 93 mm JETFAN Water Pump at speeds of 2,000 3,000 and 4,000 RPM. Performance graphs of the increase in static pressure above the base zero flow pressure are given for a range of flow rates for each rotational speed.

The visual inspection of the onset of cavitation indicated that over the range of flow rates tested, cavitation first appears at a rotational speed of 3,300 RPM. Above this speed cavitation bubbles were observed to form on the concave surface of each blade near the leading edge, and to be reabsorbed a short distance inside the blade passage. The point of reabsorption corresponds to a line drawn at right angles from the leading edge of the convex surface of the adjacent blade. This reabsorption indicates that the pressure is rising as the water enters the blade passage.

# Water Pump University Report Extracts



## CONCLUSIONS:

This series of performance tests on the 93 mm JETFAN Water Pump has illustrated the performance characteristics of this new prototype pump, and determined both the extent of cavitation and the speeds at which cavitation may occur.

In comparing the performance of the JETFAN water pump to other pump designs it must be noted that the performance detailed in this report has been achieved without the use of a complex volute or stator blades, which are commonly used to direct the flow of water from the rotating impeller into the outlet pipe in many pump designs.

## Measurement and Analysis of Circulation Control Airfoils

F. Kevin Owen  
Complere Inc.  
P.O. Box 541  
Pacific Grove, CA 93950

Andrew K. Owen  
University of Oxford  
Oxford, U.K.

### Abstract

A wind tunnel investigation has been conducted of a two-dimensional circulation control airfoil section equipped with trailing edge blowing. The tests were conducted in the NASA-Ames 2 x 2-Ft. Variable Density Transonic Wind Tunnel over a range of free-stream Mach number and unit Reynolds numbers. Detailed non-intrusive flow-field measurements of the mean flow and turbulent properties were obtained in the airfoil wake for a number of different blowing coefficients. These results have been related to the circulation control airfoil performance obtained from direct surface pressure measurements. The analysis shows that wind tunnel wall interference can have significant influence on high lift test results. This influence must be accounted for before wind tunnel test data can be used for design extrapolation or for turbulence modeling and CFD assessments. Corrections have been made for finite aspect ratio wind tunnel wall interference in order to provide interference free benchmark data for turbulence modeling and CFD code development and validation. A substantial amount of additional data awaits analysis.

### Introduction

In the study of circulation control, the sharp trailing edges of otherwise conventional airfoils are replaced with rounded or bluff surfaces, typically either circular or elliptic cross-sections, with thin tangential blowing slots located on the aft upper surface. These rounded trailing edges, allow the rear stagnation point to move. This movement is controlled by the relative blowing momentum of fluid injected through the slots, and by the properties of the external flow field. By blowing through the slot, a jet sheet is issued that, due to the balance of centrifugal force and sub-ambient static pressure within the jet, remains attached to the airfoil.

At low blowing rates, this Coanda effect entrains upper surface boundary layer flow and prevents trailing edge separation. As the blowing momentum is increased, the rear stagnation point is moved further around the trailing edge and the wake deflection angle is increased. An effective camber is introduced, and the lift is increased. Blowing rates can be adjusted until the airfoil static pressure distribution is that predicted by inviscid

potential flow. With increased blowing, the jet controls the location of the airfoil stagnation points, and therefore the circulation and lift. However, eventually there becomes a point where there is no longer a balance between the static pressure and centrifugal force and jet bow-off occurs with a corresponding dramatic decrease in lift.

Lift values greater than those predicted by inviscid potential flow theory are generated in the circulation control regime. Pneumatic camber similar to a mechanical high lift system can be obtained. However, circulation control lift augmentation is far more efficient than conventional high lift devices since they only have to overcome the viscous losses in the flow. By compensating for the viscous losses, the flow field more closely resembles the ideal inviscid case. Accordingly, lift augmentation several times those attainable with jet flap or blown devices have been achieved.

Unfortunately, the precise determination of circulation control airfoil performance for design and CFD assessment purposes is difficult to achieve. The most serious problem encountered in testing these high lift devices is the interference produced by wind tunnel test section wall separation. Due to the strong adverse pressure gradients on the airfoil upper surface, strong secondary flows can be generated in the sidewall boundary layers. The problem is further compounded by since there are significant spanwise circulation gradients present since circulation must decrease towards the wall. Even at moderate lift, these factors can generate shed vorticity more characteristic of a three-dimensional than an infinite span wing. Clearly, a great deal of research and analysis is still required in order to properly establish a reliable database for full-scale model development and CFD code validation.

### **Experimental Details**

The work described in this report was conducted in the NASA Ames 2 x 2-Ft. Variable Density Transonic Wind Tunnel at a free stream Mach number of 0.5 and at a unit Reynolds number of 3.2 million/ft. The test model spanned the test section and was held at zero angle of attack for the present work. The model was a symmetric 6-inch chord airfoil, 20% thick, 3% camber ellipse with a nominally circular arc trailing edge. An adjustable, nominally 0.010-inch, tangential blowing slot was located on the upper surface, 1-2% before the usual upper surface separation point, at the 96% chordwise location. Transition strips were attached to the airfoil section at the 17% chord on both the upper and lower surfaces. The 1.25-mm-wide strips consisted of 0.13-mm nominal diameter glass beads. Transition effectiveness was verified by the sublimation technique. A regulated 3000 psig air system was utilized to supply the internal plenum of the model, and a maximum internal pressure of 60 psig was attainable. The resulting high internal contraction ratio ensured adequate two-dimensionality of the jet exit flow. The jet exit velocity was calculated from isentropic relationships referenced to tunnel static conditions.

There were a total of 91 pressure taps on the model, 59 were positioned along the centerline. Of these taps, 24 were on the upper surface, 35 on the lower surface. The airfoil performance data were obtained by direct integration of these centerline pressure

taps. The flowfield measurements were obtained with a two-component laser velocimeter with conditional sampling capability. The effective sensing volume approximated a cylinder, 200micron diameter and 3 mm long, with its axis aligned with the cross-stream direction. Detailed measurements of the mean axial and vertical velocities, turbulent intensities, and turbulent shear stress distributions were obtained.

## Sample Results

Examples of laser velocimeter wake profile measurements for a zero angle of attack airfoil case are shown in Figures 1 and 2. These results show the effects of jet blowing on the near-wake axial velocity profiles. In the zero blowing case, there is a small wake displacement due to the airfoil camber that produces lift at zero angle of attack. There is also a large region of reversed flow typical of a blunt body re-circulation zone. With a small amount of blowing ( $C_\mu = 0.024$ ), there is a significant downward wake displacement and a fuller profile wake that has been energized by the jet. These data, and other profiles obtained at various distances downstream of the airfoil trailing edge, can be used to determine wake deflection angles, wake deficit recovery, and mixing and shear layer growth downstream.

It is evident that the Coanda effect of the flowing jet relocates the aft stagnation point upstream along the airfoil lower surface resulting in a downward displacement of the wake. This trend of increased wake displacement continues with higher blowing rates until there is no longer a balance between local static pressure difference and centrifugal force required for continued jet attachment. At this point we get what is referred to as jet blow off. Jet effectiveness is destroyed, and there is a rapid drop in wake displacement and the in the measured lift coefficient. However, in the present case, Figure 3 shows that blowing can produce effective angles of attack, determined from measured wake displacement, of almost 20 degrees in the present zero degree airfoil angle of attack case before blow off occurs.

From these data we can calculate the infinite aspect ratio lift coefficients from inviscid potential flow theory and thus assess airfoil lift performance. These results are shown in Figure 4, where the lift at zero blowing agrees well with zero offset camber predictions. However, these results are significantly higher than the lift computed from the measured airfoil surface pressure distributions. But, as expected, we have seen seed particle deposits on the test section windows, which suggest that strong secondary flows are generated in the wind tunnel sidewall boundary layers. This shed vorticity will induce unknown flow angularity in the free stream flow ahead of the model, thus changing the airfoil's effective angle of attack. However, from the wake measurements, we are able to calculate the induced flow angularity as a function of jet blowing momentum coefficient. These results, calculated assuming a semi-elliptic lift distribution, are shown in Figure 5. With this information, we are able to compute the finite aspect ratio lift coefficients that are shown in Figure 6. These results are in excellent agreement with the surface pressure, direct lift measurements shown in Figure 7.



Wake turbulence measurements indicate that large-scale fluctuations are introduced by jet blowing and that wake unsteadiness may well be present at the higher blowing rates just before jet detachment. In the no blowing case shown in Figure 8, small-scale turbulence dominates, and local RMS turbulence intensities are related to the local mean velocity gradients as in a plane-mixing layer. There is good agreement between the calculated mixing length to wake width ratio of 0.08 compared to the nominal value of 0.07 for a plane-mixing layer. However, once jet blowing is initiated, as shown in Figure 9, a wide highly turbulent core develops that is indicative of high turbulent kinetic energy production in the blown jet wake. Turbulent length scales are increased by a factor of three, an indication of large-scale turbulent mixing and/or wake unsteadiness.

### **Concluding Comments**

New circulation control test measurements and analysis have been presented that show the need for caution when attempting to use wind tunnel test results for CFD code validation, or for design purposes. In particular, the results have identified the quantitative extent of wall influence can have on circulation control test results; e.g. lift augmentation reduced from 68 to 42. The results also suggest that turbulence models must be modified to account for the effects of unsteady, large scale turbulent mixing. The agreement between the measured and the calculated finite aspect ratio lift coefficients suggests that if we know the effective angle of attack then simple inviscid theory may well be adequate for lift coefficient predictions. In turn, the analysis suggests that 2-dimensional CFD computations could well be meaningless unless the airfoil effective angle of attack is known. Full 3-dimensional calculations will probably be required to account for wall interference; i.e. effective angle of attack and effective camber.

Estimates of the errors caused by non-uniform flow due primarily to wall boundary layer separation are essential. Initial investigations suggest that angle of attack corrections of at least  $-1.5C_L$  will be required. Clearly, this can be a substantial correction factor since lift coefficients well in excess of 2.0 can be expected for high lift systems. Effects on the estimated drag coefficient are even more acute. Typical drag coefficients show errors of over 100 percent at induced angles of less than 1 degree. Indeed, at lift slopes typical of those at transonic speeds, angle of attack errors of 0.01 degree can lead to drag measurement uncertainty of more than one drag count. Clearly, in any high lift experiments, accurate estimates or measurements of induced flow angularity must be made before useful design estimates or meaningful comparisons with CFD calculations are undertaken. A detailed review and analysis of finite aspect ratio circulation control experiments must be conducted to assess wind tunnel wall effects on experimental data previously reported in the literature.

**Figure 1 Wake Velocity Profile**  
 $C_u = 0, X/C = 0.05$

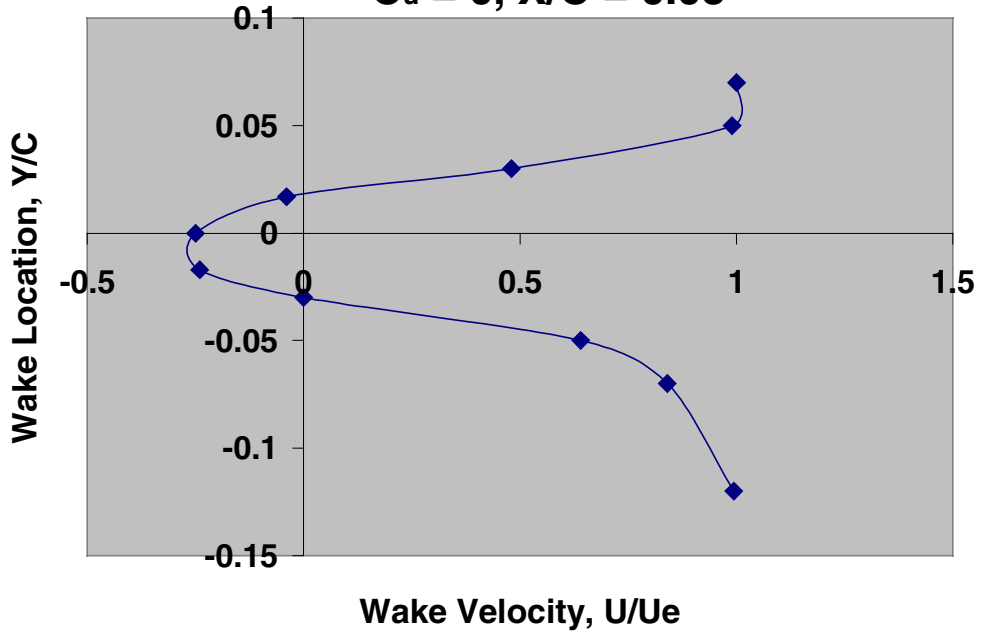


**Figure 2 Wake Velocity Profile**  
 $C_u=0.024, X/C=0.05$

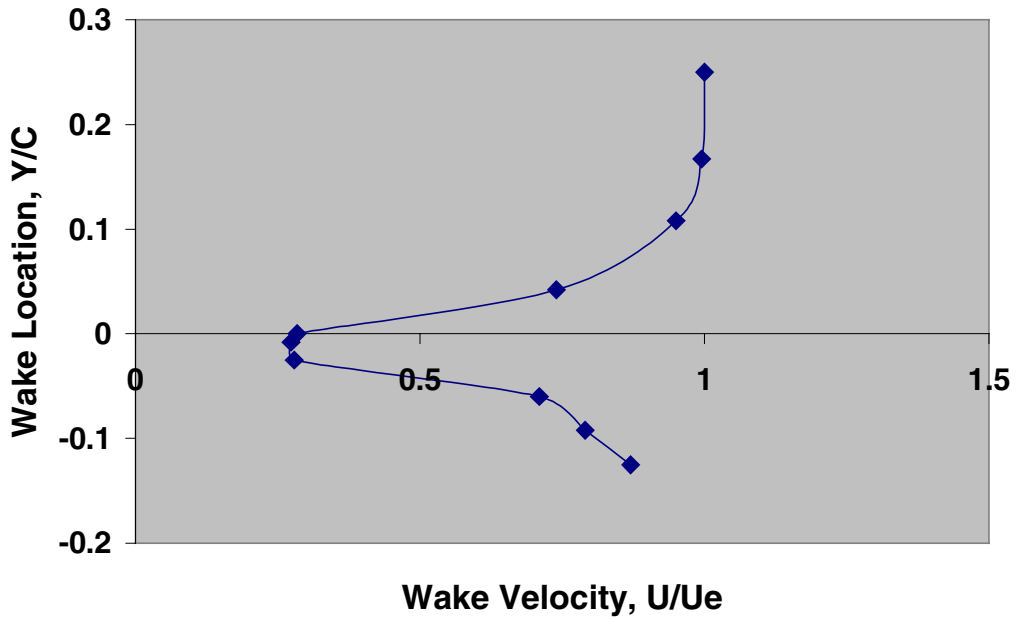


Figure 3 Measured Wake Angles

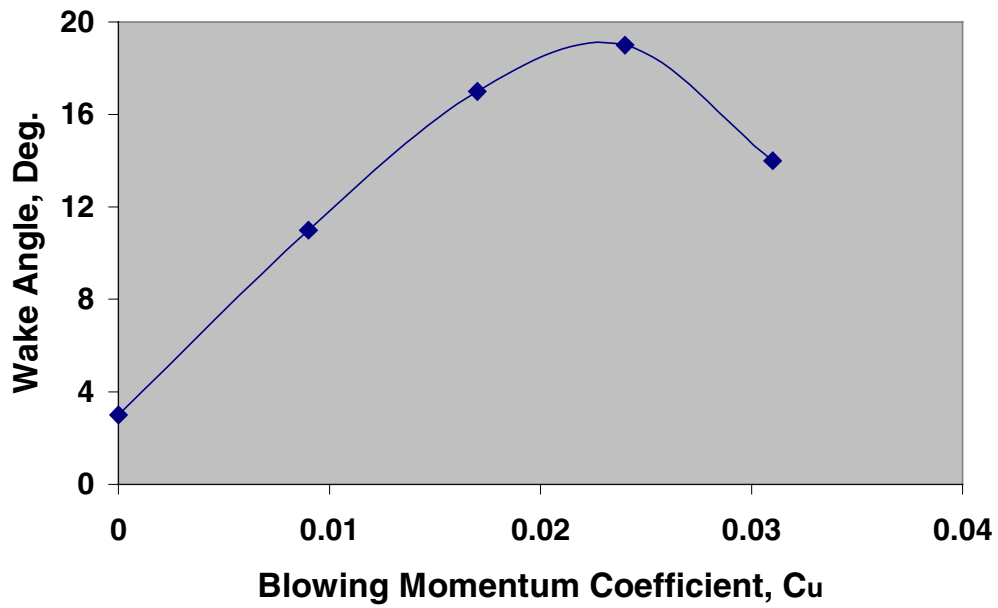


Figure 4 Infinite Aspect Ratio Lift Coefficients

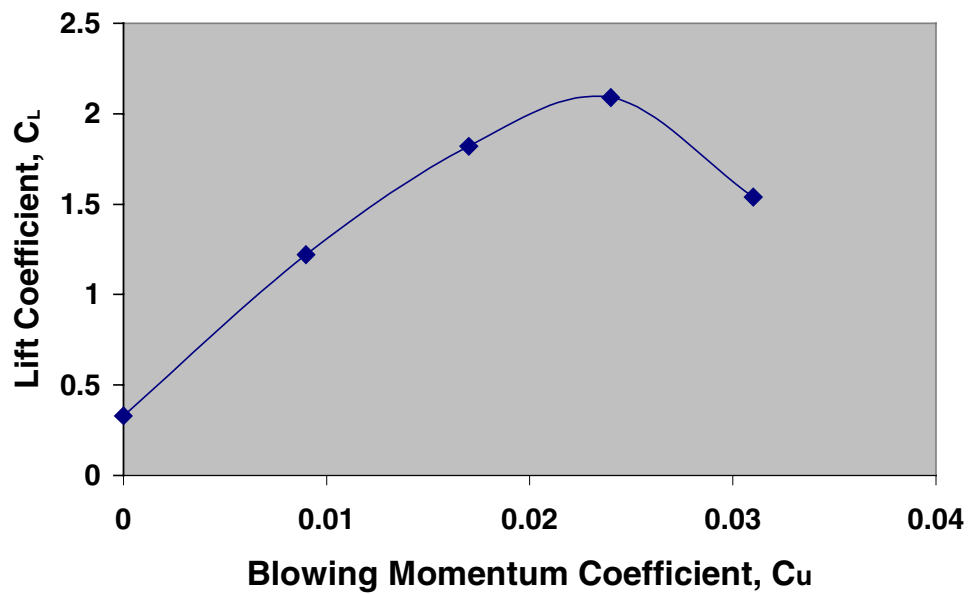


Figure 5 Induced Flow Angularity

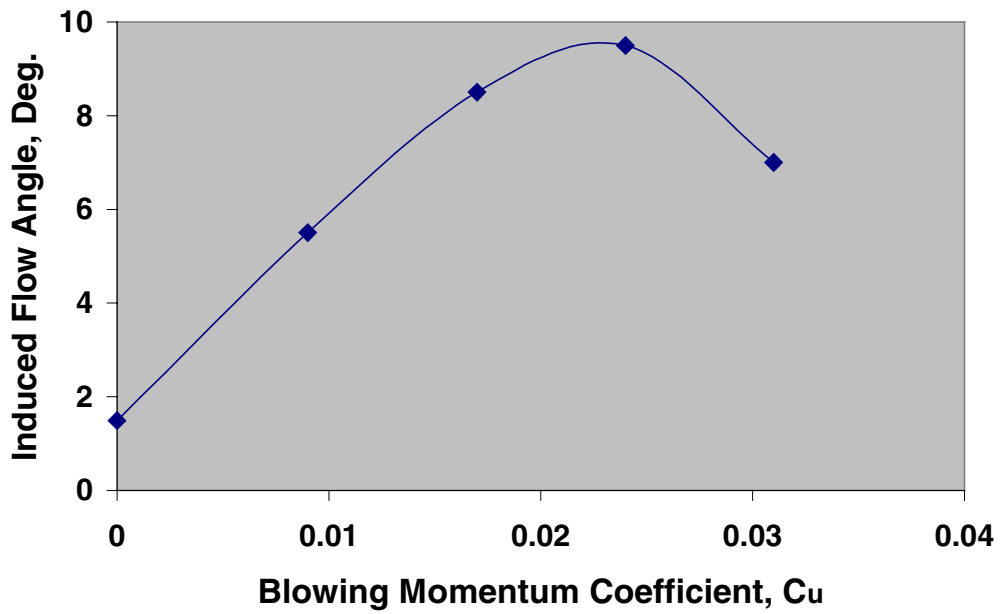


Figure 6 Calculated Finite Aspect Ratio Lift Coefficients

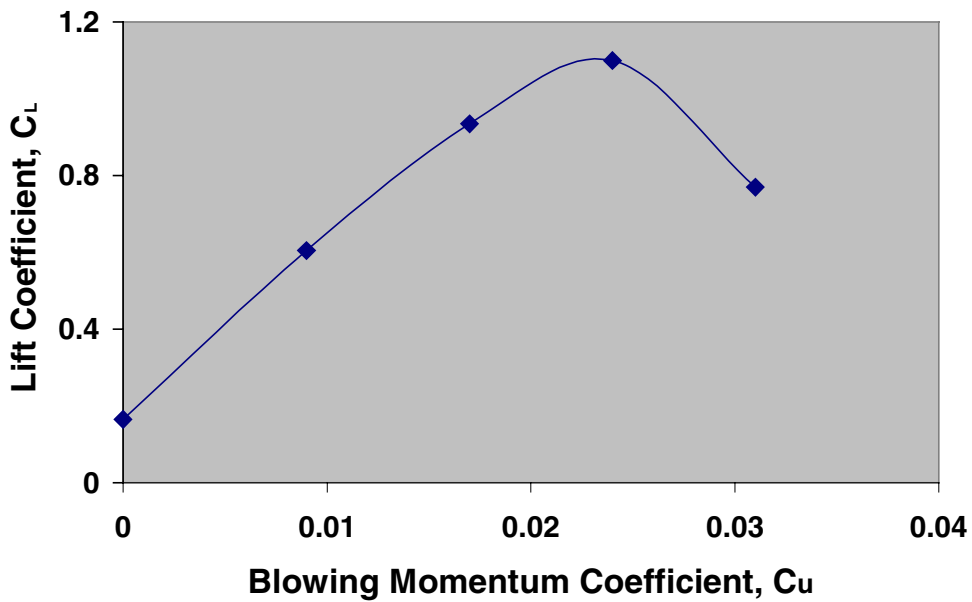


Figure 7 Measured Lift Coefficient

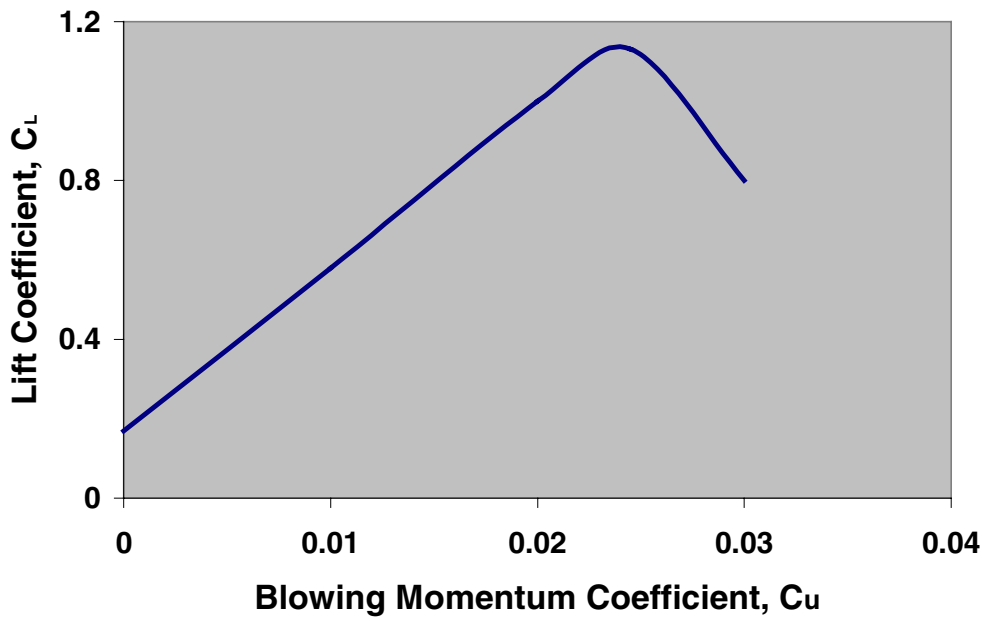
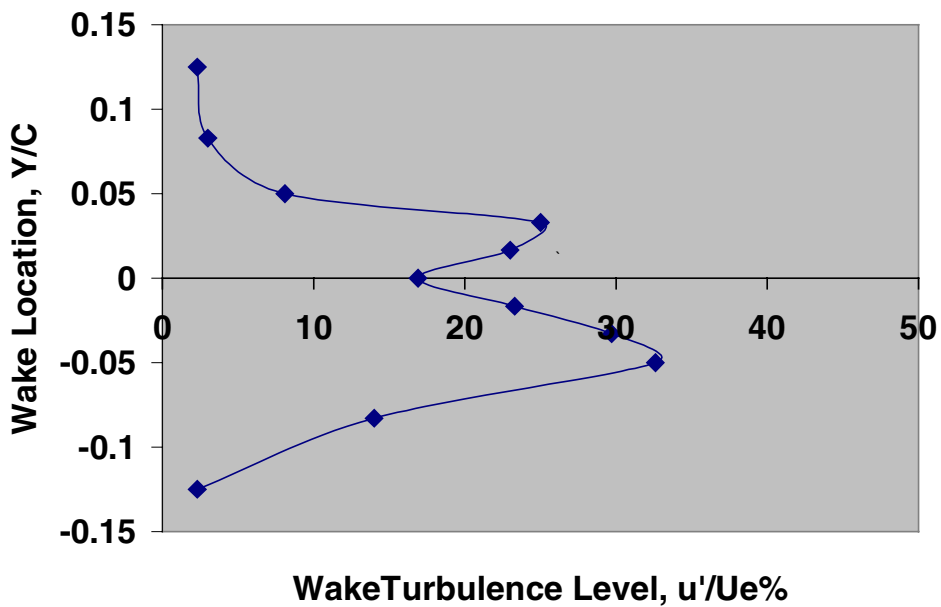
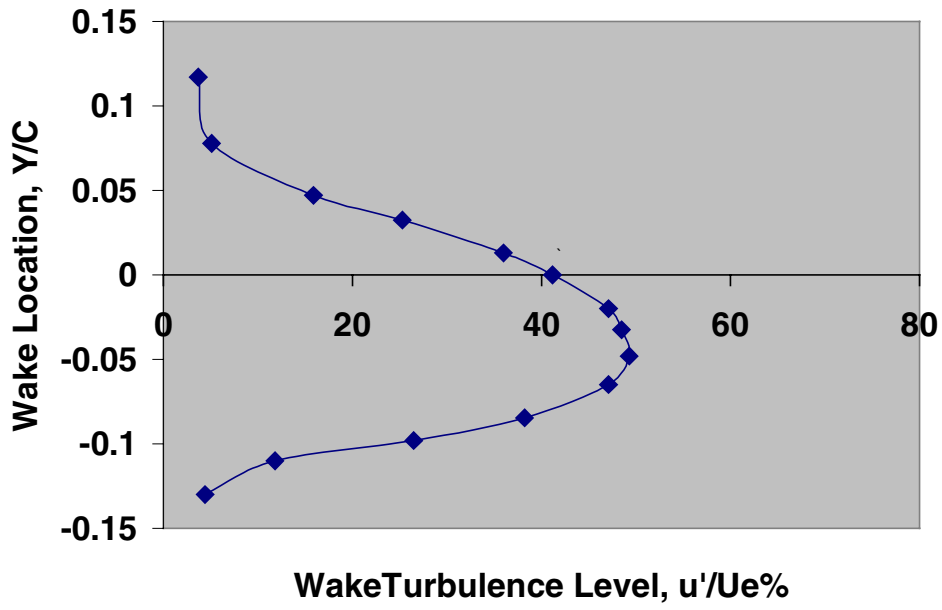


Figure 8 Wake Turbulence Profile  
 $C_u = 0, X/C = 0.17$



**Figure 9 Wake Turbulence Profile,  
 $C_u = 0.009$ ,  $X/C = 0.17$**







# The Application of Pneumatic Aerodynamic Technology to Improve Performance and Control of Advanced Automotive Vehicles

Robert J. Englar, Principal Research Engineer

Georgia Tech Research Institute; Aerospace,

Transportation and Advanced Systems Lab,

Atlanta, Georgia 30332-0844

## Abstract

Blown aircraft aerodynamic technology has been developed and applied to entrain separated flow fields, significantly reduce drag, and increase the fuel economy of Heavy Vehicles and Sports Utility Vehicles (SUVs). These aerodynamic improvements also lead to increases in stability, control, braking, and traction, thus enhancing safety of operation. Wind-tunnel results demonstrating model Heavy Vehicle drag coefficient reductions of up to 84% due to blowing and related configuration improvement are reviewed herein. Tunnel data confirming the elimination of directional instability due to side-winds plus generation of aerodynamic forces which are not currently used for control of large vehicles are also shown. These data have guided the design and modification of a full-scale road-test vehicle. Initial confirmation road test results of this patented concept on the modified blown HV rig are presented. An SAE Type-II Fuel Economy test was also conducted. Here, various blowing configurations were tested, and results were compared to a baseline reference tractor-trailer to confirm the improved fuel economy due to blowing. Full-scale wind-tunnel tests of this pneumatic technology applied to a GM Suburban SUV were also conducted, and the positive effects of blowing for drag reduction, vehicle aerodynamic stability, and operational safety are shown. Comparative results presented include wind-tunnel data for both unblown and blown configurations, full-scale blowing and fuel-economy data, and comparisons to smaller-scale blown Pneumatic Heavy Vehicle experimental results.

## Nomenclature

A	Vehicle frontal area
b	Vehicle width
c	Vehicle total length = tractor + trailer + gap
$C_D$	Drag coefficient=Drag/(qA)
$C_L$	Lift coefficient=Lift/(qA)
$C_M$	Pitching moment coefficient=Pitching moment/(qAc)
$C_N$	Yawing moment coefficient =Yawing moment/(qAb)
$C_Y$	Side force coefficient=Side force/(qA)
$C_\mu$	Jet momentum coefficient= $mV_j/(qA)$
h	Blowing jet slot height
m	Measured jet mass flow
q	Freestream dynamic pressure
$Re$	Freestream Reynolds number, based on vehicle length c

- V Freestream velocity
- $V_j$  Isentropic jet velocity
- $\rho$  Freestream or jet density
- $\psi$  Yaw (side wind) angle

## Introduction

Considerable interest has arisen recently in improving the aerodynamics of Heavy Vehicles (HVs) as a means of improving their operating costs, performance and safety. As Reference 1 from 2002 discusses, for a typical US tractor-trailer rig logging 175,000 miles a year at a fuel price of \$1.50/gallon, that yearly fuel costs could average over \$40,000 (\$29,000 if only 125,000 miles logged). Thus even a 5-10% increase in fuel economy could be meaningful. While devices which can reduce the HV's drag coefficient can significantly improve the fuel economy, it is also desirable that additional capabilities result from improved aerodynamics. These could include: increased stability (both lateral and directional); reduction in side-wind sensitivity; reduction in splash and spray; and improved

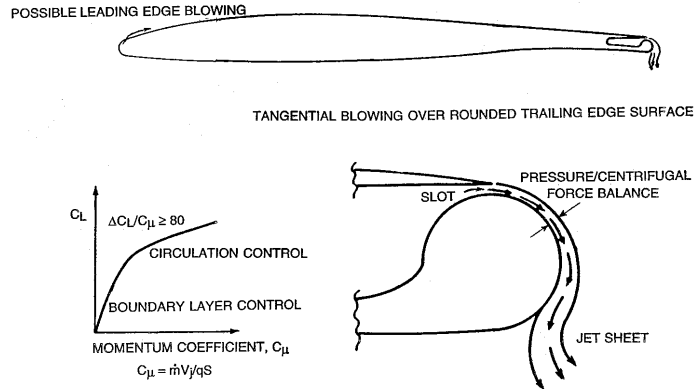


**Figure 1 - Basics of Circulation Control Pneumatic Aerodynamics on a Simple 2-D Airfoil**

traction plus aerodynamic braking. One could also include an aerodynamic means to reduce tire rolling resistance. Any such devices being considered for these applications also should be simple and robust, contain few or no moving parts, not be hampered by weather, and not increase vehicle weight or external dimensions. This paper discusses pneumatic aerodynamic devices based on the use of Circulation Control Aerodynamics which thus possess many of these desirable characteristics. These are currently under development at Georgia Tech Research Institute (GTRI) for the DOE Office of Heavy Vehicle Technology. First described below will be the basics of pneumatic aerodynamics and application to Heavy Vehicles, and then details of wind-tunnel and full-scale programs conducted, their results, and possible future applications.

### Basics Of Pneumatic Circulation Control Aerodynamics

GTRI researchers have been involved for a number of years in the development of pneumatic (pressurized air blowing) concepts to yield efficient yet mechanically simple means to control, augment or reduce the aerodynamic forces and moments acting on aircraft. This was detailed in References 2, 3, and 4 among others, but will be summarized

briefly to familiarize the reader with this technology. Figure 1 shows the basic pneumatic concept, which has become known as Circulation Control (CC) aerodynamics. Here, an airfoil's conventional mechanical trailing-edge device has been replaced with a fixed curved surface and a tangential slot ejecting a jet sheet over that surface. That jet remains attached to the curved surface by a balance between sub-ambient static pressure on the surface and centrifugal force (the so-called Coanda Effect, Reference 4). This entrains the external flow field to follow the curving jet, and thus enhances the circulation around the airfoil and the aerodynamic forces produced by it. The governing parameter is not angle of attack, but rather the blowing momentum coefficient:

$$C_{\mu} = m V_j / (q S)$$

where  $m$  is the jet mass flow,  $V_j$  the isentropic jet velocity,  $S$  is a reference wing area (or frontal area  $A$  for a ground vehicle) and  $q$  is the freestream dynamic pressure ( $q = 0.5 \rho V^2$ , with  $\rho$  being the freestream density). At lower  $C_{\mu}$  values, augmentation of the aerodynamic lift by a factor of  $\Delta C_l / C_{\mu} = 80$  has been recorded (Ref. 4), representing an 8000% return on the invested jet momentum (which in a physical sense is also equal to the jet thrust). Familiarity with blown aerodynamic systems will remind the reader that this is quite extraordinary: thrust-deflecting Vertical Take-Off and Landing (VTOL) aircraft are fortunate if they recover anything near 100% of the engine thrust expended for vertical lift (which must exceed weight), with very little, if any, augmentation of aerodynamic lift occurring.



Flight Test Results:

140% Increase in Usable Lift Coefficient,  $C_L$

30-35% Reduction in Takeoff & Approach Speeds

60-65% Reduction in Takeoff & Approach Ground Rolls

**Figure 2- A-6/CCW STOL Flight Test Confirming Pneumatic Devices for Aerodynamic Force Augmentation**

It is because of this high return on blowing, or conversely, because of the very low required blowing input and associated power required to achieve a desired lift, that Circulation Control airfoils appear very promising for a number of applications. The A-6/CC Wing Short Take Off & Landing (STOL) flight demonstrator aircraft (Figure 2 and Ref. 2)

showed the STOL performance listed, and also suggested capabilities very useful to ground vehicles: during short takeoff, it demonstrated high lift **with reduced drag**, while in the approach/landing mode, very high lift **with high drag** was shown.

These advantages led to the application of this pneumatic concept to improve the aerodynamics of an already streamlined car model (Reference 5). The resulting large jet turning over the curved rear of this vehicle is shown in Figure 3. Significant but distinctly different trends were observed during testing, depending upon which portion of the tangential slot located along the trunk break line was blown. Blowing the full-width slot produced the large jet turning shown by the multi-color tuft in Figure 3, with drag increases of greater than 70%, showing potential for pneumatic aerodynamic braking. Blowing only the outside segments of the slot weakened the corner vortex rollup, attached separated flow, lessened aft suction, and reduced drag by as much as 35%. Blowing this aft slot also yielded a lift increase of 170%. One can envision a similar slot applied to the lower rear surface that could instead yield negative lift (positive down force). This concept has been patented by GTRI and verified by a similar installation on a wind-tunnel model of a European Formula 1 race car (see Reference 6).

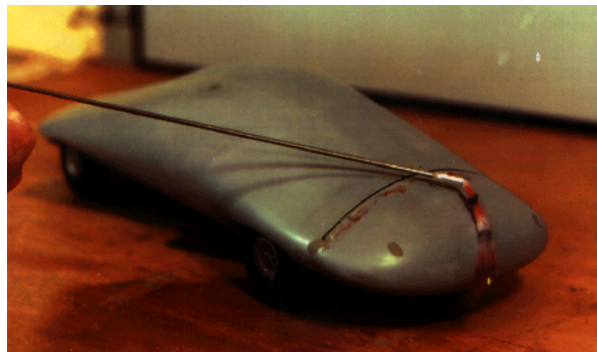


Figure 3- Pneumatic Technology on a Streamlined Car Model; Aft View, Showing Blown Jet Turning

#### DOE PNEUMATIC HEAVY VEHICLE MODEL TEST RESULTS

Based on the above results, a research program was initiated at GTRI for the Department of Energy's Office of Heavy Vehicle Technologies. The goal was to apply this pneumatic technology to tractor-trailer configurations to develop an experimental proof-of-concept evaluation leading to an on-the-road demonstration of an operating Pneumatic Heavy Vehicle (PHV). Figure 4 shows a schematic of a generic PHV with tangential blowing slots on each of the trailer's 4 curved aft edges plus blowing on the rounded upper leading edge of the trailer. Early portions of that effort, including a preliminary feasibility study and design of baseline and pneumatic wind-tunnel configurations, are detailed in Reference 6.

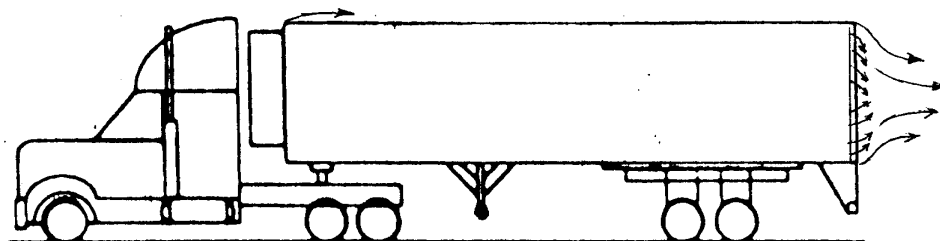


Figure 4 – Schematic of Application of GTRI Pneumatic Technology to Heavy Vehicle Trailer, Showing 4 Aft Blowing Slots and Upper Leading-edge Blowing Slot

## Wind-Tunnel Evaluations Of Baseline Unblown Heavy Vehicle Models

To develop a representative Pneumatic Heavy Vehicle configuration prior to full-scale testing, initial baseline wind-tunnel testing was conducted, which was then followed by several phases of blown test configurations. For this, an existing generic Heavy Vehicle configuration, the Ground Transportation Systems (GTS) vehicle of Reference 7 was used. The model is shown in Figure 5 before the blowing modifications were installed. It is actually representative of a faired cab-over-engine HV based on a Penske racing team car carrier, and is relatively independent of the numerous and varying cab roof fairings employed on a number of current Heavy Vehicles. Tests of this unblown model configuration did, however, demonstrate the importance of cab/trailer gap and fairing treatments. These configurations were tested in the GTRI Model Test Facility research tunnel (Refs. 6 and 8) and showed some significant drag reductions due to changes in the unblown geometry. Figure 5 shows drag reductions of up to 25% below a low-cab full-open-gap vehicle when the gap was eliminated (filled in) and the cab top was even with the trailer top (trailer leading and trailing edges are square here). An additional 15% reduction was confirmed with a round trailer leading edge (LE) facing into the open gap and a round trailing edge (TE) on the trailer (this is the unblown Pneumatic HV). These data were taken at a typical tunnel speed of 70 mph. Also very significant is the tremendous increase in  $C_D$  in Figure 6 (more than a doubling is seen) due to a side wind acting at a yaw angle on the HV. (In all of the drag data shown herein,  $C_D$  is based on projected frontal area of the vehicle,  $A$ , including the wheels).

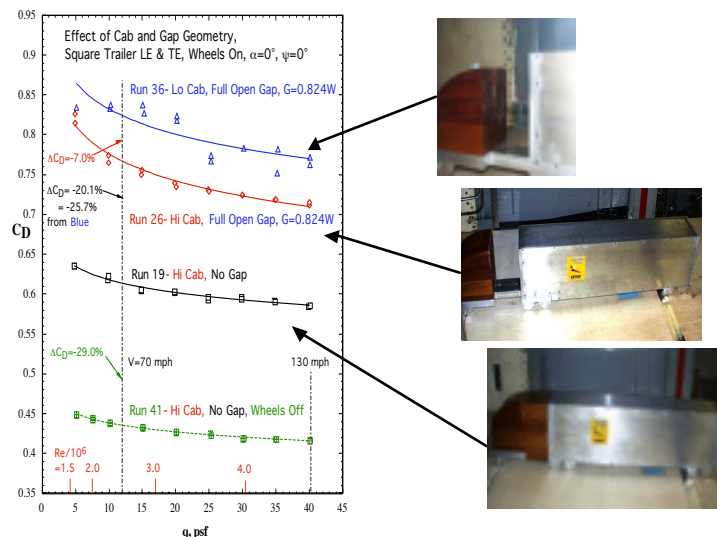


Figure 5-Test Results for Unblown HV Models, Showing Effect of Cab Height, Gap, Wheels and Reynolds Number

## Wind-Tunnel Evaluations Of Blown HV Configurations

Based on the above **unblown** configurations with reduced drag, additional wind tunnel tests were conducted to evaluate aerodynamic improvements resulting from **blown** configurations. Details of these investigations are presented in Reference 8. Unless otherwise noted, the blowing variations were run at tunnel (vehicle) wind speeds of

approximately 70-71 mph (dynamic pressure  $q=11.86$  psf and Reynolds number =  $2.5 \times 10^6$ , based on total tractor + trailer length).

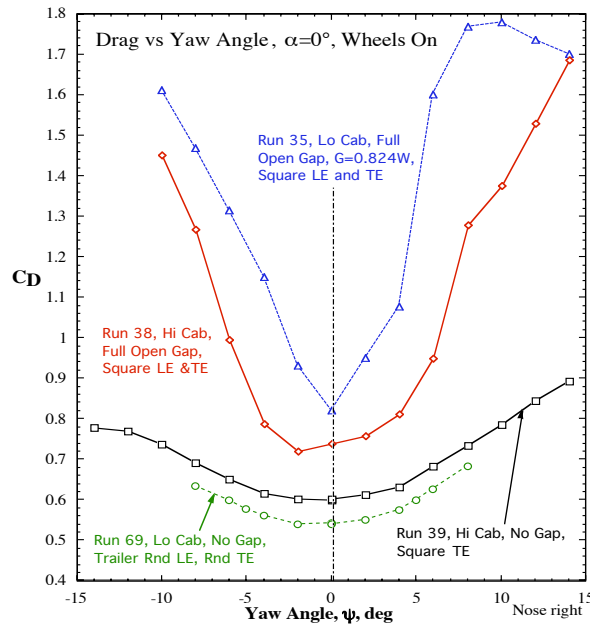


Figure 6- Effects of Side Wind on Drag for Various Unblown HV Configurations

**Drag Reductions (for Fuel Economy) or Drag Increases (for Braking & Stability)** - The blowing slot heights at each aft edge of the trailer could be varied and tested either unblown or blown in any combination of the 4, or even with leading edge slots on the trailer front face also blown. Flow visualization tufts in Fig. 7 show jet turning of  $90^\circ$  on all four aft corners, even the bottom slot blowing upwards. Figure 7 also shows the results of this jet turning on reducing or increasing aerodynamic drag by blowing various combinations of these aft slots. The combination of all 4 slots blowing together yielded the greatest drag reduction, more effective than blowing individual slots. Compared to the typical unblown baseline configuration from above (full gap between cab and trailer, square trailer leading edge and trailing edge, and cab fairing slightly lower than the trailer front) which produced a  $C_D = 0.824$  at this Reynolds number, the blown configuration reduced drag coefficient to 0.459 at  $C_{\mu} = 0.065$ . This is a 44%  $C_D$  reduction, and the internal plenum blowing pressure required was only 0.5 psig. A second blown configuration (labeled “ $90^\circ/30^\circ$  TE”) used less jet turning on the upper and lower surfaces to generate even greater drag reduction: at 0.5 psig,  $C_D$  was reduced by 47%, and at 1.0 psig ( $C_{\mu}=0.13$ ),  $C_D$  was reduced by 50%. These data are all for a smoothed bottom tractor-trailer model with low sides and half-cylinder simulated wheels.

Additional evaluation of the effectiveness of the blown configurations was made. The drag coefficient of the unblown baseline configuration above, but with the tractor-trailer gap filled in, is  $C_D = 0.627$  (not shown in Fig. 7). Addition in Figure 7 of the unblown pneumatic surfaces onto the trailer TE reduces  $C_D$  by 9.7%. Adding blowing at  $C_{\mu} = 0.065$  reduces that  $C_D$  by another 23.1%. This combination reduces  $C_D$  to 30.6% less than the square TE baseline having a smooth fairing filling in the gap.

When only the top slot, the bottom slot, or both of these slots were blown in the absence of the side jets, drag was initially reduced slightly, but then significantly increased with the addition of blowing. This represents an excellent aerodynamic braking capability to supplement the hydraulic brakes. Blowing efficiency is plotted in Figure 8, where  $\Delta C_D$  is an increment from the blowing-off value (negative  $\Delta C_D$  is reduced drag). Absolute values of  $\Delta C_D/C_{\mu}$  greater than 1.0 represent greater than 100% return on the input blowing  $C_{\mu}$ . It is seen that the 90°/30° 4-slotted configuration generates values as high as -5.50, representing 550% of the input blowing momentum recovered as drag reduction. This figure also shows the opposite trend as well, with up to 200% of the blowing momentum from top/bottom slots recovered as increased drag for braking. Obviously, these percentages will be modified when the power expended to compress the blowing air is included, but that will have to await a full-scale systems study.

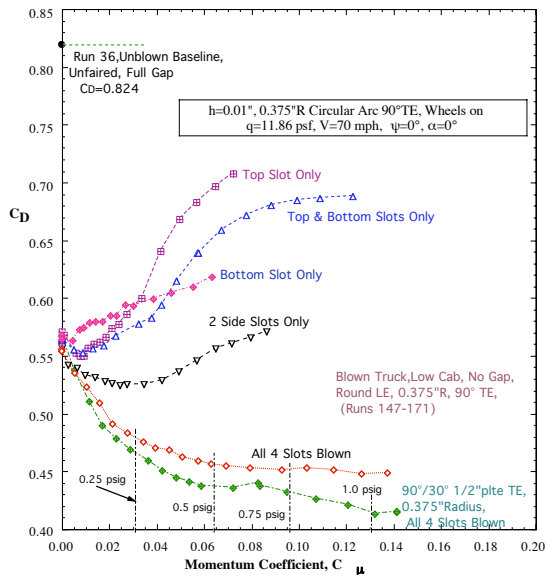


Figure 7 - Drag Reduction or Augmentation on Blown Trailer with 90° Turning Surfaces, plus Flow Visualization of Jet Turning

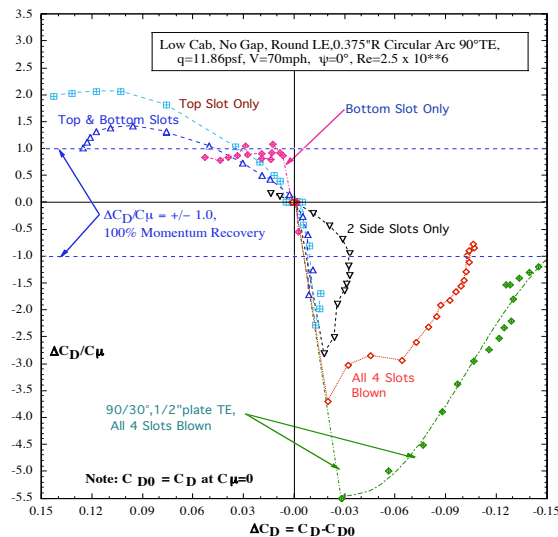
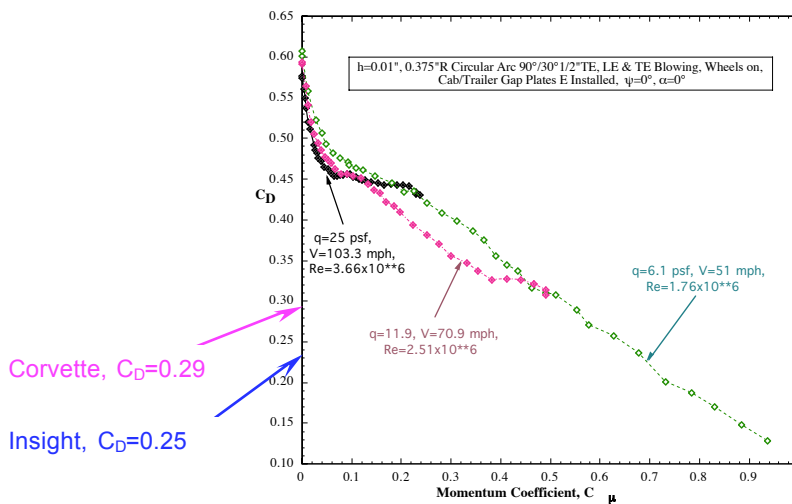


Figure 8 - Blowing Efficiency & Drag Increments due to Blowing Slot Configuration



Should additional air be available from an onboard source such as an existing turbocharger or an electric blower, additional drag reduction is possible, as shown in Figure 9. Drag coefficients of less than 0.30 are shown for faired blown HV configurations. This is in the arena of streamlined sports cars. The drag coefficient of a 1999 Corvette coupe is  $C_D = 0.29$ . Figure 9, originally intended to show that the drag curves tend to converge onto one slope independent of Reynolds number, also shows a measured drag coefficient of 0.13 for the Pneumatic Heavy Vehicle model at increased  $C_{\mu}$ . This is about half the drag coefficient value of the Corvette or a Honda Insight hybrid ( $C_D = 0.25$ ). Even though not achieved in the most efficient blowing operation range, this is an 84% drag reduction compared to the unblown baseline configuration. Note that the tractor cab in Figure 9 has “gap plates” (or fairing extensions) instead of the full “No Gap” fairing of Figure 8, and is thus much closer to an actual tractor/trailer configuration. It also has blowing on the trailer top leading edge. Figure 10 shows this alternative means of improving upon the gap problem.



**Figure 9 - Reynolds Number Effects & Increased Blowing Values, plus Leading-edge Blowing & Gap Plates**

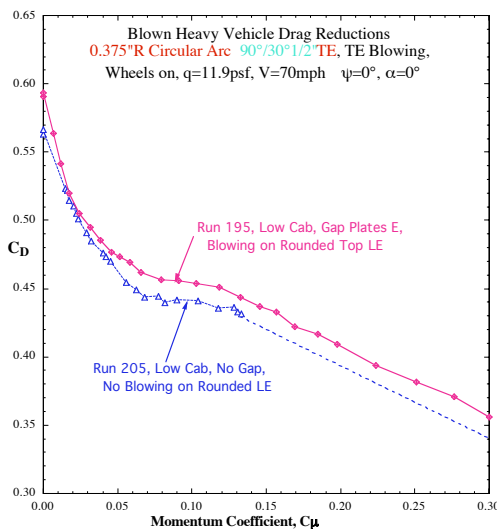


**Figure 10 – Side Plates and Trailer Top Blowing: a Practical Solution to the Cab Gap Problem**

Note, when comparing these data to other experiments which have been conducted by other researchers on similar GTS models, that these GTRI data above and below include simulated wheels which, as Figure 5 shows, add about  $\Delta C_D = 0.18$  to non-wheeled vehicles'  $C_D$  values, perhaps more, depending on how well the tunnel ground effects are treated experimentally. GTRI's measured data are recorded using test-section tangential floor blowing to eliminate the floor boundary-layer interference, as discussed in References 5, 6, and 8.

**Stability and Control** – Strong directional instability can be experienced by Heavy Vehicles at yaw angles (i.e., when experiencing a side wind) because of large side forces on their flat-sided trailers, Figure 11. This yaw sensitivity is confirmed by the unblown ( $C_{\mu} = 0$ ) yawing moment  $C_N$  shown, where yaw angle as small as  $-8^\circ$  produces a large unblown yawing moment coefficient of  $C_N = -2.0$ . [It should be noted here that this yawing moment is measured about the rigid model's midpoint at the ground, whereas on a real articulated tractor-trailer, it would be experienced at the tires of the individual units. However, comparisons of blowing on and off are being made for the same single HV unit, and apparent benefits should be valid]. Blowing only one side slot can easily correct this: with the nose straight ahead ( $\psi = 0^\circ$ ), blowing the left slot at  $C_{\mu} = 0.06$  yields the equivalent opposite yawing moment ( $C_N = +2.0$ ). With the nose yawed left (for example,  $\psi = -8^\circ$ ), blowing at  $C_{\mu} = 0.06$  returns the unstable yawing moment to  $C_N = 0.0$ . Then, increasing the blowing a bit more causes the nose to yaw in the opposite direction, to the right. The opportunity for a no-moving-part quick-response aerodynamic control system is apparent.

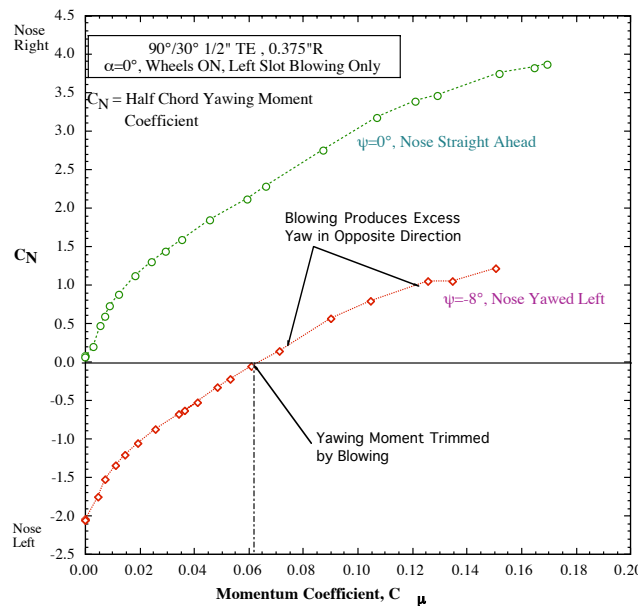


**Figure 11- Directional Control Capability Provided by HV Configuration with Left Rear Slot Blowing Only**

### Pneumatic Heavy Vehicle Fuel Economy Testing

The above model tests led to the conclusion that a full-scale proof-of-concept test series should be conducted on a Pneumatic HV test rig to determine if the above tunnel

results would also occur on the road. Based on the above wind-tunnel results, GTRI team member prototype shop Novatek, Inc. designed and fabricated the PHV blown test trailer, including blowers, drive motors, control systems and instrumentation. This configuration is shown in Figure 12 in comparison to a stock (reference) Great Dane trailer. Blown tufts confirming jet turning of 90° around the right-side trailing-edge curved pneumatic surface are shown in Figure 13.



Figure 12- PHV Pneumatic Trailer (left) and Baseline Reference Unmodified Trailer (right)



Figure 13 Right Rear Corner View, Looking Up, with Tufts Showing 90° Jet Turning

## Tuning Tests

Test vehicle fabrication and assembly were completed at GTRI and the modified trailer was then picked up by team member Volvo Trucks of North America and moved to its facility in Greensboro, NC. Here two initial Tuning Tests were conducted (Reference 10 and Figure 14). Figure 15 shows a rear view of the pneumatic trailer with the tufts confirming on-road flow turning. These tests verified the test equipment and data system operations, and indicated unofficial fuel economy increases from blowing of up to **15.3%** over the baseline trailer when on an open highway, rather than on a test track.

## Full-Scale PHV On-Track Fuel Economy Tests

On-track testing of the PHV **Test** vehicle (tractor and modified trailer) was conducted at the Transportation Research Center (TRC) test track in East Liberty, OH, along with a

**Control** vehicle (a stock Volvo/ Great Dane rig). Figure 16 shows these two vehicles while in a pit lane fuel station at the 7.5-mile banked test track at TRC. SAE Type-II fuel economy runs were conducted by the TRC/GTRI/Volvo/Novatek team members in strict accordance with SAE test procedures (as specified in SAE J1321, Oct 1986). During these tests, a total of 59 runs was made for the 6 configurations evaluated, each at 3 different speeds (55, 65, and 75 mph) and with each run covering 6 laps (45 miles) of the TRC test track. (See References 9, 11, 12, and 13 for more details). Figure 17 shows the pneumatic test tractor-trailer at speed on the TRC track.

The six sets of fuel economy runs were made at different blowing rates, including zero blowing. This allowed reference comparisons to be made after the pneumatic test trailer was re-configured into the baseline trailer and then tested to provide reference fuel economy



**Figure 14- On-road Pneumatic Heavy Vehicle Tuning Test near Volvo Facility In North Carolina**



**Figure 15- On-road PHV Test Vehicle Rear View with Jets Blowing and Tufts Turning**





**Figure 16- Test and Control Vehicles in Pits at TRC Test Track**



**Figure 17- PHV Test Vehicle on Track at 75 mph**

of the standard vehicle (all fuel economy data achieved with the other test configurations were compared to this one to determine percent fuel efficiency increase, %FEI). Figure 18 shows %FEI as a function of blowing coefficient,  $C_{\mu}$ . The %FEI improvements shown range from 4% to 5% (5% to 6% if the 1% error band is included) above the fuel economy of the baseline standard tractor-trailer, but these are seen to reduce somewhat as blowing increases to values beyond  $C_{\mu} = 0.02 - 0.03$ . Whereas responses heard from typical HV users indicate this 5-6%FEI to be quite respectable, it is less than we had anticipated based on our smaller-scale wind-tunnel tests (Refs. 6 and 8). Figure 19 compares this on-track data to the predicted fuel efficiency increase that we had expected from the drag reductions of the blown configurations. Whereas the lower blowing values were nearing 70-80% of the expected values, at greater blowing the payoff was reduced. The test team of GTRI, Novatek, and American Trucking Associations identified suspected reasons for this, and we then conducted an experimental test program to confirm these, as is discussed below.

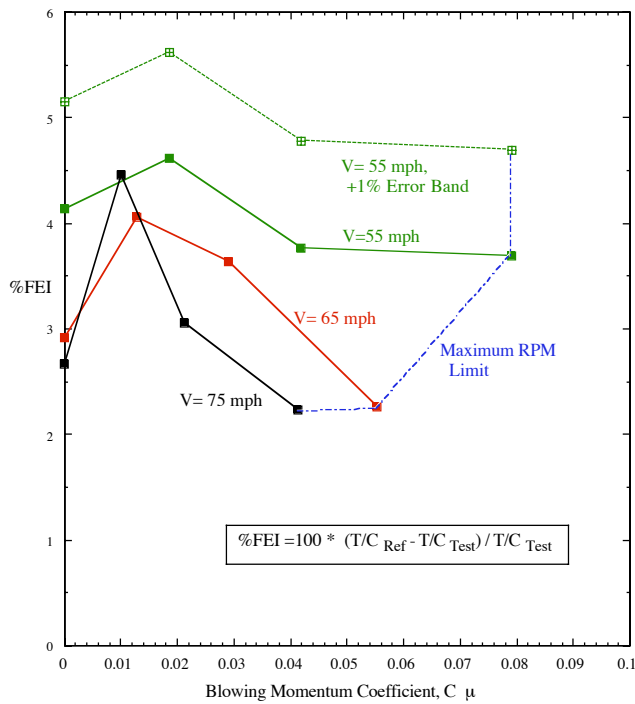


Figure 18- Measured PHV Fuel Economy Improvement, With 4 Trailer Slots Blowing

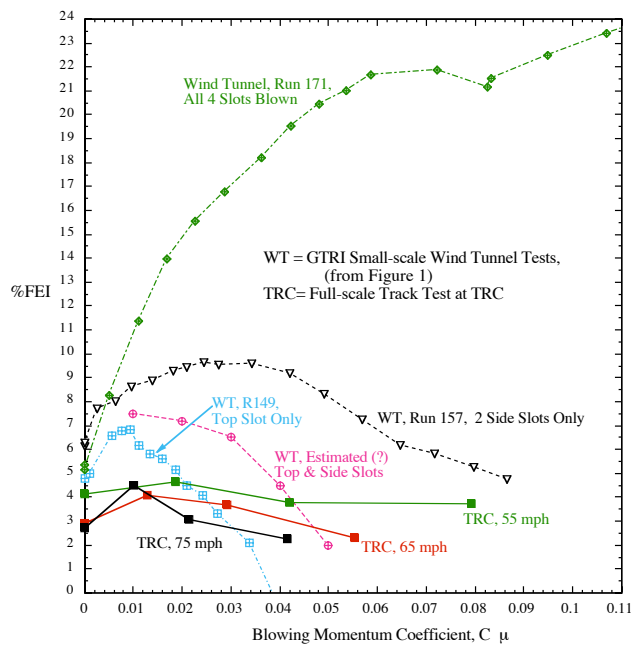


Figure 19- Comparison of Wind-tunnel Results to TRC Track Results (from Reference 11)

### Updated Wind Tunnel Evaluations

A new series of wind-tunnel runs was made on the 0.065-scale PHV model. We began with the best blown configuration from Figure 7 (now seen as Run 205 in Fig. 20), and then we sequentially downgraded the model by making changes suspected of being detrimental

when installed on the road-test truck. It was the intent of this new wind-tunnel program to determine if the geometric differences between the full-scale test vehicle and the wind-tunnel model produced the aerodynamic and fuel consumption differences discussed above. Figure 20 shows that as the configurations approached the representation of the full-scale test vehicle (Run 239), both blown and unblown drag increased. These tests are further detailed in References 14 and 15. Figure 21 compares the percentage drag reduction due to each configuration change, while Figure 22 shows the predicted change in percent Fuel Efficiency Increase (%FEI) due to each. Major problems on the full-scale rig were the lower surface fairing with aft facing step in front of the bottom blowing slot and the partial gap between tractor and trailer. A comparison in Figure 22 of Run 239 (model most like the blown full-scale test vehicle) with Run 36 (most like the standard tractor-trailer vehicle) shows that only a 2% FEI occurs for the unblown vehicle and only 7% for the blown one. This confirms the trends of Figures 18 and 19, and explains the causes of the less-than-expected track-test results. We have since conducted further testing to improve the final PHV configurations in anticipation of a second on-road fuel economy test at TRC. Note from Figure 22 that if we convert the full-scale PHV test vehicle to a blown configuration much more like the one in Run 205, we can expect Fuel Efficiency Increases of 16% unblown and 23% blown, which will be very significant results. That plan to reconfigure the test truck and retest is now underway.

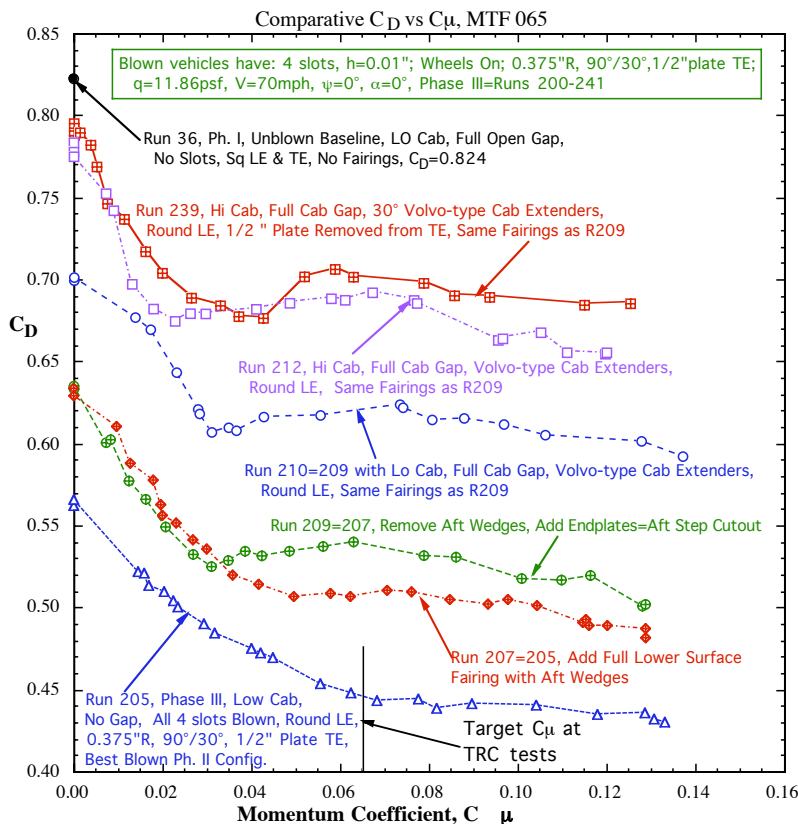


Figure 20- Updated Wind-tunnel Test Results: Drag Change with Configuration Variation and with Variations in Blowing



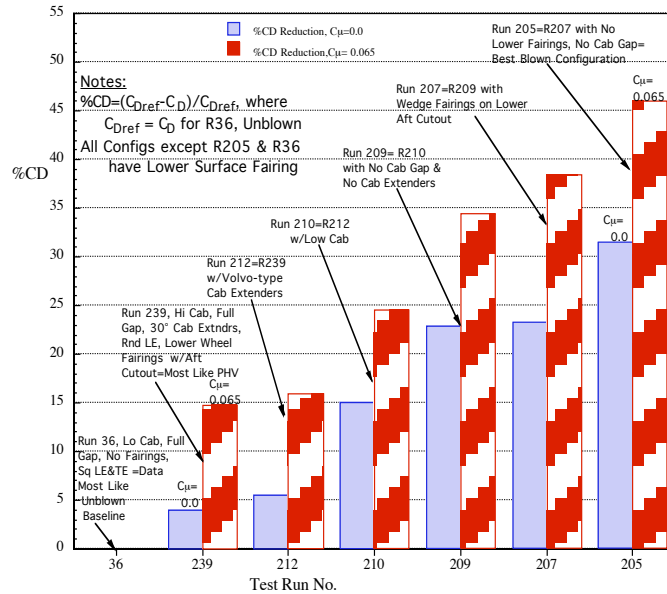


Figure 21- GTRI Model Drag Reductions Relative to Run 36 (Configuration Closest to Baseline HV); (Positive  $\Delta C_D$  here is drag reduction)

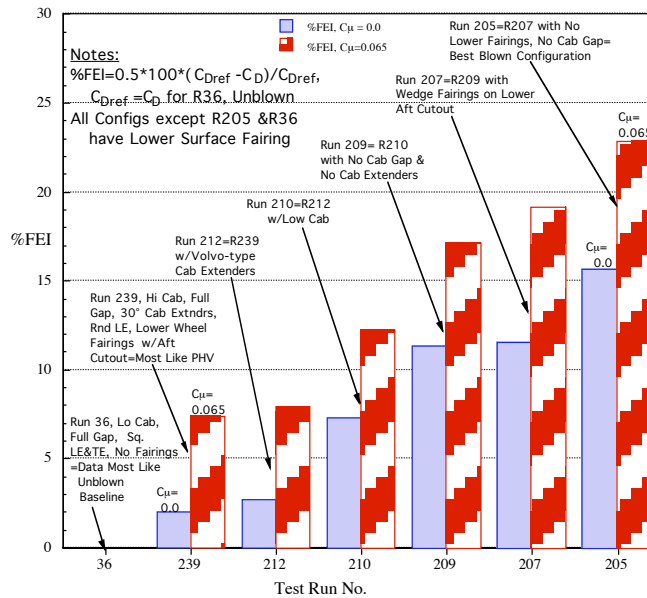


Fig. 22- Equivalent Fuel Efficiency Increase (%FEI) Relative to Run 36

### Pneumatic Sport Utility Vehicles (PSUVs)

An analysis of vehicle fuel usage rates in the United States (Figure 23 and Refs. 16 and 17) shows that as of about 2001, SUVs and light trucks consumed more total fuel in the US than either automobiles or HVs. It thus seemed quite relevant to determine if this pneumatic technology would be as beneficial to SUVs as to HVs, perhaps even more so in the total picture. To prepare for a full-scale evaluation of the pneumatic concept applied to a

Sports Utility Vehicle, we acquired the use of the Georgia Tech FutureTruck vehicle, a 2000 Chevrolet Suburban SUV. Preliminary wind tunnel testing of the conventional SUV was first conducted to determine baseline aerodynamic characteristics and flow separation point locations (Figures 24 and 25). The unmodified baseline GM Suburban SUV was installed on the 6-component balance of the Lockheed 16' x 23' subsonic wind tunnel in Marietta, GA. Figure 26 shows aerodynamic force and moment variations for the unblown vehicle as functions of yaw angle, and confirms that side winds can have a significant effect on the performance and stability of these large SUVs (much like the HVs).

The conventional Suburban was then modified into the Pneumatic SUV configuration for the blowing tests. We had received an additional aft door assembly for the Suburban, donated by the GM Technical Center. The modification was conducted at the prototype shop

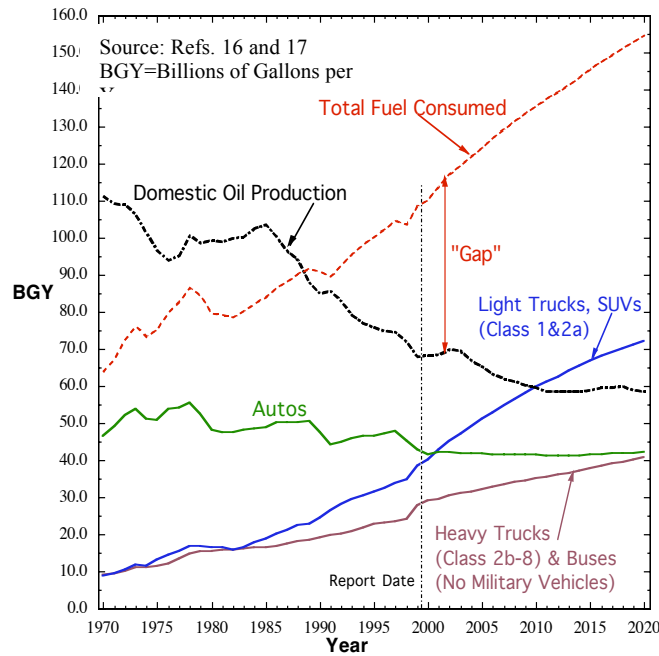


Figure 23 - Highway Energy Usage Comparisons (Billions of Gallons per Year) by Vehicle Type



Figure 24- GM Suburban Test Vehicle Undergoing Smoke Flow Visualization in the Lockheed 16' x 23' Wind Tunnel Test Section



Figure 25- GM Suburban Test Vehicle Undergoing Tuft Flow Visualization in the Lockheed Wind Tunnel

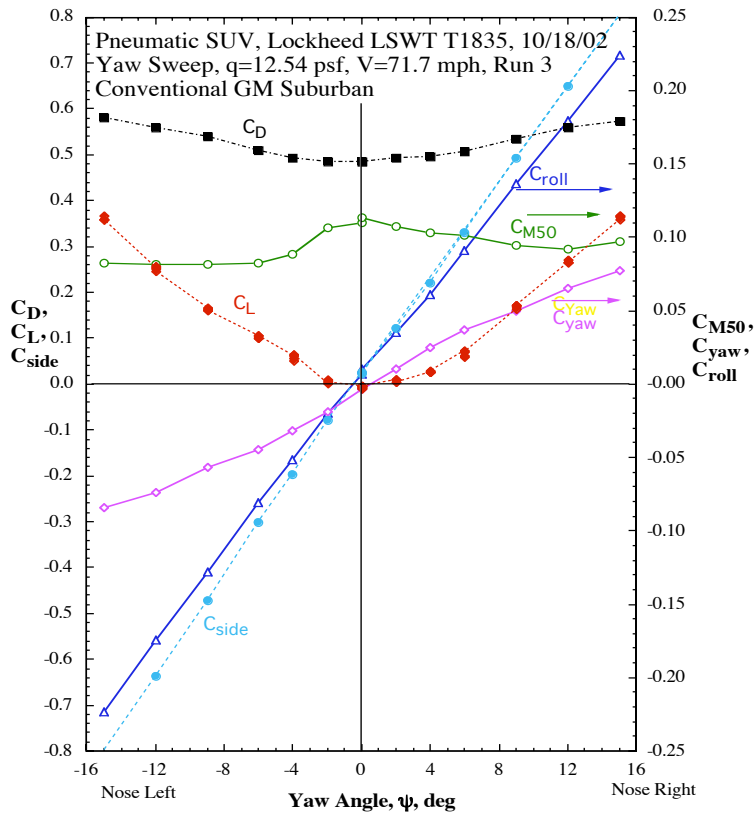


Figure 26- Resulting Aero Forces and Moments as Functions of Yaw Angle for Baseline Suburban

of our team member Novatek, Inc. in Smyrna, GA. Since it was impractical to cut away the rear sheet metal and door structure of the Suburban, we simply added blowing plenums, slots and turning surfaces onto the outside of the donated door. This modification installed on the vehicle is shown in the Lockheed Low Speed Wind Tunnel in Figure 27. The blowing slots were adjustable and the trailing-edge jet turning angles could be changed. Blowing coefficient was variable, and mass flows, pressures and jet velocities were measured to enable on-line calculation and setting of  $C_{\mu}$ .



Figure 27- Modified PSUV Blown Test Vehicle in the Lockheed Low Speed Wind Tunnel

## PSUV Test Results

Flow visualizations taken with blowing activated on the pneumatic vehicle showed significant attachment of flow over the new curved aft surfaces and a contracting of the jet wake behind the vehicle. The wind-on, blowing-on data showed different behaviors for the different trailing-edge configurations. Greater trailing-edge turning-surface angle produced greater jet turning but also greater suction on these trailing edges, the latter causing an incremental drag force. The resulting total drag is shown in Figure 28 for four different blowing configurations. Notice that for some configurations, initial drag reduction reached a minimum point, followed by drag increase with higher  $C_{\mu}$ . This drag reduction at lower blowing is on the order of 3 to 4.15 times the input blowing coefficient, representing as much as a 415% return on the jet momentum invested. Note that when increased blowing yields a rise in drag for some of the configurations, this represents an opportunity for an aerodynamic braking system. What is needed, of course, is an onboard control system to switch from drag reduction to braking if requested by the driver. Note also that the configuration with a  $45^{\circ}$  turning surface on all exposed trailing edges continued to reduce drag with increased blowing, although at a lesser rate of reduction. Also, the blowing-off drag coefficient for these non-optimized pneumatic configurations was the same as that of the stock reference Suburban tested earlier, indicating no blowing-off drag penalty for installing this system on a typical SUV.

An additional benefit of the blowing system is its ability to provide increased safety of operation. Aerodynamic braking was mentioned above, but Figure 29 shows an additional strong potential. To counteract the adverse effects of side winds on both yawing and rolling moments shown in Figure 26, we tested blowing of only one side slot, the left side. In Figure 26, the baseline SUV is directionally unstable (for instance, nose-left yaw produces nose-left negative yawing moment, which tends to yaw the vehicle more), but blowing on the left side produces an aft aerodynamic side force to the left and a restoring yawing moment that returns the SUV's stability. Figure 29 shows the amount of left-side blowing required to eliminate the destabilizing yawing moment at each of 3 side-wind angles,  $\psi$ . In each case, blowing at a slightly higher rate produced yaw in the opposite direction, so that the vehicle's stability in either direction could be controlled by varying blowing alone.

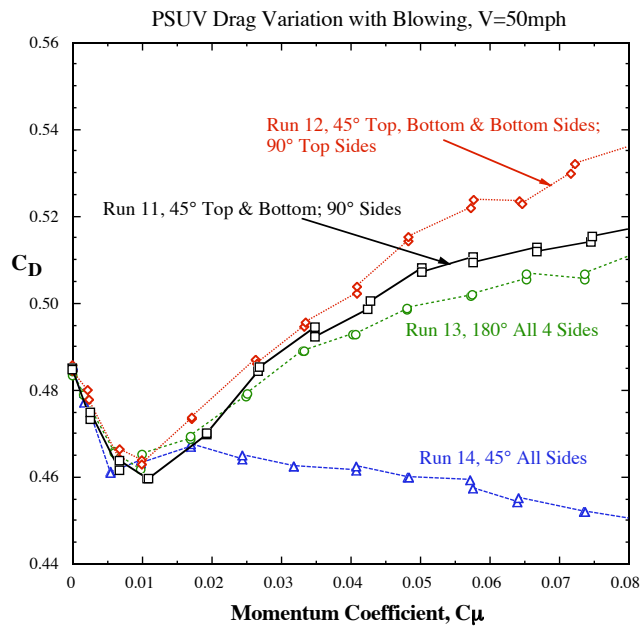


Figure 28- PSUV Drag Coefficient Changes with Varying  $C_\mu$

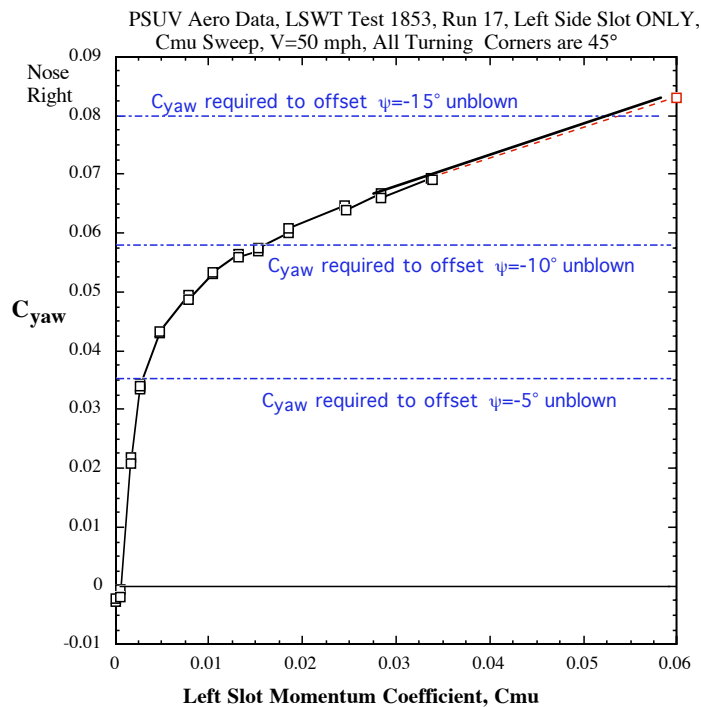


Figure 29- Yawing Moment Control by Blowing the Left Side Slot Only

It is to be noted from the above that we have not yet achieved the optimum configuration to maximize drag reduction and yawing moment generation while requiring minimum blowing input, but we have otherwise verified that blowing on SUVs can be a powerful means to reduce or increase drag as needed, and to increase vehicle stability, all with no external moving parts.

In a related application, GTRI and Novatek are also currently developing a patented aerodynamic heat exchanger that is based on these pneumatic principles (Refs. 18 and 19). This can be combined with the above devices to further reduce vehicle drag by reducing the drag associated with the conventional vertical radiator and related cooling system, while also adding favorable aerodynamic and control characteristics to the vehicle.

### **Conclusions**

Under DOE-sponsored research programs, GTRI and its teammates on the DOE Pneumatic Heavy Vehicle project have completed experimental investigations to confirm the use of pneumatic aerodynamics on these vehicles. We have verified these capabilities by designing, fabricating, and testing small-scale PHV models in 3 separate wind-tunnel tests; and by designing, fabricating and conducting 3 road or track tests of a full-scale Pneumatic Heavy Vehicle demonstrator. We have also conducted full-scale wind-tunnel tests of this technology applied to a typical Sports Utility Vehicle. It has thus been verified that these blowing concepts can: reduce aerodynamic drag; favorably modify other aerodynamic characteristics; and thus improve the performance, stability & control, handling qualities, safety of operation, and economics of both Heavy Vehicles and Sports Utility Vehicles. The very favorable capability of controlling all aerodynamic forces was shown for the PHV and Pneumatic SUV configurations, as was the ability of a no-external-moving-part pneumatic control system to restore directional stability by eliminating unstable yawing moment and providing counter-yaw in the opposite direction.

The above test programs and analyses have confirmed the following capabilities for pneumatic aerodynamics applied to Heavy Vehicles or Sports Utility Vehicles:

- Pneumatic devices, using one to four blowing slots and non-moving downstream jet turning surfaces on HVs and SUVs, have reduced drag up to 84% in tunnel tests. This is due to prevention of flow separation and increase in base pressure on the rear of the vehicle. Recent tunnel tests of a new PHV configuration soon to be tested full-scale indicate Fuel Efficiency Increase of up to approximately 23%, corresponding to about 46%  $C_D$  reduction at highway speeds.
- Specific blowing on only certain of the slots can cause a deliberate increase in drag which can be used for rapid-response aerodynamic braking.
- Specific blowing on only one side slot can cause a deliberate increase in side force and yawing moment to overcome the directional instability of these flat-sided vehicles caused by side winds and/or wind gusts.
- Blowing on only the top slot can cause a deliberate increase in lift to reduce tire rolling resistance and thus increase fuel economy; or blowing on the bottom slot only can deliberately increase down force and thus provide an increase in load on the wheels to increase both traction and braking.
- Because blowing can be quickly directed to whichever slot it is needed in, these devices provide a very-rapidly-responding pneumatic control system without external moving parts. Integrated with an onboard sensor and controls, a pneumatic system could thus

control all aerodynamic forces and moments acting on HVs and SUVs and increase operational safety.

- Pneumatic reduction of the vehicle's wake should lead to reduced spray and its effect on following vehicles, and thus also increase safety of operation.
- Low-pressure blowing required could be supplied from onboard sources such as a turbocharger or supercharger, or from an existing auxiliary engine, such as is currently used for HV refrigeration units.
- These pneumatic aerodynamic systems can be integrated with the patented GTRI/Novatek aerodynamic heat exchanger to further increase fuel economy from additional drag reduction and reduced radiator size requirements for cooling.
- Non-moving external components can yield an all-pneumatic system and components with very small (if any) component drag. These small-size aft trailer extensions should incur no vehicle length limitations.
- For safety, stability and/or economy, positive use can be made of aerodynamic forces/moments (lift, down force, side force, yaw, roll) which are currently not employed to influence Heavy Vehicle or SUV operation.

The relevance of the above results is shown by the DOE fuel usage data of Figure 23. It appears that it is time to approach this problem for Heavy Vehicles, Light Trucks, and SUVs in order to reduce the deficit ("gap") shown between US oil usage and domestic supply. The concepts demonstrated by these pneumatic vehicle results suggest that certain options are now available to do so. In addition to Heavy Vehicle and SUV application, the above results appear quite promising for other forms of automotive vehicles. Clearly, buses, motor homes, and trains are also prone to large drag values and directional stability issues due to aft flow separation and large vertical panels exposed to side winds. Of course, the application of improved blown aerodynamics to increase the performance, traction, braking and handling of race cars is a very related and promising subject.

### **Recommendations**

The above aerodynamic data confirm the Pneumatic Heavy Vehicle as a viable concept for improving the aerodynamic performance, economy, stability, handling and safety of operation of large tractor-trailers. The following recommendations are made to suggest a meaningful continuation of this program:

- Conduct additional wind-tunnel evaluations to further reduce the required blowing momentum needed from an air source onboard the tractor-trailer rig or SUV. Include slot height variation, improved blowing surface geometry, alternate jet turning surface geometry, pulsed blowing, or other innovative means.
- Feasibility studies are needed, where the above results are transferred to the HV and SUV industries and interactions occur with tractor, trailer, and SUV manufacturers, as



well as with engine manufacturers, turbocharger builders, or other possible air-supply specialists. Blowing sources and required compressor power must yet be considered.

- Conduct additional full-scale on-the-road demonstration and development of this technology with improved aerodynamic configurations

### **Acknowledgements**

The author wishes to acknowledge and thank Dr. Sidney Diamond, Dr. Jules Routbort, and Mr. Rogelio Sullivan of DOE for their continued support and encouragement of this work, as well as Mr. Victor Suski for the continued very valuable involvement of the American Trucking Associations. The technical assistance of Ken Burdges of Novatek, Inc., Skip Yeakel of Volvo, and Charlie Fetz of Great Dane is also greatly appreciated, as are the experimental efforts of GTRI Co-op students Graham Blaylock, Warren Lee, Chris Raabe, Erik Kabo, and Brian Corner from the Georgia Tech School of Aerospace Engineering, and researchers Dr. Rob Funk and Paul Habersham of GTRI.

### **References**

1. Hammache, M., M. Michaelian, and F. Browand, "Aerodynamic Forces on Truck Models, Including Two Trucks in Tandem," SAE 2002-01-0530.
2. Englar, R. J., et al, "Design of the Circulation Control Wing STOL Demonstrator Aircraft," AIAA 79-1842, August 1979.
3. Englar, R. J. and C. A. Applegate, "Circulation Control-A Bibliography of DTNSRDC Research and Selected Outside References (Jan 1969 to Dec 1983)," DTNSRDC Report 84/052, Sept., 1984.
4. Englar, R. J., "Circulation Control Aerodynamics: Blown Force and Moment Augmentation and Modification; Past, Present and Future," AIAA 2000-2541, June, 2000.
5. Englar, R. J., M. J. Smith, C. S. Niebur, and S. D. Gregory, "Development of Pneumatic Aerodynamic Concepts for Control of Lift, Drag, and Moments plus Lateral/Directional Stability of Automotive Vehicles," SAE Paper 960673.
6. Englar, Robert J., "Development of Pneumatic Aerodynamic Devices to Improve the Performance, Economy and Safety of Heavy Vehicles," SAE 2000-01-2208.
7. Gutierrez, W. T., B. Hassan, and W.H. Rutledge, "Aerodynamics Overview of the Ground Transportation Systems (GTS) Project for Heavy Vehicle Drag Reduction," SAE Paper 960906.
8. Englar, Robert J., "Advanced Aerodynamic Devices to Improve the Performance, Economics, Handling and Safety of Heavy Vehicles," SAE Paper 2001-01-2072, May 14-16, 2001.
9. Englar, R. J., "Development and Evaluation of Pneumatic Aerodynamic Devices To Improve the Performance, Economics, Stability and Safety of Heavy Vehicles," DOE Quarterly Progress Report No. 14, April 1, 2002 to June 30, 2002
10. Englar, Robert J., "Preliminary Results of GTRI/DOE Pneumatic Heavy Vehicle Tuning Tests," GTRI Report A-5871, Mar 14, 2002.
11. Englar, R. J., "Preliminary Results of the Pneumatic Heavy Vehicle SAE Type-II Fuel Economy Test," GTRI Draft Report, Sept, 2002.
12. Dotson, Robert, "SAEJ1321 Class-Eight Truck Aerodynamic and Tire Comparison Fuel Economy Tests," Transportation Research Center Report, Project 20020465, Sept., 2002.

13. Englar, R. J., "Development and Evaluation Of Pneumatic Aerodynamic Devices To Improve the Performance, Economics, Stability and Safety Of Heavy Vehicles," DOE Quarterly Progress Report No. 15, July 1, 2002 to Sept. 30, 2002.
14. Englar, Robert J., "GTRI Updated Wind-Tunnel Investigation of Pneumatic Heavy Vehicle Road-Test Configurations," GTRI Draft Report, Projects A-5871 and A-6395, Jan. 10, 2003.
15. Englar, Robert J., "Drag Reduction, Safety Enhancement and Performance Improvement for Heavy Vehicles and SUVs Using Advanced Pneumatic Aerodynamic Technology", SAE Paper 2003-01-3378, presented at 2003 SAE International Truck and Bus Meeting and Exhibition, Ft Worth TX, November 10-12, 2003.
16. "Transportation Energy Data Book: Edition 19," DOE/ORNL-6958, Sept., 1999.
17. "EIA Annual Energy Outlook 2000," DOE/EIA-0383 (2000), December, 1999 and "AEO 2001",
18. Gaeta, R. G., R. J. Englar, and G. Blaylock, "Wind Tunnel Evaluations of an Aerodynamic Heat Exchanger," Proceedings of the UEF Conference "The Aerodynamics of Heavy Vehicles: Trucks, Buses and Trains," Dec. 2-6, 2002.
19. Gaeta, R. J. and R. J. Englar, "Pneumatically Augmented Aerodynamic Heat Exchanger," Paper #18 presented at the NASA/ONR Circulation Control Workshop, Hampton, VA, March, 2004. Also to be published in Workshop Proceedings.

### **Contact**

Robert J. Englar, Principal Research Engineer  
Georgia Tech Research Institute  
Aerospace, Transportation & Advanced Systems Lab  
CCRF, Code 0844  
Atlanta, GA 30332-0844

(770) 528-3222, Office  
(770) 528-7586, Wind Tunnel  
(770) 528-7077, Fax  
[bob.englar@gtri.gatech.edu](mailto:bob.englar@gtri.gatech.edu)



**Application of Pneumatic Aerodynamic Technology to Improve Drag Reduction, Performance, Safety, and Control of Advanced Automotive Vehicles**  
 by Robert J. Englar, Georgia Tech Research Institute



Application of Advanced Pneumatic Aircraft Technology...



...Through Analytical & Experimental Development ...



..To Proof-of-Concept Full-Scale Tests

NASA/ONR Circulation Control Workshop  
 March 16-17, 2004, Hampton, VA

**Outline of Poster Presentation**

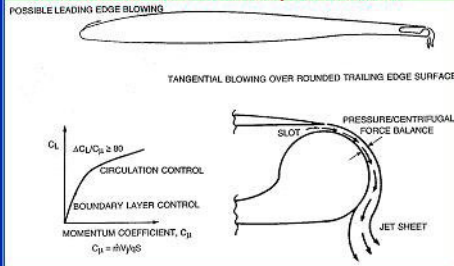
- Introduction: Pneumatic Heavy Vehicle Aerodynamic Technology
- Pneumatic Heavy Vehicles (PHV)... Multi-Purpose Aero Devices for:
  - Force & Moment Reductions or Augmentations
  - Drag Reduction (Fuel Efficiency) or Drag Increase (Aero Braking)
  - Increased Stability (Directional & Lateral)
  - Improved Safety of Operation
  - Reduced Spray Turbulence & Hydroplaning
  - No-Moving-Part Integrated System
  - Pneumatic Cooling System
- Wind-tunnel Investigations & Confirmations
- Initial Full-Scale Tuning Tests at Volvo Trucks
- SAE Type II Fuel Economy Tests at TRC
- Other Applications: Pneumatic SUV & Aero Heat Exchanger
- Conclusions: Summary of Wind-Tunnel & Full-Scale Results



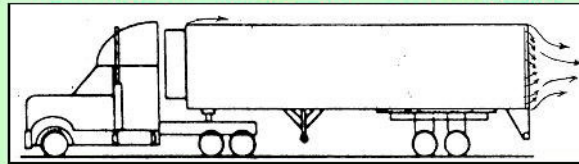
## Basics of Circulation Control Pneumatic Aerodynamics and Application to Heavy Vehicles

### Circulation Control Concept on Aircraft

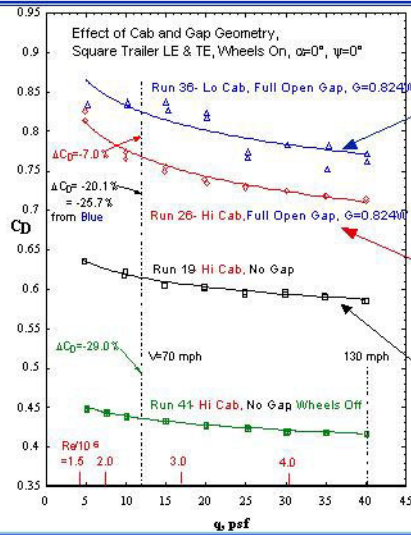
### Navy A-6/CCW Flight Test Aircraft



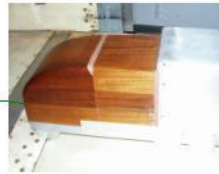
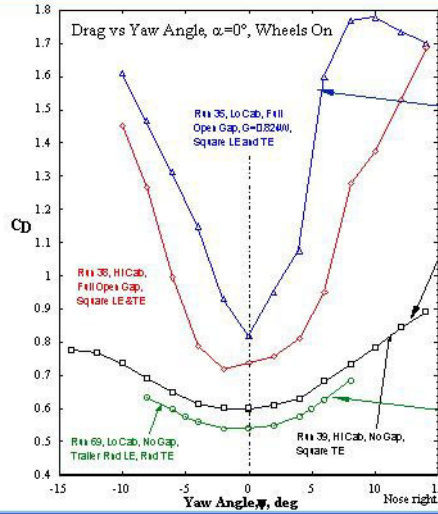
### Blowing on Front of Trailer and/or All 4 Trailing Edges



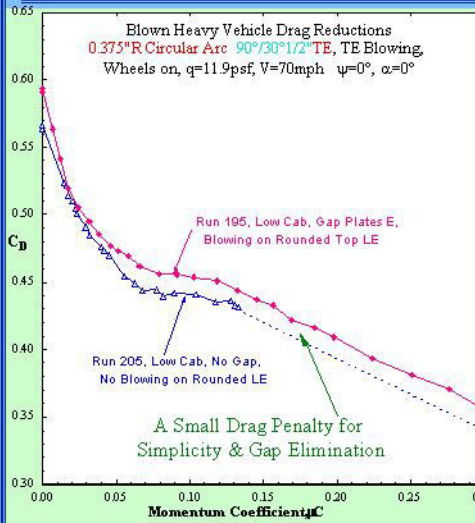
### Initial Baseline Tunnel Tests of Unblown Generic Configuration Showed Significant $C_D$ Reduction when Cab Gap was Improved



## Adverse Effects of Side Winds and Cab Gap on Drag & Stability



## A Practical Pneumatic Alternative to the Cab Gap Problem



**Cab "No-Gap" (Filled) is Effective, but Not Practical, SO....**

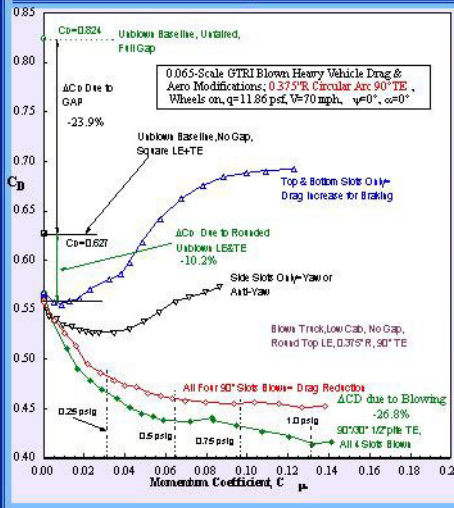
Top LE Blowing  
 Gap Side Plates with Small Clearance



**...Substitute FlexGap Side Plates and Top LE Blowing**

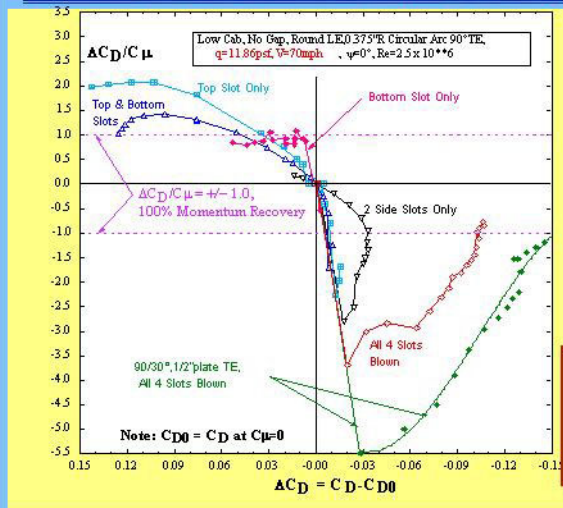


**Pneumatic Aero Development at GTRI Showed 50%(or more) Drag Reduction, Force & Moment Augmentation from Blown Configurations, and Drag Increase for Aero Braking if Desired**



4 Blown Slots & Jet Turning on Rear Doors of Wind-Tunnel Model

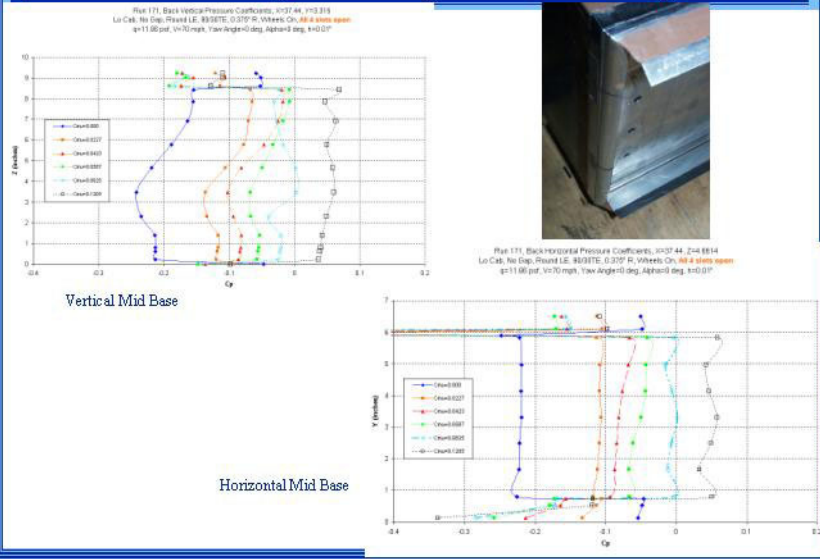
**Blowing Efficiency & Drag/Thrust Increment Due to Blowing Slot Position, shown as Fraction/Multiple of Blowing Momentum Input**



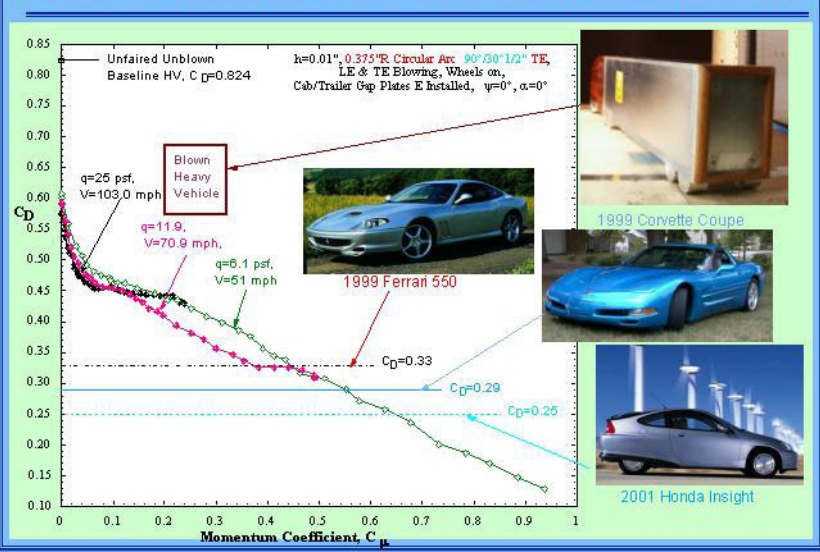
It's possible to get back 5.5 times the  $C_{\mu}$  input as a  $C_D$  Reduction.... OR 2 times the  $C_{\mu}$  input as Aero Braking increase

Figure 4. Blowing Efficiency & Drag/Thrust Increment Due to Blowing Slot Location

## The Effects of Blowing on Increasing Base Pressure for $C_D$ Reduction

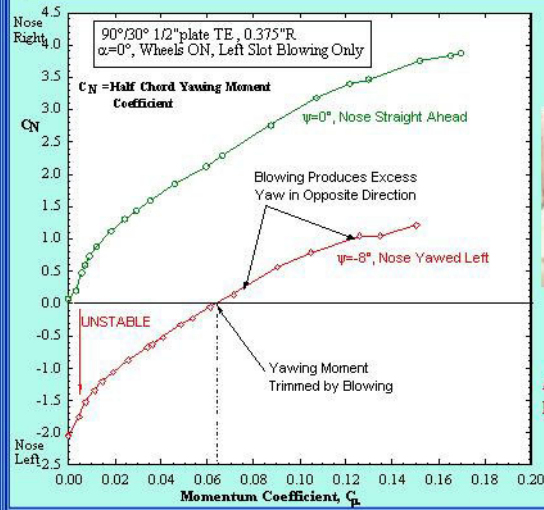


## GTRI Extended $C_{\mu}$ Tests Showed State-of-the-Art Drag Reduction!!





## Directional Control Capability Provided by Blowing of Left Side Slot Only (Similar Effects on Drag)



Yaw Nose Left, Blow HERE

Additional Gain from Side Blowing =  
 Reduced  $C_D$  due to Yaw

## Full-Scale Tests: Pneumatic Heavy Vehicle Test Trailer Compared to Stock Baseline Control Trailer from Great Dane

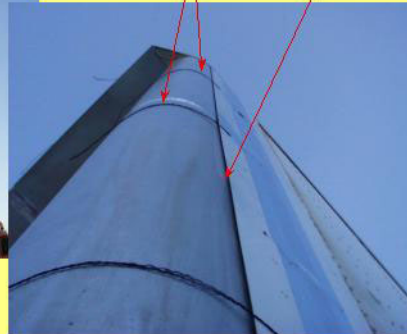


- Test PHV Features:
- 4 jet turning surfaces with plenums and blowing slots
  - NACA inlet to entrain free-stream total pressure into blowers
  - Diesel-driven external blowers feeding diffusers to plenums to slots
  - GTRI data telemetry of blowing parameters

**Static Jet Turning Displayed During Full-scale Run-up Testing**



Setting Slot Heights and Confirming Jet Turning at Low Blowing Rate on Aft Door of Trailer



Tufts  
Slots, 4 total,  
one per side

Right Rear Corner, looking up--  
Tufts Show Jet Turning to Left:  
90° on Side and 30° on Top

**On-the-Road Operation: Jet Turning Entraining the Freestream Flowfield and Reducing Vehicle Drag**



Rear View with Jets Blowing



Close-up of Tufts  
Showing Jet Turning

### Tuning Test Results (V=65 mph), Comparison to GTRI Wind Tunnel Results, and Conclusions

Configuration	WindTunnel	% C <sub>D</sub>	% Equiv. GPM	Road Test	% GPM	% Equiv. C <sub>D</sub>	% MPG
	C <sub>D</sub>	Change	Reduction	Run No.	Reduction	Change	Increase
Baseline, No Gap, Sq. LE & TE	0.627	0	0.0	13 (Gap)	0.00	0.00	0
Unblown PHV, Cmu=0	0.57	-9.1	-4.6	9	-10.21	-20.42	11.37
PHV, 4 Slots Cmu=0.05	0.44	-29.8	-14.9	5	-13.27	-26.54	15.30

**CONCLUSIONS:**

- Limited Tuning Runs confirmed up to **15.3% increase in MPG**, or about **26.5% reduction in C<sub>D</sub>**, due to blown PHV configuration, **but this first Tuning Test was not optimized** (Speed, Temps, Blowing rate, etc.)

### Test and Control Vehicles in Pits for SAE Fuel Economy Runs at Transportation Research Center (TRC), East Liberty, Ohio



Front View of Test (Blown, front) and Control (Stock, rear) Vehicles



Rear View of Test and Control Vehicles, Showing Blown Tufts Turning

**Pneumatic Heavy Vehicle(PHV) Test Rig on Track  
at 75 mph with Blowing**



**PHV Testing on the TRC Track (7.5 mile oval)**



View from Cab on Straightaway  
(2 miles long,  
NO SuperSTOL aircraft needed!)



View from Cab on 1.75-mile Banked  
Turn (outer lane for 140mph Ferraris)

Test runs showed Fuel Economy Increase of ~5-6%, or Only 10-12%  $C_D$  reduction--Why?



## Differences Between PHV Model and Road Test PHV Vehicle



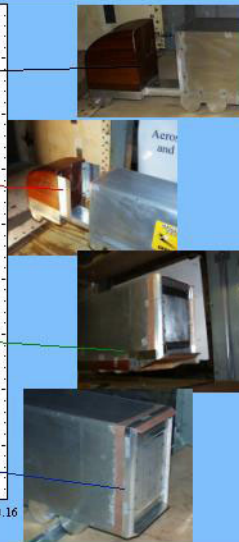
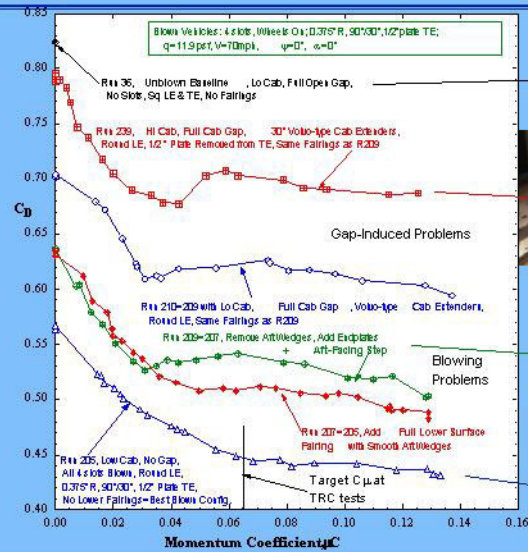
### Difference

- Cab Extender Fairing
- Trailer/Cab Gap
- LE Radius Hidden by Fairing
- Lower Aero Fairing
- Trailer Ground Clearance
- Side Winds, Gusts

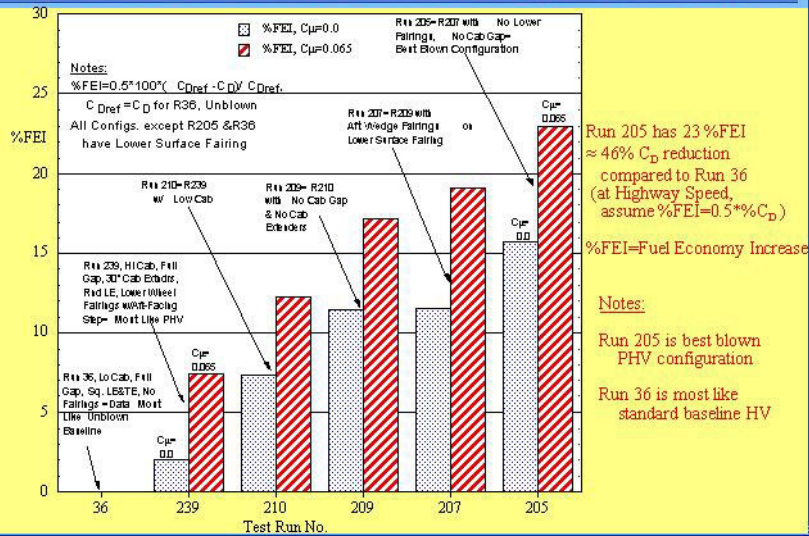
### Adverse Effect on Test Vehicle

- Less  $C_D$  Reduction from  $C_{D1}$
- Increased  $C_D$  due to Increased Vorticity
- Less  $C_D$  Reduction than WT
- Reduce Lower Jet Entrainment, Raises  $C_D$
- Higher  $C_D$ , Less Blowing Effectiveness
- Dramatically Increase  $C_D$  because of Yaw

## Tests to Determine Drag Differences: TRC Test Vehicle not like Tunnel Model

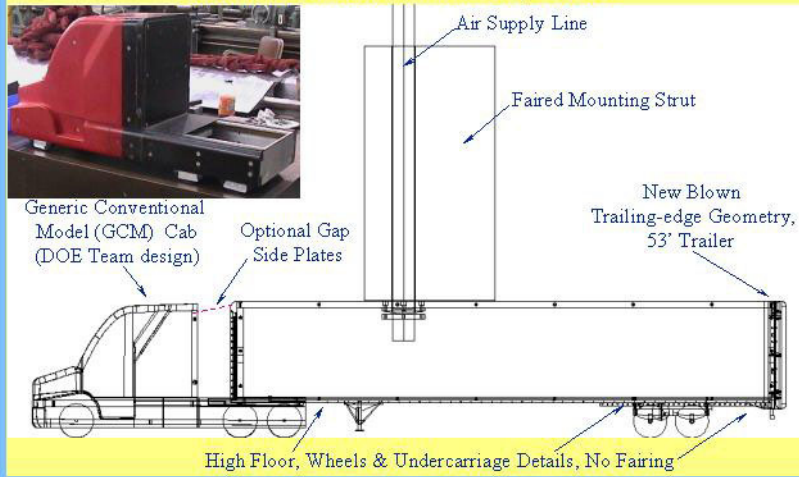


**Predicted Fuel Efficiency Increase after PHV Road Test Vehicle is Converted To Resemble Best Model Configuration (Run 205)**

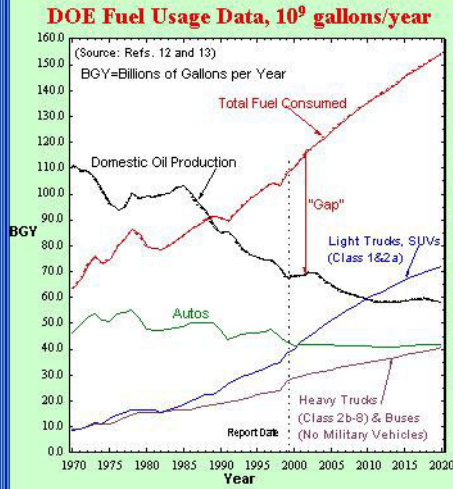


**Updated PHV Blown Wind-tunnel Model to Resemble TRC Test Rig, With New Tractor, New Top Strut Mount, New TE Geometry**

Tests of this new model now underway at GTRI



**Fuel Usage in the US (look at SUVs), and One Possible Fix:  
Increase Fuel Efficiency of SUVs**



**Blown SUV in Lockheed Tunnel**



**Full-Scale □ Tunnel Tests of Unblown SUV to Locate  
Flow Separation for Blowing Slot Location of Pneumatic SUV**



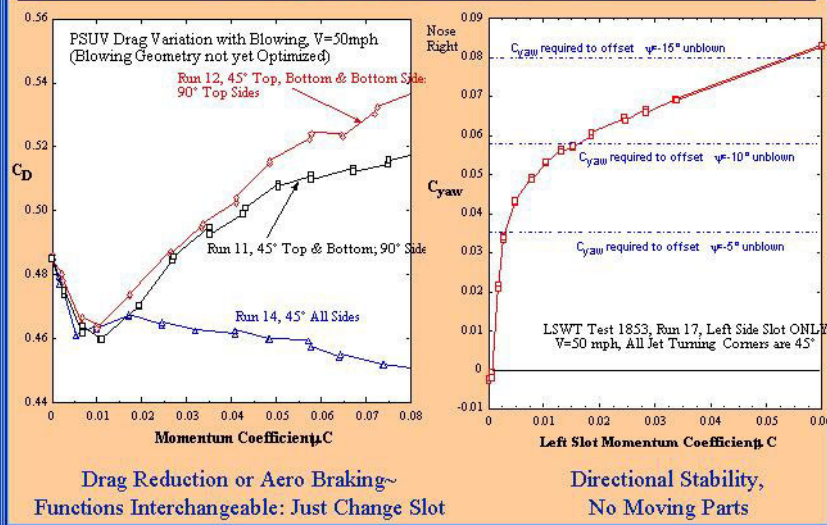
**Smoke Flow over Unblown SUV,**  
Testing in Lockheed 16' x 23' Low  
Speed Wind Tunnel, Marietta GA



**Separated Flow over Aft Door of SUV**



**Pneumatic Capabilities of Blown SUV Confirmed in WT Test;  
Blowing Configs far from Optimized**



**The Radiator Problem: Current Automotive Heat Exchangers  
are Neither Aerodynamic nor Fuel Efficient**



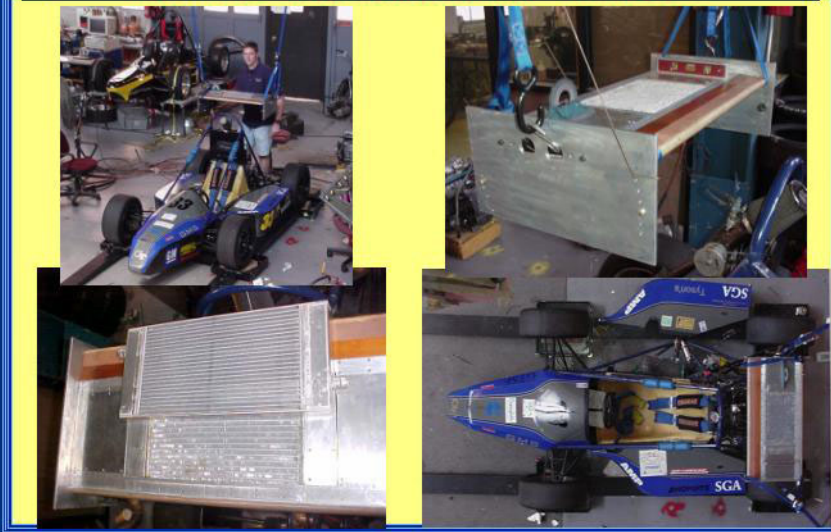
Heavy Vehicle vs Conventional Car  
~Much Larger Frontal Area and Drag



Large Frontal Area and Drag due to Radiator  
Pods on Formula 1 or Indy Racer

- Radiator Usually Vertical for Largest Pressure Drop and Heat Exchange
  - However, Largest Possible CD is from a Vertical Flat/Cusped Plate
  - $\Delta$  Pressure = 0.4 to 0.5 x dynamic pressure ~ 5 to 7 psf (at 62 to 74 mph)
  - Fan and extra power required for more mass flow and cooling
- NEW: Aerodynamic Heat Exchanger (GTRI patent) [See Poster Session 3]**

### Pneumatic Aero Heat Exchanger Radiator/Wing Applied to Formula SAE Demonstrator Race Car by GTRI



### CONCLUSIONS: Pneumatic Aerodynamic Concepts Now Demonstrated Full-Scale on PHV and PSUV

- Blowing Demonstrated on Full-Scale PHV Tests at TRC, Confirming Drag Reduction, but less than from Tunnel Tests; Reasons Now Identified
- 23% - 24% Fuel Efficiency Improvement is Possible Based on 46-48%  $C_D$  Reduction, if PHV Test Vehicle Resembles Tunnel Model Characteristics; Now Underway
- Pneumatic Yaw Stability, Side-Wind  $C_D$  Reduction, and Aero Braking Capabilities (Safety of Operation) are Confirmed, Model & Full-scale
- Pneumatic Full-scale Tunnel Tests Showed Similar Blown Capabilities for SUVs
- Pneumatic Aerodynamic Heat Exchanger: Simplicity, Reduced Drag, and Heat Transfer Effectiveness Confirmed
- Improvements Underway!!

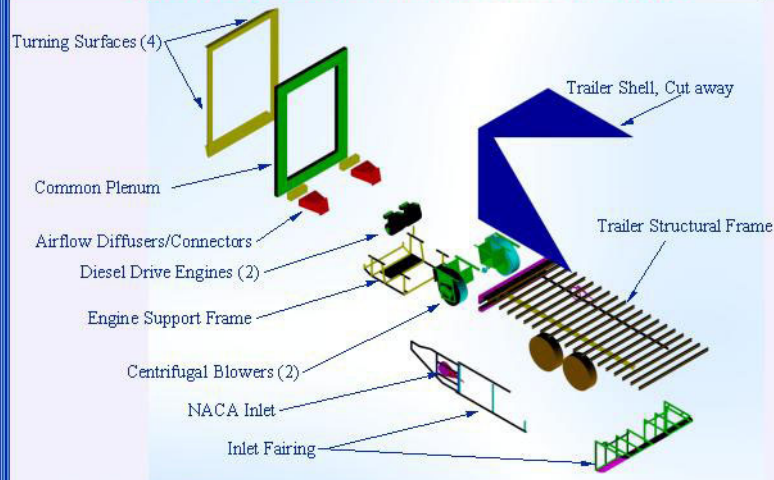
GTRI PATENTED  
CONCEPTS



**BACKUP Slides**



**PHV Trailer Modifications for Blowing Systems ~These are for the Test Prototype only, not Production Design**



Designed & Modified by Prototype Shop Novatek, Inc.

**Trailing Edge Turning Surface Geometries, Built at Novatek, Inc**



Plenums, Slots and Turning Surfaces,  
Showing 90° (left) & 30°



Right Rear Corner, looking up--  
90° Side and 30° Top

**Flow Visualization of Blowing Jets**



Tuft Showing Flow Uniformity at Diffuser Center



Combined Jet Strength and  
Wake Contraction (see Shirt)





# **Aerodynamic Heat Exchanger: A Novel Approach to Radiator Design using Circulation Control**

R. J. Gaeta  
R. J. Englar  
G. Blaylock

***Aerospace and Acoustics Technology Branch / ATAS Laboratory  
Georgia Tech Research Institute  
Georgia Institute of Technology  
Atlanta, Georgia 30332***

## **Abstract**

GTRI has recently been developing pneumatic aerodynamic concepts for application to Heavy Vehicles under a Department of Energy contract through the Oak Ridge National Laboratory (ORNL). A related application under development is a novel heat exchanger known as the Aerodynamic Heat Exchanger (AHE). This patented device employs airfoil/wing aerodynamic pressure differences to induce large mass flows across a radiator installed inside a wing. GTRI has recently completed an in-house wind tunnel test of this concept. The objective of this proposed effort was to perform a wind-tunnel evaluation of the AHE and establish the feasibility of the concept. A 2D wing was fabricated with a removable center section. A radiator core was integrated into this section of the wing. A conventional radiator core (based on a Visteon design) and two cores made from carbon foam were tested. The carbon foam cores were designed and provided to GTRI by ORNL. Hot water was allowed to pass through the inside of the wing while freestream, wind tunnel air passed over (and through) the wing. Heat rejected by the radiator was measured as well as lift and drag. Results indicated that the concept is feasible and can provide an effective means to reduce vehicle drag by reducing the drag due to conventional radiators.

## Introduction

### The Aerodynamic Heat Exchanger (AHE) Concept

A conventional automotive heat exchanger uses the stagnation pressure drop across a flat plate that is porous. Air flow from the freestream is directed either through a duct or through louvers to reach the face of the heat exchanger. This pressure difference is large, but it occurs at the price of a large drag force. A wing is a device that naturally produces a pressure difference but in a way that produces a low drag force (see Figure 1). It is true that the pressure difference is not nearly as high as the conventional flat

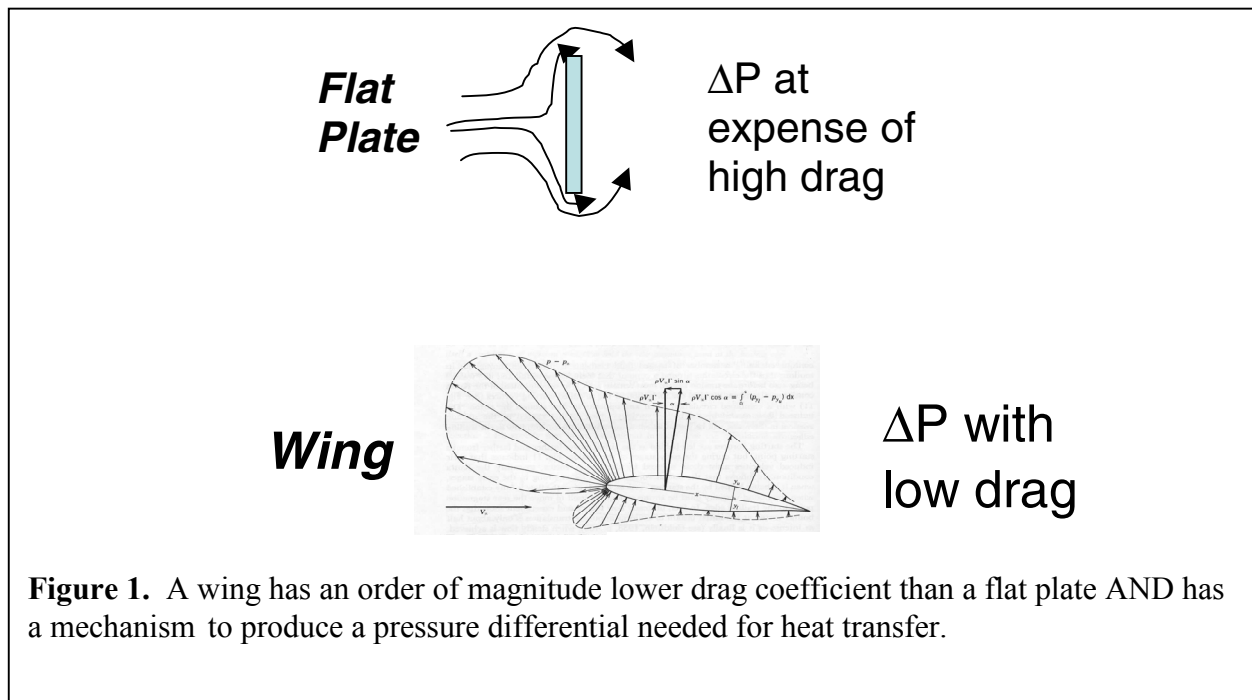
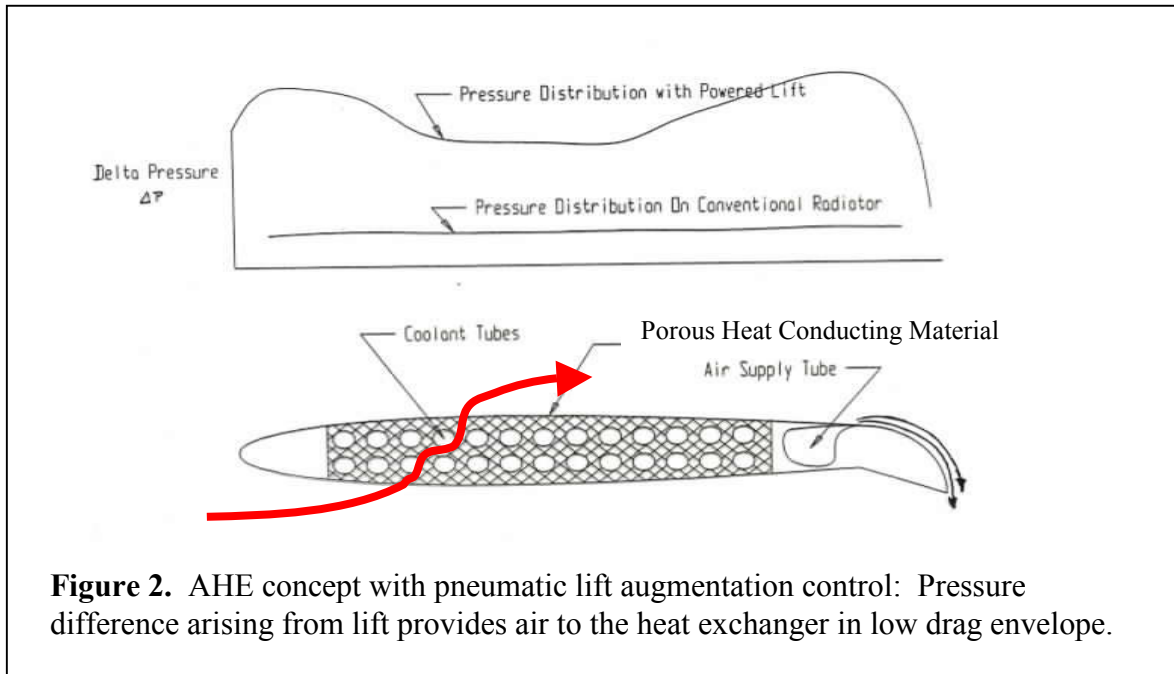


**Figure 1.** A wing has an order of magnitude lower drag coefficient than a flat plate AND has a mechanism to produce a pressure differential needed for heat transfer.

plate approach. But by using established pneumatic flow control techniques, the wing lift (or pressure difference) can be radically augmented. Figure 2 shows the AHE concept in conjunction with pneumatically augmented lift system. The lift augmentation concept here has received significant research and development attention in the literature.<sup>1,2</sup> The AHE concept is embodied in a patent that was granted to GTRI and Novatek, Inc.<sup>3</sup> Even at zero angle of attack on a symmetric airfoil, large pressure differences can be realized by increasing the wings circulation through trailing edge blowing. This process leverages the Coanda effect and can produce phenomenal increases in lift. Figure 4 shows how the lift on a symmetric airfoil can be controlled by



changing the momentum of air blown through a thin slot at the trailing edge of the wing. The design challenge for the AHE is to provide enough flow through the wing (via porosity), but still retain a high enough pressure difference to create aerodynamic force, if needed.



A proof-of-concept model was built and testing in a low speed wind tunnel at GTRI to see if this concept was a feasible solution. Several radiator core configurations were tested and heat rejection was measured. The remainder of this paper presents the testing approach and set-up along with results and discussion.

### Motivation

Current engine heat exchangers for heavy vehicles and automobiles are neither aerodynamic nor fuel efficient. This is evident visually as the radiator grill is usually the most distinctive feature on a tractor rig as seen from the front end. Passenger automobiles get their distinctive look from how the radiator grill is designed and the ram scoops on high performance race cars are necessarily evils. A common feature is the need for large amounts of air to flow through the heat exchanger. The solution for over a century has been to place this heat exchanger normal to the oncoming air stream. This is a very effective means of producing heat transfer but it is also an effective

means of creating drag [see Figure 3]. A novel approach to an alternate cooling solution is embodied in the notion of housing the heat exchanger in a low drag envelope: a wing.



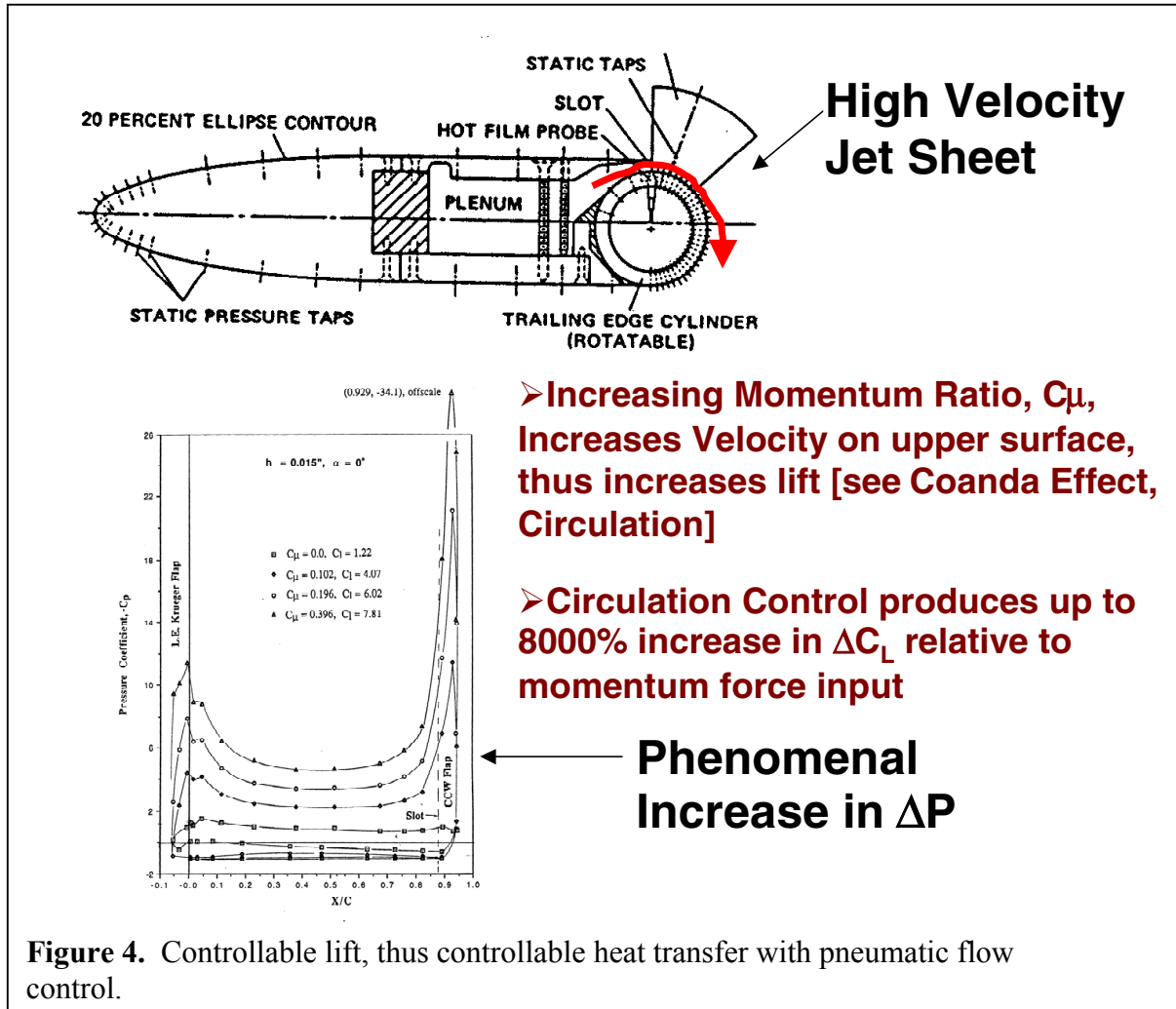
**Figure 3** Large Heavy Vehicle and passenger car: radiator presents large frontal area to flow, thus significant drag. F1 & Indy cars: pods or ram scoops are necessary evils - *speed draining drag sources*

### **Technical Approach and Experimental Set-up**

The testing of the AHE model was performed in GTRI's Model Test Facility. This facility is a closed-return wind tunnel with an operating dynamic pressure range of 5 to 50 psf. The test section is 30 by 30 inches and has a 6 component balance attached to a turntable for easy model angle changes.

#### **AHE Configurations**

The airfoil shape chosen for the model AHE concept was elliptical with a round trailing edge, similar to that shown in Figure 4. The aerodynamic reference configuration was a non-porous center section. Three porous center sections were fabricated which represented three different types of radiator cores.



Conventional Visteon Aluminum Fin Core

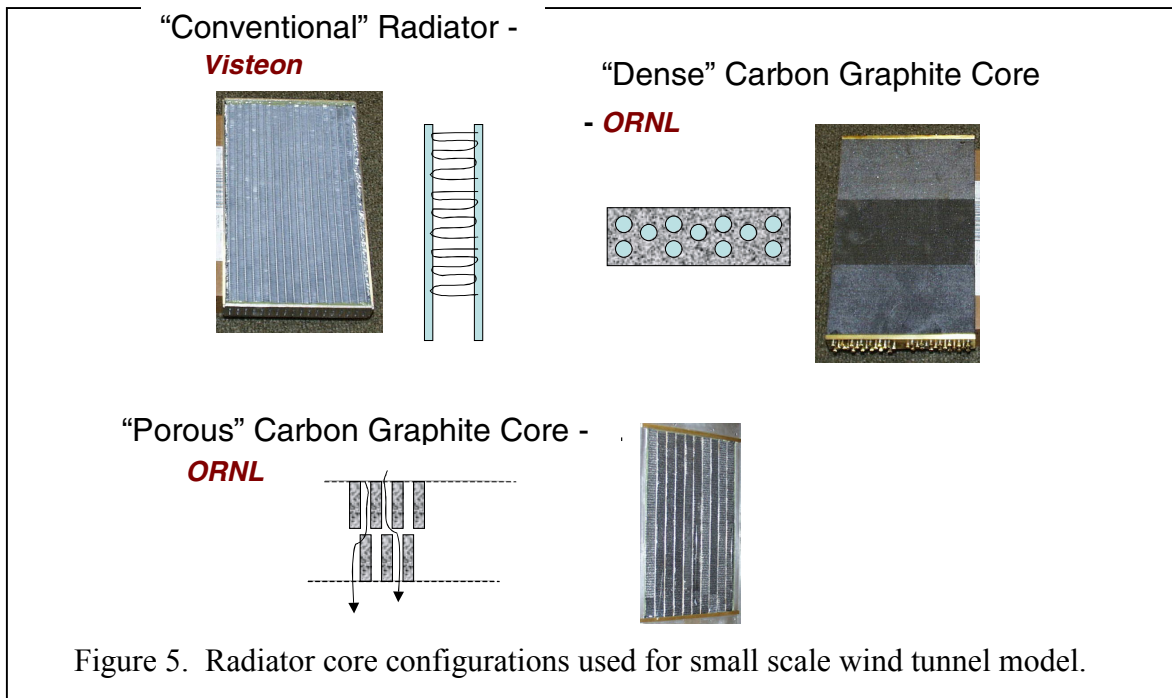
This core was a conventional aluminum finned core used in a SAE Formula car operated by the Georgia Tech Motorsports Club. It had relatively low pressure drop or a high porosity and was produced by the Visteon Company.

ORNL Very Dense Graphite Foam Core

ORNL supplied a radiator that was in the same envelope as the Visteon radiator, but was made from solid pieces of carbon-graphite foam material. This material has phenomenal heat conductivity properties. Although it is porous, the bulk density is such that it has a significant pressure drop. Brass tubes were press fit into the foam to carry the coolant through the material for heat exchange.

### ORNL Porous/Serpentine Graphite Foam Core

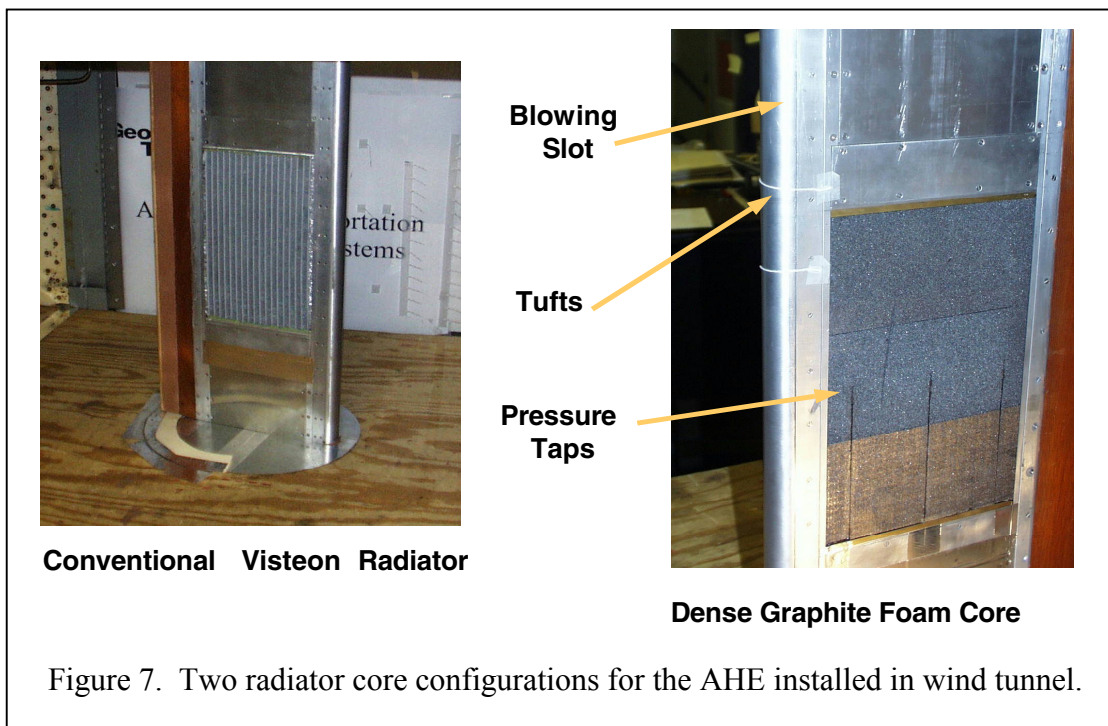
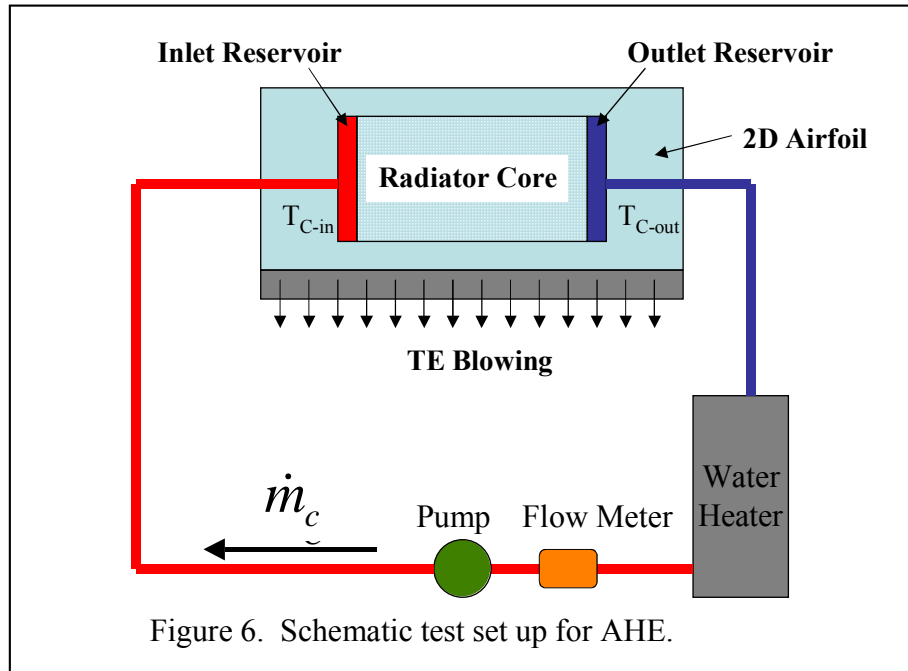
A second ORNL supplied radiator core consisted of smaller carbon-graphite foam fins arranged in such a way that flow could serpentine around them. These were brazed to narrow water channels in a matter similar to the aluminum radiator. The manufacturing of this core was such that some of the coolant passages were blocked off, so its full heat rejection potential was not realized. Furthermore, it was made about a half an inch thinner than the thickness of the wing, so a perforated sheet had to cover the wing to maintain smooth flow. Figure 5 shows all three configurations.



### Experimental Set-up

The elliptical wing with the radiator core was installed vertically in the wind tunnel and was attached to the force balance. The airfoil was connected via flexible hoses to a 3-phase electric 3600W water heater. Water was heated and pumped into one side of the radiator. It was allowed to settle in the inlet reservoir before moving through core and settling in the outlet reservoir. The outlet water was then allowed to return to the water heater closing the coolant loop. Figure 6 shows a schematic of the coolant flow path. Coolant mass flow was measured with a water flow meter. Thermocouples were placed in both inlet and exit reservoirs to monitor the temperature drop across the core. All

fluid measurements were fed into a Labview program running on a Windows platform, which stored mass flow and temperatures. Piping and thermocouples are visible. Figure 7 shows the Visteon radiator configuration and the dense carbon-graphite radiator installed in the wind tunnel.



A typical run for a given radiator configuration would include a “sweep” of slot blowing pressure at constant angle of attack and tunnel speed, to record and evaluate aerodynamic characteristics. Then, for each radiator core installed, the coolant lines were added (these would have caused balance tares during the aero runs) and temperature data were taken at constant coolant flow rates for variable blowing pressures. Variation in tunnel speeds was also conducted for the radiator airfoils at constant flow rates while varying blowing pressures. For reference, the conventional Visteon radiator was evaluated without blowing or airfoil frame but perpendicular to the freestream flow so as to simulate a standard radiator’s cooling characteristics.

In the results presented below , all aerodynamic characteristics are based on a wing planform area of  $S = 2.871 \text{ ft}^2$  , and the blowing momentum coefficient is defined as :

$$C_{\mu} = \frac{\dot{m}V_j}{qS} \quad (1)$$

Where  $\dot{m}$  = blowing mass flow from jet, measured by flowmeter, slug/sec  
 $V_j$  = isentropic jet velocity, from measured pressure and temperature, ft/sec  
 $q$  = freestream dynamic pressure =  $0.5 \rho V^2$ , lb/ft<sup>2</sup>,  $\rho$  = air density  
 $S$  = wing planform area = span x chord, ft<sup>2</sup>

It should be noted that it is assumed that the AHE radiator airfoil was to be mounted on race car (a GT Motorsports SAE car), intended also to give down force for cornering and traction. Thus the model airfoil is mounted inverted in the tunnel, with negative lift (positive downforce) towards the ground as the lifting side of the airfoil is towards the road, and negative angle of attack is leading edge downward.

A simple heat balance was used to quantify heat rejection of the coolant to the air passing through the airfoil into the tunnel. The heat transferred from the coolant can be expressed as:

$$Q = \dot{m}_c C_p (T_{c_{IN}} - T_{c_{OUT}}) \quad (2)$$

A schematic of the test set-up and measured quantities is shown in Figure 8. Measurements were made for each configuration at several freestream velocities, coolant flow rates, and blowing rates.

### **Aerodynamic Results**

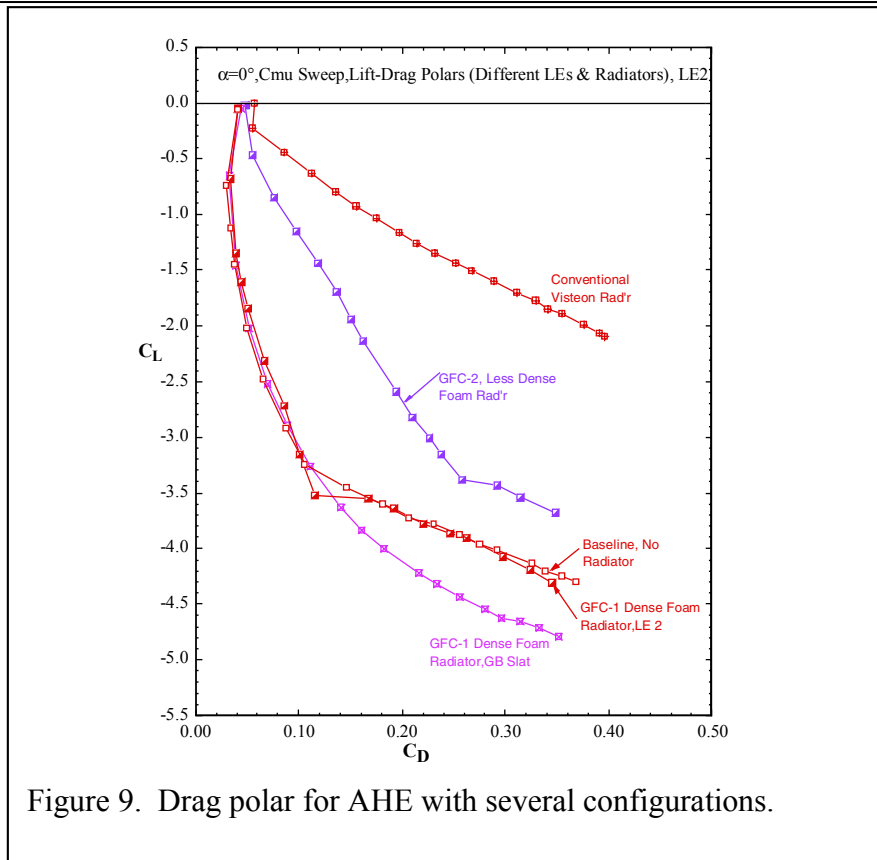
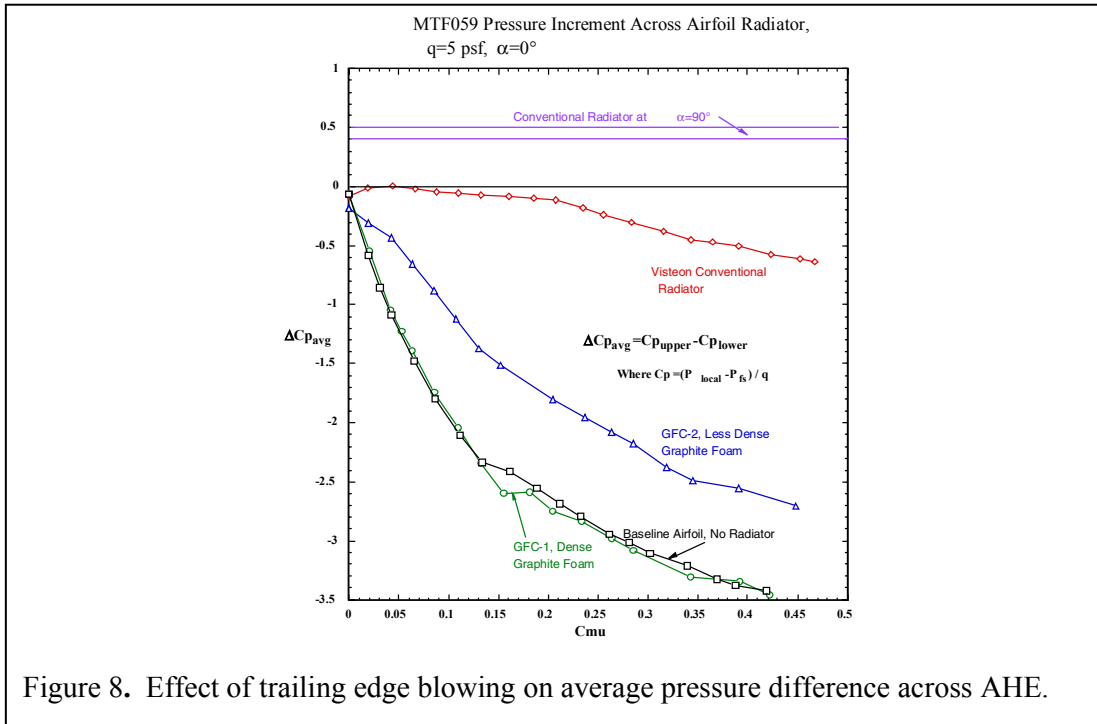
The aerodynamic portion of the tests (i.e., the radiator installed and blowing applied, but no coolant hoses connected and no coolant flowing) was conducted first to evaluate the effects of porous sections in the center of the lifting airfoil.

Figure 8 shows pressure coefficients plotted as functions of blowing, all at  $\alpha = 0^\circ$ . Increasing blowing ( $C_{\mu}$ ) dramatically increases the static pressure differential ( $-\Delta C_p$  avg) implying suction on the lifting (downforce) side. Here the pressure coefficients (defined in Fig 8) are averaged between the pressure and suction side of the radiator, and the suction rise is equal to the pressure drop. As the radiator gets more porous, the  $\Delta C_p$  is reduced. For reference, the pressure drop of the conventional radiator at  $90^\circ$  is shown ( $\Delta C_p = +0.4$  to  $+0.5$ ) and blowing is a factor of up to 7 times that. Note that the ORNL dense foam radiator performs almost exactly as the baseline blown airfoil with no radiator installed. The implication is that this foam is so dense as to allow little if any air to pass through the radiator core.

Figure 9 shows how blowing and porosity affect the lift and drag. These results conform directly to the pressure differences in Figure 9. As porosity increases, lift decreases and drag increases, but still increased blowing is very effective. As downforce ( $-C_L$ ) increase due to blowing, the high circulation around the airfoil causes the leading edge to separate (or a bubble to form there), and thus the discontinuity in the lift curves to occur. This can be corrected by improving the leading edge shape. There is still improvement to be had: the 20% Elliptic Airfoil of Ref. 5 is a thicker airfoil (i.e. has a greater LE radius) version of the current baseline blown ellipse airfoil, and it shows no sign of separation, continuing on as  $C_L$  reaches  $-8$  or more. Thus great downforce



potential is confirmed with blowing (no increase in airfoil angle of attack is necessary here) and this carries over into the heat transfer evaluations conducted with coolant flowing through the blown radiators.



## Heat Transfer Results

Results for the conventional or Visteon radiator core indicated that a maximum coolant temperature drop of about 5 degrees Fahrenheit was achieved for a flow rate of 5 gallons/min with a 64 mph freestream velocity. Figure 10 shows coolant temperature drop for the Visteon core as a function of blowing coefficient,  $C_{\mu}$ , and coolant mass flow. Note that for the smaller coolant mass flows, larger temperature drops are realized. This is due to the longer exposure of the coolant to the heat exchanger (longer residence times). It should be stated that due to fabrication anomalies, some (42%) of the coolant flow tubes were blocked off so the Visteon radiator was not flowing in an evenly distributed manner and it is quite likely that its performance was inhibited to some degree. Figure 11 shows the corresponding heat removal as a function of  $C_{\mu}$  and coolant mass flow for the various radiator configurations of the AHE. A low coolant flow rate is shown. Note that the effect of the pneumatic lift augmentation (the increasing  $C_{\mu}$ ) is to increase the heat removal rate.

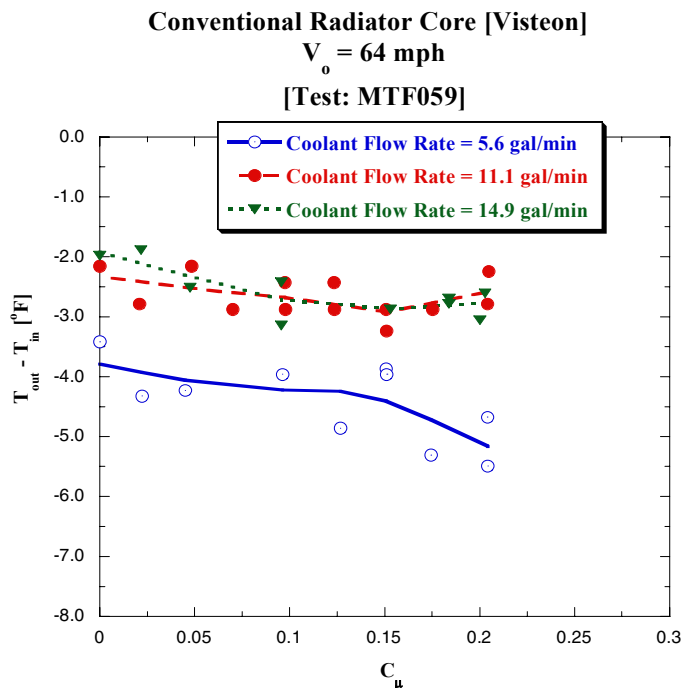


Figure 10. Effect of radiator temperature drop with respect to blowing coefficient.

Coolant Flow Rate ~ 5.5 gal/min;  $V_o = 32$  mph  
 [Test: MTF059]

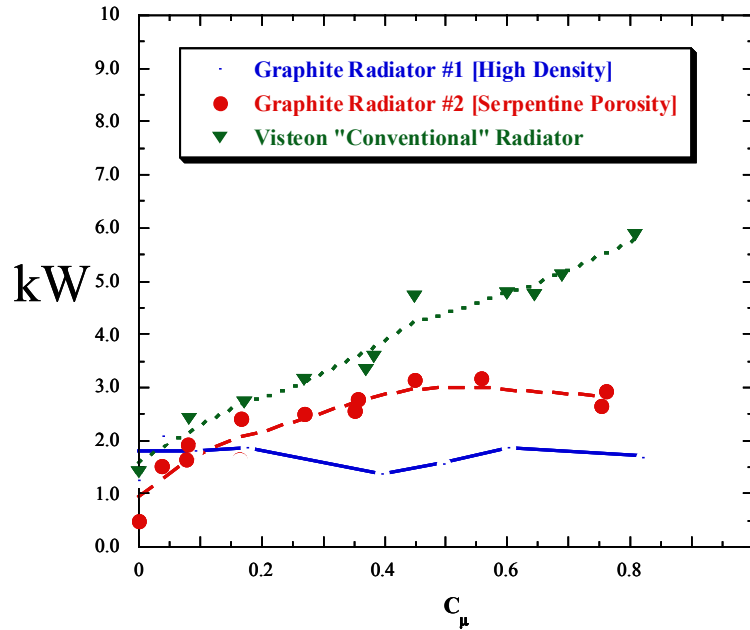


Figure 11. Low coolant flow rate results of AHE; note effect of heat removal with respect to blowing coefficient.

Figure 12 shows a comparison of heat removal for the carbon-graphite foam configurations along with the more conventional Visteon core for a coolant flow rate of about 15 gallons/min and a velocity of 64 mph. These are more realistic flow rates and freestream velocities which are encountered while cruising at highway speeds. Note that the high density graphite core performs as well as the Visteon core which is somewhat surprising since it has little or no airflow through the core. Due to the superior conductive performance of the foam, almost all of the heat transfer takes place in the form of forced convection along the surface of the airfoil (both upper and lower). This result was intriguing and suggests that the heat removal can be varied by simply varying the turbulence level of the flow over the wing surface. There are many methods (active and passive) which can accomplish this. This configuration (high density graphite) also was the best performer in relation to the aerodynamics of the device.

Coolant Flow Rate ~ 15.5 gal/min;  $V_o = 64$  mph  
 [Test: MTF059]

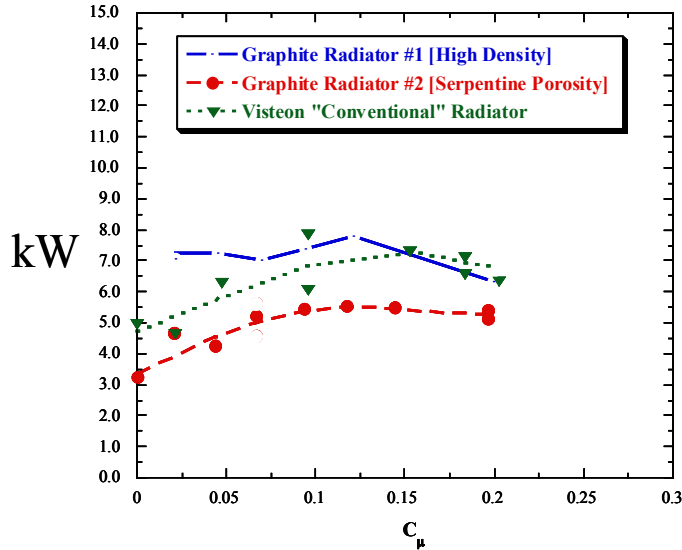


Figure 12. Heat rejection from AHE for high coolant flow rate; note independence of heat removal with respect to blowing coefficient for high density foam core.

For comparison, a typical automobile radiator removes about 15 kW in normal operation for a full-sized car engine. This model AHE produced roughly half this heat rejection but with a radiator core of less than half the typical area. And with substantially less drag [ $C_D$  of about 0.3 versus close to 1) than a conventional, normal to the flow, heat exchanger.

### Conclusions

Initial wind tunnel evaluations of the Aerodynamic Heat Exchanger concept employing both conventional and ORNL graphite foam radiator cores have been performed. This new concept has been shown to adequately transfer heat at the same or similar rates as convectional radiators at  $90^\circ$  to the flow, but at much lower drag coefficients when enclosed in a lifting surface parallel to the flowfield. The dense graphite foam core of ORNL has been shown to be both an effective heat transfer medium employing forced convection and an excellent core surface allowing almost no air to pass through the wing.

The following conclusions can be drawn from this proof-of-concept test of the AHE:

- An Aerodynamic Heat Exchanger with pneumatic lift control was successfully tested in a wind tunnel and basic concept was confirmed.
- Lift and drag are dramatically affected by the porosity of the radiator core section, but pneumatic augmentation is still a powerful control.
- Wind tunnel model demonstrated non-optimized heat rejection performance, but optimized sizing should further improve results.
- AHE has great potential for exhibiting both controllable aerodynamic force and low drag penalty for engine cooling.
- Carbon-Graphite foam enables optimal performance of the radiator core within the AHE concept.

It is important to note that system integration issues will pose a (surmountable) challenge to designers of cooling systems. Two important issues that need to be addressed are the production of steady high pressure air for the pneumatic system and coolant pump size and ducting for the AHE. It is the plan of GTRI to demonstrate this technology on the GT Motorsports SAE race car as a technology demonstrator. Initial work has highlighted the need for good system integration design. Figure 13 shows the one of the SAE Student Formula Cars with the AHE model being prepared for installation.



Figure 13. AHE preparing for installation in GT Motorsports SAE Formula car.

### **Acknowledgements**

The authors would like to acknowledge James Klett and April McMillan of ORNL for being receptive to the concept of the AHE and providing funds and material for a part of this work.

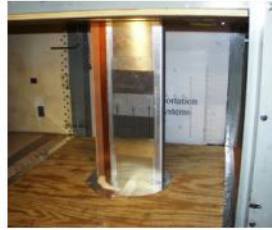
### **References**

<sup>1</sup>Englar, R. J. *Circulation Control Pneumatic Aerodynamics: Blow Force and Moment Augmentation and Modification; Past, Present, and Future*. AIAA2000-2541 presented at the AIAA Fluids 2000 Conference, Denver, Co., 19-22 June 2000

<sup>2</sup>Englar, Robert J., *Experimental Investigation of the High Velocity Coanda Wall Jet Applied to Bluff Trailing Edge Circulation Control Airfoils*, published as M.S. Thesis, University of Maryland, Department of Aerospace Engineering (June 1973).

<sup>3</sup>Burdges, K. P. and R. J. Englar U. S. Patent No. 6,179,077, "Vehicle Heat Exchangers to Augment & Modify Aerodynamic Forces," August 2000.

## Wind Tunnel Evaluation of an Aerodynamic Heat Exchanger



**Richard J. Gaeta,  
Robert J. Englar,  
& Graham Blaylock**

Aerospace and Acoustics Technologies Branch  
Georgia Tech Research Institute  
Georgia Institute of Technology  
Atlanta, GA 30332-0844  
rick.gaeta@gtri.gatech.edu

NASA/ONR  
Circulation Control Workshop  
March 16-17, 2004



Georgia Tech Research Institute

Aerospace  
Transportation  
Advanced  
Systems  
Laboratory

EA71

## The Problem: Current Automotive Heat Exchangers are Neither Aerodynamic nor Fuel Efficient



Pods or Ram Scoops used on F1 & Indy Cars are necessary evils - speed draining drag sources

For Large Heavy Vehicle and passenger car, radiator presents large frontal area to flow - thus significant drag



Georgia Tech Research Institute

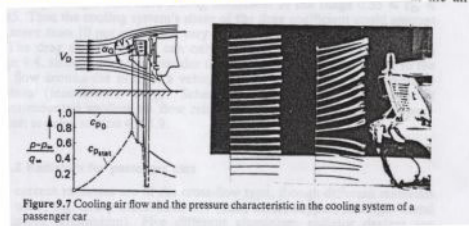
Aerospace  
Transportation  
Advanced  
Systems  
Laboratory

EA72



## Current State of the Art

Ref. : "Aerodynamics of Road Vehicles" Hucho, et al.



- > Radiator Usually Vertical for Largest Pressure Drop and Heat Exchange
- > However, Largest  $C_D$  Possible is a Vertical Flat/Cusped Plate
- >  $\Delta$  Pressure = 0.4 to 0.5 x dynamic pressure  $\sim$  5 to 7 psf = 0.03 to 0.05 psig
- > Fan & power required for more mass flow and cooling

WHAT'S BEEN DONE TO ALEVIATE THIS: Slightly inclined/angled smaller radiator core

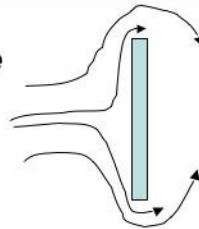
Aerospace  
Transportation  
Advanced  
Systems  
Laboratory

EA33

Georgia Tech Research Institute

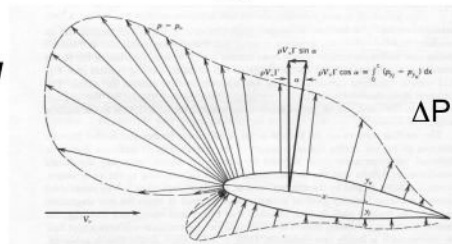
## New Concept - What if.....

Flat Plate



$\Delta P$  at expense of high drag

Wing



$\Delta P$  with low drag

A wing has an order of magnitude lower drag coefficient than a flat plate AND has a mechanism to produce a  $\Delta P$ .....

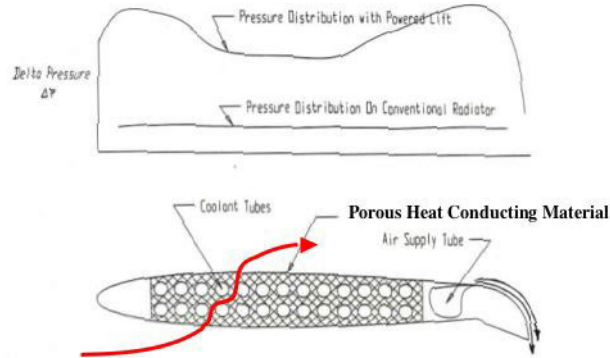
Aerospace  
Transportation  
Advanced  
Systems  
Laboratory

EA34

Georgia Tech Research Institute

.....we could Leverage Useful Work of a Wing

.....if the center of the wing was replaced with a porous material (e.g., a radiator), air would be forced to go through (get sucked through) the wing due to  $\Delta P$ .....



**The aerodynamic efficiency of wing in conjunction with the heat exchanger could provide engine cooling with low drag!**

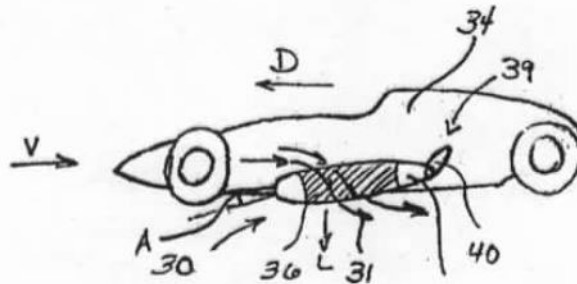
Aerospace  
Transportation  
Advanced  
Systems  
Laboratory

EA35

Georgia Tech Research Institute

The Patent: 6,179,077 B1 (GTRI & Novatek)

Aerodynamic Heat Exchanger (AHE)



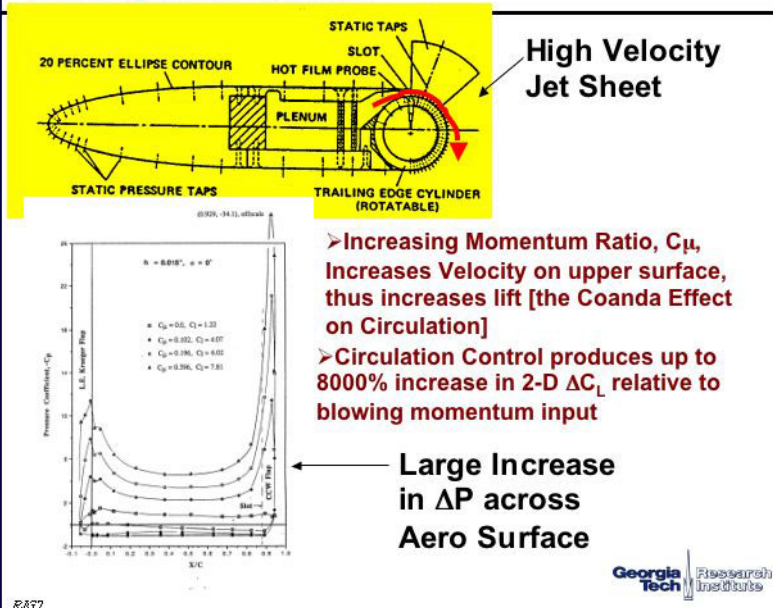
➤ GTRI and Novatek, Inc. have patented the concept of integrating a Heat Exchanger with a High-Lift Augmented Wing to produce the Aero Heat Exchanger

Aerospace  
Transportation  
Advanced  
Systems  
Laboratory

EA36

Georgia Tech Research Institute

## What is "Circulation Control" and why does it matter?



Aerospace  
Transportation  
Advanced  
Systems  
Laboratory

EA37

## Potential

- Circulation Control can generate lift (up or down force) on a "wing type" structure at ZERO angle of attack and with no moving parts
- Excellent opportunity for dual-use system (e.g., aero/cooling control for racing vehicles, side load management for heavy vehicles, integrated drag reduction for passenger vehicles like SUV's, radiator-in-wing for aircraft)



Aerospace  
Transportation  
Advanced  
Systems  
Laboratory

EA38

Georgia Tech Research Institute

## Proof-of-Concept - Wind Tunnel Test at GTRI

2-D simple elliptical wing with pneumatic high lift device on trailing edge and removable center section was tested in a low-speed wind tunnel at GTRI



3 types of radiators tested

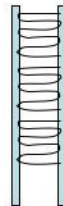
Aerospace  
Transportation  
Advanced  
Systems  
Laboratory

EX79

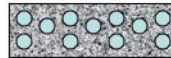


## Proof-of-Concept - Test Articles

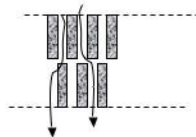
“Conventional” Radiator -  
*Visteon*



“Dense” Carbon Graphite Core -  
*ORNL*



“Porous” Carbon Graphite Core -  
*ORNL*



Aerospace  
Transportation  
Advanced  
Systems  
Laboratory

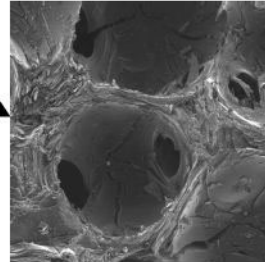
EX10



## Carbon-Graphite Foam - Incredible Heat Transfer Properties



High Heat  
Transfer Rates -  
Able to pass fluid



Specific  
Thermal Conductivity: 1.2 - 313 (W/m·K)/(g/cm<sup>3</sup>)

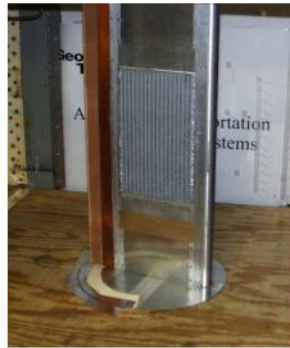
Specific  
Thermal Conductivity of Copper ~ 45 (W/m·K) / (g/cm<sup>3</sup>)

Aerospace  
Transportation  
Advanced  
Systems  
Laboratory

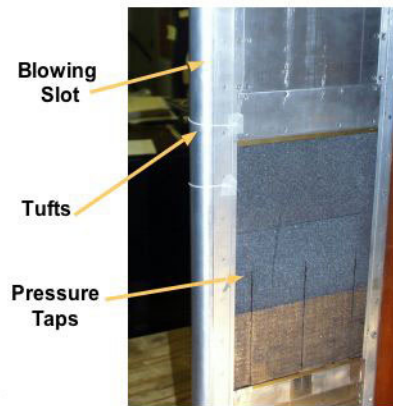
EXF11

Georgia  
Tech Research  
Institute

## Pneumatic Airfoil/ Aerodynamic Radiator Test Models



Conventional Visteon Radiator



Dense Graphite Foam Core

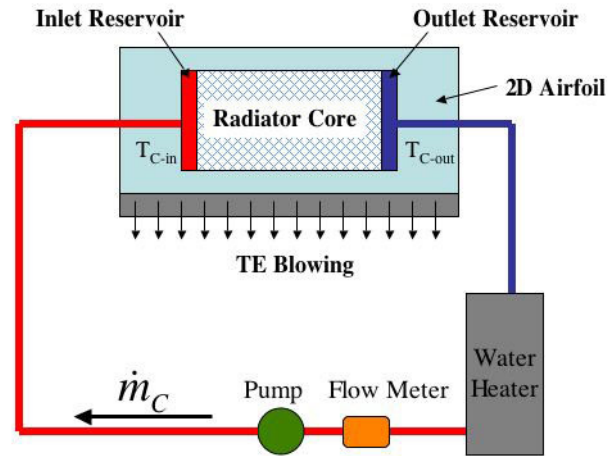
Aerospace  
Transportation  
Advanced  
Systems  
Laboratory

EXF12

Georgia  
Tech Research  
Institute



## Proof-of-Concept - Heat Rejection Measurements

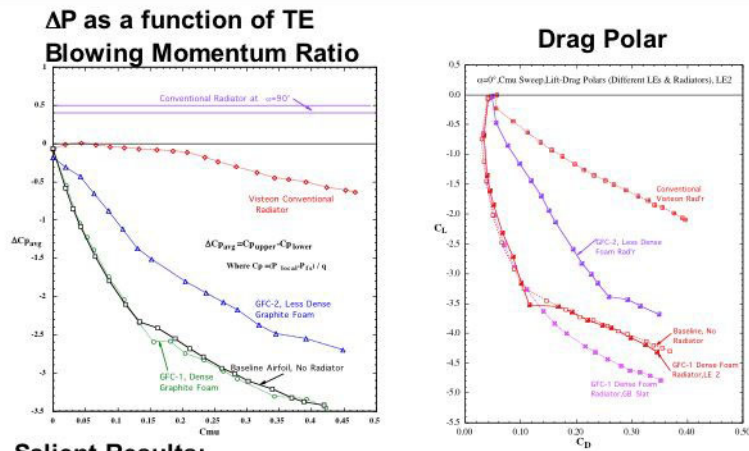


Aerospace  
Transportation  
Advanced  
Systems  
Laboratory

AE13

Georgia Tech Research Institute

## Proof-of-Concept - Aerodynamic Force Results



### Salient Results:

- Large Pressure Drop Through Carbon Foam Based Radiators
- "Dense" Carbon Foam Radiator was essentially a "hard wall"

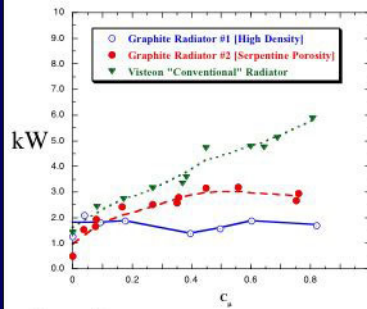
Aerospace  
Transportation  
Advanced  
Systems  
Laboratory

AE14

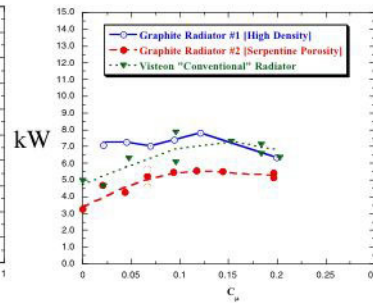
Georgia Tech Research Institute

## Proof-of-Concept - Heat Transfer Results

$V_0 = 32$  mph



$V_0 = 64$  mph



### Results:

➤ Heat Rejection is controllable with pneumatic lift augmentation

➤ "Dense" Carbon foam radiator shows great promise as purely forced convection radiator

Aerospace  
Transportation  
Advanced  
Systems  
Laboratory

EA715

Georgia Tech Research Institute

## On Road Test - Student Race Car Competition

Integration into GT Motorsports\* Formula SAE race car



\*Student Organization which competes with other schools in Formula SAE and international design (and race!) competition  
Last year: 1st Place in England (Formula Student)  
3rd Place (out of 142) in Formula SAE competition in US

Aerospace  
Transportation  
Advanced  
Systems  
Laboratory

EA716

Georgia Tech Research Institute



## On Road Test - Student Race Car Competition

- Initial installation with Visteon radiator
- Encountered head loss problems
- Used Turbocharger (not augmenting engine) as pressurized blowing air source



*Preliminary runs did not overheat engine, however coolant pump and pressure source problems needs to be overcome*

Aerospace  
Transportation  
Advanced  
Systems  
Laboratory

EXF17

Georgia  
Tech Research  
Institute

## Summary

- Pneumatic aerodynamic radiator was successfully tested in wind tunnel and confirmed basic concept
- Lift and drag are dramatically affected by porosity of radiator section, but  $C_{\mu}$  is still very powerful
- Wind tunnel model demonstrated non-optimized heat rejection performance  
*- optimization of radiator design will improve performance*
- Potential is great to have both controllable aero force AND low-drag-penalty engine cooling
- Carbon Foam enables optimal performance of the Aerodynamic Radiator

Aerospace  
Transportation  
Advanced  
Systems  
Laboratory

EXF18

Georgia  
Tech Research  
Institute

## Future Directions

---

- Important system integration issues need to be addressed
  - Source of steady high pressure air
  - Pumping of engine coolant to wing surface
- Further on-road tests with Formula SAE car will demonstrate efficacy of concept
- Further research is needed! Several racing teams as well as large heavy vehicle manufacturers and SUV manufacturers have expressed significant interest
- Fixed-wing Aircraft and UAV radiator-in-wing potential





## **Summary: 2004 NASA/ONR Circulation Control Workshop**

Ronald D. Joslin <sup>1,a</sup> and Gregory S. Jones<sup>2</sup>

<sup>1</sup>Office of Naval Research, 800 North Quincy Street, Arlington, VA 22217 USA

<sup>2</sup>NASA Langley Research Center, Hampton, Virginia 23681

### **Abstract**

This conference proceeding is comprised of papers that were presented at the NASA/ONR Circulation Control Workshop held 16-17 March 2004 at the Radisson-Hampton in Hampton, VA. Over two full days, 30 papers and 4 posters were presented with 120 scientists and engineers in attendance, representing 3 countries from industry, academia, and government laboratories. In this paper, we summarize some of the issues raised during the two-day workshop. These issues may take the form of significant benefits realized with circulation control, conflicting results between different presentations, or future directions for circulation control research. The reader must be aware that we have encouraged the authors to include preliminary results and extraneous results in this workshop for the benefit of future circulation control applications.

---

<sup>a</sup> The views expressed in this article are those of the authors and do not reflect the official policy of position of the US Office of Naval Research, the US Department of Defense, or the US Government. Distribution Statement A: Approved for public release; distribution is unlimited.

## Introduction

The previous workshop on circulation control is documented in a conference proceeding by Nielsen (1986) and in a summary of the workshop by Nielsen and Biggers (1987).

The summary paper provided a very nice description of the known flow physics associated with circulation control and the Coanda effect<sup>b</sup>, which is now considered a common flow phenomena as outlined in US patent terminology. As well, other papers in the 1986 conference carefully outline the flow physics of this control technology and will not be repeated here. With this introduction, we summarize the previous workshop to glean what future directions were projected almost 20 years ago and if these directions were addressed in this conference some 2 decades later.

Technology development activities are cyclic and depend on platform needs of the day. Apparently, the 1980's had a significant focus on circulation control based on the two workshops and the writing of Nielsen and Biggers (1987). Fixed wing and rotorcraft were the aircraft platforms of that era. The 1986 conference had sessions that dealt with viscosity and turbulence (flow physics), circulation control airfoil theory, circulation control experiments, rotorcraft, X-wing technology, fixed wing technology, and circulation control research planning (Nielsen, 1986). Because Nielsen and Biggers (1987) summarized the major discoveries of the conference, it will not be repeated here.

---

<sup>b</sup> Discovered by Henri Marie Coanda (1886-1972). September 1, 1936, H. Coanda *Device for deflecting a stream of elastic fluid projected into an elastic fluid*. US Patent # 2,052,869. (In France on October 8, 1934: *Procedure and device for the deviation of a fluid inside another fluid*, #762688)

Rather, the presentation of future directions for circulation control research will be repeated to better understand what progress has been made in this technology.

Tables 1 to 4 repeat the research needs as outlined in the 1982 and 1986 workshops (Nielsen and Biggers, 1987). Interestingly, many of the issues listed as research needs for the future have been addressed and most of the solutions to these issues are reported in this conference proceeding. Many papers in the current workshop have investigated the use of oscillatory blowing, evaluated the turbulent flow physics, looked at high speed control, conducted many experiments and compared with airfoil theory, and introduced dual-slot control. These are some of the issues raised in the 1982 and 1986 workshops and have been addressed with much success in this proceeding. The following sections summarize the results of the 2004 workshop. The highlighted authors in this paper gave the oral presentation at the workshop.

### **Day 1 – 16 March 2004**

The first day contained 19 presentations and a key note address, which are summarized in this section.

## **Part 1**

*Paper 1:* Rich, **McKinley**, and Jones (2004) presented an overview of the NASA Vehicle Systems Program and the relationship of circulation control to aspects of this program. ESTOL, Quiet technology, low emissions, and autonomous vehicles are among the platform goals of the NASA program. The primary role of circulation control to focused on lift performance improvement.

*Paper 2:* **Englar** (2004) provided an overview of many uses of circulation control via tangential blown jets. The paper discusses application such as induced-flow thrust augmentation, airfoil high lift device, helicopter rotor, the A-6 circulation control wing, the pneumatic channel wing, and a couple of automotive applications. All of these applications demonstrate performance gains using circulation control.

*Paper 3:* Englar and **Campbell** (2004) discussed the use of circulation control on a circulation controlled channel wing. The propeller driven channel wing is based on the Custer channel wing. Through wind tunnel experiments, lift coefficients of 10 to 11 were achieved using pneumatic circulation control.

*Paper 4:* **Chang** et al. (2004) presented computational results for the NCCR 1510-7067 airfoil compared with experimental results. The amount of mass flow and slot height variations were considered for a range of airfoil angle of attacks. Although some disagreement with the experimental results was presented, correct trends in performance were predicted for a variation in angle of attack and slot height; however,



reasonable agreement was observed for the surface pressures. Again consistent with all other papers, the larger slot height led to better performance.

Paper 5: **Paterson** and Baker (2004) conducted a computational study of the NCCR-1510-7067N circulation control airfoil using RANS and the detached eddy simulation (DES) approaches. The surface pressure comparison showed good agreement between the computations and experiments. The lift had about a 5% difference but poor agreement was found for the drag comparison. The DES approach yielded some complex unsteady structures in the wake region.

Paper 6: **Viswanathan** and Tafti (2004) performed RANS computations using the NCCR 1510-7607N circulation control airfoil and made comparisons with the experimental data. Similar to other computational results presented in this workshop, the surface pressures were in good agreement for low values of blowing. Considerable disagreement resulted for high mass blowing values.

Paper 7: **Swanson**, Rumsey, and Anders (2004) present a computational study of a circulation control airfoil to study the effects of turbulent models, curvature effects, and eddy viscosity levels on the trailing edge Coanda flow. Here, the NCCR 1510-7067 airfoil is used and the computed results are compared with the experimental pressures. The one-equation SA turbulence model with curvature correction and two versions of the two-equation SST model were used in this study. All models predict separation downstream of the experiments at high Mach number, over predicting the lift

performance. All models produced excess eddy viscosity in the Coanda flow region. By modifying the curvature correction coefficient, the eddy viscosity is reduced and better agreement with experiments can be achieved with this coefficient tuning. Turbulence models were found to be the key element in achieving a good match between the computations and the experiments.

Paper 8: McGowan, Gopalarathnam, Xiao, and **Hassan**. (2004) Investigated the role of existing turbulence models on the predictive performance of circulation control airfoils. The preliminary comparisons for different turbulent models with the circulation control approach indicate that the predicted solution depends on the choice of turbulence models. Further, a laminar cavity (actuation) and turbulent cavity can yield different global changes in the pressure field. The laminar cavity solutions agreed with the experimental pressure results.

Paper 9: Liu et al. (2004) presented computational results of a study that used two-dimensional steady and pulsed blowing at the leading and trailing edge of an airfoil with a 30 degree deflected flap. A mass flow rate boundary condition was used to mimic the actuators. The low subsonic flow conditions were set to match previous experimental conditions. Excellent agreement between the computational predictions and the experimental results was noted over a large range of momentum coefficients and angles of attack up to stall conditions. This is quite surprising compared with some of the other papers in this series. Insufficient numerical and modeling details were presented in most of the papers to uncover the reason for this good agreement. As

expected, significant improvements in the lift performance was observed using circulation control. Leading edge blowing was shown to increase the stall angle, while the trailing edge blowing was shown to increase the overall level of lift. Also, slot height variations were explored and indicate that smaller slot heights lead to higher lift with the same momentum coefficient. However previous studies by Munro et al. (2001) and Munro and Ahuja (2003) have shown that larger jet heights lead to preferred acoustic performance. Thus, one must trade off between acoustic and aerodynamic performance when designing the optimal slot height. The study shows that using pulsed actuation the performance of the airfoil is increased compared with the steady blowing case. Through a parameter study, it was shown that the Strouhal number has a more dominant effect on the average lift coefficient than the frequency of the pulsed jet.

Paper 10: **Fasel**, Gross, and Wernz (2004) used the direct numerical simulation (DNS) and RANS approaches to study the flow physics of circulation cylinder subject to a blown wall jet and the NCCR 1510-7067N airfoil. On the cylinder, the DNS results suggested that the flow exhibited large-scale Görtler structures. RANS results on the airfoil were in good agreement with the experimental results.

Paper 11: Cerchie Cullen, Goldstein, Han, Taubert, **Wynanski** (2004) discuss a series of circulation control experiments that made use of steady blowing, suction, and periodic excitation. The physical features of the trailing edge Coanda flow were studied using a circulation cylinder. The wake profiles were substantially reduced with flow control compared with the baseline wake. Then a NACA 0015 airfoil with a 26 percent

chord flap was used circulation control at the trailing edge of the main airfoil, affecting the flow on the flap. Oscillatory excitation produced the higher performance gains compared to steady blowing. Then an ellipse model with leading and trailing edge cylinders were employed, permitting variations in slot widths and exhaust angles. Again steady blowing, steady suction, and oscillatory flows were for circulation control. Although the three actuation types produced lift enhancement, the periodic excitation produced the largest performance gain.

Paper 12: **Alexander**, Anders, and Johnson (2004) reported the results for experiments conducted using a circulation control airfoil at transonic speeds. Slot heights and the shape of the trailing edge were varied and result compared. At a Mach number of 0.8, decreased slot height and increased Coanda surface elliptical ratio increased the effectiveness of control. At a Mach number 0.3, decreased slot height and decreased elliptical ratio increased the control effectiveness.

Paper 13: **Kondor** presented experimental results for a circulation controlled engine nacelle simulator. The axisymmetric Coanda surface was located at the exit of the nacelle with a fixed slot height. These results indicated that circulation control techniques at the exit of the nacelle could be used to turn the flow to achieve vectored thrust and improved nacelle efficiency. The limitations of these data are related to having no external flow over the nacelle.

Paper 14: **Zha** and Paxton (2004) looked at the concept of a co-flow jet system on a NACA 2415 airfoil. The circulation control concept involved blowing near the leading edge of the upper surface and suction on the same surface is employed. The results indicate a substantial improvement in lift over the entire lift curve, positive and negative angles of attack. The lift-drag polar suggested that both a drag reduction and lift enhancement were achieved with this system.

Paper 15: Munro, **Ahuja**, and Englar (2004) investigated flow-induced noise associated with circulation control airfoils. The acoustics characteristics of a conventional airfoil with a flap were compared with a circulation control airfoil. The results showed a lower noise spectrum for the circulation control wing compared with the conventional wing at the same lifting conditions. It was suggested that the internal noise of the system could be improved through careful design of the system.

## **Part 2**

### **Day 2 – 17 March 2004**

*Paper 16:* **Joslin** (2004) highlighted some of the naval platform interests in circulation control. The V-22, A-6A, and HH-2D flight demonstrations were summarized followed by a discussion of circulation control issues for undersea applications. The effects of circulation control on the submerged operating envelope and maneuvering were presented.

*Paper 17:* **Imber** (2004) presented an overview of circulation control experiments conducted at the Naval Surface Weapons Center-Carderock Division over a 26 year period. Fixed wing and rotorcraft applications were discussed pertaining to wind tunnel and flight tests. Many investigations have considered the effect of slot height, thrust, power requirements, and performance. The discussion ended with a brief presentation of the dual slot low aspect ratio circulation control airfoil experiment.

*Paper 18:* **Loth** (2004) summarized the circulation control flight test conducted at the West Virginia University in the 1970's and makes a comparison with the A-6 circulation control conducted in the late 1970's. The paper deviates slightly from the presentation because the paper seeks to address the question: Why are there no current platforms with circulation control? Loth (2004) concedes that the main issue with circulation control is associated with landing on the backside of the power curve, where to fly at

half the speed at double the power would be required. Hence, take off and landing would require large power, making circulation control an undesirable technology.

Paper 19: **Moore** presented an overview of the use of circulation control on a notional NASA platform wave vortex wing-tip turbine powered vehicle. The use of a wingtip turbine provides a unique method of providing an air source for a CC system that is not associated with the vehicle propulsion system. In addition the tip turbine may be locked in place during cruise, when compressed air is not required, to provide an endplate effect, and therefore a reduction in induced drag. The wing-tip turbine could potentially generate sufficient energy to power the circulation control system for general aviation aircraft at lift coefficients of 3.5.

Paper 20: **Frith** and Wood (2004) discussed wind tunnel results using trailing edge circulation control on a 50 degree swept delta wing for roll control. The study showed that roll control was possible while simultaneously maintaining lift. Unlike most of the results presented here which integrated pressure tap measurements for performance, the current study makes use of a six-component balance for force and moment measurements. Consistent with Liu et al. (2004), smaller height slots lead to improved performance. The experiments did show that a particular rolling moment could be achieved using circulation control.

Paper 21: **Sahu** (2004) presented results of computations of 40 mm spinning projectile circulation control application. Four unsteady synthetic jets were used to vector the



projectile. Unsteady CFD computations were conducted using a hybrid RANS/LES approach. A dual time-step sequence was used to compute a time-accurate flow field prediction. The actuators had a peak velocity of 69 m/s oscillating at 1000 Hz. With a projectile velocity of Mach 0.11 and for a non-spinning projectile, the actuator-induced change in lift of the computations agrees with the experiments over an angle of attack from 0 to 4 degrees. For a projectile velocity of Mach 0.24 and a projectile spinning at 67 Hz, time-averaged results were shown for actuator on versus off conditions. A comparison of integrated forces for actuators operating at 31 and 69 m/s clearly show that the larger actuation leads to larger impulses.

Paper 22: **Burdges** (2004) discussed the design and fabrication issues related to circulation control models. This paper highlighted several model configurations discussed by Englar (2004) during this workshop. Various wings, automobile and tractor-trailer trucks (models and actual tractor-trailer), heat exchangers, and aircraft configurations were also presented.

Paper 23: **Rogers** and Abramson (2004) presented some operational issues and modeling (or prediction) capabilities for circulation control. The utility of panels methods coupled with some experimental results was highlighted. Fixed wing, a duct, and a rotorcraft were discussed with application of circulation control.

Paper 24: **The keynote address (Wood, 2004)** and an earlier paper by Brand et al. (1997) focused on the implementation of circulation control on the Bell Boeing V-22

Osprey. While on the ground during flight idle operations, the V-22 engine exhaust impinges on the ground. Portions of these hot gases are directed toward the fuselage causing some of the sensitive subsystems (e.g., avionics) to operate in an undesirable environment. The Coanda circulation control system was developed and implemented on the nacelles to deflect these gases away from the fuselage with a penalty of 7% engine bleed to operate the system. Circulation control was incorporated into the platform with a reduced weight and cost compared with the various deflector options. The engine bleed penalty did not detract from the performance of the platform because circulation control is used while on the ground when minimum performance is required from the engine. Hence, circulation control solved a critical platform issue. Introduction of steady-blown circulation control on the V-22 clearly supports the assertion that this technology has become a technology that can be engineered into a platform. However, oscillatory control is a recent development and much basic research remains, as this proceeding suggests and some of which will be outlined at the end of this paper. First, let us summarize the discoveries of this conference.

Paper 25: **Baker** and Paterson (2004) presented a two-dimensional computational study for the general aviation circulation control airfoil studied by Jones (2004). The mean surface pressure and lift forces agreed reasonably well with the experimental results for the baseline and steady low mass flow blowing control cases. High mass flow blowing computations under predicted the experiments.

Paper 26: **McGowan** and Gopalarathnam (2004) used the Fluent software package to analyze a circulation control airfoil, (General Aviation Circulation Control, GACC). The performance trends with blowing agreed with the experiments, but the computations under predicted what was observed in the experiments. The computations clearly showed movement of the attachment line with changes in mass flow.

Paper 27: **Jones** (2004) presented experimental results from a two-dimensional airfoil with steady and pulsed blowing (General Aviation Circulation Control, GACC). With variations in mass flow and slot height, performance improvements using circulation control were presented for a range of angle of attacks. Elliptic, biconvex, and circular trailing edge shapes were evaluated for steady and pulsed blowing conditions. The lift and drag performance benefit of each of these configurations are related to the  $r/C$ . For the steady blowing conditions lift increased with increasing  $r/C$ , but also increased the drag. Pulsed blowing decreased the mass flow requirement for a given lift in the separation control regime for larger circular  $r/C$ . However, the elliptic and biconvex trailing edges had no significant change in the lift or drag results for the pulsed configuration. The dual blown configuration that was to address the cruise drag associated with the blunt Coanda surface was also highlighted. The performance benefits of blowing thru the wing are discussed in terms of equivalent drag, measured drag, and power requirements for the low speed conditions associated with high lift and low speed control.

Paper 28: **Angle**, Huebsch, and Smith (2004) presented the application of circulation control to the Bell A821201 airfoil. The objective of circulation control for this application was to minimize downwash for a rotorcraft. A wind tunnel experiment with leading and trailing edge blowing slots indicated that a maximum of 8 percent reduction in the downwash force was obtainable using circulation control. Although no direct comparison was made with experimental results, computational results were presented for leading edge, trailing edge and combined blowing. The results indicate that leading and trailing edge blowing leads to the largest performance gains.

Paper 29: **Kelso**, Laubsch, and Haraldsson presented the results from a single slot airfoil experiment conducted at a Pennsylvania State University wind tunnel. The goal of the research was to evaluate the implementation of circulation control for a wind turbine application. Variations in mass flow and slot height were evaluated in the experiment. Smaller slots led to large performance gains for the 4 slots tested.

Paper 30: **Day** (2004) presented a variety of circulation control applications, including a ceiling fan, jetfan, the notar helicopter, turbines, pumps, and hovercrafts. Benefits of circulation control were demonstrated for these applications.

### **POSTER SESSION**

Each author was provided an opportunity to make a 15-minute oral presentation to describe and augment his or her poster presentation.

Paper 31: **Owen, and Owen** (2004) presented results from a two-dimensional circulation control airfoil tested in a wind tunnel. Wind tunnel wall interference effects were shown to significantly impacting the performance. For example, correcting the wall interference, the lift was reduced by almost 30 percent. Computational comparisons must account for this wall interference.

Paper 32: **Englar** (2004) discussed the use of circulation control for advanced automotive vehicles with the goal of increased fuel economy. The aft of a heavy vehicle trailer was implemented with pneumatic blowing action. Wind tunnel tests with the blowing on yield 15-25 percent reduction in drag over the baseline case. Using 4 slots on the 4 edges of the trailer yielded the largest drag reduction of 44-50 percent. A full-scale test with a pneumatic blowing system was conducted using a modified trailer provided by Volvo Trucks of North America. Approximately 15.3 percent increase in the fuel economy was observed with the system. Finally, the incorporation of pneumatic control in a SUV was discussed. Wind tunnel tests were conducted in the Lockheed 16' by 23' subsonic wind tunnel. The GM technical center supplied an aft door assembly and was modified to incorporate the blowing slots. The test results indicate a drag reduction for low blowing, with approximately 415 percent return on jet momentum investment. For higher blowing coefficients, the drag was observed to increase with increased momentum.

Paper 33: Gaeta and **Englar** (2004) presented a wind tunnel evaluation of an Aerodynamic Heat Exchanger concept employing circulation control for racecar

applications. This new concept was shown to adequately transfer heat at the same or similar rates as convectational radiators at  $90^\circ$  to the flow, but at much lower drag coefficients when enclosed in a lifting surface parallel to the flow field.

Presentation with no documentation: **McMichael** et al. (2004) discussed the use of circulation control to control a 40 mm projectile (these experiments are related to Sahu paper 21). The aft of the projectile was designed to have a Coanda surface. Four small synthetic jets were used to vector the projectile while the projectile spins and proceeds toward its target. Control of the trajectory of the projectile is achieved by altering the pressure distribution on the projectile through a forced asymmetric control of the separation. While the projectile spins at 67 Hz, functionally, one actuator would be active for 1/4 of a spin and turned off for the remaining 3/4 of the cycle. This on/off operation of the actuator leads to asymmetric separation and an induced force to alter the trajectory of the projector.

Paper 34: Joslin and Jones (2004) have summarized the 2004 NASA/ONR Circulation Control Workshop proceeding. Our ability to design and implement circulation control concepts onto aircraft (fixed wing & rotorcraft), marine, automotive, and miscellaneous applications has been highlighted throughout this workshop. Coanda driven circulation control is a technology that has the potential of improving performance for many applications that have been described throughout this workshop. In some cases where performance requirements exceed traditional capabilities, circulation control may become the viable solution. However, the roadblocks to implementation that circulation

control faces remain in the performance requirements and optimization of a design for particular application, i.e. it's in the details. In light of the shrinking resources associated with advanced technologies, it is important to set direction that leverages off of the state of the art. The final portion of this discussion is focused on what future directions remain for circulation control.

### **Future Directions**

The workshop concluded with an open discussion of lessons learned and future direction. The state of the art for circulation control can be related to what we can and cannot predict, design, and or implement. This workshop has highlighted the successful implementation of circulation control for several applications and demonstrated performance benefits through experiment and CFD. Many of the workshop participants would suggest the technology readiness level for circulation control has reached a level that has transitioned from basic science and technology to research and development (or applied engineering). Others would say that we cannot reliably predict circulation control performance and need more basic research that focuses on the physics of Coanda surface jet separation and turbulence modeling. Both are correct, as confirmed by inconsistencies in the workshop's CFD challenge and by the key-note address (Wood, 2004) and an earlier paper by Brand et al. (1997) that focused on the implementation of circulation control on the Bell Boeing V-22 Osprey.

To understand why circulation control technologies are not routinely found on production vehicles, one must understand the tradeoffs of competing technologies. These tradeoffs include, aerodynamic requirements and performance, weight, safety,



noise, impact on other systems (e.g. mass flow from engines, controls, maintenance, etc.). While lift performance is critical to many of the vehicles described throughout the workshop, drag/thrust and the moments created by this technology are equally important. These tradeoffs were not directly addressed in this workshop. However, as part of the NASA and ONR visions described in the workshop, circulation control research of the future will be directed toward vehicles (real and notional). The benefits of circulation control technologies can be large but can only “buy it’s way on” to a vehicle through the integration process, making realistic system studies necessary.

NASA’s ESTOL vehicle will start from scratch, enabling the design and integration of engine and circulation control systems to be optimized. This paper has also highlighted the successful implementation of circulation control for some naval demonstrators and raised some issues for the practical application of circulation control for undersea platforms. Of course, it is debatable whether these issues have been addressed sufficiently for direct implementation on a new platform.

The methods for system analysis for circulation control are based on empirical techniques, CFD, and experiments. To improve the design and prediction capability the workshop participants suggested the following recommendations for direction of circulation control activity:

### Near Term Needs for Circulation Control

What Next	2 Years
CFD	<ul style="list-style-type: none"> <li>•NOT CFD on our own... Do it along with New Experimental Benchmarks (Model, metrics, ...)</li> <li>•Include Noise (CAA)</li> <li>•Not Haphazard</li> <li>•Leverage off existing Data, find the good data base (eg. LM, GACC)</li> <li>•Develop panel codes in addition to advanced methods</li> </ul>
Experiments	<ul style="list-style-type: none"> <li>•Benchmarks with vehicle as a target</li> <li>•Work toward larger experiments (realistic scales)</li> <li>•Multiple Facilities</li> <li>•Pulsed blowing (larger scales, optimized frequency, supercirculation, realistic actuation, etc.)</li> <li>•Leverage off existing Data, fill in missing holes</li> <li>•Benchmark with hardware aimed at CFD validation (evaluate Re, boundary layer turbulence, noise, etc.)</li> </ul>
Applications	<ul style="list-style-type: none"> <li>•Commission a Vehicle (<b>aircraft</b>, submarine, automobile, truck, etc.)</li> <li>•Tie to VSP sectors and needs</li> <li>•Design with Panel Codes &amp; Experience</li> <li>•Emperical methods (capture before brain trust retires)</li> </ul>

### 2004 Research Needs for Circulation Control

Wrap Up Discussion	What Should We Be Doing
CFD	Study physics of the problem with high fidelity tools; need to better model the turbulence for CC; revisit the use of standard models which are based on empiricism (perhaps) inconsistent with CC; grid studies require to sort out numerical vs modeling errors; mimic real exp conditions (include WT walls); compare grid spacing; determine metrics for comparisons
Theory (e.g., panel codes)	CFD should support entrainment to support design codes; Re-look at panel codes.
What experiments need to be done & why?	Document exp conditions, & errors, uncertainties; wall effects & IC (e.g. receptivity/stability); Improve Drag database (integrate into propulsion system); tunnel flow quality (intensity, spectra); QA on model; test with appropriate application conditions (e.g. speed, density, supersonic flow, etc); resolve pressure, fluctuating and time avg in entrainment;h/_+ studies needed

### 2004 Research Needs for Circulation Control

Wrap Up Discussion	What Should We Be Doing
What applications are TRL>5? NOTAR, Bell Thrust Deflector, A6 Flight demo	System level CC requirements, impacts on platform, application; CC trade studies; failure mode alternatives What sensitivity/fidelity do designers require; Design guides needed to support industry; a goal of reducing noise; need propulsion involved in air supply issue.
Why isn't CC in production flight applications?	Not answered at workshop.... Discussion... It must buy it's way onto an aircraft. Do the aircraft flying today have a high lift requirements that cannot be met with conventional high lift systems? (No) Will the NASA ESTOL effort have such a requirement? (Yes?)
other	Need a roadmap, bench test experiments together (& reviewing previous exp); tie CC to a vehicle/mission... Working group should be formed prior to next workshop.

## **References**

- Alexander MG, Anders SG, Johnson SK. A wind tunnel experiment for trailing edge circulation control on a 6% 2D airfoil up to transonic Mach numbers. 2004 NASA/ONR Circulation Control Workshop, March 16-17, 2004, NASA/CP-2005-213509, pp. 407-426.
- Angle GM, Huebsch WW, Smith JE. Experimental and computational investigation into the use of the Coanda effect on the Bell A821201 airfoil. 2004 NASA/ONR Circulation Control Workshop, March 16-17, 2004, NASA/CP-2005-213509, pp. 917-938.
- Baker WJ, Paterson EG. Simulation of steady circulation control for the general aviation circulation control (GACC) wing. 2004 NASA/ONR Circulation Control Workshop, March 16-17, 2004, NASA/CP-2005-213509, pp. 819-840.
- Brand AG, Jenkins JL, Wood TL. Analysis, design, and testing of the Coanda effect exhaust deflector of the V-22 tilt-rotor. Twentieth European Rotorcraft Forum, Amsterdam/October 4-7, 1997.
- Burdges KP. Design and fabrication of circulation control test articles. 2004 NASA/ONR Circulation Control Workshop, March 16-17, 2004, NASA/CP-2005-213509, pp. 733-752.
- Chang PA, Slomski JF, Marino TA, Ebert M, Abramson J. Full Reynolds stress modeling of circulation control airfoils. 2004 NASA/ONR Circulation Control Workshop, March 16-17, 2004, NASA/CP-2005-213509, pp. 141-166.
- Cerchie D, Cullen L, Goldstein J, Halfon E, Han G, Taubert L, Trouve L, Wygnanski I. Some circulation control experiments. 2004 NASA/ONR Circulation Control Workshop, March 16-17, 2004, NASA/CP-2005-213509, pp. 369-406.
- Day TR. Coanda effect and circulation control for non aeronautical applications. 2004 NASA/ONR Circulation Control Workshop, March 16-17, 2004, NASA/CP-2005-213509, pp. 949-974.
- Englar RJ. The application of pneumatic aerodynamic technology to improve performance and control of advanced automotive vehicles. 2004 NASA/ONR Circulation Control Workshop, March 16-17, 2004, NASA/CP-2005-213509, pp. 985-1024.
- Englar RJ. Overview of circulation control pneumatic aerodynamics : Blow force and moment augmentation and modification as applied to fixed-wing aircraft. 2004 NASA/ONR Circulation Control Workshop, March 16-17, 2004, NASA/CP-2005-213509, pp. 37-100.
- Englar RJ, Campbell BA. Experimental development and evaluation of pneumatic powered-lift super-STOL aircraft. 2004 NASA/ONR Circulation Control Workshop, March 16-17, 2004, NASA/CP-2005-213509, pp. 101-140.

Fasel H, Gross A, Wernz S. Investigation of turbulent Coanda Wall Jets using DNS and RANS. 2004 NASA/ONR Circulation Control Workshop, March 16-17, 2004, NASA/CP-2005-213509, pp. 337-368.

Frith SP, Wood NJ. The use of circulation control for flight control. 2004 NASA/ONR Circulation Control Workshop, March 16-17, 2004, NASA/CP-2005-213509, pp. 667-698.

Imber R. Exploratory investigations of circulation control technology : Overview for period 1987-2003 at NSWCCD. 2004 NASA/ONR Circulation Control Workshop, March 16-17, 2004, NASA/CP-2005-213509, pp. 569-612.

Jones GS. Pneumatic flap performance for a 2D circulation control airfoil, steady & pulsed. 2004 NASA/ONR Circulation Control Workshop, March 16-17, 2004, NASA/CP-2005-213509, pp. 873-916.

Kelso FJ, Laubsch KL, Haraldson RK. Low-cost high-quality wind tunnel testing of a 30% elliptical circulation control airfoil at low blowing levels for application to wind turbines. 2004 NASA/ONR Circulation Control Workshop, March 16-17, 2004, NASA/CP-2005-213509, pp. 939-948.

Liu Y, Sankar LN, Englar RJ, Ahuja KK, Gaeta. Computational evaluation of the steady and pulsed jet effects on the performance of a circulation control wing section. 2004 NASA/ONR Circulation Control Workshop, March 16-17, 2004, NASA/CP-2005-213509, pp. 295-336.

Loth JL. Why have only two circulation-controlled STOL aircraft been built and flown in years 1974-2004, 2004 NASA/ONR Circulation Control Workshop, March 16-17, 2004, NASA/CP-2005-213509, pp. 613-650.

McGowan G, Gopalarathnam A. CFD analysis of a circulation control airfoil using Fluent. 2004 NASA/ONR Circulation Control Workshop, March 16-17, 2004, NASA/CP-2005-213509, pp. 841-872.

McGowan G, Gopalarathnam, Xiao X, Hassan H. Role of turbulence modeling in flow prediction of circulation control. 2004 NASA/ONR Circulation Control Workshop, March 16-17, 2004, NASA/CP-2005-213509, pp. 275-294.

Munro SE, Ahuja KK, Englar RJ. Noise reduction through circulation control. AIAA Paper 2001-0666, Jan. 2001.

Munro SE, Ahuja KK. Aeroacoustics of a high aspect-ratio jet. AIAA Paper 2003-3323, May 2003.

Munro SE, Ahuja KK, Englar RJ. Noise reduction through circulation control. 2004 NASA/ONR Circulation Control Workshop, March 16-17, 2004, NASA/CP-2005-213509, pp. 489-544.

Nielsen JN. (editor). Proceedings of the Circulation-Control Workshop 1986, 19-21 February 1986, NASA Conference Proceedings 2432, 1987.

Nielsen JN, Biggers JC. Recent progress in circulation control aerodynamics. AIAA Paper 87-0001, Jan. 1987.

Owen FK, Owen AK. Measurement and analysis of circulation control airfoils. 2004 NASA/ONR Circulation Control Workshop, March 16-17, 2004, NASA/CP-2005-213509, pp. 975-984.

Paterson EG, Baker WJ. RANS and detached-eddy simulation of the NCCR airfoil. 2004 NASA/ONR Circulation Control Workshop, March 16-17, 2004, NASA/CP-2005-213509, pp. 167-196.

Rich P, McKinley B, Jones G. Circulation control in NASA's vehicle systems program. 2004 NASA/ONR Circulation Control Workshop, March 16-17, 2004, NASA/CP-2005-213509, pp. 1-36.

Rogers EO, Abramson J. Selected topics related to operational applications of circulation control. 2004 NASA/ONR Circulation Control Workshop, March 16-17, 2004, NASA/CP-2005-213509, pp. 753-798.

Sahu J. Time-accurate simulations of synthetic jet-based flow control for a spinning axisymmetric body. 2004 NASA/ONR Circulation Control Workshop, March 16-17, 2004, NASA/CP-2005-213509, pp. 699-732.

Swanson RC, Rumsey CL, Anders SG. Aspects of numerical simulation of circulation control airfoils. 2004 NASA/ONR Circulation Control Workshop, March 16-17, 2004, NASA/CP-2005-213509, pp. 227-274.

Viswanathan A, Tafti DK. Numerical analysis of circulation control on a NCCR 1510-7607N airfoil using RANS models. 2004 NASA/ONR Circulation Control Workshop, March 16-17, 2004, NASA/CP-2005-213509, pp. 197-226.

Wood TL. From Concept to Production of the Coanda Driven Exhaust Deflector for the V22, 2004 NASA/ONR Circulation Control Workshop, March 16-17, 2004, NASA/CP-2005-213509, pp. 799-818.

Zha GC, Paxton C. A novel airfoil circulation augment flow control method using co-flow jet. 2004 NASA/ONR Circulation Control Workshop, March 16-17, 2004, NASA/CP-2005-213509, pp. 461-488.

Table 1. Circulation control research needs : 1982 (Nielsen, 1987).

#### Computational fluid dynamics

- Airfoils : N-S/Euler, including stall, etc.
- Transient rotor-wake/inflow
- Compare circulation control rotor wake with conventional rotor wake
- Stopped rotor code (x-wing cruise mode)
  - o Unsteady aerodynamics
  - o Front-rear wing interaction
- Three-dimensional pneumodynamics code
- Turbulence modes for Coanda area
- Wing-body integration and interaction

#### Experiments

- Study Existing data (basic understanding)
- Test circulation control airfoils (fundamental physics)
- Systematic airfoil tests (data base)
- Test circulation control wing, vary sweep, Mach, blowing, etc.
- Transonic test of vehicle design

#### Aerodynamic analysis and theory

- Circulation control airfoil prediction (AMI and SAI codes)
- Transient rotor wake (empirical)
- Upgrade X-wing analytical codes

#### Aeroelasticity and loads

- Nonsteady aerodynamics/flutter
- Front wing divergence, including servo feedback
- Vibratory loads on rotor
- Coupled wing/body flutter
- Rotor system aeromechanical stability

#### Flight dynamics

- Pitch/roll rate effects
- Ground effects
  - o Rotors
  - o Wings
- Control and trim aerodynamics
  - o Transition
  - o Conversion



Table 2. Circulation control basic research needs: 1986 (Nielsen, 1987).

<b>What</b>	<b>How</b>	<b>When</b>
Develop engineering circulation control airfoil code	Analysis, database	ASAP
Investigate nonsteady effects	Test	ASAP
Oscillate blowing		
Airfoil motion effects		
Investigate basic effects of circulation control aerodynamics (coordinate experiments and theory)	Analysis, 2D test	ASAP
turbulence		
local geometry		
compressibility		
external pressure gradients		
off-design effects (manufacturing defects, erosion, ice accretion, etc)		
Improve/optimize Coanda geometry	Analysis, 2D test	Start now
Develop high-speed circulation control airfoils	Analysis, 2D test	By 1988
Compile information groups		
Geometry for success	Database	ASAP
Detailed potential of circulation control	Database & experience	ASAP
System potential of circulation control	Analysis	1987

Table 3. X-wing research needs: 1986 (Nielsen, 1987).

<b>What</b>	<b>How</b>	<b>When</b>
Extended X-wing airfoil data base to include Low-speed and high alpha Dual, differential front-rear blowing skewed flow Oscillating blowing	2D wind tunnel test	ASAP
Develop second generation X-wing airfoils with 20% improvement Improve low-speed L/D Increase drag divergence Mach number Extend stall boundaries Increase total augmentation	Data base, analysis, 2D wind tunnel tests	extended test above
Develop and test lower-surface blowing concept	Data base, analysis, 2D wind tunnel tests	1986-87
Improve computing for higher-harmonic control system	Analysis	ASAP
Improve 3D predictions Rotary wing	Analysis	1987
Stopped rotor, including wing-body interaction		
Investigate gust response of vehicle	Analysis	1986-87

Table 4. Fixed-wing research needs : 1986 (Nielsen, 1987).

<b>What</b>	<b>How</b>	<b>When</b>
Investigate safety and reliability issues	Analysis	ASAP
Use of circulation control for engine exhaust turning	Test	ASAP
Effects of circulation control wing on tail downwash	Analysis, test	ASAP
Develop small Coanda for high-speed use Low drag with zero blowing High augmentation at low speeds Use of blowing at high speeds for control	Analysis, test	ASAP
Combine circulation control with slotted flap	Test	2-3 years
Investigate circulation control surfaces	Test	2-3 years



## Workshop Program Scope

1. As technological advances influence the efficiency and effectiveness of aerodynamic and hydrodynamic applications, designs and operations, this workshop is intended to *address the technologies, systems, challenges and successes specific to Coanda driven circulation control in aerodynamics and hydrodynamics.*
2. A major goal of this workshop is to *determine the state-of-the-art in circulation control and understand the roadblocks to its application.* The 2004 workshop will address and discuss *applications, CFD, and experiments* related to circulation control, emphasizing fundamental physics, systems analysis, and applied research.

## Workshop March 15 - 16, 2004

- 120 Registered Participants
  - Representing
    - 7 Government Agencies
    - 12 Industrial Partners
    - 13 Universities
- 34 Presentations
  - 13 Experimental
  - 11 CFD
  - 2 Combined CFD & Experiment
  - 8 Applications
- Results to be published as NASA CP and as a referred AIAA Book focused on CC

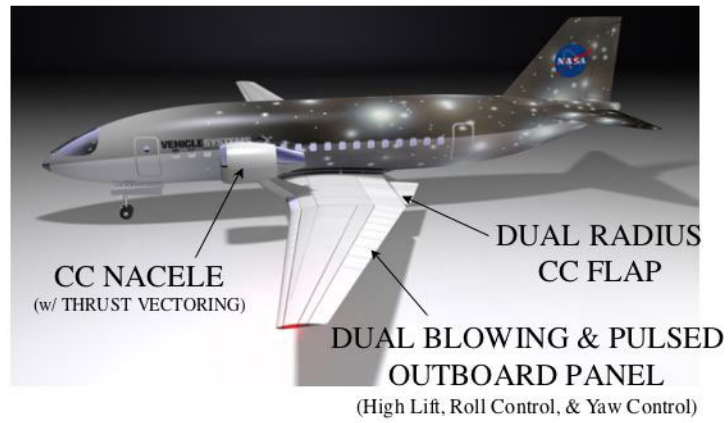
# General Outcomes

- Sponsor Visions
  - NASA vision toward aircraft vehicle eg. ESTOL focus (start from scratch instead of modifying existing platforms) ...
    - Lift Coefficient = 10,  $L/D > 25$ , engine bleed requirements, etc.
  - ONR vision refocused toward underwater vehicles
    - Addressing practical issues such as slot fouling in sea water, control with dual blowing, noise, and mass flow requirements.
- CFD ... Can't reliably predict it's performance.
  - Key is Separation on Coanda Surface (Turbulence Modeling is a critical factor)
- Experiment ... Lack of uncertainty analysis
  - Scaling parameters ( $Re$ , pulsed blowing, etc.)
- Application ... It bought it's way on to a deflector.
  - Bell showed a benefit of CC compared to Conventional control techniques

## *What did you learn from this workshop?*

- Where does the air come from? Need to include engine partners... start from scratch e.g. ESTOL vehicle.
- Disconnect between aero & noise activities... Disappointed that more noise research has not been accomplished
- Surprised at the deficiencies in CFD to capture BL/Jet physics; others believe that we have made much progress -but we need modern experiments for validation data w/ uncertainties.
- DATA (LM) available (non-electronic) for validation – we should make it available to all
- Data shows that thinner slots "can" lead to higher performance, but not universal. There is a range of h/c with good trends
- Good potential for oscillatory CC
- Much TE CC; should look at hybrid CC (e.g., mid-chord, coupled with LE AFC, etc.)
- Much of the data was at low  $Re$ , but we need more realistic (application) speeds and  $Re$ ... Scaling laws???
- Real Applications Do exist (WV GA aircraft, Bell thrust deflector, NOTAR, & A6)
- Surprised at diverse number of applications ... Automotive, Trucks, Wind Turbine, etc. (more than helicopter, fixed wing aircraft, and submarines)
- Recognize power requirements a good way to make comparison, (not just momentum i.e.  $C\mu$ )
- Inconsistencies in nomenclature/non-dimensionalization/etc... Makes modeling hard
- Why airframes do not use CC?? (Not answered here)
- Still addressing issues brought up in 1986 CC workshop (Not much progress since 86)

***NASA ESTOL CONCEPT***  
*using Simplified High Lift w/ Integrated  
Circulation Control Concepts*







2004 NASA/ONR Circulation Control Workshop  
Pre-registered Attendee List

Dr. Khaled S Abdol-Hamid  
Khaled.S.Abdol-Hamid@nasa.gov  
NASA Langley Research Center  
Hampton VA 23681

Jane Abramson  
abramsonjs@nswccd.navy.mil  
NSWC Carderock Division  
West Bethesda MD 20817

Dr. Krish Ahuja  
krishan.ahuja@gtri.gatech.edu  
Georgia Institute of Technology  
Atlanta GA 30332-0844

Michael G Alexander  
M.G.ALEXANDER@LaRC.NASA.GOV  
NASA Langley Research Center  
Hampton VA 23681

Brian Allan  
Brian.G.Allan@nasa.gov  
NASA Langley Research Center  
Hampton VA 23681

Scott Anders  
Scott.G.Anders@nasa.gov  
NASA Langley Research Center  
Hampton VA 23681

Gerald M Angle  
gangle@mix.wvu.edu  
West Virginia University  
Morgantown WV 26506-6106

Dr. Richard R Antcliff  
r.r.antcliff@larc.nasa.gov  
NASA Langley Research Center  
Hampton VA 23681

Zachary T Applin  
Zachary.T.Applin@nasa.gov  
NASA Langley Research Center  
Hampton VA 23681

Warren Baker  
wjb@wt.arl.psu.edu  
Penn State University  
State College PA 16803

Bobby L Berrier  
Bobby.L.Berrier@nasa.gov  
NASA Langley Research Center  
Hampton VA 23681

Dr. Robert E Bond  
rbond4@utk.edu  
University of Tennessee  
Knoxville TN 37996-2210

Sherilyn Brown  
S.A.BROWN@LaRC.NASA.GOV  
NASA Langley Research Center  
Hampton VA 23681

Kenneth P Burdges  
kburdges@mindspring.com  
Novatek, Inc.  
Smyrna GA 30080

Cecile M Burg  
fn.c.m.burg@larc.nasa.gov  
Georgia Institute of Technology  
Hampton VA 23681-2199

Dennis M Bushnell  
D.M.BUSHNELL@LaRC.NASA.GOV  
NASA Langley Research Center  
Hampton VA 23681

Bryan Campbell  
Bryan.A.Campbell@nasa.gov  
NASA Langley Research Center  
Hampton VA 23681

Jay Casper  
Jay.H.Casper@NASA.gov  
NASA Langley Research Center  
Hampton VA 23681

Nicolas Castro  
kieromaz@yahoo.com  
Virginia Commonwealth University  
Richmond, VA 23258

Dr. Peter A Chang  
changpa@nswccd.navy.mil  
NSWC Carderock Division  
West Bethesda MD 20817-5700

Dr. Lachlan Cullen  
lach@u.arizona.edu  
The University of Arizona/AME  
Tucson, AZ 85721

Mr. Terence R Day  
terryday1@hotmail.com, terry@vortex-  
dynamics.com.au  
Vortex Dynamics Pty Ltd  
Queensland Australia 4214

Charles Dixon  
cdixon@casinc.us  
Consulting Aviation Services, Inc.  
Kennesaw, GA 30144

Martin J Donnelly  
donnellymj@nswccd.navy.mil  
NSWC Carderock Division  
W.Bethesda MD 20817

Dr. John P Drummond  
j.p.drummond@larc.nasa.gov  
NASA Langley Research Center  
Hampton VA 23681

Charles Dunton  
Charles.V.Dunton@nasa.gov  
NASA Langley Research Center  
Hampton VA 23681

Robert J Englar  
bob.englar@gtri.gatech.edu  
Georgia Tech Research Institute  
Atlanta GA 30332-0844

Prof. Hermann F Fasel  
faselh@u.arizona.edu  
University of Arizona  
Tucson AZ 85718

James Fields  
J.Fields@larc.nasa.gov  
NASA Langley Research Center  
Hampton VA 23681

Steven Frith  
stevenfrith1978@yahoo.co.uk  
University of Manchester  
Manchester, United Kingdom M30  
7RU

Rick Gaeta  
rick.gaeta@gtri.gatech.edu  
Georgia Tech Research Institute  
Atlanta GA 30332-0844

Dr. Carl H Gerhold  
C.H.GERHOLD@LaRC.NASA.GOV  
NASA Langley Research Center  
Hampton VA 23681

Dr. Ari Glezer  
ari.glezer@me.gatech.edu  
Georgia Institute of Technology  
Atlanta GA 30332-0844

Prof. Ashok Gopalarathnam  
ashok\_g@ncsu.edu  
North Carolina State University  
Raleigh NC 27695-7910

David Greenblatt  
FN.D.GREENBLATT@LaRC.NASA.GOV  
NASA Langley Research Center  
Hampton VA 23681

Yueping Guo  
yueping.guo@boeing.com  
Boeing  
Huntington Beach, CA 92647

Andrew S Hahn  
A.S.HAHN@LaRC.NASA.GOV  
NASA Langley Research Center  
Hampton VA 23681

Rikard Haraldsson  
RHaraldsson@advan-tek.com  
Advantek International  
Boothwyn PA 19061

Dr. Hassan A Hassan  
hassan@eos.ncsu.edu  
North Carolina State University  
Raleigh NC 27695-7910

Geoffrey A Hill  
geoffrey.a.hill@nasa.gov  
NASA Langley Research Center  
Hampton VA 23681

William T Hodges  
William.T.Hodges@nasa.gov  
Army Cvl Srvc - Langley Research  
Center  
Hampton VA 23681

Dr. Thomas T Huang  
t.t.huang@ngc.com  
Northrop Grumman Newport News  
Washington, DC Wash., DC 20003

Dr. Wade W Huebsch  
Wade.Huebsch@mail.wvu.edu  
West Virginia University  
Morgantown WV 26506-6106

Robin D Imber  
ImberRD@nswccd.navy.mil  
NSWC Carderock Division  
West Bethesda Maryland 20817-5700

Stuart K Johnson  
Stuart.K.Johnson@nasa.gov  
NASA Langley Research Center  
Hampton VA 23681

Dr. Gregory S Jones  
Gregory.S.Jones@nasa.gov  
NASA Langley Research Center  
Hampton VA 23681

Dr. Ron D Joslin  
Ronald\_Joslin@onr.navy.mil  
Office of Naval Research  
Arlington VA 22217

Fred Kelso  
FKelso@advan-tek.com  
Advantek International  
Boothwyn PA 19061

Mehdi Khorrami  
mehdi@tabdemo.larc.nasa.gov  
NASA Langley Research Center  
Hampton VA 23681

Dr. Ki-Han Kim  
kimk@onr.navy.mil  
Office of Naval Research  
Potomac Maryland 20854

Shayne Kondor  
shayne.kondor@gtri.gatech.edu  
Georgia Institute of Technology  
Atlanta GA 30332-0844

Kenneth Laubsch  
klaubsch@advan-tek.com  
Advantek International  
Boothwyn PA 19061

Larry Leavitt  
Laurence.D.Leavitt@nasa.gov  
NASA Langley Research Center  
Hampton VA 23681

Prof Geoffrey Lilley  
g.m.lilley@soton.ac.uk  
Penn State University  
Hampton Va 23681

Dr. John Lin  
j.c.lin@larc.nasa.gov  
NASA Langley Research Center  
Hampton VA 23681

Dr. Yi Liu  
yi\_liu@ae.gatech.edu  
Georgia Institute of Technology  
Atlanta GA 30332-0150

Curtis Longo  
CLongo@toyota-aircraft.com  
Toyota ABDO  
Torrance, CA 90509-2729

Prof. John Loth  
loth@cemr.wvu.edu  
West Virginia University

Dr. Mujeeb R Malik  
Mujeeb.R.Malik@nasa.gov  
NASA Langley Research Center  
Hampton VA 23681

Dr. John B Malone  
John.B.Malone@nasa.gov  
NASA Langley Research Center  
Hampton VA 23681

Poorna Mane  
manep@vcu.edu  
Virginia Commonwealth University  
Richmond VA 23284

Johnny C Mau  
j.c.mau@larc.nasa.gov  
NASA Langley Research Center  
Hampton VA 23681

Gregory Z McGowan  
gzmcgowa@unity.ncsu.edu  
North Carolina State University  
Garner NC 27529

Bob McKinley  
R.E.MCKINLEY@LaRC.NASA.GOV  
NASA Langley Research Center  
Hampton VA 23681

James McMichael  
jim.mcmichael@etri.gatech.edu  
Georgia Tech Research Institute  
Atlanta GA 30332-0844

Diana McQuestion  
mcquestion@stcnet.com  
Planners Inc. (Staff)  
Hampton VA 23681

Michael McVeigh  
michael.a.mcveigh@boeing.com  
Boeing  
Philadelphia, PA 19142

Latunia Melton  
Latunia.P.Melton@nasa.gov  
NASA Langley Research Center  
Hampton VA 23681

Dr. Wade Miner  
Wade.Miner@ngc.com  
Northrop Grumman Newport News  
Newport News VA 23607

Kazuhiko Mochida  
kazmochida@toyota-aircraft.com  
Toyota ABDO  
Torrance, CA 90509-2729

Danny Molligan  
dmolligan@advan-tek.com  
Advantek International  
Boothwyn PA 19061

Mark D Moore  
Mark.D.Moore@nasa.gov  
NASA Langley Research Center  
Hampton VA 23681

Makram Mouhli  
mouhlim@vcu.edu  
Virginia Commonwealth University  
Richmond VA 23238

Tom Moul  
t.m.moul@larc.nasa.gov  
NASA Langley Research Center  
Hampton VA 23681

Charlie Novak  
charlie.novak@lmco.com  
Lockheed Martin  
Smyrna GA 30080

Michael OL  
Michael.OL@wpafb.af.mil  
AFRL  
Wright Patterson AFB, OH 45433-7542

Dr. Kevin Owen  
Compleere@cs.com  
Compleere, Inc.  
Pacific Grove, CA 93950

James Parish  
james.parish@siemens.com  
Siemens VDO Automotive  
Newport News, VA 23692

Dr. Eric G Paterson  
eric-paterson@psu.edu  
Penn State University  
State College PA 16803

Mark L Perry  
mark.l.perry@lmco.com  
Lockheed Martin  
Smyrna GA 30080

Dr. W. David Pointer  
dpointer@anl.gov  
Argonne National Laboratory  
Argonne IL 60439

Thomas W Roberts  
Thomas.W.Roberts@nasa.gov  
NASA Langley Research Center  
Hampton VA 23681

Ernest O Rogers  
RogersEO@nswccd.navy.mil  
NSWC Carderock Division  
West Bethesda MD 20817

Christopher Rumsey  
Christopher.L.Rumsey@nasa.gov  
NASA Langley Research Center  
Hampton VA 23681

Dr. Jubaraj Sahu  
jubaraj.sahu@us.army.mil  
U.S. Army Research Laboratory  
Aberdeen Proving Ground MD  
21005-5066

Dr. Lakshmi N Sankar  
lsankar@ae.gatech.edu  
Georgia Institute of Technology  
Atlanta GA 30332-0150

Dr. David M Schuster  
d.m.schuster@larc.nasa.gov  
NASA Langley Research Center  
Hampton VA 23681

Dr. Roy Scruggs  
rscruggs@casinc.us  
Consulting Aviation Services, Inc.  
Kennesaw, GA 30144

Delores Shackelford  
delores@stcnet.com  
Planners Inc. (Staff)  
Hampton VA 23681

Prof. Roger L Simpson  
simpson@aoe.vt.edu  
Virginia Tech  
Blacksburg VA 24061

Dr. Bart Singer  
Bart.A.Singer@nasa.gov  
NASA Langley Research Center  
Hampton VA 23681

Dr. Joe Slomski  
SlomskiJF@nswccd.navy.mil  
NSWC Carderock Division  
West Bethesda MD 20817-5700

Dr. James E Smith  
james.smith@mail.wvu.edu  
West Virginia University  
Morgantown WV 26506-6106

Kevin L Smith  
k.l.smith@ngc.com  
Northrop Grumman Newport News  
Newport News VA 23607

Dr. Craig Street  
C.L.STREETT@LaRC.NASA.GOV  
NASA Langley Research Center  
Hampton VA 23681

Gregory Stuckert  
gks@fluent.com  
Fluent Inc.  
Lebanon, NH 03766

Mohamad Sultan  
msultan@advan-tek.com  
Advantek International  
Boothwyn PA 19061

Charles Swanson  
Roy.C.Swanson@nasa.gov  
NASA Langley Research Center  
Hampton VA 23681

Prof. Danesh K Tafti  
dtafti@vt.edu  
Virginia Tech  
Blacksburg VA 24061

Takao Tate  
TTate@toyota-aircraft.com  
Toyota ABDO  
Torrance, CA 90509-2729

Dr. Demetri P Telionis  
telionis@vt.edu  
Virginia Tech  
Blacksburg VA 24061

Russ Thomas  
Russell.H.Thomas@nasa.gov  
NASA Langley Research Center  
Hampton VA 23681

Andy Turnbull  
A.R.Turnbull@larc.nasa.gov  
Swales  
Hampton Va 23681

Dr. Veer Vatsa  
v.n.vatsa@larc.nasa.gov  
NASA Langley Research Center  
Hampton VA 23681

Aroon K Viswanathan  
aroonkv@vt.edu  
Virginia Tech  
Blacksburg VA 24061

Prof. Vlachos P Vlachos  
pvlachos@vt.edu  
Virginia Tech  
Blacksburg VA 24060

Michael J Walsh  
M.J.WALSH@LaRC.NASA.GOV  
NASA Langley Research Center  
Hampton Va 23681

Anthony Washburn  
Anthony.E.Washburn@nasa.gov  
NASA Langley Research Center  
Hampton VA 23681

Dr. Robert E Whitehead  
bobw@nianet.org  
National Institute of Aerospace  
Hampton VA 23666

Tom Wood  
twood@bellhelicopter.textron.com  
Bell Helicopter Textron  
Fort Worth TX 76101

Kenneth Wright  
Kenneth.D.Wright@nasa.gov  
NASA Langley Research Center  
Hampton VA 23681

Dr. Israel J Wagnanski  
ijw@email.arizona.edu  
University of Arizona  
Tucson AZ 85721

Long Yip  
Long.P.Yip@nasa.gov  
NASA Langley Research Center  
Hampton VA 23681

Ken Young  
kyoung@advan-tek.com  
Advantek International  
Boothwyn PA 19061

Prof. Gecheng Zha  
zha@apollo.eng.miami.edu  
University of Miami  
Coral Gables FL 33124

Dr. John Zuk  
jzuk@mail.arc.nasa.gov  
NASA Ames Research Center  
Moffett Field CA 94035



REPORT DOCUMENTATION PAGE				Form Approved OMB No. 0704-0188	
<p>The public reporting burden for this collection of information is estimated to average 1 hour per response, including the time for reviewing instructions, searching existing data sources, gathering and maintaining the data needed, and completing and reviewing the collection of information. Send comments regarding this burden estimate or any other aspect of this collection of information, including suggestions for reducing this burden, to Department of Defense, Washington Headquarters Services, Directorate for Information Operations and Reports (0704-0188), 1215 Jefferson Davis Highway, Suite 1204, Arlington, VA 22202-4302. Respondents should be aware that notwithstanding any other provision of law, no person shall be subject to any penalty for failing to comply with a collection of information if it does not display a currently valid OMB control number.</p> <p><b>PLEASE DO NOT RETURN YOUR FORM TO THE ABOVE ADDRESS.</b></p>					
1. REPORT DATE (DD-MM-YYYY)		2. REPORT TYPE		3. DATES COVERED (From - To)	
01-06-2005		Conference Publication			
4. TITLE AND SUBTITLE Proceedings of the 2004 NASA/ONR Circulation Control Workshop				5a. CONTRACT NUMBER	
				5b. GRANT NUMBER	
				5c. PROGRAM ELEMENT NUMBER	
6. AUTHOR(S) Jones, Gregory S.; and Joslin, Ronald D. (Editors)				5d. PROJECT NUMBER	
				5e. TASK NUMBER	
				5f. WORK UNIT NUMBER 23-762-55-ME	
7. PERFORMING ORGANIZATION NAME(S) AND ADDRESS(ES) NASA Langley Research Center Hampton, VA 23681-2199				8. PERFORMING ORGANIZATION REPORT NUMBER  L-18395B	
9. SPONSORING/MONITORING AGENCY NAME(S) AND ADDRESS(ES) National Aeronautics and Space Administration Washington, DC 20546-0001				10. SPONSOR/MONITOR'S ACRONYM(S)  NASA	
				11. SPONSOR/MONITOR'S REPORT NUMBER(S)  NASA/CP-2005-213509/PT2	
12. DISTRIBUTION/AVAILABILITY STATEMENT Unclassified - Unlimited Subject Category 02 Availability: NASA CASI (301) 621-0390					
13. SUPPLEMENTARY NOTES An electronic version can be found at <a href="http://ntrs.nasa.gov">http://ntrs.nasa.gov</a>					
14. ABSTRACT As technological advances influence the efficiency and effectiveness of aerodynamic and hydrodynamic applications, designs and operations, this workshop was intended to address the technologies, systems, challenges and successes specific to Coanda driven circulation control in aerodynamics and hydrodynamics. A major goal of this workshop was to determine the 2004 state-of-the-art in circulation control and understand the roadblocks to its application. The workshop addressed applications, CFD, and experiments related to circulation control, emphasizing fundamental physics, systems analysis, and applied research. The workshop consisted of 34 single session oral presentations and written papers that focused on Naval hydrodynamic vehicles (e.g. submarines), Fixed Wing Aviation, V/STOL platforms, propulsion systems (including wind turbine systems), ground vehicles (automotive and trucks) and miscellaneous applications (e.g., poultry exhaust systems and vacuum systems). Several advanced CFD codes were benchmarked using a two-dimensional NCCR circulation control airfoil. The CFD efforts highlighted inconsistencies in turbulence modeling, separation and performance predictions.					
15. SUBJECT TERMS Circulation control; Coanda; High lift; Powered lift; Super-circulation; V/STOL; ESTOL; Advanced pneumatic flow control; Active flow control; CFD benchmarking					
16. SECURITY CLASSIFICATION OF:			17. LIMITATION OF ABSTRACT	18. NUMBER OF PAGES	19a. NAME OF RESPONSIBLE PERSON
a. REPORT	b. ABSTRACT	c. THIS PAGE			STI Help Desk (email: <a href="mailto:help@sti.nasa.gov">help@sti.nasa.gov</a> )
U	U	U	UU	520	19b. TELEPHONE NUMBER (Include area code) (301) 621-0390